Ute Linz (Ed.)

Ion Beams in Tumor Therapy

With 150 Figures, Some in Color
and 61 Tables

CHAPMAN & HALL
London · Glasgow · Weinheim · New York
Tokyo · Melbourne · Madras

Dr. UTE LINZ
Forschungszentrum Jülich GmbH
Institut für Kernphysik
D-52425 Jülich
Germany

A CIP catalogue record for this book is available from the British Library

Book Production: PRO EDIT GmbH, D-69126 Heidelberg
Typesetting: Mitterweger Werksatz GmbH, D-68723 Plankstadt
Printing, Cover: Appl OHG, D-86650 Wemding
Printed in the Federal Republic of Germany
Printed on acid-free paper

Ute Linz (Ed.)

Ion Beams in Tumor Therapy

ISBN 3-8261-0063-8

Preface

Restricting the irradiated volume to the site and shape of the tumor has been the goal of radiotherapists since the beginning of radiation therapy nearly 100 years ago. Even before appropriate particle accelerators were available it was realized that ion beams could be a means to get very close to this ideal. In 1946, the young Harvard physicist Robert Wilson published his pioneering article in which he outlined the physical rationale for the clinical usefulness of protons and other ions. But unlike X-rays, gamma radiation and neutrons which were used therapeutically very soon after their discovery, protons and heavier ions did not meet the immediate interest of therapists, despite their obvious physical advantages.

Several reasons have been responsible for the slow pick-up of this discipline. The new, expensive accelerators were restricted to a few research laboratories where they were fully occupied by high-energy physicists. None of these facilities had hospital access and there was no trained medical staff to perform the treatments. Not the least, the modest performance standards of the diagnostic techniques hampered a therapy which required precision localization.

Only in the last few years, things have begun to change. The last decade has brought great improvements in imaging techniques, such as MRI and CT, permitting tumor localization with an accuracy of a couple of millimeters. More radiotherapists became interested in ion beam therapy when the first treatment results became available which indicated clinical superiority of ions over conventional radiotherapy for certain tumor indications. In retrospect, these results must be valued especially high, because many of them were obtained with less than optimal irradiation conditions or outdated technical equipment which was not designed for medical applications in the first place.

Today, the first two hospital-based ion beam centers are operating: A proton therapy center in Loma Linda, California and a heavy ion facility in Chiba, Japan. These two, which profit from equipment specifically designed and built for therapeutic purposes, and a number of other institutions are developing innovative irradiation components to exploit clinically the unquestionable physical advantages of ion beams.

But it has to be understood that the real benefit of ion beam therapy can only be assessed when the most suitable tumor types are chosen and the highest standard of ion beam therapy is compared to the most advanced control treatment be it photons or any other modality. This evaluation, however, needs a much stronger foundation of information and knowledge, which has to come from intensive future research and clinical experience.

As the scientific knowledge of ion beam therapy is scattered throughout the literature or concealed in not easily accessible proceedings volumes, it has been the intention of this book to present a comprehensive overview on the present status of ion beam therapy and an outlook on where it is likely to go.

The title of the book implies that if focuses on therapeutic applications of accelerated protons and heavier ions. The term ion beam therapy has been preferred over the common "charged particle therapy" or the more recent "hadron therapy" to distinguish the medical application of accelerated

nuclei from that of electrons, pions, or neutrons, which share some physical and biological properties with ions, but are not specifically addressed in the book to keep the volume concise. Charged particles is only used as synonym for ions when the context is clear. Other terms that are occasionally a source of confusion are "light" and "heavy" ions. High-energy physicists or members of the ion beam community might not conceive the same when using these terms. Ions lighter than argon might be considered light by physicists in contrast to lead or uranium which they would classify as heavy. Within the ion beam community "light" ions are usually only the low-LET nuclei of hydrogen (protons) and helium. Carbon, nitrogen, and all other high-LET ions are called "heavy". By specifying the ions mostly by their name we have tried to avoid confusion on this issue.

Ion beam therapy is a highly interdisciplinary field which unifies diverse disciplines from accelerator physics to medical and biophysics, radiobiology and radiooncology. Colleagues from these various fields contributed to this book and hence permitted to examine the topic with all its clinical, biological, physical and technical facets. It has been a great pleasure to work within this international community and I am very much indebted to all those who contributed chapters to this book. I am also grateful to the Forschungszentrum Jülich for its support and permission to prepare this book. My special thanks go to Mrs. Eva-Maria Gottschlich and Ulrike Schmitt for their very careful and meticulous assistance in editing the manuscripts. Finally, I would like to apologize to all those whom I was pushing too much to meet one or the other tight deadline during the making of this publication.

Jülich, June 1995 U. Linz

Contents

List of Contributors

Dr. JOSE R. ALONSO
Lawrence Berkeley Laboratory
1 Cyclotron Rd., B 50–149
Berkeley, CA 94720, USA

Dr. JOHN O. ARCHAMBEAU
Loma Linda University Medical Center
Dept. of Radiation Therapy,
P.O. Box 2000, 11234 Anderson St.
Loma Linda, CA 92354, USA

Dr. JAN J. BATTERMANN
Academisch Ziekenhuis Utrecht
Catharijnesingel 101
NL-3511 GV Utrecht, The Netherlands

Dr. ELEANOR A. BLAKELY
Lawrence Berkeley Laboratory
1 Cyclotron Rd., MS 70-A-1118
Berkeley, CA 94720, USA

Dr. HANS BLATTMANN
Paul Scherrer Institut
Abt. Strahlenmedizin
CH-5232 Villigen, Schweiz

Prof. Dr. ANDERS BRAHME
Karolinska Institutet
Dept. of Medical Radiation Physics,
P.O. Box 260
S-17176 Stockholm, Sweden

Dr. JOSEPH R. CASTRO
Lawrence Berkeley Laboratory
1 Cyclotron Rd., B 50–149
Berkeley, CA 94720, USA

Dr. PIERRE CHAUVEL
Centre Antoine Lacassagne
Biomedical Cyclotron
227 Av. de la Lanterne
F-06200 Nice, France

Dr. WILLIAM T. CHU
Lawrence Berkeley Laboratory
1 Cyclotron Rd., B 64-227
Berkeley, CA 94720, USA

Dr. PASCAL COHILIS
Ion Beam Applications
Chemin du Cyclotron
Rue J. E. Lenoir 6
B-1348 Louvain-la-Neuve, Belgium

Dr. FRANÇOIS D'HERMIES
Centre de Protonthérapie d'Orsay
15 rue Georges Clémenceau, BT 101
F-91400 Orsay, France

Dr. Dr. JÜRGEN DEBUS
Rupprecht-Karls-Universität
Kopfklinik, Abt. Strahlentherapie
Im Neuenheimer Feld 400
D-69120 Heidelberg, Germany

Dr. LAURENCE DESJARDINS
Centre de Protonthérapie d'Orsay
15 rue Georges Clémenceau, BT 101
F-91400 Orsay, France

Dr. JOHN F. DICELLO
Clarkson University
Dept. of Physics, MS 5820
Potsdam, NY 13699, USA

Dr. Kenneth A. Frankel
Lawrence Berkeley Laboratory
1 Cyclotron Rd., MS 55-121
Donner Pavilion
Berkeley, CA 94720, USA

Dr. Eric Frau
Centre de Protonthérapie d'Orsay
15 rue Georges Clémenceau, BT 101
F-91400 Orsay, France

Dr. John Gueulette
Université Catholique de Louvain
Cliniques Universitaires St. Luc
Av. Hippocrate 10
B-1200 Bruxelles, Belgium

Dr. Jean-Louis Habrand
Centre de Protonthérapie d'Orsay
15 Av. Georges Clémenceau, BT 101
F-91400 Orsay, France

Dr. Dan T. L. Jones
National Accelerator Centre
P.O. Box 72
Faure, 7131, South Africa

Dr. Andrzej Kacperek
Clatterbridge Centre for Oncology
Clatterbridge Rd., Bebington, Wirral
Merseyside, L63 4JY, United Kingdom

Dr. Patric Källmann
Karolinska Institutet
Dept. of Medical Radiation Physics
P.O. Box 260 S-17176 Stockholm, Sweden

Dr. Barbara Kaser-Hotz
Vet. Med. Klinik
Winterthurer Str. 260
CH-8057 Zürich, Switzerland

Dr. Kiyomitsu Kawachi
National Inst. of Radiol. Sciences
Div. of Acc. Phys. & Engineering
9-1, Anagawa 4-chome, Inage-ku
Chiba-shi, 263, Japan

Dr. Shohei Koyama
Proton Medical Research Center
University of Tsukuba, Tennodai
Tsukuba City, 305, Japan

Dr. Gerhard Kraft
Gesellschaft f. Schwerionenforschung
Postfach 11 05 52
D-64220 Darmstadt, Germany

Dr. Richard Levy
Lawrence Berkeley Laboratory
1 Cyclotron Rd., MS 55-121
Donner Pavilion
Berkeley, CA 94720, USA

Dr. Patricia K. Lillis-Hearne
Brooke Army Medical Center
San Antonio, TX 78234, USA

Dr. Ute Linz
Forschungszentrum Jülich GmbH
Institut für Kernphysik
D-52425 Jülich, Germany

Dr. Bernhard Ludewigt
Lawrence Berkeley Laboratory
1 Cyclotron Rd., MS 64-121
Berkeley, CA 94720, USA

Dr. Pierre Mandrillon
Centre Antoine Lacassagne
Biomedical Cyclotron
227 Av. de la Lanterne
F-06200 Nice, France

Dr. Yasushi Matsuzaki
Proton Medical Research Center
University of Tsukuba, Tennodai
Tsukuba City, 305, Japan

Dr. Alejandro Mazal
Centre de Protonthérapie d'Orsay
15 rue Georges Clémenceau, BT 101
F-91400 Orsay, France

Dr. Daniel W. Miller
Loma Linda University Medical Center
Dept. of Radiation Therapy
P.O. Box 2000, 11234 Anderson St.
Loma Linda, CA 92354, USA

Dr. Elizabeth Y. Minakova
Institute for Theoretical
and Experimental Physics
B. Cheremushkinskaya, 25
Moscow, 117259, Russia

Dr. JOHN E. MUNZENRIDER
Massachusetts General Hospital
Radiation Oncology – Cox 3
Boston, MA 02114, USA

Dr. MARK NYMAN
Lawrence Berkeley Laboratory,
1 Cyclotron Rd.
Berkeley, CA 94720, USA

Dr. TOSHIYUKI OKUMURA
Proton Medical Research Center
University of Tsukuba, Tennodai
Tsukuba City, 305, Japan

Dr. KIYOSHI OHARA
Proton Medical Research Center
University of Tsukuba, Tennodai
Tsukuba City, 305, Japan

Dr. EROS PEDRONI
Paul Scherrer Institut
Abt. Strahlenmedizin
CH-5232 Villigen, Schweiz

Dr. JÜRGEN PROSS
Deutsches Krebsforschungszentrum
Postfach 10 19 49
D-69009 Heidelberg, Germany
present address:
Fa. Leibinger GmbH
Bötzinger Str. 41
D-79111 Freiburg, Germany

Dr. MUDUNDI R. RAJU
Los Alamos National Laboratory
Life Sciences Division, MS M888
Los Alamos, NM 87545, USA

Dr. HARIZO RANDRIANARIVELO
Centre de Protonthérapie d'Orsay
15 rue Georges Clémenceau, BT 101
F-91400 Orsay, France

Dr. TIM RENNER
Lawrence Berkeley Laboratory
1 Cyclotron Rd., B 2-431
Berkeley, CA 94720, USA

Prof. Dr. WOLFGANG SCHLEGEL
Deutsches Krebsforschungszentrum
Postfach 10 19 49
D-69009 Heidelberg, Germany

Dr. PIERRE SCHLIENGER
Centre de Protonthérapie d'Orsay
15 rue Georges Clémenceau, BT 101
F-91400 Orsay, France

Dr. UWE SCHNEIDER
Paul Scherrer Institut
Abt. Strahlenmedizin
CH-5232 Villigen, Schweiz
present address:
Sektion Physik
Am Coulombwall 1
D-85748 München Garching
Germany

Dr. MICHAEL SCHOLZ
Gesellschaft f. Schwerionenforschung
Postfach 11 05 52
D-64220 Darmstadt, Germany

Dr. REINHARD SCHULTE
Loma Linda University Medical Center
Dept. of Radiation Therapy
P.O. Box 2000, 11234 Anderson St.
Loma Linda, CA 92354, USA

Dr. LAURENT SCHWARTZ
Centre de Protonthérapie d'Orsay
15 rue Georges Clémenceau, BT 101
F-91400 Orsay, France

Dr. JEFFREY V. SIEBERS
Loma Linda University Medical Center
Dept. of Radiation Therapy
P.O. Box 2000, 11234 Anderson St.
Loma Linda, CA 92354, USA

Dr. R. P. SINGH
Lawrence Berkeley Laboratory
1 Cyclotron Rd.
Berkeley, CA 94720, USA

Dr. JANET SISTERSON
Harvard Cyclotron Laboratory
44 Oxford St.
Cambridge, MA 02138, USA

Dr. JAMES M. SLATER
Loma Linda University Medical Center
Dept. of Radiation Therapy
P.O. Box 2000, 11234 Anderson St.
Loma Linda, CA 92354, USA

Dr. JERRY D. SLATER
Loma Linda University Medical Center
Dept. of Radiation Therapy
P.O. Box 2000, 11234 Anderson St.
Loma Linda, CA 92354, USA

Dr. GARY K. STEINBERG
Stanford University Medical Center
Division of Neurosurgery
300 Pasteur Dr.
Stanford, CA 94305, USA

Dr. ARIS TILIKIDIS
Karolinska Institutet
Dept. of Medical Radiation Physics
P.O. Box 260
S-17176 Stockholm, Sweden

Dr. HIROSHI TSUJI
Proton Medical Research Center
University of Tsukuba, Tennodai
Tsukuba City, 305, Japan

Dr. HIROHIKO TSUJII
Proton Medical Research Center
University of Tsukuba, Tennodai
Tsukuba City, 305, Japan
and
National Institute of Radiol. Sciences
Research Center of Charged Particle Therapy
9-1, Anagawa 4-chome, Inage-ku
Chiba-shi, 263, Japan

Dr. MARCIA URIE
Massachusetts General Hospital
Radiation Oncology
Boston, MA 02114, USA
present address:
University of Massachusetts Medical Center
Radiation Oncology
55 Lake St. North
Worcester, MA 01655, USA

Dr. STEPHAAN VYNCKIER
Université Catholique de Louvain
Cliniques Universitaires St. Luc
Av. Hippocrate 10
B-1200 Bruxelles, Belgium

Prof. Dr. ANDRÉ WAMBERSIE
Université Catholique de Louvain
Cliniques Universitaires St. Luc
Av. Hippocrate 10
B-1200 Bruxelles, Belgium

Prof. Dr. MICHAEL WANNENMACHER
Radiologische Klinik der Universität
Im Neuenheimer Feld 400
D-69120 Heidelberg, Germany

List of Abbreviations

A

AAPM = American Association of Physicists in Medicine
AGOR = Accelerator Groningen-Orsay, Groningen, The Netherlands
AVM = Arteriovenous malformation

B

BEV = Beam's eye view
BNCT = Boron neutron capture therapy

C

CAL = Centre Antoine Lacassagne, Nice, France
CCD = Charge-coupled device
CCO = Clatterbridge Centre for Oncology, Wirral, UK
CEC = Commission of the European Communities
CGE = Cobalt-Gray equivalent
CNS = Central nervous system
COMS = Collaborative Ocular Melanoma Study
COSY = Cooler Synchrotron, Jülich, Germany
CPO = Centre de protonthérapie d'Orsay, Orsay, France
CPU = Central processing unit
CRIRR = Central Research Institute of Roentgenology and Radiology, St. Petersburg, Russia
CRT = Cathode ray tube
CT = Computed tomography
CTV = Clinical target volume
CW = Continuous wave

D

DKFZ = Deutsches Krebsforschungszentrum (German Cancer Research Center), Heidelberg, Germany
DRR = Digitally reconstructed radiograph
DTL = Drift tube linac
DVH = Dose-volume histogram

E

ECHED = European Clinical Heavy-Particle Dosimetry Association
ECR = Electron cyclotron resonance
ECRIPAC = Electron cyclotron resonance ion plasma accelerator
ECU = European Currency Unit
EU = European Union
EULIMA = European Light Ion Medical Accelerator

F

FNRS = Fonds National de la Recherche Scientifique (Belgium)
FSU = Functional subunit
FWHM = Full width at half maximum

G

GSI = Gesellschaft für Schwerionenforschung (Society for Heavy Ion Research), Darmstadt, Germany
GTV = Gross tumor volume

H

HCL = Harvard Cyclotron Laboratory, Cambridge, USA
HILAC = Heavy Ion Linear Accelerator, Berkeley, USA
HIMAC = Heavy Ion Medical Accelerator Chiba, Japan
HITAG = Heavy Ion Therapy at GSI Darmstadt, Germany
HMI = Hahn-Meitner-Institut, Berlin, Germany
HZE = High atomic-number elements

I, J

IAEA = International Atomic Energy Agency
ICRU = International Commission of Radiation Units and Measurements
INP = Institute for Nuclear Physics, Gatchina, Russia
ITEP = Institute for Theoretical and Experimental Physics, Moscow, Russia
JINR = Joint Institute for Nuclear Research, Dubna, Russia

K

KEK = National Laboratory for High Energy Physics, Tsukuba, Japan
keV = Kiloelectronvolt
KFA = Forschungszentrum Jülich, Germany
KVI = Kernfysisch Versneller Instituut (Nuclear Physical Accelerator Institute), Groningen, The Netherlands
KM = Kaplan-Meier

L

LBL = Lawrence Berkeley Laboratory, Berkeley, USA
LCR = Local control rate
LD_{50} = Lethal dose 50%
LET = Linear energy transfer
LLUMC = Loma Linda University Medical Center, Loma Linda, USA
LRFS = Local recurrence-free survival

M

MEEI = Massachusetts Eye and Ear Infirmary, Boston, USA
MGH = Massachusetts General Hospital, Boston, USA
MRI = Magnetic resonance imaging

N

NAC = National Accelerator Center, Faure, South Africa
NCOG = Northern California Oncology Group
NIRS = National Institute of Radiological Sciences, Chiba, Japan
NPTC = Northeast Proton Therapy Center, Boston, USA
NTCP = Normal tissue complication probability

O

OAR = Organ at risk
OER = Oxygen enhancement ratio

P

PET = Positron emission tomography
PLC = Programmable logic controllers
PLD = Potentially lethal damage
PMMA = Polymethylmethacrylate
PMRC = Proton Medical Research Center, Tsukuba, Japan
PROG = Proton Radiotherapy Oncology Group
PSI = Paul Scherrer Institut, Villigen, Switzerland
PTCOG = Proton Therapy Cooperative Group
PTF = Proton Therapy Facility, Moscow, Russia
PTV = Planning target volume

R

RBE = Relative biological effectiveness
REGIS = Respiration-gated irradiation system
RF = Radiofrequency
RFQ = Radiofrequency quadrupole
rms = Root mean square
RTOC = Radiation Therapy Oncology Group

S

SAD = Source-to-axis-distance
SCL = Side-coupled linac
SEM = Secondary emission monitor
SERAG = Southern Europe Radiotherapy Group
SIN = Swiss Institute for Nuclear Research, Villigen, Switzerland
SIS = Schwerionen-Synchrotron, Darmstadt, Germany
SOBP = Spread-out Bragg peak
SSD = Source-to-skin distance
SUMC = Stanford University Medical Center

T

TCD_{50} = Tumor control dose 50%
TCP = Tumor control probability
TDF = Time, dose and fractionation
TE = Tissue-equivalent
TEPC = Tissue-equivalent proportional counter
TERA = Terapia con Adroni
TLD = Thermoluminescence dosimeter
TNM = Tumor-nodulus-metastasis

U–Z

UCSF = University of California at San Francisco
VOI = Volume of interest

I. Ion Beam Therapy in Perspective

1 The History of Ion Beam Therapy

M. R. RAJU

Life Sciences Division, Los Alamos National Laboratory, Los Alamos, NM, USA

Introduction

The term "ion beam therapy" is used to include radiotherapy using protons and heavy ions, and to distinguish them from fast neutrons and negative pions (pions) that are also of interest to radiotherapy. The clinical experience of fast neutrons and pions is relevant to ion beam therapy. Hence, although this article is primarily on the historical development of ion beams, it also brings in the results of fast neutrons and pions within the context of ion beams. For further details, the reader is referred to two books on this subject [1, 2]. The ion beam therapy centers are listed in Table 1. The historical developments in the use of protons in radiotherapy and -surgery in different countries

Table 1. World-Wide Ion Beam Experience*

Institution	Country	Ion	Date First Rx	Date Last Rx	Recent Patient Total
Berkeley 184	CA, USA	p	1954	1957	30
Berkeley	CA, USA	He	1957	1992	2054
Uppsala	Sweden	p	1957	1976	73
Harvard	MA, USA	p	1961		6138
Dubna	Russia	p	1967	1974	84
Moscow	Russia	p	1969		2550
St. Petersberg	Russia	p	1975		891
Berkeley	CA, USA	Ne	1975	1992	433
Chiba	Japan	p	1979		86
PMRC, Tsukuba	Japan	p	1983		393
PSI (SIN)	Switzerland	p	1984		1574
Dubna	Russia	p	1987		31
Uppsala	Sweden	p	1989		34
Clatterbridge	England	p	1989		513
Loma Linda	CA, USA	p	1990		805
Louvain-la-Neuve	Belgium	p	1991		21
Nice	France	p	1991		338
Orsay	France	p	1991		402
N.A.C.	South Africa	p	1993		6
Indiana Cyclotron	IN, USA	p	1993		1
UC Davis	CA, USA	p	1994		4
					2,487 Light Ion Beams 13,974 Proton Beams

* from: Particles, Newsletter (Ed J. Sisterson) No. 14, July 1994. Harvard Cyclotron Laboratory, Harvard University, Cambridge Massachusetts

will be presented first, followed by that for heavy ions.

Medical Use of Protons

Berkeley

The use of ion beams in general, and protons in particular, for radiotherapy was first proposed by Wilson in 1946 [3]. Berkeley was the birth place of particle therapy, including ion beam therapy, because of the discovery of the cyclotron principle by Ernest O. Lawrence, the development of cyclotrons with increasing energy in Berkeley under his leadership, and his interest in biomedical applications in physics.

Two years after the publication of the paper by Wilson, the 184-inch cyclotron was available for experiments. Tobias, Anger, Lawrence [4] conducted extensive studies of the physical properties of protons, deuterons and alpha particles and confirmed the predictions of Wilson. They also demonstrated, after careful radiobiological investigations, the potential applications of these beams to medicine. There were some interesting reasons for the concentrated effort on pituitary treatments, rather than radiotherapy at Berkeley. Because of the difficulty in delineating tumor and normal tissue boundaries and the negative experiences with fast neutrons earlier, both Ernest O. Lawrence and his brother Dr. John Lawrence who was a medical doctor, discouraged cancer treatment and were interested in other medical applications. They were searching for a scientifically and medically worthwhile project. There were some interesting research and clinical developments taking place at that time on the nature of growth hormone and its control by the pituitary gland. The Swedish surgeon Dr. Olivecrona [5] observed some startling remissions of advanced breast cancers after surgical removal of the pituitary gland. The rationale for doing a hypophysectomy for such cases dates back much earlier. The radioresistance of the pituitary was demonstrated by Lacassagne in France as early as in 1934 [6]. Dr. John Lawrence, inspired by Dr. Cushing, was interested in influencing the function of the pituitary but found it difficult to accomplish with X-rays [7].

The pituitary is a well localized gland closely surrounded by sensitive structures and hence is an ideal and appropriate target for sharp dose localization of ion beams. Tobias and his associates [8] attempted to irradiate selectively the pituitary gland of the rat with deuterons. The rats became hypophysectomized in a similar manner to the one obtained by surgery. The first use of ion beams in humans was for pituitary hormone suppression in the treatment of patients with metastatic breast carcinoma [9]. Subsequently, pituitary suppression/ablation was applied to the treatment of proliferative diabetic retinopathy and pituitary adenomas. The improvements of the 184-inch cyclotron, driven by the high-energy physics research, led to the acceleration of protons and deuterons to much higher energies with longer ranges, thereby losing most of the favorable, Bragg-peak characteristics. However, the biomedical work was continued at Berkeley using a helium ion beam. The clinical experience of pituitary treatments in more than 800 patients was reviewed by Levy et al. [10].

Uppsala

The famous protein chemist and Nobel Laureate, Svedberg and his associates turned to Berkeley, in the late 40's and early 50's when they designed and built the 230-cm proton synchrocyclotron in Uppsala, Sweden. Like Lawrence, they wanted to use the accelerated particles, not only for nuclear chemistry but for physical and medical studies as well. Inspired by the work of Tobias et al. [4] and their pioneering studies of radiation hypophysectomy, Svedberg engaged a young biophysicist, Börje Larsson in 1954 and gave him the task of implementing the Berkeley pituitary irradiation method in Uppsala. This task was performed under the guidance of Tobias and the endocrinologist Rolf Luft who worked with Olivecrona.

The project was successfully completed in 1956, but the Swedish group could not pursue the pituitary work further for lack of funds. So Larsson turned to basic radiobiological and physiological experiments, with the available biomedical proton beam line. On the basis of this research, a collaboration was initiated with a community of

Swedish clinicians. The famous neurosurgeon, Lars Leksell in Lund, inventor of stereotactic instruments now used world-wide, participated in the development of functional radiosurgery using protons and the radiation oncologist, Sten Graffman, for proton irradiation of tumors in the 60's. This modified research program ended with two new clinical applications: stereotactic functional radiosurgery of the brain [11] and fractionated proton therapy for large tumors with the spread-out Bragg peak [12]. Larsson, Graffman, and their associates also developed innovative techniques for large field radiotherapy and treated about 60 patients [12]. They demonstrated that almost any volume in the body can be selectively and uniformly irradiated using proton beams.

Cambridge and Boston

Dr. William Sweet, chief of the neurosurgical service at Massachusetts General Hospital, became quite interested in the studies being carried out at Berkeley and Uppsala. He decided to investigate the possibility of doing such work himself or with his colleagues. Dr. Sweet helped to arrange to send Dr. Ray Kjellberg, then a junior member of the neurosurgery staff to Berkeley and Sweden, to observe the proton beam work. Dr. Sweet persuaded the Harvard cyclotron group, headed by Dr. Preston at that time, to work with them. Koehler and his associates of the Harvard cyclotron group developed precise techniques to do hypophysectomy using the Bragg peak. The Berkeley group at that time was doing hypophysectomy mostly by using the cross-fire technique rather than the Bragg peak. The uniqueness of the Harvard cyclotron program is that since the early 60's the cyclotron operation, including the staff salaries, was completely supported by the modest income generated from patient treatments and it is still functioning that way today. The Harvard cyclotron, under the leadership of Mr. Andrew Koehler, developed numerous techniques appropriate for various medical applications. Kjellberg, in collaboration with the Harvard cyclotron group, also developed techniques to treat arteriovenous malformations with protons [13]. His work used the technique developed by Leksell and his associates, who in turn used the gamma knife developed for Leksell by Larsson and his associates.

A turning point in proton radiotherapy took place during the early 1970's. Dr. Ian Constable, an ophthalmologic surgeon from Australia, joined the Massachusetts Eye and Ear Infirmary, next door to Massachusetts General Hospital, and he started working with Koehler and his associates in 1972. They conducted animal experiments using monkeys to determine normal tissue tolerance levels. They also worked out procedures to make the technique suitable for more localized intraocular lesions such as malignant melanoma, which Constable saw as more important clinically [14]. The wisdom of this choice has been supported by its wide acceptance and impressive clinical results [15]. The successful results in treating uveal melanoma led to the use of proton beams from the cyclotrons as generators for neutron and pion radiotherapy.

Suit, Goitein and their associates, in collaboration with Koehler, initiated fractionated radiotherapy using large fields of protons. Goitein and his associates developed three-dimensional treatment planning techniques [16, 17]. The spectacular clinical results for boney and cartilaginous tumors of the skull base and cervical spine also aroused international interest in proton radiotherapy [18, 19].

Russia

The use of proton beams in radiotherapy and radiosurgery in the former USSR has an interesting beginning and a long history. It started from an illness due to cancer of the esophagus of Academician Pomeranchuk. When he was irradiated with X-rays in the Oncological Centre in Moscow, without a mention of his own disease, he asked why protons are not used for radiotherapy. Wilson's paper was not known to either Pomeranchuk or to the others there. Pomeranchuk died, but his illness was instrumental in developing proton radiotherapy in Russia.

During the mid-to-late 60's, in collaboration with high-energy physicists, Prof. Ruderman initiated an ambitious proton therapy program at

Dubna and Moscow. The Uppsala group, headed by Larsson, helped the development of proton therapy in the former Soviet Union starting in 1969. A Proton radiosurgery program was initiated at the Gatchina proton accelerator facility by Konnov and his associates in 1975. The Russian group has treated about 3600 patients, approx. 25% of the total number of patients treated with protons in the world (see Chapter 12 for details). The Soviet physicists, oncologists, and neurosurgeons should be congratulated because, in spite of the difficult political situation in the USSR, they held the first international seminar on Dec. 6–11, 1977, on the uses of proton beams in radiation therapy. Another international working meeting on proton therapy was organized by the Central Research Roentgen-Radiological Institute and was held in Leningrad on October 14–18, 1986.

The particle therapy groups of the world can take pride for their success in international collaboration during the cold war years. During the last five years, the interaction of Russian colleagues with European and American scientists has become a common occurrence.

Japan

The development of particle therapy also has a long history in Japan, and there has been US-Japan cooperation in these efforts. Neutron therapy has been carried out in Tokyo and Chiba, Japan since the early 70's. Proton therapy in Japan was initiated in 1979 at the National Institute of Radiological Sciences (NIRS) in Chiba, using a 70 MeV proton beam, and also begun in 1983 at the Particle Radiation Medical Science Center (now Proton Medical Research Center, PMRC) of the University of Tsukuba using a vertical beam of 250 MeV protons. The Chiba group pioneered the development of a three-dimensional, spot-beam scanning technique to reduce the dose outside the treatment volume considerably [20].

The Tsukuba group concentrated on treating common tumors such as lung-mediastinum, esophagus, digestive tract, gynecological, genitourinary organs. They have also developed an innovative technique to compensate for inhomogeneity problems in the treatment of lung tumors by using a respiration-gated irradiation system (cf. [21] and Chapter 32).

Current Status of Protons in Radiosurgery and Radiotherapy

Pituitary Treatments

Although the initial efforts in Berkeley and Harvard were primarily focussed on pituitary suppression/ablation for treating patients with mammary carcinoma, these treatments are not common anymore in the Western countries. With the increasing availability of gamma knives and linear accelerators modified for stereotactic procedures, and the development of new methods to select hormone-dependent mammary tumors protons are less commonly used today. With the recent developments in imaging technology such as MRI and CT, it is now possible to localize accurately most microadenomas. With this ability and the concurrent development of modern transphenoidal surgical techniques, surgical procedures are increasingly used for pituitary suppression/ablation because of their immediate beneficial effect without the delay in suppression of pituitary hypersecretion that is normally experienced after radiation treatment.

The data obtained with protons and helium ions, however, are still of value for the use of gamma knives and linear accelerators. Currently, pituitary treatments are being routinely carried out using protons in Russia.

Arteriovenous Malformations

The treatment of arteriovenous malformations using protons is being continued at the Harvard cyclotron, and in Russia. With the shutdown of the ion beam facilities in Berkeley, the associates of late Fabrikant are continuing to treat arteriovenous malformations at Loma Linda. Gamma knives and linear accelerators modified for use of stereotactic radiosurgery are currently being

increasingly used for AVM treatments. While small size AVMs, with diameters less than around 3 cm can be treated as effectively by these devices as with protons, protons continue to have an important role in treating larger AVMs.

Uveal Melanoma

The proton therapy for treating uveal melanomas was the treatment of choice and is pursued at many of the centers around the world that have proton beams. Char and his associates compared helium ions with brachytherapy using I-125. The helium ion results have been found to be superior [22].

Large Field Radiotherapy

The Harvard group has made a concentrated effort to treat sarcomas of the skull base/cervical spine by taking full advantage of the dose localization characteristics of protons. Immediately adjacent, radiosensitive, critical normal structures, such as brain, brain stem, cranial nerves, etc., normally restrict the dose that can be delivered to the tumor using conventional radiations. The resulting control rate was estimated to be about 35%. The five year actuarial control rate after proton treatment was found to be 94% for chondrosarcoma patients and 63% for chordoma patients [23]. This substantial gain in the results strongly suggests that post-operative proton therapy is the treatment of choice for these tumors.

Nearly 100% local control rates were observed after treatment with protons in several small groups of patients with inoperable meningioma, craniopharyngioma, rectal carcinoma, and soft tissue sarcoma [19]. The results from the group in Tsukuba, Japan are also found to be favorable in treating some of the common tumors [21].

The impressive clinical results obtained with protons in some of the well investigated tumor sites, led to the development of medically dedicated proton therapy facilities. One such facility, which is equipped with three gantries to allow convenient treatment with a high patient turnover, was built and is now in operation at Loma Linda, California. Another such facility is in the initial stages of design at Massachusetts General Hospital, Boston, and there are plans for many more (cf. succeeding chapters).

Heavy Ions

Dr. Tobias was primarily instrumental in initiating the heavy ion therapy program at Berkeley. His interest in heavy ions dates back to his graduate student days at Berkeley. His thesis in 1942 was entitled "High Energy Carbon Particles". Zirkle had already demonstrated in 1935, the big effects of alpha particles from polonium [24] and, subsequently, those with fast neutrons. The radiobiological studies of low-energy heavy ions provided the rationale for the use of heavy ions in radiotherapy. Since the protons did not produce biological effects much different from X-rays, it was then thought that heavy ions had all the advantages of protons and, in addition, they also had a high-LET effect. This prejudice, combined with the fact that the physicists decided to raise the proton energy to 730 MeV with no possibility of getting a lower-energy proton beam, explains why Tobias and his associates at Berkeley deviated from protons. Heavy ions with ranges adequate for radiotherapy were not available until 1974, when the two existing accelerators at Lawrence Berkeley Laboratory, the heavy ion linear accelerator (HILAC) and the Bevatron were modified and connected together in order to accelerate heavy ions to energies suitable for heavy ion radiotherapy. This combined facility was known as Bevalac and it was the only biomedical, heavy-ion facility in the world until its eventual shutdown at the end of 1992.

After extensive radiobiological studies using helium ions at the 184-inch cyclotron and heavier ions at the Bevalac, a collaborative clinical study under the leadership of Dr. Joseph R. Castro, was undertaken by the University of California, San Francisco Medical Center (UCSF) and Lawrence Berkeley Laboratory (LBL). Helium ions and neon ions were selected as ions to be tested. Helium ions were used mostly for dose localization characteristics similar to protons and neon ions for both the physical and possible biological

advantages of high-LET. After shutdown of the 184-inch cyclotron in 1987, the work with helium ions was shifted to the Bevalac.

The clinical results with helium ions in treating sarcomas at the skull base and uveal melanomas were impressive and consistent with proton results. The phase I–II clinical trial with neon ions suggested improved results for several types of tumors: advanced and recurrent microscopic salivary gland carcinomas, paranasal sinus tumors, advanced soft tissue sarcomas, microscopic sarcomas of bone, locally advanced prostatic and bilary tract carcinomas [25]. These results are consistent with the notion developed earlier from fast neutron radiotherapy experience that slowly growing tumors may be effectively treated with high-LET particles.

The Bevalac was prematurely shut down. It is ironic that there is no particle therapy facility left in Berkeley, the very birth place of particle therapy. The confirmation of these favorable heavy ion clinical results has to come from heavy ion facilities that are built in Darmstadt, Germany and Chiba, Japan (see Chapters 34 and 36).

Recent developments in sophisticated imaging techniques have helped to make use of the excellent dose distributions of heavy charged particles. Because of the biological complexities of tumors and their variations, the optimum utilization of high-LET beams requires considerable research effort in developing methods to identify tumors that have a better prognosis for high LET. The clinical experience with fast neutrons is relevant to heavy ions with regard to the potential applications of high-LET radiations. In principle, for the tumors that are found to be better treated with fast neutrons as compared to conventional radiations, heavy ions should be even better than fast neutrons because of their good localization characteristics. An international and cooperative effort is required to find the appropriate role for heavy ions in radiotherapy.

Acknowledgement

I would like to thank Dr. George A. Baker, Jr. for his suggestions to improve the manuscript.

References

1 Raju, M.R. Heavy Particle Radiotherapy. Academic Press, New York, 1980.
2 Fowler, J.F. Nuclear particles in cancer treatment. Med. Phys. Handbooks 8, Adam Hilger Ltd, Bristol, 1981.
3 Wilson, R.R. Radiological use of fast protons. Radiology 47, 487–491, 1946.
4 Tobias, C.A., Anger, H.O., and Lawrence, J.H. Radiological use of high energy deuterons and alpha particles. Am. J. Roentgenol. Radiat. Ther. Nucl. Med. 67, 1–27, 1952.
5 Luft, R. and Olivecrona, H. Experiences with hypophysectomy in man. J. Neurosurg. 10, 301–316, 1953.
6 Lacassagne, A. and Nyka, W. Sur les processus histologiques de la déstruction de l'hypophyse par le radon. Comptes Rendus Soc. Biol. 117, 956–958, 1934.
7 Lawrence, J.H., Nelson, W.O., and Wilson, H. Roentgen irradiation of hypophysis. Radiology 29, 446–454, 1937.
8 Tobias, C.A., Van Dyke, D.C., Simpson, M.E., Anger, H.O., Huff, R.L., and Koneff, A.A. Irradiation of the pituitary of the rat with high energy deuterons. Am. J. Roentgenol. Radiat. Ther. Nucl. Med. 72, 1–21, 1954.
9 Lawrence, J.H. Proton irradiation of the pituitary. Cancer 10, 795–798, 1957.
10 Levy, R.O., Fabrikant, J.I., Frankel, K.A., Phillips, M.H., and Lyman, J.T. Charged particle radiosurgery of the brain. Neurosurg. Clin. N. Am. 1, 955–990, 1990.
11 Larsson, B., Leksell, L., and Rexed, B. The use of high energy protons for cerebral surgery in man. Acta. Chir. Scand. 125, 1–7, 1963.
12 Graffman, S., Brahme, A., and Larsson, B. Proton radiotherapy with Uppsala cyclotron. Experience and plans. Strahlentherapie 161, 764–770, 1985.
13 Kjellberg, R.N. Proton beam therapy for arteriovenous malformations of the brain, in Operative Neurosurgical Techniques, Vol. 1. Schmidek,H. and Sweet, W. (eds.), Grune and Stratton, New York, 1988, pp. 911–915.
14 Constable, I.J., Goitein, M., Koehler, A M., and Schmidt, R.A. Small field irradiation of monkey eyes with protons and photons. Radiat. Res. 65, 304–314, 1976.
15 Gragoudas, E.S., Goitein, M., Koehler, A.M., Verhey, L., Tepper, J., Suit, H., Brockhurst, R., and Constable, I.J. Proton irradiation of small choroidal malignant melanomas. Am. J. Ophthalmol. 83, 665–673, 1977.
16 Goitein, M. and Abrams, M. Multi-dimensional treatment planning: 1. Delineation of anatomy. Int. J. Radiat. Oncol. Biol. Phys. 9, 777–787, 1983.
17 Goitein, M., Abrams, M., Rowell, D., Pollari, H., and Wiles, J. Multi-dimensional treatment planning: II. Beam's eye-view, back projection through CT sections. Int. J. Radiat. Oncol. Biol. Phys. 9, 789–797, 1983.

18 Suit, H. Potential for proton beams in clinical radiation oncology, in Proc. of 9th ICRR Meeting, Toronto 2, 3–13, 1992.
19 Suit, H. and Urie, M. Proton beams in radiation therapy. J. Natl. Cancer. Inst. 84, 155–164, 1992.
20 Kanai, T., Kawachi, K., Matsuzawa, H., and Inada, S. Three dimensional beam scanning for proton therapy. Nucl. Instr. Meth. 214, 491–496, 1983.
21 Tsujii, H., Tsuji, H., Inada, T., Maruhashi, A., Hayakawa, Y., Takada, Y., Tada, J., Fukomoto, S., Tatsuzaki, H., Ohara, K., and Kitagawa, T. Clinical results of fractionated proton therapy. Int. J. Radiat. Oncol. Biol. Phys. 25, 49–60, 1992.
22 Char, D.H., Quivey, J.M., Castro, J.R., Kroll, S., and Phillips, T. Helium ions versus I-125 brachytherapy in the management of uveal melanoma: A prospective, randomized, dynamically balanced trial., J. Ophthalmol. 100, 1547–1554, 1993.
23 Goitein, M. Personal communication, 1994.
24 Zirkle, R.E. Biological effectiveness of alpha particles as a function of ion concentration produced in their paths. Am. J. Cancer 23, 558–567, 1935.
25 Castro, J.R. Heavy ion therapy: The Bevalac Epoch, in Hadrontherapy in Oncology, Amaldi, U. and Larsson, B. (eds.), Proc. Int. Symp. Hadrontherapy, Como, Oct 18–21, 1993, Elsevier, Amsterdam, 1994, pp. 208-216.

2 The Role of Ion Beam Therapy in Cancer Management

J. DEBUS and M. WANNENMACHER

Department of Radiotherapy, Rupprecht-Karls-Universität Heidelberg, Germany

Introduction

Over the last decades advances in the field of radiation oncology have improved the cure rates for patients with various malignancies. Clinical results of surgery alone or combined with photon radiation therapy are improving for cancers of many sites. Nevertheless, there are still about 30% of all cancer patients with localized disease where failure in the treatment of the primary tumor factually means death for the patient. Improving the local control rate of these cases by 50% would improve the overall survival rates of cancer patients by 10–15% [1]. Ion beam radiotherapy may be one tool to help achieve this goal.

Since 1957 more than 16000 patients have been treated with ion beam radiotherapy [2]. Protons and helium ions, in particular, were investigated because of their improved dose distribution. This has translated into superior clinical results for several tumor sites in comparison to conventional radiotherapy with photons or electrons. Heavier ions gained additional interest, because of their experimentally and clinically demonstrated increased biological effectiveness.

Conformal Radiotherapy and the Risk of Treatment-Related Complications

The radiation tolerance of most organs depends on the volume of normal tissue treated [3]. Conformal irradiation techniques which restrict the treatment volume to the actual target volume reduce the probability for normal tissue complications. Depending on the total dose and the fractionation pattern prescribed, these techniques might also prompt better tumor control.

There are two categories of treatment-related morbidities due to radiation therapy: the acute and subacute radiation reactions on one hand, and so-called late delayed radiation reactions, on the other hand. While acute radiation reactions (e.g., hair loss) occur within days or weeks after radiotherapy, late radiation effects (e.g., brain necrosis) may appear years later. The natural history of acute and subacute reactions is often self-limiting, whereas late radiation reactions tend to be progressive and possibly manifest as unintended severe treatment complications. The aim of treatment planning is to minimize such side effects.

As irradiation-related morbidity often develops in non-target tissues, it can be assumed that a dose distribution which spares normal tissue leads to less frequent and less severe treatment-related morbidities and complications.

It is obvious that the overall treated volume must not be smaller than the size of the medically required target volume. Defining the proper planning target volume is, therefore, a crucial step in the treatment preparation and determines the potential clinical benefit of conformal therapy.

Figure 1 illustrates schematically the difference between conventional and conformal radiation therapy. Clearly, conformal techniques can reduce the volume exposed to significant dose levels and spare organs at risk. But it has to be kept in mind that organs at risk which are part of the planning target volume may not be spared because of the risk of local relapse. The treatment

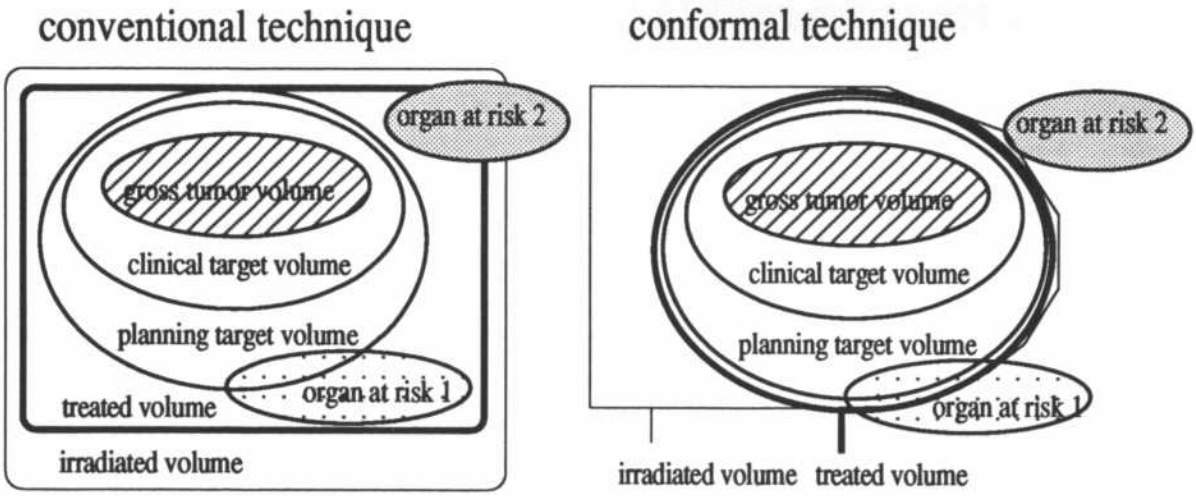

Fig. 1. Comparison between conventional and conformal technique with different radiotherapeutical volumes according to ICRU 50. While the organ at risk 2 can be completely spared by conformal techniques the organ at risk 1 is part of the planning target volume and may therefore only partially be spared

of carcinoma of the prostate stands for such a problem. As the anterior rectal wall is part of the target volume, radiation induced morbidity of the anterior rectal wall is generally put up with.

Enhanced Radiobiological Effectiveness

The radiobiological effectiveness of proton beams is nearly equal to conventional high voltage photon radiotherapy. Hence, both are comparable from the radiobiological point of view. Fast neutrons and heavy ions (e.g., carbon and neon) which are examples for high-LET radiation, exhibit an increased relative biological effectiveness (RBE) or a higher cell killing efficiency which is less dependent on oxygen saturation or the mitotic age of the cells (see subsequent chapter for details).

From early fast neutron radiotherapy it is known that high-LET radiation may improve local control [4] in selected indications (Tab. 1).

Table 1. Advantage of high-LET neutron therapy over conventional photon/electron radiotherapy [4]

Site/Histology	Number of patients	Significance
Salivary gland	150	++++
Prostate cancer	285	+++
Bone sarcomas	105	++
Soft tisse sarcomas	540	++

Patients to Profit from Precise Dose Localization

Technically, tumor conform treatment requires an accurate definition of the whole target volume, i.e., the outline of the target volume based on three-dimensional image information and the clinical knowledge of the microscopic tumor growth. Modern three-dimensional treatment planning is, therefore, a prerequisite of successful conformal treatment [5]. Defining the proper target volume is an essential step in the whole radiotherapeutical treatment. If it is too large, the risk of radiation morbidity increases and/or the total deliverable dose might not be sufficient for tumor control. Smaller target volumes bear the risk of

higher failure rates, because parts of the tumor margin might be excluded from the target volume. Despite a successive reduction of treatment volumes since the introduction of simulators, CT- and MRI-based treatment planning, local control rates have increased. But this is possibly due to the fact that up to now treatment volume contours have largely been defined by structures which are unambiguously non-target.

In general, patients will very likely profit from target volume conform irradiation and sparing of non-target tissues, if

- acute morbidity due to irradiation of non-target tissues is high, as, e.g., in prostate carcinoma, where radiation-induced rectal mucositis can be dose limiting,
- the cure rate is high but associated with significant radiation-induced morbidity as in the treatment of childhood cancer,
- the dose prescribed is limited by the late radiation morbidity of unnecessarily treated non-target tissue, as in the case of benign skull base tumors, where the tolerance of the adjacent brain structures is dose limiting,
- organs at risk have lowered tolerance due to previous radiotherapy, as, e.g., in the treatment of a local relapse or a secondary neoplasia years after the initial treatment.

It can be assumed that target conform treatment by ion beam therapy will increase the number of patients with complication-free local cure. For certain lesions, surgery might even be replaced or at least the scope of surgery reduced.

It has been shown that stereotactic single high dose irradiation (radiosurgery) of brain metastases can achieve similar tumor control rates as neurosurgical intervention with fewer cases of treatment-related morbidity [6].

A comparison of radiosurgery and conventional whole brain irradiation of solitary brain metastases revealed that radiosurgery could control 90% of the metastases locally. With conventional whole brain irradiation the corresponding value was only 45%. This example illustrates how tumor control can be improved by dose escalation in selected clinical situations after conforming the treatment volume to the target volume.

Presently and in the near future, conformal radiotherapy with ions will only be available to a very limited extent. Patients suitable for ion beam therapy, need, therefore, carefully be stratified according to the expected benefit. A system has recently been proposed by Drumm [7]. It suggests to favor patients who are likely to experience significant radiation morbidity after conventional treatment, due to unintended irradiation of non-target tissue outside the target volume. A second criterion is a high likelihood to improve the tumor control by dose escalation, and finally it should be evaluated, if modern photon treatment techniques combined with sophisticated treatment planning could achieve the required dose distribution at lower cost than ion beam therapy. Patients who meet the two former criteria and for whom the latter question can be answered with "no" are considered first priority.

There are a number of indications where the treatment of the disease is associated with the unintended but currently unavoidable irradiation of non-target tissue, e.g., mantle field irradiation in patients with Hodgkin's disease. They are always exposed to a currently unavoidable irradiation of the lung which is a non-target tissue in early stage Hodgkin's disease, and the patients may suffer from radiation-induced pneumonitis.

Currently, there are no techniques routinely available to solve this problem. Ion beams have the potential to spare such sensitive structures, at least in part.

The greatest benefit from ion beam therapy can probably be expected for the treatment of tumors located directly adjacent to an organ at risk. Chordomas of the clivus would be an extreme example, with the brain stem, the optic chiasm and the pituitary gland surrouding the target.

In randomized trials, it could be demonstrated that ion beam therapy of chordomas and chondrosarcomas of the spine and skull is superior to conventional radiotherapy (see Section III for details). Patients with constitutionally reduced radiotolerance, including young children with brain tumors may also profit considerably from ion beam treatment [8].

Patients to Profit from Increased Biological Effectiveness

For salivary gland tumors, prostate cancer, and certain sarcomas (see Tab. 1) survival and tumor control could be considerably improved with high-LET radiotherapy [4]. The late radiation effects observed with neutrons, however, are mostly attributed to the poor dose distribution of this kind of high-LET radiation from former neutron generators. They should be avoidable with heavy ions, which combine the radiobiological advantage of high-LET radiation with the ideal physical characteristics of fast protons. Patients with tumors that respond to high-LET radiation next to organs at risk should, therefore, benefit most from heavy ion beam therapy (head and neck tumors, rectum, retroperitoneal tumors).

A recent detailed study on the clinical relevance of heavy ion therapy concluded that approximately one third of all patients with localized tumors could, in principle, benefit from heavy ion radiation [7]. The selection was based on the following clinical criteria:

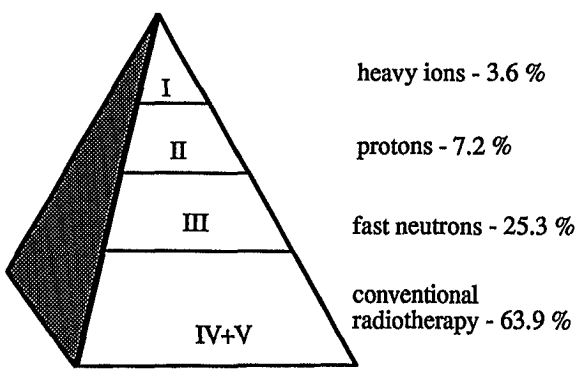

Fig. 2. The pyramid with the distribution of patients to different kinds of beam quality is based on socioeconomical data from [7]. It is assumed that there is only limited availability of ion beam therapy. The patients were stratified according to the expected benefit from improved dose distribution of ion beam therapy (I, II) or improved biological effectiveness due to high-LET effect (I, III) or the combination of both by heavy ion beam therapy (I)

- strictly locoregional tumor growth,
- tumors with no or low tendency to metastasize,
- cure rates either low or side effects with conventional therapy inacceptably high,
- patients young to middle-aged.

The study also considered the fact that heavy ion beam therapy is still not very widely available. Therefore, the author attempted a ranking of indications to select those patients for whom there is really no satisfactory alternative. It was concluded that the absolute minimum of patients with localized tumors who would require heavy ion therapy is 4% (see Fig. 2). Even this very narrow indication spectrum translates into approx. 11000 patients per year within the European Community and would require at least 4–5 heavy ion facilities.

Summary

The treatment of more than 16000 patients has demonstrated that ion beam application is feasible in clinical routine. Recent cost estimates, assuming very conservative numbers come to the conclusion that the capital cost of a proton facility is at least comparable to that of photon facilities of similar clinical capacity [7, 9]. If one further considers that higher cure rates produce less follow-up costs and bring more patients back into the work process, ion beam therapy becomes even more competitive.

The clinical data of proton and heavy ion treatment have confirmed the theoretical considerations regarding higher tumor control probability, less side effects and higher survival rates in a number of benign and malignant lesions, even though most have been obtained under suboptimal conditions as far as accelerator technology, beam delivery and treatment planning are concerned.

In the future, much more attention needs to be payed to a careful patient selection. The treatment plan should indicate that the equivalent ion dose in the target can be at least 10% higher than in the reference treatment and the dose to the organs at risk be lowered as compared to the currently available best possible photon technique.

The reference treatment should yield tumor control probabilities below 60% and be associated with a significant level of radiation-related morbidity due to non-target tissue exposure. If patient selection will follow these rules, one has a good chance to verify, where ions offer an actual advantage in local control or treatment-related morbidity.

Clinical studies with ion beams have been suggested for a number of malignancies, including carcinomas of the head and neck, prostate, uterus, rectum, soft tisse sarcomas, gliomas, meningiomas, retroperitoneal and pediatric tumors. International participation in clinical studies is now necessary to investigate the effectiveness of protons and heavier ions in Phase III studies.

Many more years are necessary until a comprehensive final judgement on the value of ion beams seems reasonable, not only because of the still limited number of clinical facilities and the long time periods needed for follow-up and detailed evaluation of a curative treatment, but also, because further diagnostic progress, advances in 3D-treatment planning, and new ways to compensate patient and target motion are being awaited. Improvements in these fields will also be responsible, at least in part, for the success of ion beam therapy.

References

1 Suit, H.D. The scope of the problem of primary tumor control. Cancer 61, 2141–2147, 1988.
2 Sisterson, J.M. World wide charged particle patient totals. Particles 14, 10, 1994.
3 Emami, B., Lyman, J., Brown, A., Loia, L., Goitein, M., Munzenrider J.E., Shank, B., Solin, L.J., and Wesson, M. Tolerance of normal tissue to therapeutic irradiation. Int. J. Radiat. Oncol. Biol. Phys. 21, 109–122, 1991.
4 Griffin, T.W., Wambersie, A., Laramore, G., and Castro, J. High-LET heavy particle trials. Int. J. Radiat. Oncol. Biol. Phys. 14, S1, S83–S93, 1994.
5 Goitein, M. 3D-treatment planning for heavy charged particles. Radiat. Environ. Biophys. 31, 241–245, 1992.
6 Engenhart, R, Kimmig, B.N., Höver, K.H., Wowra, B., Romahn, J., Lorenz, W.J., van Kaick, G., and Wannenmacher, M. Long-term follow-up for brain metastases treated by percutaneous stereotactic single high-dose irradiation. Cancer 71, 1353–1361, 1993.
7 Drumm, K. Sozioökonomische Studie zur Strahlentherapie mit geladenen Partikeln (Thesis), Rupprecht-Karls Universität, Heidelberg, 1993.
8 Gademann, G. and Wannenmacher, M. Charged particle therapy to pediatric tumors of the retroperitoneal region: A possible indication. Int. J. Radiat. Oncol. Biol. Phys. 22, 375–381, 1992.
9 Chu, W.T. Cost comparison between proton and conventional photon facilities. Particles 13, 8–9, 1994.

3 Physical and Biological Rationale for Using Ions in Therapy

U. LINZ

Forschungszentrum Jülich (KFA) GmbH, Jülich, Germany

Introduction

Since the beginning of clinical radiotherapy approximately 100 years ago, it has been the goal of radiation oncologists to restrict the irradiated volume to the site and shape of the target volume. With ion beams it is now possible to get very close to this goal (Fig. 1).

The fact, that ions of appropriate energy are suitable to irradiate a tumor at any depth of the body with a minimum dose to the surrounding healthy tissues is the strongest argument to consider protons and other accelerated ions for radiotherapy. This is achievable, because the penetration depth of ions can be taylored precisely by their initial energy and can be made to coincide with the location of the tumor to be treated. In

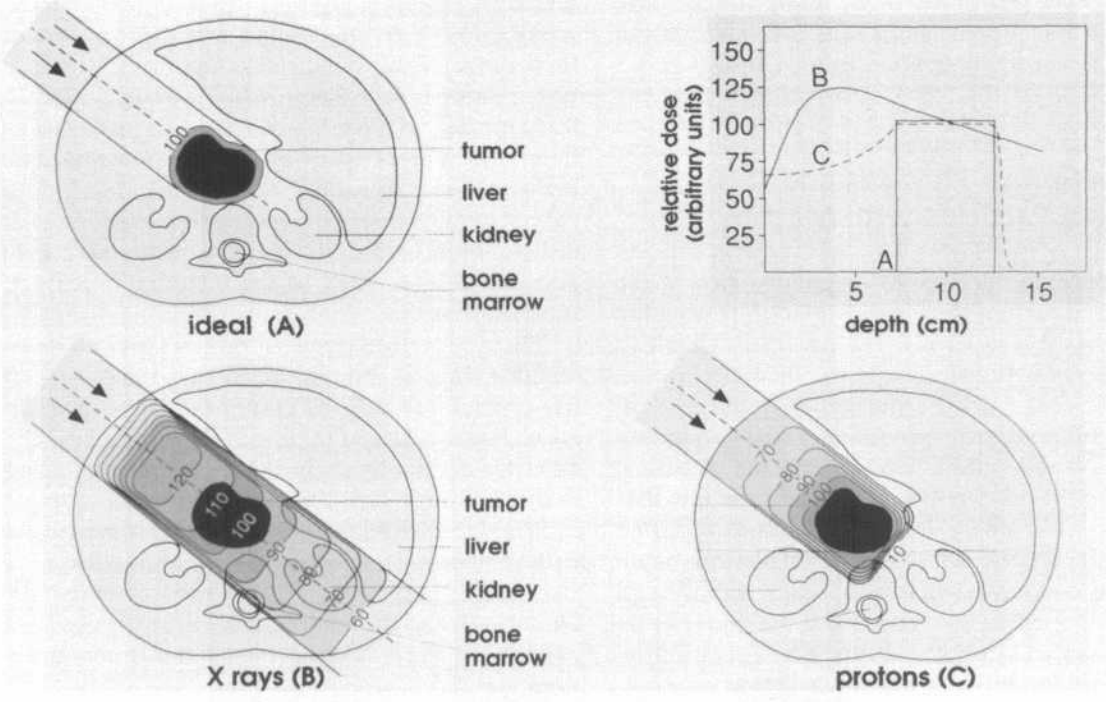

Fig. 1. Ideal vs. real radiotherapy: A) radiotherapeutically ideal situation: the full dose (100 %) is given to the tumor plus a small safety margin, while non-target structures receive no dose, B) depth-dose profile of megavoltage X-rays, C) depth-dose profile of a spread-out proton beam, D) depth-dose profiles of A, B, and C along the central beam axis

addition, the so-called Bragg peak effect prompts damage mainly at the end of the ions' range inside the tumor and keeps the radiation burden on the healthy tissue of the entrance channel low. Due to the finite path of ions, it is possible to limit the range of the radiation field to the distal part of the tumor and to spare the structures beyond from any radiation exposure.

In addition to a more favorable axis depth-dose distribution, another important feature distinguishes ions favorably from the conventional therapeutic radiations (photons and electrons): it is the lateral scattering of ions, which is negligible and leaves an incident beam greatly unchanged in size and shape when it penetrates the body.

The physical rationale to use protons and heavier ions in radiotherapy was conceived already nearly 50 years ago. In 1946, the Harvard physicist Robert R. Wilson published his pioneering paper on the radiological use of fast protons to "acquaint medical and biological workers" with some of the physical properties and possibilities of ions [1]. Since then, many others have reviewed the properties of ions that give reason for their clinical application (e.g., [2–4]).

Interaction of Photons and Charged Particles with Matter

When photons such as X- or gamma rays strike condensed matter, they release electrons from the atoms they interact with. The processes by which their energy is transferred to the medium are stochastic events, such as inelastic (Compton) scattering, photoelectric processes and – at higher energies – pair production. Due to the statistical nature of the absorption process and the fact that photons are strongly deflected (scattered) during their interactions with atoms, a photon beam entering condensed matter spreads rapidly and has no defined range. The respective axis depth-dose curve of a photon beam reveals an initial build-up domain, followed by a region of exponentially decreasing dose (Fig. 2).

In contrast to the indirectly ionizing electromagnetic radiation, all charged particles are

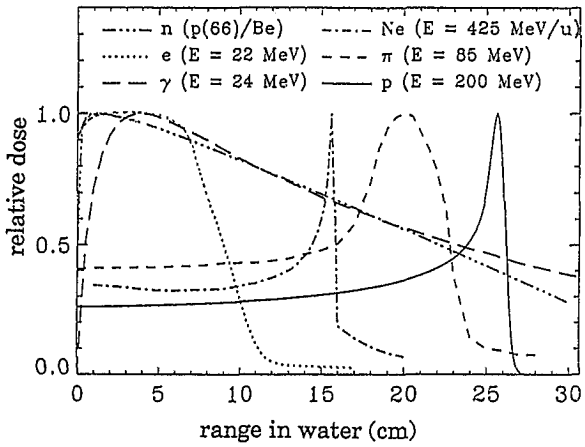

Fig. 2. Depth-dose distributions of various kinds of radiation in water

directly ionizing and all exhibit a finite, energy-dependent range.

Due to their low mass, accelerated electrons reach rapidly high velocities close to the speed of light (at energies > 1 MeV). Passing through matter, they, therefore, deposit a relatively constant energy dose per unit length for a good part of their range. Their penetration depth, however, is rather short (range R [g/cm^2]= 0.57 E_{max} [MeV]-0.16, for E_{max} > 1 MeV), as their low mass makes them also subject to strong lateral scattering. The low-intensity tail at the end of the depth-dose curves of high-energy electron beams (Fig. 2) is due to bremsstrahlung photons which are produced as a by-product of the stopping process of the electrons.

The depth-dose curve of protons and all heavier ions show a slow initial increase and a steep rise and fall towards the end of the range (Fig. 2). As a consequence of their much higher mass they experience significantly less lateral scattering than electrons.

The interaction of accelerated atomic nuclei with matter is predominantly an interaction with the target electrons (Coulomb interaction). Quantitatively, the energy loss of heavy charged particles is described by the Bethe-Bloch equation

$$\frac{dE}{dx} = Kn_o\frac{Z_{eff}^2}{\beta^2}\left[\ln\left(\frac{2m_ec^2\beta_2}{(1-\beta^2)I}\right)-\beta^2\right] \qquad (1)$$

where K is a constant, n_o the electron density of the target material, Z_{eff} the effective charge of the projectile ions, β the velocity of the projectile in units of the speed of light ($\beta = v/c$), I the mean ionization energy of the target atoms and m_e the mass of the electron.

With decreasing velocity the energy deposition increases. At the same time, the projectile scavenges electrons, thus reducing its effective charge, Z_{eff}. Together, both effects produce the sharp rise and fall – the Bragg peak – at the end of the particle track.

Most particles travel the same distance in a monoenergetic proton beam. Loss of particles due to nuclear interactions is low. But not all particles experience the same number of collisions. Their range is, therefore, somewhat different. This phenomenon is called straggling. In tissue the difference is of the order of 1% of the mean range [5]. For heavier ions, range straggling varies approximately inversely to the square-root of the particle mass. This means, helium ions show only 50% and carbon only 30% of the straggle of protons.

As the mass of an ion is at least 2000 times (for protons) higher than the mass of an electron, the projectile ions are barely deflected from their initial path during collisions with electrons. Still, multiple deflections cause lateral spreading and lead to divergence of the beam. For large parallel beams this affects only the outer edges which tend to get a little diffuse. The central axis remains unaffected, because the number of particles scattering out are compensated for by others scattering in. When applying narrow beams, however, the central dose decreases with depth, as particles scattering out are no longer compensated for.

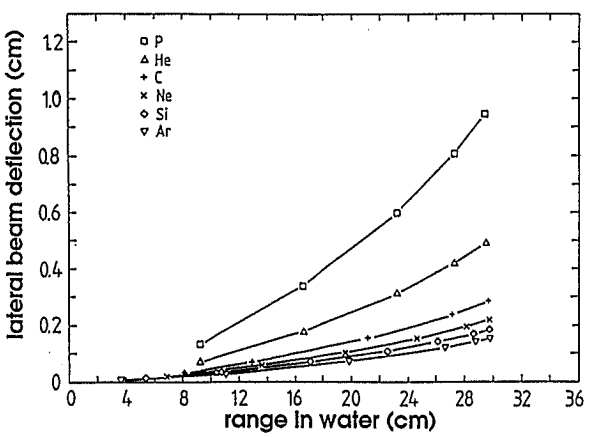

Fig. 3. Lateral beam deflection as function of penetration depth. Data from M. Phillips, LBL

The transverse spread of an infinitely narrow starting beam amounts to approximately 5% of its initial range [1]. Just as for range straggling, the deflection from the incident beam direction by multiple scattering (angular deflection) decreases with increasing charge and mass. Figure 3 illustrates this correlation graphically for several ions. For helium ions the effect is approximately a factor of two, for carbon a factor of four lower than for protons [5].

Tumor Conform Treatment

The narrow Bragg peak of a monoenergetic beam which is only a few millimeters wide, is exploited in specific radiosurgery procedures ([6–7], cf. as well Chapter 16). For most practical irradiations, however, it is necessary to spread out the radiation field laterally and in depth to cover a larger target area (Fig. 1). Up to now, this has been done by passive beam shaping devices, such as scattering foils and energy modulating absorber media which broaden the beam profile transversely and extend the Bragg-peak dose from the distal to the proximal end of the target volume, respectively (for review cf. [8]).

The charge of the ions provides another means to tailor the irradiated volume very precisely to the shape of the tumor. By deflecting a pencil-thin ion beam magnetically in horizontal and vertical directions, a tumor slice of the approximate width of the Bragg peak ($\approx$ 5 mm) can be irradiated point by point (Fig. 4). By reducing the energy stepwise and repeating the irradiation for each slice, a tumor of any arbitrary shape can be successively irradiated from its most distal to the most proximal part. This unique irradiation technique, which is only possible with protons and heavier ions, permits the ultimate in tumor conform radiotherapy, minimizing the radiation burden on healthy tissues. In addition, it facilitates

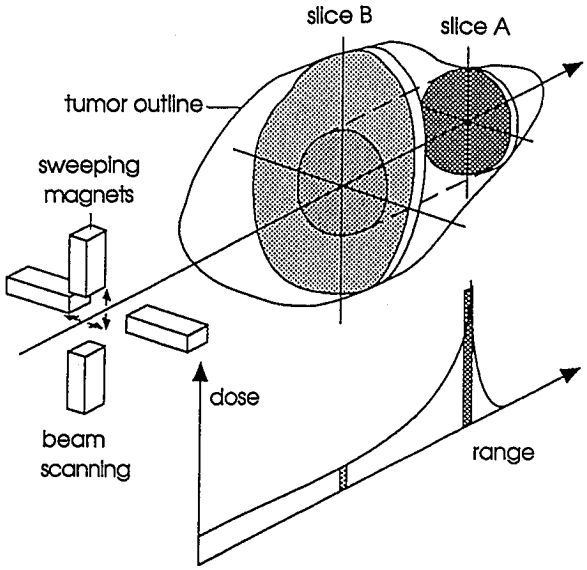

Fig. 4. Schematic view of scanning technique. Individual slices of approx. 5 mm (≈ Bragg peak width) are irradiated starting from the most distal part of the tumor and gradually moving forward. Within a slice the magnetically controlled ion beam is moved line-wise or from spot to spot to cover the desired target shape. The fact that proximal layers receive some dose (indicated by the dark central spot of slice B) when more distal layers (A) are treated has to be taken into consideration by appropriately designing the irradiation protocol (e.g., give higher dose to the lighter margin of slice B than to the preirradiated central spot)

the application of individualized treatments with local boosts or other desired non-homogeneous dose distributions. It can be applied to increase the dose in the tumor (as compared to photon irradiation) without increasing the dose in the entrance channel or to reduce unwanted radiation in the beam entrance without changing the tumor dose. Even though this irradiation mode has not yet been achieved clinically, several groups are working on its realization (cf. Chapters 35 and 36 for more details).

Linear Energy Transfer (LET)

The energy loss per unit length or LET has long been viewed as a major parameter to describe the qualitative differences of the biological effects of various kinds of radiation [9]. Numerically, the LET is identical with the stopping power of a particle for which all secondary electron energies are considered.

LET – usually expressed in keV/μm – is not a constant value. As charge and energy of a projectile ion change along the particle's path, the LET value changes, as well. The depth dependence of the LET displays the characteristic Bragg maximum. The maximum LET-value of electrons amounts to approximately 30 keV/μm. For protons, the corresponding value is roughly 100 keV/μm and for heavier ions it might be well over 1000 keV/μm.

It is the increase in stopping power of accelerated ions towards the end of their tracks which leads to more biological damage or an increase in RBE at the site of the Bragg peak. In general, the RBE rises with increasing LET up to approx. 100 keV/μm and decreases at higher LET values [24, 25].

Even though more recent systematic experiments have shown that the LET is not a good parameter to describe the full spectrum of biological radiation effects [9, 22, 23], it is still a widely used parameter to categorize ion-induced damage.

The limitations of LET become particularly prominent, when ions of different atomic number are compared [22, 26]. In this case, different biological responses can be observed for particles of the same LET (Fig. 5). This is explained by the

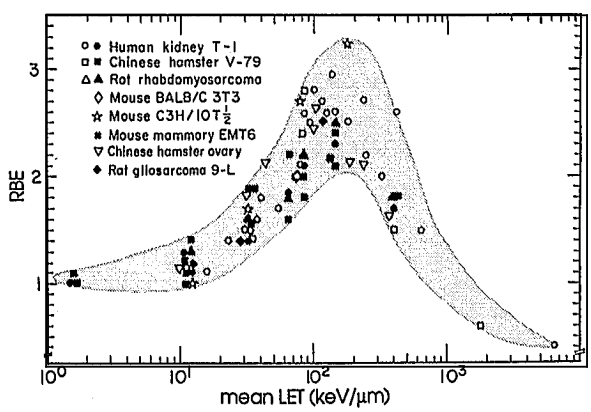

Fig. 5. Relative biological effectiveness (RBE) of ion beams as a function of linear energy transfer (LET). The compilation of data for a number of cell types shows that there is a trend but no simple relationship between the two. Adapted from [8]

fact that the energy of accelerated ions is deposited in individual "packets" of varying density along individual particle tracks rather than evenly throughout the overall irradiated volume.

Ions of the same velocity or specific energy produce tracks of secondary electrons with the same kinetic energy. However, the dose density within the track, i.e., the number of secondary electrons produced, need not be identical. According to the Bethe-Bloch equation, the deposited dose increases with decreasing velocity and the square of the effective charge (cf. eq. 1) of the beam ions. Therefore, the heavier ions which can have higher charge states have, in general, higher ionization densities than singly charged protons, for example.

Biological Properties

Relative Biological Effectiveness (RBE)

Prior to the clinical use of accelerated ions, their biological effects were studied with a number of experimental systems. In the late 50's, the Uppsala cyclotron was intensively used for such studies. Larsson and his colleagues provided a wealth of radiobiological data of protons [2, 10–13]. Similar investigations were also performed in Russia [14, 15] and the United States [16–18].

Cultured cells, plant seedlings, healthy and tumor-bearing animals were irradiated and cell survival, chromosomal aberrations, histological changes, LD_{50} etc. examined (for review cf. [4, 19]). The central question of these experiments was the biological effectiveness of the accelerated ions in comparison to certain reference radiations, mostly 250 kV X-rays or ^{60}Co gamma rays.

For protons, these studies revealed a relative biological effectiveness (RBE) close to one. This means, that the proton dose required to produce a given effect is comparable to the reference photon dose. More recent, refined studies indicate, however, that low (< 1 MeV) and very high (> 1GeV)-energy protons may have RBE-values of 2 and more, depending on the biological endpoint studied [20–23].

An elevated biological efficiency in the Bragg peak region has clearly been demonstrated for ions heavier than helium. This specific ionization density pattern is seen as the key element of the biological quality and effectiveness of particle beams [27–30]. For the same reason, RBE predictions of heavier ions cannot simply be made on the basis of LET information. Detailed knowledge of the beam composition, such as fluence, charge and velocity are required, in addition.

Oxygen Enhancement Ratio (OER)

Oxygen acts as sensitizer, rendering the cells more susceptible to radiation damage [31]. When irradiating cells with photons or low-LET ions, they demonstrate different survival behavior, depending on the presence or absence of oxygen (Fig. 6).

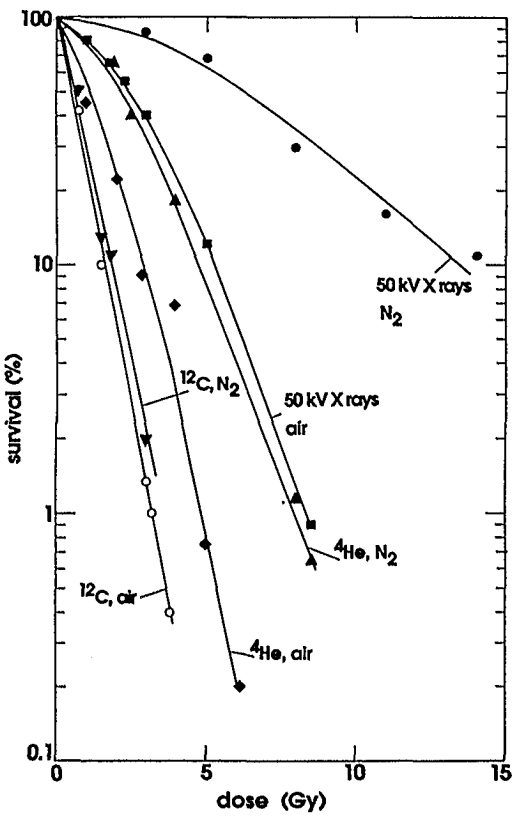

Fig. 6. Cell survival curves of T1 cells after irradiation with ions or X-rays in air or nitrogen atmosphere, respectively. Adapted from [26]

The oxygen enhancement ratio (OER) of radiation is the dose (D) required to produce a certain biological effect in the absence of oxygen (hypoxic conditions) to the dose (D_o) required to produce the same effect in the presence of oxygen (oxic conditions)

$$OER = \frac{D(\text{Effect E})}{D_o(\text{Effect E})}$$

For X-rays, the OER ranges from 2.5 to 3 which means that the killing of oxygen-deprived cells requires 2.5–3 times higher X-ray doses than killing the same cells under aerobic conditions. Many independent studies have shown that the OER-value decreases with increasing LET and approaches unity at LET-values of approx. 150–300 keV/μm [26, 32].

Radiosensitivity becomes maximal at oxygen pressures of approx. 20 mm Hg (2700 Pa). Well-vascularized normal tissues exceed this value at least by a factor of two. They are, therefore, generally fully radiosensitive as far as the oxygen effect is concerned [33].

In all experimentally-induced animal tumors studied, hypoxic cells have been found [34, 35]. For human tumors, the existence of hypoxic cells is recognized but its clinical significance is debated, in particular because of the reoxygenation phenomenon after fractionated radiotherapy [36]. Reduced oxygen partial pressures have been measured, e.g., in carcinomas of the rectum or bone metastases, but considerable intra- and inter-individual variations in oxygenation even among tumors of the same clinical stage and grade make general statements difficult [37, 38]. Still, a reduction in OER has become one of the rationales to use high-LET radiation in cancer therapy.

Variation in Radiosensitivity with the Cell Cycle

The cell cycle of eukaryotic cells is divided into several phases of growth and maturation (Fig. 7). The postmitotic rest or gap phase G_1 is followed by the S or DNA synthesis phase and a second gap, the so-called premitotic or G_2 phase which precedes the actual mitosis (M). The duration of S, G_2 and M is relatively constant for cells from

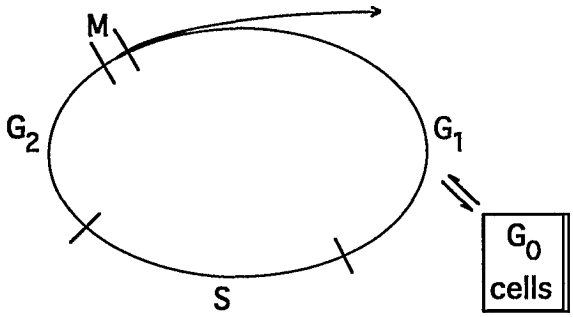

Fig. 7. The phases of the cell cycle. M = mitosis, G_1 = postmitotic gap, S = DNA synthesis phase, G_2 = postmitotic gap. Cells can leave the cycle temporarily to rest in G_o

the same species in contrast to G_1 which can vary widely.

Single-cell survival data with cells in different stages of the cell cycle showed that most cells are sensitive during mitosis and more resistant in the late S phase. The effect can be significant with survival rates differing up to a factor of ten at large doses per fraction [39].

A reduced but not completely eliminated cell-phase dependent radiation sensitivity was also observed for heavy ions. However, the extent of the effect is well reduced [4, 24]. More recent studies with synchronized cells revealed that the cell-cycle dependence recedes with increasing LET, vanishing at approximate LET-values of 200 keV/μm [40].

Sublethal Cell Damage

Survival curves of exponentially growing cells irradiated by X-rays are characterized by a shoulder due to the capacity to accumulate sublethal damage (see Fig. 6). If the irradiation scheme is divided into multiple fractions, the survival is higher or a shoulder appears with each new fraction, indicating that repair occurs after each treatment.

With increasing LET of the radiation, the shoulder recedes. Heavy ions with a LET of 100–200 keV/μm prompt an exponential survival curve. After fractionated irradiation with heavy ions, the survival curves remain exponential, i.e., no significant repair occurs (for review cf. [25]).

Comparison of Protons and Heavier Ions

Protons as well as the heavier ions are characterized by a superior depth-dose distribution as compared to photons. Whereas this improved physical dose distribution is common to all ions, protons and ions with higher atomic numbers differ in a number of other factors (see Table 2).

Multiple scattering and range straggling effects dwindle with increasing mass, improving the lateral and distal dose fall-off. Clinically exploited, this translates into higher precision of the treatment and, e.g., improved sparing of critical structures immediately adjacent to the tumor.

These physical advantages of helium and the heavier ions are offset, however, by their tendency to fragment after nuclear collisions [28, 41], causing a tailing of the Bragg peak due to the presence of lighter fragment particles which have longer ranges than the primary beam components and hence, impair the excellent physical dose distribution. This makes the clinical usage of ions with $Z > 10$ (Ne) probably less interesting.

There is another reason to be sceptical about the usefulness of ions with $Z > 10$. The biological effectiveness of ions increases with increasing Z. But only for ions with $Z < 10$ the RBE is selectively increased in the Bragg peak region [42]. The radiobiological effects from particles in the plateau region correspond to lesions of sparsely ionizing radiation, which means repair of and recovery from radiation damage can occur in this section, which usually consists of healthy tissue.

In the Bragg peak region of heavier ions survival and repair are reduced and the extent of damage becomes independent of cell cycle stages.

Table 1. Favorable properties of ions

Penetration depth in tissue well defined and adjustable
Maximum energy deposited near the end of the particle track
Beam propagation in tissue in straight line
Radiation burden on healthy tissue low
No dose beyond the target

Table 2. Comparison of properties of protons and light ions

Pros of light ions	Cons of light ions
Range straggling reduced	Peak-to-plateau ratio reduced
Lateral deflection reduced	Nuclear fragmentation
No oxygen enhancement effect (OER = 1)	Tumorigenic potential
More lethal damage (RBE > 1)	Much higher cost

These positive biological phenomena are, however, overshadowed by the observation that heavier ions have a higher tumorigenic potential than low-LET radiation (see Chapter 7). This reduces their value, e.g., in the treatment of very young patients [43, 44].

The assessment of the ions is not complete without addressing economic aspects. In this respect, protons score best. They can be produced at approximately one third of the electrical power costs of carbon ions [45].

The list of pros and cons reveals that protons and heavier ions have special physical and biological features which complement each other. But the present clinical experience (see Section III) is still too scarce and preliminary to select the clinically optimal ion. More comprehensive studies are needed before the clinical value of the various particles can be assessed with certainty.

References

1 Wilson, R.R. Radiological use of fast protons. Radiology 47, 487–491, 1946.
2 Larsson, B. Radiological properties of beams of high-energy protons. Radiat. Res. Suppl. 7, 304–311, 1967.
3 Koehler, A.M. and Preston, W.M. Protons in radiation therapy. Radiology 104, 191–195, 1972.
4 Raju, M.R. Heavy Particle Therapy. Academic Press, New York, 1980.
5 Tobias, C.A., Fabrikant, J.I., Benton, E.V., and Holley, W.R. Projection radiography and tomography, in Biological and Medical Research with Accelerated Heavy Ions at the Bevalac, 1977–80, Pirrucello, M.C. and Tobias, C.A. (eds.), Lawrence Berkeley Laboratory Report, LBL-11220, 1980, pp.335–346.
6 Lawrence, J.H. Proton irradiation of the pituitary, Cancer 10, 795–798, 1957.

7 Larsson, B., Leksell, L., Rexed, B., Sourander, P., Mair, W., and Andersson, B. The high-energy proton beam as a neurosurgical tool. Nature 182, 1222–1223, 1958.
8 Chu, W.T., Ludewigt, B.A., and Renner, T.R. Instrumentation for treatment of cancer using proton and light-ion beams. Rev. Scient. Instrum. 64, 2055–2122, 1993.
9 Zirkle, R.E. The radiobiological importance of linear energy transfer, in Radiation Biology, Hollaender, A. (ed.) McGraw Hill, New York, Vol. 1, 1954, pp. 315–350.
10 Larsson, B., Leksell, L., Rexed, B., and Sourander, P. Effect of high energy protons on the spinal cord. Acta Radiol. 51, 52–64, 1959.
11 Falkmer, S., Larsson, B., and Sténson, S. Effects of single dose proton irradiation of normal skin and Vx2 carcinoma in rabbit ears. Acta Radiol. 52, 217–234, 1959.
12 Larsson, B. and Kihlman, B.A. Chromosome aberrations following irradiation with high-energy protons and their secondary radiation: a study of dose distribution and biological efficiency using root-tips of Vicia faba and Allium cepa. Int. J. Radiat. Biol. 2, 8–19, 1960.
13 Andersson, B., Gale, C.C., Hökfelt, B., and Larsson, B. Acute and chronic effects of preoptic lesions. Acta Physiol. Scand. 65, 45–60, 1965.
14 Ueno, Y. and Grigoriev, Y.G. The RBE of protons with energy greater than 126 MeV. Br. J. Radiol. 42, 475, 1969.
15 Wainson, A.A., Lomanov, M.F., Shmakova, N.L., Blokhin, S.I., and Jarmonenko, S.P. The RBE of accelerated protons in different parts of the Bragg curve. Br. J. Radiol. 45, 525–529, 1972.
16 Robertson, J.B., Williams, J.R., Schmidt, R.A., Little, J.B., Flynn, D.F., and Suit, H.D. Radiobiological studies of a high-energy modulated proton beam utilizing cultured mammalian cells. Cancer 35, 1664–1677, 1975.
17 Tepper, J., Verhey, L., Goitein, M., Suit, H.D., and Koehler, A.M. In vivo determinations of RBE in a high energy modulated proton beam using normal tissue reactions and fractionated dose schedules. Int. J. Radiat. Oncol. Biol. Phys. 2, 1115–1122, 1977.
18 Urano, M., Verhey, L.J., Goitein, M., Tepper, J.E., Suit, H.D., Mendiondo, O., Gragoudas, E.S., Koehler, A. Relative biological effectiveness of modulated proton beams in various murine tissues. Int. J. Radiat. Oncol. Biol. Phys. 10, 509–514, 1984.
19 Blakely, E.A. Cell inactivation by heavy charged particles. Radiat. Environ. Biophys. 31, 181–196, 1992.
20 Leont'eva, G.A., Fomenko, B.S., Antipov, A.V., and Mantsygin, I.A. Action of secondary radiation from 70 GeV protons on the cellular DNA of mammals (Russ.). Radiobiologiia 24, 9–12, 1984.
21 Kabachenko, A.N., Fedorenko, B.S., and Smirnova, O.A. Evaluation of the cataractogenic effect of 9 GeV protons (Russ.). Radiobiologiia 26, 318–322, 1986.
22 Perris, A., Pialoglou, P., Katsanos, A.A., and Sideris, E.G. Biological effectiveness of low-energy protons. I. Survival of Chinese hamster cells. Int. J. Radiat. Biol. 50, 1093–1101, 1986.
23 Belli, M., Cherubini, R., Finoto, S., Moschini, G., Sapora, O., Simone, G., and Tabocchini, M.A. RBE-LET relationship for the survival of V79 cells irradiated with low-energy protons. Int. J. Radiat. Biol. 55, 93–104, 1989.
24 Skarsgard, L.D., Kihlman, B.A., Parker, L., Pujara, C.M., and Richardson, S. Survival, chromosome abnormalities, and recovery in heavy-ion- and X-irradiated mammalian cells. Radiat. Res. Suppl. 7, 208–221, 1967.
25 Barendsen, G.W. Response of cultured cells, tumors and normal tissues to radiations of different linear energy transfer, in Current Topics in Radiation Research, Ebert, M. and Howard, A. (eds.), North-Holland Publishers, Amsterdam, Vol 4, 1968, pp. 295–356.
26 Todd, P.W. Fractionated heavy ion irradiation of cultured human cells. Radiat. Res. 34, 378–389, 1968.
27 Curtis, S.B. The effect of track structure on OER and high LET, in Charged Particle Tracks in Liquids and Solids, Conf. Series 8, The Inst. of Physics and the Physical Society (England), 1970, pp.140–142.
28 Shavers, M.R., Curtis, S.B., Miller, J. and Schimmerling, W. The fragmentation of 670 A MeV neon-20 as a function of depth in water. II. One-generation transport theory. Radiat. Res. 124, 117–130, 1990.
29 Butts, J. J. and Katz, R. Theory of RBE for heavy ion bombardment of dry enzymes and viruses, Radiat. Res. 30, 855–871, 1967.
30 Kraft, G., Krämer, M., and Scholz, M. LET, track structure and models. Radiat. Environ. Biophys. 31, 161–180, 1992.
31 Gray, L.H. Radiobiologic basis of oxygen as a modifying factor in radiation therapy. Am. J. Roentgenol. 85, 803–815, 1961.
32 Barendsen, G.W., Koot, C.J., Van Kersen, G.R., Bewley, D.K., Field, S.B., and Parnell, C.J. The effect of oxygen on impairment of the proliferative capacity of human cells in culture by ionizing radiations of different LET. Int. J. Radiat. Biol. 10, 317–327, 1966.
33 Churchill-Davidson, I. The oxygen effect in radiotherapy. Proc. Roy. Soc. Med. 57, 635–638, 1964.
34 Tobias, C.A. and Todd, P.W. Heavy charged particles in cancer therapy, Natl. Cancer Inst. Monograph 24, 1–21, 1967.
35 Suit, H.D. Radiation biology: A basis for radiotherapy, in Textbook of Radiotherapy, Fletcher, G.H. (ed.) 2nd ed., Lea and Febinger, Philadelphia, pp. 75–121, 1973.
36 Brown, J.M. Sensitizers and protectors in radiotherapy, Cancer 55, 2222–2228, 1985.
37 Müller-Klieser, W., Vaupel, P., Manz, R., and Schmidseder, R. Intracapillary oxyhemoglobin saturation of malignant tumors in humans. Int. J. Radiat. Oncol. Biol. Phys. 7, 1397–1404, 1981.
38 Wendling, P., Manz, R., Thews, G., and Vaupel, P. Inhomogeneous oxygenation of rectal carcinomas in humans: A critical parameter for preoperative irradiation? Adv. Exp. Med. Biol. 180, 293–300, 1984.

39 Sinclair, W.K. Cyclic X-ray responses in mammalian cells in vitro. Radiat. Res. 33, 620–643, 1968.
40 Chapman, J.D. Biophysical models of mammalian cell inactivation by radiation, in Radiation Biology in Cancer Research, Meyn, R.E. and Withers, H.R. (eds.), Raven Press, New York, 1988, pp. 21–32.
41 Goldhaber, A.S. and Heckman, H.H. High energy interactions of nuclei, Ann. Rev. Nucl. Part. Sci. 28, 161–205, 1978
42 Blakely, E.A., Tobias, C.A., Ngo, F.Q.H., and Curtis, S.B. Physical and cellular radiobiological properties of heavy ions in relation to cancer therapy application, in Biological and Medical Research with Accelerated Heavy Ions at the Bevalac, 1977–80, Pirrucello, M.C. and Tobias, C.A. (eds.), Lawrence Berkeley Laboratory Report, LBL-Report LBL-11220, 1980, pp. 73–86.
43 Fry, R.J.M., Powers-Risius, P., Alpen, E.L., and Ainsworth, E.J. High-LET radiation carcinogenesis. Radiat. Res. Suppl. 104, pp. 188–195, 1985.
44 Alpen, E.L., Powers-Risius, P., Curtis, S.B., and DeGuzman, R. Tumorigenic potential of high-Z, high-LET charged-particle radiations. Radiat. Res. 136, 382–391, 1993.
45 S. Martin, personal communication, 1994.

4 Socio-Economic Aspects of Ion Beam Therapy

A. WAMBERSIE and J.J. BATTERMANN*

Cliniques Universitaires St-Luc Université Catholique de Louvain, Brussels, Belgium, and * Academisch Ziekenhuis Utrecht, The Netherlands

Introduction

Cancer has an increasing impact on the death rates in the western world, as well as in the developing countries [1, 2]. Although there is a prominent progress in the field of medical oncology, high cure rates are mainly related to solid pediatric tumors, leukaemias and lymphomas, and testicular tumors. But these tumors represent only about 5% of all cancers seen in the general population [3, 4].

At the moment of first admittance approximately 65% of the patients have localized tumors. About two thirds of these are cured either by surgery, radiotherapy, or a combination of both. In this group, some patients with probable but unproved subclinical metastatic disease may profit from chemotherapy or immunotherapy used as an adjuvant treatment [3, 4]. Among the other 35% of patients presenting with inoperable or metastatic disease at the moment of first admittance, only about 5% will be cured by combined treatment including chemotherapy and immunotherapy as well as radiotherapy and/or surgery.

Local control of the tumor seems, therefore, the key to more successful treatment results [5, 6]. Following Devita [5], it is even "axiomatic" to control the local disease if one aims ultimately at curing any cancer patient.

The techniques of surgery have already reached a very high level. Further improvement will be seen in a reduction of mutilating procedures (limb sparing operation, breast conserving surgery, reduction of colostomies and urinary diversions). On the other hand, wider excisions are still forseeable in relation with safer anaesthesiology, intensive care support and improvement in reconstructive surgery. The combination of surgery with irradiation, on a wider scale, will help to increase the local control rate.

Radiotherapy is still open to new developments. Further improvements can be expected from the use of better fractionation schedules, for example, or a combination with new radiosensitizers. But it is through the development of new irradiation techniques that the most promising progress may be expected. An increase in total dose to the tumor, without exceeding the tolerance dose of the normal surrounding tissues, has always been the key to a better clinical result. New techniques like stereotactic radiotherapy, intraoperative radiotherapy, high dose rate brachytherapy and conformation therapy offer already very encouraging results. These techniques can be applied in several large, well-equipped and well-staffed radiotherapy departments.

However, one of the most promising technologies seems to be the use of ion beam therapy. Application of ion beams, in safe conditions, implies large and expensive investment, as well as adequately trained staff. Therefore, only a few ion beam therapy centers are likely to open (as a rough estimate according to the CEC: one per ten million inhabitants). This in turn implies the organization and agreement upon a system of referring those patients who could benefit from this advanced technology.

Indications for Proton Beam Therapy

The rationale for proton beam therapy is an improved physical selectivity (cf. previous chapter).

Generally speaking, an improvement in physical selectivity is always an advantage. Therefore, principally all the photon patients could be potential indications for protons. However, only clinical experience will reveal to what extent the improvement in physical selectivity can be converted into a better treatment outcome.

Looking at the possible tumor sites, one can identify two main types of indications for proton beam therapy.

The first type of indications are small, rather resistant tumors, located close to critical normal structures [7].

The best example today is uveal melanoma treated in several proton therapy centers and considered to be the typical indication for proton beam therapy. Other good indications are tumors of the base of the skull [8], brain tumors in children [9] and tumors close to the spinal cord. For these localizations, the adequate depth-dose curves and the narrow penumbra of the proton beam are definitive advantages and can be fully exploited. Proton beams can also be indicated for larger and/or deep-seated target volumes, such as brain and pelvis, reducing the irradiation of sensitive structures outside the target volume.

In that respect, it is interesting to compare the types of patients treated at the Harvard Cyclotron Laboratory (HCL) on the one hand, and in Loma Linda on the other hand (Tab. 1). At HCL, the patients are included in well defined protocols, the machine availability is limited and the beam characteristics have also some limitations. Under these conditions, patient selection is always critical. In contrast, in Loma-Linda, a larger number of patients with different types of tumors can be treated, several treatment rooms are available full-time and there are nearly no limitations as far as the proton beam characteristics are concerned (e.g., energy, field size, orientation).

For small fields, as used for uveal melanoma, for instance, it is probable that the geometry of the irradiation is the major factor of success. The total dose, overall time and dose per fraction are probably of less importance. In contrast, for large fields, the current rules of radiobiology, in particular, those for fractionation should be followed as for photon beam therapy.

Table 1. Distribution of the patients treated with protons at the Harvard Cyclotron Laboratory (HCL) and the Loma Linda University Medical Center (LLUMC)

Tumor Site	HCL (a)	LLUMC (b)
Uveal melanomas and other eye tumors	33%	8%
Brain/CNS	2%	21%
Cordomas/Chondrosarcomas	6%	3%
Soft tissue sarcomas	2%	2%
Head and neck tumors	1%	6%
Radiosurgery (AVM, pituitary tumors)	50%	7%
Prostatic adenocarcinomas	3%	48%
Miscellaneous	3%	5%
	100%	100%

(a) 5949 patients by Sept. 1993
(b) first 300 patients treated by Oct. 1992

Potential Value of Heavy Ions in Cancer Therapy

Heavy ions combine the advantage of a high physical selectivity with the potential advantage of high-LET radiations (see previous chapter for details).

Radiobiological data indicate that high-LET radiations could be of interest for the treatment of some tumor types. A review of the clinical results of fast neutron therapy, another high-LET radiation, indicates that neutrons can indeed bring a benefit for several tumor types or sites, such as salivary glands, (locally extended) prostatic adenocarcinomas, or slowly growing soft tissue sarcomas [10–12]. The Berkeley experience with heavy ions is an additional argument for the use of these particles, although the clinical results were obtained from limited, selected groups of patients.

The best results obtained at Berkeley with neon ions [13] were obtained for those tumors for

which fast neutrons were also shown to be of interest (Tab. 2).

The potential value of heavy ions in cancer therapy has to be analyzed in relation with the causes of local failure after conventional radiotherapy, for which at least 4 factors can be identified:

- intrinsic cell radioresistance,
- the oxygen effect,
- cell repair,
- repopulation during the treatment.

These factors are discussed in more detail in the previous chapter. Here, they are only mentioned as to their clinical consequences. Regarding the intrinsic radioresistance of a cell population, high-LET radiation could bring an advantage for tumors particularly resistant to photons such as adenocarcinomas or sarcomas. On the other hand, it is obvious that heavy ions should not be given for tumors that exhibit an exquisite radiosensitivity to photons, (e.g., seminomas or lymphomas).

Table 2. Local control rates for various tumor types obtained with neon ions at Berkeley in comparison to conventional treatment results from various sources (RTOG = Radiotherapy Oncology Group, NCOG = Northern California Oncology Group)

Tumor Site	Local control rate	
	Neon Ions	Conventional Treatment
Salivary Gland	80% (10 patients)	28% 188 patients (Literature review)
Nasopharynx/ Paranasal sinus	63% (21 patients)	21% (97 patients (UCSF)
Sarcoma	45% (24 patients)	28% (Literature review)
Prostate	100% (9 patients)	60–70% (Literature review)
Lung	39%	22–40% (UCSF)
Glioblastoma/Brain	Median survival 17 months (13 patients)	Median suvival 9–12 months (UCSF, RTOG, NCOG)

Modified from J.R. Castro [13]

As far as the oxygen effect is concerned, the OER (oxygen enhancement ratio) is lower for high-LET radiations than for photons and this could bring a benefit for those tumors for which hypoxic cells constitute the main cause of radioresistance.

Repair of sublethal damage is also reduced with high-LET radiations, and a smaller number of fractions and/or shorter overall time can be chosen with high-LET radiations, compared to photons. High-LET therapy could thus bring a benefit for those tumors which repopulate quickly compared to the critical normal tissue.

General Principles of Patient Selection for Heavy Ion Therapy

As summarized in Table 3, there are two main groups of indications for heavy ions: those, for which the biological effect of high-LET radiation is thought to be the most important factor (A) and indications for which the high physical selectivity of the beams is thought to prevail (B). In addition, some specific indications with poor prognosis (C) can be proposed [14].

Concerning the first group of indications, it is possible to make a tentative prediction of the clinical benefit which could be expected from heavy ion beams by considering both the conclusions of the neutron studies and the heavy ion results from Berkeley.

At present, over 14 000 patients have been treated with fast neutrons alone, or in combination with photon irradiation. From the data described in the literature one can schematically distinguish [10–12]:

superior results, e.g., salivary gland tumors or prostatic adenocarcinomas;
conflicting results, e.g., head and neck tumors [15] or cervix [16];
disappointing results, e.g., brain tumors [17].

Two types of comments need to be made here. Firstly, not all patient series were randomized. One should, therefore, be careful before deriving definite conclusions from them. Secondly, neutron data probably reflect the lower limit of what could be expected with heavy ions, since – as

Table 3. General principles of patient selection for heavy ion therapy

A. The radiobiological advantage (high-LET) is thought to be the most important factor, followed by the physical selectivity of the beams:
a) high-LET radiation already demonstrated to be useful for – salivary gland tumors – paranasal sinuses – fixed lymph nodes – prostatic adenocarcinomas – sarcomas, etc. b) additional information is needed for – pelvic tumors: bladder, rectum, cervix, etc. – other tumors: stomach, biliary duct, etc.
B. The physical selectivity (dose distribution) of the beams is thought to be the most important factor followed by the radiobiological advantages of high-LET
Tumors in technically difficult situations, where high-LET radiation may be superior (e.g., slowly growing tumors): – adjacent to CNS: meningioma, pharyngioma, chordoma, optic nerve, glioma, AVM, paraspinal cord tumor, paraaortic lymph node, etc. – root of neck disease: upper esophagus, post cricoid carcinoma, etc. – thoracic disease: tumor of the lung with mediastinal disease after resection of primary tumor, mesothelioma, etc.
C. Additional indications: a) where possible subsequent surgery should be prejudiced: – tongue, avoiding mandible, etc. b) disease with very poor prognosis: – unresectable hepatoma, pancreas – retroperitoneal sarcoma, recurrent after previous radiotherapy, etc.

Modified after G.R.H. Sealy [14]

often stressed – neutrons were, in many centers, not applied under optimal technical conditions. A similar remark applies, however for other reasons, also to the neon results of Berkeley (cf. Chapter 15) for which, in addition, patient selection was insufficient.

Concerning the group of indications where the physical selectivity is considered to be the most important factor, we can expect the same results as with protons, but with the additional advantage of high-LET radiation for slowly growing tumors. In this respect, heavy ions could extend the field of indications by allowing the oncologists to envisage irradiation of groups of tumors "traditionally" considered to be radioresistant (e.g., adenocarcinomas).

Since an improved physical selectivity is, in any case, an advantage and since a high physical selectivity is more important for high-LET than for low-LET radiation, the superiority observed for some localizations with fast neutrons can be expected to be even more pronounced and clinically more relevant when the physical selectivity of heavy ions becomes available. The physical selectivity is especially important in tumors located near normal tissue, e.g., tumors adjacent to CNS.

In addition, there might be some miscellaneous indications (C), including tumors where more precise irradiation can reduce normal tissue effects, and tumors with a very poor prognosis such as unresectable hepatomas, pancreatic tumors, retroperitoneal sarcomas, or recurrences after previous irradiation.

Due to possible higher tumorigenicity of heavy ions, tumors in children are not considered as indications for heavy ions (high-LET irradiation). They should preferably be treated with proton beams (low-LET irradiation). With protons, as with heavy ions, the possibility of achieving a precise irradiation minimizes the effects on the normal tissues, and especially growth retardation [9, 18].

Boost irradiation could be another interesting field for heavy ions. In fact, one might assume that all tumors that are now treated with a boost after large-field locoregional irradiation are good candidates for heavy ions, since boost irradiation is applied to a residual malignant and usually resistant cell population against which high-LET radiation is likely to be more effective. This could include a large group of tumors such as carcinomas of the bladder, the esophagus, colorectal, and selected gynecological tumors, locally advanced pharyngeal and oral cavity tumors, especially with fixed cervical lymph nodes, or bronchus carcinoma with relatively resistant histology.

Finally, the treatment of solitary and slowly growing metastases could benefit from heavy ion

therapy. Among the possible indications are sarcomas, kidney tumors, and adenoid cystic carcinomas. These tumors tend to distribute solitary and/or slowly growing metastases to distant organs which force an immediate and efficient local therapy. Metastases in brain and vertebrae are examples of such malignancies, and they could be the only clinical sign of disease progression. In these patients, the local problems remain more important clinically than the problems of the systemic disease. A comprehensive list of tumor types or sites which could be indications for heavy ions has recently been published [19].

Estimation of the Cost of Ion Beam Treatments

Due to the wide variations in the reimbursement rates and systems, even between the countries of the European Union (EU), the only relevant way to express the cost of the ion beam treatments is by comparison with other radiotherapy techniques and other cancer treatment modalities.

Dedicated Proton Beam Therapy Facility

A rather accurate evaluation of the cost of a dedicated proton therapy facility was requested for the new program at the Massachusetts General Hospital (MGH) and simultaneously by the Belgian "Fonds National de la Recherche Scientifique" (FNRS) in 1993 [20].

In both cases, the evaluation was based on data from Ion Beam Applications S.A. (IBA), a Belgian company manufacturing cyclotrons for medicine and industry. In early 1994, IBA was selected as supplier for the equipment of the Northeast Proton Therapy Center (NPTC), planned by MGH in Boston (cf. Chapter 39).

They established the initial investment cost for a dedicated proton beam therapy facility as follows:

20 MECU for a 230 MeV compact cyclotron and 4 treatment rooms (3 with isocentric beam line (gantry) and 1 with horizontal beam);
4 MECU for the building;
1 MECU for the medical equipment (simulator, CT, treatment planning, etc.)

The annual running cost would be about 1 MECU, including maintenance, electricity, and salaries for 3 engineers and office personnel.

The salaries of the medical staff (radiotherapists, hospital physicists, radiographers) need not be included in the cost evaluation, as they are the same as in the case of X-ray treatments, at least for complex treatments, e.g., conformation therapy. The medical staff is simply "transferred" from the existing conventional therapy facilities to the proton therapy facility.

Assuming an amortization of the equipment over 25 years (which seems reasonable for this well established conventional cyclotron technology), the same for the building, and 1 MECU for the annual running cost specific to the proton facility, the study of the FNRS [20] came to the conclusion that the cost per patient, related only and specifically to the proton therapy facility, would be about 1250 ECU per patient, if 1600 patients were treated each year (600 full treatments and 1000 boosts). This amount of 1250 ECU has to be added to the other costs such as the salaries of the medical staff, the amortization of the current medical equipment, etc. (which are assumed to be the same for proton and conformation photon therapy). The amount of 1250 ECU is somewhat lower than the present reimbursement rate by the Social Security in Belgium for a conventional photon treatment. Hence, it can be concluded that the total cost of a proton treatment is less than twice the price the Social Security is presently paying for a photon treatment.

In a recent evaluation of the cost of proton therapy, based on the situation in Nice (France), Chauvel [21] compared a cyclotron (and 3 treatment rooms) with 3 photon linacs (for conformation photon therapy). Assuming an amortization over 20 years for the cyclotron and over 10 years for the linacs, he concluded that the cost per year (machines + buildings) is 1.4 to 1.8 times higher for the proton as compared to the photon therapy facililty. For 1100 patients per year, he estimated the cost per patient (machines + buildings) as 860–1140 ECU for protons vs. 640 ECU for photons. The cost of staff salaries, patient accom-

modation, patient transport, maintenance and furnitures are comparable for proton and conformation photon treatment (i.e., 8000–9000 ECU per patient, for 1100 patients treated), according to the author.

These two evaluations based on the situation in Belgium and in Nice, respectively [20, 21], agree that a proton treatment is somewhat more expensive than a complex photon treatment. The argument that protons cost exceedingly more can thus no longer be retained. Along the same line, Chu [22] came to the conclusion that proton therapy could even be cheaper than photon therapy. He based his evaluation on the assumption that one proton facility (4 treatment rooms) can treat the same number of patients as 10 photon linacs, which have to be replaced after 10–12 years which means about twice as often as a cyclotron. Chu also assumed that the number of beams per treatment could be lower for protons, that the number of fractions could also be lower, and that treatment planning is easier for protons than for photons.

In contrast, a significantly higher cost estimate was made by Suit and Urie [7] who reported that a proton beam treatment would be 2–3 times more expensive than conformation therapy with photons. A more expensive evaluation was also reported from Loma Linda in California, but it is obvious that more sophisticated and expensive choices were made in Loma Linda when designing and constructing the facility in comparison to the compact cyclotron indicated above.

In any case, when making comparisons, one should check whether the different components of the budget are taken into account in the same way (e.g., equipment amortization, salaries of the medical staff, etc.).

In addition, when comparing protons and photons, one should compare the cost of a proton treatment with a complex photon treatment performed with great accuracy with the help of all available modern technology (e.g., conformation therapy, etc.). Comparison of ion beam therapy with a single photon beam or 2 parallel opposed photon beams is, of course, not relevant.

Proton Therapy with "Physics Machines"

Several proton therapy centers are using or will use existing "physics machines" adapted for therapy applications, such as Harvard, the Russian facilities, Uppsala, Louvain-la-Neuve, Orsay, etc.

Cost evaluation must be done in each case individually, and completely different situations have to be taken into account:

- the investment needed to adapt the machines for therapy applications;
- the cost of the machine time (ECU per beam hour);
- the salaries of the machine engineers;
- the running cost and the maintenance cost.

In particular, maintenance and running costs are usually higher for these machines not initially designed for therapy and may vary widely from machine to machine. For these and other reasons, no general estimation can be made concerning the costs of proton beam treatments, using physics machines adapted for therapy applications.

Heavy Ion Therapy

Whatever the approach and the hypotheses used for cost estimation, and the way of funding the program, the cost of therapy with heavy ions is significantly higher than that of proton beam therapy. As a result, it is reasonable to expect that no more than a few heavy ion therapy centers will be installed in the world in the foreseeable future. In any case, the cost per treatment will to a large extent depend on the number of patients treated per year. In that respect, similarly to the case of proton beam therapy, one has to clearly separate the cost evaluation for a dedicated heavy ion therapy facility from that of a therapy program using an existing, high-energy physics machine.

It is difficult to derive general conclusions about the cost of heavy ion therapy from the Berkeley experience or to make general predictions from the HIMAC (Heavy Ion Medical Accelerator) project in Chiba, Japan, or from the GSI (Gesellschaft für Schwerionenforschung) project in Darmstadt, Germany. The local factors are not comparable. In particular, the HIMAC facility

offers large possibilities but is generally considered to be very expensive.

In 1990, the Commission of the European Communities (CEC) decided to support a feasibility study called EULIMA (for EUropean Light Ion Medical Accelerator) for a heavy ion therapy facility, designed and devoted exclusively to therapy applications. This hospital-based facility was planned to treat a large number of patients (up to 3000 patients a year). For the evaluation of the costs of EULIMA, the following assumptions were made [23]:

1. One heavy ion accelerator (cyclotron or synchrotron) is serving four treatment rooms:
   room 1 and 2 equipped with both a vertical and horizontal beam;
   room 3 equipped with a horizontal beam only;
   room 4 equipped with a 45° oblique beam and possibly, in a second phase, an isocentric gantry.
2. The beams can be switched rapidly and safely between the different treatment rooms.
3. On the average, 2.5 patients can be treated per hour (room set-up time 15 minutes, beam time 5 minutes, 4 minutes "contingency" reserve for possible medical or technical difficulties).
4. A full treatment consists of 12 fractions (it was assumed that hypofractionation is possible with high-LET treatment), a boost of 5 fractions.
5. Hospitalization is necessary for only 10% of patients; full treatment patients for an average of 3 weeks, boost patients for 2 weeks.

A total number of 27000 fractions per year could be derived from those figures, assuming, in addition, 10 working hours per day, 6 working days per week and 45 weeks per year (due to the high investment and running costs, one must aim for the maximum possible working hours).

With the further assumption that two thirds of the patients would receive a full treatment and one third only a heavy ion boost, 1860 patients could be treated per year for a full treatment and 930 for a boost.

Roughly 300 patients would need hospitalization, for whom 20 permanent hospital beds and approx. 200 out-patient beds ("low care" hospital beds or hotel rooms) were projected.

As cost for the equipment the following was assessed [21]:

15–20 MECU for a dedicated accelerator (cyclotron or synchrotron),
10–15 MECU for the beam delivery systems serving 4 rooms,
20 MECU for the building.

To this investment, annual running costs of approx. 17 MECU have to be added, which consist of the following:
7 MECU for machine and treatment rooms,
6 MECU for medical staff,
4 MECU for beds/patient transport.

With the figures for the investment and running costs and the above made assumptions on the patient spectrum, the cost per patients would be around 7000 ECU. For a 50% cure rate with heavy ions, the cost would then be around 15000 ECU per patient cured, which is very reasonable when compared to other radiotherapy modalities or other cancer treatment techniques (Tab. 4 and 5).

Table 4. Cost estimation of the current cancer treatment techniques. The relatively wide range depends on country and/or extent of disease

Treatment Technique	Average Cost	Range
Surgery	6500 ECU	5000–8000 ECU
Conventional radiotherapy	4800 ECU	2000–7500 ECU
Bone marrow transplantation	43500 ECU	37000–50000 ECU

Modified from [23]

Table 5. Cost of some current cancer chemotherapy and hormone therapy schemes in Belgium. Prices taken as reference are prices valid on November 5, 1994 for in-patients, according to the Belgian Social Security. Cost given are for the cytostatic agents only, and normalized for a patient with a body surface area of 1.6 m^2. Drugs such as antiemetics or anxiolytics, perfusion fluids, perfusion material, room charges, medical fees, etc. are not included. Prices are calculated for each cytostatic agent administered during one course and for the total number of courses usually given for the whole treatment. After J. Longueville, UCL, Clinique Universitaires St.-Luc, Brussels, Belgium

Head and neck cancer			
Carboplatin	400 mg/m^2 1 day	640 mg	543 ECU
5-Fluorouracil	1 mg/m^2 4 days	6400 mg	57 ECU
Total for 1 course			600 ECU
Total for 4 courses			2400 ECU
Early or advanced breast cancer			
Cyclophosphamide	600 mg/m^2 1 day	960 mg	5 ECU
Methotrexate	40 mg/m^2 1 day	64 mg	21 ECU
5-Flourouracil	600 mg/m^2 1 day	960 mg	9 ECU
Total for 1 course			35 ECU
Total for 6 courses			210 ECU
Small-cell lung cancer			
Carboplatin	330 mg/m^2 1 day	528 mg	448 ECU
Etoposide	120 mg/m^2 3 days	576 mg	83 ECU
Epiadriamycin	65 mg/m^2 1 day	104 mg	211 ECU
Total for 1 course			742 ECU
Total for 4 courses			2968 ECU

Conclusion

Ion beam therapy appears to be a promising approach in cancer therapy, able to improve local control but also survival. Due to the clear improvement in physical selectivity, proton beam therapy, used either as full treatment or as boost, can bring a benefit for a large number of patients.

On the other hand, heavy ions, which combine a high physical selectivity with the potential advantage of high-LET radiations for some tumor types, are indicated for a smaller percentage of patients for whom they could bring a significant benefit as can be derived from Berkeley and the past fast neutron experience.

Ion beam therapy – protons or heavy ions – still requires expensive investments and will be somewhat more expensive than conventional radiation therapy, at least for the near future. In order to make this additional cost tolerable for the Social Security System, it is important to optimize the machine characteristics (reliability, compactness, user friendliness, low running costs, etc.) and to rationalize the patient recruitment and referral. Only if the number of patients treated per ion beam facility is high enough, the cost per treatment will be acceptable, and not higher than the cost of accepted cancer treatments such as surgery or chemotherapy.

References

1 Muir, C.S. and Boyle, P. The Burden of Cancer in Europe. Eur. J. Cancer 26, 1111–1113, 1990.
2 Davis, L., Hoel, D., Fox, J., and Lopez, A. International trends in cancer mortality in France, West Germany, Italy, Japan, England and Wales, and the USA. The Lancet 336, 474–481, 1990.
3 Devita, V.T. Progress in cancer management. Cancer 51, 2401–2409, 1983.
4 Doll, R. Are we winning the fight against cancer? An epidemiological assessment. EACR – Mühlbock Memorial Lecture. Eur. J. Cancer 26, 4, 500–508, 1990.

5 Devita, V.T. and Korn, D. Progress against cancer. New Engl. J. Med. 315, 964, 1986.
6 Suit, H.D. Potential for improving survival rates for the cancer patient by increasing the efficacy of treatment of the primary lesion. Cancer 50, 1227–1234, 1982.
7 Suit, H. and Urie, M. Proton beams in radiation therapy, J. Natl. Cancer Inst. 84, 155–164, 1992.
8 Suit, H.D., Goitein, M., Munzenrider, J., Verhey, L., Urie, M., Gragoudas, E., Koehler, A., Gottschalk, B., Sisterson, J., Tatsuzaki, H., and Miralbell, R. Increased efficacy of radiation therapy by use of proton beam. Strahlenther. Onkol. 166, 40–44, 1990.
9 Wambersie, A., Gregoire, V., and Brucher, J.M. Potential clinical gain of proton (and heavy ion) beams for brain tumors in children. Int. J. Radiat. Oncol. Biol. Phys. 22, 275–286, 1992.
10 Battermann, J.J. and Mijnheer, B.J. The Amsterdam fast neutron radiotherapy project: A final report. Int. J. Radiat. Oncol. Biol. Phys. 12, 2093–2099, 1986.
11 Griffin, T., Pajak, T.F., Laramore, G.E., Duncan, W., Richter, M.P., Hendrickson, F.R., and Maor, M.H. Neutron vs. photon irradiation of inoperable salivary gland tumors: Results of an RTOG-MRC cooperative randomized study. Int. J. Radiat. Onol. Biol. Phys. 15, 1085–1090, 1988.
12 Schmitt, G. and Wambersie, A. Review of the clinical results of fast neutron therapy. Radiother. Oncol. 17, 47–56, 1990.
13 Castro, J.R. Light ion radiotherapy, in Kraft, G. and Grundinger, U. (eds.) Third Workshop on Light Charged Particles in Biology and Medicine, GSI = Darmstadt, Report 87–11, 1987, pp. KO 1–5.
14 Sealy, R. EULIMA, Patients Logistics, in Eulima Workshop on the Potential Value of Light Ion Beam Therapy. Chauvel, P. and Wambersie, A. (eds.) Publication EUR 12165 EN of the Commission of the European Communities, Brussels, Luxembourg and CAL Edition, 1989, pp. 487–499.
15 Griffin, T.W., Pajak, T.F., Maor, M.H., Laramore, G.E., Hendrickson, F.R., Parker, R.G., Thomas, F.J., and Davis, L.W. Mixed neutron/photon irradiation of unresectable squamous cell carcinomas of the head and neck: The final report of a randomized cooperative trial. Int. J. Radiat. Oncol. Biol. Phys. 17, 959–965, 1989.
16 Maor, M.H., Gillespie, B.W., Peters, L.J., Wambersie, A., Griffin, T.W., Thomas, F.J., Cohen, L., Conner, N., and Gardner, P. Neutron therapy in cervical cancer: Results of a phase III RTOG study. Int. J. Radiat. Oncol. Biol. Phys. 14, 885–891, 1988.
17 Breteau, N., Destembert, B., Favre, A., Phéline, C., and Schlienger, M. Fast neutron boost for the treatment of grade IV astrocytomas. Strahlenther. Onkol. 165, 320–323, 1989.
18 Gademann, G. and Wannenmacher, M. Charged particle therapy to pediatric tumors of the retroperitoneal region: A possible indication. Int. J. Radiat. Oncol. Biol. Phys. 22, 375–381, 1992.
19 Commission of the European Communities, Concerted Action: Cancer Treatment with Light Ions in Europe = EULIMA, Final Report Part 1: General Feasibility Study, Wambersie, A., Chauvel, P., Gademann, G., Gerard, J.P., and Sealy, R. Socio-economic study, CEC, Brussels, 1992, pp. 2–39.
20 Fonds National de la Recherche Scientifique: Création d'un Centre Interuniversitaire de Protonthérapie (CIUP): Examen des implications épidémiologiques, économiques et techniques. Première évaluation, Groupe de Contact FNRS Protonthérapie: Burny, A., Klastersky, J., Meulder, J.P., Minet, P., van Houtte, P. (Secrétaire), Wambersie, A. (Président), and Jongen, Y., and Groupe de Travail "Protonthérapie" Autier, P., d' Hoore, W., Fiasse, P., and Ryckewaert, G., FNRS 3.4621.93 Brussels 1993.
21 Chauvel P. Socio-economic aspects, in Application of High-LET Radiations in Cancer Treatment, Report of a Consultants' Meeting (Chiba-Japan, Nov. 1994). International Atomic Energy Agency, IAEA, Vienna (in press).
22 Chu, W.T. Cost comparison between proton and conventional photon facilities, PARTICLES – PTCOG Newsletter 13, 8–9, 1994.
23 Commission of the European Communities, Concerted Action: Cancer Treatment with Heavy Ions in Europe – EULIMA. Mandrillon, P. (Chairman), Bewley, D.K. (Secretary), Banfi, P., Battermann, J.J., Chauvel, P., Farley, F.J.M., Gerard, J.P., Kraft, G., Larsson, B., Menzel, H.G., Meulders, J.P., Ryckewaert, G., Sealy, G.R.H., Vermorken, A.J.M., Wannenmacher, M., and Wambersie, A. Final Report – Part 1: General Feasibility Study, CEC, Brussels, 1992.

II. Models and Preclinical Studies

Practical Implications of Microdosimetry

J. F. DICELLO

Clarkson University, Department of Physics, Potsdam, NY, USA

Introduction

This chapter reviews the basic physical concepts underlying the field of microdosimetry and how they apply to therapeutic proton beams. It discusses the extension of these physical concepts to problems in radiobiology and radiation oncology, and finally, it examines the microdosimetric similarities and differences of protons with other heavy charged particles and with conventional photon beams. Mathematical analyses have been kept to a minimum as have descriptions of both the experimental and theoretical methods, in recognition of the diversity of backgrounds and primary interests of the readers. Likewise, specialized aspects of the field have not been emphasized.

The Meaning of Microdosimetry

Microdosimetry is the study of the physical processes associated with the transfer of energy to matter and their relation to the subsequent chemical and biological processes. Historically, the initiation of the field is generally attributed to a group of scientists at Columbia University under the direction of H. H. Rossi [1] and other researchers who recognized the limitations of the average physical parameters for characterizing radiation fields used in biology and therapy. The absorbed dose, that is, the mean energy imparted to matter per unit mass, is the quantity most commonly specified to establish the amount of radiation delivered to a biological site or to a patient, but it is necessarily a macroscopic quantity, not in the optical sense but rather in the thermodynamic or statistical-physics sense, in other words: it is an average property of a large number of atoms or molecules. Like other macroscopic quantities describing the state of a system, such as temperature and pressure, it is a concept applicable only to macrostates near equilibrium. In contrast, most initial physical processes responsible for transferring energy to biological systems are taking place at the atomic or molecular level and are not accurately approximated by static or quasi-static situations. Such situations are classified thermodynamically as microstates or microscopic states. Hence the designation "Microdosimetry" for the name of the field. Unfortunately, the name is to some extent oxymoronic in that the term dose as an average quantity of the state should not be applied to particles traversing single atoms, a few molecules, or even a cell nucleus. Despite early attempts to arrive at a more appropriate name [1], it is nevertheless well established and the field continues to be so labelled even today.

The Need for Microdosimetry

The success of radiation therapy depends upon our ability to define a specific treatment which will control the disease while sparing normal tissues and preserving the welfare of the patient. Protocols evolved largely from clinical observations. The philosophy of conventional therapy is assumed to be to deliver the maximum uniform dose to the treatment volume with minimal effect

to adjacent normal tissues. The manner in which treatment planning is done, however, somewhat contradicts this philosophy. For high-energy, high atomic-number ions (HZE), we must modify the physical dose distributions to account for the nonuniform response as the beam penetrates the tissue. Protons, argumentatively, owe at least part of their success in comparison with HZE particles to the relative ease (cost) with which they can be used to localize the physical dose while achieving a relatively uniform response throughout the treatment volume. Yet protons and even photons produce differences in biological response throughout that treatment volume; those differences are simply smaller than in the case of the heavier charged particles. Even in the case of photon therapy, we compensate for sensitive tissues within the volume, implicitly invoking a uniform effective dose, that is, a nonuniform physical dose selected to produce a uniform biological response. The clinical experience with protons has demonstrated the advantage of precise delivery of uniform (effective) doses. The success of protons has been a major catalyst for the development of comparable treatments with X-rays using conformal therapy and radiosurgery with comparable improvements in response. Significant gains have been achieved with better localization and improved uniformity of response irrespective of the type of radiation. At the same time, the potentials of radioimmunotherapy and brachytherapy have not been fully realized in part because of microscopic nonuniformities in energy deposition. Continued improvements in radiation therapy require more detailed information concerning the variation in biological effects at the microscopic level, and this requires more detailed information concerning the interactions of the radiations and the subsequent physical processes.

Each type of particle being used for external beam therapy and each type of source in brachytherapy produce different types of response and different levels of response for the same absorbed doses. The reason for these differences in response is simple and indisputable; the distributions of the physical interactions and the energy transferred at the relevant biological sites are different. These differences are illustrated in Figure 1 for photons and alpha particles, where the number of particles and the lengths of their tracks are shown schematically for cells irradiated with equal doses. Even though the average macroscopic dose is the same, in the case of the alpha particles, the cells see fewer events per cell, per cell nucleus, or per DNA strand, with each event depositing a greater amount of energy on the average. Each type of radiation produces a different distribution of dose (energy) at the cellular and subcellular level even for the same macroscopic dose distribution. Differences in response must be caused by the differences in the distributions of energy transfer. That is not to say that there are no other factors affecting response. The same radiation delivering the same dose, for example, may produce a different response in different organs. These differences result from the differences in the structure of the targets and the subsequent biological or chemical processes, as well as differences in the initial physical interactions. There is a physical component to each process and a biological component.

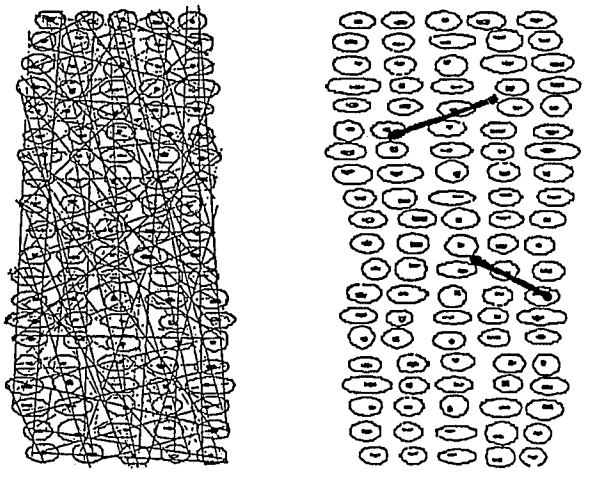

Fig. 1. A schematic representation of the relative number of secondary electrons, on the left, produced by an exposure of cells to a megavoltage photon beam in comparison with the same dose of alpha particles on the right. For the total energy per unit volume, the dose, is to be the same in both cases with much fewer tracks of shorter length from the alpha particles, because alpha particles can deposit much more energy along their tracks

All of the physical information is contained in the frequency and energy distributions for the various types of particles, and it behooves us to

study these distributions as a means of understanding the basic physical mechanisms. Microdosimetry establishes what the probability distributions are for depositing energy in a given target volume for various particle types under therapeutic conditions. It is the only internationally recognized method for describing probabilistic or stochastic processes initiated by radiation [2–5].

General Features of Microdosimetry

In the present context, there exist two basic physical quantities responsible for biological processes:

1. energy, resulting in work and the transfer of information and
2. sources and/or sinks of energy in the form of masses and charges.

In principle, we totally define the radiation field by specifying the number or frequency for the various types of particles per unit volume or per unit area (fluence) as a function of their energies and direction. In practice, the frequency distributions needed for therapeutic situations are usually difficult to obtain either experimentally or theoretically and difficult to utilize. Simpler quantities and methods are frequently invoked. The use of dose rather than the complete distributions in energies, masses, and charge is such an example. Moreover, we wish to characterize the radiation field only as an intermediary step to determine the biological consequence.

Once a particle transfers energy to a particular site, such as an atom, a molecule, or even a person, there is a certain probability that we will observe a particular physical or biological result, and there is a certain probability that we will observe nothing. The physical occurrences are called events and null events, respectively. The probability is simply the fraction of occurrences of the event of interest.

In Microdosimetry we are specifically interested in the frequency or probability of physical events which transfer energy from the radiation to relevant biological sites such as the cell nucleus or DNA as a function of the energy deposited. If the energy deposited is between E and E+dE, dE being the differential energy, we say that the differential probability in the energy interval dE is f(E)dE. If we integrate over all energies, the total probability or fraction, F, would be one corresponding to 100%. The distribution f(E) as a function of E is called either the probability distribution, the frequency distribution (frequency of events as a function of energy), or the differential (probability or frequency) distribution.

The number and type of events we observe in some specified volume is obviously related to the number of incident particles and the size and shape of the target. We, therefore, express the probability of an occurrence or event in terms of the number of particles incident on the volume of interest. The number of particles, N, incident on some specified volume divided by the cross-sectional area, a, of that volume is called the fluence, Φ. In the limit, this becomes

$$\Phi = dN/da \qquad (1)$$

where the volume for the purpose of calculating the fluence at a site is usually chosen to be a sphere [4]. The choice of specifying the volume, as in absorbed dose, or the cross-sectional area of that same volume, as in the fluence, is somewhat arbitrary because the two are directly related.

We define the differential probability in the interval between E and E+dE divided by the fluence as the differential cross section because it has units of area:

$$d\sigma(E)dE = f(E)dE/\Phi \qquad (2)$$

It should be interpreted only as the probability for a given fluence, not as the actual area of the target. There is, then, a direct and unique correlation between probabilities or frequency distributions and cross sections.

Recognizing that the amount of energy transferred by an event can be as important biologically as the event itself, we frequently discuss frequency distributions of energy transferred as distinguished from the previously discussed frequency distributions of the events which deposited the energy. These frequency distributions of energy transferred are often identified in the literature simply as energy distributions or, unfortunately, dose distributions. For such distributions,

the cross section for energy transferred would be the amount of energy transferred divided by the total amount of incident energy per unit area. This latter quantity is utilized in the literature less frequently than distributions of energy transfer.

The energy transferred or absorbed per unit mass is the dose, and the energy lost per unit path length is the linear energy transfer (LET). Note that the energy absorbed in the mass must be distinguished from the energy lost by the incident particle. The absorbed energy will usually be less than the total energy lost, significantly so in many cases, because energy can be transported outside of the mass, even in the case of a patient.

The dose, as we have noted earlier, is an average, macroscopic quantity. Nevertheless, there is energy deposited by each event in the target site even for microscopic sites, and there is a microdosimetric analogue of the dose. To avoid confusion with the macroscopic dose, this microscopic quantity is called the specific energy, z, although it has the same units as dose. Just as we were able to define a probability for an event occurring between E and E+dE, we can define a probability for an event occurring between z and z+dz as f(z)dz with the corresponding cross section for that event being

$$\sigma(z)dz=f(z)dz/\Phi \qquad (3)$$

In the macroscopic case, we frequently consider the energy *lost* per unit pathlength, the unrestricted linear energy transfer or LET [4]. For the microscopic case, we consider the energy *absorbed* in the site per unit average pathlength, x_{ave}, through the site, and we define this quantity as the lineal energy, y, usually expressing it in terms of units of keV/μm. For a volume, V, of area, A, and known shape, composition, and density, ϱ, we can calculate the mass of the volume and the average pathlength across that volume, so there is a direct and unique relationship between the specific energy and the lineal energy. Although there is no obvious advantage of the use of one or the other, historically, lineal energy is more frequently used as the independent variable.

Microdosimetric Attributes of Beams of Photons and Ions

A measured spectrum of the number of events with lineal energies within a fixed interval as a function of lineal energy is shown in Figure 2 for an energetic beam of protons. The details concerning the experimental methods and procedures are discussed in a previous publication [6].

In order to show some of the physical characteristics of this spectrum, it has been presented on a log-log plot. Note that this spectrum extends over a factor of 10000 in lineal energy with the relative number of events within that interval changing by a factor of 10000000. Typical spectra will extend from a few eV/μm to over a thousand keV/μm. Although events of higher lineal energy are relatively infrequent in the case of protons, each of such events can deposit thousands of times more energy than typical events from photons. Despite their infrequency, such large events can have significant biological consequences. They are responsible for the higher effectiveness, for example, of neutrons and pions. Even in the case of photons, the greater abundance of higher

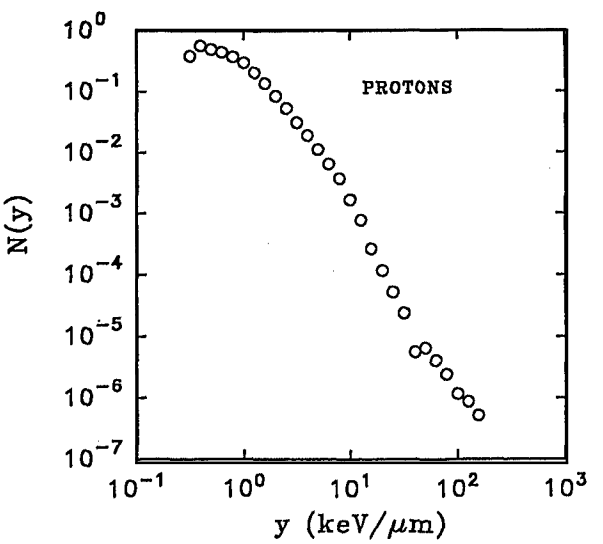

Fig. 2. The number of measured events per unit interval of lineal energy is plotted as a function of lineal energy for an energetic beam of protons incident upon a detector simulating a sphere 2 μm in diameter

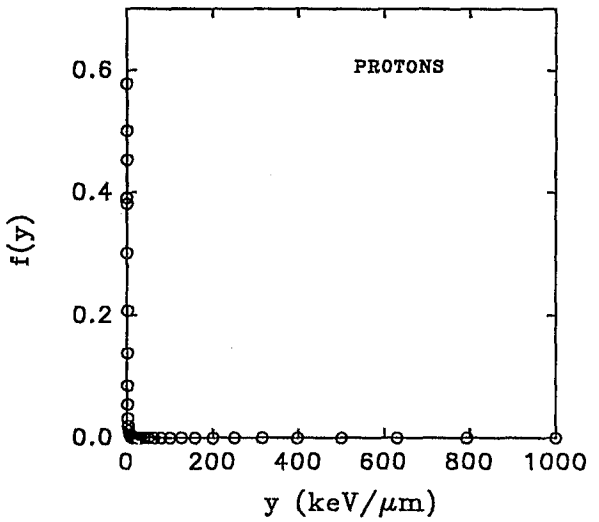

Fig. 3. The frequency distribution of events presented in Fig. 2

events from orthovoltage X-rays, in comparison with ^{60}Co gamma rays explains the higher RBE frequently observed for the lower-energy X-rays.

It is difficult to extract quantitative information directly from the presentation used in Figure 2, but those data can be used to calculate a normalized frequency (probability) distribution. In Figure 3, we have plotted the differential probability or frequency distribution for the same proton distribution shown in Figure 2. In this representation, the integral

$$\int_0^\infty f(y)dy \tag{4}$$

is the total probability equal to one (100%), and the integral between any two values of y

$$\int_{y1}^{y2} p(y)dy \tag{5}$$

is the probability that lineal energy will be deposited in the range between y_1 and y_2.

Because these integrals are simply the areas under the curves between two values of y, the area under each curve in a given region is proportional to the probability that events will occur in that interval. Such curves could provide a powerful means of examining the differences in energy deposition by the various types of radiation, except they are usually too close to the two axes to be distinguished from the axes. If we plot the data on a log-log plot, it would look similar to the distribution of data in Figure 2, but the area under the curve would no longer be proportional to the probability. To obtain a representation which will allow us to see both the structure of the curves, including those rare but important events, with the area proportional to the probability, consider

$$\int f(y)dy = \int f(y)yd(\ln y) = yf(y)d(\ln y) = kyf(y)d(\log y) \tag{6}$$

where k is the factor to convert natural logarithms to log base ten, d(ln y) and d(log y) are the differentials of the natural log of y and the log to the base ten of y, respectively. From elementary calculus, d(ln y)/dy = 1/y, and it follows that dy = yd(ln y).

This shows that, if we plot yf(y) versus log y, as we have done in Figure 4, instead of f(y) versus y, the area under the curve is still proportional to the probability of an event with lineal energy between y and y+dy. The advantage is merely

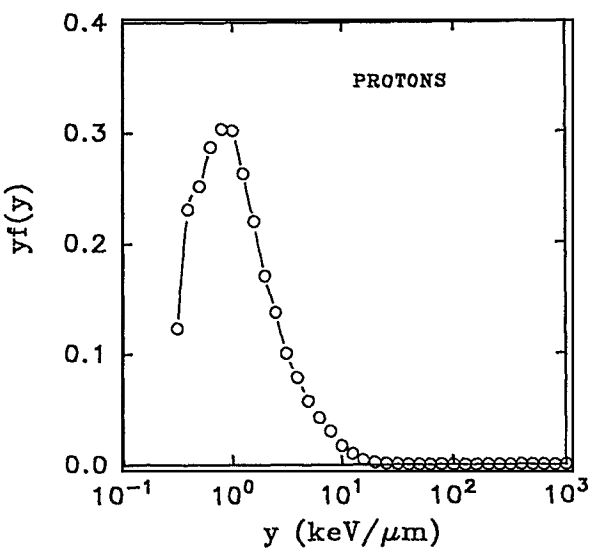

Fig. 4. The same data as presented in Figure 2 have been used to calculate the product yf(y), which is plotted versus the log of the lineal energy. In this representation, the area between two values of y is proportional to the probability of an event occurring in that region

that we can discern the structure of the distribution, and we can see better portions of the distributions that were close to the axes in the earlier representation. This proved to be a significant advantage and most data are presented in this fashion.

The mean lineal energy is simply

$$\Sigma\ (N_i y_i)/\Sigma\ N_i \qquad (7)$$

where $f_i(y) = (N_i/\Sigma N_i)$, i.e., it is the average energy deposited per μm by each event. In the literature, this is usually designated as y_f. It varies from a fraction of a keV/μm for photons to as high as several hundred keV/μm for some heavy ions. Even for a particular type of particle, the mean lineal energy will depend upon the energy distribution of the particles and the physical characteristics of the object being irradiated. For therapeutic proton beams the mean lineal energy can vary within a treatment volume from typically 1 keV/μm to well over 10 keV/μm.

Biological endpoints are frequently correlated not only with the number of events but the amount of energy deposited by those events as well. We can use the event distributions to calculate the corresponding distributions for energy deposited in the same site. The differential energy distribution is the probability of depositing a given amount of specific energy (rather than the probability of an event) between z and z+dz expressed here as Δ(z)dz. The total specific energy deposited in a given interval is simply the specific energy, z, associated with each event times the number of such events. The number of events between z and z+dz is f(z)dz, so the fractional contribution to the total energy deposited per unit mass is zf(z)dz. Again, we can use the conversion from dz to zd(ln z) as discussed above, and we have

$$z^2 f(z)d(\ln z) = kz^2 f(z)d(\log z). \qquad (8)$$

This tells us that, if we plot $z^2 f(z)$ versus log z, the area under the curve is the fractional contribution to the total energy deposited from events within that interval of specific energies. As noted earlier, this is frequently designated as the (differential) energy (deposited) distribution. Historically, researchers developed a preference for plotting lineal energy in research articles rather than

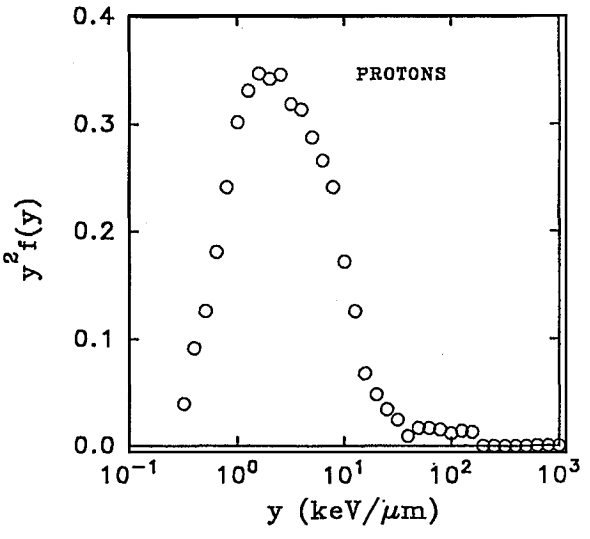

Fig. 5. The probability distribution for energy deposition as a function of lineal energy

specific energy. Because one is proportional to the other, we may just as easily plot $y^2 f(y)$ versus log y; the area under the curve would still be proportional to the fractional contribution. The curve corresponding to the event data in Figures 3 and 4 is shown in Figure 5.

The average lineal energy for this distribution

$$\Sigma\ N_i(y_i f_i(y))/\Sigma\ N_i \qquad (9)$$

is called the dose mean lineal energy and is designated as y_d. The dose mean lineal energy is admittedly a more esoteric parameter than the frequency mean lineal energy, y_f, and its physical meaning may be less easily understood. It is best appreciated as the microscopic analogue of the dose. Because the dose arose historically as the parameter best related to biological response, we might expect that the microscopic mean to be even better correlated. It is frequently considered in biological modelling.

We have discussed two basic distributions, the frequency distribution and the energy distribution, each as a function of lineal energy and specific energy. The frequency distribution is in fact proportional to the distribution of differential cross sections; it presents the probability that an event with a particular lineal energy will occur while the cross section is the probability per unit

fluence. The energy distribution presents the probability that energy will be delivered by events within a particular lineal energy interval. The latter distributions are generally the more relevant ones biologically, and the ones usually presented in research articles. We could calculate a cross section corresponding to the energy distribution, but that is seldom done.

Microdosimetric Differences in Therapeutic Beams

We now can examine therapeutic differences in the response to different types of radiations in relation to the microdosimetric distributions for the various particle types. Figure 6 presents a comparison of typical measured dose distributions for ^{60}Co, protons, and energetic heavy ion beams [7] of helium, carbon, nitrogen, neon, argon, and iron. In this figure, the total dose, proportional to the total area under each curve, is the same for each type of particle. We see immediately that the dose from the heavier ions is delivered by many more events of high lineal energies. For equivalent doses, we have fewer events with larger energy depositions per event when we irradiate with heavy ions.

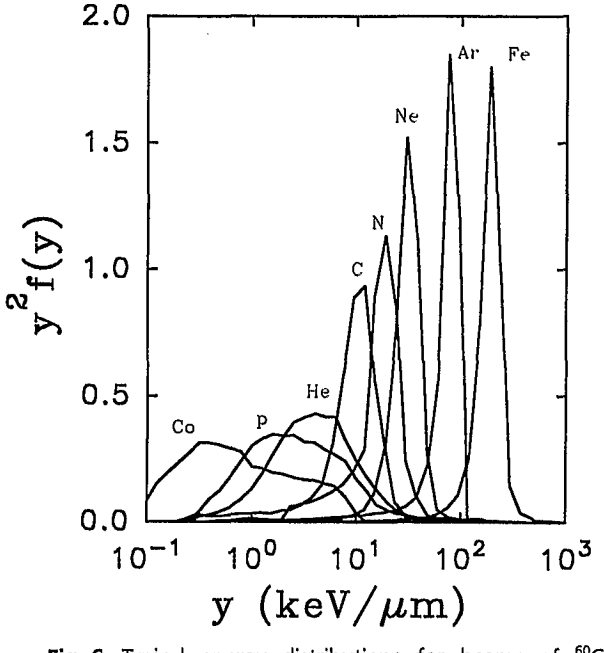

Fig. 6. Typical energy distributions for beams of ^{60}Co-photons, energetic protons, and heavy ions [7]

Proton distributions are relatively unique in comparison with other particles. A large fraction of the energy is being deposited at lower values of lineal energies, but not as low as most of the events from high energy photons. Events from protons tend to be more comparable to those from low energy orthovoltage photons. This is a partial explanation for the fact that responses to protons tend to be slightly higher than the response to cobalt-60 and more comparable to those from 250-kV X-rays. Furthermore, recall that most proton distributions exhibit a small contribution, around a percent or so, of high lineal energy events around 100 keV/μm, a region which tends to produce maximum biological damage for some biological endpoints. These higher events represent secondary protons nearing the end of their range and events from recoil ions and nuclear secondaries, including a significant contribution from secondary neutrons [8].

In a true sense, a proton irradiation might be considered to be an irradiation with a beam of intermediate quality with the simultaneous irradiation with a small dose of low energy, high-LET heavy particles, (the atomic and nuclear secondaries).

Finally, there is a great deal of variability in the energy deposited by most light ions, including protons as evidenced by the larger spread in the distribution for these lighter particles. If, for example, a large amount of energy from a single event is necessary to inactivate a cell, we immediately realize that there is some probability that such an event might be produced by relatively light particles with relatively low LETs.

Particle energy, the size and shape of the treatment volume, and the depth within that volume greatly alter the distributions of most particle types [9]. A proton beam nearing the end of its range, for example, can have a microdosimetric distribution with a mean lineal energy comparable to that of an energetic nitrogen or neon beam and almost ten times that of an energetic photon beam. A comparison of the distributions

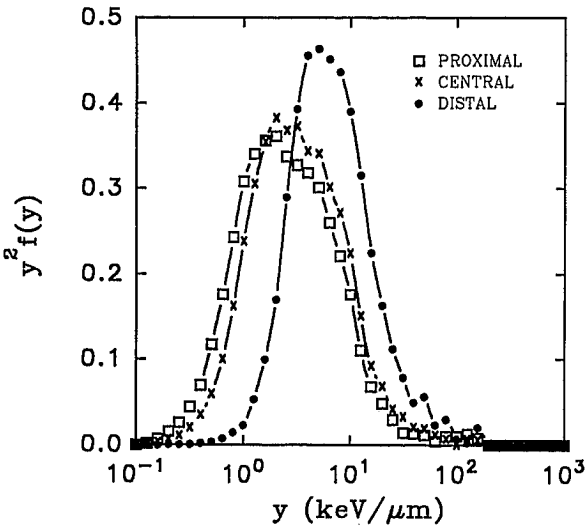

Fig. 7. A comparison of the microdosimetric distributions in the proximal, central, and distal portions of a volume irradiated with a proton beam at the Loma Linda University Medical Center

observed in the proximal, central, and distal regions of a proton beam used to treat ocular diseases at the Loma Linda University Medical Center is shown in Figure 7 for spherical targets of unit density. The shapes of these distributions differ as a function of the size and shape of the targets. Consequently the relative effectiveness of different particle types, such as iron beams versus protons, for double-strand DNA breaks can be significantly different than that for single-strand breaks simply because of differences in the distributions of energy as well as for differences in biological processes.

Calculation of Biological Response

The ultimate goal of Microdosimetry in radiation therapy is to understand responses and to be able to predict responses for individual treatments. Although there have been strides in achieving this goal, there remains much to be gained. Microdosimetry has been most successful to date in explaining cellular responses *in vitro* (e.g., [10–13]). It is only recently that significant inroads have been made at the molecular levels or, at the other extreme, in tissues and organs. In the developmental days of Microdosimetry, the need for simplifying assumptions was a major consideration; the physical cross sections for the plethora of different processes were generally unknown and were too many to be either measured or calculated in treatment planning. If we realize that even three-dimensional planning of the macroscopic dose is just beginning to be available in the clinic because of the complexity and uncertainty of the input data and the need for large amounts of computer power, we can appreciate the amount of effort needed not only to calculate the dose but also the distribution of interactions and reactions with a target molecule, to say nothing of modelling the molecule itself. Nevertheless strides are being made rapidly in applying microdosimetry to molecular biology [14, 15] and the capability of incorporating microdosimetric concepts into treatment planning appears now to exist.

Many earlier models were based upon the earlier linear quadratic approach. The basic premise in these models has been that the initiating biological event is proportional to the energy deposited or the energy squared. Kellerer's and Rossi's "Theory of Dual Radiation Action" [16] extended this concept to the microdosimetric level and, in one model based on this theory, it is assumed that the initial microscopic changes induced by the radiation are proportional to the dose mean specific energy, z_D. Such assumptions were extended [17] to account not only for the differences in radiation quality of different beams but also changes within the treatment volume taking into account the dose rate, fractionation schedules, and repair. Nevertheless, it was still difficult to take into account repopulation and organ response, particularly in complex tissues where the organ response is influenced, for example, by the unirradiated microvasculature [18]. More recently, we have begun to address the problems of organ responses from the microdosimetric viewpoint. Perhaps most importantly, this type of an approach could be implemented in newer treatment planning codes with only a modest effort.

One of the major limitations of models which correlate biological responses mainly through the mean values of the distributions, is that they fail

to take into consideration variations in the distributions themselves. It is possible that two significantly dissimilar radiations can have approximately the same dose mean specific energy but significantly different distributions and, consequently, different biological impacts. To account more precisely for the differences in the distributions themselves rather than the mean values, Bond and Varma [19, 20] proposed that there is a specific biological response associated with each event determined by the value of lineal energy (or specific energy) associated with that event. If we know the response as a function of lineal energy and if we have the probability of an event with a specified lineal energy, we can determine the net response simply by adding the expected responses weighted by the probability that each will occur. They chose to call this method "hit size effectiveness", in that each hit of a particular size has associated with it a particular effectiveness for a particular endpoint. This model introduces a level of sophistication in the calculation previously lacking and is being applied rapidly to a variety of problems. At the present time its application is limited to low doses where the occurrence of multiple events at the target can be ignored. This appears, however, not to be a limitation of the model so much as a limitation of the present mathematical techniques for it. The concept has the potential to be applied at therapeutic doses to the clinic.

There are now sophisticated models capable of simulating complex molecules such as the DNA and capable of tracking individual atomic and molecular transitions, at least for specific cases [14, 15]. Such models may not be incorporated into routine treatment codes for external beam therapy in the immediate future. Nevertheless, such analyses are becoming an integral aspect of radioimmunotherapy and brachytherapy. There is no doubt that their area of application is expanding into HZE therapy (cf. the succeeding chapter) and that it will ultimately be applied to routine clinical treatments.

Future Applications of Microdosimetry in Therapy

The future of radiation therapy lies not in achieving uniform dose, but rather in achieving uniform response in the treatment volume and uniform response from patient to patient [21]. Recent gains in conventional external beam therapy were motivated in part by the results of clinical studies with charged particles and neutrons showing the need for uniformity and localization, a need which cannot be eliminated at this time by the use of exotic particles if the underlying physical mechanisms are insufficiently understood [11]. Studies in radioimmunotherapy and in brachytherapy seem to reinforce the need for microdosimetric input [22]. The maximum gains are most certainly to be achieved with microdosimetry-based treatment planning striving for a uniform response [11]. Likewise, preclinical biological research is requiring an increasingly sophisticated knowledge of the physical distributions. From the physics viewpoint, many of the simplifying assumptions which were invoked in the early stages of Microdosimetry are rapidly becoming inadequate, and our abilities in physics and physics research must expand accordingly.

As long as there is a need to consider physical processes at the cellular and subcellular level, there will be a need for Microdosimetric studies; the two areas are equivalent.

References

1 Rossi, H. H. Microscopic distributions of radiation energy. Proc. of the Symp. on Microdosimetry, Ebert, H. G. (ed.) European Communities, Brussels, 1968, pp. 27–55.
2 International Commission on Radiation Units and Measurements, Microdosimetry. ICRU Report 36. ICRU, Bethesda, MD, 1983.
3 International Commission on Radiation Units and Measurements, The Quality Factor in Radiation Protection. ICRU Report 40, ICRU, Bethesda, MD, 1993.
4 International Commission on Radiation Units and Measurements, Quantities and Units in Radiation Protection Dosimetry. ICRU Report 51, ICRU, Bethesda, MD, 1993.
5 Lyman, J. T., Awschalom, M., Berardo, P., Bichsel, H., Chen, G. T. Y., Dicello, J., Fessenden, P., Goitein, M.,

Lam, G., McDonald, J. C., Smith, A. R., Haken, R. T., Verhey, L., and Zink, S. Protocol for Heavy Charged-Particle Therapy Beam Dosimetry. American Association of Physicists in Medicine, American Institute of Physics, NY, 1986.

6 Dicello, J. F., Lyman, J. T., McDonald, J. C., and Verhey, L. J. A portable system for microdosimetric intercomparisons by Task Group 20 of the American Association of Physicists in Medicine (AAPM). Nucl. Instr. Meth. B45, 724–729, 1990.

7 Dicello, J. F., Wasiolek, M., and Zaider, M. Measured microdosimetric spectra of energetic ion beams of Fe, Ar, Ne, and C: Limitations of LET distributions and quality factor in radiation effects and space research. IEEE Trans. Nucl. Sci. 38, 1203–1209, 1991.

8 Dicello, J. F., Schillaci, M. E., and Liu, L. Cross sections for pion, neutron, proton, and heavy ion production from 800-MeV protons incident upon aluminum and silicon. Nucl. Instr. Meth. B45, 135–138, 1990.

9 Zaider, M., Dicello, J. F., and Coyne, J. J. The effects of geometrical factors on microdosimetric probability distributions of energy deposition. Nucl. Instr. Meth. B40/41, 1261–1265, 1989.

10 Dicello, J. F., Zaider, M., and Varma, M. N. An inductive assessment of radiation risks in space. Adv. Space Res. 14, 899–910, 1994.

11 Archambeau, J. A., Slater, J. M., Coutrakon, G. B., Dicello, J. F., Miller, D. W., Preston, W., Robertson, J. B., Slater, J. D., and Slater, J. W. Proton beam irradiation for the cancer patient: An approach to optimal therapy and normal-tissue sparing. Adv. Radiat. Biol., in press 1994.

12 Robertson, J. B., Glisson, W. C., Archambeau, J. O., Coutrakon, G. B., Miller, D. W., Moyers, M. F., Siebers, J. F., Slater, J. M., and Dicello, J. F. The relative biological effectiveness of attenuated protons, in Biological Effects and Physics of Solar and Galactic Cosmic Radiation, Swenberg, C. E., Horneck, G., and Stassinopoulos, E. G. (eds.), NATO ASI Series, Plenum Press, New York, 1993; pp. 853–857.

13 Robertson, J. B., Eaddy, J. M., Archambeau, J. O., Coutrakon, G. B., Miller, D. W., Moyers, M. F., Sievers, J. V., Slater, J. M., and Dicello, J. F. Relative biological effectiveness and microdosimetry of a mixed energy field of protons up to 200 MeV. Adv. Space Res. 14, 271–275, 1994.

14 Glass, W. A. and Varma, M. N. (eds.) Physical and Chemical Mechanisms in Molecular Radiation Biology. Plenum Press, New York, 1991.

15 Vracko, M. G. and Zaider, M. A calculation of exciton energies in periodic systems with helical symmetry: Application to a hydrogen fluoride chain. Int. J. Quantum Chem. 43, 321–326, 1992.

16 Kellerer, A. M. and Rossi, H. H. The theory of dual radiation action. Curr. Top. Radiat. Res. Quart. 8, 85–158, 1972.

17 Zaider, M. and Dicello, J. F. RBE and OER. Los Alamos Report LA-7196-MS, Los Alamos National Laboratory, NM, 1978.

18 Shymko, R. M., Hauser, D. L., and Archambeau, J. O. Lack of correlation between basal cell survival and gross response in irradiated swine skin. Int. J. Radiat. Oncol. Biol. Phys. 10, 1079–1085, 1984.

19 Bond, V. P. and Varma, M. N. Stochastic, weighted hit size theory of cellular radiobiological action. Proc. 8th Symp. on Microdosimetry, Report EUR 8395, Commission of the European Communities, Brussels, 1982, pp. 424–437.

20 Bond, V. P. and Varma, M. N. An alternative to absorbed dose, quality, and RBE at low exposures. Radiat. Res. 104, 52–57, 1985.

21 Dicello, J. F. and Slater, J. M. Advanced cancer therapy with proton and heavy ion technology. Trans. Am. Nucl. Soc. 68B, 37–40, 1993.

22 Makrigiorgos, G. M., Adelstein, S. J., and Kassis, A. I. Limitations of conventional internal dosimetry at the cellular level. J. Nucl. Med. 30, 1856–1864, 1989.

6 Modelling Heavy Ion Radiation Effects

M. SCHOLZ

Gesellschaft für Schwerionenforschung (GSI), Darmstadt, Germany

Introduction

Therapy planning for charged particle beams requires the knowledge of the biological effect of a complex charged particle field. There are two factors contributing to this complexity:

- In order to achieve a flat dose distribution throughout the tumor volume, beams with different penetration depth and thus different energies have to be superimposed.
- For particles heavier than protons, nuclear reactions lead to a breakup of primary particles and thus to an increasing contribution of lighter fragments with increasing penetration depth.

Consequently, the composition of the radiation field varies significantly throughout the whole irradiated volume and will consist of a spectrum of particles with different atomic numbers and energies at any given point. The situation is even more complex, because the radiation field is not solely characterized by the physical dose deposition. RBE effects have to be taken into account and RBE is not a constant value. Experimental results show, that a single variable like LET is not sufficient to describe the RBE of a particle beam [1, 2]. Instead, two variables like, e.g., LET and atomic number or energy have to be used to characterize the RBE, which in turn depends on the biological endpoint, the level of the biological effect and may also differ for various cell types.

As a consequence, it is impossible to determine the radiobiological characteristics at each point of these radiation fields for all conditions occuring in the therapeutical practice. Therefore, biophysical models have to be used in order to interpolate or extrapolate from experiments performed under well defined conditions, e.g., track segment experiments with defined atomic number and energy.

Basic Considerations

The most obvious difference which can explain the enhanced RBE of charged particles as compared to photon fields is the different spatial energy deposition pattern. Photons deposit their energy nearly homogeneously throughout the irradiated volume, at least when considering dimensions of the order of the cell nucleus and dose levels relevant for therapy.

In contrast, charged particles deposit their energy by emission of secondary electrons in a narrow region close to their trajectory (Fig. 1). The local dose distribution around the particle path roughly follows a $1/r^2$-law, which is confirmed by experimental results as well as by numerical calculations and Monte Carlo models [3, 4, 5]. The radial extension of the dose distribution, i.e., the track radius, is defined by the highest energetic secondary electrons.

Thus, the track radius increases with increasing specific energy of the primary particle. Due to the sharp decrease of the dose, the major fraction of energy is deposited in a cylinder with a diameter of the order of 1 μm around the path of the primary particle even for highly energetic particles. The local concentration of energy deposition suggests an explanation of the higher RBE of

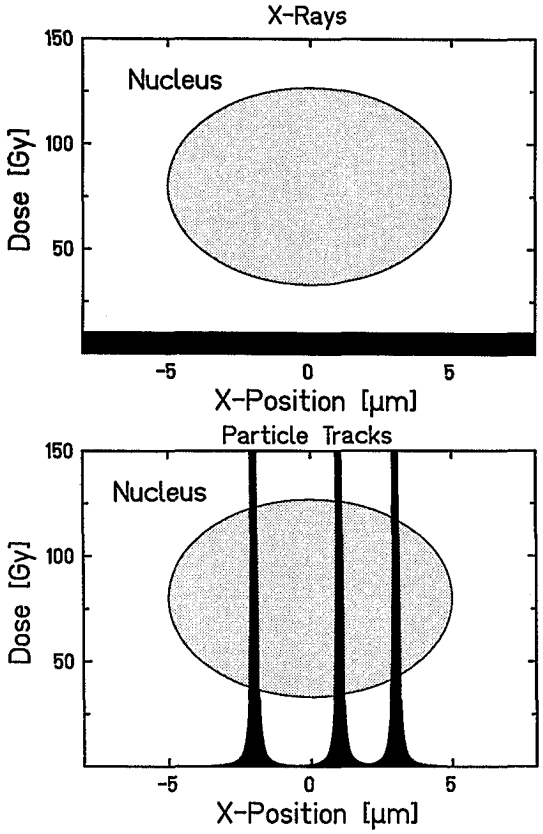

Fig. 1. Schematic view of local dose distributions after X-irradiation (top) and charged particle irradiation (bottom). The radial dose profile of charged particles follows a $1/r^2$ dependence, resulting in sharp spikes with extremely high local doses. The comparison with the size of a mammalian cell nucleus (shaded area) shows, that the dose distribution inside the nucleus is very inhomogeneous

charged particles as a consequence of a more complex and thus less repairable damage.

Mainly two different approaches to model the biological action of charged particles have been developed, which focus on the specific spatial energy deposition pattern:

1. the microdosimetric approach, which emphasizes the stochastical nature of the energy depositions by the electrons;
2. the 'amorphous' track structure approach, which is based on the radial dose distribution as a continous distribution, representing an average over many tracks.

Because the microdosimetric approach is discussed in more detail in the preceding chapter, we will focus here on the second type of models.

The Track Structure Model of Katz and Coworkers

General Considerations

The radiobiological models developed by Katz and coworkers [4, 6–8] are based on observations obtained with charged particle tracks in photoemulsions, where the spatial energy deposition pattern can be directly made visible. The work includes two major parts. As a first step, algorithms for the calculation of the radial dose distribution across the particle track are developed, utilizing a simplified kinematics of the secondary electrons. In a second step, these radial dose distributions are used to derive the biological response to charged particle radiation.

As mentioned above, the basic idea behind the radiobiological application of track structure models is that the differences in the radiobiological effects for different radiation qualities can be attributed completely to their different spatial energy deposition patterns. For X-rays as well as for charged particles, the biological damage is mainly produced by electrons. It is assumed that the action of a certain local dose deposited by electrons is independent of the physical process leading to their production. If this assumption is valid, charged particle radiobiological effects should be predictable by an appropriate convolution of the X-ray-effect curve with the radial dose distribution. This convolution is particularly easy to apply in the case of point-like targets such as, e.g., small viruses or enzymes. These objects can be interpreted as small detectors testing the local dose in the particle track. The biological effect of a local dose can directly be taken from the X-ray effect curve, which is usually exponential and determined by a single parameter like, e.g., D_{37}. Correspondingly, modelling of the inactivation of viruses and enzymes was the first successful application of the track structure principle to a radiobiological phenomenon [4].

Application to Mammalian Cell Survival

The application becomes more difficult in the case of spatially extended targets such as mammalian cells, because the cell nucleus, which is the assumed critical target, is considerably larger (diameter typically 10 μm) than the extension of the radial dose profile. Therefore, the dose distribution inside the cell nucleus is completely inhomogeneous (cf. Fig. 1). In addition, the dose-response curve after X-irradiation in general exhibits a shouldered shape, in contrast to the purely exponential dependence observed for viruses and enzymes. Therefore, several modifications and ad hoc assumptions have been suggested by Katz et al. for the prediction of mammalian cell survival after charged particle irradiation [6, 8].

In order to handle the transition from shouldered to exponential survival curves with increasing LET, two different modes of inactivation are introduced: γ-kill mode and ion-kill mode. γ-kill dominates at low LET and represents the non-linear dose-response curve showing a shoulder. Ion-kill mode describes the case of efficient energy deposition, dominating at high LET, so that a single particle traversal is capable to produce sufficient damage for cell inactivation. Accordingly, survival in the ion-kill mode is determined by a one-hit statistics and leads to purely exponential survival curves.

The energy deposited by the particles is split between the two inactivation modes. A certain fraction acts in the ion-kill mode with survival probability P_{ion} and the remaining fraction in the γ-kill mode with survival probability P_γ. The relative dose contributions for both inactivation modes are given by a free parameter, which is adjusted by fitting experimental survival curves for charged particle irradiation. Because both modes are assumed to act independently, the total survival probability is given simply by the product

$$P = P_{ion} \times P\gamma \qquad (1)$$

In the case of extended targets the target size plays an important role in order to reproduce correctly the stochastic properties of particle radiation, e.g., the number of particle traversals through the cell nucleus. Experimental results indicate, that the cell nucleus including the nuclear membrane is the sensitive target for radiation-induced inactivation. In contrast, in the Katz model a substructure with a size of approximately 1 μm is assumed to be the sensitive target for the ion-kill mode. In order to determine the biological response to the passage of a charged particle, the energy deposited in the critical target is integrated according to the impact parameter of the particle. Then, the inactivation probability is taken from the X-ray survival curve at the corresponding dose level, and inactivation cross sections are determined from the slope of the survival curves. As the target size in the model is smaller than the geometrical nuclear size, all calculated inactivation cross sections have to be scaled by a factor of nine in order to achieve a smooth transition between the low-LET and the high-LET region [8].

It has been pointed out by Katz and coworkers [6], that this model should be understood as a phenomenological model, and that literal interpretation of the parameters is not possible. Apart from this disadvantage, the model calculations reproduce the experimental results quite well, and for a long time this model was the only one able to reproduce the measured inactivation cross sections over the whole LET range up to 15000 keV/μm quantitatively correct. It was, in particular, the first model, which could explain the separation of the inactivation cross sections as a function of LET into different, Z-dependent branches for very heavy particles. The complex 'hook' structure of inactivation cross sections was attributed to the correlation between particle energy and track diameter and thus to track structure. Similarly, the model has demonstrated its qualification to describe other biological endpoints including chromosome aberrations and mutation frequencies as well.

Nevertheless, some problems arise from the approach discussed above:

1. The algorithm for the calculation of inactivation cross sections in the ion-kill mode implies an integration and thus averages the energy deposited in the critical target. Because the target has a diameter of typically 1 μm, the fine structure of the radial dose distribution is washed out by this method, and differences

between particles with the same LET, but different energy and thus different track structure will disappear.
2. The separation between γ-kill mode and ion-kill mode is artificial, and there is no direct experimental evidence supporting two completely independent modes of inactivation.
3. Due to the small target size assumed, calculated inactivation cross sections have to be scaled by a factor of nine. If the complete nucleus is assumed to be the critical target, scaling should become unnecessary.

A Unified Track Structure Approach

Calculation of Local Biological Effects

Recently, a unified track structure model has been developed, which combines to some extent principles of microdosimetry and usual track structure models [9–11]. Rather than the Katz approach which uses the integral of the energy deposited in the critical target, it is based on the integration of the local biological effect. This difference is crucial especially in the case of shouldered X-ray survival curves. The shoulder indicates, that at high doses the same dose increment is more efficient than at low doses. This consideration is assumed to apply likewise in the case of local dose depositions. A given energy deposited as high local dose in a small subvolume of the nucleus should be more efficient than the same energy deposited as low local dose in a larger subvolume. Consequently, calculations based on the total energy or average dose deposited in the nucleus will always underestimate the biological effect.

In order to determine the local biological effect, an additional, but very general assumption has to be made, which is concerned with the geometrical structure of the sensitive target. In a first approximation it is assumed, that the sensitivity is homogenously distributed within the cell nucleus, and that inactivation is the result of point-like damages, so-called 'lethal events'.

After X-irradiation, the expectation value $\overline{N}$, i.e., the average number of lethal events, depends on the dose D. The fraction of surviving cells can then be attributed to the cells, which actually carry no lethal event. Assuming that the distribution of lethal events obeys the Poisson statistics, this can be written as

$$S(D) = e^{-\overline{N}(D)} \tag{2}$$

Vice versa, the number of lethal events can be derived from the X-ray survival curve as

$$\overline{N}(D) = \ln S(D) \tag{3}$$

and rewritten, relating to the linear-quadratic model as

$$\overline{N}(D) = \alpha D + \beta D^2 \tag{4}$$

Although lethal events are assumed to be discrete, point-like events, the probability for their induction at a given position can be described by a continuous function, which depends on the distribution of sensitive sites. A homogeneous distribution corresponds to a constant probability within the nuclear volume and is defined by the event density

$$\nu(D) = \frac{\overline{N}(D)}{V} = \frac{\ln S(D)}{V} \tag{5}$$

Equation (5) allows an easy calculation of survival in the case of partially irradiated nuclei or inhomogenous dose distributions. The expectation value for the number of lethal events is obtained by an integration of the event density ν(D). For example, if only a part ΔV of the nucleus is irradiated with a constant dose D, the average number of lethal events will be

$$\overline{N_{lethal}} = \overline{N}(D)\,\frac{\Delta V}{V} \tag{6}$$

and in the case of an inhomogeneous dose distribution D(x,y,z), dependent on the position in the nucleus, $\overline{N_{lethal}}$ is obtained by an integration over the nuclear volume:

$$\overline{N_{lethal}} = \int_x\int_y\int_z \nu(D(x,y,z))\,dx\,dy\,dz = \int_x\int_y\int_z \frac{\ln S(D(x,y,z))}{V}\,dx\,dy\,dz \tag{7}$$

As in Equation (2), the fraction of surviving cells is given by the cells carrying no lethal event, and thus survival is calculated to be

$$S = e^{-\overline{N}_{lethal}} \quad (8)$$

As can be seen from Equation (7), three sets of experimental data will be required for the prediction of survival after charged particle irradiation:

1. the local dose distribution D(x,y,z), which is defined by the radial dose distribution D(r) inside the particle track and the position of particle trajectories;
2. the geometrical description of the cell nucleus, defining the sensitive volume V;
3. the X-ray survival curve S(D), which is used to derive the average number of lethal events $\overline{N}(D)$ and the event density $\nu(D)$.

Comparison with Experimental Results

Figure 2 compares model calculations with experimental results obtained at the UNILAC at GSI (Darmstadt). The comparison is based on inactivation cross sections, corresponding to the slope of the survival curve as a function of the particle fluence. There is a slight underestimation of the efficiency in the LET range from 100–300 keV/μm, but the general structure of the LET dependence is reproduced very well, even though these calculations were based on several simplifications, e.g., the same size and radiosensitivity for all cells of a population and a cylindrical shape of the cell nucleus.

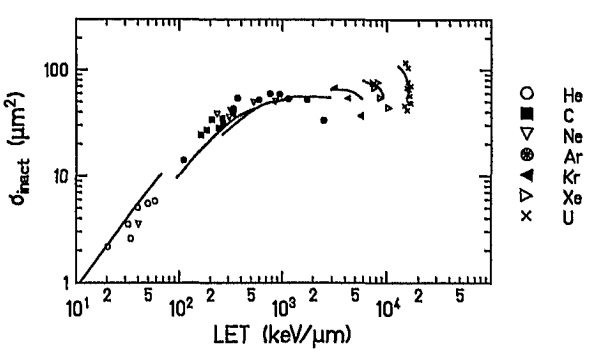

Fig. 2. Comparison of model calculations for inactivation cross sections σ_{inact} (full lines) with experimental results obtained with V79 Chinese hamster cells (symbols, redrawn from [12])

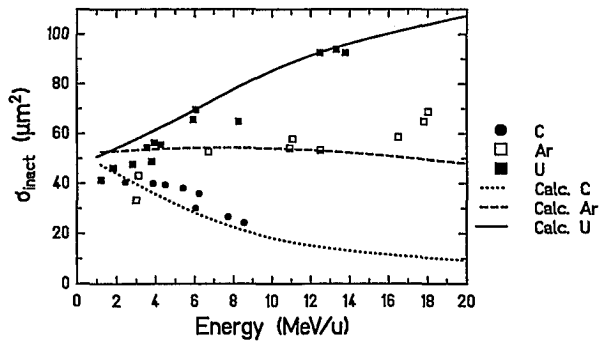

Fig. 3. Inactivation cross sections for V79 Chinese hamster cells as a function of the specific energy for carbon, argon and uranium ions

The key to the understanding of the complex hook structure at very high LET values is depicted in Figure 3, where inactivation cross sections are plotted as a function of the specific energy for three representative ion species. At low energies, all ions exhibit the same efficiency. The inactivation cross section is calculated to be 50 μm², which is equal to the effective geometrical size of the nucleus. Thus, a single traversal of any of the ions is sufficient to kill the cell with a high probability. With increasing energy, changes in LET as well as increasing track diameters are reflected in a change of the inactivation cross section σ. For the energy range shown in Figure 3, uranium ions exhibit only a slight decrease in LET, but a significant increase of the track radius. Because of the very high LET, high local doses are deposited even at large distances from the trajectory. Therefore, not only direct traversals of the nucleus, but also traversals in a certain distance can inactivate the cell. The probability of these 'indirect' inactivation events increases with the track diameter, resulting in a rise of the inactivation cross section.

The LET of argon ions declines from 3000 to 800 keV/μm for specific energies of 1 to 20 MeV/u, and despite the fact that the increase of the track radius is exactly the same as for uranium ions, the inactivation cross sections remain nearly constant over the whole energy range. This is a consequence of the much lower local doses at large distances from the track center, so that inactivation by a particle traversal outside the nucleus is very unlikely. In contrast, only the high local

doses in the center of the track have a high probability to kill the cell, and thus direct traversals are required at all specific energies for the inactivation of a cell. For carbon ions, the decreasing LET dominates the σ-E-dependence. Here, only low energetic particles deposit high local doses sufficient to kill the cell by a single traversal. As a consequence of the decreasing LET with increasing specific energy, the energy deposition per particle traversal and thus the probability of inactivation, decreases as well.

For light particles like protons, helium and carbon ions, which are more relevant for therapeutic applications, details of track structure play also an important role. This is demonstrated in Figure 4, where calculated RBE values are compared at different survival levels. At a given LET, the lighter particles are more efficient as compared to the heavier species. This higher efficiency is a consequence of the higher local doses in the track of the lighter particles, resulting from a lower energy and smaller track radius of these particles as compared to heavier ones of the same LET. In addition, the position of the RBE maxima depends on the atomic number. Whereas protons reach a maximum RBE at approx. 30 keV/μm, this maximum is shifted to approx. 90 keV/μm for α-particles and to 300 keV/μm for carbon ions. These model predictions are in good agreement with experimental results reported by several authors [2, 13, 14].

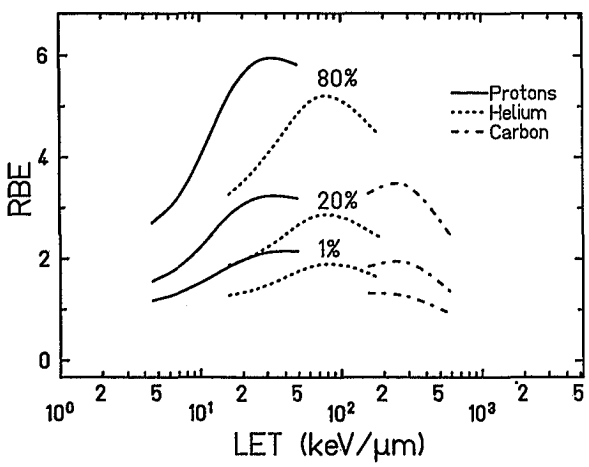

Fig. 4. Model predictions for RBE as a function of LET for protons, α-particles and carbon ions in the energy range of 1–20 MeV/u.

For LET values above 100–300 keV/μm, a rapid drop of RBE is predicted. This decreasing RBE cannot be attributed to the still increasing local dose depositions, but is related to the stochastic properties of particle radiation. For LET values above 300 keV/μm in the saturation region of the inactivation cross sections, particle fluences at the 1%-survival level lead to an average of a few particle traversals per cell nucleus. According to the Poisson statistics, this corresponds to large cell-to-cell fluctuations of the number of particle traversals, ranging from cells with no traversal up to cells with many traversals. The decrease of RBE can then be demonstrated most clearly in the case of 'overkill', where a single particle traversal deposits more energy than necessary to kill a cell. Consequently, only cells with no traversal will survive. If a cell, however, is hit by more than one particle, the additional traversals are ineffective and their energy is wasted, leading to a reduction of the RBE at high LET. However, even at lower LET values cell-to-cell fluctuations of energy depositions lead to a significant reduction of the RBE [15].

With respect to these stochastic properties it is obvious, that mean doses are not adequate to describe the biological effects of particle radiation. Instead, the concept of particle fluences and related quantities including inactivation cross sections should be used.

Biological Effects of Complex Charged Particle Fields

As mentioned at the beginning, charged particle fields applied in radiotherapy are more complex than those used for the track segment experiments discussed in the previous section. In order to calculate the biological effect of such complex fields, time consuming numerical integrations have to be performed for every point of the radiation field. Therefore, approximations which preserve the basic ideas of the model calculations but reduce the required computer time are necessary.

The basic idea of the approximations is to separate the two effects which determine the RBE of charged particle radiation:

- The energy density in the center of the track and the corresponding high local dose which lead to an enhanced relative biological efficiency of a single track.
- Cell-to-cell fluctuations of energy depositions due to the stochastic distribution of particle traversals through the nucleus which reduce the overall biological efficiency.

The separation is achieved by introducing a so-called potential or 'intrinsic' RBE, denoted as IRBE. This IRBE is a hypothetical value, describing the situation where all cell nuclei are traversed by exactly one particle. Of course, this IRBE cannot be measured directly, but it can be easily calculated. The measurable RBE is then predicted by folding the IRBE values with the stochastic distribution of the particle traversals. The advantage of this approach is, that time consuming numerical integrations have to be performed only once for the calculation of IRBE, which are than tabulated and used for the calculation of survival in complex charged particle fields by means of a very fast iterative algorithm [11].

Figures 5 and 6 show a comparison of calculations based on the approximations discussed above and corresponding experimental results. The first step from track segment experiments to the more realistic situation is to include effects of fragmentation of the primary beam and the corresponding build-up of lighter fragments due to the penetration of the beam through matter. The experiments were performed using water as tissue-equivalent absorber material. The survival curves were measured at different penetration depths of a 270 MeV/u carbon beam in water. For the survival predictions, fragment spectra were taken from a model which was adjusted to reproduce the experimental data [16]. In Figure 5, survival as a function of the particle fluence is shown for four different penetration depths. Figure 6 comprises survival values for two different particle fluences plotted versus the penetration depth, which yields the specific depth-dose distribution of charged particles, the Bragg peak. There is a good qualitative and quantitative agreement between calculation and experiments, justifying the discussed approximations.

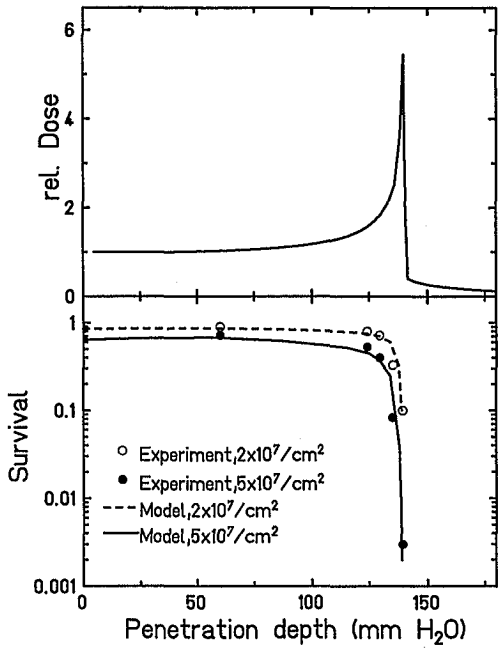

Fig. 6. Comparison of physical dose distribution (top) and biological effect (bottom) of a 270 MeV/u carbon beam penetrating through tissue, (simulated using a water column of variable thickness). Entrance particle fluences of $2 \times 10^7/cm^2$ and $5 \times 10^7/cm^2$ correspond to doses of 0.44 and 1.1 Gy at 0 mm penetration depth, respectively

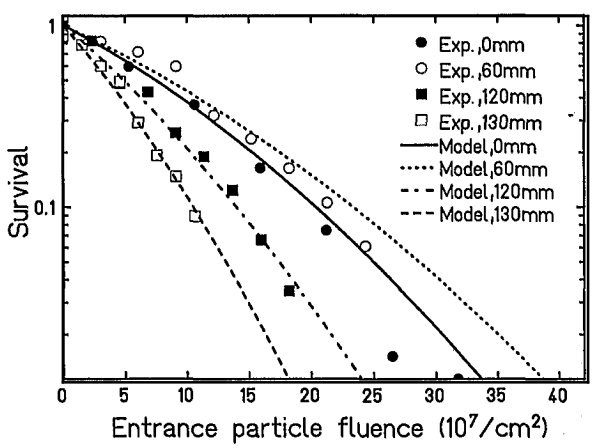

Fig. 5. Survival curves at different penetration depths of a 270 MeV/u carbon beam in water (Lines: model calculations; symbols: experimental data). Survival is plotted as a function of the entrance particle fluence at 0 mm penetration depth. Model calculations include the effects of fragmentation of the primary beam

Concluding Remarks

Investigations of track structure models reveal that many of the high-LET specific aspects, including the RBE-LET dependence, inactivation cross sections as a function of LET and energy, the Z-dependent shift of RBE maxima etc., can be attributed to the different microscopic pattern of energy depositions of charged particles as compared to photons. The approach discussed here explicitly disregards the stochastic nature of the energy depositions by individual electrons in particle tracks, but it uses the local radial dose as a mean or expectation value of the individual events. The predictions based on the average radial dose profile are in good quantitative agreement with experimental results. It seems that in standard survival experiments, where a large number of biological objects is irradiated with a large number of particles, the average radial dose profile is representative for the biological effect. As it has also been shown that the model reproduces the survival curves for decelerated beams including the effects of the lighter fragments, it is expected that similar calculations will agree with experiments applying superimposed Bragg peaks, as in the treatment of extended tumor volumes.

Differences in sensitivity and repair capacity which translate into different slopes and shoulders of the X-ray effect curves, are directly integrated into the calculations by using the X-ray curves as input for the predictions of the response to charged-particle exposure. It will be necessary to simulate the response of different cell types from tissues relevant for the therapeutic situation and to compare the response of the healthy tissue in the entrance channel with the response of the tumor cells. These calculations can help to develop guidelines for the optimization of different treatment modalities.

References

1 Goodhead, D.T., Belli, M., Mill, A.J., Bance, D.A., Allen, L.A., Hall, S.C., Ianzini, F., Simone, G., Stevens, D.L., Stretch, A., Tabocchini M.A., and Wilkinson, R.E. Direct comparison between protons and alpha-particles of the same LET: I. Irradiation methods and inactivation of asynchronous V79, HeLa and C3HT10T1/2 cells. Int. J. Radiat. Biol. 61, 611–624, 1992.

2 Belli, M., Cera, F., Cherubini, R., Haque, A.M.I., Ianzini, F., Moschini, G., Sapora, O., Simone, G., Tabocchini, M.A., and Tiveron, P. Inactivation and mutation induction in V79 cells by low energy protons: Reevaluation of the results at the LNL facility. Int. J. Radiat. Biol. 63, 331–337, 1993.

3 Varma, M.N., Baum, J.W., and Kuehner, A.V. Radial dose, LET and $\bar{W}$ for ^{16}O ions in N_2 and tissue-equivalent gases. Rad. Res. 70, 511–518, 1977.

4 Butts, J.J. and Katz, R. Theory of RBE for heavy ion bombardment of dry enzymes and viruses. Radiat. Res. 30, 855–879, 1967.

5 Krämer, M. and Kraft, G. Calculations of heavy-ion track structure. Radiat. Environm. Biophys. 33, 91–109, 1994.

6 Katz, R., Ackerson, B., Homayoonfar, M., and Sharma, S.C. Inactivation of cells by heavy ion bombardment. Radiat. Res. 47, 402–425, 1971.

7 Katz, R. Track structure theory in radiobiology and in radiation detection. Nuclear Track Detection 2, 1–28, 1978.

8 Katz, R., Dunn, D.E., and Sinclair, G.L. Thindown in radiobiology. Radiat. Protect. Dosim. 13, 281–284, 1985.

9 Scholz, M. and Kraft, G. A parameter free track structure model for heavy ion action cross sections, in Biophysical Modelling of Radiation Effects. Chadwick, K.H., Moschini, G., and Varma, M.N. (eds.), Adam Hilger, Bristol, 1992, pp. 185–192.

10 Scholz, M. and Kraft, G. Calculation of heavy ion inactivation probabilities based on track structure, X-ray sensitivity and target size. Radiat. Protect. Dosim. 52, 29–33, 1994.

11 Scholz, M., Kraft-Weyrather, W., and Kraft, G. Calculation of mammalian cell survival in complex charged particle fields, subm. to Radiat. Environm. Biophys., 1994.

12 Kraft, G. Radiobiological effects of very heavy ions: Inactivation, induction of chromosome aberrations and strand breaks. Nuclear Science Applic. 3, 1–28, 1987.

13 Thacker, J., Stretch, A., and Stephens M.A. Mutation and inactivation of cultured mammalian cells exposed to beams of accelerated heavy ions. Int. J. Radiat. Biol. 36, 137–148, 1979.

14 Kraft, G. and Kraft-Weyrather, W. Biophysical aspects of track structure, in Proc. 8th ICRR, Fielden, E.M., Fowler, J.F., Hendry, J.H., and Scott, D. (eds.), Edinburgh, July 19–24, 1987. Vol. 2, pp. 29–34.

15 Tilikidis, A., Skog, S., and Brahme, A. Influence of radiation quality changes on microdosimetric variance and dose-response relations. Radiat. Protect. Dosim. 52, 43–49, 1994.

16 Haberer, Th. Entwicklung eines magnetischen Strahlführungssystems zur tumorkonformen Strahlentherapie mit schweren geladenen Teilchen, Thesis (Univ. Heidelberg), GSI-Report 94–09, 1994.

7 Early and Late Responses to Ion Irradiation

R. SCHULTE

Loma Linda University Medical Center, Loma Linda, CA, USA

Introduction

A general trend in the development of radiation therapy has been to improve the three-dimensional dose distribution resulting in better normal tissue sparing and allowing higher doses to be delivered to tumors. The current surge of interest in ion beam therapy throughout the world reflects this trend. But even with sophisticated ion beam irradiation tumor and normal tissues adjacent to the tumor can never be completely separated, because almost all malignant and even some benign tumors infiltrate into the surrounding normal tissues. As the exact extent of this microscopic infiltration is usually unknown, the radiation oncologist must include a variable shell of normal tissue in the treatment plan, which is assumed to be infiltrated by tumor cells and needs to be treated with therapeutic doses of radiation. Particularly, when large and irregular targets are treated, the amount of normal tissues included in the high dose region may be comparable or even larger than the tumor volume itself.

Understanding the pathophysiology of normal and tumor tissue responses to ionizing radiation plays, therefore, a key role in clinical applications of ion radiation. Particularly, for the development of innovative clinical therapy protocols utilizing ion beams it is important to know and to understand the responses of normal and tumor tissues to ion irradiation in order to achieve a maximum benefit from this treatment modality.

Basic Concepts

Definition of Early and Late Tissue Responses

Tissue responses to ionizing radiation are commonly divided into early and late (alternatively, acute and delayed) effects reflecting the time after irradiation at which the biological or clinical endpoint is typically observed. The same concept is also applied to normal tissues which are classified as early or late responding tissues depending on the time after irradiation at which the clinically relevant effects occur. The latter definition, however, is not always compatible as early and late reactions can occur in the same tissue. A typical example is skin which can develop an acute erythema within a few hours followed by desquamation days or weeks after the irradiation due to depletion of the basal stem cell layer. Eventually, a delayed wave of damage is seen many months to years later evidenced by slow development of telangiectasis, fibrosis, atrophy and – in its severest form – necrosis.

Cell Depletion as the Origin of Radiation Effects in Tissues

Sufficient evidence has accumulated that both acute and late radiation effects are caused by a combination of parenchymal, endothelial and stromal cell depletion due to mitotic death. It is likely that most, if not all, normal tissues and possibly many tumor tissues show a similar pattern of response which can be divided into two distinct

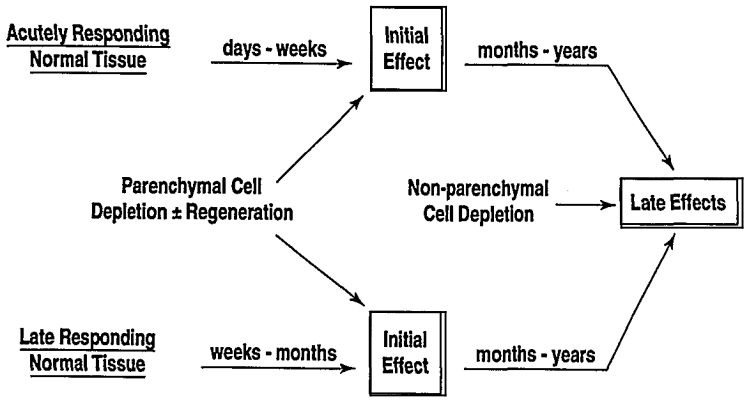

Fig. 1. Schematic illustration of the pathways leading to radiation effects in acutely and late responding tissues. Note that the two tissue types differ with respect to the timing of the initial (parenchymal) response

waves of damage (Fig. 1): the parenchymal response (e.g., mucositis, pneumonitis) which is due to depletion of normal tissue parenchymal cells or tumor clonogens, and the non-parenchymal response (e.g., fibrosis in submucosa or lung) which usually, but not necessarily, occurs after the parenchymal response. The latter is of stromal etiology and manifests as chronic tissue damage. Secondary injury may be seen at the time of non-parenchymal response in parenchymal cells of normal tissues which is related to damage of the microvasculature and loss of supply with oxygen and other nutrients. Finally, progressive atrophy and eventually necrosis may occur due to continuous loss of capillaries, endarteritis and obliteration of arteriols or even narrowing and occlusion of major arteries. There has been a long-time debate between those who believe in a mere vascular origin of late injury in normal tissues and those who claim that delayed radiation effects are primarily the result of parenchymal and/or stromal cell depletion with vascular effects secondary. It is likely, however, and there is ample evidence that in many tissues late radiation damage is caused by a combination of depletion in more than one cell compartment.

Tissue Architecture and Volume Effects

Most radiation therapists are intuitively aware of the importance of the volume factor in radiation therapy. It has long been known that the probability of normal tissue complication increases with increasing area or volume irradiated and that the probability of tumor control decreases with increasing tumor volume. Furthermore, radiation damage to larger areas or volumes of normal tissue appear to be less tolerated by patients than smaller amounts of tissue even when the average grade of tissue damage is equal.

Over the last decades, many investigators have tried to define a scientific basis for volume effects in radiation therapy [1–8]. A general concept that has emerged from these studies is that of independent tissue subunits, which means that each subunit responds to radiation as if it were isolated from all surrounding units. Withers et al. [9] suggested that some tissues are organized into functional subunits (FSUs) which are either structurally defined or undefined tissue entities. Typical structurally defined FSUs are nephrons of the kidney, or alveoli of the lung. The FSU model implies that FSUs can be repopulated when at least one single cell of an individual FSU survives. Cells from neighboring FSUs cannot substitute it.

Another important concept in the context of volume effects is that of serial and parallel tissue architecture, which is schematically illustrated in Fig. 2. The tissue or organ may be considered as an arrangement of equal-sized subvolumes which respond to radiation independent of each other. In a serial organ (Fig. 2A) loss of function in any one of these subvolumes results in a clinically relevant complication. This type of response has been called critical element response. A typical serial organ or tissue is white matter of the

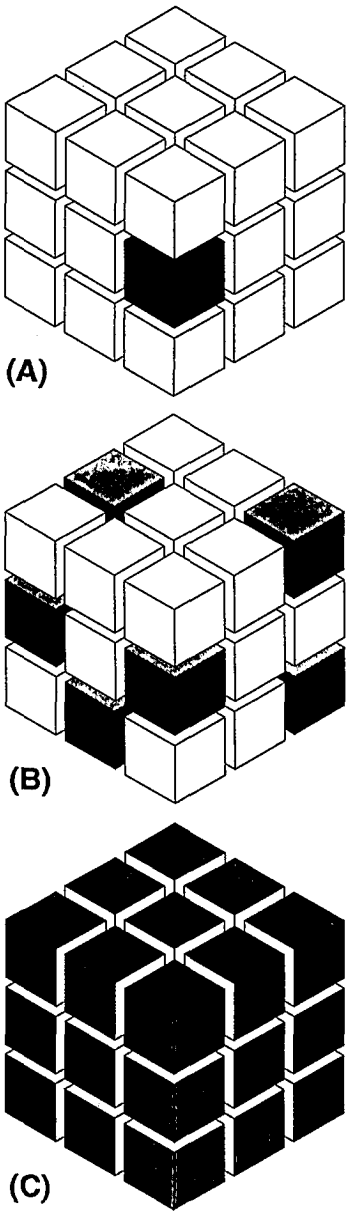

Fig. 2. Schematic representation of three different tissue radiation-response types which are related to volume effects. (A) Serial organ response; (B) parallel organ response; (C) graded response (for further explanation see text)

spinal cord. Interruption of any of the long spinal cord tracks due to necrosis within a small volume of white matter leads to a serious function loss. In a parallel organ (Fig. 2B) a clinically relevant complication can be expected when a certain fraction of subvolumes has been destroyed or has lost useful function. This type of response has also been called integral response. Examples for parallel organs include the kidney, lung, or liver.

Over the last few years several authors have stressed the importance of organization of tissues into serial or parallel arrangements of subunits for radiation tolerance and volume effects [3, 7, 9].

Serial type tissues or organs may exhibit two different types of volume effects. Firstly, when the irradiated volume is reduced below a certain size, a steep increase in tolerance is observed, for example, in rabbit brain or rat spinal cord [10–13]. This has also been observed in patients treated with functional radiosurgery, when very large single doses are needed to destroy very small amounts of brain tissue. This phenomenon may be explained by "penumbra effects": when the irradiated volume is surrounded by unaffected tissue, migration of target cells from the surrounding tissues or diffusion of oxygen, other nutritients, or response-modifying cytokines may increase the tolerance of the irradiated volume. This means that the assumption of independence of individual subvolumes may not generally hold, particularly, when neighboring tissue volumes receive largely different dose levels. Secondly, for larger volumes a less dramatic volume dependence has been observed for serial type tissues, which is predictable purely based on statistical principles including the assumption of independent subvolumes [3].

The volume effect in tissues or organs with parallel architecture is in many respects different from that of tissues or organs with serial architecture [8]. When only relatively small amounts of parallel organs, such as lung, kidney, or liver are irradiated, the functional outcome will show no volume dependence. Once, however, a critical fraction of tissue subunits in such organs has been destroyed, a steep increase in the probability of complication (i.e., loss of organ or tissue function) is observed. It should be noted that not all tissue subunits may be equally important for proper organ function and that loss of certain areas in a parallel organ may be functionally less important than others.

Both serial and parallel organs may show graded responses after irradiation (Fig. 2C). A graded response means that there is a gradual increase in the severity of acute or late reaction as a function of dose. Most acute radiation effects, e.g., skin reactions, are graded responses, but also many late effects can be categorized according to their grade (e.g., fibrosis, intellectual function loss etc.). When graded responses are defined per unit area or volume of tissue, they seem to be relatively independent of the area or volume irradiated at a given level of dose. For example, if a certain average grade of skin erythema is observed after irradiation to a certain dose it tends to be independent of the total area irradiated. On the other hand, larger areas or volumes of tissue affected by radiation are less likely to be tolerated by patients than comparably small areas.

Tissue Effects

In this section the results of experimental studies of ion irradiation effects on normal and tumor tissues will be reviewed. These studies have been an important part of the research programs leading to the clinical use of protons, helium and heavier ions at the Harvard Cyclotron Laboratory (HCL) in Massachusetts and the Lawrence Berkeley Laboratory (LBL) in California. One important aspect of these studies has been to define the RBE of ion beams with respect to tolerance doses for organ and tissue systems that were judged to impose critical dose limitations.

Clinical RBE values, which are usually based on the results of experimental studies, play an important role in present and future ion beam protocols and in treatment planning of ion beam therapy because they determine the maximum physical dose considered not to exceed an acceptable risk of complication probability in critical normal tissues and the minimum physical dose required for a sufficiently high probability of tumor control. One must remember, however, that experimentally determined RBE values depend on the particular experimental set-up and that clinical RBE values derived from these studies must be used prudently (cf. succeeding chapters).

The following review focuses on the major dose-limiting critical organs and tissues, i.e., skin and the gastrointestinal tract as indicators for early radiation effects, and lung and spinal cord as important late responding organs. For the sake of brevity, other valuable indicators for early (e.g., testes) and late (kidney, lens) reactions cannot be discussed.

Early Normal Tissue Responses

Skin

Skin, although not a critical organ in the stricter sense of the term, is an important dose-limiting tissue as its radiation side effects contribute significantly to both early and late patient morbidity. In addition, skin has been traditionally used to study RBE effects of new radiation modalities [14].

Different animal skin systems have been used such as the mouse foot [15], mouse thigh [16], or mouse flank [17]. RBE values derived from these studies are characterized by relatively large confidence intervals, typically in the order of 20–25 % of the mean value.

Raju and Carpenter [15] performed an extensive comparative study of mouse skin effects with various ions ranging in mass from protons to argon ions and using ^{60}Co-γ-rays as reference radiation. They found that the time course of development of skin reaction and subsequent healing was similar for all radiation modalities indicating that epithelial cell depletion and repopulation are not principally different when high- and low-LET radiations are compared.

Single dose RBE values for an early skin reaction of grade 1 in mouse skin obtained by these investigators are summarized in Table 1. For the lighter ions (protons and helium ions), the RBE in both the peak and the plateau region was found to be only slightly above 1.0. With increasing ion charge the RBE increases both in the peak and the plateau region and for neon and argon the RBE of peak and plateau region are approximately equivalent. The highest peak-to-plateau ratio was found for carbon ions. The RBE values

Table 1. Single dose RBE values (RBE_{sd}) for early skin reactions in mouse skin after irradiation with various ions in the peak (pk) and plateau (pl) region of a 10 cm SOBP ionization curve. From Raju and Carpenter [15]

Ion	Energy (MeV/u)	Location	RBE_{sd}	Peak-to-plateau ratio of RBE_{sd}
Proton	160	pk	1.1	0.9
		pl	1.2	
Helium	910	pk	1.1	1
		pl	1.2	
Carbon	400	pk	1.5	1.25
		pl	1.2	
Neon	400	pk	1.7	0.85
		pl	2.0	
Argon	400	pk	1.9	0.9
		pl	2.1	

reported by Raju and Carpenter are in good agreement with those reported by Leith et al. [17–19] who performed similar experiments in mice.

While the mouse skin RBE studies were performed with single doses, Leith et al. [20] investigated the response of hamster skin to various fractionation schemes with either X-rays or carbon ions using single, split or multiple exposures. RBE for acute skin reaction was obtained in the proximal portion of a 400 MeV/u carbon ion 4 cm SOBP. From the data obtained by these investigators a maximum RBE of 2.3, and an RBE at 2 Gy per fraction of 2.1 was derived. When comparing these values to the single dose RBE in Table 1, there appears to be a trend towards increased RBE values for fractionated exposures, as expected from basic principles. For protons, the fractionation effect seems to be less pronounced: a multi-fractionated dose study in mice using 20 fractions delivered with the center of a 160 MeV modulated proton beam performed by Tepper et al. [21] resulted in an RBE value of 1.1 for acute skin reactions, which corresponds to the single dose RBE value obtained by Raju and Carpenter [15].

Gastrointestinal Tract

The mouse gut microcolony method, which was originally developed by Withers and Elkind [22], has found wide application as a clonogenic assay for acutely responding tissues and has also been used for comparison of radiations of various LET values, both neutrons and heavy ions (see also Chapter 9). Briefly, in this assay the mice are sacrificed three to four days after irradiation and hematoxylin-eosin histologic sections of the jejunum are prepared. The number of regenerating crypts per circumference is then determined according to criteria established by Withers and Elkind. Assuming a Poisson distribution of the number of surviving cells per crypt, the number of surviving cells per circumference is calculated.

Table 2 summarizes the results of two such studies by Tepper et al. [21] and Goldstein et al. [23]. An increasing effectiveness of ions is seen with increasing ion charge (and mass). As the ion charge increases, the increase of RBE is first observed in the peak region of the Bragg peak ionization curve and then extends to the plateau region. For ions up to the mass of carbon, the quality of the plateau region radiation is almost independent of the ion species and is characterized by RBE values slightly above 1.0. The Bragg peak radiation of protons and helium ions is also only slightly more effective than ^{60}Co-γ-radiation, while the Bragg peak radiation of carbon and the heavier ions has high-LET character. When the different ions are compared, carbon ions are characterized – as in the case of skin (Tab. 1) – by the highest peak-to-plateau RBE ratio.

Late Normal Tissue Responses

Compared to the number of ion beam studies using early endpoints, there is a relative paucity of studies evaluating the chronic response of vitally important organs to ion beams. Late response studies are difficult to perform because they are time-consuming and expensive and often confounded by the limited life span of rats and mice. In order to be concise, only lung and spinal cord, the two late responding normal tissues in

Table 2. RBE values for single (RBE_{sd}) and fractionated doses (RBE_2 and RBE_{max}) for jejunal crypt cell survival after irradiation with various ions in different positions of the SOBP ionization curve (pk = peak, pl = plateau, dp = distal peak, mp = central peak, pp = proximal peak). Data for protons from Tepper et al. [21], all other data from Goldstein et al. [23]

Radiation Source	Energy (MeV/u)	Modulation (cm)	Location	RBE_{max}	RBE_2	RBE_{sd}	Peak-to-plateau ratio of RBE_2
^{60}Cobalt[1]	–	–	–	1	1	1	–
Proton	160	10	pk	1.2	1.3	1.2	1.1
			pl	1.2	1.2	1.1	
^{137}Cesium[1]	–	–	–	1	1	1	–
Helium	225	8	pk	1.5	1.5	1.2	1.2
			pl	1.3	1.3	1.1	
Carbon	400	10	dp	2.4	2.2	1.5	1.7
			mp	1.8	1.8	1.4	1.4
			pp	1.5	1.6	1.4	1.2
			pl	1.2	1.3	1.3	
Neon	557	10	dp	3.4	3.0	1.6	1.4
			mp	3.0	2.6	1.5	1.2
			pp	3.0	2.7	1.5	1.3
			pl	2.3	2.1	1.4	
Argon	570	10	dp	4.3	3.6	1.8	0.8
			mp	4.5	3.8	2.0	0.9
			pp	4.3	3.6	1.9	0.8
			pl	5.2	4.3	2.1	

[1] reference radiation

which most information on ion beam responses have been collected, will be discussed below.

Lung

Lung is an organ where complex cell kinetic changes determine the course of radiation injury [24]. No clinically important physiological changes are observed during the first three months after irradiation, although microscopically there seems to occur a marked increase of inflammatory cells in the alveolar septa and spaces as has been observed in hamster lung during the first month after irradiation [25]. The first wave of clinically significant damage, which is called radiation pneumonitis, shows up 3 to 6 months after irradiation. It is histologically characterized by capillary loss and type II pneumocyte depletion. After single doses exceeding 10 Gy in mice, the onset of capillary injury and pneumocyte depletion is accompanied by platelet-induced thrombosis and occlusion of many alveolar capillaries. If this acute phase of lung damage is survived, an attempt of repair is seen over the next six months with ingrowth of new capillaries which, after higher doses, is accompanied by excessive growth of collagen within septal spaces. The end result at 12 months after irradiation with single doses higher than 10 Gy is lung fibrosis, which is characterized by a reduced number of capillaries and alveolar air spaces and thickening of alveolar walls in most of the remaining alveoli.

Woodruff et al. [26, 27] investigated the late responses of hamster lung after single doses of 230 kVp X-irradiation and 375 MeV/u neon ion irradiation in the plateau region. Dose levels ranged from 2.25–15 Gy for X-irradiation and from 1.5–10 Gy for neon irradiation. Hamsters were chosen for these studies as they are free from chronic lung disease. Using morphometric techniques, these investigators found that 12 months after irradiation with either X-rays or neon ions the volume density of pulmonary septums, septal cells, collagen, and type II pneumocytes was increased, while the volume density of alveoli, empty alveolar space, and capillary

lumen was decreased. Most of these changes were dose dependent and the RBE for these histological endpoints varied between 1.6 and 1.8.

While these RBE values are not significantly different from RBE values for early endpoints (see Tables 1–2), they may not reflect clinically relevant RBE values as they were obtained after irradiation with large single doses. Travis and associates [28] investigated the influence of fractionated irradiation with 1, 4, or 7 fractions of X-rays or neons ions in the center of a 4 cm SOBP on mouse lung function. They found that the RBE increases markedly from a single dose value of 1.5 to a value of 3.3 at 2 Gy per fraction and a maximum of 4.3 in the low dose limit.

Even more pronounced than for late effects in lung, there is a fairly dramatic increase of RBE for 50% radiation myelopathy with decreasing fraction size. For carbon and neon ions the RBE increases from single dose values, which are close to those reported in early responding tissues, to values between 4 and 6 at 2 Gy per fraction and between 6 and 10 at the low dose limit. Despite the evidence that an increase of isoeffective dose with decreasing fraction size occurs after ion irradiation as well as after X-irradiation, it must be appreciated that at small doses per fraction the RBE of ions for late effects in spinal cord is considerably higher than at higher doses per fraction. Therefore, caution is necessary whenever spinal cord or other CNS tissues are exposed to multiple small fractions of high-LET ion irradiation.

Spinal Cord

Similar to lung, the central nervous system is an important dose-limiting tissue, that often compels the radiotherapist to underdose nearby tumor tissue. In particular, spinal cord is considered an important dose-limiting structure in the treatment of many head and neck and intrathoracic tumors as overdosing the cord may lead to serious and irreversible injury. Ion beams appear to be an attractive radiation modality for the treatment of such tumors, as isodoses can literally be "wrapped" around the cord.

Spinal cord studies in rats with heavy ions at LBL have been performed by Leith et al. [18, 29, 30]. Table 3 summarizes a few results which illustrate the major trends.

Carcinogenesis

The mutagenic and carcinogenic effect of ionizing radiation have long been recognized under experimental, clinical, and expositional conditions and have extensively been documented (for review, cf. e.g., [31]). Induction of secondary cancers many years after treatment with ionizing radiation, although fortunately relatively rare, is of major concern, particularly in young patients and those irradiated for benign conditions. With regard to treatment with ion irradiation an important question is whether the high-LET component will lead to a higher incidence of cancer induction than observed after low-LET X- or γ-ray irradiation.

Table 3. RBE values for single (RBE_{sd}) and fractionated doses (RBE_2 and RBE_{max}) for rat spinal cord at the isoeffective dose level (ED_{50}) for paralysis after irradiation with various ions based on data from Leith et al. [30]. Irradiations were performed in the plateau (pl) and the peak (pk) position of the SOBP ionization curve

Radiation Source	Energy (MeV/u)	Modulation (cm)	Location	ED_{50}(Gy) Single Dose	Fract. Dose	RBE_{max}	RBE_2	RBE_{sd}
230 kVp X rays	–	–	–	25.6	49	1	1	1
Helium	225	6	pk/pl	23.8	–	–	–	1.1
Carbon	400	4	pk	17.5	25.1	6.8	4.1	1.4
			pl	17.9	37.6	9.2	5.5	1.5
Neon	425	4	pk	13.8	22.5	7.7	5.3	1.9
			pl	17.5	27.2	7.2	4.5	1.5

Studies of mutation induction in vitro after exposure to accelerated ions have shown that ion beams in the LET range below 200 keV/μm are many times more effective with respect to induction of mutations and neoplastic transformation than low-LET radiations. The relationship between RBE and LET for neoplastic transformation and mutation induction shows – similar to that of cell inactivation – a peak between 90 and 200 keV/μm. In the peak region, however, the RBEs for mutation induction and neoplastic transformation appear to be higher than those for cell inactivation [32, 33].

The mutagenic and carcinogenic potential of ion beams has also been measured in animal systems [34–37] and it was found that the effectiveness of ions in producing secondary tumors per particle was approximately constant for ions with LET values larger than 100 keV/μm.

Fractionated exposure to ion beams was found to be about 1.5 times more effective than the same dose delivered in a single fraction ($p < 0.01$), which is explained by the existence of a sensitive phase for cell transformation in the cell cycle which is more likely to be hit when the number of fractions increases. Other interpretations include the effect of reduced cell killing for protracted as compared to acute exposure increasing the number of cells at risk for transformation, and the possibility that radiation acts as a promoter of cells which were initiated during prior exposures.

Tumor Responses

The response of tumor tissues to radiation is in many respects similar to that of normal tissues. There is, however, a radiobiologically important difference between normal and tumor tissues: a variable fraction of hypoxic cells is present in many tumors, particularly, in larger and rapidly proliferating tumors, which is usually not found in normal tissues (see the preceding section for details). Studies of tumor responses to ion beam irradiation have, therefore, focused on both the increased RBE and the reduced oxygen enhancement ratio (OER) of high-LET ion beams, which may result in a therapeutic benefit.

RBE values measured for different tumors confirm the general trends already described for normal tissue responses to ion beam irradiation. For helium, carbon, or neon the peak region had a higher RBE than the plateau region; for argon the RBE measured in the peak was slightly above or below that in the plateau, indicating a saturation effect in the peak region. RBE values are, generally, similar to those observed for early responding normal tissues or lower than those for late responders.

In all experiments evaluating the effect of oxygenation on the response to ion irradiation, the RBE for killing hypoxic cells was larger than that for killing oxygenated cells. The differences between hypoxic and oxic RBE values increased with increasing LET of the ion irradiation. The higher RBE for hypoxic cell kill may be interpreted in terms of the additional damage produced in the presence of oxygen due to low-energy deposition events which prevail after low-LET irradiation, while the damage due to high-energy deposition is widely unaffected by the presence or absence of oxygen. The larger RBE for hypoxic cells is also reflected in a reduction of the OER, particularly for high-LET ion beams.

Summary and Conclusions

Irradiation of deep-seated tumors with ion beams, replacing conventional X-ray or γ-ray sources, offers the possibility of increased tumor doses without increasing the dose to surrounding normal tissues. Despite the superior three-dimensional dose distribution achievable with ion beams, normal tissues can, however, never be completely excluded from the dose delivered to designated target tissues. Typically, in the treatment of malignant tumors infiltrated normal tissues have to be intentionally irradiated. Therefore, knowledge and understanding of early and late effects of ion beams is important for their clinical application.

Most early and late effects have a common pathophysiological pathway, namely, the depletion of parenchymal and stromal target cells. Early and late responses differ in the time interval after irradiation at which they occur due to

differences in cell kinetic parameters of pertinent target cells. Furthermore, tissues differ in their response to radiation according to the regenerative capacity of target cell populations, which is usually large in early responding epithelial tissues and low or absent in late responding parenchymal or stromal cell populations.

Tissue effects to radiation are also modulated by the volume of tissue irradiated. Volume effects are particularly important for conformal ion beam radiation therapy, as smaller amounts of normal tissue are included in the target volume compared to conventional radiation therapy, although these limited amounts of tissue may receive a greater dose. Volume effect models and experimental studies are needed which would allow the prediction of the complication probabilities under these circumstances.

Ion beam irradiation up to average LET values of 200 keV/μm is usually more effective at the same level of absorbed dose than low-LET X-rays or γ-rays. This increased effectiveness is observed at all levels of biological effects including cellular inactivation, mutagenesis, malignant transformation and functional tissue responses, and is usually expressed in terms of RBE values tied to a particular form of radiation. When applying the RBE concept in clinical practice one needs to be aware of the many factors besides LET that may modify the RBE. Among these factors are the depth of irradiation, dose per fraction, and tissue type. Similar to the experience with high-LET neutron beams, the RBE of ion beams tends to be larger at small dose levels and also for late effects. Another concern is the increased RBE at the distal edge of the Bragg peak for all ions lighter than neon. This may lead to an increased risk of complications when the beam is stopped on a critical structure.

Experiments with tumor tissues have suggested that Bragg peak ions with a maximum LET of about 100 keV/μm may significantly enhance the biologically effective tumor dose without substantially increasing the risk to surrounding normal tissues. Some caveats to this hope may apply: RBE values for immediately surrounding late response tissues may still be higher than those for rapidly proliferating tumor tissues, thus, diminishing the beneficial therapeutic ratio. Furthermore, reduced OERs and increased RBEs found for tumor cells under hypoxic conditions may not be of clinical significance when reoxygenation occurs during a course of fractionated radiation therapy.

It could well be that the superior three-dimensional dose distribution which is associated with significant normal tissue sparing will eventually prove to be the clinically most relevant feature of ion beams. More basic research and improved radiobiological modeling are needed in the near future to further investigate their volume effect.

References

1 Cohen, L. The tissue volume factor in radiation oncology. Int. J. Radiat. Oncol. Biol. Phys. 8, 1771–1774, 1982.

2 Wolbarst, A.B., Lee, M.C., and Svensson, G.K. Optimization of radiation therapy: Integral responses of a model biological system. Int. J. Radiat. Oncol. Biol. Phys. 8, 1761–1769, 1982.

3 Schultheiss, T.E., Orton, C.G., and Peck, R.A. Models in radiotherapy: Volume effects. Med. Phys. 10, 410–415, 1983.

4 Shymko, R.M., Hauser, D.L., and Archambeau, J.O. Field size dependence of radiation sensitivity and dose fractionation response in skin. Int. J. Radiat. Oncol. Biol. Phys. 11, 1143–1148, 1985.

5 Archambeau, J.O. and Shymko, R.M. Tissue population configuration as a modifier of organ dose response. Int. J. Radiat. Oncol. Biol. Phys. 15, 727–734, 1988.

6 Yaes, R.J. and Keland, A. Local stem cell depletion model for radiation myelitis. Int. J. Radiat. Oncol. Biol. Phys. 14, 1247–1259, 1988.

7 Niemierko, A. and Goitein, M. Modeling of normal tissue response to radiation: The critical volume model. Int. J. Radiat. Oncol. Biol. Phys. 25, 135–145, 1992.

8 Yorke, E.D., Kutcher, G.J., Jackson, A., and Ling, C.C. Probability of radiation-induced complications in normal tissues with parallel architecture under conditions of uniform whole or partial organ irradiation. Radiother. Oncol. 26, 226–237, 1993.

9 Withers, H.R., Taylor, J.M.G., and Maciejewski, B. Treatment volume and tissue tolerance. Int. J. Radiat. Oncol. Biol. Phys. 14, 751–759, 1988.

10 Berg, N.O. and Lindgren, M. Relation between field size and tolerance of rabbit's brain to roentgen irradiation (200 kV) via a slit-shaped field. Acta Radiol. 1, 147–168, 1963.

11 Hopewell, J.W. and Wright, E.A. The effects of dose and field size on late radiation damage to the rat spinal cord. Int. J. Radiat. Biol. 28, 325–333, 1975.

8 Biological Beam Characterization

E. A. BLAKELY

Lawrence Berkeley Laboratory, University of California, Berkeley, CA, USA

Introduction

Physical characterization of ion beam fields is conventionally accomplished in the practice of radiotherapy to ensure uniform clinical effects. A demonstration of a uniform physical dose across a radiation field does not always guarantee, however, a uniform clinical outcome. It is acknowledged that there are tissue-specific differences in both acute and late tissue effects to low-LET radiations, as well as considerable variability in individual radiosensitivities presumably due to inherent genetic susceptibilities [1].

The additional consideration of variations in radiosensitivity due to radiation quality can be at first somewhat staggering due to the large number of variables and the range of potential differences. The higher ionization densities of alternative radiation modalities, such as neutrons or heavy ion beams are known to be associated with greater biological effectiveness than what is measured for conventional photon therapy [2–4]. The picture becomes further complicated as published experimental data at very high LET (greater than 2000 keV/μm) indicate a reduction in the radiobiological differences between radioresistant and radiosensitive systems [5]. Most alternative radiation modalities for cancer therapy (such as protons, alpha particles, pions, or carbon ions) involve intermediate LET values (between 20 to 200 keV/μm) where the greatest variation in RBE is observed. This presents a practical problem to the clinician in choosing a specific appropriate dose regime at intermediate LET.

Neutron radiotherapy was initiated in 1938 and proton radiotherapy in 1956, yet even today there is controversy regarding the assignment of a quality factor or RBE value for neutrons and protons, especially as a function of dose or energy [6–9] For charged particles the range of changes in biological effectiveness can be even greater. After Stone's [10–12] early experience with neutron cancer radiotherapy resulted in severe adverse reactions in normal tissue, considerable attention has been given to reducing the total dose to normal tissues unavoidably in the treatment volume of alternative radiation modalities having a high-LET radiation dose component. The limiting radiosensitive normal tissue is identified in the treatment field, and a reduced dose fraction of the high-LET radiation is selected based on what is thought to be equivalent or comparable to what is tolerated in conventional photon radiotherapy. Although physical detectors of altered radiation quality are available, their use for this purpose has been limited and biological characterization has historically served as the basis for the measure of the reduction in dose fraction needed. This chapter reviews aspects of this practical approach, and discusses the need that remains in the field to standardize the protocols for biological measurements. Although not intended to be all-inclusive, several examples of techniques currently in use to measure radiobiological parameters are reviewed. Preclinical radiobiology for charged particle radiotherapy is provided as illustrative of the methodologies that have been used to complete biological beam characterization.

Representative Biological Systems

Biological characterizations for clinical radiotherapy have primarily been accomplished with cell systems in vitro and with animals in vivo [13, 14].

For reasons of practical necessity, representative biological systems have been selected for the measurement of biological effectiveness. Due to the ease of techniques and availability, emphasis has been given to the measurement of cell killing and repair using cells that grow easily in tissue culture, and using tissues having highly proliferative cell renewal systems amenable to quantitative assays. However general concern exists in the field that appropriate biological assays are not available for all of the critical tissues and endpoints that perhaps should be screened for a thorough understanding of clinical responsiveness to a particular radiation. The shortcomings of the present approach still need to be evaluated.

Essential to any of these studies is the need for deliberate coordinated physics measurements (including dose calibration, assessment of radiation field composition and uniformity, or microdosimetry) under the exact conditions of the biological exposure, and for parallel studies of the biological response to a standard low-LET reference radiation (see [15–17] and additional discussion below).

In vitro Systems

Cell systems in vitro can generally be divided into two categories: primary and established cultures. Primary cultures are those that are newly derived from normal or tumor tissues and have not undergone many passages in culture, during which changes in the cells or selection of specific cell types could have occurred. The primary normal cells, and even some tumor cells are usually difficult to grow on tissue culture plastic, as evidenced by low plating efficiencies for colony forming assays. Low plating efficiencies mean that large numbers of cells are required to measure statistically the colony forming assay endpoint. Established cultures are cell lines that have been in culture for a significant number of passages to allow convincingly a characterization of the system. Plating efficiencies are usually higher than for primary cells, probably because there is a selection for cell subpopulations that grow well under the artificial conditions in tissue culture. The question that remains is, whether the selected cells that survive are representative of the original population of cells from which the culture was derived. The answer is highly dependent on the criterion selected for the comparison.

Radiobiological characterization of accelerator-based alternative radiation modalities frequently requires comparative experiments completed over the course of several years. Since the living cell can be a very sensitive LET-detector of alternative ionization densities, it can be used to determine changes in radiation quality. For technical ease, established cultures of mammalian cells, including those of human and rodent origin have been used to examine cell killing, repair, chromosomal rearrangements, mutagenesis and transformation, and the reduction of the radiobiological oxgen effect, long thought to be a significant factor in overcoming tumor resistance [18]. The merits of this approach are that a very large matrix of data has been generated with a large assortment of established cell systems. The remaining problem is that – except where individual investigators have conducted exhaustive comparisons of various radiation modalities with the same system [14, 19] – there are in most cases, very few opportunities to make identical RBE comparisons. In many cases the low-LET reference for the RBE determination has been either cobalt-60, 100–250 kVp X-rays, or cesium-137, which confounds any strict RBE comparison since physical differences among these sparsely ionizing radiations can themselves produce up to 20% differences in the biological responses.

In vivo Systems

An early observation made in vitro was that single, acute dose responses of cell systems were not revealing all of the necessary information required for adequate treatment planning in the clinic. Dose fractionation and delayed plating studies revealed that repair of radiation damage

moderated the end effects considerably [20, 21]. Repair studies conducted in vitro are limited in scope due to technical considerations. Experiments with animals are more amenable to the dose fractionation regimes used in the clinic. Rodent tumors are a good indicator of superficial human tumors in terms of actual physical size and geometry. Extrapolations must be made to predict the effects of larger, deeper tumors found in man.

RBE Mapping Techniques

Once the decision is made about which cell is appropriate for representative biological characterization, one must next decide what geometry to use to complete the radiation exposures. Cells grown in tissue culture that attach well and make individual colonies are highly amenable to the biological characterization of accelerator-based radiations. This is primarily due to the fact that accelerators designed for physics usually have fixed horizontal beam lines that necessitate a vertical exposure geometry. If the question being asked is "what is the average biological effect over a range of beam depth?", then exposures can be made with cell suspensions. However, if one is interested in mapping the RBE as a function of depth over a few millimeters range, for example, to cover in detail the drop-off of dose in the distal portion of the Bragg peak, then cells must be held in a rigid conformation during the exposure. This can be accomplished for example by using cells attached to vessels in monolayer or held in a gelatin matrix. Illustrations of each of these approaches are described below.

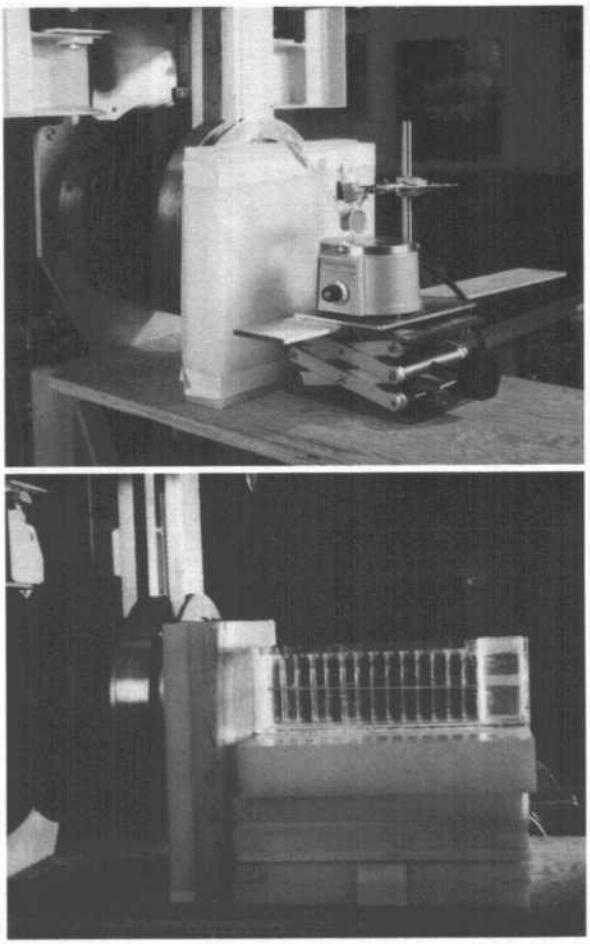

Fig. 1. Vessels for the irradiation of cells in vitro on a horizontal accelerator beam line. Upper panel: glass cylindrical chamber for cells in suspension. Lower panel: an array of tissue culture flasks with cells grown in monolayer

Cell Suspensions

Chapman et al. [22] designed a cylindrical glass chamber which allowed cells to be in a stirred suspension of less than about 2 cm width. This chamber might be placed at various depths within an extended Bragg curve (Fig. 1, upper panel). A glass sampling port allowed the removal of control, unirradiated cells prior to the start of an experiment, and subsequent sampling after a sequence of graded doses. The irradiated cell samples were immediately diluted into a test tube containing warmed medium for rapid serial dilution to the appropriate cell number required for the level of cell killing anticipated. A magnetic stir bar driven by a motor under the chamber assured a uniform cell concentration throughout the experiment. The sampling time was short enough (less than 2 minutes) that the dose fractionation was inconsequential to the survival measurement. This approach has several advantages:

1) the technique is easy and rapid,
2) the uniformity of cell treatment, handling and origin in the suspension technique is well-controlled, allowing for good reproducibility in the survival measurement,
3) there is a significant saving of beam time since the survival measurements are from accumulated doses.

Limitations include:

1) the depth of the radiation field to be studied is defined by the width of the vessel over which the survival effect is averaged,
2) the requirement for the cells to be easily held in single cell suspension without clumping or adverse plating effects,
3) restrictions on the use of the technique for the study of fractionation effects.

Cell Monolayers

The traditional radiation exposure protocol for many cultured cells has been to grow the cells in monolayer attached to tissue culture plastic petri dishes or flasks. For colony forming assays, cells are trypsinized, counted and serially diluted to the appropriate concentration for the anticipated survival. There are several variations on the monolayer protocol that have been devised to accommodate small beam diameters for eye tumor treatments for example, or to map variations in cell killing radially. Figure 1 (lower panel) illustrates a linear array of tissue culture flasks filled with either medium or water. Flasks with medium have cells grown on one of the inner surfaces. Flasks can be exposed in such arrays where each plane of cells is approximately separated by the width of one flask. Alternatively, in a variation first proposed by John Lyman, pairs or arrays of flasks can be exposed with only nominal thicknesses of additional absorber upstream to shift the

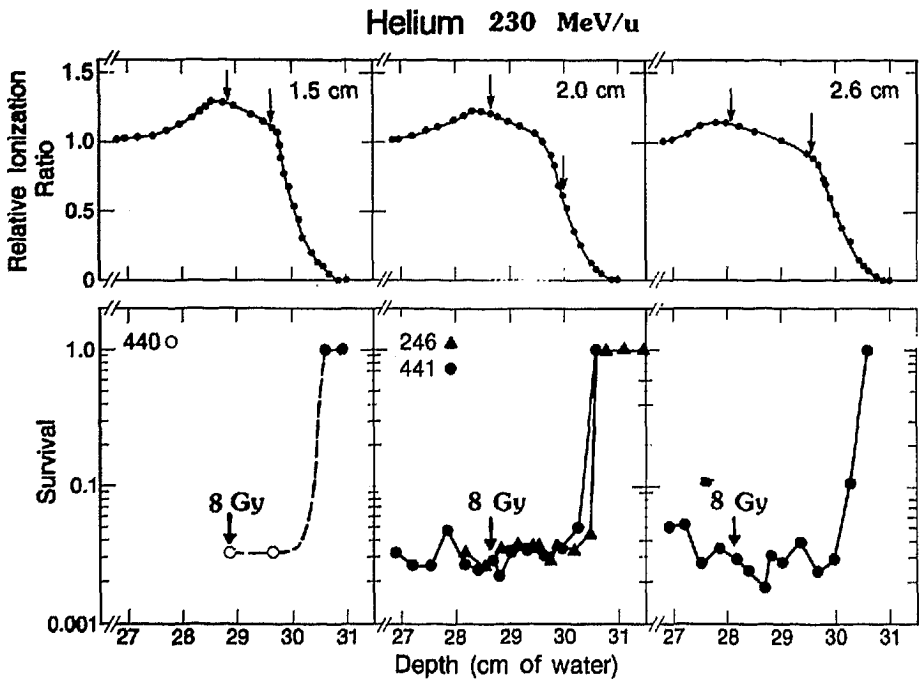

Fig. 2. Illustration of human T-1 fibroblast cell survival data obtained with the techniques described in the text over extended 230 MeV/u helium ion Bragg peaks of 1.5, 2.0 or 2.6 cm width used in the radiotherapy of uveal melanoma

full depth of range covered. This approach allows a measure of biological effects at closer spacings in the millimeter range. Figure 2 illustrates the kind of cell survival effects that were measured with this technique for high energy helium ion beam configured for eye tumor treatments.

If the diameter of the beam is limited to an area within the width of the flasks either due to accelerator constraints, or due to the configurations imposed for a specific treatment geometry under study, cells can be plated only within a small circular region on the flask. Depending on the cell line used, the cells firmly attach to the flask within one or two hours, after which the flask can be filled with additional medium. If the radiation field covers the complete surface area of the flask, the flasks can be exposed to a horizontal beam and then processed for colony formation in the traditional fashion, or allowed to grow in situ to permit an assessment of the radial uniformity of cell killing (Figs. 3 and 4). For a fixed dose, cells surviving within the irradiated field can be scored in radial sectors and plotted as a function of beam diameter to assess flatness of the biologically effective dose.

Cells in Gel

Skarsgard et al. [23] devised a creative gel technique for biological characterization involving single cells suspended in a stiff gel matrix. After

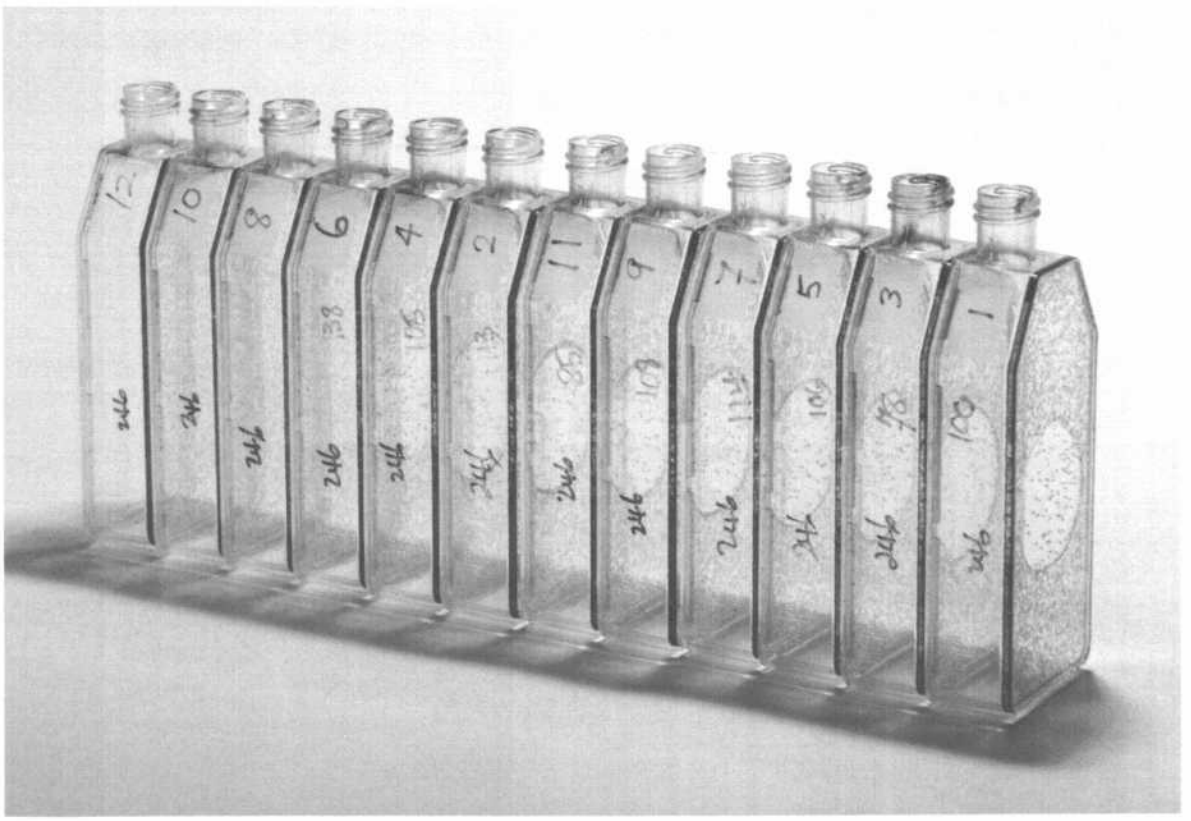

Fig. 3. Twelve 25 cm^2 tissue culture flasks that contained a uniform density of single human T-1 cells in monolayer when irradiated with the collimated 225 MeV/u helium ion beam. The flasks were irradiated in pairs with variable amounts of absorber to cover the depth of the beam range. After irradiation, the medium was replaced and the cultures were allowed to grow to clonal density. A highly collimated control region of cell killing can be seen on the right. Flasks on the left were beyond the range of the beam and show no killing

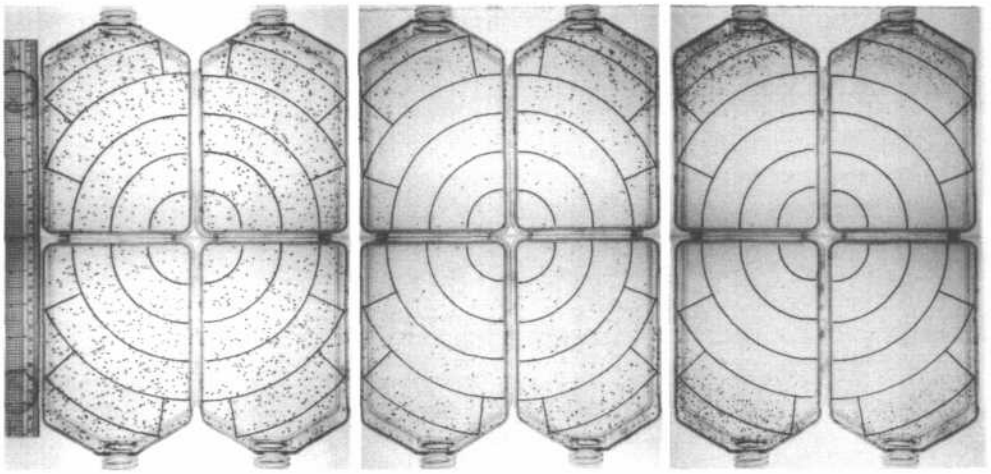

Control 1.5 Gy 3.6 Gy

Fig. 4. Three sets of four 750 cm^2 tissue culture flasks that contained a uniform density of single human T-1 cells in monolayer when irradiated with 580 MeV/u neon ions delivered in a rastered mode. Left panel: unirradiated control set; Middle panel: 1.5 Gy; Right panel: 3.6 Gy.

irradiation, the gel is extruded and sliced (Fig. 5). Each 2 mm slice contains about 10^5 cells which are resuspended by melting the gel in a tube containing warm medium for the biological assay desired. Spatial reconstruction of the biological effect can then be mapped, allowing a detailed and accurate description of the radiobiological properties of the radiations studied which were pion beams. Raju et al. [24] have adopted this approach for the study of a number of different radiation types.

The gel technique has been further refined by Skarsgard et al. [25] with the use of a cell sorter to deliver a known number of cells into the test tubes for the survival assay. Cells are identified on the basis of light scattering in the cell sorter, without the use of a cell stain. This additional step increases the accuracy and precision of this method, which offers the following merits:

1) excellent reproducibility and RBE mapping precision,
2) high resolution for dose range covered, especially at low doses,
3) ease of exposure technique,
4) reduced beam time requirements.

The only limitations involve the moderate degree of preparation and handling required for sample processing.

In vivo Assays

Since single, acute cellular responses in vitro do not provide complete information on tissue responses and their repair, most new radiation modalities have been screened with a few specific in vivo endpoints. The primary goals are to investigate dose fractionation effects after a significant number of fractions as is used in the clinic, and to assess late sequelae. Late responses to irradiation are discussed in detail in the preceding chapter. Therefore, only a few general remarks are made here regarding the selection criteria of in vivo systems.

One of the major limitations of the in vivo techniques is their degree of resolution of measurement of RBE which changes across the depth of the pristine Bragg ionization curve. This fact prevents the study of the sharp, unmoderated Bragg curve, but allows one to map RBE values over defined widths of Bragg curves that have been extended to cover the width of a tumor. The physical dimensions of the animal used in particle studies defines the width of the Bragg ionization curve that can be studied since RBE averaging is implicit over that tissue thickness.

The Withers intestinal crypt assay was an important contributor to our understanding of

Fig. 5. The gel slicing procedure. The gel is extruded and sliced at intervals of 2 mm or more. Each 2 mm slice contains 10^5 cells, which are resuspended by melting the slice in a 5 ml tube of warm medium. Photo courtesy of Lloyd Skarsgard

neutron effects [26, 27]. It is highly amenable to the exploration of dose fractionation effects. This led to its selection in the preclinical feasibility testing of heavy charged particles. The crypt assay can also be recommended as a standard protocol for interlaboratory comparisons, since it has few uncontrolled variables and good replication of the technique can be achieved. There is recent interest in using this assay to standardize some aspects of the proton therapy programs that are increasing in number world-wide (cf. also the subsequent chapter).

Traditionally skin erythema reactions have been the most immediate and visible part of a course of radiotherapy. Skin reactions have been used to investigate the time-dose relationships of radiation effects, as the biological reaction is directly proportional to the total dose delivered, and the time of appearance of the erythema reaction is inversely proportional to the time course of the irradiation. With the acquisition of sufficient information necessary for radiotherapy treatments using conventional radiations and neutrons, and with the advent of animal rights advocates who questioned the necessity of further studies, this work has received much less emphasis in the laboratory. None the less, when the novel high-LET ion beams became available, skin reaction studies were scored in rodent models because it was one of the baseline biological measurements understood and trusted by radiotherapists. Recently, there have been retrospective attempts to score acute skin reactions from patients after charged particle therapy [28]. Although skin reaction studies have large confidence limits, these data clearly indicate an RBE relationship that scales with LET value. Smaller doses per fraction per field of increasingly higher atomic number ion beams yield the same maximum acute skin reaction.

Due to the serious medical complications that can result from nervous tissue toxicities to radiation, spinal cord effects have long been a normal tissue of interest to screen for complications such as paralysis. The charged particle radiotherapy community supported the investigation of this late effect that takes more than one year to develop in rodents at clinically relevant doses to avoid duplicating the serious complications that resulted in early applications of neutron therapy. Unlike other normal tissue endpoints such as skin and intestinal crypts, the spinal cord radiosensitivity has a significantly different X-ray response, and the particle studies suggested a caution in situations in which spinal cord might be exposed to even moderate fractions of high-LET particles.

Summary of Pertinent Issues

Frustration with the variables introduced in the photon Gray-equivalent concept have led several clinical programs investigating new high-LET radiation modalities to report only physical dose. However, Gray-equivalent dose must still be considered in treatment planning to avoid normal tissue toxicities. This issue will become even more

important as alternative ion beam delivery systems are implemented to optimize tumor treatments.

In the opinion of the author, the choice of model systems should not be based on trying to be all inclusive in determining RBE. Instead, the selection should be based on having a representative radiosensitive and a radioresistant responding system. This provides the clinician with an appreciation of the range of responsiveness that may be anticipated. Depending on the treatment site, particular normal tissue toxicities should be investigated for individual organs. It would be exceedingly helpful to the international effort to compare clinical protocols and results if radiobiologists could agree with the clinicians about which representative measurements should be made. Many primary cell lines are very radiosensitive with very small shoulders on the survival curve, even after exposure to low-LET radiations. This means that there will be very little variation in RBE in primary cells, in comparison to cell lines with large shoulders on the survival (as is the case for many tumor and established cell lines) where the high-LET response collapses the shoulder.

None of the radiobiology of ion beams is worth doing unless adequate controls and sample numbers allow a statistical assessment of the significance of the results. The error analysis of a relative measurement between two independent modalities (one low-LET study and one high-LET study) is at best a challenge. The typical photon daily dose fraction is 2 Gy, and equivalent high-LET dose fractions are usually smaller. Biological endpoints must, therefore, be able to examine the biological response selected with sufficient accuracy to distinguish what may be similar responses as biological endpoints come together at low doses. Some may argue that measurement of high dose responses are adequate, since theoretical modeling would allow extrapolation to the low dose region. However, this statement assumes certainty in selection of an appropriate theoretical model to use for the extrapolation. The "stretch" to low dose response is well known to be variable with supralinear, linear and quadratic fits all represented among the various low-LET radiation responses measured. Very few low dose responses are available for high-LET radiations.

The strictest definition of RBE requires one to compare the high-LET biological response to ^{60}Co. Since cobalt sources are no longer available as commonly as was true when the RBE definition was made, the high voltage X-ray machine has gained acceptance in the field as a substitution low-LET reference. When comparing results obtained by different investigators, it is critical to correct for differences due to the choice of the low-LET reference radiation. Obviously in the need to establish a common standard, a low-LET reference that is available to the largest number of groups is desirable. The author would argue that it may even be important to propose a low-LET particle as a reference.

Once there is a solid basis for defining equivalent doses, a decision must be made regarding how the measurement should be included into the treatment planning effort. Three-dimensional analysis of isodose contours accomplished by examining all pertinent two-dimensional axial tomographs for each treatment port begin with the physical dose, but must include a consideration of criticial tissues that each may have unique values in each field. The 1987 NCI report on evaluation of treatment planning for particle beam radiotherapy [29] concluded that there was no satisfactory way of handling the potential variation of biological effectiveness in a particle beam, and they were not able to come to any conclusion about the additional need to compensate for internal inhomogeneities or for the shape of the target or the external patient surface, not the least due to the lack of sufficient particle data on individual normal tissue toxicities. These data are still required for the fullest optimization of ion beam radiotherapy, no matter what mode of beam delivery is chosen.

The main conclusion of this paper is that there is a strong need in the field of ion beam therapy to standardize the biological beam characterization and to complete parallel, coordinated physics calibration and dosimetry under the exact geometry of the biological measurements. Several candidate approaches are reviewed and recommendations are made to steer the selection of the standards. Such effort will advance the international attempt to optimize ion beam radiotherapy.

Acknowledgement

The author acknowledges the support of the Office of Health and Environmental Research, Office of Energy Research, U.S. Department of Energy under contract No. DEAC03–76SF00098.

References

1 *Second L.H. Gray Workshop on Hamilton Hall*, University of St. Andrews, Scotland, 9–12 September 1991. Int. J. Radiat. Biol. 61, 293–297, 1992.
2 Zirkle, R.E. Biological effectiveness of alpha particles as a function of ion concentration produced in their paths. Am. J. Cancer 23, 558–567, 1935.
3 Barendsen, G.W., Beusker, T.L.J., Vergroesen, A.J., and Budke, L. Effects of different ionizing radiations on human cells in tissue culture. II. Biological experiments. Radiat. Res. 13, 841–849, 1960.
4 Bewley, D.K. A comparison of the response of mammalian cells to fast neutrons and charged particle beams. Radiat. Res. 34, 446–458, 1968.
5 Blakely, E.A. Cell inactivation by heavy charged particles. Radiat. Environ. Biophys. 31, 181–196, 1992.
6 Belli, M., Cera, F., Cherubini, R., Haque, A.M.I., Ianzini, F., Moschini, G., Sapora, O. Simone, G., Tabocchini, M.A., and Tiveron, P. Inactivation and mutation induction in V79 cells by low energy protons: Re-evaluation of the results at the LNL facility. Int. J. Radiat. Biol. 63, 331–337, 1993.
7 Goodhead, D.T., Belli, M., Mill, A.J., Bance, D.A., Allen, L.A., Hall, S.C., Ianzani, F., Simone, G., Stevens, D.L., Stretch, A. Tabocchini, M.A., and Wikerson, R.E. Direct comparison between protons and alpha particles of the same LET. Part I: Irradiation methods and inactivation of asynchronous V79, HeLa, and C3H 10T-1/2 Cells. Int. J. Radiat. Biol. 61, 611–624, 1992.
8 Folkard, M., Prise, K.M., Vojnovic, B., Davies, S., Poper, M.J., and Michael, B.D. The irradiation of V79 mammalian cells by protons with energies below 2 MeV. Part I: Experimental arrangement and measurement of cell survival. Int. J. Radiat. Biol. 56, 221–237, 1989.
9 Inada, T., Hayakawa, Y., Tada, J., Kubota, N., Hiraoka, T., and Sato, S. Characteristics of neutron beam generated by 500 MeV proton beam. Int. J. Radiat. Oncol. Biol. Phys. 25, 499–504, 1993.
10 Stone, R.S. and Larkin, J.C. The treatment of cancer with fast neutrons. Radiology 39, 608–620, 1942.
11 Stone, R.S. Neutron therapy and specific ionization. Am. J. Roentgenol. 59, 771–785, 1948.
12 Sheline, G.E., Phillips, T.L., Field, S.B., Brennan, J.T., and Raventos, A. Effects of fast neutrons on human skin. Am. J. Roentgenol. 111, 31–41, 1971.
13 Skarsgard, L.D. (ed.) Pion and Heavy Ion Radiotherapy: Preclinical and Clinical Studies, Elsevier Biomedical, New York, 1983.
14 Raju, M.R. Heavy Particle Radiotherapy. Academic Press, New York, 1980.
15 Llacer, J., Tobias, C.A., Holley, W.R., and Kanai, T. On-line characterization of heavy-ion beams with semiconductor detectors. Med. Phys. 11, 266–278, 1984.
16 Llacer, J., Schmidt, J.B., and Tobias, C.A. Characterization of fragmented heavy-ion beams using a three-stage telescope detector: Measurements of 670-MeV/amu ^{20}Ne beams. Med. Phys. 17, 151–157, 1990.
17 Llacer, J., Schmidt, J.B., and Tobias, C.A. Characterization of fragmented heavy-ion beams using a three stage telescope detector: Detector configuration and instrumentation. Med. Phys. 17, 158–162, 1990.
18 Blakely, E.A., Ngo, F.Q.H., Curtis, S.B., and Tobias, C.A. Heavy-ion radiobiology: Cellular studies. Adv. Radiat. Biol. 11,195–389, 1984.
19 Hall, E.J., Roizin-Towle, L., and Attix, F.H. Radiobiological studies with cyclotron-produced neutrons currently used for radiotherapy. Int. J. Radiat. Oncol. Biol. Phys. 1, 33–40, 1975.
20 Hall, E.J. and Kraljevic, U. Repair of potentially lethal damage: Comparison of neutron and X-ray RBE and implications for radiation therapy. Radiology 121, 731–735, 1976.
21 Cohen, L., Dose-time relationship: Computation of cell lethality following fractionated radiation therapy. Int. J. Radiat. Oncol. Biol. Phys. 4, 267–271, 1978.
22 Chapman, J.D., Blakely, E.A., Smith, K.C., and Urtasun, R.C. Radiobiological characterization of the inactivating events produced in mammalian cells by helium and heavy ions. Int. J. Radiat. Oncol. Biol. Phys. 3, 97–102, 1977.
23 Skarsgard, L.D., Palcic, B., and Lam, G.K.Y. RBE mapping in pion beams using the gel technique, in Pion and Heavy Ion Radiotherapy: Preclinical and Clinical Studies, Skarsgard, L.D. (ed.), Elsevier Biomedical, New York, 1983.
24 Raju, M.R., Bain E., Carpenter, S.G., Cox, R.A., and Robertson, J.B. A heavy particle comparative study. Part II: Cell survival versus depth. Br. J. Radiol. 51, 704–711, 1978.
25 Skarsgard, L.D., Wouters, B.G., Lam, G.K.Y., Oelfke, U., and Goodman, G.B. General considerations in the biological dosimetry of heavy charged particle beams and use of the gelatin/cell sorter in vitro system at TRIUMF. To be published in Proc. of the NIRS Int. Seminar on the Application of Heavy Ion Accelerators to Radiation Therapy of Cancer, 14–16 November 1994, Chiba, Japan.
26 Withers, H.R., Chu, A.M., Mason, K.A., Reid, B.O., Barkley, J.T., and Smathers, J.B. Response of jejunal mucosa to fractionated doses of neutrons or X-rays. Eur. J. Cancer 10, 249–252, 1974.
27 Withers, H.R., Mason, K., Reid, B.O., Dubravsky, N., Barkley, J.T., Brown, B.W., and Smathers, J.B. Response of mouse intestine to neutrons and gamma

rays in relation to dose fractionation and division cycle. Cancer 34, 39–47, 1974.

28 Blakely, E.A. and Castro, J.R. Assessment of acute and late effects to high-LET radiation. To be published in Proc. of the NIRS Int. Seminar on the Application of Heavy Ion Accelerators to Radiation Therapy of Cancer, 14–16 November 1994, Chiba, Japan.

29 Goitein, M. Urie, Munzenrider, J. E., Gentry, R. Lyman, J.T., Chen, G. T. Y., Castro, J.R., Maor, M.H., Stafford, P. M., Sontag, M. R., Altschuler, M.D., Bloch, P., Chu, J. C. H., and Richter, M. P. Evaluation of Treatment Planning for Particle Beam Radiotherapy. The Radiotherapy Development Branch, Radiation Research Program, Division of Cancer Treatment, National Cancer Institute, 1987.

9 Preclinical Radiobiological Experiments

J. GUEULETTE and A. WAMBERSIE

Université Catholique de Louvain, Cliniques Universitaires St-Luc, Brussels, Belgium

Introduction

Before applying a new type of radiation in cancer therapy, two types of radiobiological experiments are required: first, the so-called "pretherapeutic" studies which are usually performed before a new facility is planned and which aim at identifying the rationale of the new radiation. Secondly, when the new facility is completed and the beam ready for application, the actual "preclinical" experiments need to be performed. They aim at the application of the new radiation under safe and optimal conditions.

For proton beams, the therapeutic benefit is first of all based on an improved physical selectivity. Pretherapeutic studies have shown that no significant benefit is to be expected from an improved biological effectiveness [1]. Only preclinical studies are thus needed today. They provide an overall check of the dosimetry and irradiation procedure, and, in addition, help to select the "clinical" RBE for which the accuracy should be better than 5 % [2].

For heavy ion beams, the therapeutic benefit is based on both an improved physical selectivity and an improved differential effect. Pretherapeutic studies are, therefore, needed in order to identify the biological rationale and to evaluate the potential benefit of the improved differential effect. Thereafter, preclinical experiments have to be undertaken. They are more important than for protons, since RBE values are high and do vary largely with dose and the biological endpoint chosen [2–10]. Moreover, for a given type of particle and energy the radiation "quality" and, hence, the RBE changes with depth. As a consequence, the selection of the clinical RBE of heavy ion beams becomes the main goal of the preclinical studies. They raise complex problems related to the choice of the biological system to be used for RBE specification and the method to be followed for the dose and volume specification.

Since RBE determinations are the common denominator of most radiobiological studies, a first section will be devoted to the concept of RBE. It appears necessary to define its different acceptations and to clarify some ambiguities about its use. The next sections will be devoted to the description of the different biological systems and their relative merit for preclinical studies.

The RBE Concept

Historical Review

In radiation therapy with low-LET radiations, the biological effect can be predicted from the dose level and the dose distribution. The specification of the type of radiation (gamma-rays, X-rays or electrons) and of the energy is of little importance since there is little RBE variation between gamma-rays, X-rays and electron beams from a few MeV to a few tens of MeV, at least for the effects relevant in radiation therapy. Therefore, dosimetry alone and dosimetric intercomparison are needed.

In the 50's and 60's, however, when 200 kV X-rays (orthovoltage) were progressively replaced by ^{60}Co γ-rays (and electrons), a dose weighting factor of 0.85 was introduced to take into account the fact that, at equal doses, the 200 kV X-rays

are somewhat more effective than high-energy radiations. As a result, the RBE concept was recommended by the ICRP and the ICRU [3, 4].

Later on, it became more and more obvious that the RBE value could be different for different systems. The RBE of 200 kV X-rays relative to ^{60}Co γ-rays was not always 0.85 but could reach values of 2 and more for some biological endpoints or very low doses, relevant in radiation protection [5]. However, it could be assumed that the conversion factor of 0.85 was sufficient to take into account the radiation quality differences between 200 kV X-rays and high-energy X- or γ-rays for the dose ranges and the effects relevant in radiation therapy [6].

The RBE problem became much more important in fast neutron therapy. RBE values of neutrons relative to γ-rays ranging from about 1.5 to 5 were observed, depending on the neutron energy, dose and biological effect. The problem is less relevant for protons (RBEs 1.0–1.2), but again significant for heavy ions for which the RBE values can go up to 10.

Definition of RBE

The relative biological effectiveness (RBE) of a test radiation, relative to a reference radiation is given by

$$RBE_{test/ref} = D_{ref} / D_{test}$$

where D_{test} and D_{ref} are the absorbed doses of the test and reference radiation, respectively, necessary to cause the same biological effect.

When comparing two radiation qualities, there is not a single RBE but a large number of RBE values, i.e., one RBE value for every set of biological system, effect and experimental conditions. Therefore, the commonly used jargon that a certain radiation has a certain RBE is fundamentally incorrect and misleading. RBE values cited in this way are ususally not the result of individual experiments but are judgements based on experimental RBEs or sometimes clinical experience. Although this practice is wide-spread and reflects some convenience of procedure for a complex issue, it cannot be stressed enough that such comparative values for different types of radiations should not be confused with true "experimental" RBE values.

Reference RBE

Due to the wide variation of the RBE with the biological system, the dose and experimental conditions, it is useful when exchanging information or prescribing the dose in non-conventional radiation beams to select reference conditons for RBE specification. These reference conditions should be as relevant as possible to the clinical situation and in that respect the following conditions appear to be most suitable:

- a dose level of 2 Gy (X- or γ-ray-equivalent) per fraction,
- a biological system and endpoint which can be considered relevant to represent the "average" or "overall" late tolerance of normal tissues.

The RBE for these reference conditions is the "reference" RBE. Reference RBE values are derived from experiments performed for late tolerance of, e.g., CNS (brain and spinal cord) [7], lung [8] or skin [9]. The reference RBE is still a radiobiological concept, although it implies that a single RBE value can represent the average or overall tolerance of a patient's normal tissue.

Clinical RBE

In contrast to the reference RBE, which is a radiobiological concept, the clinical RBE is a clinical and operational concept. The term "clinical RBE" has been particularly used in the US for neutron treatments, and is understood as the ratio of the absorbed dose which would be prescribed for a photon treatment and the dose which is actually prescribed for neutrons and for a given tumor localization [10]. The clinical RBE can also be used for all non-conventional radiation therapy modalities.

Although the clinical RBE is a dose ratio for two radiation qualities, it is not in a strict sense a RBE. It takes into account the reference RBE plus the several weighting factors (e.g., geometrical factors related to the beam penetration)

which the radiation oncologist has to consider when prescribing a dose. As in the case of selecting the target volume and the fractionation scheme, it implies the judgement and responsibility of the radiation oncologist.

Preclinical Radiobiological Studies

The radiobiological experiments discussed here concern primarily RBE determinations which should be performed prior to the clinical irradiations. This section does not deal with experiments designed to justify the rationale of using a new beam and to evaluate its potential advantage.

Cell Survival in vitro

Mammalian cells grown in monolayer have widely been used for RBE measurements, since 1956 [11]. The improvement of cell biology techniques makes it possible today to cultivate many mammalian cell lines in vitro. Particularly useful are cell lines with a high plating efficiency (60%–80%) such as V79, EMT6, or CHO, which are also relatively easy to maintain under standardized conditions. These cell lines also have a radiosensitivity and repair capacity corresponding to the average normal or tumor cells.

RBE values are generally determined after the survival data have been fitted to curves of the linear-quadratic or two-component model [12]. This allows to derive RBE values over the whole dose range. However, the derived values depend on the model, especially in the region of small doses where the different models exhibit the largest discrepancy and where the accuracy of the survival data is particularly poor. Therefore, the reliability of RBE values for small doses may be questionable as is the reliability of RBE values derived from α-ratios, which are supposed to correspond to the maximum RBE. This is especially true when comparing survival curves of high-LET and low-LET radiations which have radically different shapes (Fig. 1).

The shape of the cell survival curves reflects the repair capacity which in turn determines the influence of fractionation. The analysis of survival curves should thus help to choose the proper dose per fraction when determining the reference RBE.

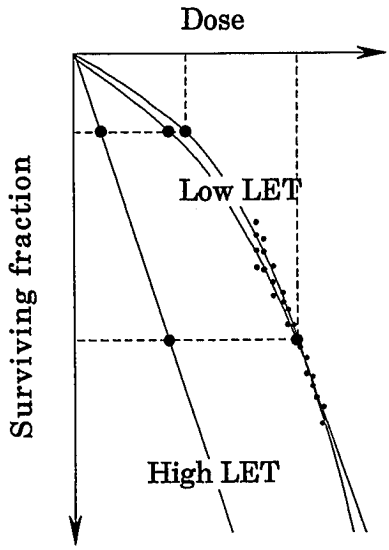

Fig. 1. Typical survival curves for high- and low-LET radiations. When the experimental points are centered on high doses it is difficult to discriminate between the different biological models. As a consequence, the RBE for small doses can vary according to the model

Growth Inhibition of Plant Roots

Growth inhibition in Vicia faba bean roots is a well documented system [13] which has been used successfully for RBE and OER determinations.

The end point (G_{10}) is the relative growth of the central root over a period of 10 days following irradiation, the mean growth of unirradiated roots being taken as reference. The sensitive part of the bean to be irradiated is the root tip. Dose delivered to other parts of the plant is of little importance for the growth of the root.
"Sutton Exhibition Long Pod" is the classical strain of Vicia faba used in radiobiology. However, it has been reported that this strain could raise technical difficulties for OER experiments involving oxygen deprivation during long periods. "Belgische Boerenbond Extra Lange Hangers" has been introduced as alternative and has proven to be more resistant to hypoxia [14].

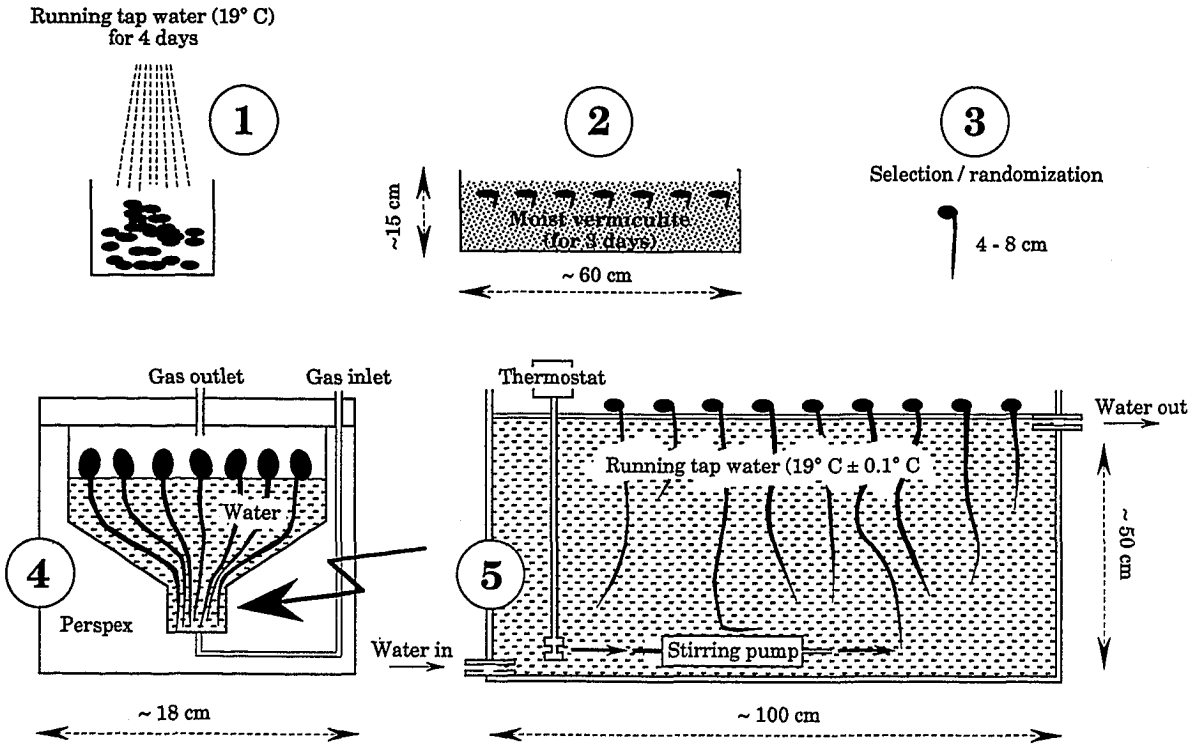

Fig. 2. Schematic illustration of cultivation and irradiation conditions of Vicia faba beans: 1) only roots of which the tip points out will be planted in vermiculite, 2) vermiculite boxes are stored in a dark place at 20 °C, 3) the roots of which the tip is twisted are discarded, 4) for irradiation in hypoxic condition, air is replaced by high-purity nitrogen (at least 30 min before irradiation), 5) after irradiation the beans are allowed to grow for 10 days in a stainless steel tank

The cultivation and irradiation technique is schematically illustrated in Figure 2. RBE or OER values are determined from the doses corresponding to 50% growth inhibition and are obtained with confidence levels of 3–5% ($p = 0.05$) as is shown in Figure 3.

Chromosome Aberrations in Vegetals

Determination of radio-induced chromosome aberrations in vegetal roots is another system which can be used for RBE determination.

While Vicia faba is most popular [15], in our laboratory we have used Allium cepa onion roots (variety "jaune paille des vertus") for many years following Markus and Kolliopoulou [16]. Allium cepa has relatively few (2N = 16), large chromosomes (≈7 μm) and exhibits frequent and regular mitoses. Past experience with this system has revealed that the best criteria for RBE studies are the number of aberrations per cell in anaphase or telophase and the number of intact cells without aberrations (Fig. 4).

In an unsynchronized cell population the relation between primary chromosome damage and the frequency of observable aberrations is complex. It is, therefore, important to make sure that the number of aberrations per cell, as well as the number of intact cells, does not depend on the incubation time between irradiation and fixation (3–9 hours). With such precautions, the system provides RBE values with an accuracy of 3–5%.

Intestinal Crypt Cell Regeneration

The regeneration of intestinal crypt cells of mice, was introduced by Withers and Elkind [17]. It was developed to quantitate the cell survival curve of

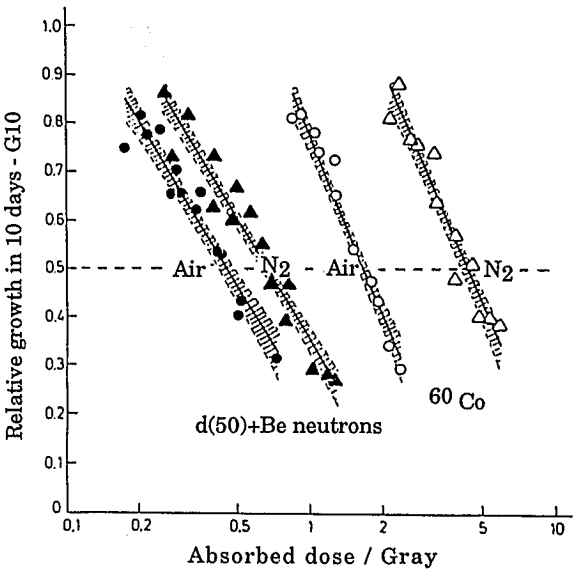

Fig. 3. Relative growth of Vicia faba root tips in 10 days as a function of dose (logarithmic scale) after irradiation under aerobic and hypoxic conditions with d(50)+Be neutrons and ^{60}Co γ-rays (the shaded areas correspond to the 95 % confidence interval). The slopes obtained under aerobic and hypoxic conditions do not show significant difference for either radiation quality (OER does not depend significantly on dose). On the other hand, the slopes of the dose-effect relations for neutrons and gamma are different, which implies an increasing RBE with decreasing dose

intestinal stem cells. In the meantime, it has been widely used to study the influence of fractionation, dose rate, effect of radiosensitizers and also to determine RBE under different conditions.

The intestinal mucosa may be described as a two-compartment tissue. The first compartment located in the lower part of the crypts contains the stem cells, which are able to proliferate. The second compartment contains differentiated cells and functional cells which are no longer able to divide and are lining the "villi" (Fig. 5). Only the stem cells (crypt cells) are radiosensitive and a single surviving stem cell can regenerate a crypt. Therefore, the number of regenerated crypts and the number of surviving stem cells can be assumed to be equal when less than 20 regenerated crypts are counted per circumference; this corresponds to a dose range of 12–20 Gy (X or γ). The conditions described hereafter are those which have been applied in our laboratory since many years.

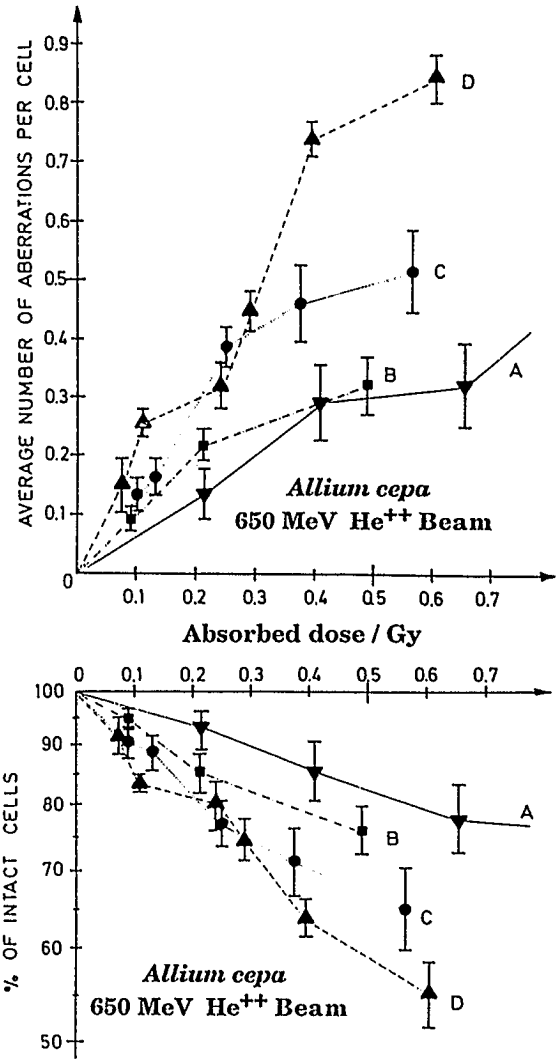

Fig. 4. Average number of chromosome aberrations per cell as a function of dose (top), and percentage of intact cells as a function of dose (bottom). The figures are derived from the same experiment and were performed in a He^{2+} beam of which the kinetic energy was modulated by a copper ridge filter between 650 and 530 MeV. The Allium cepa onion roots were positioned in the initial plateau (A) or in the beginning (B), middle (C) and end (D) of the SOBP, respectively. The indicated confidence intervals correspond to one standard deviation; the lines drawn through the experimental points serve as eye-guides, only. The data are corrected for the background (0.02 aberrations per cell or 98 % intact cells in unirradiated controls)

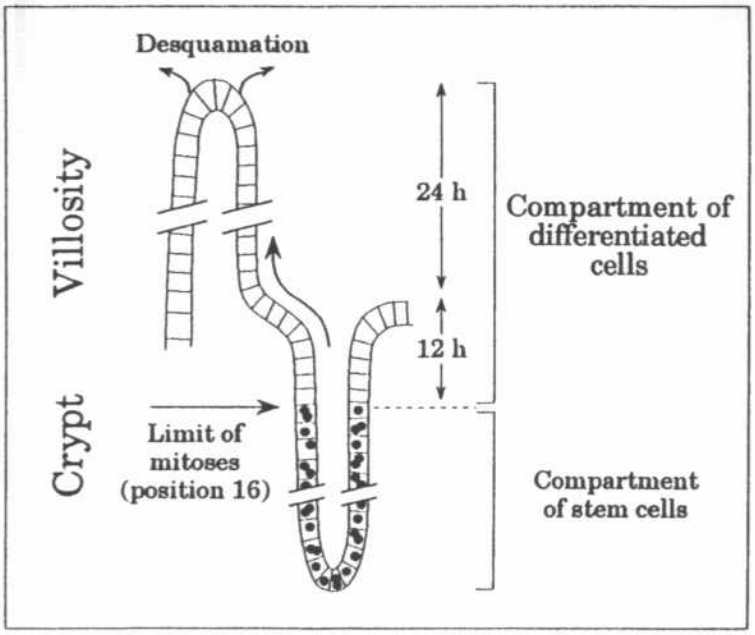

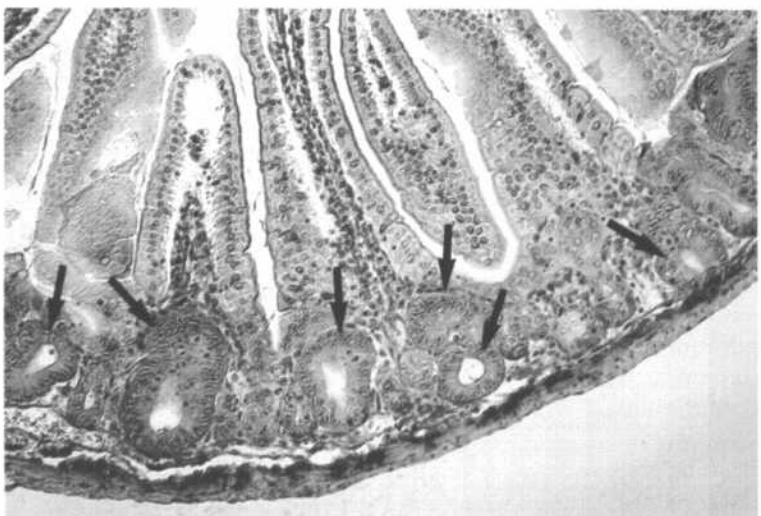

Fig. 5. Schematic view of a histological section of the intestinal mucosa, which would go both through the axis of a crypt and the axis of a villosity (top). Part of the 32 crypt cells "piled up" along the longitudinal axis are shown. The upper limit of divisions (position 16) practically demarcates the compartments of stem cells and differentiated cells. The direction and the time of the migration of differentiated cells is indicated. Transversal section of the intestinal mucosa, 3 days after irradiation with 12.6 Gy (bottom). The length of the villosities is reduced and the crypts have practically disappeared. Only few piles of apparently viable and nucleated cells are visible (regenerated crypts). They result from the multiplication of one cell which kept its proliferating capacity

Female NMRI, Balb/c or black C57 mice, typically 11–13 weeks old, are used, because of their comparable radiosensitivity. Eighty-four hours after irradiation the animals are sacrificed and a 3 cm jejunal section is taken 1 cm from the pylore. The samples are immediately fixed. They are then embedded in paraffin, sliced and stained according to the classical trichrome technique [18].

The basic experiment compares the dose-effect relationships obtained after single-fraction irradiation. As can be seen from Figure 6, the number of regenerated crypts (scoring only crypts exhibiting $\approx$ 10 surviving cells) decreases exponentially with the dose.

With 6–8 mice per dose level and 8–10 dose levels, the RBE can be determined with an accuracy of ± 3–5%.

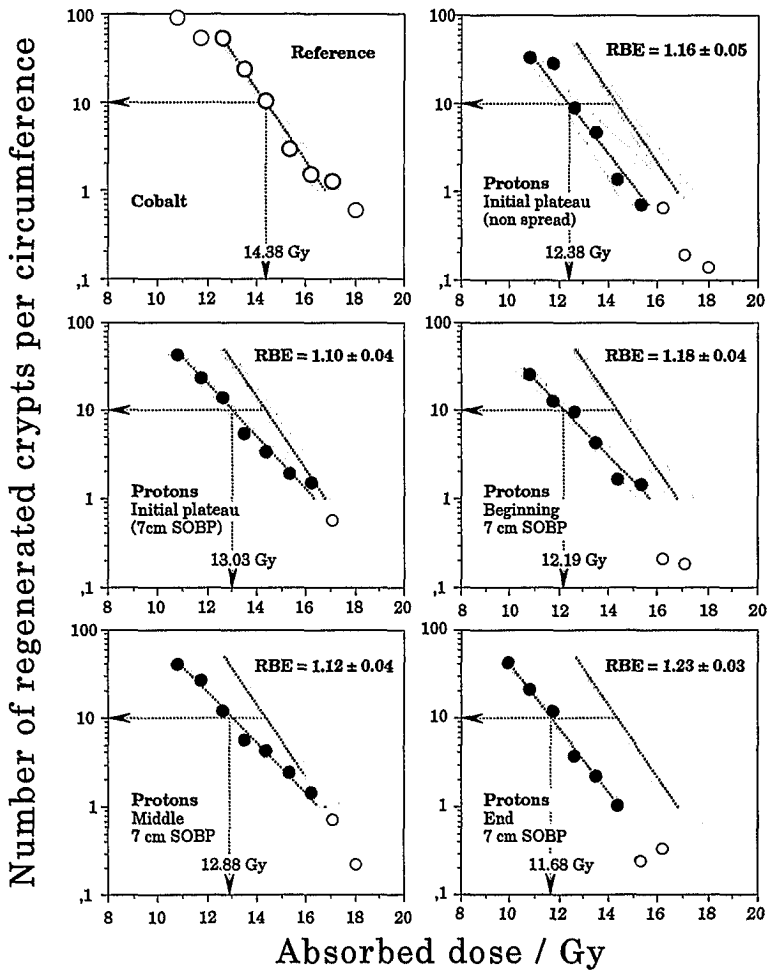

Fig. 6. Dose-effect relationships for crypt cell regeneration in mice after irradiation with ^{60}Co γ-rays and 200 MeV protons at different depths (indicated in the figure). In order to facilitate the comparison, the dose-effect relationship for ^{60}Co is redrawn on each panel. The shaded areas correspond to the confidence interval of the slope of the (exponential) curves. These experiments were performed at the National Accelerator Center (NAC) of Faure (South Africa) as part of an intercomparison program with the 75 MeV proton beam of Louvain-la-Neuve (Belgium). They were designed to "calibrate" the beam (over-all check on the dosimetry and irradiation procedures), and were associated with a dosimetry intercomparison

Mouse Lung Radiotolerance

Lung radiotolerance in mice, assessed by $LD_{50/180}$ (dose corresponding to 50% animal survival 180 days after irradiation), has been taken as a model for the evaluation of the late tolerance of normal tissues [8].

The technical issues concerning the irradiation procedure are analogous to those of intestine. The only difference is that the mice are submitted to a selective irradiation of the thorax, which implies that the beam is collimated and that the dose homogeneity inside the field is carefully controlled.

Since the animals survive the irradiation and are followed-up for 4–6 months, randomization of the animals to equalize "cage effects" and hygiene of their housing are important concerns.

Probit analysis is generally used to fit the dose-survival curves from which LD_{50} and RBE values are derived (Fig. 7). Five to seven doses (12–16 animals per step) each increasing by about 10% compared to the previous step are usually sufficient to obtain well balanced data. The useful (total) doses range from 6 to 16 Gy (X or γ) for irradiation in a single fraction and from 12 to 20 Gy (X or γ) for irradiations in 10 fractions separated by a time interval of 12 hours.

inside the target volume, i.e., in the spread-out Bragg peak region varies according to the size of the volume. The reference RBE for a specific ion at a given energy is thus not a single value typical of a certain type of normal tissue but varies with the size of the tumor.

Radiobiological Intercomparisons

Radiobiological intercomparisons are the obliged counterpart to physical dosimetry intercomparisons to determine the biological equivalence of different radiation beams. They are a prerequisite when comparing clinical results from different facilities and pooling experience. Radiobiological intercomparisons became compulsory in neutron therapy since the RBE values of the different clinical beams vary widely, depending on the nuclear production reaction and the energy of the incident particle. Moreover, type and composition of the collimator, the thickness of the target, the filtration of the beam, etc. can influence the RBE as well; sometimes, more than 5%, which is beyond the dose variability tolerable in radiotherapy.

What is true for neutrons is in principle true for heavy ions and, to a lesser extent, also for protons, since the energy of ions changes with depth, and the production and the delivery of the beams are related to numerous parameters including type of machine (synchrotron, linac), repetition rate, beam shaping (scattering, scanning, wobbling, spot scanning), etc. Even if eventual changes in the radiation quality can be traced by different types of physical measurements, including microdosimetry [24], track structure analysis [25], and TLD measurements [26] and if calculations would permit to predict the corresponding RBEs, the actual RBE values would still have to be measured.

When the beam quality differs only by a small amount, RBE differences related to the biological system are negligible. Therefore, the choice of a biological system for intercomparisons can mainly be determined by its convenience, portability and reproducibility [27].

Crypt cell regeneration in mice appears to meet these requirements and has widely been used by different authors for intercomparison of neutron [28] and proton beams. This system is more advantageous than other "simple" in vivo systems, e.g., mouse testis, mouse skin [29, 30] or in vivo cellular systems, in so far as it is particularly independent of environmental conditions, easy to handle and capable of a good precision due to its steep dose-effect relationship.

Radiobiological intercomparisons should be associated with dosimetric intercomparisons and performed according to a strict experimental protocol in conjunction with the radiobiologists and dosimetrists from the respective facilities.

References

1 Robertson, J.B., Williams, J. R., Schmidt, R.A., Little, J.B., Flynn, D.F., and Suit, H.D. Radiobiological studies of high-energy modulated proton beam utilizing cultured mammalian cells. Cancer 35, 1664–1677, 1975.

2 Mijnheer, B.J., Battermann, J.J., and Wambersie, A. What degree of accuracy is required and can be achieved in photon and neutron therapy? Radiother. Oncol. 8, 237–252, 1987.

3 International Commission on Radiation Protection (ICRP). Report of the RBE Subcommittee to the International Commission on Radiation Protection and the International Commisssion on Radiation Units and Measurements. Health Physics 9, 357–386, 1963.

4 International Commission on Radiation Units and Measurements (ICRU). Quantitative concepts and dosimetry in radiobiology. ICRU Report 30, ICRU Publications, Bethesda, USA, 1979.

5 International Commission on Radiation Units and Measurements (ICRU). The quality factor in radioprotection. ICRU Report 40, ICRU Publications, Bethesda, USA, 1986.

6 International Commission on Radiation Units and Measurements (ICRU). Dose specification for reporting external beam therapy with photons and electrons. ICRU Report 29, ICRU Publications, Bethesda, USA, 1978.

7 Van der Kogel, A.J. Late Effects of Radiation on the Spinal Cord: Dose-Effect Relationships and Pathogenesis. Thesis (University of Amsterdam). Publication of the Radiobiological Institute TNO, Rijswijk, The Netherlands, 1979.

8 Grégoire, V., Beauduin, M., Gueulette, J., De Coster, B.M., Octave-Prignot, M., Vynckier, S., and Wambersie, A. Radiobiological intercomparison of p(45)+Be and p(65)+Be neutron beams for lung tolerance in mice after single and fractionated irradiation. Rad. Res. 133, 27–32, 1993.

9 Joiner, M.C., Maughan, R.L., Fowler, J.F., and Denekamp, J. The RBE for mouse skin irradiated with 3-MeV neutrons: Single and fractionated doses. Radiat. Res. 95, 130–141, 1983.

10 Wambersie, A. and Battermann, J.J. Practical problems related to RBE in neutrontherapy, in Progress in Radio-Oncology III, Kärcher, K.H. Kogelnik, H.D., and Szepesi, T (eds.), ICRO (International Club for Radio-Oncology), Vienna, Austria 1987, pp. 155–162.
11 Puck, T.T. and Markus P.I. Action of X-rays on mammalian cells. J. Exptl. Med. 103, 653–666, 1956.
12 Tubiana, M., Dutreix, J., and Wambersie, A. Introduction to Radiobiology, Taylor & Francis, London, 1990.
13 Hall, E.J. The relative biological efficiency of X-rays generated at 220 kVp and gamma radiation from a cobalt-60 therapy unit. Brit. J. Radiol. 34, 313–317, 1961.
14 Van Dam, J., Billiet, G., Bonte, J., Octave-Prignot, M., and Wambersie, A. Influence of dose rate on fast neutron OER and biological effectiveness determined for growth inhibition in Vicia faba. Strahlenther. 159, 576–583, 1983.
15 Hall, E.J. and Cavanagh, J. The oxygen effect for acute and protracted radiation exposures measured with seedlings of Vicia faba. Br. J. Radiol. 40, 128–133, 1967.
16 Markus, B. and Kolliopoulou, H. Ein qualitativer biologischer Wirkungsunterschied nach Bestrahlung von Teilungsgewebe mit schnellen Elektronen verschiedenen Energiespektrums. Biophysik 2, 263–270, 1965.
17 Withers, H.R. and Elkind, M.M. Microcolony survival assay for cells of mouse intestinal mucosa exposed to radiation. Int. J. Radiat. Biol. 17, 261–267, 1970.
18 Beauduin, M. Fast Neutron Beams in Radiotherapy: Influence of Energy and Clinical Implications. Thesis, Université Catholique de Louvain, Brussels, 1993.
19 Gueulette, J., Grégoire, V., and Wambersie A. Courbes de survie cellulaires; facteurs d'influence, modèles et concepts. J. Chim. Phys. 91, 109–1106, 1994.
20 Van Dam, J.M. Radiobiological Characteristics of High-LET Radiations. Thesis (Katholieke Universiteit Leuven), Leuven, 1984.
21 Barendsen, G.W. RBE-LET relations for induction of reproductive death and chromosome aberrations in mammalian cells, in Proc. 6th Symposium on Microdosimetry, Brussels, Booz, J. and Ebert, H.G. (eds.), CEC Publ. London, EUR-6064 d-e-f, 1978, pp. 55–68.
22 Gueulette, J. Efficacité biologique relative (EBR) des neutrons rapides pour la tolérance de la muqueuse intestinale chez la souris. Thesis, N° d'ordre 362 (Université Paul Sabatier de Toulouse), Toulouse, 1982.
23 Field, S.B., Hornsey, S., and Kutsutani, Y. Effects of fractionated irradiation on mouse lung and a phenomenon of slow repair. Br. J. Radiol. 49, 700–707, 1986.
24 Menzel, H.G. and Pihet, P. Microdosimetric specification of radiation quality in neutron radiation therapy. Int. J. Radiat. Biol. 57, 865–883, 1990.
25 Kraft, G. Krämer, M., and Scholz, M. LET, track structure and models. A review. Radiat. Environ. Biophys. 31, 161–180, 1992.
26 Loncol T. Personal communication, 1994.
27 Hall, E.J. and Kellerer, A. Review of RBE data for cells in culture, in High-LET Radiations in Clinical Radiotherapy. Barendsen, G.W., Broerse, J., and Breur, K. (eds.), Pergamon Press, Oxford, 1979, pp. 171–174.
28 Gueulette, J., Vynckier, S., Breteau, N., Sabbatier, R., El-Akkad, S., Strijkmans, K., De Scrijver, A., Böhm, L. Jones, D.T.L., Maughan, R, Courdi, A, Brassart, N, and Chauvel, P. Variation of neutron RBE as a function of energy. Intercomparison involving 7 neutrontherapy facilities, to be published.
29 Geraci, J.P., Jackson, K.L., Christensen, G.M., Thrower, P.D., and Weyer, B.J. Mouse testes as a biological test system for intercomparison of fast neutron therapy beams. Radiat. Res. 71, 377–386, 1977.
30 Field, S.B. and Morris, C. A comparison of the RBE of fast neutrons at Edinburgh and Hammersmith. Brit. J. Radiol. 50, 923, 1977.

10 Animal Models for Radiotherapy

B. KASER-HOTZ

Veterinär-Medizinische Klinik Zürich, Switzerland

Introduction

In particle radiotherapy a primary interest has been to use animal models for the determination of biological response to different ions, different energies and specific irradiation conditions. Information can be drawn from experiments with single cells and tissue cultures but animal models have also contributed substantially to the current knowledge. The need for animal models is obvious, since many clinically relevant hypotheses cannot be tested on human beings for ethical reasons. Animal tumor models should serve as a pattern for analogous situations in human tumors [1]. This chapter gives examples of studies performed with conventional research animals and introduces companion animals as an alternative animal model which may be of use in ion beam therapy.

Conventional Research Animals

Normal Tissue Studies

Various animal models have been used to study the effect of accelerated particles on normal tissue. Most of these models have been established for the determination of RBE for neutrons [2].

The parameters investigated for charged particles were RBE for various depths along the particles' path, in the entrance region as well as in various parts of extended Bragg peaks. An excellent overview on normal tissue response to accelerated ions has been given by Leith et al. [3]. For pion therapy target volumes and shapes had to be studied in even more detail since the RBE is dependent not only on the extension of the Bragg peak but also on the shape and size of the treatment volume [4].

The mouse foot system is very useful for studying the development of the skin reaction after graded doses [5]. Over a prolonged period of time recordings on the skin reaction are made and scored according to an arbitrary scale. One leg is irradiated, the opposite serves as a control. Dose response curves can be drawn and RBE values can be derived. The mouse skin system yields results on early and late reactions. The late reactions may not be independent of the severity of early reactions. Values can be obtained for single or multiple fractionation protocols. Raju and Carpenter [6] studied skin reactions to various ionizing radiations and concluded, that there was similar temporal development of skin damage for both low- and high-LET radiation. When various ions were compared for a single dose response in the peak and plateau region a higher RBE was found in the peak region. Other systems included ventral thoracic skin of hamsters and studied the repair capacity for various physical conditions and different fractionations. For protons, Tepper et al. [7] evaluated the response of mouse leg skin to 20 fractions of irradiation given in three-hour intervals. The assay of both acute and late skin reaction indicated RBE values of 1.09–1.14 in the spread-out Bragg peak (SOBP).

In hamsters or mice, a large portion of their skin in relation to the animals' size is irradiated, the physical volume, however, is small compared to volumes treated in human radio-oncology. The

radiation may therefore differ substantially from large volume irradiations.

A wide spectrum of fractionation schemes, covering the entire range of interest in human radio-oncology can be studied with this radiobiological system and radiobiological models, e.g., the linear quadratic model, can be tested. The use of inbred and small-size animals is practical but has its limitation in transferability to humans.

The use of pig skin which resembles human skin in many features has been pioneered by Fowler [8]. Disadvantageous is the larger size of this species and the higher experimental costs compared to mice. But on the other hand, multiple fields of relatively small dimensions, typically of a few centimeters in diameter, can be irradiated on a single animal. The possibility to apply both the unknown radiation quality and the reference irradiation on the same animal reduces the statistical variation of the results.

In the treatment of deep-seated tumors in humans, skin is usually not a dose-limiting tissue for ions. But the skin irradiations may also give valuable information on the reaction of underlying connective tissue and vasculature. The sharp dose fall-off with depth makes it difficult to precisely correlate dose and effect.

The mouse gut system is a technique first described by Withers and Elkind [9]. Whole body irradiation is performed on mice applying a single or up to 20 fractions with a minimum of a 3-hour interval. The test is based on determining the survival of jejunal crypt cells after graded doses. The animals are sacrificed 3.5 days post-irradiation and sections of jejunum prepared. The regenerating crypt cells per circumference of the intestine are counted and plotted as a function of dose. At levels of 10 to 50 cells per circumference, the dose response for various radiations can be compared. RBE values for plateau SOBP are determined with this system. The whole body irradiation allows to use irradiation volumes more similar to those applied in humans. The system is, therefore, also well suited for intercomparison studies, e.g., determining the radiobiological efficiency of different treatment facilities, radiation sources and qualities.

Another system extensively studied is the spinal cord, particularly of rats [10]. Damage to the spinal cord is characteristic for late damage. It develops after a latent period of several months as muscle atrophy and myelopathy causing neurological deficits. The dose needed to produce paralysis in 50% of the animals within a group is the endpoint of this system. It was used to study the influence of the spinal cord's position within the plateau or SOBP for various ions.

Induced Tumors

Various solid tumors can be grown after subcutaneous injection of tumor cells or implantation into specific anatomical sites. Rats, mice and rabbits are most commonly used. The tumors are allowed to grow to a predetermined size and are then irradiated in vivo to graded doses. To score the tumor response, the growth delay for a specific irradiation condition is measured and compared to untreated animals. For tumors with significant shrinkage after irradiation the time until the tumor reaches the size before treatment is taken, whereas for tumors with minimal or no shrinkage the time it takes to reach a preset volume is measured. Tumor control probabilities and RBE values can be determined with this system.

A modification of the described in vivo system is the following: the tumors are irradiated in vivo and then removed from the animal and processed to a single cell suspension, and colony forming ability determined in vitro. This system is more convenient, cheaper and faster, than growth measurements or the dilution technique, where tumor cells are removed from the animal after treatment and then injected into a recipient animal. This last technique has been used for the study of pion radiobiology with Ehrlich tumor cells [11].

All the above-mentioned systems have in common, that they permit large numbers of exposures with relatively modest efforts, resulting in sound data with small statistical errors. The use of inbred strains of animals and pure tumor cell lines further contributes to the good reproducibility of the results.

However, the shortcomings of induced animal tumors is the fact that physiologically, the tumor

environment in these transplanted tumors may be quite different from spontaneous tumors in humans.

Companion Animal Research

Tumors of Interest

Spontaneous tumors in dogs and cats provide an opportunity to study new therapeutic agents and cancer biology. The pet population is a vastly underutilized resource of animals available for study. In clinically related anti-cancer protocols pets can be used as alternative models, reducing the need for traditional research animals. Privately owned animals can be entered into experimental studies with informed consent from the owner. Animal owners are willing to cooperate in humane experimental approaches to therapy when hope for cure can be offered.

Many canine and feline animal tumors behave biologically very similarly to their human counterpart. Common aspects of human and animal tumors include similarity of histological types, cell kinetics, tumor volume and anatomical site of occurence. Tumor volumes are of similar proportion relative to the body size for dogs and man. The weight and surface area of dogs are sufficiently large so that small extrapolations can be made to adjust for the increased size of humans. In contrast to chemically or virally induced tumors, naturally occuring malignancies display the same relationship between tumor and tumorbed, vascularization and surrounding healthy tissue, as is encountered in human cancer. Compared to human patients, canine patients which have not undergone previous or concurrent therapy to complicate the analysis of response, can be selected.

The expenses of clinical trials in dogs are greater than in mice, but are much smaller than in man. Pet dogs are supported and cared for by their owners, limiting the costs for follow-up care. Animal owners are not expected to pay for the actual treatment, but they are expected to bring their dogs for follow-up exams and permit a necropsy at time of euthanasia. Most animals are euthanized once the quality of life is judged to have deteriorated. This allows a final, thorough examination before euthanasia. For dogs on experimental protocols a 98% follow-up rate for at least a year and a 85% necropsy rate have been reported from the Colorado State University-Animal Cancer Center [12].

Spontaneous animal tumors can serve in preclinical trials, designed very similarly to those for man. Animals can be assigned to different doses, and estimates of the therapeutic ratio can be made. Accordingly, judgements of optimal dose can be made prior to entering more expensive human clinical trials. Dose-effect curves and RBEs for multifractionated treatments can be obtained for various tissues. With respect to conformal therapy, animals may be used to study partial volume effects. It is also possible to randomize animals to a single treatment modality, such as surgery, radiation therapy or a combination of the two, which is ethically more difficult to justify in humans.

Tumors which have served as models for human cancer biology and treatment, i.e., tumors with potential relevance include canine osteosarcoma, soft tissue sarcoma, oral melanoma, oral squamous cell carcinoma, nasal tumors, mammary carcinoma, brain tumors and malignant non-Hodgkin's lymphoma [13].

Spontaneous animal tumors have been extensively used to determine dose response for irradiation, hyperthermia and the combination of the two [12–17]. For example dose response curves for tumor control and normal tissue reaction for canine oral carcinomas were determined for radiation alone and for the combination of radiation and heat (Fig. 1).

For studies on ion beam therapy nasal and oral tumors and soft tissue sarcomas appear to be suitable. Squamous cell carcinoma of the oral cavity is the second most common malignant oral tumor in dogs and carries a better prognosis than malignant melanoma (most common oral tumor) or fibrosarcoma for local control and long-term survival [16–20]. Squamous cell carcinomas usually originate from gingival epithelium and are characterized by rapid growth, early invasion of bone and late distant metastases. Dogs with rostrally located tumors have longer survival times than dogs with caudally located tumors. Canine oral

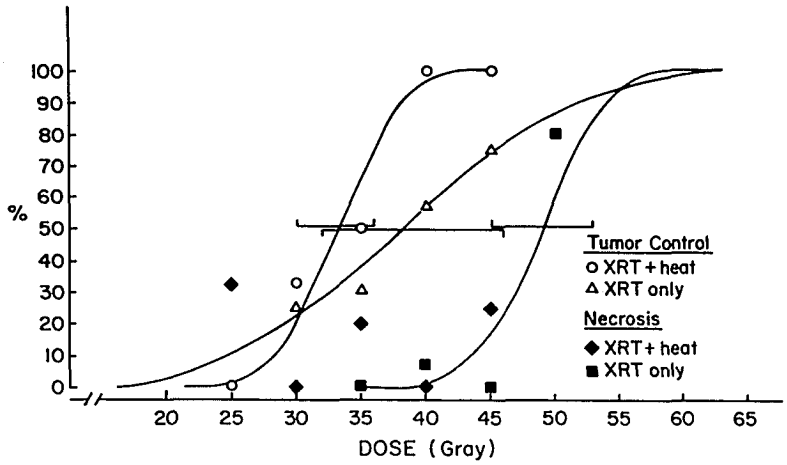

Fig. 1. Dose response curves for tumor control and probability for necrosis after irradiation (XRT only) of hyperthermia plus radiation (XRT + heat). From (24) with permission

squamous cell carcinomas are considered radiosensitive [21–25].

Tumors of the nasal cavity and paranasal sinuses are locally invasive but metastasize rarely. Carcinomas account for two thirds, sarcomas for one third of the nasal tumors. The disease usually presents in a relatively advanced stage in a critical location near the brain and eyes. Bone invasion occurs early and curative surgery is virtually impossible. The only improvement in survival has been gained with radiation therapy alone or in combination with surgical debulking [26–28]. These tumors are particularly challenging for conformal radiotherapy.

The incidence of soft tissue sarcomas in dogs is much greater than the rate in humans with 350 cancers per 100,000 dogs at risk [29]. The term "soft tissue sarcomas" refers to a group of tumors with similarities in pathological appearance, clinical presentation, and behavior. Soft tissue sarcomas tend to have poorly defined margins and infiltrate through and along fascial planes [30]. Local recurrence after conservative surgery is common. Soft tissue sarcomas are generally thought to be resistant to conventional doses of irradiation [31, 32]. Although higher doses have higher control rates, the chances of normal tissue complications also increase.

Experience at PSI

At PSI soft tissue sarcomas, oral tumors and nasal/paranasal tumors are selected to study conformal proton radiotherapy with a dynamic application technique.

In preparation for this study, spontaneous tumors in dogs and cats are irradiated with the 72 MeV proton beam used for the treatment of ocular melanomas. These treatments allow us to study acute and late reactions of fast protons in various tissues of dogs and cats and to estimate tumor control compared to results of photon beams in veterinary medicine. To our knowledge, ion beam therapy has not been studied in canine and feline tumors.

Ten animals have been treated so far and we feel the procedure is now well established. Six of the treated animals had squamous cell carcinomas, three had melanomas and one had a recurrent basal cell tumor. The proton beam's diameter of 3 cm and its depth range of 3 cm were considered limiting factors and enabled the treatment of small tumors only. The current protocol for human ocular tumors at PSI is 60 Gy given in 4 fractions over 4 days. We chose to treat twice a day to a total dose of 40.5 CGE over 4 days. This relates to a biological effective dose for late effects of 66.6 Gy and for early effects and tumor response of 53.0 Gy in treatments with 35 fractions. A RBE of 1.1 is used to convert physical dose to biologically effective dose. Especially in

cats, the volume irradiated is greater in relation to body size as compared to the volume irradiated in human ocular tumors. Even so performed in the beam for ocular melanoma treatment, the project aims at data concerning proton therapy for larger tumors outside the eye. The finer fractionation protocol was chosen as preparation for humans and dogs which will be treated with a more conventional fractionation protocol on a gantry.

All animals had skin in their treatment fields. They developed various degrees of edema, erythema and moist desquamation 10 to 14 days after completion of radiation therapy. The skin reactions healed within the next 2 weeks. Hair loss was apparent in the second to fourth week. During the same time period dark colored skin would lose pigmentation. Four weeks after completion of therapy acute reactions had subsided and a hairless, pigment free, but dry and non-edematous skin was present at the irradiation field. Mucosa appeared to respond earlier than skin. On the last day of treatment mild erythema and hyperemia could be observed – progressing to mucositis, which peaked 7 to 10 days after irradiation. In none of the animals ulceration or necrosis was observed, neither for the skin nor the mucosa. The acute reactions were graded between 2 and 3 according to the acute radiation morbidity scoring criteria of the Radiation Therapy Oncology Group [33]. Some animals required local treatment, but the acute effects were well tolerated by animals and judged transient and manageable also by the owners. Hair grew back within 4–6 months, often in a different color. Some animals were treated only a few months ago, so we are continuing to collect information on late effects. One animal with a squamous cell carcinoma on the toe and thus with bone tissue in the treatment field developed a coarse bone pattern with decreased bone density 6 months after treatment. There was no lameness or pain on palpation. One year after treatment this dog remains free of tumor and lameness. No other late reactions have been observed until now.

It is premature to report in detail on tumor response. The squamous cell tumors appeared to be very radioresponsive. Within the first month after treatment the tumor mass shrank substantially and reepithelization occurred.

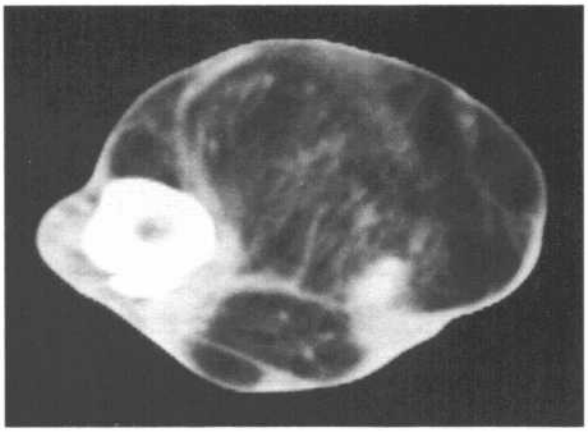

Fig. 2. CT of infiltrative lipoma at the level of the distal tibia

For the high energy proton beam our first goal is to test the feasibility and safety of all aspects of the dynamic application technique. The long-term goal is the determination of early and late normal tissue reactions in dependence of dose. Only dogs are entered in the study, because tumor volume and animal size are more comparable to human patients than in the case of cats. The animals undergo a thorough clinical work-up to

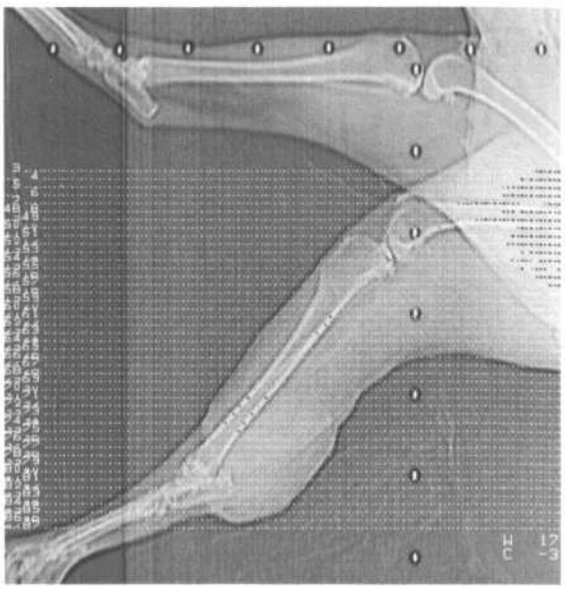

Fig. 3. Scout view of the dog in treatment position

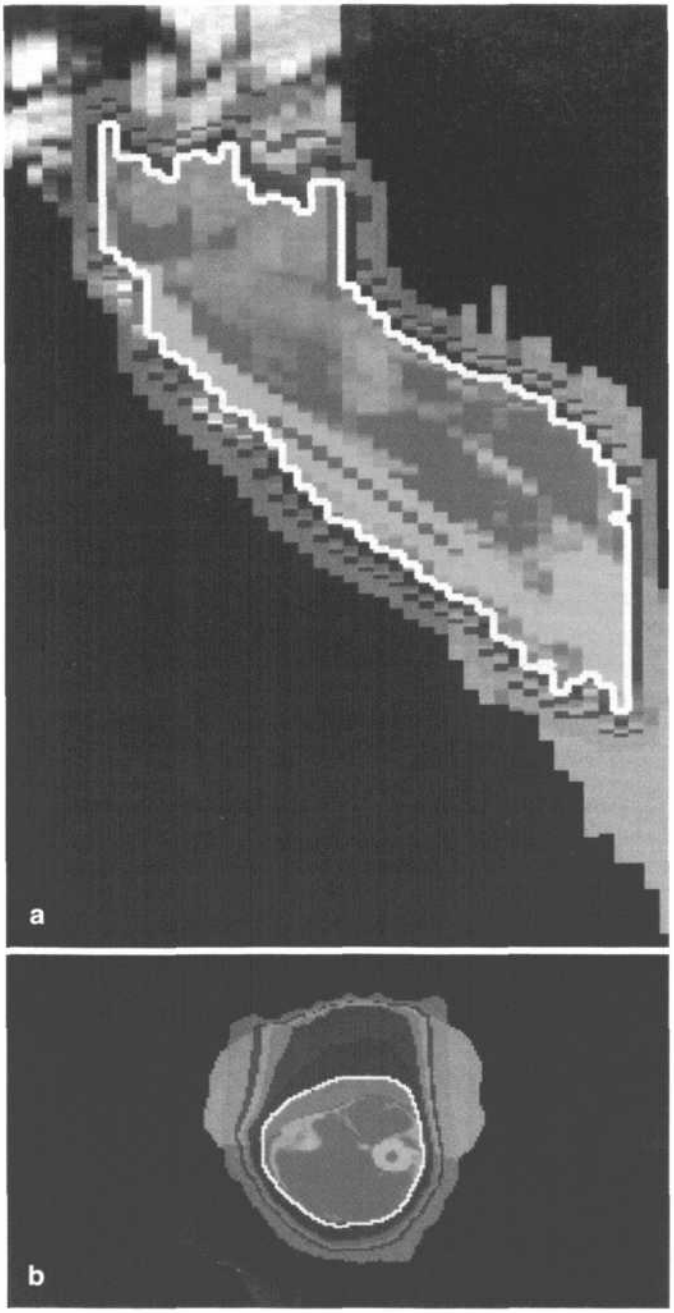

Fig. 4a, b. 3D-treatment planning of the dog's tumor. Dose distribution is overlayed (color-wash) over the reconstructed CT-image. **a)** saggital, **b)** cross-section

exclude those, which might not tolerate the course of therapy due to other serious diseases or evidence of limited organ function. To characterize the primary tumor, radiography and computed tomography are performed. Ultrasonography is used where indicated for further definition of tumor extent and lymph node involvement. Thoracic radiographs are made routinely to exclude animals with pulmonary metastases.

The WHO has provided staging criteria for a

variety of animal tumors [34]. These criteria are used to stage the disease.

The treatment volume is chosen on the basis of physical examination, CT information and tumor histology. The same safety margins found to be appropriate for cure with photons are applied. Special consideration is given to the individual anatomical location to make full use of the advantages of conformal proton radiotherapy.

In veterinary medicine a commonly used protocol is 49.5 Gy given in 15 fractions over a period of 19 days. This accelerated and hypofractionated scheme has evolved empirically, mostly guided by the idea to limit the number of anaesthesias. For the dynamic proton study a dose escalation study is planned beginning with 12 fractions of 3.5 CGE to a total dose of 42 CGE within 26 days. A drawback might be the necessity to adapt the treatment protocol to the PSI accelerator schedule which will direct Mondays, Tuesdays and Fridays as days of treatment. Additional fractions will be given on Thursdays increasing the total dose to 45.5 CGE, 49 CGE, 52.5 CGE, and 56 CGE.

Follow-up is of prime importance for clinical evaluation, statistical conclusions and comparison, and for future veterinary and human clinical studies. The treated dogs are examined the first, second, third and forth week, the third, sixth, ninth, twelfth month and every sixth month thereafter. The animals undergo physical exams at every reexamination. Thoracic radiographs and CTs are planned at half-year intervals. Special procedures, ultrasonography or more frequent CTs are done as indicated.

The acute effects are scored according to the radiation morbidity scoring criteria established by RTOG [33]. The potential late effects will also be evaluated and scored. The course fractionation scheme of the protocol should be particularly sensitive to detecting late effects. The endpoint for tumor response is the lack of tumor progression at 1 year as evidenced by physical examination and CT scans. Once the status of the animal deteriorates, owners are asked to have their animal be euthanized. This provides the final physical exam. A gross histological exam can be performed at the time of necropsy and histological samples are taken from various locations in the irradiated field to correlate tissue response with dose.

A dog with an infiltrative lipoma of the hind leg was the first patient to be treated on the gantry at PSI, just before the 1994 fall shutdown of the accelerator. The purpose of this treatment was – besides offering an alternative to amputation – to verify that voxel scanning does not yield

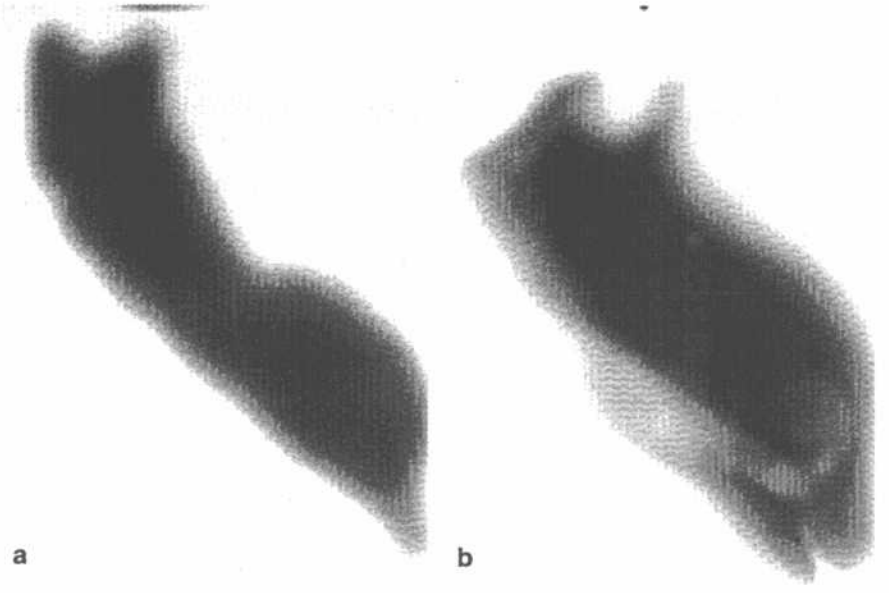

Fig. 5. Radiographic films taken during irradiation of the dog according to the treatment plan, shown in Figure 5. **a)** before the leg, **b)** behind the leg

a significantly different RBE than the 1.1 described in the literature.

A simple treatment geometry, namely a single vertical port, was chosen. The dog was fixed in treatment position in a mould on the table, produced from polyurethane foam. In this position serial CT slices were taken as a basis for treatment planning (Figs. 2 and 3). The target volume was defined to encompass the entire leg from the metatarsi to the distal femur region (Fig. 4). For partial sparing of the lymph drainage, the target contour excluded a small strip of skin at the cranial side of the leg. The prescribed dose was 36 CGE, assuming a RBE of 1.1, in 10 fractions over 16 days. The dose was measured by an ionization chamber in a homogeneous Plexiglass block, and the dose distribution checked by exposing films in various depths of the block (Fig. 5).

The dog tolerated treatment and acute reactions, including moist desquamation, well.

Conclusions

Small, experimental animal models have proven very useful to study fundamental radiobiological questions concerning normal tissues and tumors for various treatment modalities. This knowledge can be supplemented with valuable information gained from treatments of spontaneous, well-selected animal tumors in carefully designed protocols.

References

1 Herbermann, R.B. Counterpoint. Animal tumor models and their relevance to human tumor immunology. J. Biol. Resp. Modif. 2, 39–46, 1983.

2 Field, S.B. A historical survey of radiobiology and radiotherapy with fast neutrons. Curr. Top. Radiat. Res. 11, 1–86, 1976.

3 Leith, J.T., Ainsworth, E.J., and Alpen, L. Heavy ion radiobiology: Normal tissue studies. Adv. Radiat. Biol. 10, 192–227, 1983.

4 SIN, Medical Newsletter 6, 1984, PSI, Villigen, Switzerland, 1984.

5 Douglas, B.G. and Fowler, J.F. Effect of multiple small doses of X-rays on skin reactions in the mouse and a basic interpretation. Radiat. Res. 66, 401–426, 1976.

6 Raju, M.R. and Carpenter, S.G. A heavy particle comparative study. Part III. OER and RBE, Br. J. Radiol. 51, 712–719, 1978.

7 Tepper, J., Verhey, L., Goitein, M., Suit, H.D., and Koehler, A.M. In vivo determinations of RBE in a high energy modulated proton beam using normal tissue reactions and fractionated dose schedules. Int. J. Radiat. Oncol. Biol. Phys. 2, 1115–1122, 1977.

8 Fowler, J.F., Morgan, R.L., Silvester, J.A., Bewley, D.K., and Turner, B.A. Experiments with fractionated X-ray treatment of the skin of pigs: Fractionation up to 28 days. Br. J. Radiol. 36, 188–196, 1963.

9 Withers, H.R. and Elkind, M.R. Microcolony survival assay for cells of mouse intestinal mucosa exposed to radiation. Int. J. Radiat. Biol. Phys. 17, 261–267, 1970.

10 Van der Kogel, A.J. Mechanisms of late radiation injury in the spinal cord, in Radiation Biology in Cancer Research. Meyn R.E. and Withers H.R. (eds.), Raven Press, New York, 1980, pp. 461–470.

11 Jühling-Pohlit, L., Latz, D., Pohlit, W., and Thonke, A. The RBE of euoxic and hypoxic Ehrlich ascites tumor cells irradiated with negative pions in vitro and in vivo. Radiother. Oncol. 19, 57–72, 1990.

12 Gillette, E.L., personal communication, 1994.

13 MacEwen, E.G. Spontaneous tumors in dogs and cats: Models for the study of cancer biology and treatment. Cancer and Metastasis Rev. 9, 125–136, 1990.

14 Dewhirst, M.W., Sim, D.A., and Wilson, S. Correlation between initial and longterm responses of spontaneous pet animal tumors to heat and radiation or radiation alone. Cancer Res. 43, 5735–5741, 1983.

15 Gillette, E.L. Hyperthermia effects in animals with spontaneous tumors. Nat. Cancer Inst. Monogr. 61, 361–364, 1984.

16 Richardson, R.C., Anderson, V.L., and Voorhees, W.D. Irradiation-hyperthermia in canine hemangiopericytoma: Large animal model for therapeutic response. J. Nat. Cancer Inst. 73, 1187–1194, 1984.

17 Thrall, D.E. and Dewhirst, M.W. Use of radiation and/or hyperthermia for treatment of mast cell tumors and lymphosarcoma in dogs. Vet. Clin. North Am. Small Animal Pract. 15, 835–843, 1985.

18 Thrall, D.E. Orthovoltage radiotherapy of oral fibrosarcomas in dogs. J. Am. Vet. Med. Ass. 179, 159–162, 1981.

19 Brewer, W.G. and Turrell, J.M. Radiotherapy and hyperthermia in treatment of fibrosarcomas in the dog. J. Am. Vet. Med. Ass. 181, 146–150, 1982.

20 Oakes, M.G., Hedlund, C.S., Lewis, D.D., and Hosgood, G. Canine oral neoplasia. Comp. Cont. Educ. Pract. Vet. 15, 15–31, 1993.

21 Bradley, R.L, MacEwen, E.G., and Loar, A.S. Mandibular resection for removal of oral tumors in 30 dogs and cats. J. Am. Vet. Med. Ass. 184, 460–463, 1984.

22 Salisbury, S.K. and Lantz, G.C. Long-term results of partial mandibulectomy for treatment of oral tumors in 30 dogs. J. Am. Anim. Hosp. Ass. 24, 285–294, 1984.

(23) Salisbury, S.K., Richardson, D.C., and Lantz, G.C. Partial maxillectomy and premaxillectomy in the treatment of oral neoplasia in the dog and cat. Vet. Surg. 15, 16–26, 1986.

24 Gillette, E.L, McChesney, S.L., Dewhirst, M.W., and Scott, R.J. Response of canine oral carcinomas to heat and radiation. Int. J. Radiat. Oncol. Biol. Phys. 13, 1861–1867, 1987.
25 Evans, S.M. and Shofer, F. Canine oral nontonsillar squamous cell carcinoma. Prognostic factors for recurrence and survival following orthovoltage radiation therapy. Vet. Radiol. 29, 133–137, 1988.
26 Thrall, D.E. and Harvey, C.E. Radiotherapy of malignant nasal tumors in 21 dogs. J. Am. Vet. Med. Ass. 183, 663–666, 1983.
27 Adams, W.M., Withrow, S.J., Walshaw, R., Turrell, J.M., Evans, S.M., Walker, M.A., and Kurzmann, I.D. Radiotherapy of malignant nasal tumors in 67 dogs. J. Am. Vet. Med. Ass. 191, 311–315, 1987.
28 Roberts S.M., Lavach J.D., Severin G.A., Withrow S.J., and Gillette E.L. Ophthalmic complications following megavoltage irradiation of the nasal and paranasal cavities in dogs. J. Am. Vet. Med. Ass. 190, 43–478, 1987.
29 Dorn, E.R. Epidemiology of canine and feline tumors. J. Am. Anim. Hosp. Ass. 12, 307–312, 1976.
30 MacEwen, E.G. and Withrow, S.J. Soft tissue sarcomas, in Clinical Veterinary Oncology. Withrow, S.J. and MacEwen, E.G. (eds.), J.B. Lippincrott Co., Philadelphia, 1989, pp. 167–176.
(31) Mc Chesney, S.L., Gillette, E.L., Dewhirst, M.W., and Withrow, S.J. Influence of WR 2721 on radiation response of canine soft tissue sarcomas. Int. J. Oncol. Biol. Phys. 12, 1957–1963, 1986.
32 McChesney, S.L., Withrow, S.J., Gillette, E.L., Powers, B.E., and Dewhirst, M.W. Radiotherapy of soft tissue sarcomas in dogs. J. Am. Vet. Med. Ass. 194, 60–63, 1989.
33 Seegenschmiedt, M.H. and Sauer, R. Systematik der akuten und chronischen Strahlenfolgen. Strahlenther. Onkol. 169, 83–95, 1993.
34 Owen, L.N. TNM Classification of Tumours in Domestic Animals, Ed. 1. Geneve, Switzerland, World Health Organization, 1980.

III. Clinical Results and Indications

11 Proton Therapy with the Harvard Cyclotron

J. E. MUNZENRIDER

Massachusetts General Hospital, Boston, USA

Introduction

The Harvard Cyclotron began its life as a research instrument in Cambridge, Massachusetts, USA in 1948. Initial animal experimentation designed to study the biological effects of the 160 MeV synchrocyclotron proton beam commenced in 1959, and in 1961 human proton therapy was initiated with that beam at the Harvard Cyclotron Laboratory (HCL). In collaboration with the Neurosurgery Department of the Massachusetts General Hospital, Boston, promising clinical results in patients with intracranial targets were achieved. A Biomedical Annex was constructed in 1963 specifically for patient treatment; single fraction stereotactic proton radiosurgery continues there to the present day.

A second clinical collaboration for fractionated proton beam radiotherapy, with the Radiation Medicine Department of the Massachusetts General Hospital and the Retina Service of the Massachusetts Eye and Ear Infirmary was initiated in 1974. A second treatment room was developed at HCL in 1978, specifically to allow large field treatments to be carried out.

The HCL is currently dedicated primarily to clinical use; 15–22 patients are treated there each day, with the beam available for clinical use four and a half days each week, fifty-two weeks per year. The patient population treated through September 30, 1993 is listed in Table 1.

Initial research support for the Stereotactic Radiosurgery Program was obtained from the U.S. Office of Naval Research and later from the National Aeronautics and Space Administration, and the National Science Foundation. Single fraction treatments have been self-supporting from patient treatment fees for many years. Since the inception of the fractionated proton treatment program, the National Cancer Institute has supported research in the clinical application of the proton beam in fractionated proton beam radiotherapy. Superiority of protons for patients with uveal melanomas and skull base chordomas and chondrosarcomas was relatively quickly recognized, and such patients are currently charged for the treatment. Patients with other tumor types continue to be treated under research protocols with support from the NCI.

The 160 MeV proton beam has a maximum range in tissue of 16 cm. Addition of preabsorbing material, such as water or plastic, can reduce the residual range of the beam to that appropriate for a given clinical situation.

Table 1. Patients Treated at Harvard Cyclotron Laboratory 1961 to September 1993

	Patient number	Percentage (%)
Radiosurgery	2982	50
Fractionated treatment	2967	50
Uveal melanoma	1957	(66)*
Chordoma, chondrosarcoma	354	(11.4)
Prostate cancer	166	(5.6)
CNS	103	(3.5)
Soft tissue sarcoma	94	(3.2)
Head and neck	67	(2.3)
Bone sarcoma	68	(2.3)
Other sites	158	(5.3)

* numbers in parenthesis are % of fractionated patients

Table 2. Current Treatment Categories

Ocular Tumors
Uveal melanomas
Angiomas and hemangiomas
Choroidal metastasis
Retinoblastomas
Skull Base, Vertebral/Paravertebral Tumors
Chordoma, chondrosarcomas
Other histologies
Head and Neck Tumors
Paranasal sinus
Nasopharynx
CNS Tumors
Benign meningiomas
Malignant meningiomas
Glioblastomas
Acoustic neuromas
Large arteriovenous malformations (AVMs)
Pelvic Tumors
Prostate cancer (T3-T4)
Anal & rectal carcinomas
Sacral chordomas & sarcomas

Planning and treatment techniques currently employed for fractionated proton beam therapy at the HCL, a broad overview of results in patients with uveal melanomas, skull base and cervical spine chordomas and chondrosarcomas, Stage T_{3-4} prostatic cancer, and some CNS tumors will be presented in this chapter. Treatment categories currently in effect at the HCL are listed in Table 2. In Chapter 39 of this volume, plans for proton beam therapy at the Northeast Proton Therapy Center in Boston are discussed.

Ocular Tumors

Charged particle beams are ideal for treatment of intraocular neoplasms: relatively large radiation doses can be concentrated in the tumor, and uninvolved intraocular and orbital structures can largely be spared. Extensive experience has been developed at the Harvard Cyclotron Laboratory in ocular proton beam therapy, primarily of uveal melanomas, involving a collaborative effort between that laboratory, the Radiation Oncology Department of Massachusetts General Hospital (MGH), and the Retina Service of the Massachusetts Eye and Ear Infirmary (MEEI) [1].

Preclinical Studies

Studies on normal and simulated tumors in monkey eyes used single proton doses of 50–100 Gy through 7 or 10 mm diameter beams. Opaque areas of edematous retina and choroid developed within 20 hours in each eye, while the non-irradiated retina and choroid appeared entirely normal [2]. A marked fractionation effect was seen: 125 Gy/5 fx produced the same effect at 24 hours and at 1 year as did a single dose of 30 Gy [3]. Chorioretinal changes persisted within the irradiated area, but normal retinal architecture was preserved immediately outside the discrete retinal proton scar at 42–51 months [4].

Planning and Treatment Techniques

A computerized treatment planning program has been used for all patients, whether or not they had undergone surgical tumor localization [5–7]. Treatment decisions are routinely based on clinical evaluation only, since diagnostic accuracy of current non-invasive ophthalmologic techniques is quite high [8]. Input data for the treatment planning program include:

- ultrasound-measured axial eye length and tumor height, and
- tumor configuration drawn manually on the computer from presurgical tumor sketches and/or fundus photographs.

If surgical tumor localization is done, the clip position is determined visually from measurements taken at the time of surgery for clip placement, and from simulator radiographs usually performed on the second or third day following surgery. A transparency with appropriate magnification shows the desired clip position, and the projection of the proton beam onto the front of the eye. This transparency can be used for treatment set-up. Individualized brass apertures are specified from the treatment planning program directly to a computer-controlled milling machine for fabrication. Compensators are not employed.

Planning and treatment techniques have been generally similar at all centers using protons for

ocular radiotherapy. Anterior lesions involving the ciliary body and the peripheral choroid have been treated with a light field only, verifying tumor location for treatment by transillumination after initial computerized planning from fundus photographs, tumor sketches and ultrasound. A light field set-up has also been used for metastatic choroidal lesions involving the posterior pole.

Patients are seated for treatment, the head immobilized with an individually molded bite block and face mask. Retractors are employed to limit the volume of eyelid irradiated. Voluntary fixation on an external light source positions the eye for radiographic or light field set-up and during treatment, with video monitoring of eye position during the 1–2 minute treatment.

Clinical Results

Between July 1975 through October 1993, uveal melanomas in 1957 patients were treated at the Harvard Cyclotron Laboratory. Approximately half the patients were female. Using the Collaborative Ocular Melanoma Study (COMS) size categories [8], 7% of patients had small tumors, 62% medium tumors, and 31% large tumors. Over 80% of treated eyes had initial visual acuity of 20/200 (6/60) or better. Standard dose has been 70 Cobalt Gy Equivalents (CGE = proton Gy times RBE 1.1) in five fractions in 7–9 days. Local control of tumor within the treated eye was 96.3 ± 1.5% and 95.4 ± 3.3% at 60 and 84 months, respectively. Two failures occurred after 48 months, and none after 6 months; 236 and 82 patients were available for follow-up at those times after treatment. Two failures occurred in the full dose (70 CGE) region, with 10 recurring at the margin of the irradiated volume [9]. Five year survival approximates 80% for all patients [1, 10, 11]. Survival in proton treated patients is at least as good as in patients undergoing primary enucleation [12, 13].

Visual acuity is improved or preserved in over 50% of treated eyes; a lesser degree of visual preservation is observed in eyes with larger and with more posteriorly placed tumors. Visual prognosis in conservatively treated eyes has been found to be significantly associated with tumor height, distance of the posterior tumor margin from the optic disc and/or fovea, pretreatment macular retinal detachment, initial visual acuity, and radiation dose to both disc and fovea and to the lens [14, 15].

Acute reaction occurs only if the eyelid cannot be completely retracted from the irradiation field; in such cases, moist eyelid desquamation usually involves a discrete (2–5 mm by 8–15 mm) lid segment, which heals in two to four weeks. Some scarring and permanent lash loss usually occurs in such areas. Late complications include rubeosis iridis with neovascular glaucoma, occurring from 2 months to 5.2 years (median 1.4 years) after treatment, which can be treated successfully in the majority of patients. Macular vasculopathy, macular edema, optic atrophy and radiation papillopathy can be seen in small percentages of patients [1]. Cataracts develop in some patients, predominantly those with large choroidal or ciliary body tumors in whom a large portion of the lens has been irradiated. Successful cataract extraction with restoration of vision after intraocular lens implantation has been reported [16].

Uveal melanoma patients were also treated from 1978 through 1992 at Lawrence Berkeley Laboratory with helium ions in a collaboration between the Radiation Oncology and Ocular Oncology Departments of the University of California-San Francisco. Results with doses of 50, 60, 70 or 80 CGE (CGE, equal to helium ion dose in Gy times RBE factor 1.3) have been encouragingly similar to those described above for proton beam therapy (cf. Chapter 15 for details). That group began treating patients with a cyclotron at the University of California-Davis, in May, 1994. Similar results are also being achieved at PSI [17].

Angiomas, hemangiomas and metastatic intraocular tumors are other examples of malignancies which have been treated at HCL. Doses have been 25–35 CGE in 4–5 fractions for the blood vessel tumors, and 28 CGE in 2 fractions for metastatic lesions. Palliation of ocular symptoms in patients with metastatic disease can be achieved very efficiently. A light field treatment plan can be prepared from fundus photographs, tumor sketches, and ultrasound obtained at the first clinic visit. After fabrication of the treatment

aperture, the first of two treatments can be given at the initial particle facility visit.

Charged particle dose localizing qualities are particularly attractive for the treatment of retinoblastomas [18]. Significant reduction in normal tissue volume treated can be achieved, which might reduce the incidence of second malignant tumors in patients with the hereditary form of the disease. Previously untreated retinoblastomas in 14 eyes showed good acute tolerance and tumor regression. Patients are planned with the 3D-planning system described below, and have received 40–46 CGE in 20–23 fractions over 5–5 1/2 weeks. Targets have included individual tumors, retina posterior to the equator in cases with posterior multifocal disease, or the entire retina and vitreous in more advanced cases. No dose is given beyond the midline with a single lateral proton portal, resulting in a much smaller volume of bone and other nontarget tissues being irradiated than would be treated with photon techniques. The dose distribution for treatment of retinoblastoma with a single lateral proton beam is shown in Figure 1, and illustrates how the dose can be conformed to the target in the orbit, with lesser doses to the skin, subcutaneous tissue, and bone.

Significance of Particle Therapy of Ocular Tumors

Uveal melanomas can be treated conservatively with a high degree of success, using particle beam techniques, with good expectation for visual preservation, eye retention [19], and low complication rates. Even for very large tumors, treatment can be justified if vision is poor or absent in the fellow eye; in such cases expectations for visual preservation must be low, and the probability that enucleation will be necessary in the future approximates 20%.

Further follow-up of particle-treated uveal melanoma patients will be needed to determine the ultimate impact of such therapy on survival and long-term visual outcome. Available evidence, however, strongly suggests that survival is not compromised, local control is achieved in almost all treated eyes, and useful vision is preserved in the majority of patients.

Additional clinical experience and possibly clinical trials are required to clarify the role of particle beam therapy relative to other conservative techniques in the treatment of other ocular tumors, such as retinoblastomas, angiomatous tumors, and metastatic lesions.

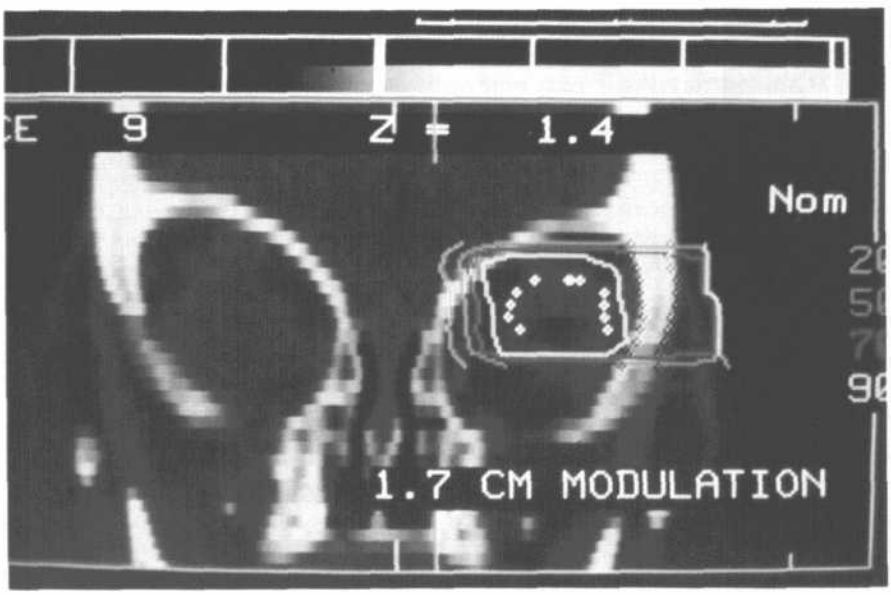

Fig. 1. Dose distribution with a single lateral proton portal to a retinoblastoma patient. Note target defined in globe, absence of dose across midline, and localization of the 90% isodose line within the globe

Planning and Treatment Techniques with Other Tumors

Both planning and treatment techniques for patients with other tumor types are markedly different from those used for eye tumors. Proton beam dose distributions are perturbed by inhomogeneities, such as bone or air cavities, to a much greater extent than is the case for conventional X-ray beams. Tissue density in the volume to be irradiated must be accurately known for proton therapy, to allow compensation for tissue inhomogeneities, both in planning and treatment [20–22].

Metallic markers, either small gold screws or coated lead spheres surgically implanted into the skull prior to treatment planning in patients with head and neck, intracranial or skull base lesions, serve as fiducials for patient positioning [23]. A treatment planning CT scan is performed on the immobilized patient in the treatment position [24], with tumor and normal tissues of concern throughout the treatment volume then being defined on each CT section.

The "beam's eye-view" feature of the interactive treatment planning program is employed to define appropriate apertures to treat the defined tumor volume, while minimizing dose to dose-limiting normal tissues [25]. Fields are defined with brass or Cerrobend apertures, while dose at depth is determined by portal-specific lucite compensators. Apertures and compensators are individually fabricated for each field. Up to 12 aperture-compensator sets have been required for some patients. Most patients receive a portion of their treatment through two or more X-ray portals, to achieve some skin sparing, and to allow treatment five days per week (HCL beam has been available only four days per week for the fractionated proton therapy program). Prior to plan implementation, 3D-dose distributions throughout the treated volume are reviewed, allowing necessary corrections prior to actual treatment.

Patients are treated in their immobilization device, their position having been radiographically verified prior to each treatment. Set-up accuracy and reproducibility is ± 2 mm with skeletal fiducial [24], and ±1 mm when small surgically placed skull fiducials are employed [26].

Full 3D-dose distributions can be displayed on the monitor or printed out as hard copy, with either conventional isodose lines or color shades with the appropriate scale. Up to four different plans can be compared simultaneously. Dose-volume histograms can be produced for any structure which has been defined on the planning scan. A full data set for each patient is archived at the completion of treatment, and can be recalled for clinical or research purposes at any time after treatment has been completed [27, 28].

Clinical Results with Other Tumors

Chordomas and Chondrosarcomas

A large number of patients with cervical spine and skull base chordomas and chondrosarcomas have been treated at the Harvard Cyclotron, using 3D-planned combined proton and X-ray treatment [29, 30]. The HCL 160 MeV proton beam is particularly suitable for treating such tumors, although lack of a gantry has required some patients to be treated in the upright position. Between February 1974 and December 1991, 45 patients with cervical spine and 209 patients with skull base chordomas and chondrosarcomas were treated. Tumor volumes ranged from 3.3 to 318 ml; median volume was 70 ml for cervical spine and 40 ml for skull base tumors. Tumor dose ranged from 56.8 to 80 CGE, with median dose being 69.9 CGE for patients with cervical spine tumors and 68.4 CGE for skull base patients. Local recurrence-free survival (LRFS) for the skull base tumor patients was 77 ± 5% at five years, significantly better than for cervical spine tumor patients (58 ± 14%, $p = 0.0076$). Skull base chondrosarcoma patients had significantly better LRFS than did chordoma patients (95 ±4% vs. 62 ± 9%, $p = 0.0001$). In skull base chordoma patients, males fared significantly better than did females. No significant difference in LRFS was observed between cervical spine chordoma and chondrosarcoma patients ($p > 0.05$). Improved cause-specific survival for skull base tumor patients relative to patients with cervical spine tumors, and for skull base chondrosarcoma

patients relative to skull base chordoma patients was also observed ($p < 0.05$ for both comparisons).

Relatively few complications have occurred, considering the high doses delivered. In skull base patients, significant brain injury was seen in approximately 6% and severe visual complications in approximately 2%. Post-treatment pituitary insufficiency can occur in 10–15% of patients, being partial in most, although a few have developed panhypopituitarism. Unilateral hearing loss also has developed in 10–15% of skull base patients. Neurovisual and neuroendocrine sequelae of treatment have been described [31, 32].

Treatment with conventional radiotherapy following surgery results in locally progressive disease and ultimately death in most patients [33]. Local recurrence-free survival achieved with the 3D-planned combined proton and photon techniques in these patients are superior to results described in the literature. Similar encouraging results have been reported from LBL [34].

A randomized prospective clinical trial was initiated in 1985 through the NCI and the RTOG (Radiation Therapy Oncology Group), as a collaboration between MGH-HCL and UCSF-LBL. Tumor control and treatment sequelae were to be prospectively assessed after doses of either 66.6 or 72 CGE, given predominantly with protons or helium ions.

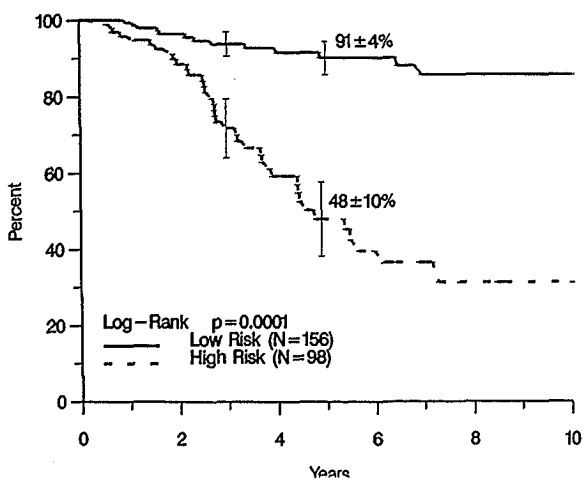

Fig. 2. Local control (local recurrence-free survival) for lower risk patients (male skull base chordomas and all skull base chondrosarcomas) and for higher risk patients (female skull base chordomas and all cervical spine patients) with chordomas and chondrosarcomas of the skull base and cervical spine

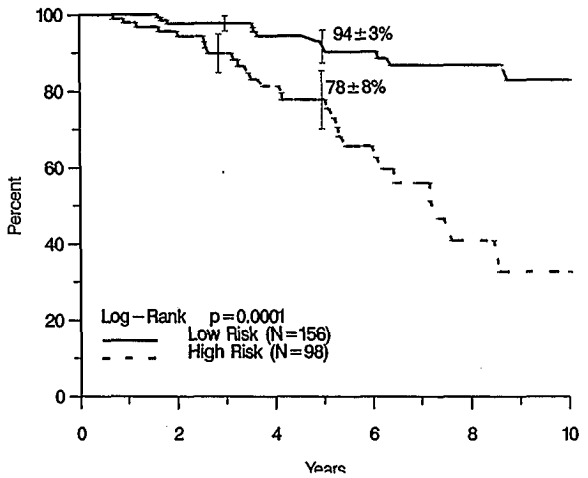

Fig. 3. Overall survival for lower risk patients (male skull base chordomas and all skull base chondrosarcomas) and for higher risk patients (female skull base chordomas and all cervical spine patients) with chordomas and chondrosarcomas of the skull base and cervical spine

As the study progressed, it became apparent that this population contained two separate groups, in terms of the risk of both local failure and survival. Treatment failure was significantly more likely to occur in female skull base chordoma patients, as well as in patients with cervical spine tumors, regardless of sex or histology. Lower risk patients (male skull base chordomas and all skull base chondrosarcomas) had a 91 ± 4% probability of local control at five years, compared to 48 ± 10% for higher risk patients (female skull base chordomas and all cervical spine patients), $p = 0.0001$. Cause-specific survival was 94 ± 3% for the lower risk group, and 78 ± 8% for the higher risk patients. Local control (LRFS) and overall survival for both groups are shown in Figures 2 and 3, respectively.

Accordingly, the protocol was modified; lower risk patients would continue to be randomized between the original dose levels (66.6 vs. 72 CGE), using the standard normal tissue dose constraints, while higher risk patients (female skull

base chordomas and cervical spine tumors of either sex or histology) would be randomized between 72 and 79 CGE. Dose constraints for the 72 CGE arm would remain unchanged, but be increased by 5% for patients randomized to the 79.2 CGE arm. One hundred forty-seven patients were randomized through September, 1993, 118 at MGH-HCL, and 25 at UCSF-LBL. Patient treatment has been terminated at LBL, but Loma Linda will be participating in this trial.

Complication rates have been acceptable, especially in view of the major morbidity followed by an invariably fatal outcome in patients with uncontrolled tumor growth. Neurological, visual, endocrine and auditory problems can appear at various times after treatment, dictating that initial and continued multidisciplinary surveillance with specialists in those areas be performed, to allow identification and appropriate treatment of tumor recurrence, extension or metastasis as well as of treatable complications.

In summary, 3D-planned high dose radiation therapy delivered with combined proton and megavoltage X-ray techniques following appropriate surgery appears to represent the best management policy currently available for patients with chordomas and low-grade chondrosarcomas of the skull base and cervical spine. This potentially hazardous treatment is expensive, time-consuming and demanding for both the patient and those involved in their care. Nonetheless, it offers major improvements in outcome, relative to that anticipated with conventional megavoltage X-ray techniques, or with surgery alone.

Prostate Cancer

Initial results in 66 prostate cancer patients treated with a perineal proton boost following high energy X-ray whole pelvic irradiation were encouraging. Doses ranged up to 75 CGE, 10–20% greater than those then being given with conventional megavoltage X-ray techniques, and were associated with no greater rectal or bladder morbidity than would have been expected after treatment to conventional doses with X-rays [35]. A Phase III clinical trial based on that experience was initiated in 1981, and closed in June, 1992 after 203 patients had been enrolled. Patients with T_{3-4} N_{x-0} M_0 disease received 50.4 Gy to the pelvis, followed by a randomly assigned boost to either 67.4 Gy with X-rays or 75.6 CGE with protons.

Local control at five years for the entire group was 90%, with overall survival 81% (median follow-up 41 months, range 14–74 months) in an interim analysis [36]. Trial design had estimated local control at 5 years with the lower dose to be approximately 70%. Another interim report on this trial has been presented in October 1994. Mild (grades 1 & 2) rectal bleeding occurred in 16% of patients treated to the lower dose (X-rays only), and in 34% of patients boosted to the higher dose with the perineal proton portal ($p = 0.013$). Dose volume histogram analysis in 41 patients showed that the total volume of anterior rectum receiving ≥75 CGE correlated significantly with the probability of remaining free of rectal bleeding. No rectal bleeding was experienced by 80% of 27 patients in whom >40% of the anterior rectum received ≥75 CGE, while only 40% of 14 patients in whom >40% of the anterior rectum received ≥75 CGE remained free of rectal bleeding [37].

Intracranial Tumors

Techniques for treatment of skull base tumors are also appropriate for the fractionated treatment of patients with discrete CNS tumors, such as meningiomas, craniopharyngiomas, acoustic neuromas, and some gliomas.

Thirty-two meningioma patients with recurrent or incompletely excised meningiomas have received doses ranging from 55.8 to 71.6 CGE with combined photon and proton treatment. No tumor progression has been documented in 26 patients with benign histology, although two of six atypical or malignant meningioma patients did show progression. Some of these patients are included in a report on results in 36 patients with benign meningiomas treated at MGH between 1968 and 1986 [38]. There was a trend toward improved local control in patients treated with combined photon and proton techniques and 3D-planning. A Phase III clinical trial has been initi-

ated, to evaluate prospectively local control and morbidity after proton and photon treatment of incompletely excised or recurrent benign meningiomas to doses of 55.8 CGE or 63.0 CGE. Patients will also be entered into this protocol from LLUMC.

Twelve craniopharyngioma patients have received doses ranging from 52.7 to 63.4 CGE. No tumor progression or complications have been seen in 10 patients (median follow-up in excess of 5 years). One did require cyst evacuation after treatment. Two died, one with blindness and dementia, and the other without obvious tumor progression from complications of diabetes mellitus. Superior dose distributions for craniopharyngiomas can be achieved with proton techniques, relative to those possible with X-rays. However, conventional megavoltage X-ray treatment to moderate doses, of the order of 50.4 Gy in 28 fractions, produces acceptable results, and further treatment of patients with these tumors at the HCL is not currently planned.

Early experience in treating high grade gliomas engendered little enthusiasm for use of once-daily fractionated proton beam techniques in that group of patients. Three of four such patients died of progressive tumor growth at 11, 30, and 62 months after treatment; another died at two months with leukopenia and sepsis following chemotherapy at another hospital. We recently demonstrated that a dose of 90 CGE in 50 fractions over 5–5 1/2 weeks to the CT-enhancing volume of patients with glioblastoma multiforme was well tolerated: all nine patients entering the protocol completed the treatment. Although none survived beyond 26 months, recurrent tumor was seen only in the lower dose volume immediately outside the volume treated to 90 CGE, suggesting that the target volume designed from the CT-enhanced scan had underestimated true tumor extent. A new protocol has been developed, combining findings from CT, MRI, and PET in the initial definition of the target volume. The dose fractionation schedule described above will be employed in that protocol.

Arteriovenous Malformations

The most common indication for single fraction proton or helium ion beam treatment in recent years has been for arteriovenous malformations [39–40]. Although benign, these vascular abnormalities can result in major CNS morbidity or even death from uncontrolled hemorrhage. If surgical treatment is not possible, single fraction radiosurgery is a viable option for smaller (<5 cm) lesions: fractionated radiotherapy may be beneficial for larger malformations. Such treatment may be given with protons, although other centers have employed the ^{60}Co Gamma Knife or specially modified linear accelerators to deliver stereotactic irradiation to small intracranial targets.

It may be difficult to demonstrate any advantage for particle beams in treating small CNS lesions, since few if any symptoms may be manifest after injury to a small volume of the CNS. However, it is likely that particle beams will be particularly advantageous for fractionated treatment of larger AVMs, as suggested by a comparative treatment planning study recently presented by Miralbell and Urie [41].

Assessing the Value of Proton Therapy: Clinical Trials through PROG

Suit et al. [42] have discussed criteria for assessing the value of proton therapy: "In planning the clinical trials for proton radiation therapy, special attention has to be directed toward definition of the control arm and to select tumors for which there are excellent prospects of administering doses which are higher by >10% than is feasible with high technology photon therapy."

The initiation of proton therapy at several new proton therapy centers may accelerate the accrual of patients into cooperative clinical trials. An administrative mechanism to facilitate and coordinate such trials has been set up by the American College of Radiology and the U.S. National Cancer Institute. They established the Proton Radiotherapy Oncology Group (PROG)

to
1. stimulate cooperative clinical trials by the various proton therapy centers in the US and abroad,
2. organize and manage the clinical trials,
3. provide data management for the trials,
4. encourage the prompt reporting of trial results.

The initial PROG trial will extend a two-dose level trial for patients with skull base and cervical spine chordomas and chondrosarcomas, as discussed above. Other active PROG protocols include treatment of recurrent and incompletely excised benign meningiomas, advanced paranasal sinus carcinomas, and T3/4 carcinomas of the tonsil. New protocols will be developed for atypical and malignant meningiomas, for high-grade gliomas, and uveal melanomas, as well as tumors at other sites. Initial PROG members include MGH, UCSF-LBL, and LLUMC. Participation by other centers in North America and abroad will be encouraged. Despite initiation of cooperative clinical trials by PROG, it is not likely that the true efficacy of proton radiation therapy will be assessed before the end of this century. Testing proton therapy against various tumor sites is really just now beginning, and radiation therapy clinical trials require long observation periods to properly assess the end-points of local control, patient survival, and acute and chronic morbidity.

Summary and Conclusions

Protons are not "magic bullets". Proton beam therapy is not a revolutionary development in the treatment of malignant disease. It is better considered as an evolutionary advance in radiotherapy practice, similar to improvements in dose distributions which were made possible when kilovoltage X-rays were supplanted by megavoltage photons, and, in some cases, by the availability of electron beam techniques.

The impressive clinical successes achieved by the Massachusetts General Hospital and the Massachusetts Eye and Ear Infirmary in the proton therapy program at the Harvard Cyclotron, particularly in patients with uveal melanomas and with bony and cartilaginous tumors of the skull base and cervical spine, continue to fuel the burgeoning interest in the United States and throughout the world in ion beam radiotherapy for the treatment of human malignancies.

References

1 Gragoudas, E.S., Seddon, J.M., Egan, K. Glynn, R., Munzenrider, J., Austin-Seymore, M., Goitein, M., Verhey, L., Urie, M., and Koehler, A. Long-term results of proton beam irradiated uveal melanomas. Ophthalmol. 94, 349–353, 1987.

2 Constable, I.J., Koehler, A.M., and Schmidt, R.A. Proton irradiation of simulated ocular tumors. Investig. Ophthalmol. 14, 547–555, 1975.

3 Constable, I.J., Goitein, M., Koehler, A.M., and Schmidt, R.A. Small field irradiation of monkey eyes with protons and photons. Rad. Res. 65, 304–314, 1976.

4 Gragoudas, E.S., Zakov, N.Z., Albert, D.M., and Constable, I.J. Long-term observations of proton irradiated monkey eyes. Arch. Ophthalmol. 97, 184–191, 1979.

5 Gragoudas, E.S., Goitein, M., Koehler, A.M., Verhey, L.J., Tepper, J.E., Suit, H.D., Brockhurst, R., and Constable, I. Proton irradiation of small choroidal malignant melanomas. Am. J. Ophthalmol. 83, 655–673, 1977.

6 Gragoudas, E.S., Goitein, M., Verhey, L.J., Munzenrider, J., Suit, H.D., and Koehler, A. Proton beam irradiation: An alternative to enucleation for intraocular melanoma. Ophthalmol. 87, 571–581, 1980.

7 Goitein, M. and Miller, T. Planning proton therapy of the eye. Med. Phys. 10, 275–283, 1983.

8 The Collaborative Ocular Melanoma Study group. Accuracy of diagnosis of choroidal melanomas in the collaborative ocular melanoma study. COMS Report No. 1, Ophthalmol. 108, 1268–1273, 1990.

9 Munzenrider, J.E., Verhey, L.J., Gragoudas, E.S., Seddon, J.M., Urie, M., Gentry, R., Birnbaum, S., Ruotolo, B.S., Crowell, M.S., McManus, P., Finn, S., Sisterson, J., Johnson, K., Egan, K., Lento, D., and Bassin, P. Conservative treatment of uveal melanoma: Dose distribution to tumors with local recurrence after proton beam therapy. Int. J. Radiat. Oncol. Biol. Phys. 17, 493–498, 1989.

10 Gragoudas, E.S., Seddon, J.M., Egan, K.M., Polivogianis, L., Hsieh, C., Goitein, M., Verhey, L., Munzenrider, J., Austin-Seymour, M., Urie, M., and Koehler, A. Prognostic factors for metastasis following proton beam irradiation of uveal melanomas. Ophthalmol. 93, 675–680, 1986.

11 Gragoudas, E.S., Seddon, J.M., Egan, K.M., Glynn, R.J., Goitein, M., Munzenrider, J.E., Verhey, L.J., Urie, M., and Koehler, A. Metastasis from uveal mela-

noma after proton beam irradiation. Ophthalmol. 95, 992–999, 1988.
12 Seddon, J.M., Gragoudas, E.S., Albert, D.M., Hsieh, C., Polivogianis, L., and Friedenberg, G.R. Comparison of survival rates for patients with uveal melanoma after treatment with proton beam irradiation or enucleation. Am. J. Ophthalmol. 99, 282–290, 1985.
13 Seddon, J.M., Gragoudas, E.S., Egan, K.M., Glynn, R.J., Howard, S., Fante, R.G., and Albert, D.M. Relative survival rates after alternative therapies for uveal melanomas. Ophthalmol. 97, 769–777, 1990.
14 Seddon, J.M., Gragoudas, E.S., Polivogianis, L., Hsieh, C.-C., Egan, K.M., Goitein, M., Verhey, L., Munzenrider, J., Austin-Seymour, M., Urie, M., and Koehler, A. Visual outcome after proton beam irradiation of uveal melanoma. Ophthalmol. 93, 666–674, 1986.
15 Seddon, J.M., Gragoudas, E.S., Egan, K.M., Glynn, R.J., Munzenrider, J.E., Austin-Seymour, M., Goitein, M., Verhey, L., Urie, M., and Koehler, A. Uveal melanomas near the optic disc or fovea: Visual results after proton beam irradiation. Ophthalmol. 94, 354–361, 1987.
16 Gragoudas, E.S., Egan, K.M., Arrigg, P.G., Seddon, J.M., Glynn, R.J., and Munzenrider, J.E. Arch. Ophthalmol. 110, 475–477, 1992.
17 Zografos, L., Perret, C., Egger, E., Gailloud, C., and Greiner, R. Proton beam irradiation of uveal melanomas at Paul Scherrer Institute (former SIN). Strahlenther. Onkol. 166, 114, 1990.
18 Mukai, S. Management of retinoblastoma. Sem. Ophthalmol. 8, 281–291, 1993.
19 Egan, K., Gragoudas, E.S., Seddon, J.M., Glynn, R.J., Munzenrider, J.E., Goitein, M., Verhey, L., Urie, M., and Koehler, A. The risk of enucleation after proton beam irradiation of uveal melanoma. Ophthalmol. 96, 1377–1383, 1989.
20 Goitein, M. and Abrams, M. Multi-dimensional treatment planning: Delineation of anatomy. Int. J. Radiat. Oncol. Biol. Phys. 9, 777–787, 1983.
21 Goitein, M. Compensation for inhomogeneities in charged particle radiotherapy using computed tomography. Int. J. Radiat. Oncol. Biol. Phys. 4, 499–508, 1978.
22 Urie, M.M., Goitein, M., and Wagner, M. Compensating for heterogeneities in proton radiation therapy. Phys. Med. Biol. 29, 553–566, 1983.
23 Gall, K.P., Verhey, L.J., and Wagner, M. Computer-assisted positioning of radiotherapy patients using implanted radiopaque fiducials. Med. Phys. 20, 1153–1159, 1993.
24 Verhey, L.J., Goitein, M., McNulty, P., Munzenrider, J.E., and Suit, H.D. Precise positioning of patients for radiation therapy. Int. J. Radiat. Oncol. Biol. Phys. 8, 289–294, 1982.
25 Goitein, M., Abrams, M., Rowell, D., Pollari, H., and Wiles J. Multi-dimensional treatment planning: II. Beam's eye-view, back projection and projection through CT sections. Int. J. Radiat. Oncol. Biol. Phys. 9, 789–797, 1983.
26 Rosenthal, S.R., Urie, M.M., and Thornton, A. Advances in head and neck immobilization for radiotherapy. (Abst.) Med. Phys. 20, 868, 1993.
27 Urie, M.M., Fullerton, B., Tatsuzaki, H., Birnbaum, S., Suit, H.D., Convery, K., Skates, S., and Goitein, M. A dose response analysis of injury to cranial nerves and/or nuclei following proton beam radiation therapy. Int. J. Radiat. Oncol. Biol. Phys. 23, 27–39, 1992.
28 Austin, J.P., Urie, M.M., Cardenosa, G., and Munzenrider, J.E. Probable causes of recurrence in patients with chordoma and chondrosarcoma of the base of skull and cervical spine. Int. J. Radiat. Oncol. Biol. Phys. 25, 439–444, 1993.
29 Munzenrider, J.E., Austin-Seymour, M., Blitzer, P.J., Gentry, R., Goitein, M., Gragoudas, E.S., Johnson, K., Koehler, A.M., McNulty, P., Moulton, G., Osborne, E., Seddon, J.M., Suit, H.D., Verhey, L.J., and Wagner, M. Proton therapy at Harvard. Strahlentherapie 161, 756–763, 1985.
30 Austin-Seymour, M., Munzenrider, J.E., Goitein, M., Verhey, L., Urie, M., Gentry, R., Birnbaum, S., Ruotolo, D., McManus, P., Skates, S., Ojemann, R., Rosenberg, A., Schiller, A., Koehler, A., and Suit, H. Fractionated proton radiation therapy of chordoma and low-grade chondrosarcoma of the base of skull. J. Neurosurg. 70, 13–17, 1989.
31 Slater, J.D., Austin-Seymour, M., Munzenrider, J.E., Birnbaum, S., Carroll, R., Klibanski, A., Riskind, P., Urie, M., Verhey, L., and Goitein, M. Endocrine function following high dose proton therapy for tumors of the upper clivus. Int. J. Radiat. Oncol. Biol. Phys. 15, 607–611, 1988.
32 Habrand, J.L., Austin-Seymour, M., Birnbaum, S., Wray, S., Carroll, R., Munzenrider, J., Verhey, L., Urie, M., and Goitein, M. Neurovisual outcome following proton radiation therapy. Int. J. Radiat. Oncol. Biol. Phys. 16, 1601–1606, 1989.
33 Cummings, B.J., Hodson, D.L., and Bush, R.S. Chordoma: The results of megavoltage radiation therapy. Int. J. Radiat. Oncol. Biol. Phys. 9, 633–642, 1983.
34 Berson, A.M., Castro, J.R., Petti, P., Phillips, L., Gauger, G.E., Gutin, P., Collier, J.M., Henderson, S., and Baken, K. Charged particle irradiation of chordoma and chondrosarcoma of the base of skull and cervical spine: The Lawrence Berkeley Laboratory experience. Int. J. Radiat. Oncol. Biol. Phys. 15, 559–565, 1988.
35 Duttenhaver, J.R., Shipley, W.U., Perrone, T.L., Verhey, L.J., Goitein, M., Munzenrider, J., Prout, G.R. Parkhurst, E.C., and Suit, H.D. Protons or megavoltage X-rays as boost therapy for patients irradiated for localized prostatic carcinoma: An early phase I-II comparison. Cancer 51, 1599–1604, 1983.
36 Dugan, T.C., Shipley, W.U., Young, R.H., Verhey, L., Althausen, A.F., Heney, N.M., McManus, P.L., and Abraham, E.H. Biopsy after external beam radiation therapy for adenocarcinoma of the prostate: Correlation with original histological grade and current prostate specific antigen levels. J. Urol. 146, 1313–1316, 1991.

37 Benk, V.A., Adams, J.A., Shipley, W.U., Urie, M., McManus, P.L. Efird, J.T., Willett, C.G., and Goitein, M. Late rectal bleeding following combined X-ray and proton high dose irradiation for patients with stages T3-T4 prostate carcinoma. Int. J. Radiat. Oncol. Biol. Phys. 26, 551–557, 1993.
38 Miralbell, R., Linggood, R.M., de la Monte, S., and Munzenrider, J. E. The role of radiotherapy in the treatment of subtotally resected benign meningiomas. J. Neurooncol. 13, 157–164, 1992.
39 Kjellberg, R.N., Hanamura, T., Davis, K.R., Lyons, S.L., and Adams, R.D. Bragg peak proton beam therapy for arteriovenous malformations of the brain. N. Engl. J. Med. 309, 269–274, 1983.
40 Fabrikant, J.I., Levy, R.P., Steinberg, G.K., Phillips, M.H., Frankel, K.A., Lyman, J.T., Marks, M.P., and Silverberg, G.D. Charged-particle radiosurgery for intravascular malformations. Neurosurg. Clin. North Am. 3, 99–139, 1992.
41 Miralbell, R. and Urie, M.M. Potential improvement of three-dimensional treatment planning and proton beams in fractionated radiotherapy of large cerebral arteriovenous malformations. Int. J. Radiat. Oncol. Biol. Phys. 25, 353–358, 1993.
42 Suit, H.D., Urie, M.M., and Efird, J.T. Proton beams in clinical radiation therapy. Principles & Practice of Oncology 6, 1–15, 1992.

12 Clinical Results of Proton Therapy in Russia

E. I. MINAKOVA

Institute for Theoretical and Experimental Physics, Moscow, Russia

Introduction

The clinical application of proton beams has been a subject of medical research in Russia for over 25 years. There are three proton therapy facilities in Russia in

- Dubna (the Joint Institute for Nuclear Research, JINR),
- Gatchina (the Institute for Nuclear Physics, INP) and
- Moscow (the Institute for Theoretical and Experimental Physics, ITEP).

Each of the three facilities has a different physical environment (Tab. 1) which has to some extent determined their clinical programs.

More than 3600 patients had been irradiated at these three facilities by June 1994.

The treatment categories can be grouped into four programs:

- a radiation oncology program which started in Dubna in 1967 and in Moscow in 1969.
- a radioneurosurgical and neurooncological program which started in Moscow in 1972 and in St. Petersburg in 1975.
- an endocrinological program (an important branch of the radioneurosurgical program) which started in St. Petersburg in 1975 and in Moscow in 1976.
- an oncoophthalmological program which started in Moscow in 1976.

Radiation Oncology Program

The radiation oncology program has been directed by the Cancer Research Center in Moscow. Clinicians from other medical centers, e.g., the Moscow Research Institute of Roentgenology and Radiology, the Research Institute of Urology took part in this program at various phases.

During the first phase of this research the physical, medical and technical equipment and the dose delivery system were tested under realistic conditions irradiating skin cancer, solitary soft-tissue metastases or metastases in lymph nodes (with the primary tumor cured), vulva tumors, etc. Visual control and histological post-irradiation investigations showed that morphological changes in the tumors and radiation reactions in tissues surrounding the target were adequate for the treatment plans.

The Early Phase

Among the earlier treatments were, e.g., 37 adult patients (75 % of them older than 60) with carcinoma of the vulva (clinical stage I–IV; $T_1N_0M_0$–$T_{4(m)}N_3M_0$) who were given combined radiotherapy: proton irradiation of the primary tumor at the ITEP and conventional irradiation of the locoregional lymph nodes. All patients had somatic counterindications to surgical treatment. In about 90 % of the patients clinical local control was achieved. The 5-year survival rate was 51 % without complications or treatment related morbidity. The combined proton therapy proved to be the only successful treatment for such cases [1].

Table 1. Three Russian Proton Therapy Facilities

Institution Place	Accelerator	Date of First Treatment	Reconstruction Interval	External Beam Data		Number of Treatment Rooms	Patient Total by June 1994
				Energy MeV	Max. Intens. pp s		
Institute for Theoretical and Experimental Physics (ITEP), Moscow	Synchrotron	1969 reopening 1975	1972–1975	70–200	2×10^{10}	3	2700
Joint Institute for Nuclear Research (JINR), Dubna	Synchrotron; Phasotron after reconstruction	1967 reopening 1987	1974–1987	660[a)]	2×10^{13}	3[b)]	>110
St. Petersburg's Institute for Nuclear Physics (INP), Gatchina	Synchrocyclotron	1975	–	1000 not variable	5×10^{9}	1	>850

a) The proton energy can be degraded down to 100–200 MeV.
b) There are also other beam channels: negative pions up to 80 MeV, neutrons of ca. 350 MeV and a reserve gamma-unit with a ^{60}Co-source.

It is known that proton beam irradiation ensures a much more favorable ratio of tumor to normal tissue dose for deep-seated tumors, in particular. The results obtained from the early investigations (approx. 100 patients) made it possible to begin assessing the treatment efficiency of broad proton beam therapy of malignant sinovioma, osteogenic sarcoma, of deeper seated tumors of the larynx, the cervix uteri, lung, esophagus and prostate.

First attempts to irradiate larynx cancer with protons failed. Large fractions (5.0–6.0 Gy per fraction, total dose of 75 Gy during 10 weeks) had to be applied due to the beam time schedule of the JINR accelerator. Complete primary tumor resorption was achieved, but late radiation complications with necrosis of the larynx cartilage occurred which made subsequent surgery necessary. Of a total of 14 patients, 6 lived three years and 3 lived 5 years after the irradiation without recurrence and metastases. Retrospectively, it is assumed that the complications were due to the fractionation regime. The high dose fractions very likely exceeded the tolerance of the delicate, regenerating larynx cartilage [2].

Single-Fraction Preoperational Irradiations

The results of single-fraction preoperational irradiations of limb osteogenic sarcomas (doses ≥ 100 Gy) at the ITEP proton synchrotron proved to be dramatic. The high intensity of the ITEP synchrotron beam made it possible to accumulate high doses rather fast even in large volumes. The goal was to ablate the radioresistant tumor before the amputation of the limb [3]. Approximately 3–10 months later all 14 patients had metastases in the lung. A subsequent analysis showed that the tumor boundaries in the limbs were not well

enough defined and that there were cold spots in the dose profile. In addition, some patients possibly had remote metastases prior to irradiation. It remained unclear, if proton irradiation is capable to ensure tumoricidal radiation doses.

The single-fraction presurgical irradiation of 16 patients with skin melanomas was more successful. More than half of them had disease-free survival periods of 5 years [2].

Cancer of the Cervix Uteri

Radiation therapy is the basic method for 90% of the patients with cervix uteri cancer and it is the only treatment for 75% of the patients in Russia.

Until June 1994 more than 180 patients with cervix uteri cancer in clinical stages I–III had been treated at the ITEP and the JINR. The first phase of the clinical trials comprised 110 randomly chosen patients for a combined preoperative transvaginal proton irradiation of the primary tumor in 3 large fractions and a conventional irradiation of the small pelvis (with protection of the uterus). A control group of patients was only administered to the standard conventional radiation therapy without proton boost. Total dose delivered to the tumor core (point "A") was 35–45 Gy for both groups.

No significant differences in the cumulative survival rates in trial (81%) and control (78%) group were observed during 15 years of follow-up period. Acute and late morbidity levels were acceptable.

A phase II unrandomized clinical investigation started in 1980, comparing a radical gamma-therapy or a combined proton-gamma therapy in more than 50 patients with cervix uteri cancer of stages I–III. The total dose at point "A" was 60–70 Gy. The survival rate was 88% after 3 years (some patients died due to remote metastases without local recurrence). A comparison of the results of the proton boost therapy with a combination treatment of intracavitary implants and external locoregional conventional irradiation showed no significant difference in the survival rate. The proton boost irradiation yielded, however, considerable improvements for the patients' quality of life: while proton therapy led to no complications at all, the combination of intracavitary implants with external irradiation resulted in rectitis and cystitis in 14–20% of the cases, and recto- and vesicovaginal fistulas in 1–5% of the cases, respectively. Moreover, proton transvaginal irradiation required no cervical canal expansion or premedication and decreased the irradiation times to 1–2 min [4].

At Dubna, this method was attempted in 26 patients.

Prostate Cancer

The first phase of the clinical trials to assess the efficacy of combined proton boost and conventional radiation therapy of pelvis-limited prostate cancer was performed between 1981 and 1985. For 17 patients with various clinical stages, a split-course scheme with X-rays and protons was set up.

The conventional external therapy was performed as standard "box" technique. Proton spread-out Bragg peak (SOBP) irradiations were performed using one transperineal portal.

The second phase of unrandomized clinical investigations with new clinical protocols for stages T_{1-2} and stages T_{3-4} was started in 1987. The proton boost therapy group comprised 88 patients. Control groups included patients administered to megavoltage photon irradiation (105 patients), and patients administered to a standard conventional external ^{60}Co gamma therapy only (68 patients). A comparative study of the 261 cases performed in 1990 revealed no statistically significant differences in complete and partial tumor regression rate between these methods for T_{1-2} stages. On the other hand, there was a pronounced advantage of combined proton-boost irradiation for advanced T_{3-4} cancer. The 5-year local recurrence-free survival rates were 87.5% for the proton group, 76.4% for the megavolt photon group and 69.8% for the ^{60}Co patient group, and remote metastases were established in 14.4%, 25.8% and 47% of the cases, respectively. Treatment-related morbidity included urological complications. They were 1.5%, 8.3% and 17.5%, respectively, for the different groups [5, 6]. Some patients were found to have bone metastases after 12–27 months.

In the case of cured primary foci and the presence of metastases of the skeleton, proton "hypophysectomy" was applied with the intention to relieve pain. Stereotactic proton irradiation of the pituitary (100–130 Gy in a single fraction) for advanced prostate cancer patients has been applied since 1972.

More than 100 patients with estrogen-resistant prostate cancer stages III and IV have since been irradiated at the ITEP. Proton "hypophysectomy" does not only lead to a recovery of the hormonal status with a response to estrogenic agents. It further ensures a mean survival of 20.6 months for incurable patients [7].

Cancer of the Thorax

In 1970, Dubna began to develop equipment and a proton therapy procedure for broad beam irradiation of thoracic tumors.

Until 1974 a total of 56 patients received treatment. There were 23 lung cancer patients and 33 cases of oesophageal cancer.

A group of 14 patients with peripheral lung cancer (stages II) or with solitary metastases in the lung (primary tumor cured) was involved in a phase I clinical trial using 130 MeV proton beams. Patients in a sitting position were irradiated twice a week (due to limited availability of the accelerator) with anteposterior fields and Bragg peaks superimposed in the tumor center. Tumor dose per fraction was 4 Gy, total doses were up to 52 Gy (tumor sizes μ 55 mm). 6 patients were irradiated preoperationally (lobectomy) with tumor doses of 27–33 Gy. Future studies will stipulate a more precise proton therapy of these tumors with rotational beam portals where the Bragg peak position will be controlled and adjusted in accordance with the proton range calculations based on calibrated computer tomography data.

Static multi-field and rotational proton irradiation was used to irradiate the esophagus tumors (clinical stages III–IV) in a phase I clinical trial. The tumors, situated in the middle third of the esophagus, ranged in size from 70–160 mm. The target doses were 4 Gy per fraction, two fractions per week, up to a total tumor dose of 48–60 Gy. Local radiation reactions did not differ from traditionally treated patients. Six and 3 patients were alive 1 and 3 years, respectively, after the irradiation. Local control and survival rate were comparable to conventional therapy. Proton beam therapy, however, did not cause serious side effects, as were observed after conventional radiation therapy of lung and esophagus tumors [8]. Five more patients with esophageal cancer had been irradiated until June 1994, after extensive reconstruction of the accelerator.

For these cases a new method was used. The esophagus was irradiated with the proton beam moving in several steps along the target length. The Bragg peak position was matched to the tumor using the signal from a miniature removable silicon diode, inserted into the esophagus. The radiological depth from the patient's surface to the tumor was first measured for every single angular position. The data were then used to set the Bragg peak position with the beam energy degrader in the sessions to follow. The reproducibility of the patient's position was checked with X-ray computer tomography [9]. The clinical results have not yet been reported, but the method described seems to be challenging for the treatment of such tumors.

Breast Cancer

According to statistical data, lung, stomach, skin and breast cancer are the most frequent localizations of malignant tumors in Russia. The high frequency of breast cancer was also a reason to look into proton therapy in order to improve the results of radiation treatment. Single-session pituitary stereotactic proton irradiations of patients with generalized breast cancer began in Moscow in 1972 [10]. 100 incurable patients with generalized breast cancer were treated until 1979. Fast pain relief in the skeleton – in 70% of the patients – objective stabilization or resorption of bone metastases, and improved quality of life were reported [11]. This method was later widely used in Moscow as part of a combined radiation treatment of breast cancer ("hypophysectomy" with proton beams at the ITEP plus conventional ^{60}Co or proton irradiation of the lymph nodes, soft tissues, bones and solitary liver metastases).

The mean survival reached 36.4 months in a group of more than 190 patients [12].

Direct irradiation of primary nodal breast cancer with SOBP was started in 1982. Proton therapy was the only treatment for 18 patients ($T_{1-2}N_0M_0$). All patients had 5-year local recurrence-free survival without remote metastases. All women had a good cosmetic effect and organ preservation.

Another 87 patients ($T_{1-4}N_{1-3}M_{0-1}$) were treated using both combined proton boost therapy and photon irradiation of the whole breast and eventually any locoregional metastases. The full course of radiation was given within 11–14 days. Patients having bone metastases, were administered to the proton stereotactic "hypophysectomy", as well. 78% of the patients in this group were alive for more than 4 years. A comparison of the clinical results of the proton boost therapy (in combination with pituitary suppression) with conventional procedures proved the advantage of protons in the therapy of nodal breast cancer in $T_{1-2}N_{0-3}M_{0-1}$ stages [13].

Since 1975, the Central Research Institute of Roentgenology and Radiology (CRIRR) in St. Petersburg has treated 102 patients with generalized and 48 patients with primary, locally disseminated breast cancer ($T_3N_2M_0$–$T_{4B}N_{1-2}M_1$) and different metastases, by means of proton "hypophysectomy" plus external conventional irradiation of the primary tumor and the metastases. A 5-year survival rate of more than 30% was reached in the second group [14].

Radioneurosurgical and Neurooncological Program

For more than two decades proton beams have been used in Russia for the treatment of benign and malignant brain diseases. The program is jointly coordinated by the Burdenko Neurosurgical Institute in Moscow and the Polenov Neurosurgical Institute in collaboration with the CRIRR in St. Petersburg. The experience of these centers exceeds 1500 cases.

Narrow (5–30 mm diameter) proton beams, have been used for the following indications:

1. Stereotactic radiosurgery of vascular diseases of the brain.
2. Stereotactic large-fraction proton therapy of intracerebral, deep-seated, midline malignant and benign tumors.
3. Stereotactic proton radiosurgery of pituitary adenomas.
4. Functional stereotactic radiosurgery.

Stereotactic proton radiosurgery of the pituitary gland ("normal" and adenomatous) proved to be a highly efficient treatment for a variety of endocrine and hormone-dependent metabolic states (including hormone-responsive metastatic cancer), so that these directions formed a separate endocrinological proton therapy program (in collaboration with the Endocrinological Research Center in Moscow and the Institute for Advanced Medical Training in St. Petersburg).

Two techniques of proton irradiation were applied:

- through-and-through technique, with unmodulated high energy (200 and 1000 MeV) proton beams using the plateau of the depth dose curve,
- Bragg peak irradiation using the unmodulated or spread-out Bragg peak (180 MeV, Moscow).

Arteriovenous Malformations

Arteriovenous malformations (AVMs) are the traditional target for stereotactic proton radiosurgery world-wide (cf. as well Chapter 16). Approximately 330 angiographically visible AVMs have been irradiated in St. Petersburg since 1978 and Moscow since 1983.

Deep-seated, inoperable AVMs or AVMs located in functionally important areas of the brain have usually been treated by stereotactic proton therapy alone. In some cases intravascular embolization of the AVM feeder vessels or a partial resection of the AVM was carried out prior to proton therapy.

A single through-and-through irradiation has been used at Gatchina. The preradiosurgical volumes of the malformations ranged from 1 to 10 cm^3 in the main group. The size of a single irradi-

ated area was 5–10 mm (included in 50% isodose), and the maximum dose varied between 40 and 80 Gy. In some cases 2–3 fields of irradiation were used.

In almost 50% of the cases, the AVMs were located in the medio-basal region of the brain. The highest number of patients with complete response was observed among those who had malformation volumes of less than 2.0 cm^3 (68%), while complete obliteration was angiographically documented in only 38%, when the malformation volume was 10 cm^3. Neither treatment-related complications, nor decline of neurological symptoms was recorded. The first experience with the treatment of cerebral arterial aneurysm (6 patients) was unsatisfactory, presumably due to the fact that the dose level was kept very low in order not to risk vessel breakage [15, 16].

Bragg peak proton radiosurgery has been used for AVM treatment in Moscow. Preradiosurgical volumes of the malformations varied from 1–48 cm^3. Bilateral opposed portals (6–8) and narrow beams (15–30 mm diameter) were used. The target was included in the 50–80% isodose of the resulting dose field. The dose level (usually 30–50 Gy in 1 or 2 fractions) was chosen according to size and location of the target (brain stem, thalamus, corpus callosum, basal ganglia, some critical areas of the cerebrum cortex).

Total obliteration rate was approximately 60% for all volumes of AVMs, partial obliteration was observed in 25%. For larger and partially irradiated AVMs different degrees of thrombosis of the pathological vessels were observed. Four cases of serious radiation reactions of the brain occured (AVMs located in the wall of the ventricle of the brain and in the basal ganglia) which could be treated by drugs only [17, 18].

Spontaneous Arteriosinusal Fistulas

Another type of vessel pathology cured with proton beams in Moscow are spontaneous arteriosinusal fistulas of the cavernous sinus (sASF) causing severe changes in eye and orbit (40 patients since 1983). Single-session plateau irradiations were performed with 50–60 Gy (beam diameter up to 12 mm). Within short time ophthalmological and neurological improvement or complete recovery was observed in almost all cases. No complications were recorded. Angiography revealed total and partial obliterations in 95% of the cases [18, 19].

Meningiomas

For large fraction proton therapy meningiomas of the cavernous sinus were chosen as primary indication because complete surgical resection is very often impossible and they are too radioresistant for conventional radiation therapy alone. Depending on the size and shape of the tumors, spread-out Bragg peak or through-and-through methods were used for the treatment of approx. 80 patients in Moscow since 1982. Tumors, mostly 20–30 mm in diameter, were treated with 60–70 Gy in 2–4 fractions during 1 or 2 weeks. The target margin was usually confined within the 50% isodose. In some cases the treatment was postoperational.

Total clinical effectiveness (stabilization and improvement of symptoms) was achieved in 87% of the observations. Objective local control (CT-assisted follow-up) was recorded in 84% of the cases. There was no case of damage to the sensitive anatomical structures of the cavernous sinus. Some relapsing meningiomas were only partially irradiated. In one case (female patient with a tumor of more than 35 mm in diameter) the irradiation resulted in brain necrosis. A total dose of 68.7 Gy was delivered in 3 fractions from 5 portals in ipsilateral temporofrontoparietal region during 10 days. Treatment related morbidity symptoms and objective images (CT and MRI) indicating brain damage were obtained 2 months later. The patient received three courses of medicinal therapy and 8 months later the clinical symptoms had completely disappeared as did the abnormal changes of the CT [20, 21].

Narrow proton beams do not only help to overcome the radioresistance of meningiomas. They permit to irradiate selectively tumors with orbital spreading.

The following beam conditions were used in these cases: frontal through orbit (1 portal),

through lobe area (2 portals) plus through parietooccipital regions of the skull (4 portals). Thereby, it was possible to create a dose field which optimally covered both the intracavernous part of the tumor and its intraorbital part.

The patients were irradiated in blind-eye side lying position. The total dose of 50–65 Gy was delivered in 3 fractions (dose on eye: 6 Gy). Pain remission, regression of exophthalmus and restitution of proper eye movement was observed after the irradiation [17, 22].

Besides meningiomas, some other histological types of tumors of the cavernous sinus were treated such as pituitary adenoma invading parasellar structures and pseudotumoral Tolosa-Hunt Syndrome. Patients with steroid-resistant recurrent Tolosa-Hunt Syndrome recovered completely after the irradiation of their cavernous sinus and they remained without local recurrence for periods up to ten years [23].

Other Intracerebral Tumors

Large-fraction proton therapy is a very promising treatment for small intracranial tumors, particularly for those which are inaccessible to open radical surgery. The following types of tumors fall into this category: primary intracerebral low-grade glioma, germinoma, pineocytoma, hamartoma, various craniopharyngiomas (17 patients in total), secondary metastatic tumors of the brain (4 patients) in Moscow. The specific location of these targets (pineal region, internal capsule, brain stem, third ventricle, basal ganglia) and the vicinity to critical normal tissues are the limiting factors for conventional therapy. Spread-out Bragg peak stereotactic large fraction proton therapy with beam diameters of 20–30 mm doses of 30–60 Gy was used. The treatment was delivered in 2–4 fractions within 1–2 weeks. The target was usually included in the 50%–80% isodose. The proton irradiation was complemented with conventional radiation in some cases.

The best results were obtained with the very radiosensitive germinomas. The tumors disappeared completely within two weeks. Pineocytomas and hamartomas disappeared within 1–1.5 years. Patients with metastases of lung carcinoma responded well to the combined radiation treatment. The size of astrocytomas grade I (remnant after surgery) started to decrease 6 months after the proton irradiation. Acute and late morbidity was acceptable, treatment-related mortality was not recorded [21].

Pituitary Adenomas

The first intracranial tumors to be treated with proton beams in St. Petersburg and Moscow were pituitary adenomas. Twenty years of clinical experience have revealed that proton irradiation is best suited for microadenomas, macroadenomas with endosellar localization and no or only local invasion of the dura mater and for adenomas with a little suprasellar extension or sharply asymmetrical parasellar growth. For the latter two indications it is necessary to use Bragg peak irradiation. Precise irradiation must be used for radical treatments of hormone-secreting and non-secreting adenomas with curative intent and for the irradiation of unresected parts of the tumor (after non-radical surgery).

If contraindications to surgery exist, partial irradiation of large adenomas might be recommended to minimize the mass syndrome (palliative radiation therapy). There are no age-related or somatic contraindications to stereotactic proton therapy of pituitary adenomas [24].

The total number of observations amounts to approx. 300 in St. Petersburg and 650 in Moscow. Stereotactic through-and-through radiosurgery is used in Gatchina, while both through-and-through and Bragg peak irradiations are used in Moscow.

The largest group – more than 500 patients – were diagnosed with Cushing disease. These patients were generally treated with 70–100 Gy in a single fraction.

More than 90% of the patients examined had complete clinical and biochemical remission wich lasted for many years of follow-up. No hormonal replacement therapy was necessary and no radiation-induced tumors were observed [25]. Today, proton pituitary irradiation complements the complex treatment of Cushing disease including medicinal and hormonal treatment and, if necessary, one-sided adrenalectomy.

The second largest group (a total of about 320 in both centers) were patients with acromegaly. For targets less than 15 mm in diameter a similar through-and-through technique was used as in the case of the pituitary adenomas. Patients with adenomas larger than 15 mm were treated with the Bragg peak technique. The maximum dose of 50–120 Gy was delivered in 1–3 fractions within 1–2 weeks.

Clinical and metabolic improvements were observed for 50% of the patients within the first year and for 80% after 3–5 years with normalization of the serum growth hormone level. The results depended, e.g., on tumor size, the presence of suprasellar or parasellar tumor spread, and the invasion of the dura mater.

Nelson's syndrome, prolactinomas, thyreotropinomas, non-functioning adenomas did not differ significantly from the well-known radiation experience of proton therapy of pituitary adenomas (cf. as well Chapter 16). Transient complications (extraocular palsies) were exceptional. When local failure was indicated by a definite increase of the tumor volume in CT or MRI scans, the irradiation was repeated and in some cases transnasal surgery was performed [21, 26]. The improved anatomic resolution which is now possible with CT and MRI scanning provides better localization of pituitary adenomas and a more accurate assessment of extrasellar tumor extensions. This should result in an improved local control rate and less treatment failures due to unsatisfactory treatment planning.

More than 50 patients with diabetic proliferative retinopathy and progressive endocrine ophthalmopathy treated with through-and-through technique (100–120 Gy) in St. Petersburg and Moscow showed stabilization and regression of their retinopathy and visual acuity was preserved or improved. Patients with progressive ophthalmopathy responded less favorably [26].

Functional Brain Disorders

Stereotactic proton radiosurgery of functional disorders of the brain is not extensively developed in Russia. The number of patients in these categories is very limited (5 patients with epilepsy in St. Petersburg and 1 patient with epilepsy and 2 observations of trigeminal "gangliotomy" in Moscow). The proton therapy experience in this field has not yielded clear answers as to the value of the technique. However, it can be assumed that modern methods of diagnostics and localization of epileptic foci and small functional structures will provide a possibility for more precise stereotactic proton radiosurgery [26].

Oncoophthalmological Program

The program started in 1977 after a series of preclinical studies with animals. Narrow proton beams from the ITEP synchrotron were used for precision radiation therapy of malignant eye tumors. This clinical program is headed by the Moscow Helmholtz Institute of Eye Diseases. More than 570 patients were administered to Bragg peak proton therapy during 17 years. Eye tumor patient follow-up varied from 1 to 12 years.

Melanoma or cancer of the eye lid and conjunctivae ($T_3N_0M_0$–$T_{3-4}N_1M_0$) with the extension to the upper or lower vaults located on the edge of the cornea, the epicanthus and lacrimal carunculae. The tumors' diameter and height were 18–20 and 6–8 mm, respectively. Large-fraction irradiation consisted of 3–5 fractions per week, 15–20 Gy per fraction up to a total dose of 60–100 Gy.

Local control, i.e., complete or partial resorption and stabilization, was 97% for eye lid cancer and 98% for conjunctival cancer. The eye was preserved in 95% of the patients. Exenteration had to be performed in 2.3% of the patients who showed no treatment effect. Proton therapy was therefore an alternative tool for exenteration operation of the orbit and enucleation of such tumors [27].

Intraocular melanoma ($T_{2-3}N_0M_0$) of the ciliary body and choroid (more than 100 patients) is routinely treated as a one-field irradiation. 15 Gy are administrated per fraction, 4–5 fractions are given during a 2-week period (total dose: 60–80 Gy).

Local control was recorded for 78% of the cases during a 7-year period (22.4% complete, 55.6% partial resorption and stabilization). In

22% of the observations – corresponding to tumors of more than 15 mm in diameter – no response was recorded and enucleation had to be performed. Visual functions were preserved in 50% of the patients with the preserved eye. Some patients had postirradiational glaucoma. Mortality following distant metastases amounted to approx. 10%. Proton therapy of such tumors is clearly seen as a meaningful alternative to enucleation of the diseased eye [28].

Fifty percent local control was achieved in patients treated for secondary malignant orbital tumors after enucleation following melanoma of the choroid after 5–7 years. The patients were irradiated in a sitting upright position using one portal and Bragg preak irradiation mode. The procedure consisted of 4–5 fractions given within 8–10 days. The tumor (maximum diameter 12–30 mm) was included in the 80% isodose. The total tumor doses amounted to 80–100 Gy. This method was developed as an alternative to the crippling interference-subperiosteal exenteration of the orbit [29].

Conclusion

Both, organizational and technical conditions of the clinical work at the Russian proton facilities have not been optimal for the treatment of patients. First, the present proton therapy facilities are away (5–150 km) from the specialized clinical centers which host the patients during pre- and post-irradiation periods. The non-medical accelerators have had peculiar time schedules and unstable running conditions which often interfered with traditional fractionation schemes and finally, the fixed horizontal beam lines greatly reduced the number of accessible portals. A number of other technical problems have also limited the types of clinical indications for proton therapy.

At the ITEP the technical circumstances are slightly more suitable for clinical practice. As a result 75% of all Russian patients have been irradiated here and ITEP has turned out to be the only center in Russia to run all four clinical programs.

Technical, economical and organizational solutions to overcome the difficulties characteristic for the first stage of proton therapy have been found. Particularly designed medical accelerators with rotational gantries and techniques for 3D-conformal therapy provide an optimistic outlook on proton therapy. The technical capabilities of proton therapy do not differ from those of modern electron accelerators. However, all the advantages of proton beam irradiation prevail [30, 31].

The practical basis of a new phase of proton therapy in Russia will be the construction of a special proton therapy facility at the Moscow Cancer Research Center, designed at ITEP.

Acknowledgement

I am very grateful to Drs. Khoroshkov and Breev for their assistance in preparing this article, and to all the clinicians and physicists for their efforts and patience in treating more than 3600 patients.

References

1 Kiseleva, V.N., Ruderman, A. I., and Lebedev, A.I. The use of proton beam at the ITEP in the treatment of oncogynecological patients. J. Voprosy oncologii 6, 34–41, 1983 (Russ.).
2 Ruderman, A.I. Proton therapy experience in the USSR, in Proc. I. Int. Seminar on The Uses of Proton Beams in Radiat. Therapy, Atomizdat; Moscow, 1979, Vol. 3, pp. 3–10.
3 Blokhin, N. N., Ruderman, A.I., Trapeznikov, N.N., and Yarmonenko, S.P. New approaches to preoperative irradiation of malignant tumors. J. Vestnik AMS USSR, 3, 46–49, 1971 (Russ.).
4 Kiseleva, V.N., Ruderman, A.I., Lomanov, M.F., Lebedev, A.I., and Sorokina I.I. Long-term results of cervix uteri cancer therapy using proton beam irradiation, J. Med. Radiol. 6, 49–54, 1988 (Russ.).
5 Makarova, G.V., Ratner, T.G., Cheban, N.L., Mazurov, S.T., and Shuvalov, E.L. Clinical trials of X-ray and proton therapy for prostatic carcinoma. Preliminary Results of Therapy in Phase I-II studies, J. Cancer Res. Clin. Oncol. 116, 505, 1990.
6 Makarova, G.V., Ratner, T.G., Shuvalov, E.L., Cheban, N.L., and Romanov, V.A. Do protons improve the prostate cancer local control? Preliminary clinical analyses, in Proc. Proton Radiotherapy Workshop. Blattmann, H. (ed.), PSI-Report 111, 1991, p. 121.

7 Lopatkin, N.A., Khazanov, V.G., Minakova, E.I., and Krymsky, V.A. Proton irradiation of the pituitary in combined antiandrogenical treatment of cancer of the prostate. J. Khirurgia 3, 1–3, 1988 (Bulg.).

8 Astrakhan, B.V. Radiation therapy of oesophagus and lung cancer at the medical proton beam of the JINR Laboratory of Nuclear Problems, in Proc. I. Int. Seminar on the Uses of Proton Beams in Radiat. Therapy, Atomizdat, Moscow, 1979, Vol. 3, pp. 140–148.

9 Abazov, V.M., Astrakhan, B.V., Budjashov, Yn.I., Molokanov, A.G., Mytsin, G.V., Poidenko, V.K., Savchenko, O.V., and Zorin, V.P. Medical facility for radiation therapy with JINR proton phasotron beams. Communication JINR, Dubna, 1994.

10 Minakova, E.I. Single large-dose proton irradiation of the pituitary for dyshormonal malignant tumors, in High Energy Proton Beams and Radiation Therapy of Malignant Tumors. Preprint JINR, E-9035, Dubna, 1975, pp. 124–141.

11 Minakova, E.I., Davidova, I.G., Savinskaya, A.P., Shuvalov, E.L., Karetnikov, Yu.P., Chaklina, E.A., and Kamchatova, N.A. Clinical and physiological analysis of the results of pituitary proton irradiation of patients with dyshormonal tumors, in Proc. I. Int. Seminar on the Uses of Proton Beams in Radiat. Therapy, Atomizdat. Moscow, Vol. 3, 1979, pp. 36–48.

12 Monzul, G.D. and Ryabukhin Yu.S. Combined treatment of disseminated breast cancer with proton irradiation of the pituitary and zone gamma-ray teletherapy of the skeleton. J. Voprosy Oncologii 4, 427–433, 1990 (Russ.).

13 Monzul, G.D., personal communication.

14 Konnov, B.A., Konnova, L.A., and Melnikov, L.A. Proton "hypophysectomy" in patients with locally disseminated mammary carcinoma. J. Med. Radiol. 2, 45–47, 1994 (Russ.).

15 Melnikov L.A., Konnov B.A., and Yalynych, N.N. Radiosurgery of cerebral AVM, in Proc. Int. Workshop on Proton and Narrow Photon Beam Therapy. Oulu, Finland, 1989, pp. 92–95.

16 Konnov, B.A., Yalynych, N.N., Melnikov, L.A., Garmashov, Yu.A., and Pak, V.A. Proton stereotactic therapy of arteriovenous malformations of the brain. J. Med. Radiol. 10, 4–6, 1993 (Russ.).

17 Minakova, E.I. Review of twenty years of clinical proton therapy experience in Moscow, in Proc. 2nd Int. Charged Particle Therapy Workshop, Loma Linda, 1987, pp. 1–23.

18 Krymsky, V.A., Minakova, E.I., and Luchin, E.I. Proton beam irradiation of spontaneous arterio-sinusal fistulas of the cavernous sinus and deep-seated cerebral arteriovenous malformations, in Proc. Int. Workshop on Proton and Narrow Photon Beam Therapy, Oulu, Finland, 1989, pp. 101–102.

19 Krymsky, V.A., Serbinenko, F.A., Minakova, E.I., Luchin, E.I., and Rubtzova, E.A. Ophthalmological symptoms regress after proton irradiation of the arteriosinusal fistulas in the cavernous sinus, in Report Abstr. Int. Symp. Diseases of the Orbit, Moscow, 1989, pp. 149–151 (Russ.).

20 Luchin, E.I., Minakova, E.I., Krymsky, V.A., Gabibov, G.A., and Valsky, V.A. Stereotactic proton beam radiation therapy of cavernous sinus meningiomas, in Proc. Intern. Heavy Particle Therapy Workshop. Blattmann H. (ed.), PSI-Bericht-111, 1991, pp. 163–166.

21 Minakova, E.I., Luchin, E.I., Kirpatovskaya, L.E., and Shishkina, L.V. Narrow proton beam stereotactic radioneurosurgery and large-fraction radiotherapy at ITEP. Clinical results. Int. J. Radiat. Oncol. Biol. Phys. 1995, in press.

22 Luchin, E.I., Minakova, E.I., and Krymsky, V.A. Proton beam irradiation of cavernous sinus meningiomas, in Int. Workshop on Proton and Narrow Photon Beam Therapy, Oulu, Finland, 1989, pp. 99–100.

23 Luchin, E.I., Minakova E.I., and Krymsky, V.A. Proton beam irradiation effect in Tolosa-Hunt syndrome. J. Med. Radiol. 8, 55–57, 1987 (Russ.).

24 Minakova, E.I., Twenty years clinical experience of narrow proton beam therapy in Moscow, in Proc. Int. Heavy Particle Therapy Workshop. Blattmann H. (ed.), PSI-Report 69, 1990, pp. 154–157.

25 Marova, E.I., Starkova, L.E., Kirpatovskaya, L.E., Kolesnikova, I.S., Bukhman, A.I., Rozhinskaya, L.Ya., and Belchenko L.V. Results of treatment of Icenko-Cushing disease with proton beam irradiation of the pituitary body, J. Med. Radiol. 8, 42–49, 1987 (Russ.).

26 Konnov, B.A., Melnikov, L.A., Zargarova, O., Lebedeva, N., Yalynych, N.N., and Karlin, D. Narrow proton beam therapy for intracranial lesions, in Int. Workshop on Proton and Narrow Photon Beam Therapy. Oulu, Finland, 1989, pp. 48–55.

27 Brovkina, A.E. and Zarubey, G.D. Management of ocular tumors with a medical proton beam. J. Med. Radiol. 8, 61–66, 1987 (Russ.).

28 Brovkina, A.F. and Zarubey, G.D. Ciliochoroidal melanomas treated with a narrow medical proton beam. J. Archiv. Ophthal. 104, 402–404, 1986 (Russ.).

29 Zarubey, G.D. and Kubynina, N.A. Possibilities of proton beam therapy for the treatment of secondary malignant orbital tumors, in Report Abstr. Int. Symp. Diseases of the Orbit, Moscow, 1989, pp. 149–151 (Russ.).

30 Minakova, E.I. and Monzul, G.D. Perspectives of clinical investigations in the Moscow Proton Therapy Facility, in Proc. Proton Radiotherapy Workshop. Blattmann, H. (ed.), PSI-Report 111, 1991, pp. 109–112.

31 Minakova, E.I. The Russian Proton Therapy Program, in Hadrontherapy in Oncology, Amaldi. U and Larsson, B. (eds.), Proc. Int. Symp. Hadronther. Como, Italy, Oct. 18–21, 1993, Elsevier, Amsterdam, 1994, pp. 102–108.

13 Treatment of Eye Tumors

P. CHAUVEL

Biomedical Cyclotron and Radiotherapy Department, Centre Antoine-Lacassagne, Nice, France

Introduction

A close collaboration between the Massachusetts Eye and Ear Infirmary, the Massachusetts General Hospital Department of Radiation Medicine and the Harvard Cyclotron Laboratory gave rise to the treatment of eye tumors (mainly uveal melanoma) using a proton beam in July 1974 in Boston (Massachusetts). In 1978 the Lawrence Berkeley Laboratory (Berkeley, California) started treatments using helium ions the characteristics of which are close to those of protons. In 1984, Continental Europe joined this effort with the opening of the OPTIS facility at the Paul Scherrer Institut (formerly SIN) in Villigen, Switzerland. Since then, a constant increase in the number of facilities treating eyes has been noted: Clatterbridge (United Kingdom) and Uppsala (Sweden) in 1989, Loma Linda (California, USA) in 1990, Nice and Orsay (France) in 1991. Up to now the total number of patients treated in these institutions is around 5500.

Uveal Melanoma

Epidemiology and Natural History

Uveal melanomas are infrequent tumors usually occuring in the second part of life (mean age in our series of 450 treated patients: 56 years) mainly in whites. In 1947, incidence in the USA was reported to be 5.2 per million and year [1]. For the period 1942–53, Jensen reported an incidence in Denmark of about 7.5 per million and year [2]. A study by Wilkes et al. [3] found a significant difference for the incidence in people under the age of 50 (3/1M/year) and over 50 (21/1M/year). Uveal melanomas are much less frequent than choroidal nevi reported to range from 1 to 2% in various clinical studies to 6.5% in eyes studied post-mortem [4, 5].

Diagnosis and Staging

The diagnosis of uveal melanoma is generally performed by specially trained ophthalmologists working in ocular units. The diagnosis is essentially based on non-invasive modalities, because these intraocular tumors are not readily accessible to biopsy. Clinical examination, including indirect ophthalmoscopy is associated to slit-lamp biomicroscopy, fundus photos, fluorescein angiography, ultrasonography (A and B scans), to assess the nature of the tumor. CT scan and magnetic resonance imaging are often performed not only to help the diagnosis but to have a better representation of the tumor shape, size and relationship to adjacent structures.

Physical examination, liver function tests and/or liver ultrasonography or CT scan are also performed before the treatment, to evaluate the metastatic situation. These examinations allow diagnosis and staging. In the TNM classification, the stage is mainly based on tumor dimensions as listed in Table 1. Nodal and metastatic extensions are quoted as present or not.

Cytological data obtained from fine needle aspiration refine the prognosis: spindle cell melanomas are less aggressive (mortality within 5

Table 1. Tumor classification on the basis of the tumor dimensions

	Diameter r [mm]	Thickness d [mm]
T1 a	≤ 7	≤ 2
T1 b	$7 < r \leq 10$	$2 < d \leq 3$
T2	$10 < r \leq 15$	$3 < d \leq 5$
T3	> 15	>5
T4	extrascleral extension	

years 15%) than epithelioid tumors (mortality within 5 years 40 to 60%) and mixed tumors have an intermediate degree of malignancy. The site of the tumor may also affect the prognosis: ciliary body tumors are generally larger, more likely to metastasize and to yield complications [6].

Therapeutic Approaches Other Than Ion Beam Therapy

During the last 20 years the treatment possibilities have changed a lot. Proton therapy, new isotopes available for brachytherapy and elaborate local excision procedures have come up during this time. Due to the rapid advancement of these techniques, their relative place in the whole spectrum of treatment modalities is more and more difficult to assess.

The treatment policy of uveal melanoma remains rather controversial, depending on the characteristics of the tumor, the accessibility of the different techniques and on the specialist to whom the patient is referred. This seems to be mainly due to the fact that the long term survival results are only partly influenced by a successful local treatment and that there is no clearcut definition when to use which procedure. This means that, for instance, the chances of local control of a retro-equatorial uveal melanoma 5 mm thick and 10 mm in diameter, will be the same using local resection, brachytherapy or proton therapy. But these chances are certainly different if one of the techiques is performed by a not sufficiently trained team. In that case, the best choice of treatment is the best expert!

Surgery

For a long period surgery was the only treatment for uveal melanomas, and it meant almost exclusively enucleation and exenteration. Progress in knowledge, instrumentation and new techniques have improved the situation. Whereas early stage melanocytic tumors, presumably malignant and apparently dormant seem to justify a simple periodic observation, all other tumors have to be treated as early as possible in order to decrease the metastatic rate, and their stage determines the respective procedure.

Photocoagulation

Xenon or argon lasers [7–9] may be used for the treatment of small flat tumors (excluding the ciliary body) if they are at least 2 mm away from the optic disc or the fovea. 65% complete regression and acceptable visual outcome were reported for these kinds of tumors [10]. But photocoagulation should be mainly considered as salvage treatment for limited, flat, marginal relapses occurring after either brachytherapy or proton therapy. The risk of metastasis is comparable to that after enucleation [9].

Local Resection

Since 1972, surgical procedures have been developed for some limited tumors which allow to resect the malignancy while sparing the vision [11–13]. The techniques vary from full thickness eye wall resection to more conservative procedures [14] sparing retina and external sclera. It is difficult to give formal results for these procedures, as the patient numbers are still small and the follow-up periods short. Nevertheless, the majority of the patients seem to retain a diminished but useful vision without major complications and the local control seems to be as good as for proton therapy. The classical indications for local resection are small anterior tumors, but some ophthalmologists have started to perform larger tumor resections, as well.

Enucleation

For a long time, enucleation was the only possible treatment of uveal melanoma. The survival rate was 40% over the untreated patient series [15],

justifying the mutilation. But the place of enucleation remains controversial [16–18], not the least due to the work of Zimmerman and associates [19–22]. They showed a peak mortality of 8% 2 years after enucleation as compared to a death rate of 1% per year in non-enucleated patients. This increase was attributed to metastases, and it was thought that the surgical procedure could play a role in cell spreading. Therefore, no-touch techniques were described [23–25] and are widely used nowadays in order to prevent this possibility. Despite these careful procedures metastatic death occurs in 30 to 45% of the patients and it is presently impossible to know if surgery gives more metastasis than conservative treatments. Some randomized clinical trials are in progress and will perhaps clear up the problem. Combined with prothesis, enucleation is cosmetically acceptable for the treatment of large tumors.

Exenteration

This substantial procedure remains the only possible approach in case of large extraocular extensions invading the orbital content and/or eyelids [26] as primary or salvage treatment.

Brachytherapy

In 1929, Moore [27] treated the first patient (a monophthalm) by implantation of radon seeds into the sclera in front of the tumor. This treatment led to tumor regression. In 1932, Stallard used the same isotope in a wax shell. Sixteen years later, he began to use cobalt plaques sutured to the sclera next to the tumor [28–30]. From a series of 100 patients 69 were successfully treated, and 16 were enucleated. Lommatzsch [31] developed a new plaque using 106-ruthenium (106Ru/106Rh), a β-emitter which reduced the dose to non-target tissues. The survival rate of patients with tumors distant from disc and/or macula (> 1 to 2 diameters), less than 5 mm thick and 15 mm wide was comparable to that of an enucleation series. 18% of the eyes were enucleated following brachytherapy (70% spindle cell tumors). 26% of the patients retained a vision of >5/10. These results [32] were considered encouraging and the plaque technique grew up. Packer [33] introduced 125-iodine-impregnated gold scleral plaques which were initially described by R. Sealy [34]. They have become the standard for the Collaborative Ocular Melanoma Study (COMS) in the United States [35]. Their choice is based on sound scientific principles: 125-I can totally be shielded, minimizing the radiation hazard to the clinical personnel; it allows a marked reduction of the radiation dose laterally and posterior to the plaque, and it has demonstrated its effectiveness to promote tumor shrinkage.

It was hoped that 125-I-plaques would lower the incidence of radiation retinopathy and optic neuropathy observed with other radiation sources. However, it turned out that the long-term evaluation was not so favorable. A progressive increase in complications was observed for good short-term results with a fast tumor shrinkage [36]. In a series of 64 patients with a mean follow-up of 65 months, 95% had a tumor ≤ 8 mm. The local recurrence rate was 12.5% (8/64); 17% of the patients died of metastasis, neovascular glaucoma developed in 11%, radiation retinopathy in 23% and cataract in 45%. 17% of the patients required enucleation for either tumor growth or neovascular glaucoma. Some recurrences might be explained by technical inadequacies, including insufficient plaque size, as initially, the plaques were only 1 mm larger than the tumor base diameter.

Considering that the tumors treated by brachytherapy are generally smaller than those referred to charged particles, the complication rates are significant and certainly not superior to those of protons.

Ion Beam Therapy

General Considerations

The incentive to use ions in radiotherapy is to treat the tumor volume with a homogeneous dose distribution while decreasing the dose delivered to healthy surrounding tissues. The particular depth dose curve of protons and heavier ions gives two important advantages: a low entrance dose and a sharp distal fall-off at the end of the

particles' range. In addition to these characteristics, the possibility to spread the Bragg peak very homogeneously to yield a flat depth dose distribution all along the tumor thickness is a very useful feature. The length of this plateau can be adapted to the length of the target volume, from the whole path to a small portion (Fig. 1).

The treatment of eye tumors has been among the first applications of ion beams. The small volume of this sense organ and the close vicinity between tumor and critical structures such as optical disc and nerve, macula, and lens have been a challenge for the potential advantages of this technique.

Fiducial Placement

Uveal melanomas are usually invisible and always radiotransparent. Therefore, markers have to be inserted into the eye to permit tumor measurement and irradiation modelling. After opening the conjunctiva under general anaesthesia, the ophthalmologist looks for an extrascleral extension and then, after locating the tumor base by transillumination, sutures four to five 2.5 mm diameter tantalum rings (clips) around the tumor periphery. The set-up of the clips may be verified by indirect ophthalmoscopic examination, using an indentator to push the clips which become visible as protrusion under the retina.

Once the clips are sutured, the distances between the clips and the tumor base and the clips and the limbus can be measured. These measurements will be compared to those calculated by the treatment planning system. The clips are the only evidence of the tumor in the eye. A clear drawing of tumor and clip position is made and if possible the clip position is marked on a fundus photo. After the surgical procedure an ultrasound measurement of the distances between clips and optic disc is recommended, if the tumor is close to the posterior pole or reaches it.

Treatment Simulation

The treatment of eye tumors with proton beams requires a very accurate determination of the tumor volume, shape, site, relationship to critical

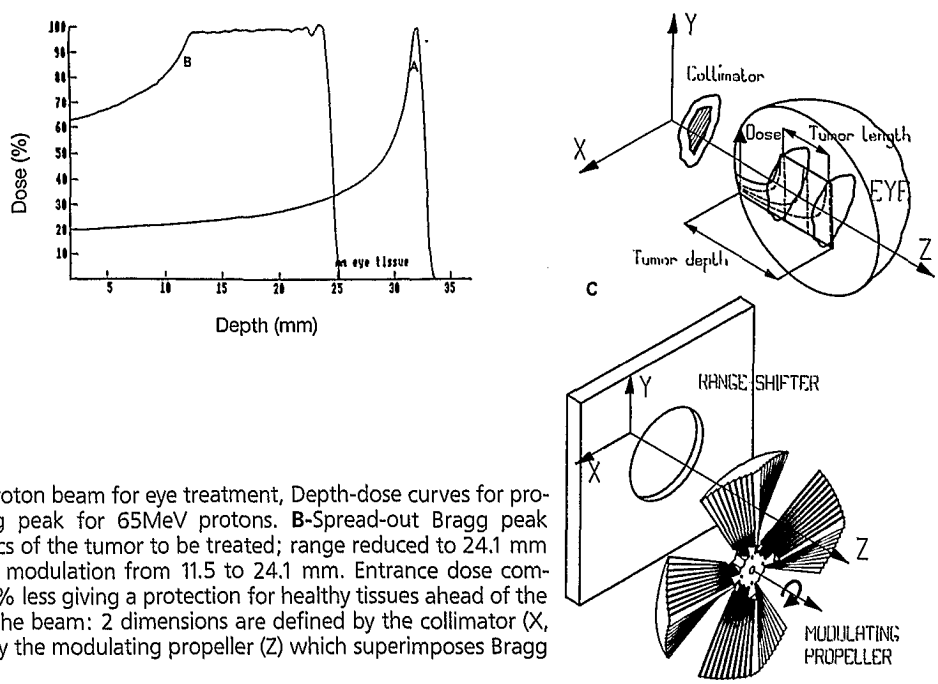

Fig. 1. Adaptation of the proton beam for eye treatment, Depth-dose curves for protons in eye tissue **A**-Bragg peak for 65MeV protons. **B**-Spread-out Bragg peak adapted to the characteristics of the tumor to be treated; range reduced to 24.1 mm (calculated on distal 90%), modulation from 11.5 to 24.1 mm. Entrance dose compared to plateau dose is 37% less giving a protection for healthy tissues ahead of the tumor. **C**-Conformation of the beam: 2 dimensions are defined by the collimator (X, Y), 3rd dimension is given by the modulating propeller (Z) which superimposes Bragg peaks at different energies

structures and a reliable reconstruction of all these elements for treatment planning and dosimetry.

Special treatment chairs permit accurate repositioning of the order of 0.1 mm in x, y, z directions, chair rotation and head tilting. Fixation of the patient is ensured by a bite block and a facial thermoplastic mask mounted on the same support and attached to the treatment chair. A counterweight pushes the head from behind into the mask for immobilization. The chair is mounted in front of the "optical bench" (Fig. 2) which is an assembly of the elements necessary to adjust the proton beam to the need of the patient and to monitor the dose delivered to the tumor. The size of the chair is adjustable to any adult size.

After centering the eye on the beam axis represented by the crosshairs of the X-ray tubes and laser alignment systems, couples of orthogonal X-ray films are taken from different lines of sight. The direction which permits the best possible positioning of tumor and critical structures relative to the beam and minimizes the dose to healthy tissues is then selected as treatment position.

The clip positions for each visual angle are entered in the treatment planning program. The macular position is a reference position to which other positions are compared. For patients with poor vision it might be necessary to use the contralateral eye for fixation. In this case, the diode position is adjusted by adding the interpupillary distance to the diode position on a paper with polar coordinates. But this might only give an estimate, as the vision is not always parallel under close sight conditions.

During simulation as well as during treatment, a TV camera views the eye with high magnification. In order to recognize possible movements during eye fixation, the contour of the limbus is drawn directly on the screen of the treatment room monitor and transmitted to the control desk monitor.

After this first simulation a phase of treatment planning including eye modelling, tumor reconstruction, choice of treatment position, calculation of dose distribution and treatment parameters follows.

A document issued from the computer showing the clip position towards the crosshairs and the collimator is compared to the X-ray films obtained after repositioning the patient, in order to verify that the treatment position and twist angle (rotation of the eye around its axis) have not changed or have accurately been planned. This step is very crucial because it modifies the tumor position in the collimator and could cause an underdosage of part of the volume, if not performed properly. Once a good position and twist are obtained, position and thickness of the eyelid(s) in the beam are checked. This is another important step which affects the range calculation.

To avoid problems when performing the final simulation, the concept of "second simulation" was introduced at the Centre Antoine Lacassagne. This simulation is performed with a shadow paper collimator allowing to use one or two

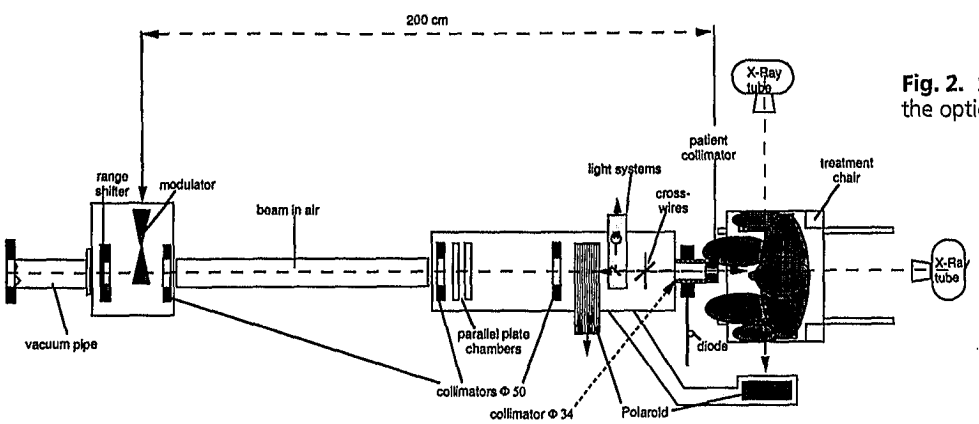

Fig. 2. Schematic drawing of the optical bench in Nice.

blepharostats to tract the lid(s) out or the beam or to treat intentionally through the lid taking into account its thickness. This way, the risk to build a wrong brass collimator, modulator or range shifter is minimized.

A final simulation is performed with the collimator mounted (Fig. 3). If a wedge is used in addition, its position in the collimator and beam is checked by taping a thin tungsten wire to the ridge and taking a low voltage X-ray film of the assembly.

Treatment Planning

The treatment planning systems used by the various teams involved in ophthalmic applications of proton beams are derived from a program developed by Goitein et al. [37, 38]. This program yields the following information:

- 3D-representation of normal structures,
- 3D-reconstruction of the tumor,
- 3D-representation of these structures in a beam's eye-view,
- visualization from arbitrary angles,
- contouring of target volume and aperture of the beam in this view,
- 3D-calculation of dose distribution,
- calculation of dose-volume histograms,
- calculation of range and modulation,
- files for numerically controlled milling machines to produce beam shaping elements (collimator, modulating wheel, range shifter).

The eye is pictured as a line-drawn 3D-model according to individual measurements of the axial length, thickness of sclera and lens, diameter of the limbus and distance of the cornea from the posterior lens. These measurements are made by sonography.

The tumor viewed from the beam ("beam's eye view") is contoured and a safety margin defines the apertures of the collimator. The depth of penetration of the beam, the width of the spread-out Bragg peak are also specified. These parameters can be adjusted in order to optimize the dose distribution which may be represented in any plane orientation (aligned or off the beam axis).

In order to obtain a better protection of some critical structures, it is possible to introduce one or more wedge filters into the beam. They modify the depth dose distribution and may allow to treat a parapapillar tumor without damaging the optic nerve. Their use has to be carefully checked, especially when a combination of two partially overlapping filters is anticipated, in order to avoid possible underdosage of part of the tumor volume.

Modelling the eye is easy, as long as the eyeball is regular and the measurements are correct. If, for instance, adjustments of the axial length

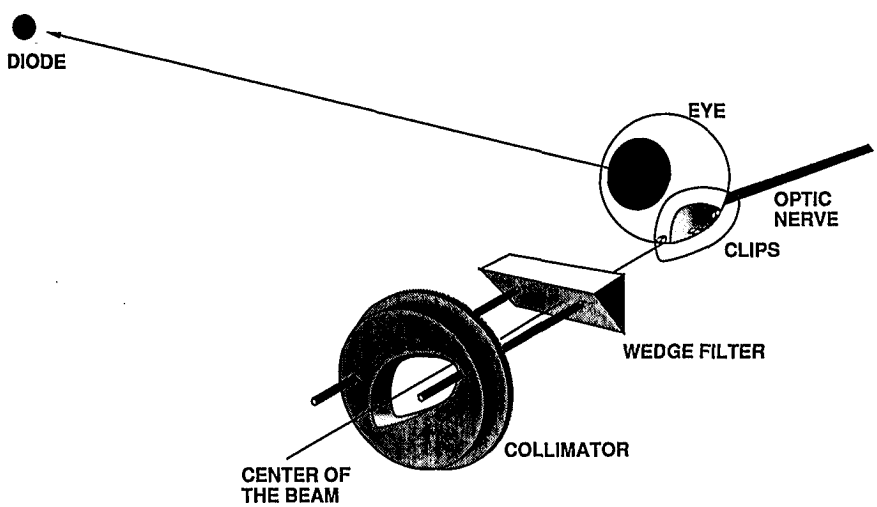

Fig. 3. Schematic representation of the eye treatment technique

are necessary, a CT scan in macular vision position might help to remeasure eye length, diameter, sphericity etc. But correlations are complicated, because the eye model does not accept asymmetric or ovoid shapes. Some compromises have to be made at present. But new versions of the program offering new modelling options are upcoming.

Dose-volume histograms (DVH) [39, 40] are calculated for the main structures of the eye. They contribute to a better understanding of the dose distribution in a whole organ or parts of it. The DVHs are the first step towards a more accurate analysis of the tumor control rates and an evaluation of the normal tissue complication probability (NTCP) [41, 42].

Treatment

The European centers give the treatment routinely in four fractions over four days. The total dose are 60 CGE (Cobalt Gray Equivalent = physical dose × RBE). This is a slight difference from the American protocol (see Chapter 11) which prescribes 70 CGE in five fractions. Each fraction is applied following the same procedure including the final simulation of the accurate position of patient and clips relative to the beam. During the treatment the eye remains under control of a TV system. If any significant movement is observed, the treatment is interrupted, the set-up renewed and the treatment continued. In Nice, the average time to deliver one fraction is 20 seconds.

Results

The treatment of uveal melanoma with protons can be considered as one of the most successful cancer treatments [43–46]. The 5-year local control rate is impressive: 96.3 ± 1.5% in 1989 and 97 ± 1% in 1992 for Boston from a series of more than 1000 patients, 96.8% for Berkeley from a series of 307 patients. These numbers were recently confirmed during the PTCOG (Proton Therapy Co-Operative Group) meeting held in Chester in May 1994 [47].

The probability of eye retention at 5 years was 89.1% in Boston and 83% in Berkeley. As main reason for the somewhat lower values, the development of neovascular glaucoma and rubeosis iridis were indicated. Tumor regrowth was responsible for only a small number of enucleations.

The factors influencing recurrence were described as ciliary body invasion (9/270 versus 11/788 for other tumors), large tumor dimensions (7/710 for a tumor diameter ≤ 15 mm versus 13/343 if > 15 mm, 5/539 for a tumor height ≤ 5 mm versus 15/514 if > 5 mm) and male sex (16/525 males versus 4/532 women).

36% deaths from metastases and a 5-year survival of only 59% were reported for patients with ciliary body involvements despite an actuarial local control rate of 98% [6]. Neovascular glaucoma and enucleations (26%) were also more frequent among patients with ciliary body tumors.

A total number of 166/1078 patients (15.4%) died of metastatic disease in the Boston series [48] compared to 42/261 (16.1%) in the Berkeley series [46]. The 5-year probability of metastatic growth was 23.8% in Boston, but only 11% in Berkeley.

The visual outcome of patients is quite difficult to assess. It depends on previous visual status, size and site, and distance to disc and fovea to name only a few parameters. Of a series of 218 patients [44], 194 developed some degree of radiation maculopathy. At the end of the third year after treatment 87% presented with macular edema, 76% with microvascular changes (microaneurysms and/or telangiectasia), 70% with intraretinal hemorrhage, 64% with capillary nonperfusion. A visual acuity of at least 20/200 was observed in 90% of the treated eyes after 1 year and 67% after 3 years, respectively. From a series of 286 patients treated in Berkeley, 49% had a vision ≤ 20/200, the length of follow-up ranging from 6 to 90 months [49].

New Approaches

Local control of uveal melanomas with protons must be considered as excellent. But some progress could be expected for the visual outcome. Discussions among the ophthalmologists partici-

pating in the South Europe Radiotherapy Group (SERAG) which uses the cyclotron in Nice, initiated a study to ameliorate these functional results by modifying or adapting some technical parameters, even at the risk of a higher rate of marginal relapses, knowing that this has not affected the prognosis of metastases in the past.

Since 1992, lucite wedge filters with reduced distal safety margins have been used [50] to lower the dose to critical posterior structures (Fig. 4). In order to avoid any mistake in eyelid thickness evaluation, almost all patients are treated through a bolus made from wax and/or sonographic gel covered by a plastic foil which defines a plane to measure entrance to the beam more easily.

A number of experiments [51, 52] have also been performed on human melanoma and other cell lines in order to advance the understanding of the biological depth-dose distribution of proton beams used for eye treatments. It is suspected that the increase of the relative biological effectiveness observed at the end of the Bragg peak and its variations along the spread-out peak may enhance the dose delivered to critical structures located at the end of the beam path, partly explaining the relatively poor functional results obtained with proton beams. It is also possible that the eye density of 1.05 g/cm^3 used for the range calculations is incorrect. It is known that sclera, for instance, has a higher density than vitreum and, consequently, different densities should be considered for the different tissues crossed by the particles.

Several studies on these subjects are now in progress trying to give protons the best chance to compete with other techniques and to achieve both local control and sparing of vision.

Tentative Indications for Ion Beam Therapy

Considering the different techniques used in uveal melanoma treatment, it seems that the best indications for proton therapy are the following:

- posterior pole tumors close to the disc and/or macula regardless of size (as long as their volume is < 40% of the eye volume),
- large tumors which are not suited for plaques independent of location in the eye,
- extrascleral extensions with a very poor general prognosis.

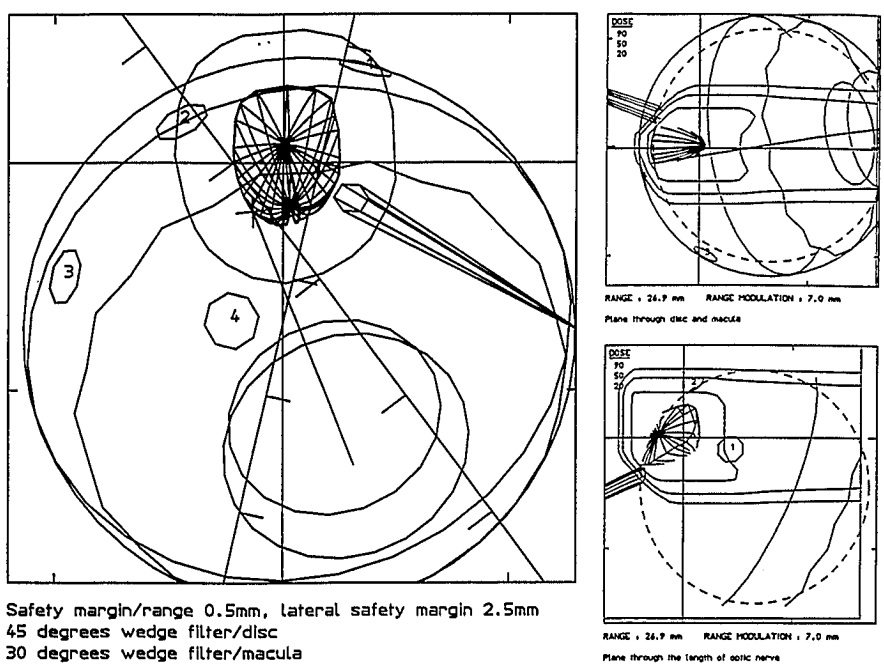

Fig. 4. Example of the treatment planning for a posterior pole tumor (reduced distal margin and use of 2 wedge filters)

Treatment of Other Ocular Lesions

Conjunctival Melanoma

Conjunctival melanoma mainly benefits from surgery and low energy X-ray therapy. Multirelapsing tumors often lead to a salvage enucleation of exenteration, although the eye itself is not affected by the melanoma. Radiotherapy (including low-energy X-rays, electrons, protons) has been used to treat some of these melanomas but give a more or less significant dose to the inner eye. A modified proton treatment which allows a homogeneous irradiation of the whole conjunctiva with a total protection of the eye has been proposed by our team [53].

The fractionation schedules generally used give 30 CGE in the non-invaded conjunctiva and thereafter a boost of 15 to 30 CGE on the positive margin or visible tumor. The most used schedule gave 4 fractions of 7.50 CGE/week.

The target volume to be considered is very large. It includes bulbar and lid conjunctiva and at least half of the total surface of the conjunctiva, to avoid further relapses at the margin of the treated volume. The beam has to pass through the lid but must respect the internal structures of the eye, in order to preserve the visual outcome. The possible complications or sequellae are mainly eyelid retraction due to fibrosis and/or sclerosis, eye dryness when the upper lid is in the field and lachrymal duct stenosis if the internal chantus is irradiated.

The technical principles of the treatment are:
- clip insertion on the eye for localization of the target volume and repositioning purposes,
- bolus set-up on the lid aiming to give a homogeneous flat entrance for the proton beam collimated to the size of the tumor,
- use of a spherical compensator (1 mm steps) milled in plexiglass in order to adapt the range of the proton beam to the shape of the bulbus,
- compensator set up on a collimator shaped to the tumor volume characteristics (at least half a conjunctiva in surface).

The first results obtained are encouraging with a good local control in the treated area. Distant relapses (in the non-irradiated conjunctiva) may lead us to propose a prophylactic treatment of the whole conjunctiva for these multirelapsing tumors.

Vascular Malformations

Protons may also be used in the treatment of vascular malformations as encountered in von Hippel-Lindau syndrom or choroidal angiomas. These benign lesions often affect the posterior pole of the eye and give retinal detachment leading to blindness. They have to be treated as carefully as possible in order to limit the dose delivered to normal critical structures, knowing that retreatment might be required. The technique used in Nice is similar to the treatment of uveal melanoma with clip insertion and simulations. The aim of the treatment is to induce a fibrosis in the malformation. Hence, it is sufficient to include a good part of the lesion, but not necessarily the whole structure. As a consequence, the lateral and distal safety margins are reduced and the dose delivered is either 17.70 Gray in four fractions on four days or 42.50 Gray in 14 fractions over 3.5 weeks. The results obtained are satisfying and seem to avoid adverse developments.

References

1 Dorn, H. F. and Cutler, S. J. Morbidity from cancer in the United States. Public Health Monograph no. 56, Washington DC, US Government Printing Office, 1959.
2 Jensen, O.A. Malignant melanomas of the uvea in Denmark, 1943–1952. Acta Ophtalmol. (suppl.) 75, 57–220, 1963.
3 Wilkes, S.R., Robertson D.M., Kurland, L.T., and Campbell, R.J. Incidence of uveal malignant melanomas in the resident population of Rochester and Olmsted County, Minnesota. Am. J. Ophthalmol. 87, 639–641, 1979.
4 Ganley, J.P. and Comstock G.W. Benign nevi and malignant melanomas of the choroid. Am. J. Ophthalmol. 76, 19–25, 1973.
5 Hale, P.N., Allen, R.A., and Straatsma, B.R. Benign melanoma (nevi) of the choroid and ciliary body. Arch. Ophthalmol. 74, 532–538, 1965.
6 Decker, M., Castro, J.R. Linstadt, D.E. Char, D., Petti, P.L., Quivey, J.M., and Ahn, D. Ciliary body

melanoma treated with helium particle irradiation. Int. J. Radiat. Oncol. Biol. Phys. 19, 243–247, 1990.
7 Meyer-Schwickerath, G. The preservation of vision by treatment of intraocular tumors with light coagulation. Arch. Ophthalmol. 66, 458–466, 1961.
8 Shields, J.A. Current approaches to the diagnosis and management of choroidal melanomas. Surv. Ophthalmol. 21, 443–463, 1977.
9 Vogel, M.H. Treatment of malignant melanomas with photocoagulation: evaluation of 10 year follow-up data. Am. J. Ophthalmol. 74, 1–11, 1972.
10 Meyer-Schwickerath, G. and Bornfeld N. Photocoagulation of choroidal melanomas. 30 years experience, in Lommatzsch, P.K. and Blodi, F.C. (eds.), Intraocular Tumors. Springer Verlag, Berlin, 1983, pp. 269–276.
11 Peyman, G.A. and Apple, D.J. Local excision of choroidal malignant melanoma. Full thickness eye wall resection. Arch. Ophthalmol. 92, 219–222, 1974.
12 Peyman, G.A. and Raichand, M. Full-thickness eye wall resection of choroidal neoplasms. Ophthalmol. 86, 1024–1036, 1979.
13 Peyman, G.A., Juarez, C.P., Diamond, J.G. and Raichand, M. Ten years experience with eye wall resection for uveal malignant melanomas. Ophthalmol. 91, 1720–1725, 1984.
14 Foulds, W.S. Results of local excision of uveal tumors, in Lommatzsch, P.K, and Blodi, F.C. (eds.), Intraocular Tumors, Springer Verlag, Berlin 1983, pp. 374–377.
15 Packard, R.B.S. Pattern of mortality of choroidal melanoma. Br. J. Ophthalmol. 64, 565–575, 1980.
16 Manschot, W.A. and van Peperzeel, H.A. Choroidal melanoma: Enucleation or observation? A new approach. Arch. Ophthalmol. 98, 71–77, 1980.
17 Shields, J.A. and Augsburger, J.J. The management of choroidal melanomas. Am. J. Ophthalmol. 90, 266–268, 1980.
18 Siegel, D., Myers, M., and Steinhorn, S.C. Survival rates after enucleation of eyes with malignant melanoma. Am. J. Ophthalmol. 87, 761–765, 1979.
19 Zimmerman, L.E. Changing concepts concerning the malignancy of ocular tumors. Arch. Ophthalmol. 78, 166–173, 1967.
20 Zimmerman, L.E., McLean, I.W., and Foster W.P. Does enucleation of an eye containing a melonoma prevent or accelerate the disseminaton of tumor cells? Br. J. Ophthalmol. 62, 420–425, 1978.
21 Zimmerman, L.E. and McLean, I.W. An evaluation of enucleation in the management of uveal melanomas. Am. J. Ophthalmol. 87, 741–760, 1979.
22 Zimmerman, L.E. Metastatic disease from uveal melanomas: The 1980 William Bowman lecture. Br. J. Ophthalmol. 100, 34–54, 1980.
23 Fraunfelder, F.T., Boozman, F.W., Wilson, R.S., and Thomas, A.H. No-touch technique for intra-ocular malignant tumors. Arch. Ophthalmol. 95, 1616–1620, 1977.
24 Wilson, R. S. and Fraunfelder F.T. No-Touch cryosurgical enucleation: A minimal trauma technique for eyes harboring extraocular malignancy. Ophthalmol. 85, 1170–1175, 1978.
25 Grange, J. D., Ducourneau, D., Taillanter-Francoz, N, Patricot, L., and Gérard, J.P. Technique d'énucléation en vase clos pour mélanomas malins de la choroïde. Bull. Soc. Ophthalmol. Fr. 81, 679–681, 1981.
26 Shields, J. A. Diagnosis and Management of Intraocular Tumors. The CV Mosby Co., St. Louis, 1983.
27 Moore, R. F. Choroidal sarcoma treated by the intraocular insertion of radon seeds. Br. J. Ophthalmol. 14, 145–156, 1930.
28 Stallard, H.B. Malignant melanoma of the choroid treated with radioactive applications, in Boniuk, M. (ed.) Ocular and Adnexial Tumors. The CV Mosby Co., St. Louis, USA, 1964.
29 Stallard, H.B. Radiotherapy for malignant melanoma of the choroid. Br. J. Ophthalmol. 50, 147–155, 1966.
30 Stallard, H.B. Malignant melanoblastoma of the choroid. Med. Prob. Ophthalmol. 7, 16–38, 1968.
31 Lommatzsch. P.K. Treatment of choroidal melanoma with 106Ru/106Rh beta-ray applicators. Surv. Ophthalmol. 19, 85–100, 1974.
32 Lommatzsch, P.K. Results after beta-irradiation (106Ru/106Rh) of choroidal melanomas: 20 years experience. Br. J. Ophthalmol. 70, 845–851, 1986.
33 Packer S. and Roter, M. Radiotherapy of choroidal melanoma with iodine-125. Ophthalmol. 87, 582–590, 1980.
34 Sealy, R., Le Roux, P.L.M., Rapley, F., Hering, E., Shackleton, D., and Sevel, D. The treatment of ophthalmic tumors with low energy sources. Br. J. Radiol. 49, 551–554, 1976.
35 Earle, J., Kline, R.W., and Robertson, D.M. Selection of iodine-125 for the Collaborative Ocular Melanoma Study. Arch. Ophthalmol. 105, 763–764, 1987.
36 Packer, S., Stoller, S., Lesser, M.L., Mandel, F.S., and Finger, P.T. Long-term results of iodine-125 irradiation of uveal melanoma. Ophthalmol. 99, 767–774, 1992.
37 Goitein, M. and Miller, T. Planning proton therapy of the eye. Med. Phys. 10, 275–283, 1983.
38 Gragoudas, E.S., Goitein, M., Verhey, L., Munzenrider, J., Suit, H.D., and Koehler, A. Proton beam irradiation, an alternative to enucleation for intraocular melanomas. Ophthalmol. 87, 571–581, 1980.
39 Chen, G.T.Y. Dose-volume histograms in treatment planning. Int. J. Radiat. Oncol. Biol. Phys. 14, 1319–1320, 1988.
40 Lyman, J.T. Complication probabilities as assessed from dose-volume histograms. Radiat. Res. Suppl. 104, 13–19, 1985.
41 Niemierki, A. and Goitein, M. Calculation of normal tissue complication probability and dose-volume histogram reduction schemes for tissues with a critical element architecture. Radiother. Oncol. 20, 166–176, 1991.
42 Lyman, J.T. Normal tissue complication probabilities: variable dose per fraction. Int. J. Radiat. Oncol. Biol. Phys. 22, 247–250, 1992.
43 Munzenrider, J.E., Gragoudas, E.S., Seddon, J.M., Sisterson, J., McNulty, P., Birnbaum, S., Johnson, K., Austin-Seymour, M., Slater, J., Goitein, M., Verhey, L.J., Urie, M., Ruotolo, D., Egan, K., Osuna, F. Con-

servative treatment of uveal melanoma: probability of eye retention after proton treatment. Int. J. Radiat. Oncol. Biol. Phys. 15, 553–558, 1988.

44 Guyer, D.R., Mukai, S., Egan, K.M., Seddon, J.M., Walsh, S.M., and Gragoudas, E.S. Radiation maculopathy after proton beam irradiation for choroidal melanoma. Ophthalmol. 99, 1278–1285, 1992.

45 Linstadt, D., Castro, J., Decker, M., Quivey, J., Char, D., and Phillips, T. Long-term results of helium ion irradiation of uveal melanoma. Int. J. Radiat. Oncol. Biol. Phys. 19, 613–618, 1990.

46 Nowakowski, V.A. Ivery, G., Castro, J.R., Char, D.H., Linstadt, D.E., Ahn, D., Phillips, T.L., Quivey, J.M., Decker, M., Petti, P., and Collier, J.M. Uveal melanoma: Development of metastases after helium ion irradiation. Radiol. 178, 277–280, 1991.

47 Abstracts of the XX PTCOG Meeting, Chester, May 16–18, 1994

48 Gragoudas, E.S., Egan, K.M., Seddon, J.M., Walsh, S.M., and Munzenrider, J. Intraocular recurrence of uveal melanoma after proton beam irradiation. Ophthalmol. 99, 760–766, 1992.

49 Linstadt, D., Char, D.H., Castro, J.R., Phillips, T.L., Quivey, J.M., Reimers, M., Hanningan, J., and Collier, J.M. Vision following helium ion radiotherapy of uveal melanoma: A Northern California Oncology Group study. Int. J. Radiat. Oncol. Biol. Phys. 15, 347–352, 1988.

50 Chauvel, P., Brassart, N., Hérault, J., Courdi, A., Caujolle, J.P., Grange, J.D., Mouries, O., Diallo-Rosier, L., Mosci, C., Polizzi, A., Porta, A., Menci, E., Bornfeld, N., Friedrichs, W., Sahel, J., Bacin, F., Gérard, J.P., Sauerwein, W., Scolaro, T., Carrie, C., Kantor, G., Rozan, R., Teissier, E., Bensadoun, R.J., Lagrange, J.L., and Demard, F. Technical considerations about proton therapy and visual conservation for uveal melanomas: The experience of the "SERAG", in Proc. Int. Symp. on Intraocular and Epibulbar Tumors, Firenze, March 3–5, 1994, in press.

51 Blomquist, E., Russell K.R., Stenerlöw B., Montelius, A., Grusell, E., and Carlsson, J. Relative biological effectiveness of intermediate energy protons. Comparisons with ^{60}Co gamma-radiation using two cell lines. Radiother. Oncol. 28, 44–51, 1993.

52 Courdi, A., Brassart, N., Hérault, J., and Chauvel, P. The depth-dependent response of human melanoma cells exposed to 65 MeV protons. Br. J. Radiol. 67, 800–804, 1994.

53 Chauvel, P., Caujolle, J.P., Sauerwein, W. Friedrichs, W., Brassart, N., and Herault, J. Proton therapy as a possible salvage treatment for conjunctival melanomas, in Proc. Intern. Symp. on Intraocular and Epibulbar Tumors, Firenze, March 3–5, 1994, Frezzotti, R., Balestrazzi, E., Falco, L., and Esente, S. (eds.), Moduzzi Editore, 1994, pp. 171–510.

14 Proton Therapy of Thoraco-Abdominal Tumors

H. Tsujii[1), 2)], H. Tsuji[1)], T. Okumura[1)], K. Ohara[1)], S. Koyama[1)], and Y. Matsuzaki[1)]

[1)] Proton Medical Research Center, University of Tsukuba, Tsukuba-shi,
[2)] National Institute of Radiological Sciences, Chiba, Japan

Introduction

By taking advantage of the excellent dose localization properties of proton beams, various types of tumors have been treated with proton therapy and a paramount advantage has been demonstrated in selected tumors, e.g., uveal melanoma, intracranial small lesions, chordoma and chondrosarcoma of the skull base and cervical spine, and prostate cancers [1]. Only limited experiences, however, have been accumulated in the treatment of deep-seated tumors. The Proton Medical Research Center (PMRC) of the University of Tsukuba, has unlike other proton facilities worldwide placed major efforts on the treatment of thoraco-abdominal tumors [2], which are usually hard to cure with conventional photon therapy. The following will give an update on the experience with these tumors, emphasizing, in particular, irradiation techniques, local control and survival rates.

Treatment Conditions and Patient Selection

For proton therapy at the PMRC, a booster synchrotron of the High Energy Physics Research Laboratory (KEK) is available which is shared with various physics groups. Its primary energy of 500 MeV is degraded to 250 MeV (corresponding to a range of 38 cm in water) by passing the beam through a graphite absorber. For generating a spread-out Bragg peak (SOBP), several types of ridge filters are used, and the beam range is determined using a pair of wedge-shaped degraders. The treatment facility has two separate treatment rooms for horizontal and vertical beam lines.

Treatment planning is based on serial computed tomography (CT) scans which are obtained at the University Hospital. Precise positioning and immobilization of the patients with thoraco-abdominal tumors is achieved using a universal cradle made of polyurethane material which fits the upper half of the body. The target volume is manually outlined on each CT slice displayed on a computer monitor. Dose calculations are carried out, field outlines are constructed, and a beam-shaping compensator (bolus) is designed. The compensating bolus which determines the distal depth of the SOBP is fabricated by a numerically controlled milling machine using a water-equivalent solid material. The collimator which shapes the lateral edges of the field is made using an array of brass.

At the PMRC a fractionation pattern of 11 fractions (Thu, Fri, Mon–Fri, Mon–Thu) per 3 weeks has been used. This unusual schedule is determined by the operation schedule of the accelerator. Thoraco-abdominal tumors are either treated by proton therapy alone or in combination with photons. In photon therapy five fractions are given per week using 10 MV X-rays or ^{60}Co gamma-rays. Based on radiobiological studies with cell cultures and animals [3], an RBE (relative biological effectiveness) value of 1.0 relative to Cobalt-60 is employed. When defining a target volume the smallest margins possible (mostly <5 mm) are added around the tumor. The dose level at the target boundary is set to 90%, and the prescribed dose to 100%. Each

treatment day the field placement is aligned radiographically using our special positioning system which consists of a fluoroscopy and real-time digital image processing unit [4].

For the treatment of lung and liver tumors which move longitudinally with respiration, we have developed a respiration-gated irradiation system (ReGIS) using a strain gauge semiconductor sensor to monitor the respiration movement of the chest or abdominal wall and to synchronize the irradiation control system with the respiration cycle [5]. An output timing signal is transferred from the system to the accelerator permitting synchronized irradiation. The timing signal for irradiation is set during the expiratory phase for a duration of 1.5 to 2.0 seconds. This novel method (cf. Chapter 32) allows to minimize irradiation to surrounding normal tissues.

As of March 1994, a total of 272 patients with malignant tumors had been treated with proton beams (alone or in combination with photons) with curative intent. This series included 128 patients with thoraco-abdominal tumors who were followed-up until death or for at least 6 months. The patients were selected for proton therapy, either because they refused surgery, because of advanced age, or because the tumors were unresectable for medical or technical reasons. Patients with distant metastases or previous external irradiation were excluded from the study.

The treatment results were expressed in local control which was defined as no evidence of local disease progression or persistence determined by serial clinical and radiographic observations. Clinical staging was done according to the UICC TNM classifications. For survival analysis, the Kaplan-Meier method was used. Treatment complications were scored from 0 (none) to 5 (fatal), and the score 3 or higher was considered as a major complication that should definitely be avoided.

Results

Lung Cancer

Of 21 lung cancer patients treated with curative intent, 4 patients had clinical stage I, 11 stage II, and 6 patients had stage III disease. There were 18 males and 3 females. Eleven were squamous cell carcinomas, 9 were adenocarcinomas and one was an adenoid cystic carcinoma. Eight patients were initially treated with photons (36–45 Gy/20–25 fx) followed by proton beams (40–50 Gy/10–20 fx), whereas 13 patients were treated with protons alone, applying total doses of 70–93 Gy in 20–27 fx. Despite these high doses, radiation-related side effects were relatively low and only one patient developed severe symptoms of radiation pneumonitis which resulted in a significant fibrotic change which could be observed on X-ray films. In some patients who were irradiated with a single portal from anterior or posterior direction, a fibrotic change was clearly demonstrable along the proton path until the end of the SOBP. The local control estimated from serial diagnostic images was 73.9% [15,21]. The overall actuarial survival rate at 3 and 5 years was 47.6% and 27.2%, respectively (Fig.1). There were no significant survival differences between squamous cell carcinoma and adenocarcinoma.

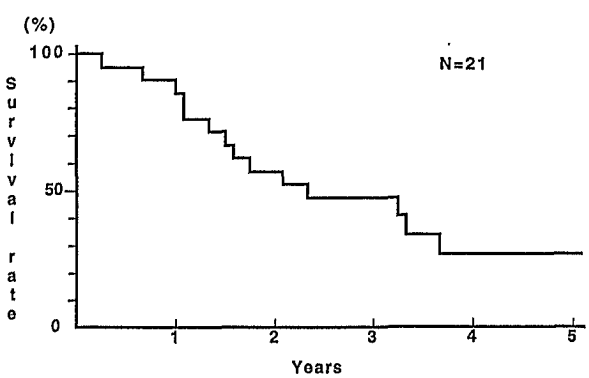

Fig. 1. Survival curve for 21 patients with lung cancer

Mediastinal Tumor

The first patient to be treated for a locally advanced malignant thymoma was a 66 year old woman who had a big anterior mediastinal tumor with multiple hilar lymph node metastases. She was inoperable because of a long history of severe asthma. She was treated with protons (50 Gy/16 fx/21 days) from the anterior direction. After completion of the treatment, she developed a moist skin reaction which eventually healed completely with conservative treatment. Four years after irradiation, she is still without any evidence of recurrence or side effects.

The second patient treated so far, was a 31 year old woman who also had a big anterior mediastinal tumor which extended posteriorly to form a paravertebral mass involving the descending aorta and pleura with pleural and pericardial fluid. Because of the advanced disease, she was initially irradiated with X-rays (40 Gy/22 fx) followed by proton beam irradiation (30 Gy/12 fx). The tumor regressed gradually and the collected fluid disappeared. She temporarily complained of dry cough which was consistent with a radiographic finding of paramediastinal pneumonitis. One and a half years after the treatment the patient is doing well with no evidence of recurrence.

Esophageal Cancer

Twenty-eight patients were treated for esophageal carcinoma. There were 3 patients with stage I, 13 patients with stage II, and 12 patients with stage III disease. Except for one patient with adenocarcinoma, all patients had squamous cell carcinomas. Seven patients were treated with proton beams alone with 75–87 Gy in 21–28 fractions. The other 21 patients were first treated with X-rays (31–50 Gy in 17–28 fractions) followed by 9–20 fractions of proton irradiation to yield total doses of 70–87 Gy. Three to six months after proton therapy almost all patients developed radiation ulcers of various severity, but except for one they all healed with conservative treatments. The treatment regime currently employed are 40–50 Gy of X-rays at a fraction size of 2.0 Gy followed by 25–35 Gy at 2.5 Gy per fraction of protons up

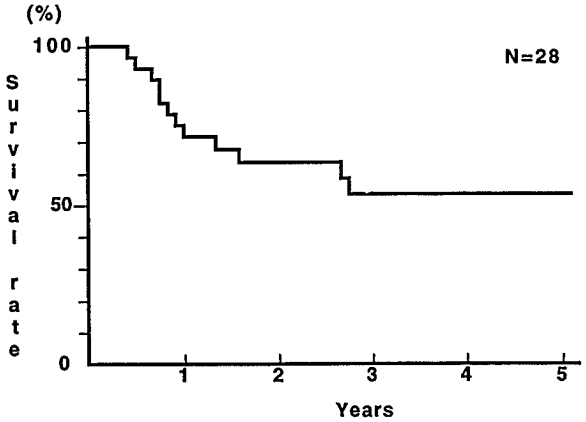

Fig. 2. Survival curve for 28 patients with esophageal cancer

to a combined dose of 75 Gy. Local control confirmed by repeated fiber-endoscopic examinations was obtained in 82.1% (23/28). The actuarial 5-year survival was 53.7% for all patients, 100% for stage I, 49.2% for stage II, and 46.7% for stage III.

Gastric Cancer

Five patients were treated for gastric cancer. The proton irradiation was only given to the primary lesions neglecting the lymphatic areas. In 3 of the 5 patients local control was obtained. One of the three was treated with X-rays and protons, the other two patients were treated with protons alone (83 Gy/30 fx and 86 Gy/28 fx, respectively). The overall survival at 3 and 5 years was 61.0% and 30.0%, respectively. Although most patients developed some degree of gastric ulcers, they all healed with conservative treatment.

Hepatocellular Cancer

72 patients with hepatocellular carcinoma (HCC) were followed for 10 months or more after being treated with a substantial, high dose of proton beams alone. The diameter of the main tumor as determined by CT scans was 3 cm in 18 patients, 3 to 5 cm in 37 patients, and 5 cm in 17 patients.

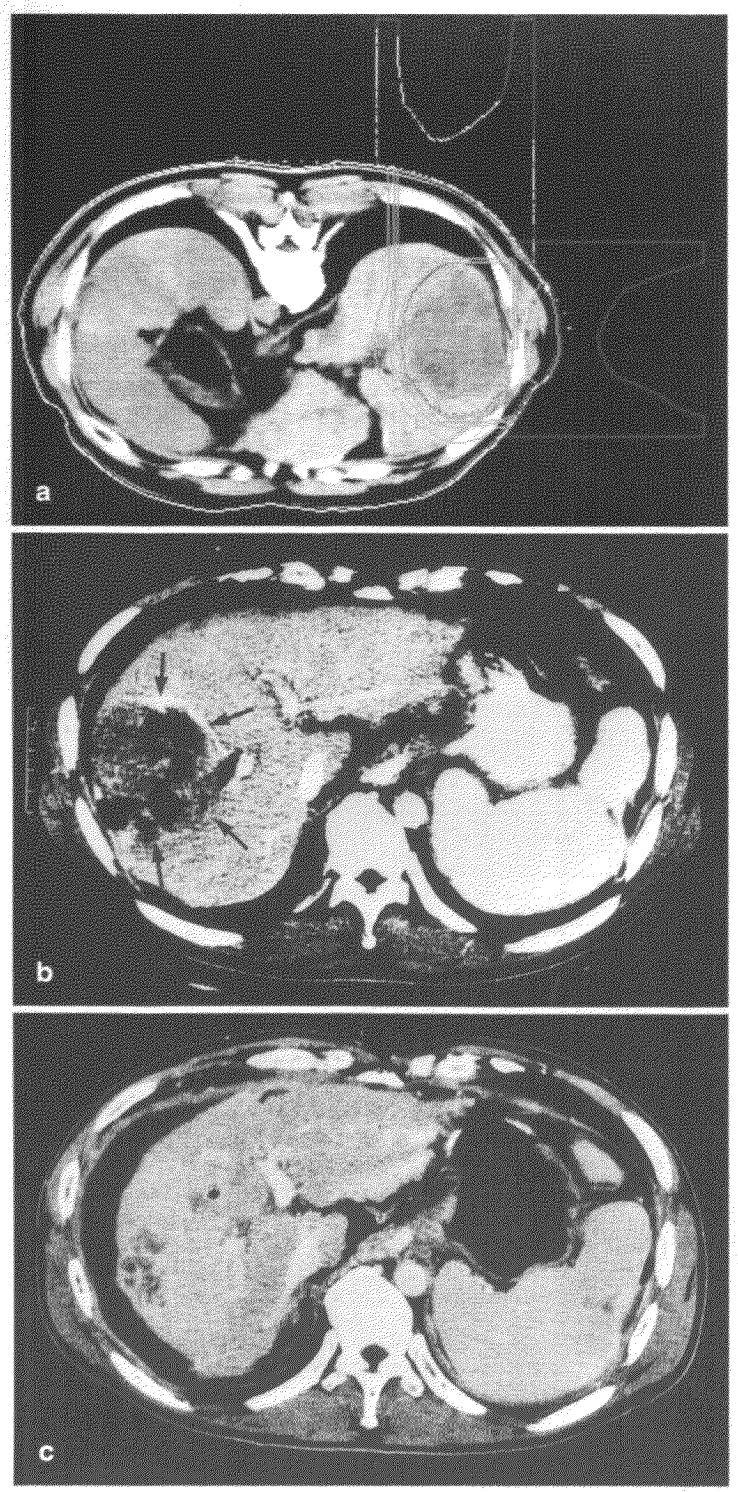

Fig. 3. An example of heptocellular carcinoma (HCC) treated with proton beams. The patient had Child C cirrhosis. He was irradiated from posterior and lateral directions lying in prone position (**a**). Note the huge tumor involving the right lobe of the liver (**b**), which was irradiated with 81 Gy/27 fx/52 days. One year after completion of proton therapy the tumor had regressed significantly (**c**)

The clinical stage of the accompanying liver cirrhosis was assessed by Child classification according to the hepatic function: 27 patients were Child A (good function), 30 patients were Child B (moderate function), and 15 patients were Child C (poor function). Initially, the majority of the selected patients had poor hepatic function, but with growing experience, patients with moderate to good hepatic function were increasingly referred to proton therapy. 65% of the patients had solitary tumors (43 nodular type and 4 invasive type). The rest developed multiple tumors which are characteristic of HCC.

The total doses ranged from 60–88 Gy given in 16–30 fractions with 3.0–4.5 Gy per fraction. During the early period of the trial, more than 20 fractions were employed, which were gradually decreased to 16. The most recent fractionation regimen prescribes 68.8 Gy in 16 fractions over 4 weeks with a fraction size of 4.3 Gy.

Of 72 patients, 35 patients underwent intraarterial injection therapy with 5–10 ml of iodized oil contrast medium (Lipiodol) mixed with 5–15 mg of Mitomycin C, followed by definitive proton therapy. The intratumoral retention of the iodized oil helped to localize the tumor and position the fields. Alternatively, irridium seeds were implanted at the edge of the tumor boundary and visualized under fluoroscopy.

Since 1990 the respiration-gated irradiation system (ReGIS) has been used to minimize irradiation of the surrounding liver tissue. With this technique, the high radiation dose has exellently been restricted to the actual target volume (Fig. 3).

The overall 3-year survival rate was 43.0%. For patients with Child A it was 62.1%, for Child B and C it was 38.0% and 0%, respectively. For 65 patients with Child A or B, and a clinical stage comparable to operable cases, the 3-year survival rate was 52.0%. The majority of deaths of Child C patients occurred as a result of hepatic failures, whereas no patient of Child A died of hepatic failure. In-field tumor control was obtained in 84.7% of the cases, with higher radiation doses yielding higher local control (Tab. 1).

Table 1. Response of in-field hepatocellular carcinomas according to radiation dose (TDF)

TDF	No	Control	Recurrence	Unknown
<160	15	9	4	2
160–180	38	33	4	1
>180	19	19	0	0
Total	72 (100%)	61 (84.7%)	8 (11.1%)	3 (4.2%)

Summary

As described earlier, well selected tumors have a distinct benefit from the improved dose distribution achievable with proton beams. However, there is only limited experience with thoraco-abdominal tumors. So far, only the PMRC has treated these tumor sites to a larger extent by proton therapy. Based on preliminary local control data and survival rates, it seems very likely that primary malignancies of the esophagus, lung and liver benefit from the improved dose distribution of proton beams. For gastric and mediastinal tumors, it is difficult to judge the results because patient numbers are still too small. For 2 patients with mediastinal tumors, however, only proton beams delivered a high enough dose, sparing the surrounding healthy lung tissues and spinal cord at the same time. Hence, proton therapy could have a distinct advantage for intramediastinal tumors which require high doses in the immediate vicinity of sensitive tissues.

Conventional radiotherapy of HCC has shown only limited success. Surgical resection rate is only in the range of 10–30% [2, 6] due to an often accompanying liver cirrhosis and poor liver function. Furthermore, postoperative recurrence in the residual liver occurs very frequently. Despite such discouraging backgrounds, however, there is evidence that hepatic resection prolongs survivals [6], and this is the rationale for applying proton radiotherapy. At PMRC, primary HCC has been extensively treated with proton therapy with some remarkable results.

Of 72 patients only 4 developed in-field tumor regrowth, 2 of whom received a TDF value which was lower than what is currently applied (160).

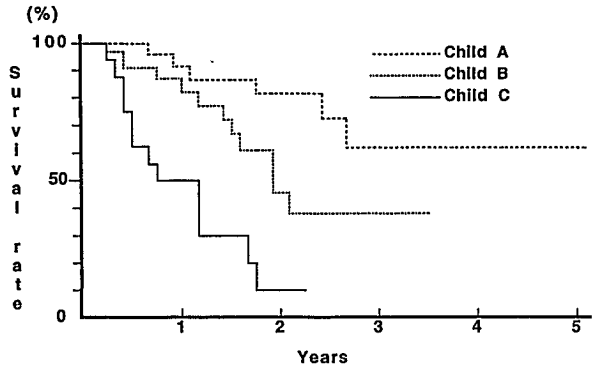

Fig. 4. Survival curves of patients with HCC according to Child's clinical staging

The current trial has demonstrated that proton beams can achieve an ablative radiation dose which warrants high control rates with acceptable toxicities.

At PMRC an increasing number of tumor types including thoraco-abdominal tumors are treated. But a systematic replacement of photons by protons may raise some problems. The clinical benefit has to justify the increased cost and necessary efforts. A new radiotherapy network is required to coordinate the work of huge proton facilities and, finally, the benefit of the physical selectivity of proton beams will only be fully exploited if the accuracy in patient positioning and dosimetry reaches the same level as with photons. Proton accelerators should also be as simple to use and as reliable as modern linear accelerators for electrons. The recent progress in accelerator technology seems to meet these requirements, and there is a good chance that in the near future more difficult and highly demanding types of cancer including thoraco-abdominal tumors will be treated with proton beams.

Acknowledgements

This work was supported in part by Grants-in-Aid (Tsujii-han) for Scientific Research from the Ministry of Education, Science and Culture, and Grants-in-Aid (Miyamoto-han) for Cancer Research from the Ministry of Health and Welfare in Japan.

References

1 Suit, H.D. and Urie, M. Proton beams in radiation therapy. J. Nat. Cancer Inst. 84, 155–159, 1992.
2 Tsujii, H., Tsuji, H., Inada, T., Maruhashi, A., Hayakawa, Y., Takada, Y., Tada, J., Fukumoto, S., Tatsuzaki, H., Ohara, K., and Kitagawa, T. Clinical results of fractionated proton therapy. Int. J. Radiat. Oncol. Biol. Phys. 25, 49–60, 1992.
3 Ando, K., Koike, S., Kawachi, K., Hiraoka, T., Ohara, H., Yokota, M., Inada, T., Hirokawa, Y., Sato, S., Eguchi, K., and Urano, M. Relative biological effectiveness of the therapeutic proton beams at NIRS and Tsukuba University. Nippon Acta Radiol. 45, 531–535, 1985.
4 Tsujii, H., Maruhashi, A., Inada, T., Hayakawa, Y., Takada, Y., Tada, J., Sato, M., Hosano, K., and Akisada, M. Real-time field positioning for proton therapy at Tsukuba, in Proc. Int. Heavy Particle Therapy Workshop. Blattmann, H. (ed.), PSI, Villigen, 1989, pp. 43–46.
5 Inada, T., Tsuji, H., Hayakawa, Y., Maruhashi, A., and Tsujii, H. Proton irradiation synchronized with respiratory cycle. Nippon Acta Radiol. 52, 1161–1167, 1992.
6 Okuda, K., Ohtsuki, T., Obata, H., Tomimatsu, M., Okazaki, N., Hasegawa, H., Nakajima, Y., and Ohnishi, K. Natural history of hepatocellular carcinoma and prognosis in relation to treatment. Cancer 56, 918–928, 1985.

15 Indications for Heavy Ions – Lessons from Berkeley

P. K. LILLIS-HEARNE* and J. R. CASTRO

Lawrence Berkeley Laboratory and The Medical Center at the University of California, San Francisco, CA, USA

Introduction

Radiation therapy with ions was initially proposed by R. Wilson in 1946 [1], and the first charged particle treatment was carried out at the University of California, Berkeley Radiation Laboratory in the 1950's [2]. Beginning in 1975 ions ranging from protons through silicon became available for clinical use at the Lawrence Berkeley Laboratory as part of a collaborative study with the University of California, San Francisco Medical Center (UCSF-LBL). Interest in the use of ions for the treatment of tumors arose because of the unique physical properties of these ions and their biological effects (Tab. 1). Charged particles such as protons, helium, carbon and neon have advantageous sharp lateral and distal beam edges that are maintained throughout their depth of penetration in tissue. Heavier particles such as neon and silicon ions have higher linear energy transfer (LET) than low-LET photons and are more effective in cell killing [3]. As is described in more detail in Chapter 3, these ions show an increased effectiveness on slow growing tumors since there is less repair of potentially lethal and sublethal cellular damage and less variation in cell killing through different phases of the mitotic cell cycle [4–6]. These particles also have greater ability to kill hypoxic cells [7], which was expected to be of great clinical significance. Preclinical work had shown an increased relative biological effectiveness (RBE) at depth and a low oxygen enhancement ratio (OER) with silicon ions. However, as evaluated in the intestinal crypt system, silicon showed very little difference in effectiveness between the plateau, mid and distal peak of the beam suggesting it would offer minimal advantage for deep-seated tumors [3]. Argon has an even lower OER than silicon but it also has depth dose characteristics that are less desirable [4].

Table 1. Ions of clinical interest

Ion species	Max. positive charge	Relative mass	RBE
Proton	1	1	1.1
Helium	2	4	1.2–1.4
Carbon	6	12	2.0–3.0
Neon	10	20	2.5–3.5
Silicon	14	28	3.0–4.0

The RBE value for protons is the one used at MGH in Boston. The values of the heavier ions are used clinically at UCSF-LBL and represent approximate values for an 8 cm spread-out Bragg peak and a fraction size of 2.0–3.0 GyE. RBE values differ for different tissues, fraction sizes and position in the entrance region, Bragg peak or tail of the beam

Carbon ions showed a significant gain in cell kills in the peak region of the beam compared to the plateau, which is ideal for normal tissue tolerance. However, the carbon RBE for tumor response was lower than for neon ions which also show some normal tissue sparing with fractionation [3]. The physical dose distribution for neon ions, and the low OER in the distal peak of the beam were factors in the selection of neon ions for high-LET clinical trials. Helium, representing low-LET radiation, was chosen primarily for its

* present address: Brooke Army Medical Center, San Antonio, TX, USA

dose distribution advantage and because it was easier to produce in the LBL accelerator than protons. Helium ions are uniquely suited for a precise localization of the radiation dose with limited irradiation of adjacent critical structures such as the brain, cranial nerves and the spinal cord. For many tumors it has been possible to deliver 10–35% higher doses than is possible with standard radiation therapy [8] resulting in an increase in local and regional control rates.

The use of these ions in clinical practice required not only extensive biological studies, but also technical developments in patient immobilization, beam delivery, patient dosimetry and the use of CT and later MRI for tumor targeting. Development of a 3-D computerized treatment planning system was critical to successful charged-particle treatment planning and delivery [9–12]. Ion beams used at LBL included helium, carbon, neon, silicon and argon ions with energies ranging from 230–670 MeV/u. However, carbon, silicon and argon ions were used in a limited fashion only, as part of phase I toxicity studies. Time and beam availability did not permit any significant clinical testing of these beams. The majority of the clinical studies at UCSF-LBL was accomplished with helium and neon ions. The choice of beam in clinical trials depended on availability, and whether it was desirable to exploit the high-LET of neon ions, or the dose localization properties of helium ions.

The Clinical Procedure at Berkeley

Indications for the use of heavy ions can perhaps best be illustrated by a brief review of LBL's clinical experience. It reveals the importance of clinical factors including histology, tumor site and volume, extent of resection or whether a treatment is for primary or recurrent disease. But it also points at the questions that remain to be answered.

After a thorough history and physical examination, treatment planning began with an individually constructed immobilization device. Generally, a thermoplastic splinting material was used. A planning CT (and in later years, an MRI), in the treatment position whenever possible, was accomplished and the physician outlined the target volume on each image slice. A VAX II/780 computer was then used to produce multiplanar

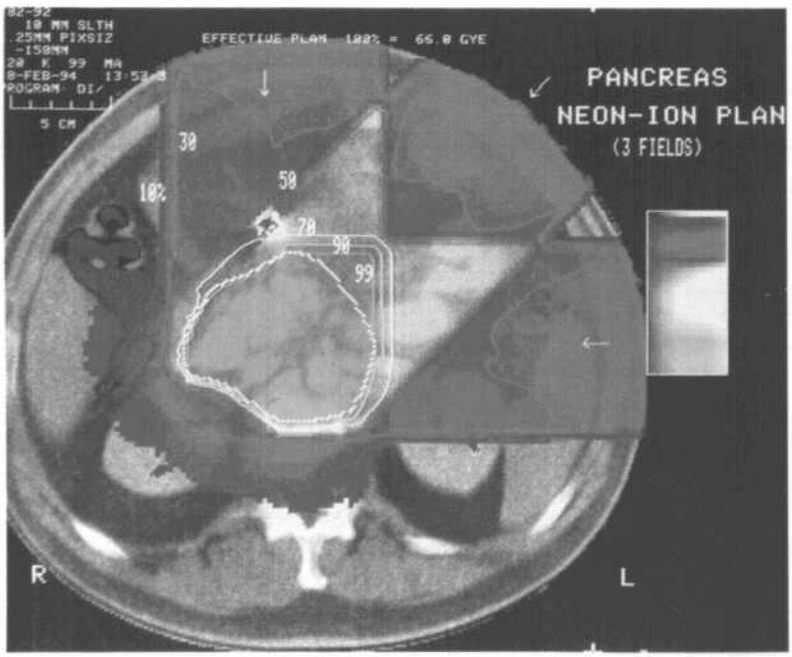

Fig. 1. An example of a biologically corrected (GyE) neon ion 3-field plan for treatment of carcinoma of the pancreas. Normally isodose plans would be prepared for several CT slices of interest in the target volume. Only one is shown here for brevity. A physical isodose plan in Gy was also prepared for each patient.

physical and biologically corrected dose distributions (Fig. 1). Tissue compensators and beam collimators were designed based on CT data using the LBL treatment planning system. In later years, dose-volume histographic analysis of critical structures was also available to assist with treatment planning. Digitally reconstructed radiographs and other portal alignment aids were also prepared from the treatment planning program. To assist in accurate beam delivery, laser lights, close-up TV monitoring and daily portal films were used. The actual treatment times were as short as possible to minimize the possibility of patient motion during treatment. Typically, the times ranged from 1–3 minutes, whereas preparatory set-up times were in the range of 10–30 minutes, depending on complexity of the set-up. Improvements in tumor targeting and treatment planning, increased knowledge of late effects and improved beam delivery techniques resulted in better clinical results in the later years [8].

The biologically corrected isodose distibution at UCSF-LBL were defined in terms of Gray-equivalents (GyE), with 1 GyE of charged particle irradiation being biologically equivalent to 1 Gray of low-LET megavoltage irradiation.

Selected Clinical Results

Skull Base Tumors

From 1977 through 1992, 223 patients were irradiated with helium and neon ions at UCSF-LBL for tumors either arising in or extending to the skull base [8, 13, 14]. Histologies including primary or recurrent squamous cell carcinoma of the nasopharynx or paranasal sinuses extending to the skull base, major or minor salivary gland tumors, chordomas, chondrosarcomas, osteo- and neurofibrosarcomas and paraclival meningiomas.

One hundred twenty-six patients with tumors arising in the skull base were irradiated with heavy ions. One hundred nine of these patients were treated with helium ions. Seventeen, who received part of their therapy with neon ions, are also included in the analysis.

The daily dose was 2.0 GyE, given in 4 fractions per week to total doses of 60–80 GyE (mean: 68 GyE). The RBE value used for helium ions was 1.3 for most tissues except for CNS, where 1.6 was used. For neon, the corresponding values were 2.5 and 4.5, respectively. Applying these factors, the limiting doses to brain stem were calculated to be 60 GyE, 55 GyE to the optic chiasm, and 45 GyE for cervical spinal cord. Due to limitations of beam availability, helium ion treatments were often combined with photon treatments for 30–70% of the total dose.

The Kaplan-Meier [15] local control rate (KM-LCR) for the entire group of 126 patients with primary skull base tumors was 71% at 5 years and 51% at 10 years. KM survival at 5 years was 77% and 62% at 10 years. Follow-up ranged from 4–191 months with a median of 51 and a mean of 58 months (Table 2). Clinicians will recognize that local control and survival appeared improved compared to historical data in all tumor histologies. Specific numerical comparison of overall survival is problematic since patients referred to LBL were often considered poor candidates for conventional photons where outcome was expected to be unsatisfactory.

In the group of 55 patients treated between 1977 and 1986, before the availability of MRI for tumor delineation, local control was 60%. This increased to 78% in the 71 patients treated during the years from 1987 through 1992 representing the influence of improved treatment planning, immobilization and treatment delivery.

The incidence of serious complications was acceptable given the levels of dose required for these tumors in critical locations. Just as outcome had improved with experience, so too, complication rates decreased in later years [8]. During the years from 1977 through 1986, when treatment

Table 2. Results of skull base therapy with ions at Berkeley

	5-year KM-LCR (%)	5-year KM survival (%)
Meningioma	85	82
Chondrosarcoma	78	83
Chordoma	63	75
Other Sarcoma	58	71

Follow-up: 4–191 months, median 51 months

planning relied on CT and treatment techniques were less well developed, 41% (12/29) had RTOG/EORTC grades 3, 4 or 5 complications. From 1987 through 1992, when MRI was used to delineate the tumor volume and image correlation techniques were developed to transfer data between MRI and CT, the complication rate declined to 20% (11/55). This decline also reflected better knowledge of late effects, and reduction in the maximum total tumor dose to 72 GyE. Complications observed were mainly injury to the central nervous system including cranial nerves, brain stem or temporal lobes. Temporal lobe injuries were manifested by MRI changes (in some cases asymptomatic), memory deficits or the development of seizures. With recognition of these changes, additional efforts were made to spare as much of the temporal lobe as possible by using multiple ports and non coplanar beams. There were 3/85 patients with grade 5 complications, all of whom had had previous treatment. Continued optimization of ion beam therapy for skull base tumors should lead to serious complication rates of not more than 5% in patients that have not been previously irradiated.

Total resection remains the optimal approach to treatment of meningioma of the skull or spine but is often not possible when disease is located in the orbits, near the clivus, sella or cavernous sinus, or in the spine. Multiple reported series have shown the benefit of postoperative treatment in subtotally resected lesions [16–20]. Twenty-six patients with meningioma in the skull base or spine were treated between 1981 and 1992 at Berkeley [21]. The total doses ranged from 53–80 GyE (mean 63 GyE) and were delivered with helium. The 10-year LCR and survival rates were 84% and 80%, respectively. There were 2 intercurrent deaths from other malignancies at 46 and 82 months and both of these patients had local control of their meningioma. Four patients with massive and/or recurrent tumors had evidence of tumor progression and subsequently died. These results are quite excellent in view of the fact that only patients with either malignant meningiomas or massive recurrences ultimately failed. Based on this series of patients we believe that at least 60 GyE are needed for control of small to moderate meningiomas and possibly higher doses for larger ones. The generally accepted fractionation for photons is 50–55 Gy at 1.8–2 Gy per day [21].

In the group of patients with tumors invading the skull base from the nasopharynx, paranasal sinuses or salivary glands, the general trend was also to favorable local control and survival rates. Feehan et al. [22] reported on 11 patients with locally recurrent nasopharyngeal cancer showing excellent results. All patients had previously received full course irradiation to a median dose of 70.2 Gy and were treated at UCSF-LBL for recurrence. The median ion dose was 50.3 GyE (range 31.8–62.3 GyE). Some patients had also received varying regimens of chemotherapy. The group as a whole demonstrated a KM-LCR rate of 45% at 2 years and a median survival of 27 months. For 12 patients treated with locally advanced (T4) primary cancer of the nasopharynx with skull base invasion, treatment to the primary and regional nodes started with photons to 50 Gy and was then completed with an ion boost to a cumulative mean tumor dose of 72 GyE (range 68–80 GyE). They had a 2-year KM-LCR of 83%. Follow-up ranged from 10–81 months.

In the entire group, patients with recurrent disease fared worse, having a 2-year KM-LCR of 50% and 5-year survival of 20% versus 80% and 50%, respectively, for patients treated for primary tumors.

For patients with tumors either partly or completely surrounding the brain stem or spinal cord, a specialized technique was developed at Berkeley [14]. Dividing the target volume into 2 or more portions and using a combination of beams allowed a reasonably homogeneous dose distribution to encompass the target, yet also spared critical CNS structures. This technique requires careful treatment planning based on metrizamide contrast CT and/or MRI, accurate compensation for tissue inhomogeneities and verifiable patient immobilization to within ± 2 mm. In the initial report of 47 patients with varying histologies treated with this technique, local control was 62% and complications 13%. Radiation injury to the spinal cord or brain stem was low occurring in only 3 patients. Median follow-up was 20 months (range 6–90 months).

Potentially High-LET Responsive Tumors

Beginning in 1979, a phase I–II clinical trial was undertaken at UCSF-LBL using neon ions. Linstadt et al. [23] reported on the initial 239 patients who had received neon ions to a dose of at least 10 Gy (physical dose), or at least 40% of their total dose. The purpose of the initial trial was to develop techniques for therapy planning and delivery, evaluate the acute and late toxicity of neon ion irradiation, and study the response of a variety of malignancies. Generally, patients were selected for treatment when their tumors were not expected to respond favorably to conventional irradiation. By May of 1992, a total of 299 patients had completed therapy receiving at least 10 Gy of neon ions. Compared with historical results, the 5-year actuarial survival, disease-specific survival (DSS) and local control rates suggested that neon is of benefit in several tumor types, namely advanced or recurrent macroscopic salivary gland tumors, paranasal sinus tumors, advanced soft tissue sarcomas, macroscopic sarcoma of bone, locally advanced prostate carcinoma and biliary tract carcinoma (Tab. 3). Again clinicians will recognize that these results are quite excellent and merit further study. Comparisons with historical data are made cautiously with all the usual caveats of the danger in doing so, not the least of which is to ascertain that patients in various series are indeed comparable.

Unresectable or Locally Recurrent Salivary Gland Tumors

At UCSF-LBL 18 patients were treated with a 5-year KM-LCR of 61% and corresponding DSS of 59% [23]. Similar excellent results were reported with neutrons from single institutions [24–26] and in a phase III randomized RTOG/MRC trial in 1993 [27]. The significant differences between photon and neutron results, coupled with the neon ion results, are sufficient to establish high-LET radiation as the treatment of choice for this type of malignancy.

Table 3. Treatment outcome comparing neon beam, neutron, and conventional X-ray therapy for selected types of tumors. Data from [23, 30, 32]

Tumor and endpoint studied	Neon (%)	Neutrons (%)	X-rays (%)
Macroscopic salivary gland carcinoma (Long-term local control)	61	60–70	25–36
Macroscopic paranasal sinus carcinoma			
(Long-term survival)	69	30+	32–40
(Long-term local control)	69	50–86	N/A
Macroscopic soft tissue sarcoma (Long-term local control)	56	50–54	30–50
Macroscopic sarcoma of bone (Long-term local control)	48	49–55	21–33
Locally advanced prostate carcinoma	91	N/A	N/A
Biliary tract	44	N/A	18

Paranasal Sinus Tumors

Twelve patients have been treated with neon ions for paranasal sinus tumors, achieving an actuarial 5-year DSS and local control of 69%. All patients with microscopic disease remained disease-free and 3 patients with gross disease failed 11, 37 and 76 months after treatment [23].

Advanced Soft Tissue Sarcoma

Between 1978 and 1989, 32 patients with unfavorable soft tissue sarcoma underwent ion beam irradiation with curative intent [23, 28, 29]. Twenty-two patients had tumors located in the trunk and 10 patients had tumors in the head and neck area. Macroscopic tumor was present in 22. Two patients had tumors felt to have been caused by prior therapeutic irradiation. Follow-up times for surviving patients ranged from 4–121 months (median 27), and the 3-year KM-LCR was 62% with corresponding KM survival rate of 50%. All patients with microscopic disease were locally

controlled, whereas local control was only 48% when macroscopic disease was present. Patients with retroperitoneal tumors fared particularly well with 5-year KM-LCR of 64% and survival rates of 62%. Complications were acceptable. Overall, these results are promising and deserve further investigation.

Bone Sarcoma

Uhl et al. [30] reported on 17 patients with unfavorable bone sarcoma including osteosarcoma, Ewings sarcoma and recurrent osteoblastoma. Four patients had radiation induced tumors. Most patients had tumors located near critical structures and gross disease was present in all but 2. Six patients were treated for recurrent disease. The 5-year KM-LCR was 48% and survival 41%. The results of this preliminary work support further investigation.

Sacral Chordoma

Schoenthaler et al. [31] reported on 14 patients treated for sacral chordoma in whom the median follow-up was 5 years. These patients were treated to a mean dose of 75 GyE. Most patients were treated after attempted resection but only a few had gross total resection, with macroscopic disease present in 10. The KM survival at 5 years was 85% and the KM-LCR 55%. A trend toward increased local control was seen in patients treated predominantly with neon (62%) versus helium (34%), supporting the high-LET advantage of the former.

Prostate Cancer

Twenty-three patients most with either poor or moderately differentiated stage B2 (8 pts.) and C (15 pts.) prostate tumors have been treated at Berkeley using neon ions for the cone-down "boost" portion of the therapy after pelvic irradiation with photons.

KM-LCR in this group of patients is projected at the 84% level at 7.5 years post treatment. KM survival is 85% at 5 years post therapy and 64% at 7.5 years. High-LET ion irradiation appears to diminish the local failure rate in locally advanced tumors to the level of 10–15%. However, at the neon doses given (approx. 10 Gy), 3 of the 23 patients have had rectal injuries possibly attributable to the neon ion treatment. One patient had a very large tumor with the result that a larger than usual volume of rectum was treated. Anal sphincter stricture developed leading to colostomy. Another patient developed an anterior rectal wall ulcer leading to a rectovesical fistula requiring a colostomy and ileal conduit. A third patient had a colostomy following development of a rectal ulcer inferior to the neon target volume. These results indicate that caution should be used in treating locally advanced prostate cancer with heavy ions. After pelvic radiation therapy to 45–50 Gy, the prostate should receive in the range of 5–7 Gy (physical dose) or approximately 15–20 GyE of neon ion irradiation.

Bile Duct Carcinoma

Initial phase I–II studies revealed encouraging results in treating adenocarcinoma of the bile ducts. Linstadt et al. [23], and Schoenthaler et al. [32] subsequently published retrospective results on patients who had received radiation therapy for bile duct carcinoma at UCSF-LBL between 1977 and 1987. Thirty received photons only to a mean dose of 54 Gy and 18 received helium and/or neon to a mean dose of 60 GyE. Thirty-six patients had gross residual disease and none had negative margins. With minimum follow-up for survivors of 2.5 years, ion treated patients fared better with an overall actuarial 2-year survival of 44% vs. 18% for photon treated patients ($p = 0.05$). Median actuarial survival for the patients treated with ions was 23 months versus 12 months for those treated with photons. Local control was also improved for all heavy ion patients as manifested by a median disease-free survival of 20 months versus 4.5 months ($p = 0.05$). There was a trend to increased survival, disease-free survival and local control in the neon-ion treated patients. But as the numbers in the various subgroups were small, further investigation is needed, before final conclusions can be drawn.

Other Tumors

Improved outcome, theoretically postulated with high-LET beams, was not realized in several tumor groups treated at Berkeley. Though dose localization for esophageal tumors with helium ions was clearly shown to be superior to photons [33], clinical results in an early trial of 32 patients with squamous cell esophageal cancer and 18 patients with adenocarcinoma of the stomach were disappointing [34]. These patients received 60–70 GyE at 2.0–2.3 GyE per fraction. All patients had unresectable locally advanced disease without evidence of distant metastasis. Median survival for the patients with esophageal cancer was 9 months and 7 months for the patients with gastric cancer. Most patients developed local failure after therapy.

It should be noted that the esophageal cancer patients were treated in the early LBL years and did not receive systemic chemotherapy. With the demonstrated safety of the delivery of high doses of heavy ions a new trial of combined chemotherapy and heavy charged-particle irradiation in esophageal and gastric neoplasms should be considered.

The initial results obtained in the treatment of pancreatic carcinoma were encouraging [35] and based on this, a prospective randomized trial comparing definitive helium radiation with split course conventional photon radiation was carried out. Patients received 60 Gy of photons or 60–70 GyE helium, both given concurrently with bolus 5-fluorouracil. There was no significant difference in the overall survival of each treatment arm though helium treated patients did show slightly higher rates of local control [36]. Four of 5 helium treated patients who survived longer than 18 months subsequently died of local failure without distant metastasis suggesting perhaps that more aggressive local treatment might result in improved survival.

A subsequent trial of neon ion irradiation combined with 5-fluorouracil, adriamycin and mitomycin C chemotherapy did not yield superior results, and treatment of pancreatic cancer with heavy ions was abandoned at UCSF-LBL in the mid 1980's. Retesting of this difficult to treat tumor with heavy ions awaits better chemotherapy, both for enhanced local effect and control of distant metastases. The use of dynamic ion beams conformal therapy [37, 38] might help to reduce the late gastrointestinal toxic effects.

In 1985, results of the Northern California Oncology Group (NCOG) phase I–II trial of the use of heavy charged particles for glioma were reported [39]. The aim of the study was to determine local tumor response, quality and length of survival, as well as normal brain tissue tolerance to heavy particles. A total of 39 patients with a variety of gliomas (33 de novo and 6 with biopsy confirmed recurrence) were treated. Initially, a group of 11 patients was treated with helium ions. The next group of 12 patients received a portion of their treatment with either carbon or neon ions as a boost after helium or low-LET standard radiation. Another group of 10 patients was treated with neon ions alone to doses of 16–18 Gy. Overall, the results with glioblastoma appeared similar to those obtained historically with standard radiation, with a median survival of about 11 months. A subsequent trial utilizing neon ions alone for glioblastoma of the brain, randomized to doses of 20 or 25 Gy, was carried out without significantly prolonging survival (median 13.5 months) or local control.

Future Directions

The use of protons and helium ions in the treatment of unresectable or partially resectable neoplasms in critical locations such as the orbit, eye, skull base, juxtaspinal area, retroperitoneum or pelvis has clearly been demonstrated to be of value. Delivering higher tumor doses while preserving adjacent critical normal tissues has resulted in higher rates of local control and survival compared to previous results with megavoltage X-ray or electron beam therapy. In the future, these results should be compared with those of dynamic conformal photon therapy, to determine the best application of these modalities for various tumor sites.

The Berkeley experience with heavy ions has shown that there may be a role for this modality in the treatment of slow growing malignancies such as adenocarcinoma, or sarcoma. Unfortu-

nately, lack of beam time at LBL limited the amount of information that could have been obtained regarding clinical use of these ions. High-LET ions such as carbon, neon or silicon ions have not had sufficient study to prove or disprove their merits in clinical therapy. Neon ions, while giving promising initial results, have had significant late effects on normal tissues.

While much has been learned regarding the clinical potential of particles in radiotherapy, it is likely that a further generation of use will be needed to fully assess their role in clinical practice. High-LET charged-particle radiotherapy would certainly be aided by better modeling of LET effects, but more radiobiological and dosimetric studies are required to achieve this goal. Studies dealing with dose specification in particle fields, biological models for estimating tissue-specific RBE values and the means to incorporate them into treatment planning are needed. Combined effects of chemotherapeutic agents and particle radiation, as suggested by Linstadt's preliminary work with neon and iododeoxyuridine, should be pursued [40]. The late normal tissue effects of high-LET radiations should be minimized and may be obviated by selecting an ion such as carbon and using dynamic conformal therapy. Both of these should provide less damage to normal tissues in the beam entrance region and give a better therapeutic ratio. Coupled with predictive assays to select patients with tumors likely to be helped by high-LET radiation, such data would help to put ion beam therapy on a more rational basis for the next 25 years.

References

1 Wilson, R. Radiological use of fast protons. Radiology 47, 487–491, 1946.

2 Tobias, C.A., Anger, H.O., and Lawrence, J.H. Radiologic use of high energy deuterons and alpha particles. Am. J. Roentgenol. Rad. Ther. Nucl. Med. 67, 1–27, 1952.

3 Phillips, T.L., Ross, G.Y., Goldstein, L.S., and Ainsworth, J. In vivo radiobiology of heavy ions. Int. J. Radiat. Oncol. Biol. Phys. 8, 2121–2125, 1982.

4 Tobias, C.A., Blakely, E.A., Alpen, E.L., Castro, J.R., Ainsworth, E.J., Curtis, S.B., Ngo, F.Q.H., Rodriguez, A., Roots, R.J., Tenforde, T., and Yang, T.C.H. Molecular and cellular radiobiology of heavy ions. Int. J. Radiat. Oncol. Biol. Phys. 8, 2109–2120, 1982.

5 Blakely, E., Castro, J., Austin-Seymour, M., Chen, G., Lommel, L., Yezzi, M., Chang, P., and Tobias, C. Clinical and cellular radiobiological studies of silicon ion beams. Int. J. Radiat. Oncol. Biol. Phys. 2 (Suppl.), 131, 1984.

6 Blakely, E., Chang, P., and Lommel, L. Cell-cycle dependent recovery from heavy ion damage in G1-phase cells. Radiat. Res. 104, 145–157, 1985.

7 Blakely, E.A., Ohara, H., Chang, P.Y., and Lommel, L. Response of aerobic and hypoxic human lung squamous cell carcinoma cells to neon ions 1987, LBL-Report No. 20345, Biology and Medicine Division, LBL.

8 Castro, J.R., Linstadt, D.A., Bahary, J.P., Petti, P.L., Daftari, I., Collier, J.M., Gutin, P.H., Gauger, G., and Phillips, T.L. Experience in charged particle irradiation of tumors of the skull base:1977–1992. Int. J. Radiat. Oncol. Biol. Phys. 29, 647–655, 1994.

9 Frass, B.A., McShan, D.L., Diaz, R.F., Ten Haken, R.K., Aisen, A., Gebarski, S., Glazer, G., and Lichter, A.S. Integration of magnetic resonance imaging into radiation therapy treatment planning: I. Technical considerations. Int. J. Radiat. Oncol. Biol. Phys. 13, 1897–1908, 1987.

10 Kessler, M.L., Pitluck, S., Petti, P., and Castro, J.R. Integration of multimodality imaging data for radiotherapy treatment planning. Int. J. Radiat. Oncol. Biol. Phys. 21, 1653–1667, 1991.

11 Saunders, W.M., Char, D.H., Quitvey, J.M., Castro, J.R., Chen, G.T.Y., Collier, J.M., Cartigny, A., Blakely, E.A., Lyman, T.J., Zink, S.R., and Tobias, C.A. Precision, high dose radiotherapy. II. Helium ion treatment of tumors adjacent to critical central nervous system structures. Int. J. Radiat. Oncol. Biol. Phys. 11, 1339–1347, 1985.

12 Chen, G.T.Y., Singh, R.P., Castro, J.R., Lyman, J.T., and Quivey, J.M. Treatment planning for heavy ion radiotherapy. Int. J. Radiat. Oncol. Biol. Phys. 5, 1809–1819, 1979.

13 Castro, J.R. and Reimers, M.M. Charged particle radiotherapy of selected tumors of the head and neck. Int. J. Radiat. Oncol. Biol. Phys. 14, 711–720, 1988.

14 Castro, J.R., Collier, M., Petti, P.L., Nowakowski, V., Chen, G.T.Y., Lyman, J.T., Linstadt, D., Gauger, G., Gutin, P., Decker, M., Phillips, L., and Baken, K. Charged particle radiotherapy for lesions encircling the brain stem or spinal cord. Int. J. Radiat. Oncol. Biol. Phys. 17, 477–484, 1989..

15 Kaplan, E.L. and Meier, P. Nonparametric estimation from incomplete observations. J. Am. Stat. Assoc. 53, 457, 1958.

16 Forbes, A.R. and Goldberg, I.D. Radiation therapy in the treatment of meningioma: The joint center for radiation therapy experience 1970–1982. J. Clin. Oncol. 2, 1139–1143, 1984.

17 Taylor, B.W., Marcus, R.B., Friedman, W.A., Ballinger, W.E., and Million, R.R. The meningioma controversy: Postoperative radiation therapy. Int. J. Radiat. Oncol. Biol. Phys. 15, 299–304, 1988.

18 Glaholm, J., Bloom, H.J.G., and Crow, J.H. The role of radiotherapy in the management of intracranial meningiomas: The Royal Marsden experience with 186 patients. Int. J. Radiat. Oncol. Biol. Phys. 18, 755–761, 1990.
19 Miralbell, R., Linggood, R.M., de la Monte, S., Covery, K., Munzenrider, J.E., and Mirimanoff, R.O. The role of radiotherapy in the treatment of subtotally resected meningiomas. J. Neurooncol. 13, 157–164, 1992.
20 Goldsmith, B.J., Wara, W.M., Wilson, C.B., and Larson, D.A. Postoperative irradiation of subtotally resected meningiomas. J. Neurosurg. 80, 195–201, 1994.
21 Kaplan, I.D., Castro, J.R. and Phillips, T.L. Helium charged particle radiotherapy for meningioma: Experience at UCLBL. Int. J. Radiat. Oncol. Biol. Phys. 28, 257–261, 1994.
22 Feehan, P.E., Castro, J.R., Phillips, T.L., Petti, P., Collier, M., Daftari, I., and Fu, K. Recurrent locally advanced nasopharyngeal carcinoma treated with heavy charged particle irradiation. Int J. Radiat. Oncol. Biol. Phys. 23, 881–884, 1992.
23 Linstadt, D., Castro, J., and Phillips, T.L. Neon ion radiotherapy: Results of the phase I/II clinical trial. Int. J. Radiat. Oncol. Biol. Phys. 20, 761–769, 1991.
24 Saroja, K.R., Mansell, J., Hendrickson, F.R., Cohen, L., and Lennox, A. An update on malignant salivary gland tumors treated with neutrons at Fermilab. Int. J. Radiat. Oncol. Biol. Phys. 13, 1319–1325, 1987.
25 Koh, W.J., Laramore, G., Griffin, T., Russel, K., Griffen, B., Parker, R., Davis, L., and Pajak, T.F. Fast neutron radiation for inoperable and recurrent salivary gland cancers. Am. J. Clin. Oncol. 12, 316–319, 1989.
26 Catterall, M. and Errington, R.D. The implications of improved treatment of malignant salivary gland tumors by fast neutron radiotherapy. Int. J. Radiat. Oncol. Biol. Phys. 13, 1313–1318, 1987.
27 Laramore, G.E., Krall, J.M., Griffin, T.W., Duncan, W., Richter, M.P., Saroja, K.R., Moar, M.H., and Davis, L.W. Neutron versus photon irradiation for unresectable salivary gland tumors: Final report of an RTOG/MRC randomized clinical trial. Int. J. Radiat. Oncol. Biol. Phys. 27, 235–240, 1993.
28 Linstadt, D.E., Castro, J.R., Phillips, T.L., Petti, P.L., Collier, J.M., Daftari, I. Schoenthaler, R., and Raynor, A. Charged particle irradiation of soft tissue sarcomas (Abstr.), in Ninth Ann. Meeting of the Europ. Soc. Therap. Radiol. Oncol. 1990, Montecatini, Terme, Italy.
29 Reimers, M., Castro, J.R., Linstadt, D., Collier, J.M., Henderson, S., Hanninghan, J., and Phillips, T.L. Heavy charged particle therapy of bone and soft tissue sarcoma. A phase I–II trial of the University of California Lawrence Berkeley Laboratory. Am. J. Clin. Oncol. 96, 488–493, 1986.
30 Uhl, V., Castro, J.R., Knopf, K., Phillips, T.L., Collier, J.M., Petti, P.L., and Daftari, I. Preliminary results in heavy charged particle irradiation of bone sarcoma. Int. J. Radiat. Oncol. Biol. Phys. 24, 755–759, 1992.
31 Schoenthaler, R., Castro, J.R., Petti, P.L., Baken-Brown, K., and Phillips, T.L. Charged particle radiation of sacral chordomas. Int. J. Radiat. Oncol. Biol. Phys. 26, 291–298, 1993.
32 Schoenthaler, R., Castro, J.R., Halberg, F.E., and Phillips. T.L. Definitive postoperative irradiation of bile duct carcinoma with charged particles and/or photons. Int. J. Radiat. Oncol. Biol. Phys. 27, 75–82, 1993.
33 Zink, S.R., Lyman, J.T., Castro, J.R., Chen, G.T.Y., Collier, J.M., and Saunders, W.M. Treatment planning study for carcinoma of the esophagus: helium ions versus photons. Int. J. Radiat. Oncol. Biol. Phys. 14, 993–1000, 1988.
34 Castro, J.R., Saunders, W., Chen, G.T.Y., Collier, J.M., Pitluck, S., Woodruff, K.H., Cartigne, A., Friedman, M., Phillips, T.L., and Austin-Seymour, M. Helium charged particle radiotherapy of locally advanced carcinoma of the esophagus, stomach and biliary tract. Am. J. Clin. Oncol. 6, 629–637, 1983.
35 Castro, J.R., Quivey, J.M., Lyman, J.T., Chen, G.T.Y., Phillips, T.L., Tobias, C.A., and Alpen, E.A. Current status of clinical particle radiotherapy at Lawrence Berkeley Laboratory. Cancer 46, 633–641, 1980.
36 Linstadt, D., Quivey, J.M., Castro, J.R., Andejeski, Y., Phillips, T.L., Hannigan, J., and Gribble, B.A. Comparison of helium-ion radiation therapy and split course megavoltage irradiation for unresectable adenocarcinoma of the pancreas. Final report of a Northern California Oncology Group randomized prospective clinical trial. Radiology 168, 261–264, 1988.
37 Chu, W.T., Renner, T.R., and Ludewigt, B.A. Dynamic beam delivery for three-dimensional conformal therapy, in Proc. EULIMA Workshop on the Potential Value of Light Ion Beam Therapy, Chauvel, P. and Wambersie, A. (eds.), Nice, France, Nov. 3–5, 1988, pp. 295–328.
38 Castro, J.R., Petti, P., Daftari, I.K., Collier, J.M., Renner, T., Ludewigt, B., Chu, W., Pitluck, S., Fleming, T., Alonso, J., and Blakely, E. Clinical gain from improved beam delivery systems. Radiat. Envir. Biophys. 31, 233–240, 1992.
39 Castro, J.R., Saunders, W.M., Austin-Seymour, M., Woodruff, K.H., Gaucher, G., Chen, G.T.Y., Collier, J.M., Phillips, T.L., and Zink, S.R. A phase I–II trial of heavy charged particle irradiation of malignant glioma of the brain: A Northern California Oncology Group study. Int. J. Radiat. Oncol. Biol. Phys. 11, 1795–1800, 1985.
40 Linstadt, D., Blakely, E., Phillips, T.L., and Castro, J.R. Radiosensitization produced by iododeoxyuridine with high linear energy transfer heavy ion beams. Int. J. Radiat. Oncol. Biol. Phys. 15, 703–710, 1988.

16 Radiosurgery with Ion Beams

R. P. Levy[1,2,3], K. A. Frankel[1,2,3], and G. K. Steinberg[3]

[1] Lawrence Berkeley Laboratory, Berkeley, CA, [2] Loma Linda University Medical Center, Loma Linda, CA, and [3] Stanford University Medical Center, Stanford, CA, USA

Introduction

The clinical application of ion beam irradiation has been the subject of biomedical research and clinical development since 1946, when Wilson [1] first proposed the therapeutic use of fast protons based on their unique physical characteristics. After completion of the 184-inch synchrocyclotron at the University of California at Berkeley – Lawrence Berkeley Laboratory (LBL) in 1947 [2], Tobias and Lawrence and their colleagues [3–5] began the study of the biological effects of fine focal beams of protons, deuterons and helium ions, with particular emphasis on reaction to radiation injury in the brain [6, 7]. Since 1954, more than 6000 patients world-wide have been treated with stereotactic charged particle radiosurgery. The great majority of these patients have been treated at LBL [7–10], the Harvard Cyclotron Laboratory – Massachusetts General Hospital (HCL) [11, 12], the Institute of Theoretical and Experimental Physics (ITEP) in Moscow [13], and the Institute of Nuclear Physics (INP) in St. Petersburg [14]. Proton radiosurgery programs have recently been initiated at Loma Linda University Medical Center (LLUMC) and at the University of Uppsala.

Clinical applications were constrained initially by the limitations of neuroradiological techniques for treatment planning, stereotactic localization and dose distribution [6]. Early clinical trials, therefore, were restricted to pituitary ablation treatment, wherein small, well-defined intracranial target volumes could be localized accurately by existing neuroradiological procedures. In 1954, the first stereotactic irradiation procedures utilizing ion beams in clinical patients were performed at LBL for pituitary hormone suppression in the treatment of metastatic breast carcinoma [4, 15, 16]. Shortly thereafter, charged particle radiosurgery was applied to the pituitary ablation treatment of patients with proliferative diabetic retinopathy [17] and to the treatment of pituitary adenomas [16, 18, 19]. With the development of improved techniques of stereotaxis and cerebral angiography, the radiosurgery approach, using Bragg peak protons, was applied to the treatment of arteriovenous malformations (AVMs) at HCL by Kjellberg et al. [11] in 1965. More recently, the advent of high-resolution computed X-ray tomography (CT) and magnetic resonance imaging (MRI) has made it possible for reliable stereotactic localization and irradiation techniques to be applied to the treatment of a diverse collection of disorders [20]. The expanded application of ion beams in radiosurgery of intracranial lesions promises new and innovative approaches in radiation oncology and neurosurgery.

In this chapter, the methods and clinical experience with helium ion and proton radiosurgery in North America are reviewed. The emphasis on helium ions reflects the authors' long-term clinical experience. The Russian experience with proton radiosurgery is described in Chapter 12 of this volume.

Methods

The methods of charged particle radiosurgery have been progressively refined during the past four decades to reflect concurrent theoretical and technical advances in physics, neuroradiology and computer science. To utilize fully the unique physical characteristics of charged particle beams for effective treatment, the target volume must be defined and located precisely within a reproducible three-dimensional frame of reference, the physical properties of the materials to be traversed by the beam must be determined accurately, and the patient must be positioned accurately with respect to the beam [6]. Treatment planning consists of a series of stages involving sequential stereotactic neuroradiological imaging studies, computer-assisted correlations among the different types of radiological imaging information and calculations of the dose distributions.

Bragg Peak Radiosurgery

In this section, we consider Bragg-peak radiosurgery for AVMs, a condition for which cerebral angiography plays a major role in target definition and localization [6, 8, 21]. The methods of target delineation and treatment planning currently being used in the LLUMC-LBL-Stanford University Medical Center (SUMC) collaborative proton radiosurgery program are described [22]. As of October 1994, 32 patients with AVMs had been treated at LLUMC using these techniques. Many aspects of the methods described in this section, however, are also applicable to the treatment of other intracranial disorders for which angiographic data are of little consequence.

Neuroradiological Procedures

Patients are immobilized for stereotactic neuroimaging, treatment planning and (subsequent) proton treatment procedures by a non-invasive relocatable head immobilization system, consisting of a vacuum-assisted dental fixation device, a vacuum-secured stereotactic head frame and interchangeable CT and angiographic localization devices. Biplanar orthogonal cerebral angiography is performed for each arterial vessel complex supplying the AVM. CT scanning without and with contrast is performed in precisely matched 2-mm-increment axial slices. The CT imaging data set is then input to the LLUMC treatment planning system. MRI studies are performed using standard T1 and T2 pulse sequences in axial, coronal and sagittal planes.

Image Correlation and Iterative Target Delineation

Initial AVM target contours are defined on selected orthogonal angiographic films for each arterial vessel complex studied. AVM contours, external fiducials from the angiographic and CT localizer boxes and implanted titanium skull screw fiducials are digitized and their coordinates entered into an image correlation software program. The program then interpolates angiographically defined contours into CT space on a 2-mm slice-by-slice basis. This procedure results in a craniocaudal stack of quadrilaterals in non-contrast CT space in the treatment planning system. The corners of each quadrilateral are determined by the AVM nidus' angiographic extrema in anteroposterior and left-right dimensions in the corresponding axial plane. Target contours are also defined on MRI and contrast-CT, and then transferred to the non-contrast CT image set in the planning system. After targeting inconsistencies among the different imaging modalities are resolved, further consideration is given to any radiobiological or anatomical factors (e.g., proximity to radiosensitive structures, such as optic chiasm or hypothalamus) that might influence the final delineation of the target volume. The goal is to define a final set of contours for the target volume and for adjacent sensitive normal brain structures on each CT slice in the region of interest.

Treatment Planning

The general technique of treatment planning for charged particle radiosurgery of AVMs has been described previously [6, 8, 21, 23, 24]. By using individually shaped collimators, tissue-equivalent boluses and range modifying absorbers, each proton beam can be tailored to place a uniquely shaped high-dose volume stereotactically within the brain (Fig. 1). Typically, a set of six separate potential beam ports, reflecting multiple entry angles and converging on the target volume, are planned individually. Usually, three or four of these beam ports are selected, with the assistance of dose-volume histogram analysis, to comprise the optimal composite treatment plan. The goal is to match the 90% isodose surface to the edge of the target volume to the extent possible, while minimizing the dose to sensitive adjacent brain structures. The comparative physical advantage of charged particles vis-à-vis photons for shaping the dose to conform to the target volume becomes progressively greater with increasing target diameter and irregularity of the lesion [25], as is illustrated in Figure 2.

Plateau Beam Radiosurgery

When an ion beam of sufficiently high energy, and hence greater depth of penetration, is available, radiosurgery can be performed with the plateau ionization portion of the beam. In this treatment configuration, the beam passes completely through the head, depositing plateau region radiation in the brain. The Bragg peak

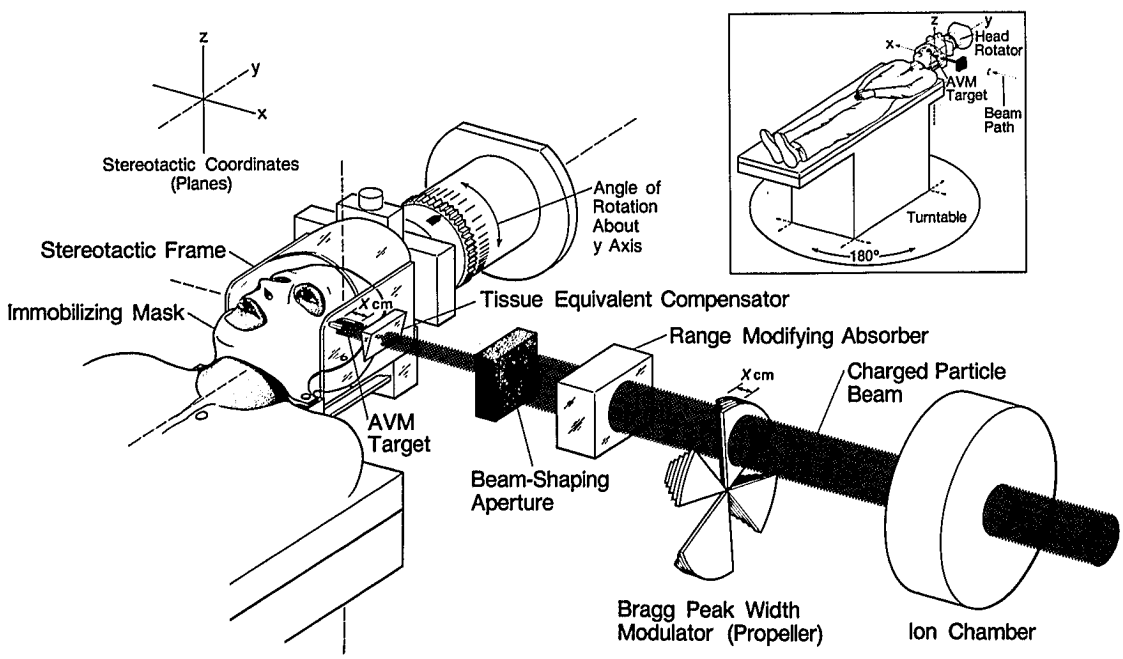

Fig. 1. Schematic diagram of charged particle beam delivery system at LBL for stereotactic radiosurgery. The patient positioning system allows translation along three orthogonal axes and rotation about the y and z axes. The width of the Bragg ionization peak is spread to the prescribed size by interposing a modulating filter of comparable maximum thickness (x cm) in the beam path, shown here as a variable thickness propeller. The range in tissue of the Bragg peak region is determined by a range modifying absorber. An individually designed aperture, specifically tailored to the size and configuration of the lesion, shapes the beam in cross-section. Tissue-equivalent compensators adjust for irregular target contours, skull curvature and tissue inhomogeneities. Multiple entry angles and beam ports are chosen so that the high-dose regions of the individual beams intersect within the defined target, with the lowest possible dose to sensitive adjacent normal brain tissues. From R.P. Levy et al. [24]

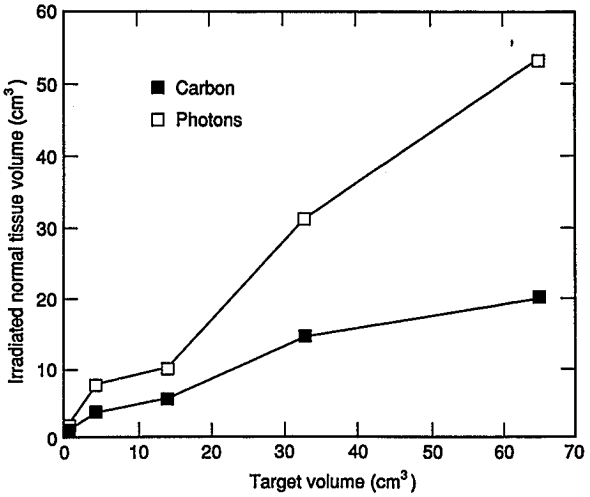

Fig. 2. The volume of brain tissue outside the target volume that receives 80% or more of the dose delivered to the target volume plotted as a function of target volume. These data are derived from dose-volume histograms for defined target volumes using photon irradiation (^{60}Co gamma rays or X-rays) and carbon ion (400 MeV/u) irradiation for stereotactic radiosurgery of target volumes ranging from 0.5 to 65 cm^3. For all volumes examined, focused photon irradiation resulted in irradiation of 2 to 3 times more normal brain tissue surrounding the target volume than did carbon ion beams. From M.H. Phillips et. al. [25]

dose is absorbed in the wall of the treatment room opposite the beam line. This method was developed by Lawrence and his colleagues [4, 5, 17, 26] at LBL in 1954 for irradiation of the pituitary gland with plateau beams of protons and helium ions.

With the plateau beam (or through-and-through) irradiation technique, consideration of the tissue inhomogeneity normally encountered in the head is not important, but accurate stereotactic localization of the intracranial target volume and precise isocentric technique are essential. The plateau beam radiosurgical system developed at LBL used a stereotactic positioning table and head holder in combination with individually fabricated plastic head masks for immobilization. Following delineation of the target volume, the ion beam was centered on the sella turcica by means of orthogonal localization radiographs and port films, and the beam contour was shaped by a brass aperture. During irradiation, the head was turned in pendulum motion around a horizontal axis while the patient was positioned sequentially at 12 discrete angles around a vertical axis. The irradiation arcs were directed such that the dose fall-off was very rapid in the anteroposterior direction and toward the optic chiasm; the dose fall-off decreased more slowly laterally toward the temporal lobes (Fig. 3). With this method, the optic chiasm, hypothalamus and outer portions of the sphenoid sinus received less than 10% of the central axis pituitary dose [26]. For small lesions, the dose distributions from plateau beam irradiation are comparable to those produced with stereotactic radiosurgical systems using X-rays or gamma rays.

Clinical Applications

Extensive clinical experience has been obtained with pituitary hormone suppression, pituitary adenomas and AVMs over the four decades since the first patient was treated with charged particle radiosurgery [6, 8, 20]. The emphasis here on helium ion irradiation reflects the authors' experience at LBL and SUMC.

Pituitary Hormone Suppression

Charged particle radiosurgery of the pituitary gland has been shown to be very effective for inducing suppression of normal pituitary function with minimal associated risk of injury in adjacent neural structures [6, 7]. The primary goals of hypophysectomy with ion beams have been control of the metastatic spread of selected hormone-responsive carcinomas (e.g., breast and prostate cancer) [4, 15, 1] and regression of proliferative diabetic retinopathy [17, 27]. In North America, pituitary ablation treatment is no longer in common use. In the case of metastatic breast carcinoma, for example, modern anti-estrogenic drugs are now available for selective use guided, in part, by reliable estrogen-receptor classification of tumors. In the case of diabetic retinopathy, pituitary ablation treatment has also fallen out of favor. Nonetheless, the extensive clinical experi-

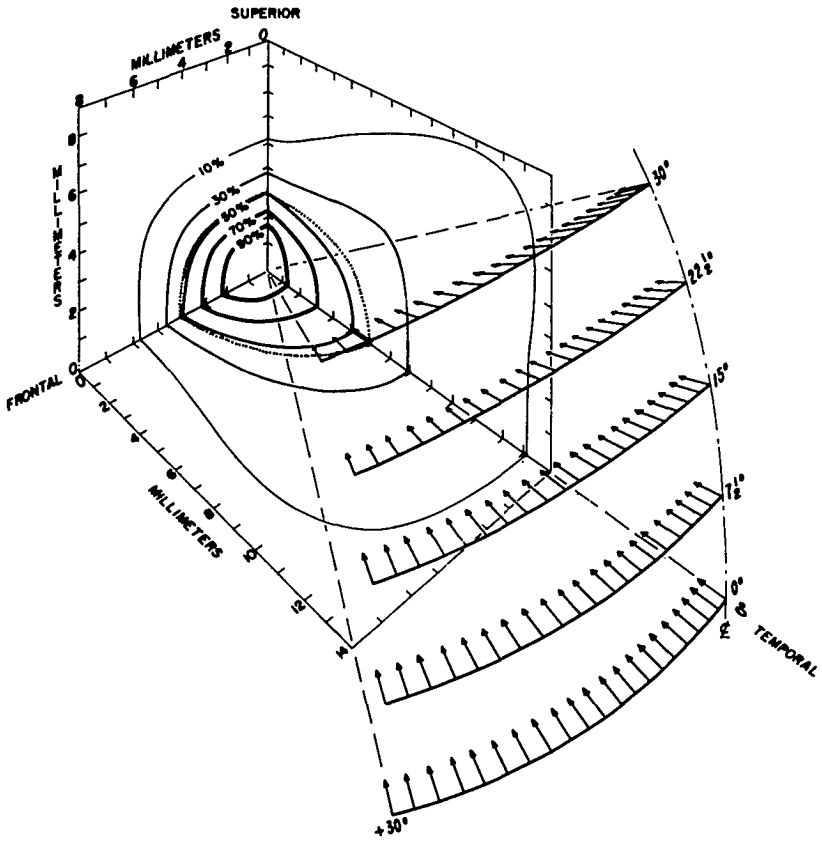

Fig. 3. Three-dimensional isodose contours for one octant of the plateau helium ion (230 MeV/u) radiation field used to treat pituitary adenomas at the LBL 184-inch synchrocyclotron. From C.A. Tobias et. al. [26]

ence accrued has served to provide considerable information about radiation tolerance of the pituitary gland, parasellar tissues, cranial nerves and temporal lobes [7].

Hormone Dependent Metastatic Carcinoma

Between 1954 and 1972 at LBL, stereotactically directed plateau beams of protons (initial 26 cases) or helium ions (157 cases) were used for pituitary ablation treatment in 183 patients with metastatic breast carcinoma [16]. Patients received 180 to 220 Gy in six to eight fractions over 2 to 3 weeks in the early years of the clinical program and in three or four fractions over 5 days in later years. Many patients experienced long-term remissions. Eight cases of focal radiation necrosis limited to the adjacent portion of the temporal lobe occurred; all were from an earlier group of patients who had received higher doses to suppress pituitary function as rapidly as possible [7]. Clinical temporal lobe injury and transient cranial nerve involvement occurred in four patients. Comparable results have been reported with Bragg peak proton radiosurgery in 31 patients at the Harvard cyclotron [28].

Diabetic Retinopathy

Between 1958 and 1969 at LBL, 169 patients with proliferative diabetic retinopathy received stereotactic plateau beam helium ion pituitary irradiation. The first 30 patients were treated with 160 to 320 Gy delivered in six to eight fractions over 11 days to effect total pituitary ablation; the subsequent 139 patients underwent subtotal pituitary ablation with 80 to 150 Gy. Most patients had a 15

to 50% decrease in insulin requirements; this result occurred sooner in patients receiving higher doses, but ultimately both patient groups had comparable insulin requirements. Moderate to good vision was preserved in at least one eye in 59 of 114 patients at 5 years after pituitary irradiation [29]. Of 169 patients treated, 69 (41%) ultimately required thyroid replacement and 46 (27%) required adrenal hormone replacement. There were four deaths from complications of hypopituitarism. Focal temporal lobe injury was limited to an early group of patients that had received at least 230 Gy to effect rapid pituitary ablation in advanced disease. Four patients in this high-dose group developed extraocular palsies. Neurological injury was rare in patients receiving doses less than 230 Gy [29]. Kjellberg et al. [27] reported comparable results following stereotactic Bragg peak proton radiosurgery in 183 patients.

Pituitary Adenomas

Since 1958, more than 2000 patients with pituitary adenomas have been treated with charged particle radiosurgery [9, 12, 18, 19, 30, 31]. This treatment has been applied to acromegaly, Cushing's disease, Nelson's syndrome and prolactin-secreting tumors, as well as to nonfunctioning and selected other adenomas. The therapeutic goals are control of tumor growth and hormonal hypersecretion, with acceptably low hormonal and neurological complications. These goals have been met with remarkable success over the past 35 years, especially considering the limitations of the available neuroradiological imaging methods during the early years of these investigations. The great majority of patients were treated before the advent of CT and MRI, and adenoma assessment and target volume determination, therefore, relied on relatively crude neuroradiologic procedures such as polytomography and pneumoencephalography. The clinical and metabolic follow-up data describing the response of pituitary adenomas to ion beam radiosurgery have been reported extensively; the reader is referred to references [6] and [7] for more detailed reviews. In this section, the emphasis is limited to selected clinical studies and complications of treatment.

Acromegaly

At LBL, stereotactic helium ion plateau beam radiosurgery was very effective for the treatment of acromegaly in 318 patients [9, 30, 31]. The maximum dose to the pituitary tumor ranged from 30 to 50 Gy, most often delivered in four fractions over 5 days. The choice of dose varied according to the extent of disease and the corresponding size of the target volume. Maximum pituitary doses were selected so that the temporal lobe cortex received no more than 15 Gy. The mean serum growth hormone (GH) level in a cohort of 234 of these patients decreased nearly 70% within 1 year and continued to decrease thereafter (Fig. 4). Normal levels were sustained during more than 10 years of follow-up.

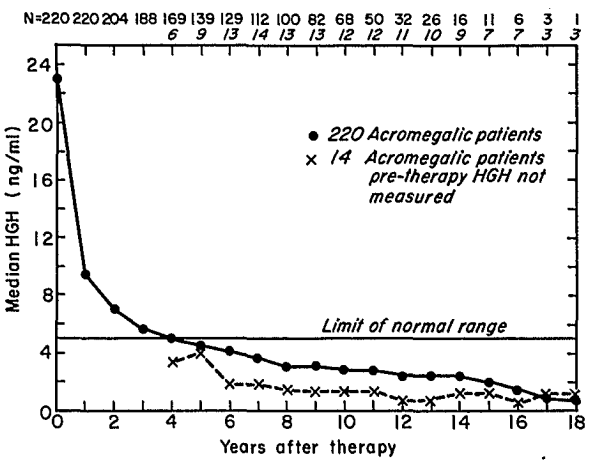

Fig. 4. Median plasma human growth hormone (HGH) levels in 234 patients with acromegaly treated with stereotactic plateau beam helium ion radiosurgery. The numbers of patients used to calculate the median plasma levels before radiosurgery and for each time interval thereafter are shown at the top of the graph. Fourteen patients did not have pretreatment HGH measurements, but their HGH levels measured 4 to 18 years after radiosurgery were comparable with those of the other 220 patients. The 20 patients in the series who subsequently underwent pituitary surgery or additional pituitary irradiation were included until the time of the second procedure. From J.H. Lawrence et. al. [30]

Comparable long-term results were observed in a cohort of 65 patients who were irradiated with helium ions because of residual or recurrent metabolic abnormalities persisting after surgical hypophysectomy. Patients with microadenomas (<10 mm diameter) had lower initial GH levels, responded more rapidly to treatment, and had a good prognosis for cure; a lower incidence of post-treatment hypopituitarism was also observed in these patients. The more invasive tumors were slower to respond, but by 4 years after irradiation they were associated with GH levels not statistically different from levels found in patients with microadenomas.

Treatment failures generally resulted from failure to assess accurately the degree of extrasellar tumor extension [9, 31]. With recent advances in MRI and CT scanning, the radiosurgical target can now be better delineated, which in turn should lead to improved rates of tumor cure and control. These same imaging improvements also make possible more reliable determination of tissue inhomogeneities in the brain and adjacent tissues and correspondingly more precise positioning of the Bragg ionization peak within the target volume.

Kjellberg et al. [12, 18] treated about 600 patients with acromegaly using Bragg peak proton irradiation at the Harvard cyclotron. Using a nomogram based on lesion size and complication rate in a large number of treated patients, maximal central doses selected were inversely related to beam diameter; intrasellar tumors typically received single doses of 60 to 120 Gy. Therapy resulted in objective clinical improvement in about 90% of a cohort of 145 patients 24 months after irradiation. By this time, 60% of the patients were in remission (GH level < 10 ng/ml); after 48 months, 80% were in remission. About 10% of patients failed to enter remission or to improve and required additional treatment, usually transsphenoidal hypophysectomy.

Cushing's Disease

Cushing's disease was treated in 83 patients at LBL using stereotactic helium ion plateau beam irradiation [9, 19, 31]. Mean basal cortisol levels and urinary fluorogenic corticosteroids returned to normal values within 1 year after treatment, and these indices remained normal during more than 10 years of follow-up. All five teenage patients were cured by doses of 60 to 120 Gy without hypopituitarism or neurological sequelae; however, nine of 59 older patients subsequently underwent bilateral adrenalectomy or surgical hypophysectomy due to relapse or failure to respond to treatment. Of the nine treatment failures, seven occurred in the earlier group of 22 patients treated with 60 to 150 Gy in six alternate-day fractions; when the same total doses were given in three or four daily fractions, 40 of 42 patients were cured [9].

Kjellberg et al. [12] treated more than 175 Cushing's disease patients with single-dose Bragg peak proton irradiation. Doses were inversely related to the beam diameter selected (typically, 60 to 120 Gy). Complete remission with restoration of normal clinical and laboratory findings occurred in about 65% of patients followed up for 24 months; another 20% were improved to the extent that no further treatment was considered necessary.

Complications

Variable degrees of hypopituitarism developed in about one third of patients following stereotactic helium ion radiosurgery, although endocrine deficiencies were rapidly corrected in most cases with appropriate hormonal replacement therapy [7, 9]. In retrospect, larger portions of the pituitary gland were designated for radiosurgical treatment to assure sufficient dose to the adenoma than would now be indicated based on current MRI and CT techniques. Other sequelae were limited most frequently to patients who had received prior photon irradiation. These sequelae included mild or transient extraocular nerve palsies, partial visual field deficits and seizures due to focal temporal lobe injury [7, 9]. After appropriate adjustments of dose schedules, temporal lobe and cranial nerve injury were rare sequelae, in the range of 1% or less, and no other permanent sequelae occurred. A very low incidence of significant adverse sequelae has also been reported in pa-

tients treated with Bragg peak proton irradiation by Kjellberg and his colleagues [12].

Arteriovenous Malformations

Since 1965, more than 1500 patients have been treated in the United States with charged particle radiosurgery for AVMs of the brain, primarily at LBL [8, 10, 23, 24], HCL [11, 32] and, since 1993, LLUMC [22]. The therapeutic goals are to achieve:

1. reduction or elimination of intracranial hemorrhage
2. stabilization or reversal of progressive neurological dysfunction
3. lower frequency of seizures
4. improvement in frequency and intensity of headaches.

Between 1980 and 1992, we treated 455 patients with intracranial vascular malformations using Bragg peak helium ion beams at the LBL 184-inch synchrocyclotron and Bevatron. In this section, we describe the patient population, clinical and neuroradiological outcome and complications in this cohort, with emphasis on patients with angiographically demonstrable AVMs treated through the collaborative LBL-SUMC radiosurgery program [8, 10].

LBL-SUMC Series

Patient Selection

Fifty-two percent of AVM patients were female and 48% were male. Seventeen percent were aged 6–20, 61% were 21–40, 18% were 41–60, and 4% were over 60 years. About 40% of the patients had no interventional therapy prior to radiosurgery, but the majority had undergone microsurgery, embolization, or both. Twenty-five percent of AVMs measured greater than 25 cm^3. Many patients presented with more than one symptom; 70% had hemorrhaged, 13% had neurological deficits unassociated with hemorrhage, 41% had seizures, and 47% had headaches. Seventy percent were graded clinically as excellent before radiosurgery, 28% as good, and 2% as poor. Nearly half (44%) had AVMs located in the brain stem, corpus callosum, thalamus or basal ganglia, and most of the remainder had large malformations in critical areas of the cerebrum – sensory, motor, language, or visual areas of the cortex.

Clinical Follow-Up and Outcome

Clinical evaluation, performed 24 to 72 months (mean, 38 months) after radiosurgery, found that 63% of patients presenting with seizures and 68% of patients presenting with headaches had improvement of these symptoms [10]. These improvements appeared to result from improved regional cerebral blood flow, stabilization of hemodynamic imbalance and reversal of vascular steal, associated with progressive thrombosis of the malformation [8, 10]. Clinical outcome was excellent in 58% of patients, good in 36% and poor in 9%. Worsening clinical grade generally resulted from intracranial hemorrhage or treatment-associated sequelae; a few patients have worsened from intercurrent medical disorders. Seven percent of patients died from disease progression (including AVM hemorrhage) or unrelated illness.

Neuroradiological Response

Cerebral angiography was performed at yearly intervals to evaluate response. The first hemodynamic changes observed include a decrease in blood flow through the AVM, due to progressive obliteration of the small shunting vessels, with a decrease in size of the feeding arteries and draining veins. This stage is followed by a progressive decrease in AVM volume until stabilization or complete obliteration of the AVM occurs.

Angiographic follow-up evaluation was performed in 86 consecutive patients treated from 1983 to 1986 in the LBL-SUMC series, as part of a dose-searching protocol [10]. In retrospect, many of these patients were treated with somewhat higher doses than would now be considered optimal. Two years after radiosurgery, complete obliteration of the AVM occurred in 70%, partial obliteration (10 to 99% obliteration) in 23%, and no change in 7%. By 3 years after treatment, 90% of the patients had complete AVM obliteration.

tion, 6% had partial obliteration, and 4% had no change. The rate and extent of obliteration appeared to be threshold phenomena directly related to AVM volume and radiation dose. Smaller AVMs had significantly higher rates of obliteration than larger ones ($p < 0.005$ after 1 and 2 years). AVMs smaller than 4 cm^3 thrombosed more rapidly and more completely than larger lesions ($p < 0.05$ for the comparison with AVMs 4 to 25 cm^3 and $p < 0.001$ for the comparison with those greater than 25 cm^3). Intermediate-sized AVMs were obliterated more rapidly and more completely than large AVMs ($p < 0.05$). Complete obliteration occurred more frequently in malformations treated with higher doses (30 to 45 GyE in one or two fractions) ($p < 0.05$ after 1 and 2 years). AVMs treated with intermediate doses (24 to 28 GyE) also responded well at 2 and 3 years. Preliminary results with doses $\leq$ 20 GyE, however, indicate significantly lower response rates.

Complications and Sequelae

Serious early sequelae have been negligible following radiosurgery [7, 8, 10, 24]. A few patients with previous seizures had transiently increased seizure activity, which was readily controlled by adjustment of anticonvulsant medications. No patients experienced nausea, vomiting or hyperpyrexia. No deaths occurred from the irradiation procedure.

Late treatment-associated sequelae can be classified as white matter changes or vasculopathy and include vasogenic edema, occlusion of functional vasculature and radiation necrosis [7, 8, 10, 24]. The manifestations and incidence of clinical sequelae depend, in part, on the region of the brain involved, the volume of normal brain tissue affected, the radiation dose, the presence of prior tissue injury and the timing and nature of therapeutic measures. Clinical complications following radiosurgery were most common in patients with

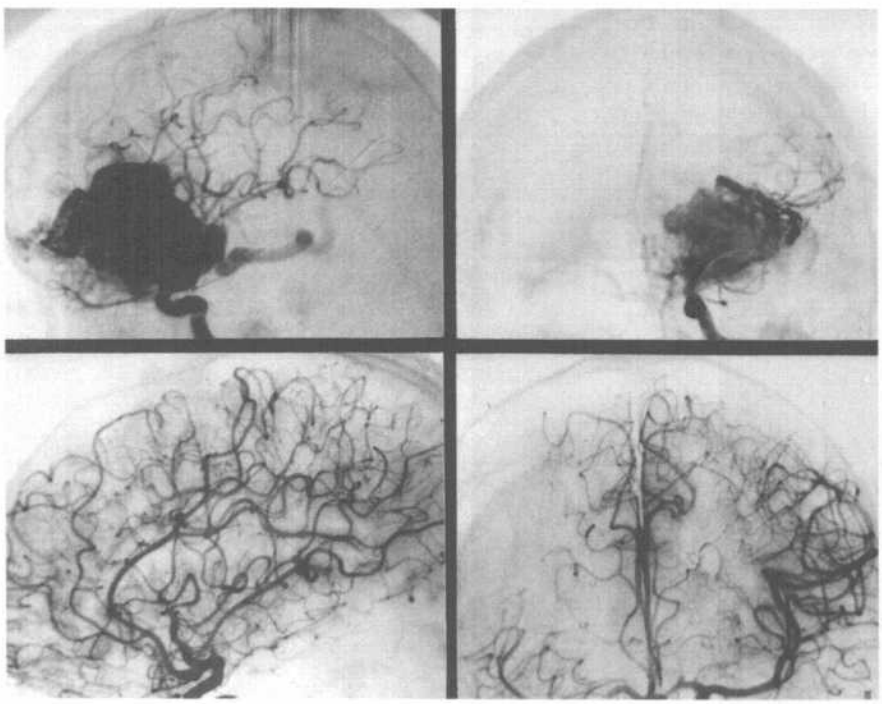

Fig. 5. Cerebral angiograms from a 23-year-old man with a large (40 cm^3) left frontotemporal AVM. Upper, lateral and anteroposterior views of the internal carotid artery angiogram demonstrate the AVM supplied by branches of the anterior and middle cerebral artery circulations. The vascular steal is prominent. Lower, comparable views taken 18 months after helium ion radiosurgery (dose, 28 GyE) demonstrate complete obliteration of the AVM. Normal cerebral blood flow has been restored, with marked reversal of the vascular steal. From R.P. Levy et. al. [6]

AVMs in the brain stem, thalamus or basal ganglia. Hemiparesis was the most common major complication and visual field deficit was the most common minor complication. Adverse sequelae were limited almost exclusively to patients who received doses above 25 GyE and whose AVM volumes were more than 14 cm^3. Complications have been rare (2%) in the approximately 250 patients treated with lower doses since 1986. Many uncertainties remain, however, regarding optimal radiosurgical treatment parameters for malformations of various sizes and locations in the brain [8, 10, 24].

MGH-HCL Series

Kjellberg and associates [11, 30] of MGH used single-fraction Bragg peak proton therapy at HCL to treat more than 1300 patients with vascular malformations of the brain [28]. Irradiation generally was delivered with parallel-opposed treatment fields. Doses (typically, 10 to 50 Gy) were selected according to diameter of the AVM, using a nomogram based on lesion size and complication rate in a large number of treated patients [11]. Findings of follow-up evaluation in 1000 patients with AVMs, 2 to 24 years after treatment with proton beam therapy, were reported [30]. In 104 patients, the clinical outcome was unrelated to either hemorrhage or radiosurgery. Of the remaining 896 patients, 818 (91.3%) were unchanged or improved; 27 (3%) had moderate deficits from hemorrhage or proton beam therapy, but functioned independently at pretreatment levels; seven (0.8%) had severe deficits and were dependent to varying degrees; two (0.2%) were vegetative; 39 (4.4%) were dead (37 from hemorrhage and two from treatment complications); three (0.3%) were lost to follow-up after surviving hemorrhage. Analysis by actuarial life table methods showed 98.4% 24-year survival for patients with AVMs <3 cm in diameter and 93% 24-year survival for all patients; these data were then compared to a 24-year survival of 77% reported for an untreated historical control group. Of the 37 patients who died from hemorrhage, 22 died within the first 2 years after treatment; 33 lethal hemorrhages occurred in patients with AVMs >3 cm in diameter. An additional 101 patients survived hemorrhage. Complications of treatment occurred in 17 patients (6 months to 6.5 years after treatment), but only seven in the last 925 patients following downward adjustments in treatment doses. In general, treatment doses used in this patient series were significantly lower than those used in the LBL-SUMC series described above.

LLUMC-SUMC Series

The LLUMC-SUMC collaborative program represents the most recent development in charged particle radiosurgery for AVMs. Using the modern methods of iterative target delineation and treatment planning described above, 28 patients with 32 discrete (non-adjacent) AVM target volumes were evaluated and treated from December 1993 through August 1994. Ten small AVMs (mean, 5.2 cm^3; range, 0.9 to 9.9 cm^3) were treated with 24.3 ± 2.4 GyE in one or two fractions. Twenty-two larger AVMs (mean, 40.9 cm^3; range, 11.6 to 114.0 cm^3) were treated with 20.9 ± 2.3 GyE in two fractions. Transient focal seizures occurred acutely in two patients, but no other acute or delayed sequelae have been observed to date. Long-term clinical follow-up is in progress.

Future Directions

Arteriovenous Malformations

An increasing number of AVM patients are now being evaluated for multistage procedures, including embolization and/or partial microsurgical resection, to reduce AVM size and blood flow prior to charged particle radiosurgery, since smaller and slower flow AVMs respond more rapidly and completely to radiosurgery and are associated with a lower risk of radiation-related complications [8, 10, 20]. This multimodality approach is proving useful for treatment of selected large and complex hemispheric AVMs, which now comprise the majority of cases referred for ion beam radiosurgery in North America.

Additionally, the role of microsurgery and embolization in patients who previously underwent charged particle radiosurgery is evolving rapidly. Thus far, in the LBL-SUMC program, these procedures have been performed in 30 patients, whose follow-up angiograms had shown little apparent change 2 to 3 years after helium ion radiosurgery. In nearly all cases, the AVMs were found at surgery to be markedly less vascular and more easily resected than had been anticipated had they not undergone prior radiosurgery. Similarly, the obliterative response to embolization was much greater than anticipated. Complete obliteration of the AVM has been ultimately achieved in a majority of these initial apparent non-responders. Selected patients with residual AVMs are treated with a second course of ion beam radiosurgery. Preliminary results in this group are encouraging. Several AVMs have already been obliterated completely following a second radiosurgical treatment. Long-term follow-up is in progress.

The rapid development of improved anatomic resolution with modern MRI and CT scanning now makes it possible to localize more accurately abnormal vascular structures and to identify sensitive adjacent neural structures [22]. It appears, in retrospect, that many of the complications of radiosurgery seen in the past could be attributed to suboptimal target delineation and unnecessary inclusion of normal tissues in the target volume [8, 21, 25]. As three-dimensional target delineation improves, it is anticipated that higher doses to the target volume, associated with higher cure rates, can be given without significantly increasing the risk of sequelae. These same imaging improvements also make possible more reliable determination of tissue inhomogeneities in the brain and adjacent tissues and correspondingly more precise positioning of the Bragg ionization peak within the target volume.

Neoplastic Disorders

Historically, stereotactic irradiation regimens have not been designed to exploit the differential response between normal cells and tumor cells that is the biological basis for the use of fractionated external beam irradiation [20]. Recently, however, the use of fractionated stereotactic irradiation for the treatment of neoplastic intracranial disorders has been reported [33]. With the development of stereotactic immobilization systems capable of reliable serial repositioning, this new approach offers the potential for improved treatment outcome by combining the excellent dose localization and dose distribution characteristics of charged particle radiosurgery with the favorable radiobiological properties of fractionated irradiation [20]. This approach is currently under investigation for the charged particle irradiation treatment of larger or invasive benign tumors, and for primary and secondary malignant brain tumors. It is anticipated that the application of more extended fractionation schedules will result in a lower incidence of cranial nerve neuropathy (for example, in acoustic neuroma treatment) and parenchymal brain injury, without compromising the treatment's effectiveness against neoplastic cells.

Acknowledgements

The authors wish to acknowledge the late Professors J.I. Fabrikant, R.N. Kjellberg and J.H. Lawrence for their pioneering contributions to the field of ion beam radiosurgery.

This work was supported by the Director, Office of Energy Health and Environmental Research, U. S. Department of Energy under Contract No. DE-AC03–76SF00098.

References

1 Wilson, R.R. Radiological use of fast protons. Radiology 47, 487–491, 1946.
2 Brobeck, W.M., Lawrence, E.O., MacKenzie, K.R., McMillan, E.M., Serber, R., Sewall, D.C., Simpson, K.M., and Thornton, R.L. Initial performance of the 184-inch cyclotron of the University of California. Phys. Rev. 71, 449–450, 1947.
3 Tobias, C.A., Anger, H.O., and Lawrence, J.H. Radiologic use of high energy deuterons and alpha particles. Am. J. Roentgenol. Radium Ther. Nucl. Med. 67, 1–27, 1952.

4 Tobias, C.A., Lawrence, J.H., Born, J.L., McCombs, R.K., Roberts, J.E., Anger, H.O., Low-Beer, B.V.A., and Huggins, C.B. Pituitary irradiation with high-energy proton beams: A preliminary report. Cancer Res. 18, 121–134, 1958.
5 Tobias, C.A., Roberts, J.E., Lawrence, J.H., Low-Beer, B.V.A., Anger, H.O., Born, J.L., McCombs, R., and Huggins, C.B. Irradiation hypophysectomy and related studies using 340-MeV protons and 190-MeV deuterons, in Proc. Int. Conf. on the Peaceful Uses of Atomic Energy, Geneva, 1955, pp. 95–106.
6 Levy, R.P., Fabrikant, J.I., Frankel, K.A., Phillips, M.H., and Lyman, J.T. Charged-particle radiosurgery of the brain. Neurosurg. Clin. North Am. 1, 955–990, 1990.
7 Rodriguez, A., Levy, R.P., and Fabrikant, J.I. Experimental central nervous system injury after charged-particle irradiation, in Radiation Injury to the Nervous System. Gutin, P.H., Leibel, S.A., and Sheline, G.E. (eds.), Raven Press, New York, 1991, pp. 149–182.
8 Fabrikant, J.I., Levy, R.P., Steinberg, G.K., Phillips, M.H., Frankel, K.A., Lyman, J.T., Marks, M.P., and Silverberg, G.D. Charged-particle radiosurgery for intravascular malformations. Neurosurg. Clin. North Am. 3, 99–139, 1992.
9 Linfoot, J.A. Heavy ion therapy: Alpha particle therapy of pituitary tumors, in Recent Advances in the Diagnosis and Treatment of Pituitary Tumors. Linfoot, J.A. (ed.), Raven Press, New York, 1979, pp. 245–267.
10 Steinberg, G.K., Fabrikant, J.I., Marks, M.P., Levy, R.P., Frankel, K.A., Phillips, M.H., Shuer, L.M., and Silverberg, G.D. Stereotactic heavy-charged-particle Bragg-peak radiation for intracranial vascular malformations. N. Engl. J. Med. 323, 96–101, 1990.
11 Kjellberg, R.N., Hanamura, T., Davis, K.R., Lyons, S.L., and Adams, R.D. Bragg-peak proton beam therapy for arteriovenous malformations of the brain. N. Engl. J. Med. 309, 269–274, 1983.
12 Kjellberg, R.N. and Kliman, B. Lifetime effectiveness – A system of therapy for pituitary adenomas, emphasizing Bragg peak proton hypophysectomy, in Recent Advances in the Diagnosis and Treatment of Pituitary Tumors. Linfoot, J.A. (ed.), Raven Press, New York, 1979, pp. 269–288.
13 Minakova, Ye.I. Twenty years clinical experience of narrow proton beam therapy in Moscow, in Proc. Int. Heavy Particle Therapy Workshop, Paul Scherrer Institut, Villigen, Switzerland, Blattmann, H. (ed.), PSI-Bericht 69, 1990, pp. 158–162.
14 Konnov, B., Melnikov, L., Zargarova, O., Lebedeva, L., Yalynych, N., and Karlin, D. Narrow proton beam therapy for intracranial lesions, in Proc. Int. Workshop on Proton and Narrow Photon Beam Therapy, Oulu, Finland, 1989, pp. 48–55.
15 Lawrence, J.H. Proton irradiation of the pituitary. Cancer 10, 795–798, 1957.
16 Lawrence, J.H., Tobias, C.A., Born, J.L., Wang, C.C., and Linfoot, J.H. Heavy-particle irradiation in neoplastic and neurologic disease. J. Neurosurg. 19, 717–722, 1962.
17 Lawrence, J.H., Tobias, C.A., Linfoot, J.A., Born, J.L., Gottschalk, A., and Kling, R.P. Heavy particles, the Bragg curve and suppression of pituitary function in diabetic retinopathy. Diabetes 12, 490–501, 1963.
18 Kjellberg, R.N., Shintani, A., Frantz, A.G., and Kliman, B. Proton beam therapy in acromegaly. N. Engl. J. Med. 278, 689–695, 1968.
19 Linfoot, J.A., Lawrence, J.H., Born, J.L., and Tobias, C.A. The alpha particle or proton beam in radiosurgery of the pituitary gland for Cushing's disease. N. Engl. J. Med. 269, 597–601, 1963.
20 Levy, R.P. and Fabrikant, J.I. Clinical applications of stereotactic radiosurgery, in Physical Aspects of Stereotactic Radiosurgery. Phillips, M.H. (ed.), Plenum Publishing, New York, 1993, pp. 239–278.
21 Phillips, M.H., Frankel, K.A., Lyman, J.T., Fabrikant, J.I., and Levy, R.P. Heavy-charged particle stereotactic radiosurgery: Cerebral angiography and CT in the treatment of intracranial vascular malformations. Int. J. Radiat. Oncol. Biol. Phys. 17, 419–426, 1989.
22 Levy, R.P., Schulte, R.W.M., Frankel, K.A., Steinberg, G.K., Marks, M.P., Lane, B., Heilbronn, L.H., Meinass, H.J., Galindo, R.A., Slater, J.D., and Slater, J.M. CT slice-by-slice target volume delineation for stereotactic proton irradiation of large intracranial arteriovenous malformations: An iterative approach using angiographic, CT and MRI data. Int. J. Radiat. Oncol. Biol. Phys., in press.
23 Fabrikant, J.I., Lyman, J.T., and Hosobuchi, Y. Stereotactic heavy-ion Bragg peak radiosurgery: Method for treatment of deep arteriovenous malformations. Br. J. Radiol. 57, 479–490, 1984.
24 Levy, R.P., Fabrikant, J.I., Frankel, K.A., Phillips, M.P., and Lyman, J.T. Stereotactic heavy-charged-particle Bragg peak radiosurgery for the treatment of intracranial arteriovenous malformations in childhood and adolescence. Neurosurgery 24, 841–852, 1989.
25 Phillips, M.H., Frankel, K.A., Lyman, J.T., Fabrikant, J.I., and Levy, R.P. Comparison of different radiation types and irradiation geometries in stereotactic radiosurgery. Int. J. Radiat. Oncol. Biol. Phys. 18, 211–220, 1990.
26 Tobias, C.A. Pituitary radiation: Radiation physics and biology, in Recent Advances in the Diagnosis and Treatment of Pituitary Tumors. Linfoot, J.A. (ed.), Raven Press, New York, 1979, pp. 221–243.
27 Kjellberg, R.N., McMeel, J.W., McManus, N.L., and Koehler, A.M. Pituitary suppression in diabetic retinopathy by proton beam in surgically "unfit" patients, in Symposium on the Treatment of Diabetic Retinopathy. Goldberg, M.F. and Fine, S.L. (eds.), Airlie House, Warrenton, VA (U S Public Health Service Publication No. 1890), Arlington, 1968, pp. 249–276.
28 Kjellberg, R.N., personal communication, 1989.
29 Lawrence, J.H., unpublished.
30 Lawrence, J.H. Heavy particle irradiation of intracranial lesions, in Neurosurgery. Wilkens, R.H. and Rengachary, S.S. (eds.), McGraw-Hill, New York, 1985, pp. 1113–1132.

31 Lawrence, J.H. and Linfoot, J.A. Treatment of acromegaly, Cushing disease and Nelson syndrome. West. J. Med. 133, 197–202, 1980.
32 Kjellberg, R.N. and Candia, G.J. Stereotactic proton beam therapy for cerebral AVMs. Harvard Radiosurgery Update, Chestnut Hill, MA, 1990 (abstract).
33 Brenner, D.J., Martel, M.K., and Hall, E.J. Fractionated regimens for stereotactic radiotherapy of recurrent tumors in the brain. Int. J. Radiat. Oncol. Biol. Phys. 21, 819–824, 1991.

17 Early and Delayed Complications of Ion Beam Therapy

J.-L. Habrand, P. Schlienger, A. Mazal, L. Schwartz, L. Desjardins, F. d'Hermies, E. Frau, and H. Randrianarivelo

Centre de Protonthérapie d'Orsay, Orsay, France

Introduction

Among approximately 15000 patients treated so far with ion beams, the rate of reported severe complications has been extremely low. Nevertheless, the balance between tumor control and morbidity remains crucial and approaches to further improve the treatment outcome will remain of utmost importance in the development of this radiotherapeutic technique.

This section gives a review on clinical complications and sequelae published in the literature for proton and heavy ion treatment along with the authors' preliminary personal experience with protons at Orsay.

Complications and Sequelae After Ion Beam Therapy of Ocular Tumors

Early complications from suturing the tantalum rings seem to be very limited. A few incidents of transcient diplopia have been reported in which the surgeon had to disinsert the inferior oblique for ring placement. Keratopathy in patients receiving high doses to the cornea have been described as early complications and also lid epithelitis, epilation and epiphora (by punctum occlusion) have been observed during the irradiation and in the following weeks in patients where a complete lid retraction during the treatment was not possible.

Delayed complications observed after proton or helium ion irradiation of uveal melanomas [1–3] are summarized in Table 1.

The most serious complication is the neovascular glaucoma. It manifests as increased intraocular pressure accompanied by a neovascular proliferation involving the anterior chamber angle and compromising the drainage of the Schlemm canal. The cause of this proliferation is still unclear and probably not correlated with a direct action of the ionizing radiation. It might be induced by the production of an angiogenic factor from hypoxic retinal tissue overlying the tumor. When established, neovascular glaucoma is fre-

Table 1. Delayed complications following proton beam and helium irradiation of uveal melanomas reported in 3 studies [1–3]

Parameter	Saunders [1]	Gragoudas [2]	Desjardins [3]
No. of patients	75	786	146
Mean follow-up (months)	3	18	12
Particle	He	H	H
No. (%) of patients with			
Maculopathy	11 (15)	159 (20)	51 (35)
Optic neuropathy	–	74 (9)	7 (5)
Neovascular glaucoma	10 (13)	73 (9)	10 (7)
Cataract	6 (8)	191 (24)	33 (23)
Vitreous hemorrhage	2 (3)	53 (7)	3 (2)

quently refractory to medical measures and requires enucleation of the affected eye. Fortunately, this complication is described in less than 15% of patients treated with helium and less than 10% after proton treatment.

Radiation retinopathy is a delayed vaso-occlusive microangiopathy that can take various pathological and clinical manifestations [4]. Many findings are similar to those observed in diabetes mellitus associated retinopathy although papillopathy is more common after irradiation.

Radiation maculopathy is a major concern in posterior tumors as was assessed by the group of the Massachusetts General Hospital in Boston [5]. They evaluated the risk in 218 eyes treated at the Harvard Cyclotron Laboratory (HCL) before January 1988 with the following result: 89% of the patients developed a wide variety of fundoscopic changes affecting the macula. Early modifications (i.e., within 1 year) were macula edemas which affected 9 out of 10 patients at 3 years if the tumor was located less than 2 disc-diameters from the macula and microvascular changes (telangiectasias or microaneurysms) which occured in 3 out of 4 patients after 3 years. Delayed manifestations included intraretinal hemorrhages (70% at 3 years), lack of capillary perfusion by fluorescein (64%), intraretinal lipid deposition (55%), nerve fiber layer infarcts (48%) and vascular sheathing (36%). Two thirds of the infarcts, 40% of the hemorrhages, and lipid deposits but only 25% of the vascular sheathing, and less than 10% of the edema and microvascular changes regressed spontaneously.

To overcome the enhanced complication rate of posterior tumors, a randomized study was initiated by the Boston Group in 1989. It comprised small melanomas located less than 6 mm from the macula and/or fovea, and compared two dose levels (50 and 70 CGE). The results of this study are still pending. Recently, however, a retrospective review conducted in children has found a very low α/β value for retina (< 1.7 Gy) which would suggest a possible protective effect of smaller dose per fractions [6].

Cataract can develop after conventional radiotherapy with doses as low as 5 to 10 Gy. According to data collected by the Seattle group, a single dose of 10 Gy represents a 50% risk to develop cataract within 5 years; if 10 Gy were fractionated the risk was approx. 5%, and 20% after 12 to 16 Gy of fractionated dose. The low incidence reported following charged particle irradiation was explained by the limited follow-up of patients and by the fact that in most patients only part of the lens was irradiated. A recent evaluation by Meecham estimated the risk for cataract at 7 years follow-up to exceed 90% when more than half of the lens was in the beam [7].

From two large series, the risk of enucleation unrelated to tumor recurrence, was estimated to be approx. 10% after helium [8], and 6% [6] after proton therapy. According to Munzenrider et al. [10], this compares favorably with other conservative radiotherapeutical approaches including radioactive plaques.

Table 2 lists a number of prognostic factors for visual loss as evidenced by multivariate analysis in 2 studies [11, 12]. In both studies, tumor height played a significant role for the visual outcome. This is very likely due to the fact that thick tumors usually occupy a large part of the eye and induce necrosis, inflammation and exudation. Distance to the posterior structures also appeared of importance. It reflects the deleterious influence of radiation maculopathy and optic neuropathy on vision.

Following ion beam radiotherapy, vision can be theoretically affected by 4 major mechanisms [13]:

Table 2. Prognostic factors for visual loss after treatment of uveal melanoma with protons. Results from 2 series [11, 12]. RR = relative risk, D = optic disc, DD = disc diameter, F = fovea, CGE = Cobalt Gray-equivalent

Parameter	Egger [11]	Seddon [12]
No. of patients	466	440
Follow-up (months)	>3	mean 19
Fractionation (CGE)	4×15	5×14
Tumor height	$p > 0.001$	<5 mm, RR 5.26
Distance to posterior structures	$p \leq 0.001$ (disc)	<2 DD, RR 1.86 (disc)
	$p \leq 0.005$ (fovea)	RR 2.18 (fovea)
		RR 2.59 (D + F)
Vision before treatment	$p \leq 0.01$	<20/40, RR 1.73
Macular detachment	–	RR 1.67

1. Direct action of ionizing radiation on the retinal cells (photo receptors, pigment epithelium, and neurons)
2. Radiation vasculopathy that favors hypoxia and degenerative processes of visual cells and is also implicated in the capillary proliferation in the anterior chamber angle
3. Retinal detachment by subretinal fluid expansion
4. Cataract

The potential role of the retinal arterial blood supply in the development of post-radiation scotomas was pointed out by Meecham et al. [13]. They found that the deficit usually needed several months to develop and that it extended both into regions of the periphery and such that had received doses of more than 50 Gy. This distribution was consistent with injuries of blood vessels passing through the target volume.

Ion Beam-Associated Damage to the Central Nervous System

Cranial Nerves and/or Nuclei

Irradiation of sarcoma of the base of the skull is one of the major indications for proton and heavy ion therapy [14, 15]. Cranial nerves and their nuclei in the brain stem are among the most critical structures at risk with this type of radiation. Urie et al. [16] conducted an analysis on 27 patients with such tumors, treated with high doses (67.8–74.7 CGE) of proton radiation at the HCL between 1981 and 1984. Only non-diabetic patients were analyzed. Follow-up ranged from 54.6 to 110 months. Dose-volume histograms were constructed for individual cranial nerves and "near maximum" doses, i.e., the highest doses received by at least 5% of the volume were compared. The analysis showed that 17 nerves were impaired in 5/27 (18%) patients. The minimum dose for injury was 59.3 CGE and the average was 74.2 CGE. At 60 CGE the complication rate was estimated to be as low as 1%; at 70 CGE it was 5%. The latency period was not influenced by the dose received. Half of the lesions manifested within the first 24 months and none after 60 months. This study failed to show any difference in radiosensitivity between the various cranial nerves; nerve number VIII was affected 4 times, number V 3 times, numbers II, VI, and VII twice, and numbers II, IV, VI, IX, XI once, respectively; no lesions of nerves X and XI were observed.

A previous analysis by Habrand et al. [17] on tolerance of the optic nerve and chiasm in 20 consecutive patients, had shown that the risk could be markedly enhanced by predisposing factors such as damage to the microvasculature induced by diabetes mellitus. Castro et al. [15] have also published damages to the optic nerves and chiasm following high dose helium and neon therapy for tumors arising in the base of skull. Among 85 patients with no evidence of disease who were followed-up for 1 to 15 years, 8/85 (9%) patients presented a cranial nerve injury, including 3 unilateral and 1 bilateral visual loss. One reason for this apparently low rate might have been the fact that "unavoidable" damages to optic nerves or chiasms that were abutting the tumor were not included in this listing.

Brain and Spinal Cord

Tolerance values of brain and spinal cord as estimated by the collaborative task force of the NCI [18] are reported in Table 3. According to Yoshii et al. [19] there is a correlation between the latency period for brain injuries and the dose administered. Injuries manifested within 10 to 20 months following a dose $\leq$ 100 TDF (equivalent to 60 Gy delivered in 5 daily sessions of 2 Gy), and within 40 to 60 months after ~~TDF 70~~. This was based on the observation of 19 injuries in 106 brain tumor patients treated with photons plus or minus a proton boost. In the proton group, brain necrosis was observed only after much higher doses than in the photon group (TDF 114 versus 70).

Castro et al. [20] reported 2 cases of spinal cord injury and one of brain stem necrosis among 47 patients treated with helium ions for lesions encircling the brain stem and/or the spinal cord. The major cause of complications was attributed

Table 3. Tolerance doses in Gy for normal tissues at risk in the irradiation of intracranial malignancies. The risk corresponds to 5 % complications in patients treated at 1.8 Gy per fraction. These constraints, used at the Centre de Protonthérapie d'Orsay, are mainly taken from [18]

Organ	Extent of Irradiation			Type of Complication
	Area			
Skin	10 cm^2	30 cm^2	100 cm^2	
	70	60	55	Necrosis, ulceration
	–	–	50	Telangiectasias
	Locus			
Spinal cord	Surface	Center	Opposite	Myelitis, necrosis
<5 cm length	64	53	48	
>5 cm length	60	50	45	
Brain stem	64	53	48	Necrosis
	Volume			
	1/3	2/3	3/3	
Brain	60	50	45	Necrosis
Optic nerve	55	50	50	Blindness
Chiasm	55	50	50	Blindness
Lens	10	10	10	Cataract
Retina	45	45	45	Amblyopia
Middle Ear	55	55	55	Serous otitis
Parotid	–	32	32	Xerostomia
Temporomandibular joint	65	60	60	Trismus
Cranial base	70	70	70	Necrosis

to an underestimate of the RBE value of He. Increasing the RBE value of helium for CNS from 1.3 to 1.8 resulted in no further complications.

Accuracy in treatment planning and treatment set-up are also of paramount importance when brain stem and spinal cord are encompassed in the planning volume. The risk of radionecrosis seems to be very low when a steep dose gradient can be achieved throughout the structure (e.g., 64 CGE to the surface of these structures and 50–53 CGE to the center). In this context, the field abutment technique needs to be mentioned as a possible cause for overdosing (cf. Chapter 29). In this technique, used for example, for tumors encircling the brain stem or spinal cord the distal range of one proton beam abuts the lateral penumbra of an another beam. An overshooting of the beam past the junction consequently results in a local overdosage. Moving the

junction during the course of treatment could help limit this risk.

Patients previously irradiated are another risk goup susceptible to life-threatening necroses. Three of five fatal complications (grade 5) reported by Castro had been irradiated in the past [15].

Endocrine dysfunction following high dose proton therapy of skull base sarcomas was one of the most frequent complications of 14 patients treated at the HCL for a tumor of the upper clivus with the hypothalamic-pituitary axis included in the treatment fields, 4 developed hormon abnormalities 14 to 45 months after irradiation [21]. The 5-year projected rate of this type of complication was 37%. The DVHs of patients with and without complications showed no obvious difference, presumably because only simple DVHs could be obtained due to the poor spatial resolution of the pituitary in CT scans.

Fractionated Ion Beam Therapy of Pelvic Malignancies

Proton boosts have been recommended in the radiotherapeutic management of prostate carcinoma to minimize dose to rectum and bladder. The Boston Group postulated that a perineal proton beam used with a water-filled balloon placed in the rectum could spare the posterior part of the rectum. The sharp distal fall-off of the dose beyond the prostate volume could also save the bladder [22]. This technique has been tested since 1976 in conjunction with precise target localization using gold seed implantation into the prostate gland.

A preliminary study was conducted with 180 patients treated between 1972 and 1979 with one of two approaches [23]:

1. X-rays only: 50 Gy of high energy photons in 5 1/2 weeks in a 4-field box technique to the pelvis, followed by 18 Gy to the prostate volume only (fraction size: 1.8 Gy).
2. X-rays + protons: 50 Gy of X-rays in a 4-field box technique, followed by 24 CGE of protons through a perineal port.

Despite the higher dose, the second group revealed no additional complications: dysuria and hematuria were recorded in 10%, urethral stricture in 5% and proctologic symptoms in 20% of the patients.

The encouraging results reported with protons led to a randomized study in T_3–T_4 prostatic carcinomas, in which patients were allocated to receive either 67.2 Gy only with 10–25 MV photons, or a total of 75.6 CGE with photons (50.4 Gy) followed by protons (25.2 CGE). Although definitive long-term results on tumor control and functional outcomes are still pending, a preliminary analysis of rectal tolerance in 191 patients has been published by Benk et al. [24]. Dose-volume histograms of the anus, the anterior rectum, the posterior rectum and total rectum were calculated for each patient. Rectal bleeding was selected as an end point. Interestingly, the probability of not developing rectal bleeding within 5 years after treatment was significantly lower ($p = 0.013$) in the "X-rays + proton" arm (66%) than in the "X-rays only" arm (84%). The result correlated with the volume of the anterior rectum treated at high dose: patients who had received 75 CGE or more to at least 40% of this structure showed a statistically significant higher risk ($p = 0.003$) for bleedings.

Fractionated Ion Beam Therapy of Abdominal Malignancies

Liver

Preliminary results of the hepatic tolerance to protons are available from Tsujii and coworkers (25, see also Chapter 14). They evaluated a group of 24 patients with hepatocellular carcinomas treated with 50 to 87 Gy (mean 76.5) physical proton dose, given in 2.5 to 4 Gy fractions. At the time of treatment, all patients suffered from liver cirrhosis of variable severity; according to the Child-Turcott classification, 11 had grade A, 7 grade B, and 6 grade C. All patients were inoperable because of local extension or poor general condition. Multiple field arrangements were designed to focus the beam on the tumor volume

and to minimize the safety margin to 5–10 mm. Despite the poor baseline conditions of the patients, none experienced any serious side effects which would have required discontinuation of irradiation. No fatigue, loss of appetite, nausea, pains, or pleural effusion were reported. Merely 7/24 (29%) patients demonstrated transcient elevation of aspartate or alanine aminotransferase of twice or more the baseline values. It was concluded that this was a safe procedure even for patients with poor liver condition.

Liver tolerance to light ion therapy was also evaluated by Austin-Seymour et al. [26] in 11 patients that had been treated at Lawrence Berkeley Laboratory (LBL) for carcinoma of the pancreas or the biliary system. The patients received whole liver coverage plus an additional boost with helium or neon ions. According to an averaged RBE of 1.3 and 2.7, respectively, the total dose ranged from 18 to 24 CGE to the whole liver, and 53.5 to 70 CGE to the primary tumor. 1/11 (9 %) patients died of radiation hepatitis. A DVH intercomparison suggested that for 18 Gy-equivalent administered to the whole gland at 2 Gy/fraction, an additional cone-down boost had to be restricted to 30% or less of the hepatic volume, if the additional dose exceeded 30–35 Gy.

Intestine

Intestinal complications have been reported sporadically. This is in part due to the fact that only few intra-abdominal malignancies have been treated by ion beam therapy. Small and large bowel injuries have been reported following pion therapy of pelvic tumors [27] and retroperitoneal sarcomas. But these studies should be regarded as preliminary evaluations of clinical normal tissue tolerance to this particular type of radiation. As a matter of fact, Greiner et al. reported no further complications when the pion dose was reduced to less than 36 Gy and the treated volume limited to 500 ml [28].

Radiosurgery with Ion Beams

Radiosurgery differs in several aspects from conventional external beam radiotherapy: it generally deals with small volumes (≤ 5 ml) which are exposed to single fractions of high doses with the aim of inducing focal tissue necrosis (cf. the previous chapter).

Besides the knowledge of dose and volume dependence gathered in the 60's and early 70's from radiobiological and clinical studies on brain tissue tolerance to single fractions, it is owing to the stereotactic approach introduced by neurosurgeons that the complication rate of radiosurgery is so remarkably low.

Acute side effects are generally limited to an increased seizure activity in patients with seizures at presentation. Very rarely, severe headaches, vomiting, and elevated temperature have been reported. Delayed effects can be various forms of vasculopathy or radionecrosis [29].

Vasogenic edema seems related to injuries to the endothelium of small vascular shunts that permit fluid diffusion to the surrounding tissues; white matter is commonly affected. On T2-weighted MRI, these areas appear with enhanced signal. These modifications are generally asymptomatic. Only 10 to 15% of the patients show symptoms. In the LBL series with helium ions, such complications were never observed for doses <25 Gy-equivalent.

Arterial occlusions result from injuries to the arterial vasculature included in the treatment field. They reveal no sign of edema on MRI. Aneurysms were reported in the follow-up of patients with arteriovenous malformations (AVMs). The suggested pathophysiology was an increased pressure in the arterial branches as a consequence of the AVM obliteration. Venous thrombosis seemed extremely rare.

Radionecrosis was described in less than 5% of patients receiving 25 to 45 CGE, although doses as low as 15 CGE have been incriminated to cause cerebral radiation necrosis [30].

Most complications have been reported for lesions situated in the brain stem, thalamus, or basal ganglia. Of 17 such patients treated at LBL for AVMs, symptoms were minor in 7 and major

in 10 ranging from visual deficit, diplopia, hearing impairment, to ataxia and/or paresis.

Kjellberg [31] reported his experience with protons in 2118 patients treated over 25 years. In pituitary adenomas, visual field disturbances, e.g., were observed in less than 2% of the treated patients.

Hypopituitarism was seen in about one out of 10 patients. One patient developed brain sarcoma several years after therapy. In arteriovenous malformations the complication rate fell to 0.5% after changes of dose and field size.

These results are difficult to compare with those of other stereotactic approaches since the indications can differ markedly, the complications are generally not reported with actuarial statistics, and the end points – clinical, radiological or both – can be different, too. But problems in AVM treatment can obviously also be kept below 10% with gamma knife [32] or linear accelerator [33].

Conclusion

Over 13000 patients have been treated with protons, and 3500 with pions and heavy ions worldwide. Large patient series are becoming available with follow-up periods exceeding 5 years. A remarkably low rate of complications and late sequelae has been reported given the large doses generally administered. Major improvements regarding treatment planning, patient set-up, knowledge of normal tissue tolerance, and RBE will help to reduce these risks, further.

References

1 Saunders, W.M., Char, D.H., Quivey, J.M., Castro, J.R., Chen, G.T.Y., Collier, J.M., Cartigny, A., Blakely, E.A., Lyman, T.J., Zink, S.R., and Tobias, C.A. Precision, high dose radiotherapy: Helium ion treatment of uveal melanoma. Int. J. Radiat. Oncol. Biol. Phys. 11, 2, 227–233, 1985.

2 Gragoudas, E.S., Seddon, J.M., Egan, K.M., Glynn, R.J., Goitein, M., Munzenrider, J., Verhey, L., Austin-Seymour, M., Urie, M., and Koehler, A. Proton irradiation of uveal melanomas: The first 1000 patients, in Tumors of the Eye. Bornfeld, N., Gragoudas, E.S, Höpping, W., Lommatzsch, P.K., Wessing, A., and Zografos, L., (eds.), Kugler Publishing, Amsterdam, 1991, pp. 489–495.

3 Desjardins, L., d'Hermies, F., Frau, E., Levy, C., Epelbaum, M., Schlienger, P., Habrand, J.L., Schwartz, L., Mazal, A., Delacroix, S., Nauraye, S., Ferrand, R., and Asselain, B. Expérience et résultats préliminaires de la protonthérapie du mélanome de la choroïde à Orsay. Les 300 premiers cas. Ophthalmol. (Paris), in press.

4 Guyer, D.R., Mukai, S., Egan, K.M., Seddon, J.M., Walsh, S.M., and Gragoudas, E.S. Radiation maculopathy after proton beam irradiation for choroidal melanoma. Ophthalmol. 99, 1278–1285, 1992.

5 Seddon, J.M., Gragoudas. E.S., Egan, K.M., Glynn, R.J., Munzenrider, J.E., Austin-Seymour, M., Goitein, M., Verhey, L., Urie, M., and Koehler, A. Uveal melanomas near the optic disc or fovea. Ophthalmol. 94, 354–361, 1987.

6 Coucke, P.A., Schmid, C., Balmer, A., Mirimanoff, R.O., and Thames, H.D. Hypofractionation in retinoblastoma: An increased risk of retinopathy. Radiother. Oncol. 28, 157–161, 1993.

7 Meecham, W.J., Char, D.H., Kroll, S., Castro, J.R., and Blakely, E.A. Anterior segment complications after helium ion radiation therapy for uveal melanoma: Radiation cataract. Arch. Ophthalmol. 112, 2, 197–203, 1994.

8 Castro, J.R., Nowakowski, V., Linstadt, D., Collier, J.M., Petti, P.L., Lyman, J., Phillips, T.L., Char, D., Gauger, G.E., Woodruff, K., Chu, W., Ludewigt, B., Renner, T., Singh, R.P., Pitluck, S., and Whitcomb, T. Heavy charged particle therapy at the Lawrence Berkeley Laboratory, in Proc. EULIMA Workshop on the Potential Value of Light Ion Beam Therapy, Chauvel P. and Wambersie A. (eds.), EC Publ. No. EUR 12165 EN, 1989, pp. 219–232.

9 Egan, K.M., Gragoudas, E.S., Seddon, J.M., Glynn, R.J., Munzenrider, J.E., Goitein, M., Verhey, L., Urie, M., and Koehler, A. The risk of enucleation after proton beam irradiation of uveal melanoma. Ophthalmol. 96, 1377–1383, 1989.

10 Munzenrider, J.E., Gragoudas, E.S., Seddon, J.M., Sisterson, J., McNulty, P., Birnbaum, S., Johnson, K., Austin-Seymour, M., Slater, J., Goitein, M.M., Verhey, L., Urie, M., Ruotolo, D.M., Egan, K., and Osuna, F. Conservative treatment of uveal melanoma: Probability of eye retention after proton treatment. Int. J. Radiat. Oncol. Biol. Phys. 15, 553–558, 1988.

11 Egger, E., Zografos, L., Perret, C., Bercher, L., Chamot, L., and Gailloud, C. Proton beam irradiation of uveal melanomas at PSI: 7 years of experience, in Proc. Proton Radiotherapy Workshop. Blattmann, H. (ed.), PSI-Bericht-111, 1991, pp. 80–83.

12 Seddon, J.M., Gragoudas, E.S., Polivogianis, L., Hsieh, C.C., Egan, K.M., Goitein, M., Verhey, L., Munzenrider, J., Austin-Seymour, M., Urie, M., and Koehler, A. Visual outcome after proton beam irradiation of uveal melanoma. Ophthalmol. 93, 666–674, 1986.

13 Meecham, W.J., Char, D.H., Chen, G.T.Y., Juster, R., Castro, J.R., Stone, R.D., and Saunders, W.M. Correlation of visual field, treatment fields, and dose in helium ion irradiation of uveal melanoma. Am. J. Ophthalmol. 100, 658–665, 1985.
14 Austin-Seymour, M., Munzenrider, J., Goitein, M., Verhey, L., Urie, M., Gentry, R., Birnbaum, S., Ruotolo, D., Mc Manus, P., Skates, S., Ojeman, R.G., Rosenberg, A., Schiller, A., Koehler, A., and Suit, H.D. Fractionated proton radiation therapy of chordoma and low-grade chondrosarcoma of the base of the skull. J. Neurosurg. 70, 13–17, 1989.
15 Castro, J.R., Linstadt, D.E., Bahary, J.P., Petti, P.L., Daftari, I., Collier, J.M., Gutin, P.H., Gauger, G., and Phillips, T.L. Experience in charged particle irradiation of tumors of the skull base: 1977–1992. Int. J. Radiat. Oncol. Biol. Phys. 29, 4, 647–655, 1994.
16 Urie, M.M., Fullerton, B., Tatsuzaki, M.D., Birnbaum, S., Suit, H.D., Convery, K., Skates, S., and Goitein, M. A dose response analysis of injury to cranial nerves and/or nuclei following proton beam radiation therapy. Int. J. Radiat. Oncol. Biol. Phys. 23, 27–39, 1992.
17 Habrand, J.L., Austin-Seymour M., Birnbaum, S., Wray, S., Carroll, R., Munzenrider, J., Verhey, L., Urie, M., and Goitein, M. Neurovisual outcome following proton radiation therapy. Int. J. Radiat. Oncol. Biol. Phys. 16, 1601–1606, 1989.
18 Emami, B., Lyman, J., Brown, A., Coia, L., Goitein, M., Munzenrider, J.E., Shank, B., Solin, L.J., and Wesson, M. Tolerance of normal tissue to therapeutic irradiation. Int. J. Radiat. Oncol. Biol. Phys. 21, 109–122, 1991.
19 Yoshii, Y., Takano, S., and Tsurushima, H. Normal brain damage after radiotherapy of brain tumors. Clin. Oncol. 3, 278–282, 1991.
20 Castro, J.R., Collier, J.M., Petti, P.L., Nowakowski, V., Chen, G.T.Y., Lyman, J.T., Linstadt, D., Gauger, G., Gutin, P., Decker, M., Phillips, T. L., and Baken, K. Charged particle radiotherapy for lesions encircling the brain stem or spinal cord. Int. J. Radiat. Oncol. Biol. Phys. 17, 477–484, 1989.
21 Slater, J.D., Austin-Seymour, M., Munzenrider, J., Birnbaum, S., Carroll, R., Klibanski, A., Riskind, P., Urie, M., Verhey, L., and Goitein, M. Endocrine function following high dose proton therapy for tumors of the upper clivus. Int. J. Radiat. Oncol. Biol. Phys. 15, 607–611, 1988.
22 Shipley, W.U., Tepper, J.E., Prout, G.R., Verhey, L.J., Mendiondo, O.A., Goitein, M., Koehler, A.M., and Suit, H.D. Proton radiation as boost therapy for localized prostatic carcinoma. J. Am. Med. Assoc. 241, 1912–1915, 1979.
23 Duttenhaver, J.R., Shipley, W.V., Perrone, T., Verhey, L.J., Goitein, M., Munzenrider, J.E., Prout, G.R., Parkhurst, E.C., and Suit, H.D. Protons or megavoltage X-rays as boost therapy for patients irradiated for localized prostatic carcinoma. An early phase I/II comparison. Cancer 51, 1599–1604, 1983.
24 Benk, V.A., Adams, J.A., Shipley, W.U., Urie, M.M., McManus, P.L., Effird, J.T., Willett, C.G., and Goitein, M. Late rectal bleeding following combined X-ray and proton high dose irradiation for patients with stages T3-T4 prostate carcinoma. Int. J. Radiat. Oncol. Biol. Phys. 26, 551–557, 1993.
25 Matsuzaki, Y., Osuga, J., Saito, Y., Chuganji, Y., Tanaka, N., Shoda, J., and Tsujii, H. A new effective and safe therapeutic option using proton irradiation for hepatocellular carcinoma. Gastroenterology 106, 1032–1041, 1994.
26 Austin-Seymour, M., Chen, G.T.Y., Castro, J.R., Saunders, W.M., Pitluck, S., Woodruff, K.H., and Kessler, M. Dose-volume histogram analysis of liver radiation tolerance. Int. J. Radiat. Oncol. Biol. Phys. 72, 31–35, 1986.
27 Schmitt, G., von Essen, C.F., Greiner, R., and Blattmann, H. Review of the SIN and Los Alamos pion trials. Radiat. Res. 104, Suppl. 272–278, 1985.
28 Greiner, R.H., von Essen, C.E., Blattmann, H.J., Pedroni, E., Studer, U.E., Thum, P.A., and Zimmermann, A. Pion Therapy at the Swiss Institute For Nuclear Research (Abstr.). Int. J. Radiat. Oncol. Biol. Phys. 12, Suppl. 1, 98, 1986.
29 Fabrikant, J.I., Levy, R.P., Steinberg, G.K., Phillips, M.H., Frankel, K.A., Lyman, J.T., Marks, M.P., and Silverberg, G.D. Charged-particle radiosurgery for intracranial vascular malformations. Neurosurg. Clin. North Am. 3, 99–139, 1992.
30 Kaufman, M., Swartz, B.E., Mandelkern, M., Ropchan, J., Gee, M., and Blahd, W.H. Diagnosis of delayed cerebral radiation necrosis following proton beam therapy. Arch. Neurol. 47, 474–476, 1990.
31 Kjellberg, R.W. and Abe, M. Stereotactic Bragg peak proton beam therapy, in Modern Stereotactic Neurosurgery. Lunsford, L.D. (ed.), Nijhoff M. Publishing, Boston, 1988, pp. 463–470.
32 Steiner, L. Radiosurgery in cerebral arteriovenous malformations, in Textbook of Cerebrovascular Surgery. Flam, E. and Ferri, J. (eds.), Springer Verlag, New York. 1986, pp. 1161–1215.
33 Colombo, F., Benedetti, A., Pozza, F., Marchetti, C., and Chiergo, G. Linear accelerator radiosurgery of cerebral arteriovenous malformation. Neurosurg. 24, 833–840, 1989.

18 Future Directions of Clinical Ion Beam Radiation

J. M. SLATER

Loma Linda University Medical Center, Loma Linda, CA, USA

Background

Ionizing radiation has been used for therapeutic purposes since 1896, within months of Roentgen's discovery of X-rays [1], and has developed into one of the two most successful modalities for treating localized cancer. Historically, this success story can be divided into four eras of roughly 30 years each. These time periods might be thought of as the discovery era (1895–1925), the kilovoltage era (1925–1955), the megavoltage era (1955–1985), and a fourth, the ion beam era, which is now in progress.

In each era, developments occurred in physics laboratories which led to the subsequent eras. Roentgen's discovery of X-rays was followed by identification of subatomic particles, emission of gamma rays, atomic structure characteristics, and engineering advances which provided new capabilities for measuring the characteristics of X-rays, gamma rays and the other subatomic particles. Such discoveries, along with milestones such as the development of the Coolidge X-ray tube, made kilovoltage-era achievements possible [2]. The concept of accelerating charged particles in small steps and using subatomic particles as carriers of energy (rather than the secondary windings in the transformer) overcame the insulation properties that severely limited the energy capabilities of high-tension accelerators of the kilovoltage era and provided further bases for developing the megavoltage and ion beam eras [3]. The Betatron, linac and cyclotron all evolved from the concept that a type of transformer could be devised wherein the energized particles formed the secondary windings. In addition, E.O. Lawrence developed the first proton cyclotron at the University of California, Berkeley [4]. The device and its successors generated high-energy neutrons and led, eventually, to the first clinical neutron trials. By 1946, 150+ MeV protons were available and Robert Wilson published his insight that accelerated protons would be superior to photons for clinical therapy [5]. Heavy particle therapy experimentation began at Lawrence Berkeley Laboratory in the early 1950s [6]. During the megavoltage era, linear electron accelerators became widely available to clinics, as did the Betatron. These technological developments occurred in tandem with a greater understanding of cancer biology; together, these advancements resulted in major improvements in cancer patient survival. This progress continued through the megavoltage era as particle energies increased with the development of high-megavoltage electron accelerators [7]. Another improvement in cancer patient survival was demonstrated with the clinical use of ion beams from heavy charged particle accelerators [8–12]. Radiation oncologists realize that increasing the total doses of ionizing radiation is essential for improving local control of many tumors that presently are not controlled.

The major improvements in tumor control seen as these eras progressed, related to the more favorable distribution of energy deposited in the patient as each increase in photon energy occurred, allowing in turn increased doses to the target volume. It is now clear, however, that further increases in the energy of photon or electron beams is no longer a satisfactory approach. New particles, with more favorable characteristics, are

essential for optimal improvements in cancer control by radiation.

This need for further major improvements in the therapeutic aspect of cancer patient management, along with the major successes achieved with ionizing radiation to date, has led to the ion beam era. This era might be said to have begun in January 1985, when an international group of 93 scientists responded to an invitation to meet at Fermi National Accelerator Laboratory. The purpose of the initial meeting was to develop the design requirements for a heavy charged particle medical facility, including the accelerator, beam transport system, beam delivery system, the building housing the equipment, and the nature of the clinical studies to be conducted. The group, known as Proton Therapy Cooperative Group (PTCOG), included from its inception members from North America, Asia, and Eastern and Western Europe. Heavy ions and protons have been under discussion ever since. PTCOG has continued to meet on a twice yearly basis; protons have gained the major attention partly due to their lower linear energy transfer properties and partly due to their significantly lower costs compared to ion beams.

Current Status

Successful control of localized tumors by traditional radiation is constrained by dose limitations imposed by the unavoidable integral dose received in normal tissues outside the target volume. Energized subatomic particles having clinically more favorable attributes for depositing their energy within a patient are now being investigated to overcome this limitation of photon and electron beams. Many subatomic particles are now available, each having its own characteristics for depositing energy. To avoid losses of time and resources involved in working with all of the available particles, it is imperative that we first define the optimum clinical requirements needed from a new therapy beam. Next, we need to evaluate each of the particles in terms of their ability to satisfy the defined clinical requirements and their potential for clinical use at this time. Finally, we need to work on an international basis to develop the ideal technology for accelerating and delivering the particle(s) selected, and follow with coordinated clinical trials and superb quality assurance programs.

The macrodosimetric properties of the particles to be evaluated should be the primary priority in determining their therapeutic utility; the microdosimetric characteristics, which greatly influence biological effects, should become the secondary priority. The minimal macrodosimetric attribute should be the ability to control each beam in three dimensions. Microdosimetric characteristics should include minimum ionization density of the particle track as it traverses normal cells; moderate increases in the ionization density of the track should ideally begin as the particles enter the target region. There are other macro- and microdosimetric requirements, too numerous to discuss here, which should be met, but the foregoing are fundamental. Subatomic charged particles of the hadron family, and heavier ions, possess the greatest potential to fulfill these requirements.

To date, more than 17600 patients have been treated with particle beams in facilities around the world; more than 14000 of them with protons (cf. Chapter 1 for more details). Patient totals will rise in the future, not only as patients are treated in existing facilities but also as new, expanded or modified facilities, currently being constructed or planned worldwide, are employed (see Tab. 1 and Chapter 139). The rapid increases in facilities and patients treated indicates the worldwide increasing recognition of the superiority of these heavy charged particles for therapeutic purposes.

Cost is the only meaningful constraint to the development of this form of irradiation. The physics of heavy charged particles supports their superiority for therapeutic use. Development of the first hospital-based clinical proton treatment facility at Loma Linda University Medical Center in 1990 established that the technology is now available to develop a highly integrated facility with the sophistication, reliability, safety, efficiency and friendly environs essential for a successful hospital operation. The financial aspects of this pioneering patient-dedicated facility have been demonstrated to be acceptable; new facil-

Table 1. New particle therapy facilities (adapted from Particles, The Newsletter of the Proton Therapy Co-operative Group 14, July 1994)

Place	Particle	Opening Date
Villigen, Switzerland (PSI)	p+	1994
Chiba, Japan (HIMAC)	ion	1994
Vancouver, Canada (TRIUMF)	p+	1994
Berlin, Germany (HMI)	p+	1995
Munich, Germany	p+	1995/6
Darmstadt, Germany (GSI)	ion	1996
Moscow, Russia (ITEP)	p+	1996
Jülich, Germany (KFA)	p+	1997
Groningen, Netherlands (KVI)	p+	1997?
MGH Boston, MA, USA (NPTC)	p+	1998
North Carolina, USA (NC STAR)	p+	1999?
Italy (TERA)	ion	2000?
Novosibirsk, Russia	p+	?
Chicago, Illinois, USA	p+	?
Clatterbridge, UK	p+	?
Tsukuba, Japan	p+	?
Krakow, Poland	p+	?

ities will experience significantly lower costs. The LLUMC experience relieves the substantive concerns regarding future development of proton therapy.

Ion Beam Therapy: The Future

The process of developing a clinical ion beam facility is essentially the same as is followed to develop any new modality for clinical use. Consideration of the clinical requirements imposed on a new modality is essential if the facility is to be successful. Several factors must be considered:

Basic Need for Utilization

Surgery and radiation therapy are the only two modalities currently available for effectively treating either local or regional gross cancer. The basic need for improving the treatment and management of cancer is undisputed: American Cancer Society statistics for 1993 indicate that 1.2 million new patients will be diagnosed with cancer in 1994, and that there will be an expected 500000 survivors [13]. No data are reported for morbidity because of the difficulty of adequately assessing that outcome. It is commonly known, however, that patients frequently delay early diagnosis because they fear the morbidity that results from the cancer and its treatment, further supporting the need for improving current therapeutic capabilities.

Efficacy

The effectiveness of ion beams for treating ocular melanomas, pituitary adenomas and chordomas and chondrosarcomas of the base of skull, has been demonstrated [14–20] and preceding chapters). Selecting the most appropriate particle for specific therapeutic purposes, however, includes consideration of the macrodosimetric, microdosimetric and financial characteristics of each particle. The vast majority of subatomic particles are too unstable to consider for clinical use, with present technology, leaving very few to select from (Table 2).

To ensure appropriate control of energy deposition for most clinical purposes, the particle should have a charge and a mass many times that

Table 2. Families of particles

Familiy	Particles
Photon	Photon*
Lepton	Electron*
	Muon
	Tau
Hadron	
Mesons	Pion*
	Kaon
	Eta
Baryons	Proton*
	Neutron*
	Lambda
	Sigma
	Xi
	Omega

* Clinically applicable

of electrons. This leaves for our consideration charged particles of the hadron family and the heavier ions.

Morbidity and Associated Risks

The risks associated with ion beam radiation largely relate to the repair capabilities of normal cells traversed by the particles and the potential for oncogenic transformation of cells surviving their exposure. Studies thus far have not detected significant differences between photon and proton beam oncogenic transformation capabilities; oncogenic transformation in mammalian cell cultures has been shown to be directly related to the density of the ionization track of the particle used, and appears to decrease with fractionated dose schedules [21].

Operational Reliability

The total system should be designed to remain operational 100% of the time, or as close to that as possible; mechanical failures resulting in short delays of patient treatments during any given day are considered acceptable if their occurrence is not routine. The ability to develop this level of reliability within a hospital setting has been demonstrated at the Loma Linda University Proton Facility (LLUPROF), where the "uptime" has exceeded 98% since the facility opened in October 1990.

Efficiency

A clinically successful hospital-based proton therapy system must be efficient. The high initial costs must be amortized by clinical funds from relatively large numbers of patients to reduce individual costs; inefficiencies in operations may preclude success in an otherwise worthwhile program.

Patient requirements should dictate the design of the clinical support portion of the facility. The use of gantries and/or fixed beam treatment rooms determines the design of the treatment portions of the facility. Efficiency refers to the entire facility design; every patient activity and each support activity must be performable with ease and should flow in a logical sequence, free of functional obstructions. The director should be able to unify and lead the entire operation in a manner akin to a conductor leading an orchestra. The conceptual design of the building, therefore, is fundamental to success in this aspect of efficiency. By outlining each activity to be performed on a patient, in preparation for the patient's treatment, the optimal room layout for convenience and efficiency can be determined. Associated with the facility's conceptual design is the engineering design that translates the concept into a functioning entity. Engineering designs based upon physical, clinical and operational design requirements should assure development of a successful hospital-based, heavy charged particle facility. The ultimate success of any new heavy particle facility will depend on the facility design, its quality of operations, and the clinical results it produces.

Functionality, which refers to the facility's responsiveness to clinical demands, is an integral aspect of efficiency. All anatomic sites must be targeted precisely in both patient set-up and treatment. Patients' needs and feelings must be considered. The facility should be designed with a friendly, inviting and comforting environment. The equipment should be sufficiently sophisticated to permit each treatment room to be operated by the attending nursing and technologist staff. Engineering and physics staff should be available for unusual circumstances. Physician staff should be involved with the verification of each set-up and should aid technologists and nurses with difficult patient positioning and medical support needs.

Financial Considerations

Self-sustaining operations are essential for a successful program at most institutions. This means that the facility should be designed to accommodate a volume of patients that will make self-sustenance possible, and that the particle selected is cost-effective, both in its initial and operational

expenses. The stability of the particle, and its mass, affect the initial costs and the operational expenses.

Summary

Photon therapy has been developing for nearly 100 years. Enormous improvements in the treatment of cancer and some benign diseases have resulted. Patient morbidity from radical surgical procedures has been greatly reduced by the photons' capability to selectively destroy undesirable abnormal cells while sparing sufficient normal cells to enable repair to proceed. Its success as a modality is immense and undeniable in spite of the controversial periods it has experienced.

Photon therapy, however, as the mainstream modality for delivering ionizing energy for human disease, has reached a plateau that further energy changes and delivery techniques have not been able to surmount. Technology has progressed and with it has come the opportunity to use other particles for carrying ionizing energy; particles having increased controllability and new energy deposition attributes. One of them likely will emerge as the primary, mainstream particle while others will function in secondary, support roles, much as electrons and radioisotopes now support photon beams. The primary particle will combine maximal controllability with minimal ionization density, attributes which allow it to be focused on target volumes with minimal effect on normal tissues and thus maximize its clinical applicability. Radioresistant tumors will require more densely ionizing characteristics, which suggests the need for more than one type of ion beam. Based upon the significant success of photon and electron beams and the capability of present technology, the proton most closely approximates the combination of attributes suggested for the mainstream particle, and therefore seems most appropriate to replace the photon as the primary particle in radiation oncology. Cost analyses of the Loma Linda experience further support the proton as the primary particle for current therapeutic purposes.

It is extremely unlikely that any single particle will adequately satisfy the physician's demands. Protons, heavy ions and neutrons [22, 23] have all demonstrated success in specific clinical applications. Modulation of the ionization density of the target volume may be achieved by mixing ion beams of different characteristics to optimize the therapeutic ratio in some clinical situations. Ultimately, the physician needs to have the ability to use the particle, or combination of particles, that will yield the highest probability of disease control and minimize the undesirable side effects.

References

1 Freund, L. Elements of General Radiotherapy for Practitioners. Rebman Company, New York, 1904, pp. 229–243.
2 Coolidge, W.D. A powerful roentgen-ray tube with a pure electron discharge, Phys. Rev 2, 409–413, 1913.
3 Glasser, O., Quimby, E.H., Taylor, L.S., Weatherwax, J.L., and Morgan, R.H. Physical Foundations of Radiology, 3rd ed. Paul B. Hoeber Inc., New York, 1961, pp. 14–21.
4 Heilbron, J.L. and Seidel, R.W. Lawrence and his Laboratory. University of California Press, Berkeley, 1989, pp. 45–102.
5 Wilson, R.R. Radiological use of fast protons. Radiology 47, 487–491, 1946.
6 Tobias, C.A., Roberts, J.E., Lawrence, J.H., Low-Beer, B.V.A., Anger, H.O., Born, J.L., McCombs, R., and Huggins, C. Irradiation hypophysectomy and related studies using 340 MeV protons and 190 MeV deuterons. Peaceful uses of Atomic Energy 10, 95–96, 1956.
7 Kaplan, H.S., Historic milestones in radiobiology and radiation therapy. Semin. Oncol. 6, 479–489, 1979.
8 Kligerman, M.M., Black, W.C., Yuhas, J.M., Doberneck, R.C., Bradbury, J.N., and Kelsey, C.A. Current status of clinical pion radiotherapy. Radiology 125, 489–492, 1977.
9 Kjellberg, R.N., Sweet, W.H., Preston, W.M., and Koehler, A.M. The Bragg peak of a proton beam in intracranial therapy of tumors. Trans. Am. Neurol. Assoc. 87, 216–218, 1962.
10 Minakova, E.I., Kirpatovskaia, L.E., Liass, F.M., Snigireva, R., and Krymskii, A. Proton therapy of pituitary adenomas. Med. Radiol. Mosk. 28, 7–14, 1983.
11 Castro, J.R. and Quivey, J.M. Clinical experience and expectations with helium and heavy ion irradiation. Int. J. Radiat. Oncol. Biol. Phys. 3, 127–131, 1977.
12 Larsson, B., Leksell, L., and Rexed, B. The use of high energy protons for cerebral surgery in man. Acta Chir. Scand. 125, 1–7, 1963.
13 Boring, C.C., Squires, T.S., Tong, T., and Montgomery, S. Cancer statistics 1994 CA. A Cancer Journal for Clinicians 44, 7–26, 1994.

14 Gragoudas, E.S., Seddon, J.M., Egan, K., Munzenrider, J., Austin-Seymour, M., Goitein, M., Verhey, L., and Koehler, A. Long-term results of proton beam irradiated uveal melanomas. Ophthal. 94, 349–353, 1987.
15 Saunders, W.M., Chen, G.T.Y., Austin-Seymour, M., Castro, J.R., Collier, M., Gauger, G., Gutin, P., Phillips, T.L., Pitluck, S., Walton, R.E., and Zink, S.R. Precision, high-dose radiotherapy: II. Helium ion treatment of tumors adjacent to critical central nervous system structures. Int. J. Radiat. Oncol. Biol. Phys. 11, 1339–1347, 1985.
16 Schoenthaler, R., Castro, J.R., Halberg, F.E., and Phillips, T.L. Definitive postoperative irradiation of bile duct carcinoma with charged particles and/or photons. Int. J. Radiat. Oncol. Biol. Phys. 27, 75–82, 1993.
17 Schoenthaler, R., Castro, J.R., Petti, P.L., Baken-Brown, K., and Phillips, T.L. Charged particle irradiation of sacral chordomas. Int. J. Radiat. Oncol. Biol. Phys. 26, 291–298, 1993.
18 Suit, H.D., Goitein, M., Munzenrider, J.E., Verhey, L., Gragoudas, E., Koehler, A.M., Urano, M., Shipley, W.U., Linggood, R.M., Friedberg, C., and Wagner, M. Clinical experience with proton beam radiation therapy. J. Canad. Assoc. Radiol. 31, 35–39, 1980.
19 Suit, H.D., Goitein, M., Munzenrider, J., Verhey, L., Urie, M., Gragoudas, E., Koehler, A., Gottschalk, B., Sisterson, J., Tatsuzaki, H., and Miralbell, R. Increased efficacy of radiation by use of proton beam. Strahlenther. Onkol. 166, 40–44, 1990.
20 Uhl, V., Castro, J.R., Knopf, K., Phillips, T.L., Collier, J.M., Petti, P.L., and Daftari, I. Preliminary results in heavy charged particle irradiation of bone sarcoma. Int. J. Radiat. Oncol. Biol. Phys. 24, 755–759, 1992.
21 Hei, T.K., Chen, D.J., Brenner, D.J., and Hall, E.J. Mutation induction by charged particles of defined linear energy transfer. Carcinogenesis 9, 1233–1236, 1988.
22 Laramore, G.E., Krall, J.M., Griffin, T.W., Duncan, W., Richter, M.P., Seroja, K.R., Maor, M.H., and Davis, L.W. Neutron versus photon irradiation for unresectable salivary gland tumors: final report of an RTOG-MRC randomized clinical trial. Int. J. Radiat. Oncol. Phys. 27, 235–240, 1993.
23 Russell, K.J., Caplan, R.J., Laramore, G.E., Burnison, C.M., Maor, M.H., Taylor, M.E., Zink, S., Davis, L.W., and Griffin, T.W. Photon versus fast neutron external beam radiotherapy in the treatment of locally advanced prostate cancer: results of a randomized prospective trial. Int. J. Radiat. Oncol. Biol. Phys. 28, 47–54, 1994.

IV. Medical Accelerators and Beam Line Design

19 Design Criteria for Medical Accelerators

J. R. ALONSO

Lawrence Berkeley Laboratory, Berkeley, CA, USA

Introduction*

Radiation therapy with beams of protons and heavier ions has reached the stage where intensive clinical research must be performed to develop protocols for best application of this modality for the treatment of cancer and other lesions. Results from many years of research, both clinical and radiobiological, and many thousands of patients treated have demonstrated the effectiveness of the dose localization abilities of these beams, and have hinted at benefits from high-LET radiation. Until recently, all the progress in the field has taken place at accelerator facilities in large laboratories or universities, accelerators built originally for physics research to which medical facilities have been added. The new treatment facilities at Loma Linda, USA and Chiba, Japan break this pattern, and are the first accelerators designed and built primarily for ion treatments.

To continue the rapid progress made in recent years, more hospital-based facilities that are optimized for patient treatments are necessary. Two primary goals should be kept in mind in planning such facilities: they should permit the treatment of large numbers of patients easily and efficiently to accrue statistics and develop the necessary protocols; and they should both assist in the development of, and incorporate into clinical use the best possible beam delivery technology to take maximum advantage of the properties of ion beams.

To accomplish these goals efficiently, careful attention must be paid to the specifications for the performance of the technical components of the treatment facility, including the accelerator, beam delivery, and patient handling systems. Very important is the order in which these specifications are determined: first must be the requirements for clinical performance, then the beam delivery system that will meet these requirements, and finally the accelerator that will provide beams tailored to the specified beam delivery system.

Clinical Specifications

As part of a joint study program sponsored by the US National Cancer Institute [1] to evaluate specifications and designs for a dedicated proton therapy facility, clinical groups from UCSF (University of California at San Francisco) and MGH (Massachusetts General Hospital), with assistance from staff members of the Lawrence Berkeley and Harvard Cyclotron laboratories developed a set of clinical specifications that could be used as the basis for the beginning of a design effort. Although these specifications were written with protons in mind, the clinical requirements for heavier ions, such as helium, carbon, or neon would be essentially the same. The only area where a real technological challenge would exist in meeting the specifications would be in providing isocentric delivery for ion beams. These

* Material for this chapter is drawn largely form LBL report 33749 "Performance Specifications for Proton Medical Facility by W.T. Chu, J.W. Staples, B.A. Ludewigt, T.A. Renner, R.P. Singh, M.A. Nyman, J.M. Collier, L.K. Daftari, H. Kubo, P.L. Petti, L.J. Verhey, J.R. Castro and J.R. Alonso, March 1993.

beams. These specifications, reported recently by Gall et al. [2] can be classified into several groupings, and are described below.

Position and Precision of Stopping Beam

The basic aim of ion beam therapy is to be able to place stopping particles in any point of the body, and so to define a treatment volume that conforms as closely as possible to the generally irregular, three-dimensional shape of the diseased tissue to be treated, while keeping the dose to adjacent normal tissue to its lowest possible value. Table 1 lists the accuracy and range of parameters desired to effect this placement. The maximum range, roughly 32 cm in tissue, is expected to be able to handle over 95% of the desired ports. While shallow-penetration beams can be obtained by simply degrading the energy of the beam, such degrading also spoils the good properties of the beam, losing the precision that is most likely required for these shallow-field treatments, such as for ocular melanomas. Achieving shallow ranges, then, must be accomplished without degradation of beam quality.

Table 1. Range and precision requirements of the stopping beam

Parameter	Desired Specification
Deepest range of penetration	32 g/cm^2
Shallowest range of penetration	3.5 g/cm^2
Precision in setting the deepest range	0.1 g/cm^2
Steps of range adjustment within a given field	0.5 g/cm^2
Maximum field size in a	
fixed-beam room	40 cm × 40 cm
gantry room	26 cm × 20 cm
Sharpness of distal dose fall-off	0.1 g/cm^2 above limit set by range straggling
Sharpness of lateral penumbra	2 mm above limit set by multiple scattering in the patient
Effective SAD (Source-to-axis distance)	> 3 m

Precision in setting the distal extent of the field (around 0.3% of the maximum range) relates to the accuracy of setting the beam energy; from an accelerator standpoint achieving this accuracy is not a problem, typical accelerator energy resolution and energy control is of the order of 0.1% or better, it is more critical to know accurately the electron density of the material to be traversed to reach this stopping point. This accuracy must be folded into the treatment planning process, the translation of CT numbers to electron density and the careful accounting for thickness of material traversed. The depth steps called for relate to the natural thickness of the Bragg peak and expected depth dimension of the voxels that would be used in the planning and delivery of treatment. As these range changes will occur many times during the treatment, this requirement constrains the time allowed to effect range changes, be they by changing the energy of the accelerator or by inserting energy degrading material in the beam.

Field size is related to the largest dimension one wishes to treat at one time. For example, an esophagus field may require a rectangular band with 40 cm extent along one axis. It is unlikely that whole-body irradiations will be performed with proton beams, so the full 40 cm × 40 cm field would not be used at one time. Nonetheless, the call for this maximum field extent sets the size of instrumentation, collimators, and beam spreading system. Typically, such large fields will be obtained by placing the patient further away from the point of origin of the spreading system, allowing more drift for the beam. This is easily obtained in a fixed-beam port, but not so in a gantry, thus the smaller field specification for the gantry port, in an attempt to contain the size and cost of the gantry. The 3-meter SAD also relates to the gantry size, lower numbers can lead to shorter beam delivery systems, or "nozzles" as they are sometimes referred to, but will increase the skin dose. As there is not the same skin sparing with protons that one encounters with high-energy photons, this could be a serious consideration in treatment planning. The goal of minimizing gantry size and preserving large SADs can be achieved by integrating the beam spreading into the magnetic deflection system of the gantry, in the manner being implemented at the PSI proton

therapy facility (cf. Chapter 23). This integration process, however, is extremely complex, both in magnet systems for the gantry as well as in achieving desired control over field size, shape and dosimetry. One should note another aspect of the PSI implementation: field spreading is performed in only one transverse direction, patient translation is used to provide the other coordinate. This "line scanning" concept was not endorsed by the UCSF/MGH clinicians, who felt it important that the whole treatment field be illuminated without moving the patient.

Sharpness of the placement of stopping beam particles is limited by certain physical effects associated with the interactions of particles as they slow down in tissue, namely the small-angle collisions between these particles and the electrons and nuclei in the tissue. These effects, multiple Coulomb scattering and range straggling, are well-understood, and can be folded into treatment planning programs. The specifications on sharpness relate then to additional spoiling of beam quality that may result from beam spreading techniques upstream of the patient. Specifically, the introduction of energy spread in the beam, due to a poorly compensated compound scattering system, or even the presence of excessive scattering material close to the patient or the patient collimator will introduce emittance growth in the beam that will lead to loss of sharpness in the stopping region of the beam. However, as these emittance growth mechanisms add in quadrature to the normal multiple scattering and range straggling phenomena, some lattitude is allowed in delivery system design; but this will be dependent on each particular field geometry.

Dose Deposition and Dosimetry

The desire of the clinicians is to complete a treatment in the shortest possible time, commensurate with accuracy and safety. Typical times for treatment should be less than two minutes for most fields, which will probably be treated to a dose of around 2 Gy. The 25 cm × 25 cm field specified in Table 2 represents a mean field size, defining a typical particle density, or dose rate. The depth in this specification is important, as placing particles in a shallower field leads to a higher rate of energy deposition. These factors together translate into the required beam current from the accelerator.

Table 2. Dose and dose rate requirements

Parameter	Desired Specification
Average dose rate	1 Gy/min for a 25 cm × 25 cm field at a depth of 32 g/cm^2
Time structure of the beam	suitable for beam scanning
Dose compliance	± 2.5% for each volume element in the entire treatment field
Dose accuracy	± 2%
Dosimetry reproducibility	day-to-day: ± 1.5% week: ± 3.0%

The clinicians recognized that an active scanning system will ultimately provide the best control over the treatment field, shape, and quality. The time structure requirement places great constraints on the accelerator parameters and performance, as will be shown below. The basic requirement is that the ability to scan the beam across the treatment field is not restricted or constrained because of beam time structure. For instance, if the accelerator produces very short pulses with a very low duty factor (e.g., a few milliseconds of beam at a 10 Hz rate) one will not be able to sweep the beam continuously across the field unless the sweep rate is very slow, less than a few beam widths per second. This would produce unacceptably long treatment times, and so precludes using a scanning system for this type of accelerator. For accelerators which deliver long duty factor beams, the critical element is the control over the intensity of the beam at all times during the time the beam is coming to the treatment room. If there are irregular spikes in the beam, these can lead to field inhomogeneities and lack of dose deposition control.

Clinical dose-response data indicate that 5% changes in dose represent about the smallest increment for which a clinical effect can be detected. This was used to establish the tolerance allowed on dose delivery and measurement in the treatment field, or the dose compliance to that specified in the treatment plan. For the simplest passive beam delivery systems this specifies the

requirement on the field uniformity, for more advanced systems, in which one may wish to tailor the actual dose delivered to each voxel of the treatment field, it specifies the control required over beam delivery to each coordinate, and the ability to measure this dose accurately.

The dose accuracy specification relates to the required precision of the calibration procedures and measurements themselves, as well as to the linearity and stability of the dosimetry system employed. The dose detected by an ionization chamber in the nozzle upstream of the patient will be different from what actually is delivered to the relevant voxel in the patient, owing to different energy and particle density profiles at the two locations. One must rely on calibrations, then, or calculational models based on empirical measurements of ratios of response of the ion chambers or other dosimeters in the nozzle with a standard dosimeter placed in a phantom configured to match the actual voxel under treatment.

Experience has shown that in a typical charged particle treatment beam line employing many redundant channels for dose measurement, there will be a daily variation observed in the ratios of all the different channels. These variations arise from many sources: slight irregularities in beam tuning, electronic drifts, slight positional errors in placement of instrumentation, environmental variations (temperature, pressure). The tolerances specified have been shown to provide an acceptable excursion in the measured ratios that do not contribute to a measurable loss of accuracy in clinical parameters.

Controls, Safety, Availability

The control system is a critical part of the treatment facility (see Chapter 27 for details). It must ensure that the beam line instrumentation, beam shaping devices and positions are all those specified in the patient prescription. It must control all parameters of the treatment: scanning magnet currents, collimator settings, range adjustments, accelerator settings, beam currents, and assure compliance of these parameters with requested values at all times. It must collect all the data generated by the dosimeters during the treatment and verify that ratios of all measurements are within acceptable limits. It must control the termination of the irradiation, either normal termination when desired dose values have been reached, or rapid termination in the event of the detection of a parameter that is out of range. It must also be able to resume the treatment from the point it was prematurely terminated once the problem has been corrected, and deliver the remaining dose to the prescribed accuracy. It must provide archiving services, to keep a record of all parameters associated with each treatment.

Many man-years of effort have been required to generate control systems for existing research facilities, but the quality control requirements for hospital-based clinical facilities will add significant time and effort to new control system development. The costs for the control system will be a very large fraction of the total technical system costs, much more than what one would encounter in a normal accelerator facility.

Added costs as well accrue from the requirement for 95% overall system availability. Although high for a research establishment, in which flexibility of configuration and always pushing the performance limits seems to be the norm, this level of reliability can be, and has been achieved where required. Both the Harvard Cyclotron and the LBL 184-inch synchrocyclotron, when used as dedicated clinical accelerators, had availability statistics at least as good as the required 95%.

Facility Requirements

Early work with charged particle beams has all been done with static, mostly horizontal beam lines. This has generally required the patient to be treated in a seated position, or in awkward recumbent orientations. Although the seated position does allow for "isocentric" delivery by rotating the patient around the beam axis, immobilization and patient comfort are more difficult. In addition, the very important requirement of coordinating the patient orientation with the diagnostic images on which the treatment planning is based, indicates that a supine treatment position is highly preferred. This means that the

beam must be brought around the patient, in the form it is done for conventional megavoltage treatments. Much of the cost and technological challenge in bringing ion beam treatments into the realm of practicality have revolved around the development of effective, inexpensive and practical gantry systems. (cf. Chapter 23). It should be noted that the UCSF/MGH team recognized the value of static horizontal ports for specialized applications, namely ocular treatments, and very large fields that could not easily be obtained with a gantry system.

Support areas required in a facility designed to handle many patients include systems for ensuring smooth patient flow, maximizing the throughput in the treatment rooms, ensuring positional accuracy of the patients and providing for storage of patient-related hardware such as collimators, compensators and immobilization devices. All of these factors require careful planning and study, and inevitably much space. Noteworthy on the alignment accuracy issue, is the HIMAC facility in Japan, in which a CT scanner has been installed in each treatment room in such a way that the patient can be scanned, then translated accurately to the treatment position, with the coordinates determined from the scan being transferred to the delivery system controller.

The biggest problem in establishing shielding requirements has turned out not to be the attenuation of neutrons and other radiations, but that of compliance with moving regulations. As the field is still very young, standards for allowed high-energy neutron fluxes in a hospital environment are still being adjusted. This has led to overly conservative specifications for shielding at facilities like Loma Linda, and added significantly to the costs in concrete and floor space. Hopefully, this situation should become more stable in the coming years.

Performance Specifications

Beam delivery systems are covered extensively in a subsequent chapter, so it suffices to state here that accelerator performance must be matched to those delivery systems most suitable for placing stopping particles in an arbitrarily-shaped three-dimensional volume. The best candidates are the raster scanner employing a small beam spot and tight control over the scanner sweep velocity and beam current, and the voxel scanning system which places a planned dose at each coordinate in the field. Suitable also, but not to the same degree, although presenting significantly fewer technical challenges, is range-stacking with a passive scattering system and a multileaf collimator. The performance specifications discussed below are matched to the needs of these three delivery systems. The discussion will be kept general, to include accelerators suitable for both protons and heavier ions, and, although problems with particular accelerator technologies will be mentioned, particular judgments as to the suitability of accelerator types will be kept to a minimum.

Beam Energy

To achieve a range of 32 g/cm^2 in tissue, a beam of approximately 225 MeV protons, 430 MeV/u carbon or 610 MeV/u neon is required. The maximum energy of the beam from the accelerator should, however, allow for energy loss in material placed in front of the patient, to include scattering systems, dosimetry devices, range modulators, and compensators. The active scanning systems are less burdensome in this regard, but the scattering systems will introduce significant energy loss. The amount of material required for scattering depends on the scattering angle, which is closely related to the maximum field size and the SAD, and so to gantry dimensions. For most accelerator types, the top energy is relatively soft, the cost of adding a few more MeV is not that great, so specifying a comfortable energy margin, of approx. 10% over the required energy, is recommended. This translates into 250 MeV for protons. The maximum energy for a light ion machine is closely related to the heaviest ion that will be used in therapy, and whether there is a desire to push this particle to the maximum depth. As the normal tissue damage from plateau irradiation of heavier ions may be substantial, the heavier ions may be preferrable for shallower irradiations, thus requiring less energy. If neon is the heaviest ion to be contemplated for full-range

treatments, then a 670 MeV/u top energy would be satisfactory.

It could be noted that 250 MeV for protons can be conveniently reached with linacs, cyclotrons or synchrotrons. However, the high rigidity of ion beams, 8.7 T-m in our 670 MeV/u example, pretty much rules out cyclotrons as a viable accelerator technology for light ion therapy.

Energy changes take two forms: the establishment of the highest energy for each treatment corresponding to the deepest portion of the treatment port, and then the changes that are necessary to treat the shallower portions of the target volume. Adjustment of this energy can be performed in the treatment room itself; this has been the normal mode of operation for many years, and allows the transport of a fixed-energy beam to the treatment room. However, the use of large amounts of degrading material leads to degradation of beam quality and to a substantial neutron background in the treatment room. In fact, the clinical specifications quoted above are carefully given so they could not be met with a configuration in which the beam enters the treatment room at a significantly higher energy than what is required to reach the distal end of the treatment field. Either, then, the beam must be degraded in the transport line, and cleaned up with emittance and momentum selection systems (at a significant loss of intensity, and activation of material in the transport gallery), or the beam must be extracted from the accelerator at or close to the desired maximum energy. Tuning for the maximum energy can be done without much demand for haste, it must be ready after the patient has been installed and aligned in the treatment position. A minute or two is satisfactory for this set-up. However, once the treatment has started, the energy changes to treat the shallower voxels must be performed quickly, within a second or two at most. With a synchrotron this requires extracting the beam on subsequent pulses at different field settings (so-called pulse-to-pulse energy variation), for the cyclotron and linac, in which energy might be variable only in fairly large discrete steps, the degrading material must be switched quickly. In all cases the beam transport lines must track the new energy of the beam, a non-trivial requirement considering the large number of bends and focusing elements in the transport line, and the very large dynamic range required for the overall energy changes, and the precision required for beam stability at isocenter (see below). It should be noted, on this point, however, that synchrotrons with many discrete magnets do track very large energy gains of particles with high precision and speed; the same techniques of common excitation of families of magnets and very tight control will have to be applied to these transport lines.

The energy spread of the beam affects the distal fall-off of the treatment field, although this effect is for most accelerators insignificant compared to the range straggling suffered by the beam as it penetrates to its end-of-range point. Of greater importance is the aperture of the transport magnets: a poorly defined beam will require very large aperture magnets for efficient transport, adding weight and power costs to the transport and gantry systems. A typical accelerator will have an extracted beam of $\pm$ 0.1% energy spread. Placing this same specification on the momentum selection and clean-up system for the degrader used to tailor the beam from a fixed-energy accelerator will specify the width of the momentum selection slits, and hence the beam loss that will be experienced when this selection takes place. The accelerator must be capable of delivering the added beam current to ensure that the dose rate of the beam surviving the clean-up process is still within the specification for maximum treatment time. This could be very significant, for large energy changes as much as a factor of 100 to 1000.

The energy precision specification relates to the ability to match the required distal edge of the field. To meet the requirement of $\pm$ 0.1 g/cm^2 (Tab. 1) one should have a proton energy adjustable to $\pm$ 0.4 MeV, or about $\pm$ 0.2% of the maximum beam energy. With typical synchrotron systems this represents a flat-top field accuracy of around $\pm$ 5 Gauss (out of 10 to 15 kG), well within the state of normal practice.

Often times the absolute accuracy of the beam energy is difficult to obtain, however, this is not relevant in our case, as we only need to set the beam range to correspond to a given desired range. This number can be obtained by empirical measurements, translating a range value into a particular magnetic field value, so high-precision knowledge of the absolute beam energy is not important.

Lateral Beam Quality

As was the case with the energy spread, the typical emittance of beams coming directly from the accelerator is very small, and contributes little to the lateral penumbra experienced in the treatment field. The penumbra specification is affected primarily by the material the beam traverses in the nozzle, most particularly whatever material is within a meter or two of the patient. The beam emittance primarily affects the size and weight of the transport magnets and gantry systems. Typical beam emittance from an accelerator will be around 5 πmm mrad (unnormalized), producing beams that can be transported with dipole magnet gaps of less than 5 cm. Again, the goal of a degrading/clean-up system from a fixed-energy accelerator should be to produce beams presented to the gantry transport system with emittances close to this value. In the absense of any tissue that would increase the beam size, the smallest beam spot (for protons) that can be obtained at isocenter is around 1 cm FWHM. Beam emittance contributes somewhat to this, because of the large distance from the last focusing magnet to isocenter, but the main contribution to beam size is the material the beam penetrates, even in the cleanest scanning system: vacuum windows, ion chambers, and air.

The accuracy of a treatment system, particularly one in which a small beam spot is swept across the treatment field, is strongly dependent on the positional stability of the beam spot. If the spot has motion at isocenter, because of improper extraction tuning or system noise or ripple, the precision required for the treatment to define the field boundary, and more particularly, to ensure conformity of the dose to the prescription inside the field, will suffer. This problem can be particularly difficult to control considering the very long moment arm between the last magnetic element and isocenter, maybe as much as 3 m or more. Acceptable motion of the beam spot at isocenter is ± 1 mm (about 10 % of the best beam size), and an angular variation of ± 1 mrad. This places great stress on the stability of the magnet elements, and on excellent control over the extraction process from the accelerator. Synchrotron extraction, in particular, can be prone to beam sweeping, and pulse-to-pulse variations. Great care must be taken in the design process to control these effects. The stability requirement at isocenter also constrains the design of the beam transport systems to be as insensitive as possible to beam motion or fluctuations.

Beam Intensity and Time Structure

The beam current must be adequate to meet the specification for maximum dose rate of 1 Gy/min for a 25 cm × 25 cm field at a depth of 32 g/cm^2. This dose rate corresponds to approximately 10^{12} protons per minute actually stopping within the treatment field. One must fold into this the efficiencies of the system, i.e., beam lost in the transport system, and more importantly beam lost in the beam spreading system. For a well-designed scattering system, efficiencies of approx. 20 % are encountered. These factors translate into a requirement for a proton current of the order of 10^{11} protons per second from the accelerator. This number is then carried back to specify the performance of the injector and ion source, folding in repetition rate, as well as transfer and acceleration efficiencies. One would think that a scanning system would require less beam owing to higher efficiencies of utilization. In practice, it is difficult to achieve a higher overall efficiency, or stated differently a shorter treatment time for the same beam current. The reason is that the scanning systems often place greater constraints on the rate of use of the particles, by either switching the beam on and off to move between voxels, or by adjusting the rate of spill to correspond to sweep speeds. The result is that not all the particles available are used in the treatment. This situation is still more desirable than the scattering system, as in the scattering system the beam is actually lost in material close to the patient, specifically the scattering foils and collimators, producing background radiation and an additional body-burden to the patient. The specification of 10^{11} protons per second (≈ 15 nA) can be met by any of the accelerator technologies: linacs typically produce beam currents far in excess of this number, cyclotrons now produce currents in the hundreds of microamperes, while synchrotrons can

reach this intensity figure, producing beams of the requisite characteristics provided care is taken in the design and optimization of accelerator parameters.

Duty factor refers to the fraction of time the beam is on. This can be divided into two basic regimes: macroscopic and microscopic. The dividing line between "micro" and "macro" occurs somewhere between the millisecond and microsecond time scale, so megahertz and higher frequencies are typically considered "microstructure", while lower frequencies will be "macrostructure". The macroscopic nature of the beam can be either CW ("continuous wave" or 100% duty factor), or pulsed. Cyclotron – at least isochronous cyclotron – beams are typically CW, synchrotrons with slow extraction systems produce beams with typically 25% duty factor and spills of a few hundred milliseconds to a second or two. Conventional (room temperature) linacs are typically very short duty factor machines, beam pulses last around a millisecond, with repetition rates of a few hertz to a few tens of hertz. These linacs are generally optimized for injection into synchrotrons, where very short pulses at low repetition rates are desired. High duty factor linacs have been built, but are very expensive because of the high-power RF systems needed to produce the field gradients necessary for efficient acceleration, this power requirement is largely wasted for the very small beams needed for therapy. Superconducting linacs would be a better match, but this technology, particularly for protons or ions is expensive and furthermore is far from mature at this point.

The importance of macroscopic duty factor is in the matching of the accelerator with the beam delivery system to be used, particularly in active delivery systems. Passive systems do not sweep the beam across the treatment field, so time structure in the beam is relatively unimportant, except to assure accuracy in cut-off when the desired dose is reached. If the sweep rate of the scanning system is matched to the length of the beam pulse, then a straightforward relationship will exist allowing a painting of the field once per beam spill. A good match exists with the synchrotron spill length of a few hundred milliseconds and scanning rates for magnet systems of conservative design. CW beams place no constraint on the delivery system; beam is simply switched off and on according to the needs of the scanner. Very low duty factor machines interface very poorly with a scanning system, sweep rates cannot match a millisecond pulse, so a short-pulse machine would have to work with a voxel scanner with one or several pulses to be delivered for each voxel. The issue will then be one of control of the number of particles in each pulse to achieve the required level of dose accuracy per voxel. This is not easy for this type of machine, but a practical system could be designed if the pulse repetition rate were at least 100 Hz to 1 kHz. Again, because of the requirement to fill large structures with RF power, rapid repetition rates are difficult to achieve in this type of linac.

Another concern with very short-pulse machines is the high instantaneous dose rate which can lead to saturation of the dose monitoring ion chambers. The critical time constant for these chambers is around a millisecond (the clearing time of ions produced in the gas), if this dose rate exceeds 20 Gy/s integrated over a millisecond [3], ion recombination, hence chamber nonlinearity will result. Unless the beam is made very large, as for a scattering system, beam currents will have to be kept very low to prevent this nonlinearity, extending the treatment times well beyond the specified requirement.

Microscopic beam structure is completely unavoidable for any accelerator extracting beam without turning off the RF. The only machines for which this would be possible is the synchrotron, but often even here the RF is left on to provide greater control over the beam during the resonant extraction process. The RF-structure ranges from nanoseconds for linacs to tens of nanoseconds for cyclotrons to microseconds for synchrotrons, with pulse trains typically filling only 10% of the time. The question one must ask is whether this time structure is important for the treatment. From the biological standpoint effects attributable to accelerator RF-structure have not been reported, but it is not clear that this specific question has really been addressed with adequate experiments. On the physical side, the question to ask is whether this structure will affect the uniformity of a scanned field. One only needs to look at the time

between pulses, the distance the beam is swept by the scanning system in this time, and the size of the spot being swept to see that this will not be a problem. Fastest sweep rates may approach 1000 cm/s, or 1 cm in a millisecond. If the beam structure is 1 MHz, about 1000 pulses will strike the target while the beam moves one beam width. Similarly, ion chamber saturation is not an issue as long as the integrated current (in one millisecond) is below the critical density.

Beam Control and Safety Aspects

Control of the beam current is critical to ensure the specified dose compliance. In the most straightforward case, the scattering system, the beam is typically delivered at a high dose rate until 90% of the desired dose is delivered, then the beam current is reduced to allow for accurate topping off of the dose and a clean cut-off of the beam. Dose rate control to the 10% level is adequate, as long as reliable attenuation of the beam is achievable and an absolute cut-off of the beam can take place in a few milliseconds. The situation is more demanding for interfacing with scanning systems. For a raster scanner sweeping at 1000 cm/s, accurate response is needed with a bandwidth of at least 1 kHz to control the dose delivered to each coordinate along the sweep path. By sweeping over the field several times, and again topping off at a lower dose rate, better accuracies can also be achieved. Most important in this process is having good, fast and accurate, dosimetry to be able to assess the dose accumulated at each coordinate, so as to calculate the correction doses to be given in the final passes. Within each sweep, a dynamic range of at least a factor of 10 in instantaneous current is required, with a tracking accuracy of at least 10%, to assure proper dose compliance. Voxel scanning requires the ability to modulate the beam on and off very rapidly, perhaps as high as at a megahertz rate, to correspond to filling each voxel to the required level.

Very fast on-off control is best performed with kickers in the transport line, and does not rely on accelerator response, although most accelerators can easily turn beam off in a millisecond. Linear control of the instantaneous beam current is quite difficult with short-pulse linacs, but can be done in a relatively easy fashion with feedback systems for both cyclotrons and synchrotrons. In the cyclotron, beam current modulation is obtained either by direct control of the ion source, although this is more difficult than the other option: optics manipulations in an axial injection line, such as variable transmission through an iris via a rapidly varying focusing or deflecting element. This scheme requires an axial injection line instead of an internal ion source, but such an arrangement has many advantages in any case. Linear control for the synchrotron is best obtained by modulating the resonant extraction system parameters, although this is a very sensitive and difficult exercise to perform properly and maintain the desired control over the beam.

To achieve the level of conformation of the dose to the prescribed values at each coordinate in the treatment field, we must have extremely good control over the dose deposition rate at all times. Particularly in a scanning system, where the exercise of treating to a prescribed dose is repeated for each coordinate, the presence of uncontrolled beam spikes can be extremely bothersome. Such spikes can come from ion source bursts in cyclotron or linac systems, or from any area where the beam is being throttled back, and where a small parameter change can cause a sudden increase in beam current. Most difficult to control, however, is the structure that accompanies resonant extraction in synchrotrons. Beam being accelerated in the synchrotron is in inherently stable orbits, but to extract the beam, a resonance is excited to render these orbits unstable and allow growth in oscillations that will lead to the beam spilling out through the exit channel. Because this process is basically introducing an instability, and attempting to control the growth of this instability to control the rate of particles flowing out from the synchrotron, it is inherently difficult to control. Any small amount of noise, for example ripple on the magnet power supply, will cause beam to emerge in an uncontrolled fashion bearing the frequency of this noise. Achieving damped feedback response is very difficult. In spite of all this, the problem is not insurmountable, provided proper care is

taken in designing the synchrotron and its extraction system. Quiet and controlled spills have been obtained from modern synchrotrons.

The level of control needed can be estimated from the dose compliance requirement, and the characteristics of the delivery system. Again, for a scattering system, where the whole field is being irradiated at once, beam spikes are less of a problem. A spike that has duration shorter than the system cut-off time must have less than 2% of the total for the whole field. For scanning systems the constraints are much more severe. If there are 10^4 separate volume elements in the target volume, and a dose compliance of 2% must be achieved for each element, then a spike cannot contain more than 2% of the dose for that element, or 2×10^{-6} of the total dose. If the total treatment contains about 10^{12} protons, then each spike must contain less than 10^6 protons. From the standpoint of measuring current spikes, this is a very small amount of charge.

System safety requires the ability to rapidly cut off the beam, either to effect normal termination of the treatment, or to respond to an emergency or detected system abnormality. Following the analysis developed above, cut-off for a scattering system that occurs in a few milliseconds will ensure adequate patient safety, with little chance of patient overdose. For scanning systems, the desired cut-off time is less than 10 microseconds, to account for a sudden spike at a rate approximately 100 times the normal rate at a voxel. This type of cut-off can be effected with a fast kicker in the transport line to divert the beam away from the transport channel, to be followed by clamping of the beam through shut-off of the extraction system, cutting magnet power to a transport magnet, or shutting off the ion source. All these will shut beam off in about 1 to 10 milliseconds, thus determining the required length of the pulse to the fast kicker. For the scattering system, the kicker would not be required to ensure proper safety.

Summary

Design criteria for accelerators for proton or ion therapy are driven first of all by the clinical requirements for the treatment fields to be employed, and then more directly by the technology that is employed to obtain these fields namely the beam delivery system employed. The basic principle is to best apply the dose localization characteristics of the charged particles, so one would want to adopt a beam delivery system that allows placement of stopping particles in an arbitrarily shaped three-dimensional volume, a volume that corresponds to the most desirable target as defined by the clinician. This type of field profile can be achieved with a properly designed passive system, or by different scanning techniques.

Scanning systems place very severe demands on the accelerator performance. Very fast response times for feedback systems with large dynamic ranges are needed to control beam current, and great care must be given to safety considerations to detect and shut off beam in the event of a system irregularity.

Developments have not progressed to the point where clinicians or physicists can feel completely comfortable in directly applying scanning technology in a hospital setting. In the opinion of the author, the best approach to adopt today is to specify an accelerator system which will begin its career treating with a scattering system, but which will be adaptable to a scanning system when this technology has progressed to a suitable level of maturity.

References

1 National Institutes of Health, National Cancer Institute Grants R01 CA 56931, M. Goitein, Principal Investigator, and R01 CA 56932, J. Alonso Principal Investigator.

2 Gall, K.P., Verhey, L., Alonso, J., Castro, J., Collier, J.M., Chu, W., Daftari, I., Goitein, M., Kubo, H., Ludewigt, B., Munzenrider, J., Petti, P., Renner, T., Rosenthal, S., Smith, A., Staples, J., Suit, H., and Thornton, A. State of the art? New proton medical facilities for the Massachusetts General Hospital and the University of California Davis Medical Center. Nucl. Instr. Meth. Phys. Res. B79, 881–884, 1993.

3 Chu, W.T., Renner, T., and Ludewigt, B.A. Instrumentation for treatment of cancer using proton and light-ion beams. Rev. Sci. Instr. 64, 2055–2122, 1993.

20 Pros and Cons of Various Accelerator Types

P. MANDRILLON

Laboratoire du Cyclotron, Centre Antoine Lacassagne, Nice, France

Introduction

Improving the quality of radiation therapy by using new irradiation technologies is one of the radiotherapist's constant concerns. The use of accelerators for delivering protons, heavier ions and secondary beams as neutrons brings further improvement in dose distribution and in interesting biological properties.

Accelerators have been present in this field since the early history of radiotherapy and they could play a major role in the future as part of hospital-based facilities with specific beam transport and beam delivery systems. Modern accelerator technology exists today to meet all of the clinical requirements within a reasonable budget. Various types of dedicated accelerators are planned or already under construction, but it is worth mentioning that the physician is not only concerned with the choice of an accelerator in the medium energy range but wants a system which yields the best conformation therapy and a minimum of dose in non-target tissues. These aspects are closely related when designing the "equipment" for an ion beam treatment facility.

Medical Requirements

The choice of the accelerator for ion beam therapy is strongly dependent on the medical requirements which could be summarized as follows:

1. The treatment unit should be installed in a large hospital in order to make the benefits of ion beam therapy available to a large number of cancer patients and to provide the medical and scientific staff for high level diagnosis and treatment.
2. The accelerator has to be highly reliable, easy to operate and eventual repair time should be short.
3. The beam delivery system should permit scanning of the beam.
4. Irradiation should be possible from any angle, e.g., by a rotating isocentric gantry.
5. Ion ranges from a minimum of 3 cm to a maximum of approx. 30 cm are required (this specification fixes the energy range).
6. A dose rate of 5 Gray/minute in a 2 liter volume is necessary which fixes the necessary intensity (Tab. 1) of the accelerator.
7. Irradiation of 30×30 cm^2 maximum field size.

The magnetic rigidity listed in Table 1 fixes the bending radius of the particles which determines the size of the accelerator and the beam delivery system.

Table 1. Energy, magnetic rigidity and required intensity for various ions ranging 20 cm in tissue and giving a dose rate of 2.5 Gy min^{-1}

Ion	Energy MeV/u	Magnetic rigidity Tm	Intensity required pps
p	175	2.00	2×10^{10}
He	175	4.00	5×10^{9}
C	330	5.67	10^{9}
O	400	6.34	7×10^{8}
Ne	470	6.98	5×10^{8}

From the energy required and the intensity needed, it is quite clear that proton machines and light ion machines will differ in size and cost. Three kinds of accelerators – cyclotron, linac and synchrotron – seem feasible for proton therapy, whereas for light ion therapy the cyclotron is close to the limit for carbon already and the synchrotron is considered the better choice for heavier particles. Each of these accelerator types has its advantages and disadvantages for therapy, but the beam delivery systems make the deficits particularly obvious.

The beam delivery system warrants that the tumor is irradiated in three dimensions. To achieve this task it requires the following features:

- lateral deflection of the beam
- variable range
- variable exposure time to achieve uniform radiation doses
- position-sensitive monitors
- rapid switch-off in case of malfunction

A number of factors affect the choice of the beam delivery system, including the time structure, the extracted beam emittances and energy dispersion of the output beam.

Characteristics of the Various Accelerator Types

Cyclotrons

Since its early history in Berkeley the cyclotron has been used for medical purposes. For several aspects, including simple design and operation, compactness and high ion intensities, cyclotrons are good candidates.

Fixed energy makes the design simple. The magnet can be optimized and trimming coils are not necessary. The accelerator operates at a fixed radiofrequency and all the settings of the beam lines are predetermined. No sophisticated controls are needed. A simple programmable logic controller (PLC) is sufficient. Operation is easy and this, in turn, reduces the manpower costs.

The dimensions of a cyclotron can be reduced by choosing a high magnetic field. But this has two important consequences: negatively charged ions cannot be accelerated due to electromagnetic stripping but superconducting magnets which have only about half the weight of room temperature magnets can be considered.

An isochronous cyclotron provides a continuous beam (CW) with ample intensity. This is a key factor for reliability. The beam intensity is easily controlled and the beam can be very stable – an important advantage for a dynamic beam spreading system. To fully benefit from these advantages, an external injection system should complement the cyclotron for flexibility. The MEDICYC cyclotron [1] in Nice, e.g., has an axial injection at 33 kV and uses a few volts on the bunching cavity as feedback control of the extracted beam intensity. With this approach, a beam stability better than 1% has been achieved (Fig. 1).

Acceleration of the particles in the cyclotron takes only 10–20 μs. By acting on the injection process, the beam can rapidly be turned on and off. It is also possible to set up a dynamic control of the beam intensity with a fast ionization chamber in the extracted beam as reference. This way, the beam can be stabilized at any required level

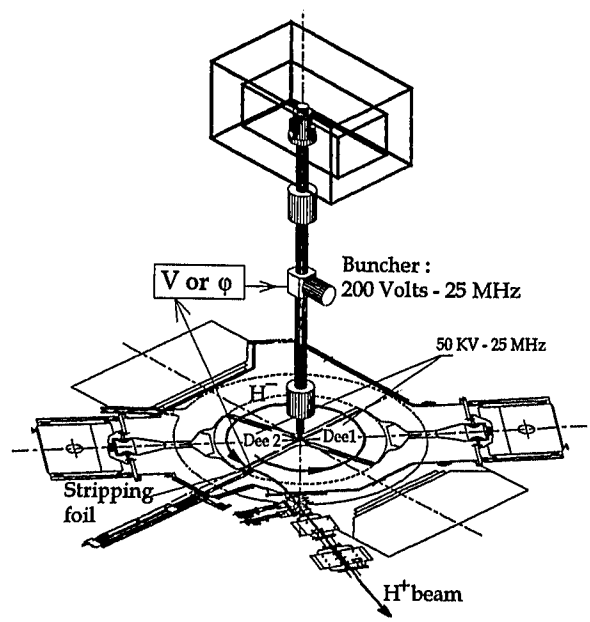

Fig. 1. MEDICYC intensity fine adjustment φ and control (V)

with response times of less than 100 μs. This process can be fully automatic. A separate safety circuit has to ensure that misoperation of this servomechanism does not overdose the patient. In case of failure, the beam of such a system can be turned off in less than 100 μs.

The lateral deflection of the beam for irradiating large fields can be obtained either by passive scattering using contoured scatterers [2] or by active methods using a magnetic field to deflect the beam. The passive method is safe and simple, but demands higher ion energies to compensate for the range losses in the scatterer.

At the PSI, a discrete (spot or pixel) scanning technique [3], has been developed (see also Chapter 35). It uses a pencil beam which deposits individual dose spots and is shifted stepwise by a kicker magnet located within the gantry.

Recently, Farley [4] has proposed a simple method for dynamic beam spreading, which should be easy to implement with a cyclotron (cf. Fig. 2). It requires

- an upstream modulator for scanning in range at 50 Hz to spread the beam to a Gaussian spot
- a magnet which scans the spot linearly along a line perpendicular to the axis at a low frequency (typically 1Hz, i.e., only low power is needed in the magnet, which can have a small gap because the deflection is only in one plane),
- a motor-driven transport system which moves the patient steadily at 5 mm/sec (patient collimator and bolus move with the patient, too)

This system is said to produce a continuous scan, called a raster scan, with uniform intensity.

Synchrotrons

A synchrotron produces pulsed beams and the energy of the extracted beam can be varied from one cycle to the next in steps of a few MeV. Hence, modulating the Bragg peak to scan a target in depth can be achieved without absorbers, avoiding scattering and momentum spread degradation of the beam.

The weight of the different magnets (dipoles, quadrupoles) is low. This makes the transport and assembly easy and reduces the statical conditions for the building.

The required intensities can be achieved, if the synchrotron is fed by an adequate injector. Losses might occur when using the traditional resonant extraction system, because small perturbations from variations in the excitation of the magnets

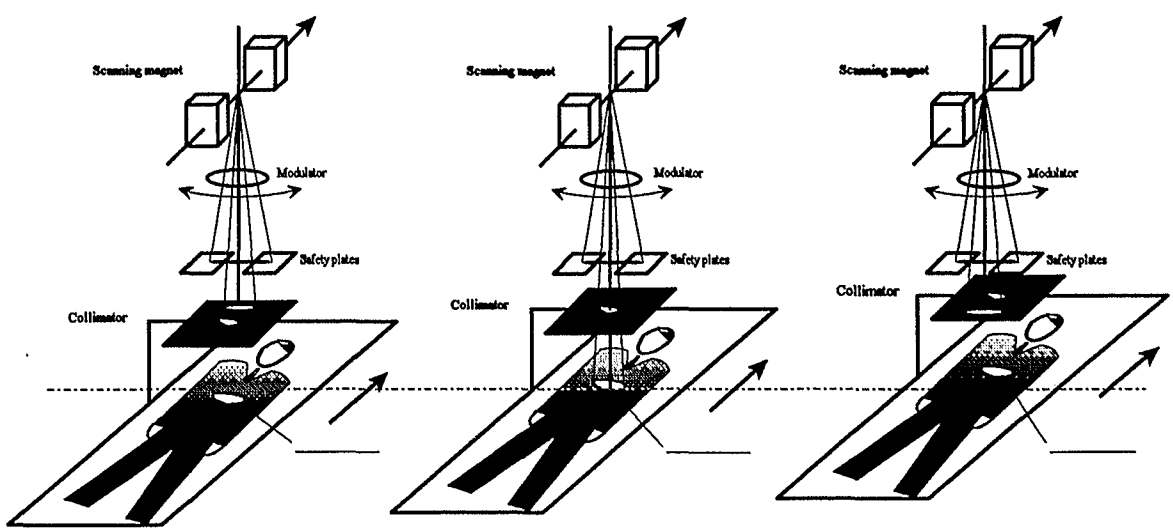

Fig. 2. A simple dynamic beam spreading mode (according to [4])

can induce time-modulations of the extracted beam intensity. An alternative is a non-resonant extraction as in H^- synchrotrons where charge-exchange extraction processes are used.

Synchrotrons request rapid magnetic field variations and operation is more complex than operating a cyclotron. Moreover, undesired intensity variations require careful control. Nevertheless, many sophisticated synchrotrons are running smoothly for high energy physics applications at a high reliability level.

The variable energy of a synchrotron is certainly a strong argument for this kind of accelerator, because it allows to irradiate tumors in discrete slices of equal range (cf. preceding chapter for more information). A synchrotron-supported scanning system can operate approx. twice as fast as a similar system connected to a CW accelerator (cyclotron). This requires, however, more power in the scanning magnets. The HITAG facility at GSI, Darmstadt, plans to use such a scanning system associated with the slowly extracted beam from their SIS-synchrotron (cf. Chapter 36 for more details).

Linear Accelerators (Linacs)

For proton therapy in the 200 MeV range, linacs are the third class of possible accelerators. Ambitious extrapolations from electron linac technology using a high frequency structure, have been proposed to shorten the length of the accelerator tube, thus reducing the costs for a hospital-based facility.

The output energy of a linac is usually fixed. But recently an interesting variable energy concept has been proposed which suggests to adjust the energy by switching on and off the power of short tank modules in the last section of the linac structure [5, 6]. Attractive as it seems, this novel design requires careful optimization of the structure and detailed calculations of transverse emittances.

Linacs can provide high ion intensities delivered in short beam pulses. This time structure has important consequences for the beam delivery system, in particular, for any dynamic beam spreading device. Discrete spot scanning, is well suited for a linac. In combination with a system which varies the output energy, even a three-dimensional spot scanning with pulse-to-pulse energy variation should be feasible.

Examples of Dedicated Designs

A Cyclotron with a Room Temperature Magnet

The Belgium industrial company Ion Beam Applications (cf. Chapter 22 for more details) has chosen a high field design (2.15 T on the extraction radius) produced by conventional coils (cf. Fig. 3 and Tab. 2). This cyclotron and the associated gantry will be installed in the coming years in the new proton therapy facility to be built at Massachusetts General Hospital in Boston (USA).

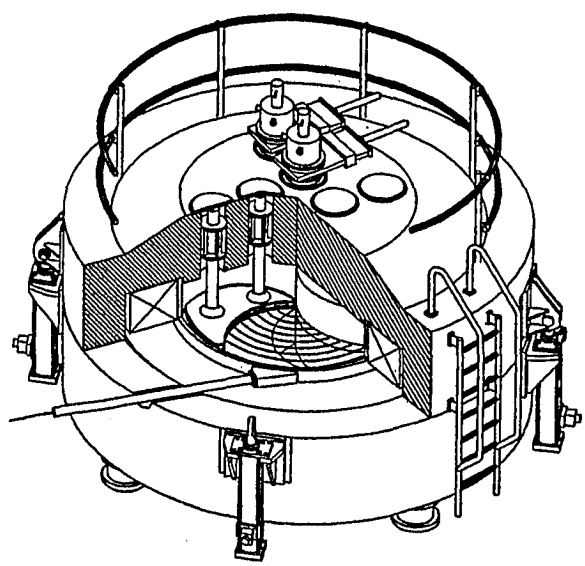

Fig. 3. IBA 235 MeV room temperature cyclotron

Table 2. Basic parameters of the IBA 235 MeV cyclotron

Magnet	
Number of sectors	4
Yoke external diameter	4.30 m
Current density in the coil	155 A/cm^2
Total weight	220 tons
Power	200 kW
RF	
Number of dees in opposite valleys	2
Frequency	107.17 MHz
Harmonic mode	4
Dee voltage injection	60 kV
Dee voltage extraction	130 kV
RF power	85 kW
Miscellaneous	
Injection	internal source

Compact Superconducting Cyclotron Designs

Figure 4 depicts a sketch of a compact superconducting sector-focused cyclotron for a continuous beam of 238 MeV protons. It has three spiral sectors with a supplementary groove along the center of each sector, making it more like a six-sector

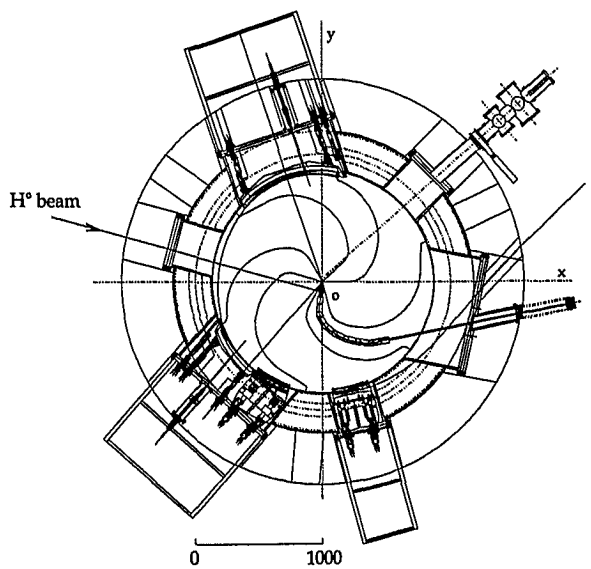

Fig. 4. The CAL/Siemens-238 MeV superconducting cyclotron

Table 3. Basic parameters of the CAL/Siemens-238 MeV superconducting cyclotron.

Magnet	
Number of sectors	3 resp. 6 ("pseudo sectors")
Yoke external diameter	3.10 m
Current density in superconducting coil	6 800 A/cm^2
Total weight	80 tons
Power including refrigerator	35 kW
RF	
Number of dees (galvanically connected)	3
Frequency	110 MHz
Harmonic mode	3
Dee voltage injection	80 kV
Dee voltage extraction	130 kV
RF power	120 kW
Miscellaneous	
Injection (2 options)	axial or radial (neutral beam + central stripper)

machine, avoiding the well known ν_r=3/2 resonance (this technique has been well established by AGOR, Groningen). Three RF cavities, galvanically connected in the central part, are operating on the third harmonic of the particle frequency. They provide a high energy gain per turn, completing the acceleration in about 400 turns. Table 3 summarizes the main characteristics of this design, jointly developed by Siemens and the Cyclotron Laboratory of CAL in Nice [7].

Blosser and associates [8] of Michigan State University (USA) have designed a 250 MeV four-sector compact superconducting cyclotron for proton therapy. Magnet hills and dees repeat with 90-degree spacing in this design and an internal ion source produces the protons.

A new 3-sector superconducting isochronous cyclotron is being designed by the LASA/Milan and the Cyclotron laboratory of CAL in Nice in the frame work of the TERA project [9].

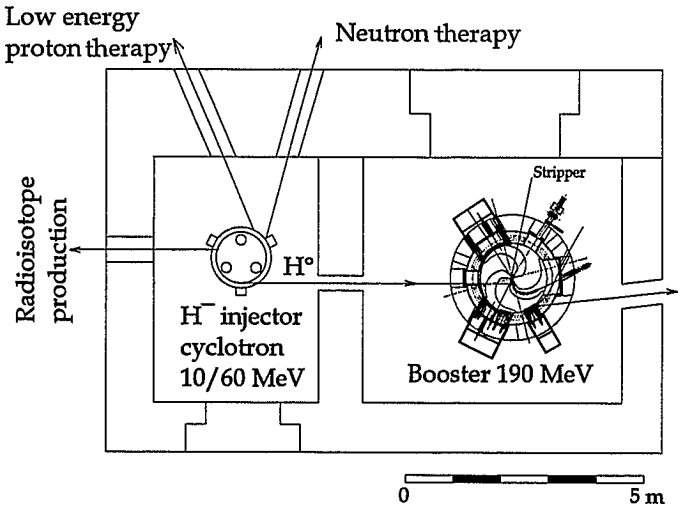

Fig. 5. Boosting an existing cyclotron

Booster Cyclotron

Several neutron therapy centers which apply their accelerators also for low energy proton therapy are examining the potential for boosting the proton energy to the 200 MeV range.

With minor modifications any cyclotron can accelerate negatively charged ions. From such a beam, it is easy to extract neutral particles by a thin stripper. This beam will have good optical properties, in particular, a small divergence, allowing transport over long distances and traversing the magnetic field of a compact superconducting accelerator. At the appropriate radius, the neutral beam penetrates a second stripping foil yielding singly charged protons [10]. An interesting feature is that all commercial cyclotrons for radioisotope production accelerate negatively charged ions. They could act as injector for such a booster (Fig. 5).

The Loma Linda Accelerator – An Outstanding Example

The first high energy proton accelerator built in a hospital environment is located at Loma Linda, California. It is a zero-gradient proton synchrotron yielding a variable energy beam from 70 MeV up to 250 MeV. It has eight 45-degree dipole magnets arranged to four straight sections providing space for injection, acceleration and extraction systems. The 30 keV proton beam from the duoplasmatron source is injected into a 2 MeV radiofrequency quadrupole (RFQ) operating at 425 MHz. Acceleration to 250 MeV is achieved via a simple ferrite-loaded RF cavity operating on the first harmonic. The beam is extracted from the synchrotron by using half-integral resonance. The cycle time is 2, 4 or 8 seconds and the extraction time is variable between 0.4 and 10 sec. The design intensity is 10^{11} protons/sec. This design is a result of a collaboration between the Loma Linda University Medical Center, the Fermi National Laboratory and the Science Applications International Corporation (SAIC) Company.

Compact Synchrotron

A very compact synchrotron [11] operating with pulsed high magnetic fields has recently been presented by the Budker Institute of Nuclear Physics in Novosibirsk (Russia). The main parameters are listed in Table 4. This design is one of three possible candidates for a compact accelerator studied by the TERA collaboration in Italy [12].

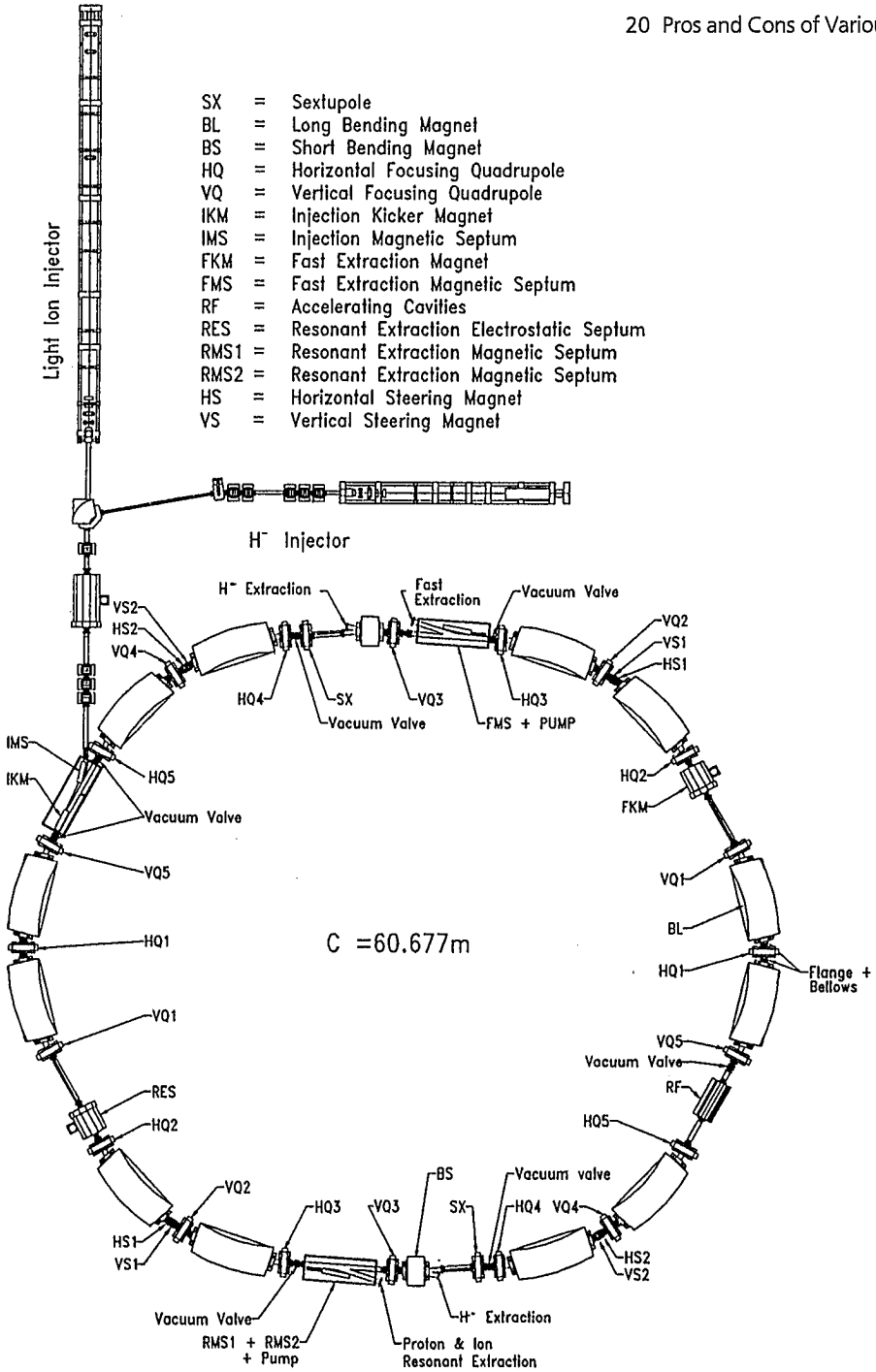

Fig. 6. Layout of the TERA synchrotron. From [12]

Table 4. Main parameters of a compact synchrotron designed by the Budker Institute of Nuclear Physics (INP), Novosibirsk, Russia

Circumference	6.4 m
Max. field in bending magnet	4.0 T
Energy range	80–200 MeV
Repetition rate at 200 MeV	1 Hz
Energy consumption	80 kW

Multi-Task Synchrotron

The TERA collaboration proposes also a multi-task synchrotron for its Hadron Therapy Center which should be able to provide: 250 MeV protons and light ion beams up to $^{16}O^{8+}$ with energies up to 400 MeV/u (Fig. 6). The concept which has been proposed by ITEP in Moscow [13] and Ron L. Martin of ACCTEK Assoc. in the United States (see also Chapter 22) considers the acceleration of H^- which simplifies the extraction, but requires a low magnetic field and a very good vacuum in order to avoid electromagnetic stripping of the H^--ions.

Ion Therapy Machines

The Heavy Ion Medical Accelerator (HIMAC) in Chiba, Japan, is the first hospital-based facility in the world to treat patients with heavy ions. Accelerator and facility are described in detail in Chapter 34. Only one remarkable feature should be mentioned. This is the fact that it has two synchrotron rings which can be used simultaneously or alternatingly with the same or with different ion types.

A synchrotron solution was also studied for EULIMA, a European initative for a light ion medical accelerator [14]. It is projected for pulsed beams with an average intensity of 10^9 particles/s and energies ranging from 100–400 MeV/nucleon. Two possibilities were investigated: a separate function machine (SFM) of 59 m circumference which offers more flexibility for developments, and a combined function machine (CFM) with a circumference of 48.6 m, if space is crucial. The maximum number of injected turns is 20, with an efficiency close to 50%. An injected intensity of about $2x10^9$ ions was proposed for both machines using an electron cyclotron resonance (ECR) ion source feeding a small RFQ linac, followed by a conventional linac (5 MeV/u) with a repetition rate of about 1 Hz. Table 5 displays the preliminary parameters of these designs. The layouts are depicted in Figure 7.

Table 5. Basic parameters of the EULIMA synchrotrons

	SFM	CFM
General layout :		
Circumference	59.08 m	48.64 m
Length of short straight sections	1.50 m	1.50 m
Length of long straight sections	4.00 m	3.20 m
Bending radius	4.53 m	5.24 m
Lattice:		
Q_h	1.67	1.66
$Q_v$max	1.76	1.80
$\beta_h$max	11.41 m	7.10 m
$\beta_v$max	10.97 m	9.44 m
D	5.40 m	3.16 m

New Linacs

Standing Wave Design

The use of a conventional S-band standing wave electron linac structure to accelerate low current protons up to 250 MeV for proton therapy was first suggested in 1991 by the California-based company AccSys Technology [5]. An updated design considering commercially available RF power tubes has recently been presented [6]. The low energy sections, consisting of a RFQ and a drift tube linac (DTL) operate at 357 MHz. The main DTL operates at 714 MHz. The 70 MeV beam from the DTL is injected into a series of conventional side-coupled linac (SCL) cavities operating at 2856 MHz. These 10 short tanks can be turned on and off to vary the proton beam energy between 70 and 250 MeV.

Crandall and Weiss [6] have recently proposed a compact linac structure consisting of a RFQ operated at 750 MHz, to accelerate a 80 keV pre-accelerated beam to 5 MeV, a coupled-cavity DTL operated at 3 GHz to reach 70 MeV and a

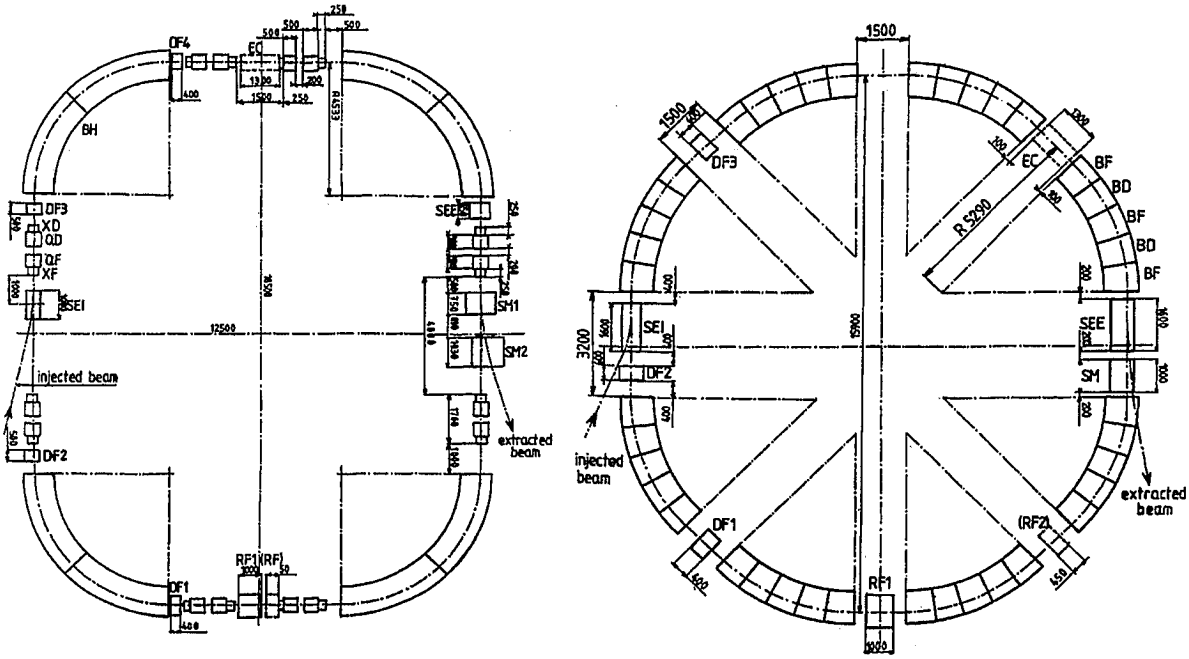

Fig. 7. General layout of the SFM (left) and CFM (right) EULIMA synchrotrons. From [14]

SCL operated at 3 GHz to reach the final 200 MeV.

Traveling Wave Design

Based on an electron linac structure using short wavelength (3 GHz instead of the traditional 200 MHz for a proton linac), a new geometry accelerating in traveling wave mode has been proposed by D. Tronc [15]. This mode removes the coupling cells and permits simultaneous acceleration and focusing. But the focusing problems need to be further investigated and the author suggests a test to confirm the results of the simulations.

Booster Linac

A classical linac structure has recently been proposed as a booster for the 62 MeV cyclotron of the Douglas Centre for Oncology, Clatterbridge, UK, permitting to implement a high energy proton therapy program at 200 MeV.

Conclusions

Designing a cost-effective accelerator which is easy to install in a hospital and simple to operate is a challenge to the accelerator community. An important factor to reduce the total cost of such a facility is certainly a small footprint of the accelerator, its associated switchyard and gantries. Compactness will, therefore, be one of the crucial demands for any new design, be it linac, cyclotron or synchrotron.

In the coming years new medical experience with high energy charged particles will be available, e.g., from two dedicated, hospital-based proton accelerators (the synchrotron in Loma Linda and a cyclotron at MGH) and the dedicated HIMAC facility in Japan. They will soon have treated a large number of patients and will gain experience with new technical developments. The work of these and other users will very likely yield new insights as to the pros and cons of synchrotrons and cyclotrons and will facilitate the task to tailor the next generation of medical accelerators.

References

1 Mandrillon, P., Farley, F., Brassart, N., Herault, J., Susini, A., and Ostojic, R. Commissioning and implementation of the MEDICYC cyclotron programme, in Proc. 12th Int. Conf. on Cyclotrons and their Applications, Berlin, May, 1989, pp. 156–159.

2 Gottschalk, B. and Wagner, M.S. Contoured scatterer for proton dose flattening. Harvard Cyclotron Laboratory, Internal Report 3/29/89, 1989.

3 Pedroni, E., Bacher, R., Blattmann, H., Boehringer, T., Coray, A., Egger, E., Phillips, M., and Scheib, S. The 200 MeV proton therapy project at PSI: A status report, in Proc. Int. Heavy Particle Therapy Workshop, Blattmann, H. (ed.), PSI-Report 69, pp. 1–8.

4 Farley, F. Supertwist gantry and dynamic beam spreading. Presented at PTCOG XIX, October 31–November 2, 1993, Cambridge, USA.

5 Hamm, R.W., Crandall K.R., and Potter, J.M. Preliminary design of a dedicated proton therapy linac, in Proc. of the IEEE Particle Accel. Conf. San Francisco, May 6–9, 1991, pp. 2583–2585.

6 Crandall, K. and Weiss, M. Preliminary design of a compact Linac for TERA, July 1994, TERA Internal note.

7 Mandrillon, P., Farley, F., Fiétier, N., Tang, J.Y., Anton, F., and Savoy, R. A compact facility for high-energy proton therapy based on a superconducting cyclotron, in Proc. of EPAC 94, June 27–July 1, 1994, Suller, V. and Petit-Jean-Genaz, Ch. (eds.), London, World Scientific, Singapore, pp. 2604–2606.

8 Blosser, H.G. Proposal for manufacturing a prototype superconducting cyclotron for advanced cancer therapy. NSCL-MSU, February 1993.

9 Acerbi, E., Alessandria, F., Bellomo, G., Birattari, C., Castiglioni, M., De Martinis, C., Fiétier, N., Giove, D., Mandrillon, P., and Sorbi, M., Preliminary results on the superconducting cyclotron, Internal Report TERA 94/36 ACC 21, October 1994.

10 Mandrillon, P. and Farley, F. Cyclotrons as booster for high energy proton therapy. To be published.

11 Averbukh, I., Bayanov, B., Below, V., Chernyakin, A., Jull, I., Karasyuk, V., Marusov, V., Palchikov, V., Ruvinsky, S., Silvestrov, G., Sokolova, S., Vecheslavova, G., Volokhov, V., Vsevolozhskaya, T., and Willewald, G. Status of compact proton therapy facility project. Presented at EPAC 94, London, June 27–July 1, 1994.

12 Amaldi, U. and Silari, M. (eds.) The TERA project and the Center for Oncological Hadrontherapy. INFN-LNF-SIS Ufficio Pubblicazioni, Frascati, Italy,1994.

13 Khoroshkov, V.S., Onosovsky, K.K., Breev, V.M., Goldin, L.L., Kleinbock, Y.L., Lomanov, M.F., Lyulevitch, V.I., Vorontsov, I.A., Klenov, G.I., Rybalko, V.S., and Ivanov Yu.S. Soviet Project of PTF. Proc. of the NIRS Int. Workshop on Heavy Charged Particle Therapy and Related Subjects, Chiba, Japan, July 4–5, 1991, pp. 204–212.

14 Mandrillon, P., Carli, C., Farley, F., Fietier, N., Ostojic, R., Pinardi, M., Postiau, N., Rocher, C., Ryckewaert, G., and Tang, J.Y. Feasibilities studies of the EULIMA light ion medical accelerator. Proc. EPAC 92, Berlin, March 24–28, 1992, pp. 179–184.

15 Tronc, D. Compact proton therapy unit predesign. Proc. of the IEEE Part. Accel. Conf., Washington, D.C., May 17–20, 1993, p.1768.

21 Shielding and Radioprotection

J. V. SIEBERS

Loma Linda University Medical Center, Loma Linda, CA, USA

Introduction

The health physics concerns for ion beam therapy include the challenges present at both conventional radiation therapy facilities and nuclear physics facilities. Like the conventional radiation therapy facility, ion beam therapy facilities must allow access to an uncontrolled population, thus radiation shielding must lower dose levels sufficient for general population occupancy. Similar to the nuclear physics facilities, high energy secondary neutron fluences exist which have large attenuation lengths and must be protected against. The limited and expensive space available in hospital locations make construction of adequate, yet cost-effective shielding an important feature of facility design.

The primary radioprotection concerns for biomedical particle accelerators are shielding from the high energy neutrons produced by interactions of the primary protons with the accelerator, beam line, and ultimately the patient. The shielding situation is complicated by the need for convenient, prompt patient access, requiring effective design of mazes or labyrinths. As well as radioprotection against the prompt radiation hazard produced by the beam, particle energies are sufficient to produce a residual radiation hazard from radioactivation of beam line components. This exposure also must be limited.

The methods used to determine the shielding requirements for ion beam therapy are similar to those used for conventional radiation therapy. Shielding must reduce dose levels below limits set by governing bodies, usually following the recommendations of the ICRU. In determining the shielding, use factors, transmission factors, and other room/facility-dependent factors may be taken into account. The difficulties for ion beam therapy arise from the fact that the source term is not typically limited to the treatment head and patient as in conventional therapy, but instead results from a largely distributed source consisting of the accelerator, beam transport system, the treatment head, and the patient.

This chapter will cover the radiation protection concerns for ion beam therapy facilities, with principle emphasis on shielding from the secondary neutrons. An introduction to shielding methodology is given, a discussion of shielding materials, as well as a review of attenuation parameter measurements and calculations. As rapid entry to patients in treatment rooms is particular to therapy, design of hallways is also discussed. Performance of facility design calculations is discussed, as well as a section on radioactivation of beam line components.

Shielding Basics

The neutrons produced by ion beam bombardment of materials have a large angular dependence and a broad energy spectrum. Calculated energy spectra for 230 MeV proton bombardment of a Fe target are shown in Figure 1 for several angular intervals [1]. Such spectra must be shielded against for personnel protection.

The dose-equivalent fall-off in shielding material from a point source of neutron production is expressed as

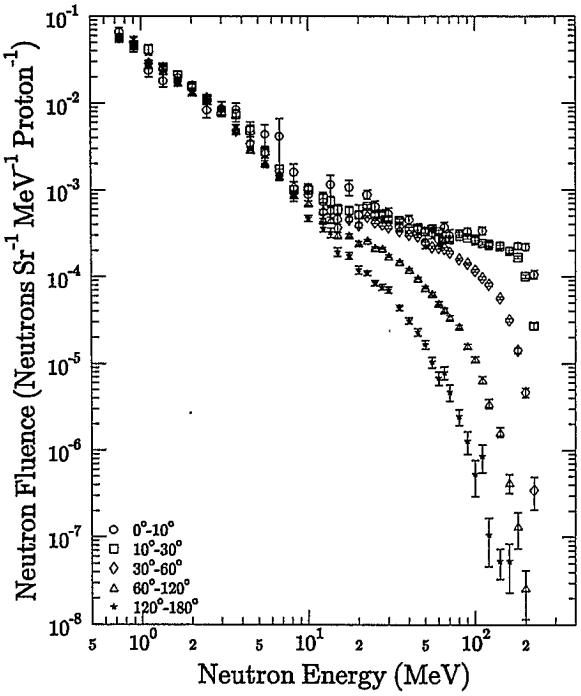

Fig. 1. Neutron spectra produced by 230 MeV proton bombardment of a stopping length iron target. Spectra were calculated using the computer code LAHET by Siebers [1]

$$H(t,\Theta) = \frac{H_0(\Theta)}{r^2} e^{-\frac{t}{\lambda(\Theta)}} \qquad (1)$$

with $H(t,\Theta)$ being the dose-equivalent at depth t in the shielding at angle Θ with respect to the incident beam direction, $H_o(\Theta)$ the dose-equivalent at angle Θ extrapolated to zero shield depth, r the distance from the target material to the point of interest, and $\lambda(\Theta)$ the attenuation length. An equivalent expression exists for the absorbed dose attenuation with $H(t,\Theta)$ and $H_o(\Theta)$ being replaced with $D(t,\Theta)$ and $D_o(\Theta)$, respectively. The attenuation length for absorbed dose may differ from the dose-equivalent attenuation length due to the energy dependence of the neutron radiation quality factor and the changing neutron spectrum with shield depth.

Using Equation [1], the thickness t of shielding required at angle Θ to reduce the dose rate to a value of H (Sv/h) from a location where N (protons/h) interact with a target material, with a distance between the source and the shielding wall entrance of l, can be determined:

$$H = H_o(\Theta)\, N/(t + l)^2\, e^{-\frac{t}{\lambda(\Theta)}} \qquad (2)$$

The shield thickness t can then be solved for using computer methods. One only requires knowledge of $\lambda(\Theta)$ and $H_o(\Theta)$ for the beam species, energy, and target combination. Unfortunately, even given the broad experience with particle accelerators in the therapy energy range, the values of $\lambda(\Theta)$ and $H_o(\Theta)$ are still highly uncertain.

A number of variables are involved in determination of shielding attenuation parameters, $\lambda(\Theta)$ and $H_o(\Theta)$, including incident beam type, incident beam energy, target material, target geometry, angle of interest, and shielding composition. Direct measurements of the attenuation properties of a bulk shielding material provide the most accurate determination of attenuation parameters for that shielding material. However, due to the number of variables involved, one can rarely directly apply measurement results to the shield design. One must, therefore, rely significantly on calculations of the shield attenuation properties. This requires detailed knowledge of the atomic and nuclear interactions produced by the secondary neutrons and photons in the shielding material, and the transport of these secondaries through the shield. This may be completed through use of Monte Carlo techniques or through solution of the Boltzmann transport equation.

Shield Materials

For the neutron shielding for medical accelerator applications, shielding material choices are typically limited to concrete, loaded or heavy concrete, earth, and steel. Other materials, including polyethylene, water, and lead are occasionally used, however, the cost of supporting these materials or the bulk material cost itself results in minimization of their use.

Concrete is most often used as a shielding material since it is an inexpensive, structurally sound, easy to use material with good nuclear

properties. The silicon and calcium have sufficiently large inelastic neutron cross sections above 20 MeV to attenuate the high energy fluence, while the large hydrogen content from bound water provides an effective means for slowing down neutrons below a few MeV. Being a mixture of a stone aggregate, sand, and a cementing agent, the properties of concrete can vary significantly. Bulk densities of concrete typically fall in the range of 2200–2300 kg/m^3, but selection of special aggregates increases it from 1300–4800 kg/m^3 [2]. The variability in bulk density between batches of concrete made from the same plant or in the same locality is usually within acceptable limits for shielding applications.

The use of concrete as shielding material has been explored greatly for the use in nuclear reactor shield designs where low energy neutrons dominate the spectra [2]. In reactor applications, the effect of water content in concrete on the neutron spectrum below 1 MeV is dramatic, with a decrease in the water content by 1/3 resulting in an increase in neutron leakage by a factor of 3. Similarly, variation in the water content of high energy neutron shielding modifies the low energy neutron spectrum. However, since attenuation lengths in shields for ion beam facilities are dictated by the inelastic interactions of the high energy neutrons [3, 4], the bulk shield density is of primary importance and the hydrogen content only determines the shape of the low energy equilibrium spectrum. Conversion between types of concrete with different aggregates can typically be accomplished by expressing the shield thickness in terms of the mass-thickness (kg/m^2).

Radiation therapy installations are typically based below ground level to take advantage of the shielding provided by the surrounding earth on at least a single wall, and typically located in a corner to gain the shielding advantage from two walls. On other walls, the containment required for earth shielding usually limits the shielding material use to concrete.

With the primary interaction mechanism for high energy neutrons being inelastic interactions and only the bulk density of the shielding material being of primary importance, use of a high density material such as steel is useful in the design of compact radiation shields. Below the threshold for inelastic interactions in steel (600 keV), few mechanisms exist for further neutron energy loss, since energy degradation by elastic interactions with iron atoms in steel is highly inefficient. To be effective, high Z (atomic number) shielding must be followed by 0.5–1 m of concrete to remove the low energy neutron component.

As concrete is the most widely used shielding material for attenuation of secondary neutrons produced in target materials, discussion will be limited to this material.

Attenuation Parameters

Measurements

To measure the attenuation properties of concrete, absorbed dose and dose-equivalent values are measured as a function of depth in the material. Preferably, a good geometry situation, with a semi-infinite planar secondary fluence incident upon a semi-infinite planar shield, or a spherical geometry with a point source located in the center of a sphere of shielding material is used. Dose and/or dose-equivalent are then measured as a function of depth and angle in the shield. The resultant measured dose values at a given angle in the shield are then fit with Equation (1) to provide the effective source term and attenuation length. These values can then be used in facility shielding calculations.

Few measurements of attenuation properties of concrete have been made in the therapy energy range. Recently, attenuation parameters have been measured for 230 MeV protons impinging upon Fe, Al, and Pb target materials. Dose and dose-equivalent were measured as a function of concrete depth at angles of 0°, 22°, 45°, and 90°. Results of these measurements are displayed in Figure 2 for the Al and Pb target materials. The Fe target results are similar to the Al and Pb results. Minimal differences in the dose values exist for different target materials at depths greater than 1100 kg/m^2. This suggests that high energy neutron production is target material independent, as would be expected for direct interactions between the incident protons and

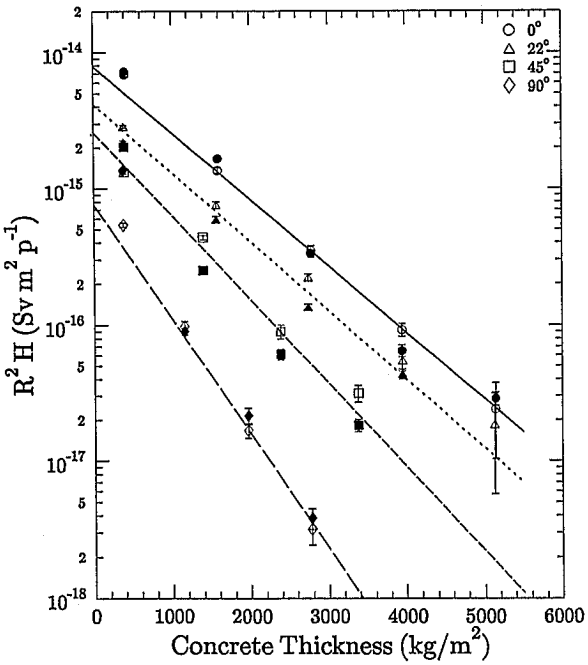

Fig. 2. Dose-equivalent values measured for 230 MeV bombardment of stopping length Al (open symbols) and Pb targets (filled symbols) as a function of depth in a concrete shield

neutrons bound in the target nuclei [1, 5, 6]. The result of this is that for deep shielding penetrations, attenuation parameters of the concrete are target material independent. At depths less than 1100 kg/m^2, the dose and dose-equivalent contributions from low energy neutrons vary strongly with the target Z, due to the strong target material dependence of low energy neutron production. At depth in the shield, this component is attenuated away, leaving only the equilibrium neutron spectra produced by the high energy neutrons.

Absorbed dose and dose-equivalent attenuation parameters for concrete were determined by fitting the Al, Fe, and Pb data to Equation (1). As similar results were found for each target material, results for all targets were combined and fit to a common curve. These target-independent results for 230 MeV proton bombardment are listed in Table 1. The attenuation length and production term decrease with increasing angle. For shielding design of a 230 MeV proton facility, these results could be used directly, for any target material. Design at other energies requires either additional measurements or calculations.

Table 1. Measured and calculated absorbed dose (D_o) and dose-equivalent (H_o) attenuation parameters for 230 MeV protons impinging upon Fe. The calculations were performed using the Monte Carlo code LCS for a fit to concrete depth ranging from 1000–4000 kg/m^2 in each angular interval

Experiment			Calculation		
Angle	D_o (10^{-15}Gym^2/p)	λ (kg/m^2)	Angle	D_o (10^{-15}Gym^2/p)	λ (kg/m^2)
0 °	1.12 ± 0.08	860 ± 21	0 °–10 °	1.36 ± 0.06	1013 ± 24
			10 °–30 °	1.05 ± 0.03	1043 ± 19
45 °	0.27 ± 0.05	700 ± 50	30 °–60 °	0.506 ±0.025	867 ± 19
90 °	0.077 ± 0.010	532 ± 20	60 °–120 °	0.212 ± 0.026	600 ± 21
			120 °–180 °	0.204 ± 0.026	436 ± 15
Angle	H_o (10^{-15}Svm^2/p)	λ (kg/m^2)	Angle	H_o (10^{-15}Svm^2/p)	λ (kg/m^2)
0 °	7.8 ± 0.5	891 ± 18	0 °–10 °	13.2 ± 0.8	991 ± 28
22 °	4.2 ± 0.5	860 ± 30	10 °–30 °	10.0 ± 0.4	1040 ± 21
45 °	2.2 ± 0.5	730 ± 60	40 °–50 °	4.58 ± 0.24	895 ± 21
90 °	0.76 ± 0.07	519 ± 15	85 °–95 °	2.0 ± 03	534 ± 26

Calculations

Shielding attenuation parameters are calculated using a variety of methods. Each method starts with an estimation or determination of the spectrum of secondary particles (neutrons) produced by ion beam bombardment of the target material. This could be through neutron spectrum measurements, however, neutron spectrum calculations are typically used. The neutron spectra are then either convolved with monoenergetic neutron attenuation data to determine the attenuation parameters, or are transported into a geometry, where the dose or dose-equivalent is determined as a function of shield depth. Similar to the measurement case, these dose values as a function of depth and angle are then fit to determine the attenuation parameters.

The calculation methods used to transport incident spectra into shielding material can be divided into two categories, discrete ordinates and Monte Carlo techniques. In discrete ordinates calculations, the neutron spectrum in a given angular interval is broken up into several energy groups. The transport of neutrons from one group to another progresses as the neutrons progress through the shield, approximating a solution to the Boltzmann transport equation. Examples of discrete ordinates codes are ANISN, TORT, and TWO-DANT [7–9].

In the Monte Carlo technique, primary and secondary interaction products are stochastically transported through the shielding media. The computation of interaction probabilities is based upon either measured or calculated cross-sections. Resultant interaction products determined using the cross-section information are then transported further through the specified shielding geometry. Due to the stochastic nature of the Monte Carlo technique, a large number of initial particles incident upon the target material must be used to get sufficient statistics. This typically takes considerable computing resources. Examples of Monte Carlo codes useful for ion beam shielding design are HETC, LCS, and FLUKA [10–12].

Table 2 lists attenuation parameters of concrete for protons at several energies and angular regions for several recent calculations. Several other shielding calculations have been completed [13–15], however, the tabulated results represent recent values. In Hagan's calculations, the High Energy Transport Code (HETC) was used to compute the secondary neutron source term. This was followed by transport calculations using the discrete ordinates code ANISN to determine the dose-equivalent at depth in the shield. Siebers used the LAHET Code System (LCS), a Los Alamos revision version of the HETC code coupled with MCNP, a low energy neutron transport code, to compute both the secondary neutron produc-

Table 2. Attenuation parameters for concrete from calculations by several authors (see ref. [5, 6, 17–19])

Energy (MeV)	Angle	H_o (10^{-15}Svm^2/p)	λ (kg/m^2)
Hagan et al., Fe target			
150	0°–15°	7.9	910
150	5°–30°	5.3	870
150	30°–45°	2.3	810
150	45°–60°	0.87	770
150	60°–90°	0.20	720
150	90°–180°	0.0086	740
200	0°–15°	15	1020
200	15°–30°	10	980
200	30°–45°	3.9	970
200	5°–60°	1.5	870
200	60°–90°	0.49	790
200	90°–180°	0.05	710
250	0°–15°	23	1090
250	15°–30°	16	1050
250	30°–45°	7.3	990
250	45°–60°	3.1	920
250	60°–90°	0.87	870
250	90°–180°	0.11	770
Siebers, Fe target			
230	0°–10°	13.2 ± 0.8	991 ± 28
230	10°–30°	10.0 ± 0.4	1040 ± 21
230	40°–50°	4.58 ± 0.24	895 ± 21
230	85°–95°	2.0 ± 0.3	534 ± 26
Braid/IAEA, Cu target			
50	0°–30°	1.4	470
50	90°	0.18	320
100	0°–30°	1.8	770
100	90°	0.48	460
200	0°–30°	7.4	880
200	90°	1.3	690
230	0°–30°	8.7	925
230	90°	1.6	731
300	0°–30°	12	1010
300	90°	2.3	810

tion and to transport the secondaries into the shielding material. IAEA used Braid's method to determine the secondary neutron production by integrating thin target neutron production over the proton slowing down spectrum. The neutron spectra were then convolved with monoenergetic neutron attenuation data to determine the dose-equivalent attenuation parameters.

The similarity of the calculated attenuation parameters in Table 2 is initially striking. However, the target secondary neutron production used as the input for all of these calculations is based on the Bertini intranuclear cascade model (INC), as embodied in either the HETC or an analytical representation based upon HETC results [10, 16]. In the INC model, particle-nucleus interactions are treated as a series of two-body collisions in the nucleus. Resulting collision products are determined based upon theoretical and experimental particle-particle total and differential cross-section data. The same cross-sectional data were used for all source calculations, resulting in the same approximate source term for each calculation. Since the source term is similar in all of the calculations, the similarity in the resultant attenuation results is not surprising.

The applicability of calculation models can be determined by a direct intercomparison between shielding measurements and the calculations performed with similar source, material, and geometry conditions. Such a comparison has recently been completed [1, 17]. The calculations very nearly modelled the measurement geometry, with a stopping-length Fe target surrounded by a 1 m air sphere, followed by a 5 m diameter concrete shielding sphere. The solid spherical concrete shield was divided into concentric spherical shells for scoring the neutron and photon fluence as a function of depth in the concrete shield. Dose and dose-equivalent were computed by multiplying the fluences by fluence-to-dose conversion factors. The values in a given angular bin as a function of depth were then fit with Equation (1) to determine the attenuation length and the source term Resultant values listed in Table 1 are for fits on the calculated and measured data over the same shielding depth intervals. Choice of depth interval in the fitting process is important since the neutron spectrum hardens with increasing shield penetration, resulting in larger attenuation lengths. The LAHET-based Monte Carlo calculation predicts the measured dose and dose-equivalent in the shield with fair accuracy. Attenuation lengths are slightly overestimated in the forward direction, but overall agreement between the measured and calculated values are quite good.

A compilation of attenuation lengths and production terms for forward and lateral shielding as a function of incident proton beam energy is displayed in Figures 3 and 4. In these figures, the open symbols are for the forward direction while the closed symbols are for lateral shielding. Also plotted are the curves suggested by IAEA-report number 283 [18] and Braid et al. [19] for forward and lateral shielding. In these graphs, no corrections for target material differences were made since measurements indicate that these differ-

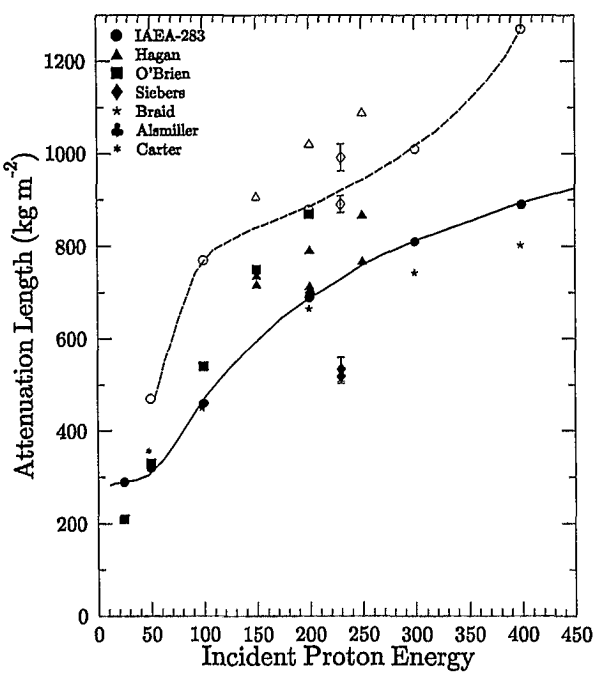

Fig. 3. Attenuation length as a function of incident proton energy for forward (open symbols) and lateral shielding (filled symbols). The curves indicate the values recommended in IAEA report 283 [18], with the dashed line for forward directed neutrons and the solid line for lateral neutron shielding

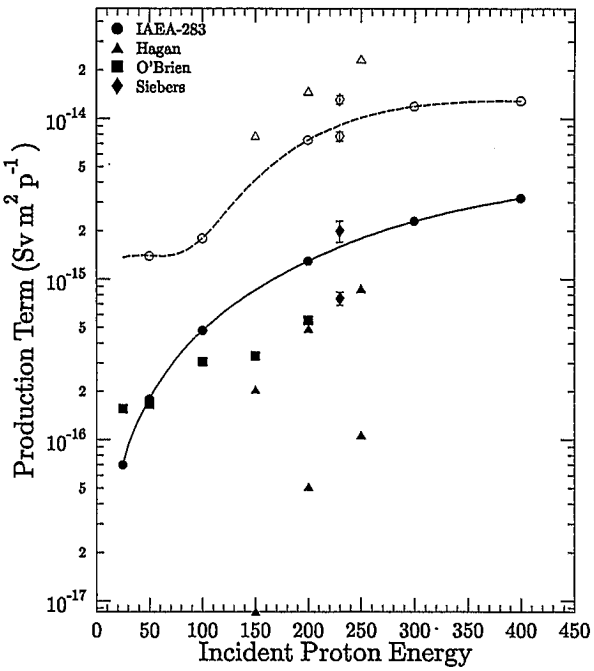

Fig. 4. Secondary neutron dose-equivalent production term as a function of incident proton energy for forward (open symbols) and lateral shielding (filled symbols). The curves indicate the values recommended in IAEA report 283 [18]. The dashed line is for the forward directed neutrons and the solid line for lateral directed neutrons

ences are minimal for large shielding penetrations. Overall, agreement between the IAEA/Braid-recommended curve and the measured values are substantial, with the measured values at 230 MeV only being slightly below the curves.

Alternative Calculation Methods

All calculation methods covered to this point have used calculations for both the source and the transport. As measured neutron spectra are now available for a number of proton energies incident upon a number of targets [20–27], these spectra can be used as input to either the discrete ordinates or the Monte Carlo calculations. The resultant attenuation parameters calculated would then at least have the right source term.

Hallways, Mazes, Ducts

In addition to the shielding material required for the walls, floors, and roofs of ion beam therapy facilities, access to irradiation areas must be allowed for both measurement devices and the patient by means of hallways and ducts. While use of a thick shielding door similar to those in use at many nuclear physics installations eliminates the need for a special maze to reduce the neutron fluence, the need for rapid patient access during irradiation procedures necessitates their use. Mazes in ion beam treatment facilities typically must have a large cross-sectional area, sufficient to allow a patient gurney or bed to enter the treatment room.

Due to the high penetrability of material and low reflectivity (albedo) of neutrons above 20 MeV, only neutrons produced below 20 MeV need to be considered in maze transmission problems. Measurements of maze transmission are made using activation foils, plastic scintillators, or other neutron-sensitive instrumentation. Several calculation codes exist for determining maze transmission, including AMC, SAM-CE, ZEUS, as well as the traditional Monte Carlo codes MORSE, HETC and LCS [10, 28–31]. All of them follow the secondaries through the various legs of the maze. In general, the calculation schemes do a good job in predicting the maze transmission and estimate the dose within a factor of two [32, 33].

General conclusions from maze measurements and calculations show:

1. Typical mazes will have at least two 90-degree angles requiring at least two bounces for the neutrons to escape the area.
2. The high energy component of the neutron spectra falls off more quickly than the low energy portion, with the energy spectra rapidly falling off with 1/E.
3. The neutron spectra intensity in the first leg of the maze follows an inverse square fall-off, while the dose fall-off in higher order legs (2 and greater) follows a sum of exponentials, with the source term requiring re-evaluation at the end of each leg.

Due to their small cross-sectional areas, duct calculations are typically more straight forward than maze calculations. Ducts are small access locations (30 cm or less) that allow entry of wires/cables, water, air and power into the radiation area. Again, duct calculations are understood from the experience in reactor design. Generally, the flux attenuation in a circular duct can be taken to be $d^2/(8L^2)$ (d = diameter, L = Length). For bends in the duct near 90°, an additional attenuation proportional to csc (Θ) due to the reflected neutron fluence is utilized. Rectangular ducts are typically estimated by use of circular ducts with the same cross-sectional area. Duct calculations usually assume the duct is empty, yet in reality, the duct is typically filled with some material thereby reducing the duct transmission through attenuation. For safety sake, mazes and ducts should not point directly at a source of secondary neutrons, nor at areas occupied by personnel.

Actual Shielding Calculations

In determining the shielding required for a given area of the facility, estimations of the locations of the beam losses, the dose limits, and the estimated type and duration of occupancy of each location must be determined. Once these parameters are known, a shielding code that convolves the various sources with production and attenuation terms over the desired geometry can then be used to determine the shielding. These calculations can be performed in a manner similar to calculations that are performed for conventional radiotherapy installations. An example of such a code is PTF-shield developed for a shielding study for the University of California-Davis Medical Center Proton Therapy Facility [33].

Several facility design criteria do greatly affect the shielding design. For a given beam energy and shielding material, the shielding attenuation lengths and source terms per proton are independent of the acceleration technique. The beam losses, however, depend significantly on the beam line design and the acceleration technique. For example, if a 250 MeV proton cyclotron is used for therapy with less penetrating beams obtained by slowing the beam down in an absorber, then shielding must exist to shield against the neutrons produced in the energy degrader. For a synchrotron, however, the acceleration energy can be changed to produce lower penetrating beams, eliminating this source of neutron production. Similarly, the type of beam delivery system affects the neutron source term. For passive scattering systems, proton energy lost in the scatterers results in neutron production, With only 30–50% of the beam in the useful patient field, the residual 50–70% of the beam is stopped in apertures and collimators, resulting in significant neutron production. With active scanning techniques (raster or voxel scanning), both the neutron production in the scattering system is avoided and the beam-use efficiency is greater resulting in lower neutron production. These examples show that the acceleration techniques and the choice of the beam delivery system greatly affect the production of secondaries that must be shielded from.

Due to the uncertainty in patient loads, field types, irradiation angles, beam energies, and beam loss locations, estimations of the quantity of secondary radiation that must be shielded against may be the single most uncertain part of facility shielding calculations. As with any shielding design, adequate safety factors must be built into the design to account for errors in values used in the calculations and to account for possible future increased secondary production due to use changes and equipment upgrades. Furthermore, one must forecast as to what the dose limits will be in the future and ensure that the facility is adequately shielded. For example, adjustments in the radiation quality factor for the secondary neutron radiation must be taken into account. The neutron quality factor, as determined from fluence to dose-equivalent conversion factors, was recommended to be doubled by the ICRU in 1987. This change has not promulgated through to regulations in many countries, however, is likely to do so in the near future. This alone causes a factor of two uncertainty in the source term.

Shielding Verification

Shielding verification is the process, after a facility is constructed, of ensuring the dose levels outside the shield are within acceptable limits. Two classes of verification measurements are customarily required:

1. Commissioning measurements: these include measurements of the dose/dose-equivalent at sites of interest for given test conditions which are needed for obtaining use permits. These measurements are often done with active dosimeters (Bonner Spheres, Long Counters, scintillators, or gas proportional counters). While these measurements do provide reassurance that the shielding is adequate, they do not reveal the dose levels for long-term exposure for the use conditions that the area is under.
2. Long-term verification measurements: these measurements are typically made with integrating type dosimeters (TLDs, film, track etch dosimeters) over long periods of time. These will give dose profiles at locations with the dose averaged out over periods of months.

Often, an energy correction must be made to the response of both active and integrating dosimeters to correct for the high energy component of the neutron spectrum (>10 MeV), for which the response of most detectors is significantly suppressed. Unfortunately, commercial instrumentation that responds adequately to high energy neutron spectra is virtually non-existent. Use of a tissue-equivalent proportional counter (TEPC) and analyzing the event size spectra to determine both the absorbed dose and radiation quality is tedious, however, provides accurate results.

Activation

Following termination of beam delivery, residual radiation is present in beam delivery areas due to the activation of items the beam intercepts. This includes the beam line components such as detectors and beam collimators, as well as patient apertures, patient compensators, and the patient. Fixed objects located in the beam line typically are activated to the highest levels, however, since these components are rarely accessed, and then only by trained personnel, the exposure hazards are minimal. Items between twice the background but less than 0.1 mSv/h 30 cm from the surface must be handled as radioactive material. Items that exceed an exposure of 0.1 mSv/h 30 cm from the surface must be handled by qualified personnel. Items producing excessive exposure can usually be allowed to decay before handling, with half-lives of components typically being less than 3 hours.

For the most part in ion beam therapy facilities, activation of removable beam line components (patient apertures and compensators) is minimal due to the low beam currents and short irradiation times, however, in facilities where high beam currents and long irradiation times are used, activation may be a significant concern. As usual, personnel should be trained in the importance of using time and distance as primary methods of reducing radiation exposure.

References

1 Siebers, J.V. Shielding Measurements for a 230 MeV Proton Beam. PhD thesis, University of Wisconsin-Madison, 1990.
2 Hungerford, H.E., Honig, A., Desov, A.E., DuBois, F., and Davis, H.S. Concretes, cements, mortars, and grouts. Jaeger, R.G., Blizard, E.P., Chilton, A.B., Grotenhuis, M., Honig, A., Jaeger, Th.A., and Eisenlohr, H.H. (eds.). Engineering Compendium on Radiation Shielding, Volume II. Springer Verlag, New York, 1975.
3 Patterson, H.W. and Thomas, R.H. Accelerator Health Physics. Academic Press, New York, 1973.
4 Tesch, K. A simple estimation of the lateral shielding for proton accelerators in the energy range 50 to 1000 MeV. Radiation Protection Dosimetry, II, 162–187, 1985.
5 Siebers, J.V., DeLuca, P.M. Jr., Pearson, D.W., and Coutrakon, G. Shielding measurements for 230-MeV protons. Nucl. Sci. Eng. 115, 13–23, 1993.
6 Hagan, W.K., Colborn, B.L., Armstrong, T.W., and Allen, M. Radiation shielding calculations for a 70–250 MeV proton therapy facility. Nucl. Sci. Eng. 98, 272–278, 1988.
7 Engle, W.W. Jr. A users manual for ANISN, a one-dimensional discrete ordinates transport code with anisotropic scattering. Technical Report K-1693, Union Carbide Corporation, Computing Technology Center, 1967.

8 Rhoades, W.A. The TORT three-dimensional discrete ordinates neutron/photon transport code. Oak Ridge Report ORNL-6268, Oak Ridge National Laboratory, November 1987.
9 Alcouffe, R.E., Brinkley, F.W. Jr., and Marr, D.R. User's guide for TWO-DANT: A code package for two-dimensional, diffusion-accelerated, neutral-particle transport. Technical Report LA-10094-M, Los Alamos National Laboratory, February 1990.
10 Armstrong, T.W., Alsmiller, R.G. Jr., Chandler, K.C., and Bishop, B.L. Monte Carlo calculations of high-energy nucleon-meson cascades and comparison with experiment. Nucl. Sci. Eng. 49, 82–92, 1972.
11 Prael, R.E. and Bozoian, M. Adaptation of the multistage preequilibrium model for the Monte Carlo method (I). Los Alamos Report LA-UR-88–3283, Los Alamos National Laboratory, 1988.
12 Ranft, J. and Routti, J.T. FLUKA and MAGKA, Monte-Carlo programs for the calculation of nucleon-meson cascades in cylindrical geometries. Technical Report CERN LABII-RA/71–4, CERN, November 1971.
13 Alsmiller, R.G. Jr., Santoro, R.T., and Barish, J. Shielding calculations for a 200-MeV proton accelerator and comparisons with experimental data. Technical Report ORNL-4754, Oak Ridge National Laboratory, 1975.
14 Smith, H.A. Shielding calculations and beam dump shielding considerations for the Indiana University cyclotron facility. Internal Report 74–6, Indiana University Cyclotron Facility, 1974.
15 Lundqvist, H. Radiation protection calculations for a proton cyclotron in the energy range 100–400 MeV. Technical Report GWI-R 18/72, Gustaf Werner Institute, University of Uppsala, Uppsala, Sweden, 1972.
16 Alsmiller, R.G. Jr., Leimdorfer, M., and Barish, J. Analytical representations of nonelastic cross sections and particle-emission spectra from nucleon-nucleus collisions in the energy range 25 to 400 MeV. Technical Report ORNL-4046, Oak Ridge National Laboratory, 1967.
17 Siebers, J.V., DeLuca, P.M. Jr., Pearson, D.W., and Prael, R.E. Shielding calculations for 230-MeV protons using the LAHET code system. Accept. for publ. by Nucl. Sci. Eng. (1995).
18 International Atomic Energy Agency. Radiological Safety Aspects of the Operation of Proton Accelerators. IAEA Technical Report Series 283. International Atomic Energy Agency, Vienna, Austria, 1988.
19 Braid, T.H., Rapids, R.F., Siemssen, R.H., Tippie, J.W., and O'Brien, K. Calculations of shielding for large cyclotrons. IEEE Trans. Nucl. Science, NS-18, 1971.
20 Meier, M.M., Goulding, C.A., Morgan, G.L., Moss, C.E., and Ullmann, J.L. Neutron yields for stopping and near stopping length targets for 256-MeV protons. Nucl. Sci. Eng. 104, 339–363, 1990.
21 Meier, M.M., Amian, W.B., Goulding, C.A., and Moss, C.E. Differential neutron production cross sections for 256-MeV protons. Nucl. Sci. Eng. 110, 289–298, 1992.
22 Meier, M.M., Amian, W.B., Goulding, C.A., and Moss, C.A. Neutron yields from stopping length targets for 256-MeV protons. Nucl. Sci. Eng. 110, 299–301, 1992.
23 Broome, T.A., Perry, D.R., and Stapleton, G.B. Particle distributions around a copper beam stop for 72 MeV protons. Health Physics 44, 487–499, 1983.
24 Bertini, H.W. Secondary particle spectra from the interaction of 30–340 MeV protons on complex nuclei: Experimental data and comparisons with theory. Phys. Rev. 162, 976–982, 1967.
25 Fasso, A. and Hofert, M. Distribution of secondary particles around various target materials exposed to 50 MeV protons. Nucl. Instr. Meth. 133, 213--218, 1976.
26 Nakamura, T., Fujii, M., and Shin, K. Neutron production from thick targets of carbon, iron, copper and lead by 30 to 50 MeV protons. Nucl. Sci. Eng. 83, 444–458, 1983.
27 Wachter, J.W., Burrus, W.R., and Gibson, W.A. Neutron and proton spectra from targets bombarded by 160 MeV protons. Phys. Rev. 161, 971–981, 1967.
28 Maerker, R. and Chain, V.R. AMC: A Monte-Carlo code utilizing the albedo approach for calculating neutron and capture gamma-ray distributions in rectangular concrete ducts. Technical Report ORNL-3964, Oak Ridge National Laboratory, August 1967.
29 Cohen, M.O., Gruber, W., Lichtenstein, H., Steinberg, H.A., and Troubetzkoy, E.S. SAM-CE, a three-dimensional Monte Carlo code for the solution of the forward neutron and forward and adjoint gamma-ray transport equations. DNA report, DNA 2830-F Rev B., Defense Nuclear Agency, 1973.
30 D'Hombres, M.M., Devillers, C., Gervaise, F., De Sereville, B., and Tardy-Joubert, P. Propagation des neutrons dans les tunnels d'accès à un accélérateur de haute énergie à protons. Report CEA-R-3491, Centre d' Etudes Nucléaires de Saclay, 1968.
31 Prael, R.E. and Lichtenstein, H. Users guide to LCS: The LAHET Code System. Los Alamos Report LA-UR-89–3014, Los Alamos National Laboratory, 1989.
32 Stevenson, G.R. Neutron attenuation in labyrinths, ducts, and penetrations at high-energy proton accelerators, in Proc. Theory and Practices in Radiation Protection and Shielding, Ingersoll, D.T. (ed.), Knoxville, April 22–24, 1987, American Nuclear Society, pp. 408–417.
33 Orthel, J.L., Knowles, H.B., and Hill, B.W. Final report for LBL/UCDMC proton treatment facility shielding and activation study. Technical Report, G.H. Gillespie Associates, Del Mar, California, 1993.

22 Commercial Concepts for Ion Beam Therapy Facilities

P. COHILIS

Ion Beam Applications (IBA) s.a., Louvain-la-Neuve, Belgium

Introduction

There are only a few centers around the world offering a treatment of tumors based on ion beam irradiation, and in fact most of them propose only proton therapy. Proton therapy is, indeed, the only ion beam therapy technique which is beginning to be used on a nearly routine basis. For therapy with heavier ions only limited clinical experience is available and research and feasibility studies still have to be done. Therefore, this chapter will concentrate on commercial concepts for proton therapy facilities.

Most of the centers offering the possibility of treating tumors with proton beams use equipment initially designed for nuclear physics research. In fact, the development of proton therapy as a clinical tool has been hampered by the complexity, the size and the cost of proton therapy facilities. Indeed, to be medically effective, protons require high energy accelerators not adapted, in the past, to the hospital environment. Pioneering institutions had to work with complex and inadequate equipment.

Today things are changing. A number of specialists and commercial companies are proposing, or working on, systems specially dedicated to proton therapy. The objective is, or should be, to meet all the clinical specifications of a state-of-the-art proton therapy facility in the most simple, reliable and cost-effective manner.

One of these specially dedicated facilities is already in use, at the Radiation Oncology Department of the Loma Linda University Medical Center (LLUMC), Loma Linda, California, USA, since the end of 1990 [1]. Another one, the Northeast Proton Therapy Center is under construction at the Massachusetts General Hospital (MGH), in Boston, Massachusetts, USA. Operation of the NPTC is scheduled to begin in 1998 [2]. These two facilities were proposed by two different companies or groups of companies and are based on different concepts, particulary, from the point of the accelerator design. Both will be presented in the next paragraphs, together with a description of a few conceptual systems which have not yet been implemented commercially.

It should be noted that the various systems may differ because of different concepts regarding the gantries, the nozzles, the patient positioners or the safety and control systems for example. However, the concept proposed for proton acceleration is probably the one which best distinguishes individual systems from each other. This concept may have important consequences regarding beam performance, cost, power consumption, and complexity to name a few. Therefore, the type of accelerator used for proton acceleration will be a key concept for classification.

Design Requirements

Any design of a proton therapy equipment should take into account all of the following concepts [1]:

- Simplicity. In contrast to what is frequently the case for nuclear physics research, the equipment designed for routine in-hospital use should be easy-to-operate and automated (as much as possible push-button operation, automatic tuning, control systems with friendly interfaces). The

need of a team of several engineers and technicians to start-up the machine during several hours each morning is certainly not compatible with the objectives of a proton therapy center!

- Reliability. Excessive downtime can compromise patient safety and convenience, and affects the cost of the treatment because it reduces patient throughput and requires maintenance specialists and/or a large inventory of spare parts.
- Safety. The safety of the patient and personnel is paramount. Each component of the equipment and the beam characteristics at strategic points must be monitored and configured correctly before the safety system allows the beam to enter the treatment zone.
- Flexibility. As much as possible, the design should be adaptable to changing concepts and ideas, especially in the treatment zone.
- Cost. This is strongly related to other concepts, such as simplicity and reliability, for example. The simpler and more reliable the system is, the higher the patient throughput and the lower the operating and maintenance costs will be. A judicious arrangement location of the different rooms composing the facility can also help to reduce the costs.
- State of the art clinical specifications. A recent paper [2] defines what is required of a state of the art facility. These specifications concern, e.g., the range in the patient, the range modulation and adjustment, the average dose rate, the field size, the dose uniformity, the distal dose fall-off and the lateral penumbra. The design which meets these requirements best will be the state of the art in proton therapy.

Description of Commercially Available Turnkey Systems

A Synchrotron-Based Proton Therapy System

The proton therapy system at Loma Linda is of this type. It was jointly built by a team of the Fermi National Accelerator Laboratory in Chicago, Illinois, the Loma Linda University Medical Center, the Lawrence Berkeley Laboratory and SAIC (Science Applications International Corporation), a private company based in San Diego. As the Loma Linda University Medical Center system is already described in another chapter of this book (see Chapter 33), we will not discuss it here. Instead, the paragraph on conceptual systems will present a design for a "next generation" of synchroton-based proton therapy equipment.

A Cyclotron-Based Proton Therapy System

The Northeast Proton Therapy Center at the Massachusetts General Hospital in Boston, USA, will be equipped with a cyclotron-based proton therapy system custom-designed for in-hospital operation. The equipment is under construction and will be ready by 1998. It is a complete turnkey therapy center based on a compact, automated, high-energy cyclotron and isocentric gantries. It is fabricated by IBA (Ion Beam Application s.a., Belgium) and a number of subcontractors, for example General Atomics in the USA and Sumitomo Heavy Industries in Japan.

The basic configuration of the IBA proton therapy system comprises the following elements:

- A 235-MeV isochronous cyclotron, able to deliver beams of up to 1.5 μA, but hardware-limited to 300 nA, in order to limit the maximum possible dose rate to the patient.
- An energy selection system transforming the fixed energy beam extracted from the cyclotron into a variable energy beam (235 to 70 MeV range) provided with energy spread and emittance limitations and verification.
- A beam transport and switching system connecting the exit of the energy selection system to the entrance points of a number of gantries and fixed beam lines. At strategic points along the beam transport system, the beam characteristics are monitored with non-interceptive multiwire ionization chambers, e.g., for automatic tuning.
- Three gantries fitted with a nozzle, and a system consisting of two horizontal beam lines, of which one (for large fields) is equipped with a

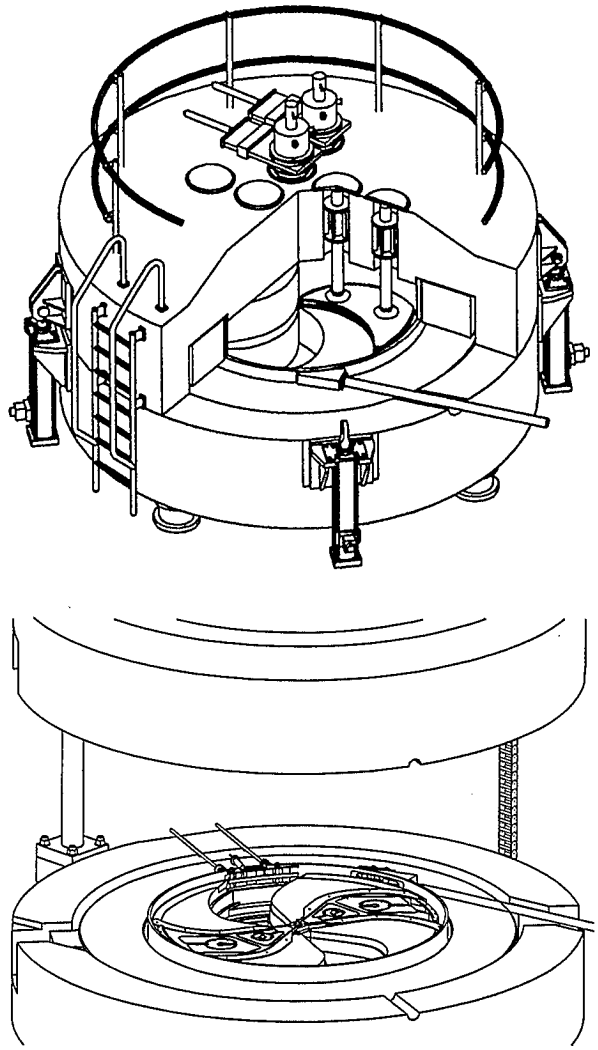

Fig. 1. Schematic view of the IBA 235 MeV cyclotron (**a**). This cyclotron splits at the median plane allowing easy maintenance (**b**)

nozzle. For beam spreading on the gantries and on the horizonal large field line, both beam scattering and beam wobbling are available.
- A global control system which comprises an "accelerator control unit" plus three independent, but networked "irradiation control stations". Through the network, each of the irradiation control systems can also take control of the PLC (programmable logic controllers) based accelerator control unit directing the cyclotron, the beam line and the gantry optics.
- A global safety management system independent of the global control system. This safety management system uses a combination of hardwired interlocks and independent PLCs to achieve a safety level meeting applicable standards.
- A robotic patient positioning system. Combined with the gantry, the equipment provides complete 4π coverage of the patient.

The advantages of this system, and in particular, the choice of a cyclotron for proton acceleration are the following according to IBA:

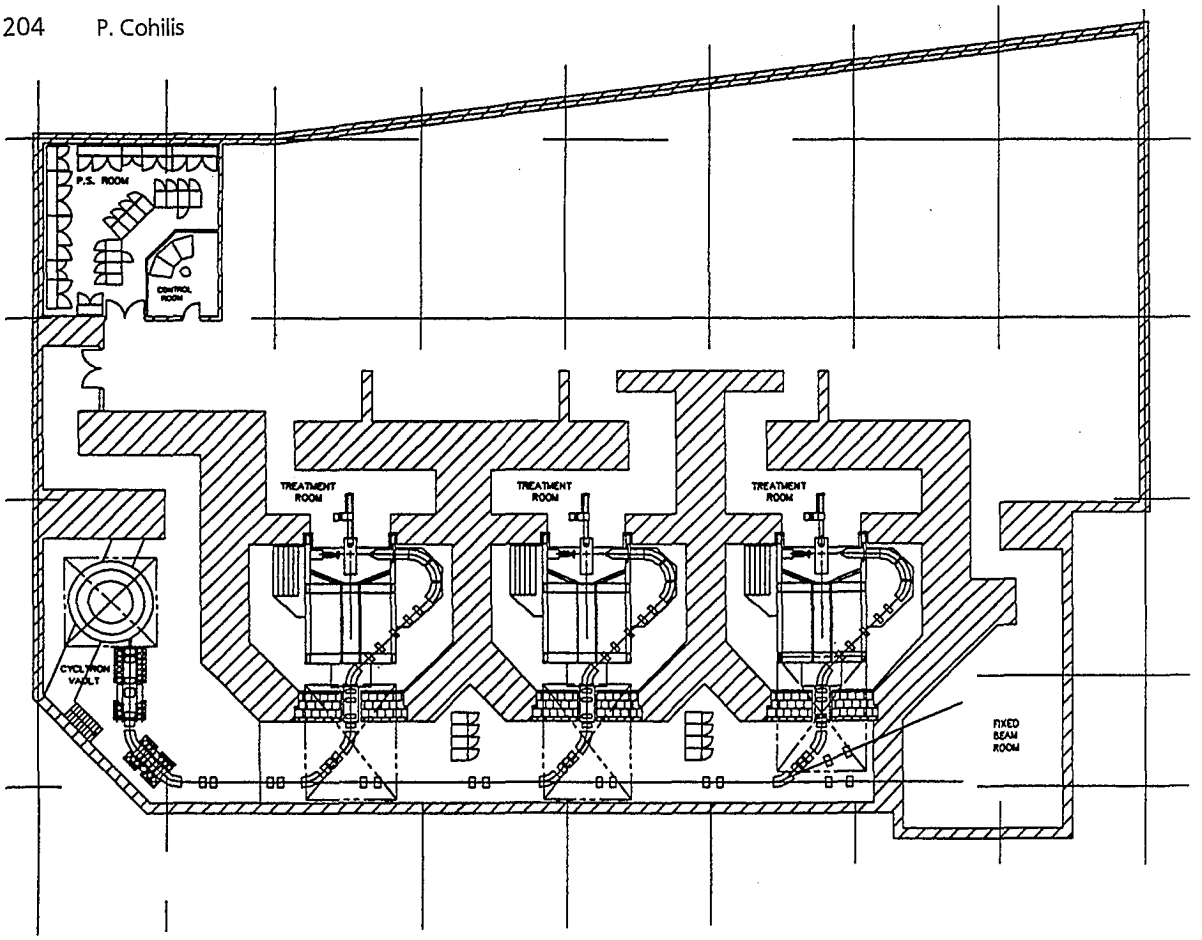

Fig. 2. Example of an IBA proton therapy center

- Simplicity, reliability and operability. An isochronous cyclotron is probably the simplest and most inexpensive way to produce 235 MeV protons. This technology is well-known and widespread. The cyclotron operates in CW (continuous wave) mode. The machine parameters are constant in time and only 5–7 of them are adjustable. None of these parameters requires operator tuning during machine operation or during the morning start-up: reference values are stored by the control system and fine-tuned using well-developed computer algorithms. There is no need for fast computer algorithms, as there are no time-critical tunings but only the need to compensate for slow drifts.
- Scanning ready. The high-intensity, continuously extracted beam can be intensity-controlled from the ion source within 15 μsec turn-on/turn-off time, and only 30 μsec separate the beam leaving the source and reaching the patient. The beam is, therefore, perfectly suited for beam scanning and wobbling. The high intensity easily allows for respiration gating without extending treatment times, even for very large fields.
- Safety. The extracted beam is characterized by a fixed energy, a low energy dispersion and a fixed, low emittance. The accelerator is unable to produce an extracted beam with incorrect energy, energy dispersion or emittance pattern. The safety system ensures the safety of the patient and personnel. The choice of PLCs offers the best choice in reliability, performance and cost.
- Maintenance. The cyclotron splits at the median plane allowing easy maintenance. The

upper yoke can be raised within minutes by hydraulic jacks, giving free access to all machine components. Thanks to the moderate vacuum requirements and the generous pumping system, full energy beam can be resumed within 30 minutes after starting evacuation.

Figure 1 presents a schematic view of the IBA cyclotron while Figure 2 shows an example of a proton therapy facility equipped with the IBA system. Additional details concerning this commercial system may be found in [3] and [4].

Description of Alternative Conceptual Systems

A H^--Synchrotron-Based Proton Therapy System

ACCTEK Associates, Inc. (La Grange, Illinois, USA) promotes a system for proton therapy which is based on a H^--synchrotron with charge-exchange extraction. The company provides, as well, a rotating vertical beam delivery system, a raster scanning system, and systems for proton radiography and computed tomography.

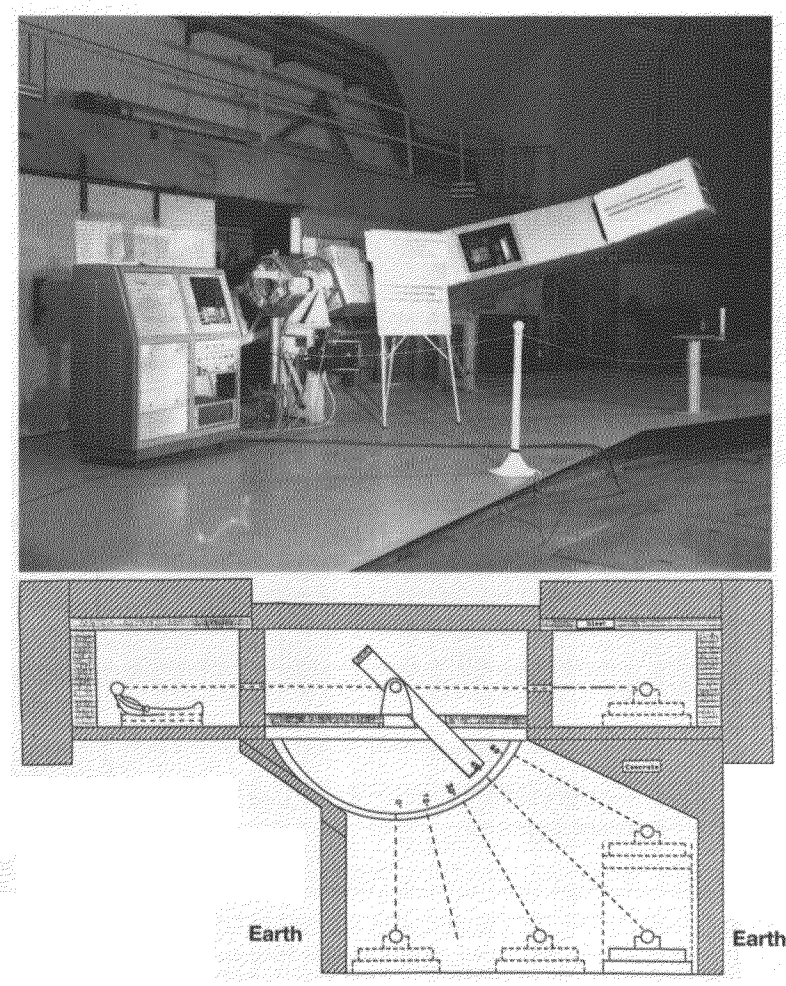

Fig. 3. The rotating magnet system for beam delivery proposed by ACCTEK (top) and a schematic view of the system serving three treatment rooms (bottom)

More details about the equipment may be found in [5]. According to ACCTEK the advantages are the following:

- Regarding the accelerator, the proposed system has probably a lower cost than a cyclotron or the more compact, higher field proton synchrotrons. The extraction system is simple, inexpensive and flexible, and many extraction ports are possible. Compared to proton synchrotrons and cyclotrons, the extracted beams have a very low emittance, making small aperture transport and gantry systems possible. The proposed system offers superior control of the extracted beam current in comparison to proton synchrotrons, and compared to cyclotrons, it offers energy variability on a pulse-to-pulse basis without degradation of the beam quality.
- The rotating vertical beam delivery system is an alternative to an isocentric gantry at much lower cost. Along with horizontal beams it can accomplish nearly everything desired for proton therapy. In addition, it will have a very significant impact on reducing the shielding requirements for therapy.
- The raster scanning beam delivery system will provide higher beam utilization efficiency, permit 3D-dose deposition, and make the patient alignment procedure simpler and faster by eliminating the necessity of a bolus and by using proton radiography for alignment. Raster scanning is required for practical real-time radiography and computed tomography.
- For radiography and computed tomography a 300 MeV beam of protons is desirable. Their use will impact therapy by providing real-time radiography for alignment and for improved treatment planning with proton computed tomography.

A "Second Generation" Synchrotron-based Proton Therapy System

A design concept for a next generation of synchrotron-based proton therapy equipment is proposed by SAIC (Science Applications International Corporation, San Diego, California, USA) and PAC (Particle Accelerator Corporation, Downers Grove, Illinois, USA). This design builds up on the experience gained from the Loma Linda facility. It includes the following:

- An accelerator system based on a "next generation" proton synchrotron delivering a 70 to 250 MeV beam. The "next generation" label is given by comparison to the Loma Linda synchrotron. The main objective of the new generation is to achieve higher intensity performances.

  According to the proposers, it is the request for rapid energy changes in therapy that speaks for a synchrotron. In addition, the extracted beam size is relatively small allowing for small bore magnets to be used. The accelerator is coupled with a radiofrequency quadrupole (RFQ) accelerator which will serve as injection system. The RFQ will be of an improved design, as compared to the Loma Linda type, allowing for a reduction of the momentum spread at the injection point, and hence, a reduction of the beam loss at injection.

- A beam transport system transporting the beam to the treatment rooms. The switchyard is based on three y-shaped magnets that shuttle the beam into any of four treatment lines. The gantry lines are on the right and on the left, and the fixed-beam room is straight ahead.
- Gantry systems allowing to support and position the bending, focusing and steering magnets and the beam nozzle, in order to focus the proton beam precisely on the patient from any desired angle in the plane of rotation. The gantry concept is the proven corkscrew configuration (cf. Chapter 23). This configuration incorporates achromatic beam transport and accommodates the necessary nozzle components.
- A patient positioner system. The gantry allows the beam to be rotated throughout a full circle of 360° (4π radians), enabling the tumor to be irradiated from any therapeutically desirable angle. Axial position of the patient is accomplished by the patient positioning system, which moves the patient perpendicular to the beam along the gantry axis.

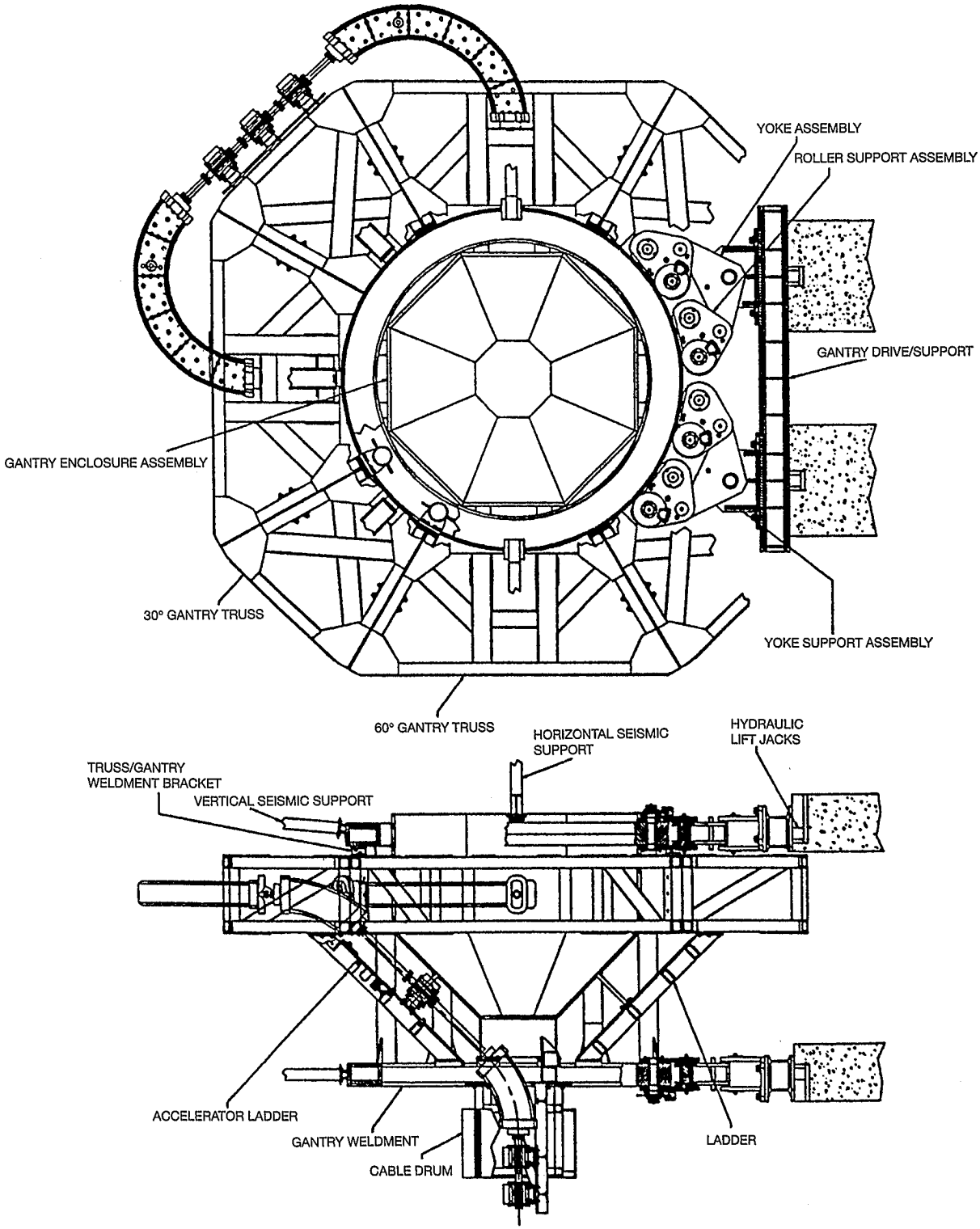

Fig. 4. The SAIC gantry system assembly

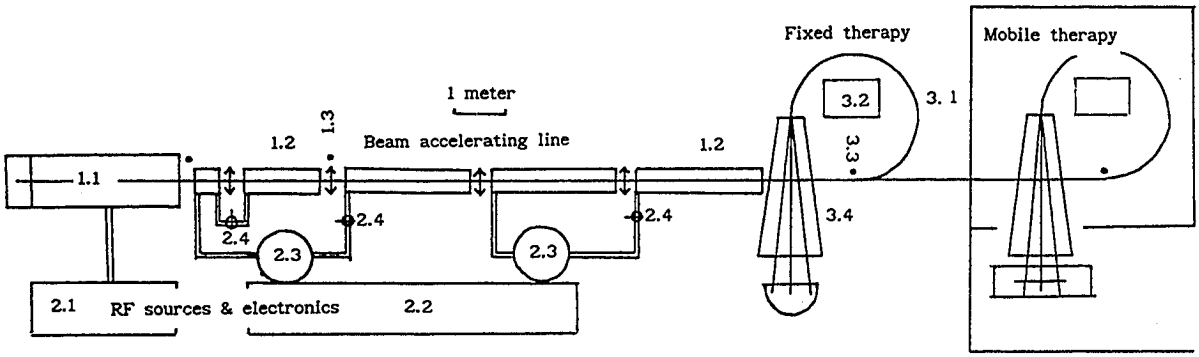

Fig. 5. The linac-based proton therapy system proposed by D. Tronc: beam line (1.1, 1.2, and 1.3), RF sources (2.1, 2.2, 2.3 and 2.4), therapy fixed head (3.1, 3.2, 3.3, and 3.4), and therapy mobile head. See [8] for more details

According to the authors, the proposed gantries are of a new generation, as compared to the Loma Linda type. Improvements concern the positional accuracy of the beam, an easier alignment of the gantry, the motion control, and a reduction of installation and/or operating costs.

Figure 4 presents the SAIC gantry system assembly. More details about the whole equipment may be found in [6].

A Linac-Based Proton Therapy System

A predesign of a compact proton therapy unit based on a H-coupled traveling wave linac has recently been published by D. Tronc, General Electric Medical Systems (Buc Cedex, France) [8]. The main idea is to make use of existing RF-linacs, e.g., the industrial standard for acceleration of electrons for radiotherapy, to accelerate protons of low and variable velocity and high rigidity. The conceptual guidelines for this compact therapy unit which, according to the author, delivers a high quality beam and is able to spread the use of protons within hospitals, are presented in detail in [7] and [8]. They are based on innovations, such as simpler accelerating RF geometries, improved focusing, and an original combination of head optics and treatment bed access. In particular, the treatment cell is a chamber large enough to allow bed rotations and human assistance at set-up location. The patient moves symmetrically to the magnet inside this treatment cell which is part of the rotating head. This non-isocentric choice – similar to the PSI patient positioner, (cf. Chapters 23 and 35) – allows reproducible error at the level of the rollers' rotation mechanism, the linac-head colinear adjustment being electronically controlled.

A Superconducting Cyclotron for Proton Therapy

The design of a compact facility for proton therapy based on a superconducting cyclotron was presented by the Siemens AG (Erlangen, Germany) at the EPAC '94 Conference in London [9].

A Proton Therapy Center Based on an ECRIPAC

The electron cyclotron resonance (ECR) plasmas are well known, e.g., inside ion sources. However, an ECR plasma cannot only produce highly stripped ions but can also accelerate them in situ up to very high energies of several hundreds of MeV/nucleon. Such an ECR ion plasma accelerator (ECRIPAC) could be extremely compact (length approx. 1 m), remarkably economic and technologically simple. A conceptual design of a proton ECRIPAC is presented in detail in [10].

The physical basis of the ECRIPAC concept has been known for several decades [11] but methods for putting it into practice have not been successful up to now. If the construction and operation of a future prototype based on [10] can be achieved, the ECRIPAC could be considered a revolutionary competitive device for proton acceleration in the framework of proton therapy.

Addendum

Table 1 presents the addresses and telephone numbers of commercial companies active in the proton therapy field.

Table 1. Commercial Companies Proposing Proton Therapy Equipment and/or Conceptual Designs

Name	Address	Phone and FAX
ACCSYS Technology, Inc.	1177 Quarry Lane Pleasanton, CA 94566 USA	TEL.: 1 510 462 6949 FAX: 1 510 462 6993
ACCTEK Associates, Inc.	901 S. Kensington LaGrange, IL 60525 USA	TEL.: 1 708 252 6786 FAX: 1 708 252 4007
Electus Technology, Inc.	P.O. Box 608 Loma Linda, CA 92354 USA	TEL.: 1 909 799 8300 FAX: 1 909 799 8348
GE Medical Systems s.a.	283 rue de la Minière, B.P. 34 78533 Buc Cedex France	TEL.: 33 1 30 70 43 21 FAX: 33 1 39 56 41 35
IBA s.a.	6 rue J.E. Lenoir B-1348 Louvain-la-Neuve Belgium	TEL.: 32 10 47 58 58 FAX: 32 10 47 58 10
Maxwell Brobeck Division	4905 Central Avenue Richmond, CA 94804 USA	TEL.: 1 510 524 8664 FAX: 1 510 524 8472
SAIC	4161 Campus Point Court San Diego, CA 92121 USA	TEL.: 1 619 458 5285 FAX: 1 619 546 6800
Siemens AG	KWU-Umwelttechnik GmbH Erlangen Germany	TEL.: 49 09131 18 4683 FAX: 49 09131 18 9166
PAC	4513 Cornell, Avenue Downers Grove, IL 60515 USA	TEL.: 1 708 969 0750 FAX: 1 708 969 0750

References

1 Slater, J.M., Miller, D.W., and Slater, J.W. Developing a clinical proton accelerator facility: Consortium-assisted Technology Transfer. Proc. of the IEEE Particle Accelerator Conference, May 6–9, 1991, San Francisco, California, p. 532.

2 Gall, K.P., Verhey, L., Alonso, J., Castro, J., Collier J.M., Chu, W., Daftari, I., Goitein, M., Kubo, H., Ludewigt, B., Munzenrider J., Petti, P., Renner, T., Rosenthal, S., Smith, A., Staples, J., Suit, H., and Thornton, A. State of the Art? New proton medical facilities for the Massachusetts General Hospital and the University of California Davis Medical Center, Nucl. Instr. Meth. Phys. Res. B79, 881–884, 1993.

3 Jongen Y., Laisné, A., Beeckman, W., Dufour, J.P., Marie, H., Verbruggen, R., Wollnik, H., Takahashi, N., Satoh, S., Sano, M., and Takayama, T. Progress report on the IBA-SHI small cyclotron for cancer therapy, Nucl. Instr. Meth. Phys. Res. B79, 885–889, 1993.

4 The IBA Proton Therapy System, Brochure describing the Proton Therapy System proposed by Ion Beam Applications s.a., available upon request from IBA, Chemin du Cyclotron, rue J. Lenoir 6 – B 1348 Louvain-la-Neuve – Belgium.

5 Martin, R.L., The ACCTEK proton medical accelerator and beam delivery system for cancer therapy and radiography. Proc. 2nd Europ. Part. Accel. Conf. (EPAC 90), June 12–16, 1990, Nice, pp.103–105.

6 Conceptual Design for a Second Generation Synchrotron Based Proton Therapy Facility. Document presenting the conceptual design proposed by Science Applications International Corporation and Particle Accelerator Corporation, available upon request from SAIC, 4161 Campus Point Court, San Diego, California 92121, USA.

7 Tronc, D. Traveling wave acceleration of protons. Nucl. Instr. Meth. Phys. Res. A327, 253–255, 1993.

8 Tronc, D. Compact proton therapy unit predesign. Proc. of the IEEE Part. Accel. Conf., May 17–20, 1993, Washington, D.C., p. 1768.

9 Mandrillon, P., Farley, F., Fietier, N., Tang, J.Y., Anton, F., and Savoy, R. A compact facility for high energy proton therapy based on a superconducting cyclotron, in Proc. of EPAC 94, Suller, V. and Petit-Jean-Genaz, Ch. (eds.) London, June 27 – July 1, 1994, World Scientific, Singapore, pp. 2604–2606.

10 Geller, R. and Golovanivsky, K.S. Design of a compact ECRIPAC device for 1–400 MeV/amu heavy ion bunches production. Nucl. Instr. Meth. Phys. Res. B68, 7–16, 1992.

11 Brunet, A., Geller, R., and Jacquot, B. 2ème Colloq. Int. sur Interaction des Champs Oscillants et Plasmas, Saclay, France, 1968, p. 677.

V. Beam Preparation and Control

Concepts for Gantry Systems

E. PEDRONI

Paul Scherrer Institute, Division of Radiation Medicine, Villigen, Switzerland

Introduction

Experience with proton therapy has been acquired in the past in research laboratories using protons with horizontal beam lines. It is only with the installation of the Loma Linda proton facility in California in 1991 that protons have been made available on an isocentric gantry and in a hospital environment [1].

The success of photons in hospitals is strongly related to the possibility of applying the beam on the supine patient using multiple fields delivered by an isocentric gantry. It is only through the overlapping of multiple beams at the target volume that photons can be used at all for the treatment of deep-seated tumors.

The questions which we want to discuss in this chapter are:

- Why should we not use the same strategy for proton therapy and apply protons using isocentric gantries?
- What are the possible draw-backs of such an approach?
- What are the technical solutions available?

The Purpose of a Proton Isocentric Gantry

The term "proton gantry" means a structure supporting a beam line which rotates around the patient. The purpose of such an instrument is to provide the application of a proton beam on the supine patient from many directions without the need to change the patient's position during the treatment.

As a first rule, for any precision radiation treatment, the patient position during treatment should be kept invariant with respect to gravity, in order to avoid possible internal shifts of organs. Uncontrolled changes of the patient anatomy would otherwise rapidly spoil the precision of the treatment. The obvious exception to this rule are treatments in the rigid skull where organ shifts are negligible.

The most preferred patient treatment position is the supine position. It is most comfortable for sick patients and also the usual orientation for taking CT and MRI images used for treatment planning.

The freedom to apply the beam on the gantry from any direction is expected to bring some significant advantages. The most obvious is to reduce the dose burden to sensitive structures surrounding the target volume. By choosing a different beam direction one can often avoid sensitive structures and by distributing the entrance dose of the beam over a larger area of the body one can also reduce the local dose at given points to be below the tolerance level. Having the flexibility to choose the direction of the beam freely is, therefore, an important tool for minimizing the risks of treatment complications.

Optimizing the beam direction pursues another goal, namely, to avoid having the beam traverse complex density heterogeneities which could produce unacceptable errors in the dose distribution. Possible examples are range uncertainty errors due to the combined effect of multiple Coulomb scattering and of range modifications due to body density heterogeneities [2]. These effects cannot completely be corrected

with compensators outside the patient's body [3] nor with dynamic variations of the energy of a scanned beam. They can only be predicted by Monte Carlo calculations but are difficult to control. The choice of the beam direction is, therefore, a factor which can be used to improve both the tolerance and the precision of the treatment.

The major drawback of a proton gantry is the size (several meters in diameter) of the rotating structure supporting the beam. Since proton therapy requires a maximum beam energy of 200–250 MeV, the beam lines have to be designed for a correspondingly large magnetic rigidity. The bending radius of such a beam using non-superconducting magnets operating below saturation limits is of the order of 1.3 m. The magnetic elements used for transporting the beam are correspondingly bulky, making the rotating structure large and heavy. This is probably the major obstacle to a rapid permeation of proton therapy into the hospital environment. Optimizing the design of proton gantries is, therefore, a crucial issue for the future development of this modality.

Fig. 1. The patient positioning system used at Harvard for non-invasive treatment of various intracranial disorders. Courtesy of the producer Product Genesis Inc. [5]

Alternatives to a Gantry Solution

For treatments in the skull it is not strictly necessary to rotate the beam around the patient. Since the skull is rather rigid, it can be scanned in a CT in supine position and then be rotated in space without changing the properties relevant to the penetration of the beam and the precision of the treatment. An elegant patient positioning unit based on this idea is in use for stereotactic treatments in a horizontal beam line at Harvard University. This very precise positioning system, developed by the company Genesis Inc., is illustrated in Figure 1. It permits rotation of the patient around the body axis, in addition to rotation of the patient table in the horizontal plane, thus providing two independent rotations of the patient skull with respect to the beam [4].

Another alternative to the gantry solution is to treat the patient in the upright position, or sitting on a chair, using a horizontal beam line. The patient support is then rotated around the vertical axis. This way, the patient is maintained in an invariant position with respect to gravity and the beam can be applied from many directions without the need of a gantry. The major problems encountered when using this solution are that CT-images of the patient must be taken in this unusual position and that reproducible immobilization of the patient during each treatment fraction is difficult. The first problem may be solved by modifying the CT-equipment to have the axis of rotation in the vertical direction. This solution was adopted at Harvard and Berkeley for proton and ion therapy in the 80's. The remaining problem is precise positioning of the patient in the modified CT. Immoblilization moulds for the upright or seated position are more difficult to manufacture than for the supine position and they are less precise since, as treatment proceeds, the patient gets more and more relaxed and tends to sink inside the mould.

Another possible alternative to a gantry is to use multiple fixed beam lines, each with a different fixed beam direction. The simplest solution is the combination of horizontal and vertical beam lines. This arrangement was adopted for the proton therapy facility in Tsukuba. A similar solution has been chosen for the very recent installation of the ion therapy facility HIMAC at Chiba (see Chapter 34). The magnetic rigidity of a thera-

peutic light ion beam is a factor of two to three larger than for proton therapy and a gantry for ion therapy would, therefore, be rather gigantic.

To further enhance the flexibility in the choice of the beam direction, one can use fixed beam lines in combination with a small pitch rotation of the patient table. If the pitch rotation angle is maintained below some limit (e.g., ±15°) the deformation of the patient anatomy is expected to be small enough not to affect the precision of the treatment.

When we discuss fixed beam line arrangements, we have to ask: how many beam lines, how many angles and how many rooms are optimal? One also has to consider carefully, if one wants a single fixed beam line for each treatment room or many beam lines for the same room (with the option to have the beam lines converging on the patient table). The first solution clearly reduces the costs per room, but scheduling the treatments in different "dedicated" rooms is difficult to mangage. If the use of the rooms is not well optimized, the saving of investment costs is jeopardized by an under-usage of the whole facility.

The option to have more beams in the same room offers more flexibility but is more expensive. There are not only additional installation

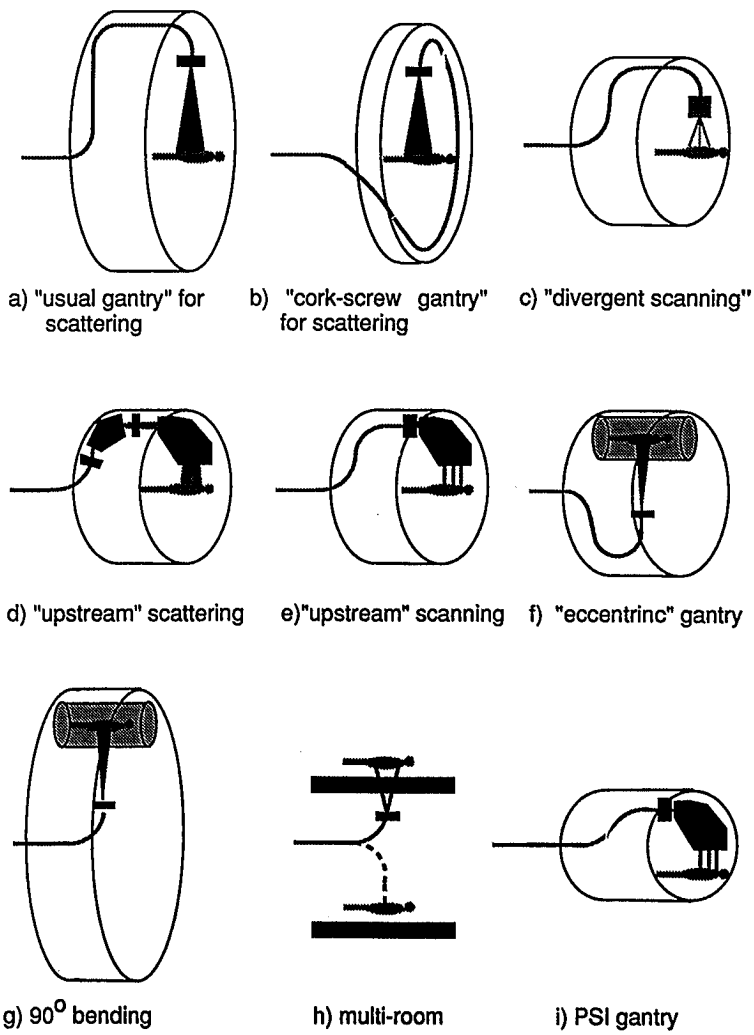

Fig. 2. Comparison of different gantry types (see text)

costs for the increased number of beam lines; one also has to worry about the extra work of performing all the necessary set-up and calibration procedures repeatedly on each single beam port. As a first approximation, it is probably reasonable to assume that a solution with two converging beam lines has similar total costs as an isocentric gantry.

Gantry Designs

The choice of the beam delivery technique and the design of the isocentric gantry are strongly related. The different solutions can, therefore, be classified according to the beam spreading technique used. In Figure 2, sketches of the different concepts discussed in the following section are given for comparison.

The 'Conventional Gantry' for the Scatter Foil Technique

This is the most straightforward design. The basic principle of this gantry design is depicted in Figure 2a. The beam is first bent away from the axis and then bent back, to come in perpendicular to the supine patient along the radial direction of the rotating structure. The devices used for spreading and shaping the beam in the patient are placed at the end of the beam line following the last bending magnet. The beam is scattered at least 3 or 4 m ahead of the patient in order to provide sufficient uniformity of the spread beam over all possible target sizes. The radius of the rotating structure must, therefore, be of the order of 5–6 m. This is probably the major disadvantage of this solution.

The conventional gantry discussed here is dedicated to the scatter foil technique, but, in principle, this design can accommodate any other dose application method including the most advanced beam scanning techniques. The passive scattering method represents the state of the art of proton beam delivery [5]. It is known to work reliably and is the most common for patient treatments. However, many of the presently proposed installations offer the option for an upgrade to a dynamic beam scanning technique as part of their design.

For the second hospital-based proton facility in the world, which will be realized at the Massachusetts General Hospital in Boston, USA, the choice has fallen in favor of a conventional gantry for scattering (Chapter 39) with mechanical and ion optical design carefully optimized to provide both scanning and scattering beam delivery techniques. Figure 3 shows the cross-section of the gantry for the Northeast Proton Therapy Center (NPTC), designed by IBA in Belgium [6].

The 'Cork-Screw' Gantry

The cork-screw gantry concept was invented in Harvard by Koehler [7]. The major difference to the previous design is given by the different beam path within the gantry structure (Fig. 2b). The bending of the beam is confined to a plane perpendicular to the gantry axis. This requires a larger total bending angle of the beam but allows for a reduced gantry volume, saving space and lowering shielding costs.

Three identical cork-screw gantries have been built at Loma Linda, presently the only hospital-based proton facility in the world and the only place where proton treatment is performed using a gantry [1]. Figure 4 shows a photograph of a patient treatment at the Loma Linda gantry. The cork-screw design has also been adopted for the proposed TERA project in Italy [8].

The 'Supertwist Gantry'

A possible disadvantage of the cork-screw gantry is the short distance between the isocenter and the coupling point of the beam with the gantry. An intermediate design between cork-screw and normal gantry which allows for a better utilization of the space in the isocenter region has recently been presented by Farley [9].

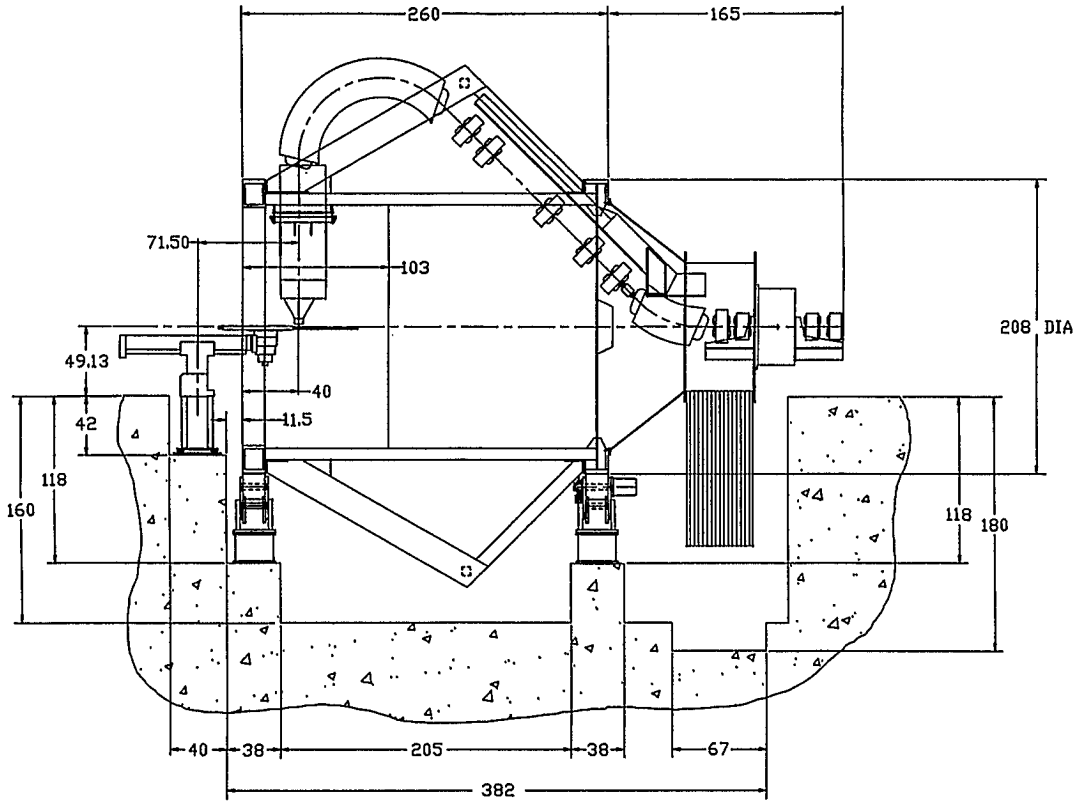

Fig. 3. View of the IBA gantry for the new proton therapy facility in Boston, USA. Courtesy of I. Jongen [7]

The 'Uppsala' Gantry

The design proposed by Graffman et al. [10] is a 'conventional' gantry with a very short distance between the last bending magnet and the patient, designed specifically for the spot scanning technique (Fig. 2c).

The basic idea behind this concept is to apply a focused proton pencil beam directly on the patient and to scan the beam under computer control using two magnets placed upstream of the patient following the last bending magnet. For the variation in range a range shifter system with moving double wedges is conceived in front of the patient. The drift space after the double magnetic scanning system is minimal and the divergence of the beam is correspondingly large with a source-to-skin distance (SSD) of less than one meter. A possible disadvantage of this approach is the increased skin dose due to the short SSD whilst the advantage of this solution is the reduced size of the rotating system resulting in a radius of the order of 3 m.

The 'Upstream Scattering' Gantry

By placing the devices for lateral broadening of the beam ahead of the last bending magnet, one can try to eliminate the long drift distance between the last bending magnet and the isocenter and reduce the radius of the rotating structure (Fig. 2d).

Due to the large deterioration of the phase space (multiple scattering and energy spread) caused by the spreading and range modulation devices, the beam optics in this case is rather dif-

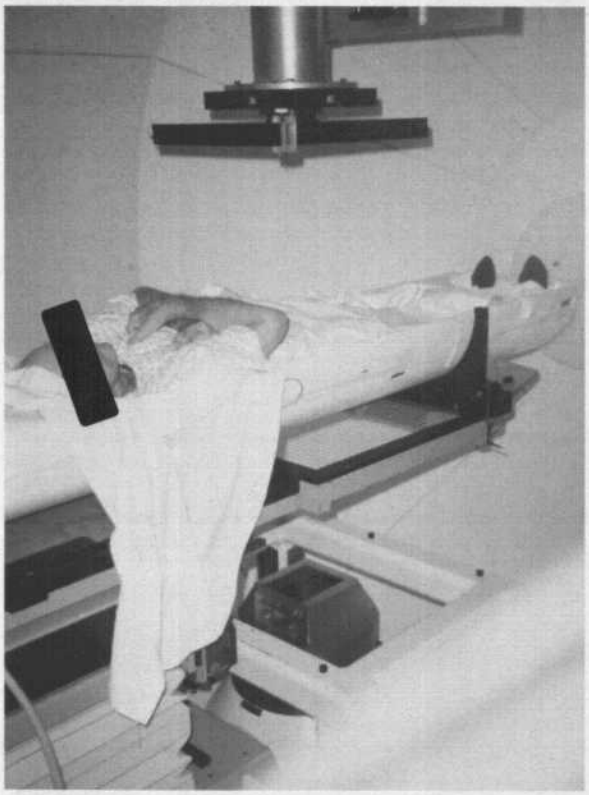

Fig. 4. Photograph of a patient being treated on the Loma Linda gantry, the only gantry presently operational in the world. Courtesy of J.M. Slater [1]

ficult to handle. The scattered beam must be transported through the last portion of the gantry while preserving a good homogeneity of the dose field at the isocenter. In order to accommodate a maximum field size capable of covering most targets, the last bending magnet has to be designed not only with a large pole face but also with an unusually large pole gap.

Gantry solutions which place scatterers in the beam before bending it onto the patient were studied and proposed independently by Enge [11] and Jongen [6]. The gantry radius for these solutions is estimated to be of the order of 3 or 4 m. The major disadvantage of the upstream scattering design is the large size of the last bending magnet needed to contain the broadening of the beam in both lateral directions, which results in an increase in weight and power consumption.

The 'Upstream Scanning' Gantry

If the beam optics is combined with dynamic scanning of the beam and the beam is only scanned in the dispersive direction of the last bending magnet, the gap of the magnets can be as small as permitted by the size of the unscanned beam (Fig. 2e). The other transverse direction can then be scanned mechanically, either by moving the patient or by rotating the last bending magnet and the nozzle. Designs based on these ideas were proposed independently by Pedroni [12] and Jongen [6].

The 'Eccentric' Gantry

A possible reduction of the gantry diameter can be achieved by mounting the patient support eccentrically on the gantry (Fig. 2f).

A gantry design with a cylindrical patient chamber mounted eccentrically on the gantry was studied by the proton therapy group of Tsukuba [13]. It is shown in Figure 5. The devices for the passive scattering method, which are usually mounted along the radius of the rotating structure, can here be distributed along its diameter, thus reducing the radius of the gantry by about a factor of two. The price paid for this solution is the extra mechanics needed to keep the patient support horizontal at all times, and an important safety issue has to be solved, namely, quick access to the patient chamber, in case of failure of the motors which rotate the gantry.

Gantries with a 90° Bending Magnet

The possibility of reducing the rotating beam transport system to a single 90° bending system, which directs the beam onto a patient support rotating with the magnet, was discussed in an early phase of the Italian TERA project. The special merits of this design (Fig. 2g) would be low weight of the rotating structure and extreme simplicity of the beam transport system. If used for the scattering foil technique, the diameter of the structure would, however, be as big as for the "long throw" solutions (Fig. 2a and b) discussed above.

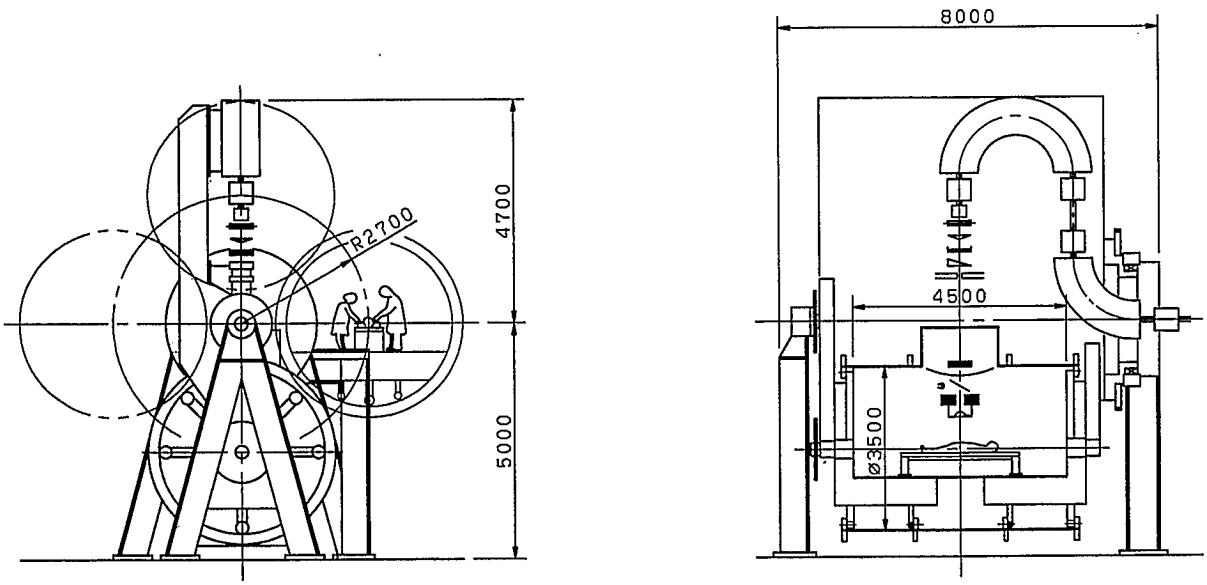

Fig. 5. Sketch of the proposed gantry for Tsukuba. Courtesy of S. Fukumoto [16]

A similar idea has been proposed by Martin [14]. His solution conceives a single rotating 90° bending magnet and limits the use of the angle of rotation to a few selected directions which brings the beam directly into different treatment rooms (Fig. 2h, see also Chapter 22). That way, he avoids moving the patient support in space.

Superconducting Solutions

Important developments in the future may be based on superconducting [15] and pulsed magnets [16]. These new technologies could be used to reduce drastically the size the beam transport system and the accelerator. Blosser proposed to rotate the whole accelerator, a superconducting cyclotron, around the patient. That such a solution is possible in principle has been demonstrated by the successful operation of his gantry for neutron therapy at the Harper Hospital in Detroit [15]. For proton therapy, one would, however, need to rotate a cyclotron of much higher energy.

The Compact Gantry at PSI

Figure 6 shows the cross-section of the PSI gantry. The beam is first bent by two 35° bending magnets shifted parallel to the gantry axis at a distance of 1.27 m, and then bent towards the patient with a 90° bending magnet. The patient table is mounted on the front wheel of the gantry and is off-center by 1.1 m. When the gantry rotates the patient table at the nominal isocenter (defined as the crossing point of the beams in the reference frame of the patient table) moves on a circle of 1.1 m. A mechanical counter-rotation maintains the patient table horizontal at all times during rotation of the gantry. By mounting the table eccentrically on the gantry and by integrating the scanning of the beam into the beam optics of the beam transport system, the diameter of the rotating structure could be reduced to 4 m, the smallest size proposed so far for a gantry using non-superconducting technology.

The PSI gantry is specifically designed for the spot scanning technique (see succeeding chapter). The scanning of the beam is performed in

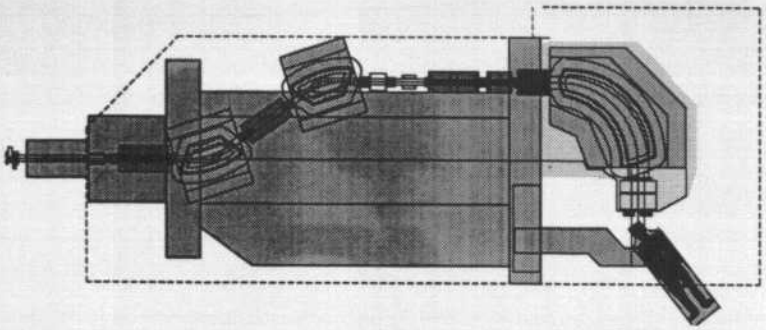

Fig. 6. Cross-section of the PSI gantry

one transverse direction by the action of a sweeper magnet placed before the last 90° bending magnet. A range shifter system moves the Bragg peak in depth. The third scanning motion is performed by moving the patient table itself.

The 90° bending magnet has been carefully designed to achieve a parallel scanning of the swept beam at the isocenter. The PSI scanning system is in this way completely Cartesian, with an infinite source-to-skin distance. The beam optics of this gantry is described in more detail in the literature [17].

The PSI facility started its operation in summer 1994. It will soon be the second facility in the world working with a proton gantry. Figure 7 shows a photograph of the gantry during commissioning.

General Considerations for Gantry Designs

One of the most important issues to be considered in the design of the gantry is the beam optics. At the coupling point of the beam to the gantry the beam should be symmetric in phase space and achromatic in order to allow the transport of the beam through the gantry independent of the gantry angle. For the spot scan technique, one should try to focus the beam directly at the isocenter in both transverse directions, whereas with scatterer foils the focus should be at the starting point of the beam spreading system. Both solutions require a double non-dispersive focusing of the beam at the end of the gantry beam

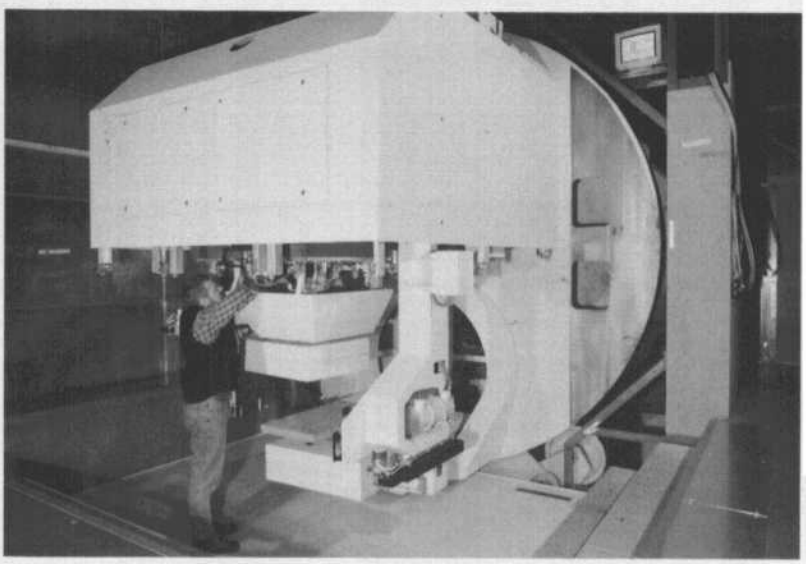

Fig. 7. Photograph of the PSI gantry during commissioning in summer 1994

line. If both scanning and scattering techniques are planned for the same gantry, two different beam optics solutions must be simultaneously available in the same layout.

Another important issue is mechanics. This includes precision of the mechanical design of the gantry and the patient table. The structure should be very rigid in order to avoid misalignment errors of the beam line elements during rotation.

The degrees of freedom necessary to direct the beam on the supine patient need also careful considerations. For example, the PSI gantry allows for an additional horizontal rotation of the patient table for treatments in the head. This permits to direct the beam onto the patient's head essentially from any direction.

At least 3 meters of free space are needed to rotate the beam line and the nozzle under the patient table. One should, therefore, pay attention to the potential risk of patients or personnel falling into the "pit" underneath the patient table. A moving platform covering the gantry pit or a protection shell mounted around the patient table can be used to eliminate this hazard. A false floor solution capable of covering the gantry pit permanently in all treatment situations is difficult to realize, especially if one chooses to treat the patients with two independent beam angles and mounts nozzle and diagnostic devices very close to the patient. The alternative in this case is to treat with an open pit and to provide the necessary safety by not allowing the patient to leave the couch during treatment in the highest position, i.e., when being treated with the beam coming from below.

The devices to control the positioning of the patient with respect to the beam are also important design components. The solution adopted at PSI is to position the patient outside the treatment room using a dedicated CT-unit. The patient, already positioned in the couch, will then be transported into the treatment room on a special vehicle. The mechanism of the CT-table, the proton gantry and the patient transporter have been designed to allow an automated and reproducible transfer of the coordinates between all these devices. The positioning of the patient will also be checked directly on the gantry using a retractable X-ray device or by directly using the proton beam for proton radiography images ([18], see also Chapter 31).

Conclusions

The design of a proton gantry is a complex task and requires careful optimization of many different parameters. These are not only purely technical aspects, such as the type of accelerator or the beam quality, but also more general considerations, such as the scope of the facility, whether a major center with broad research activities or a small facility for special indications under strong economical constraints is to be planned. The field has just started to unfold, so that significant progress can be expected in the future.

References

1 Slater, J.M., Miller, D.W., and Archambeau, J.O. Development of a hospital-based proton beam treatment center. Int. J. Radiat. Oncol. Biol. Phys. 14, 761–775, 1988.

2 Schneider, U. and Pedroni, E. Proton radiography as a tool for quality control in proton therapy. Med. Phys. 22, 353–363, 1995.

3 Urie, M., Goitein, M., and Wagner, M. Compensating for heterogeneities in proton radiation therapy. Phys. Med. Biol. 29, 553–556, 1984.

4 Product Genesis Inc., 300 Bent Street, Suite 200, Cambridge, MA 02141, USA*.

5 Chu, W.T., Staples, J.W., Ludewigt, B.A., Renner, T.R., Singh, R.P., Nyman, M.A., Collier, J.M., Daftari, I.K., Kubo, H., Petti, P., Verhey, L.J., Castro, J.R., and Alonso, J.R. Performance Specifications for Proton Medical Facility, Lawrence Berkeley Laboratory Report, LBL-33749, March 1993.

6 Jongen, Y. Ion Beam Applications, Chemin du Cyclotron 2, Louvain-La-Neuve, Belgium*.

7 Koehler, A.M. Preliminary design study for a cork-screw gantry. Proc. 5th PTCOG Meeting, April 1987, Berkeley. Lawrence Berkeley Report LBL-22962, pp. 147–158.

8 Amaldi, U. and Silari, M. (eds.) The TERA Project and the Center for Oncological Hadrontherapy. Published by INFN – LNF – Divisione Ricera, SIS – Ufficio Pubblicazioni, Frascati (Roma) Italy, 1994.

9 Farley, F.J.M. Advanced European medical facilities, published in Proc. 4th European Particle Accelerator Conference, Suller, V. and Petit-Jean-Genaz, Ch. (eds.), London, June 27–July 1, 1994, World Scientific, Singapore, pp. 417–421.

10 Graffman, S., Brahme, A., and Larsson, B. Proton radiotherapy with the Uppsala cyclotron: Experience and plans. Strahlentherapie 161, 764–770, 1985.
11 Enge, H. Deuteron Inc., 25 Hillside Rd., Lincoln MA 01773, USA.*.
12 PSI Life Science Newsletters of 1989 through 1993, PSI, Villigen, Switzerland.
13 Fukumoto, S. Proton Medical Center, University of Tsukuba, Japan, private communication.
14 Martin, R.L. ACCTEK Inc. 901 S. Kengsinton, Lagrange IL 60525, USA.*
15 Blosser, H.G., Medical cyclotrons. Physics Today, 70–73, October 1993.
16 Picardi, L., Ronsivalle, C., Vignati, A., Silvestrov, G., Vsevoloszkhaya, T., and Bartolini, R. Preliminary design of a very compact protosynchrotron for proton therapy. To be published in Proc. 4th European Particle Accelerator Conference, Suller, V. and Petit-Jean-Genaz, Ch. (eds.) London, June 27–July 1, 1994, World Scientific, Singapore, pp. 2607–2609.
17 Pedroni, E. and Enge, H. Beam optics design of a compact gantry for proton therapy. Med. Biol. Eng. Comp. 33, 271–277, 1995.
18 Pedroni, E., Bacher, R., Blattmann, H., Böhringer, T., Coray, A., Lomax, A., Lin, S., Munkel, G., Scheib, S., Schneider, U., and Tourovsky, A. The 200 MeV Proton therapy project at PSI: Conceptual design and practical realization. Med. Phys. 22, 37–53, 1995.

* presentations and material distributed at PTCOG (Proton Therapy Cooperative Group) meetings. Information available form the editor of the Newsletter 'Particle': Janet Sisterson, Harvard Cyclotron Laboratory, Cambridge, MA 02138, USA.

24 Beam Spreading Methods

B. LUDEWIGT

Lawrence Berkeley Laboratory, University of California, Berkeley, CA, USA

Introduction

Beams of heavy charged particles, protons and heavier ions, have the potential to achieve a higher degree of dose localization than is possible with conventional radiation, due to the sharp peak in the depth-dose distributions of monoenergetic beams and their lower lateral scattering. The Bragg peak must be spread out into a high dose region which covers the entire target volume. This is achieved by modulating the range of the beam, i.e., generating radiation fields containing a mix of particles with different residual energies. Various methods for shaping the depth-dose distribution are described in the following section.

Ion beams are generally tightly focused for the transport into the treatment room where the beam must be spread laterally in order to generate a large radiation field. Passive beam delivery systems, which are based on scattering foils for spreading the beam across the entire treatment volume were the first to be used clinically. A more recent approach are dynamic beam spreading systems, such as raster scanning, which move a beam spot in a predetermined way across the treatment area. Both methods will be discussed as will three-dimensional pencil beam scanning methods.

Tumor sites treated with ion beams include small ocular melanomas and large sites like prostate and biliary tract. The required radiation fields vary accordingly from 1 cm^3 to several liters and differ in their specifications for dose uniformity and lateral dose fall-off. A variety of beam spreading methods are used to serve these diverging needs. Important considerations for the design of beam spreading systems are the sharpness of the lateral and the distal dose fall-off, the beam utilization efficiency, neutron production, beam fragmentation, accuracy of the delivered dose distributions, and patient safety. Constraints are presented by the accelerator, the beam transport system, and the available space in the treatment room.

Before choosing a particular beam spreading system it is essential to ask how well the high dose region is expected to conform to the target volume and how much flexibility is desired in shaping the dose distribution. As has been shown recently [1], the conventional goal of delivering uniform dose distributions with the sharpest possible dose fall-off does not necessarily represent the best treatment. In order to optimize the biological effect, that is to maximize the tumor control probability for an acceptable level of complication probability, it may be necessary to deliver more complex dose distributions. This can only be achieved by three-dimensional pencil beam scanning.

The development of beam scanning systems has also been motivated by the desire for isocentric rotating gantries with a small diameter. The large diameter of conventional isocentric gantries, such as the ones built at Loma Linda University Medical Center (LLUMC) [2], is largely due to a long drift space required by the beam spreading system to generate large fields. New ways are being explored to reduce the overall gantry diameter by incorporating the beam spreading system into the gantry itself.

Range Modulation

The depth-dose distribution deposited by a monoenergetic ion beam in water or tissue and described by the Bragg ionization curve [3] exhibits a sharp peak at the end of the range. The width of the unmodulated peak, which is only used for treating very small lesions, depends on the energy spread of the beam and the energy straggling introduced in the tissue. For most clinical applications the Bragg peak must be spread out in depth in order to cover the target volume. The range of the beam particles must be modulated in such a way that the desired depth-dose profile results.

For proton beams a uniform dose coverage of the target volume is usually desired since it is assumed that the biological effectiveness does not significantly change as a function of depth. A uniform or "flat" distribution can be produced by superimposing individual Bragg curves that are spaced 1 to 5 mm apart depending on the width of the Bragg peak. The weights of the individual contributions (beam weights) can be determined by a least-squares fitting procedure which minimizes the difference between the desired dose level and the sum of the individual contributions at all points in the spread-out Bragg peak.

For ions heavier than protons the dependency of the biological effectiveness on the ionization density or linear energy transfer (LET) must be taken into account. Towards the end of the range the cell killing probability is markedly increased. This needs to be compensated for by reducing the dose towards the distal end if uniform cell killing throughout the target volume is to be achieved [4, 5].

Bragg peaks are spread out by inserting absorbing material of different thicknesses before the beam enters the patient. The desired depth-dose distribution results when the fraction of time each section is in the beam (assuming a constant beam current) is proportional to the beam weight for the corresponding residual range. For treatments with helium ions at LBL [5] a computer-controlled device was used to insert absorber plates from a binary set of thicknesses. In this method, whenever the dose corresponding to the beam weight has been delivered at a particular setting, the absorber thickness is changed and the Bragg peaks are sequentially stacked in depth. This method makes it easy to change or adjust a depth-dose distribution by changing the beam weights contained in a control system data file.

Widely used is the so-called modulator wheel, a fan-shaped stepped and rotating absorber, which was first proposed by Wilson [6] and later

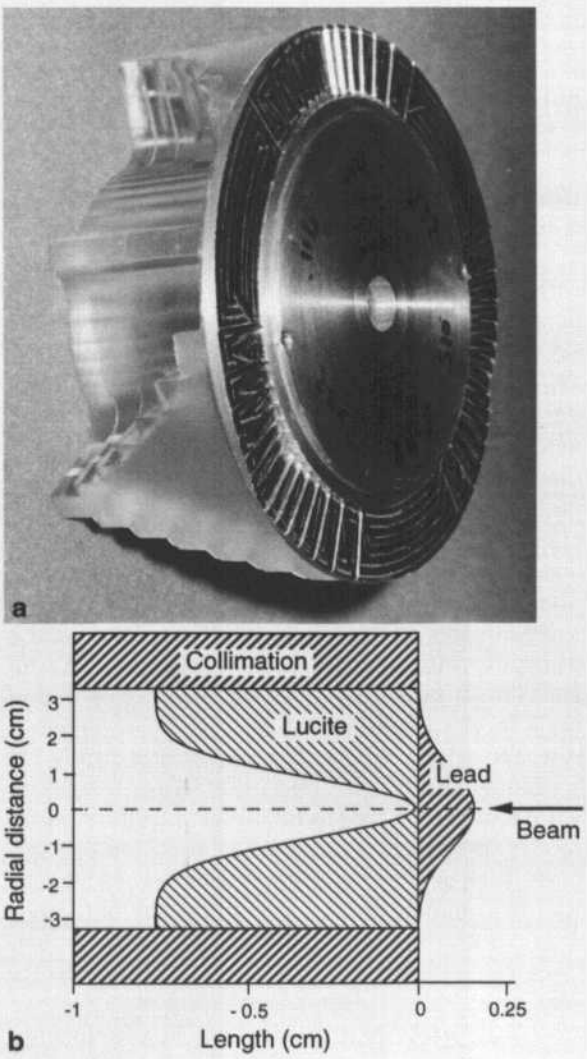

Fig.1 a) Modulator wheel with scattering compensation. The beam passes through the stepped part off axis. Courtesy of M. Wagner, HCL. **b)** Schematic cross section of a bimaterial contoured filter. Courtesy of B. Gottschalk, HCL

implemented at the Harvard Cyclotron Laboratory (HCL) [7], at LBL, and more recently at LLUMC [8] and other facilities. A new and special version is shown in Figure 1a. The beam is intercepted by the stepped part of the modulator with the thickest section pulling the beam back to the proximal end of the spread-out Bragg peak (SOBP). The modulator wheel is rotated at typically 100 rpm in a cyclotron beam while the pulse structure of a synchrotron may require ten times that frequency. It is designed such that the angular coverage of a specific thickness is proportional to the beam weight assigned to the corresponding range. The simplicity of the mechanical device and the fact that the target volume is filled simultaneously at all depths are the main advantages of this method compared to sequential beam stacking.

For heavy ion beams the degradation of the beam quality due to fragmentation in the scattering and range shifting material is an important concern. For the same reduction in range a high-Z (atomic number) material produces less fragmentation than a low-Z material. On the other hand the heavier material produces more scattering. As a result the use of high-Z materials is often advantageous for heavy ion beams whereas low-Z materials are preferred for proton beams. Bar ridge filters [9], which consist of narrow parallel ridges (Fig. 2), have been machined from brass for the range modulation of heavy ion beams. Particles going through different sections of a ridge lose different amounts of energy. By giving the ridges the correct shape the desired depth-dose distribution is produced. Care must be taken to avoid imaging the ridges and to ensure complete mixing of the particles with different residual ranges at the patient location. A bar ridge filter must be made from metal in order to limit the height of the ridges. This is important to make them sufficiently narrow and to machine them precisely. Metal bar ridge filters have also been used with proton beams [10–12].

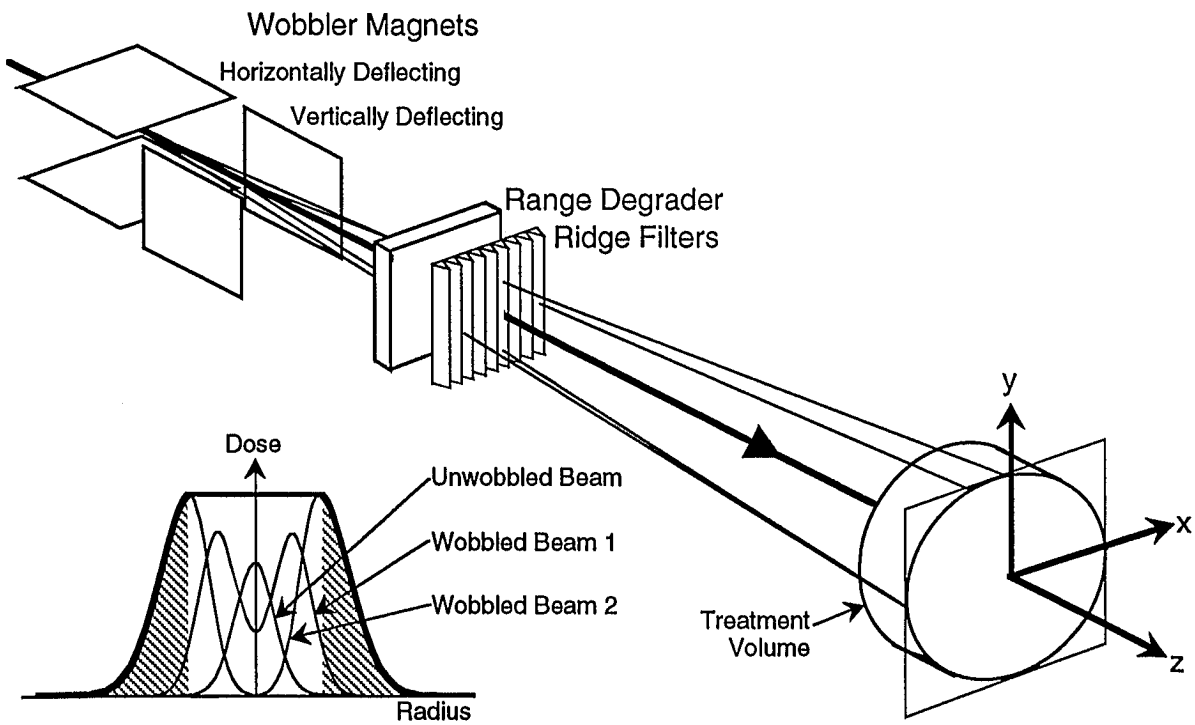

Fig. 2. Scheme of the LBL wobbler beam delivery system

Scattering Systems

A narrow ion beam is most simply spread into a large radiation field for patient treatments by directing it through a scattering foil. Multiple Coulomb scattering leads to approximately Gaussian distributions for the scattering angle and subsequently produces a two-dimensional, Gaussian dose distribution at isocenter [9, 13]. For a radiation treatment only the innermost part of the Gaussian distribution can be used since the dose distribution must be sufficiently uniform. This results in a low beam utilization efficiency, about equal to the uniformity in percent [9]. For example, for a required dose uniformity of ± 2.5%, which corresponds to the part of the Gaussian distribution larger than 95% of the peak value, the beam utilization efficiency is 5%. The single scatterer method is often used for generating small treatment fields where the beam utilization efficiency is not important. Examples are eye treatment beam lines at the Harvard cyclotron, the Loma Linda University proton therapy facility, the Crocker cyclotron at UC Davis and others.

For the generation of larger fields a higher beam utilization efficiency is needed. Double scattering methods have been employed for spreading proton [12, 14, 15] and heavier ion beams [16]. A first scatterer spreads the beam such that the projected full width at half maximum at the patient location is about equal to the desired field size. A second scatterer is needed to transform the Gaussian distribution into a "flat" one with steep lateral fall-offs. In the past this was facilitated by mounting occluding rings onto the second scatterer in order to absorb particles from the center of the distribution. This method, which is described in detail in references [9] and [14], achieves a beam utilization efficiency of typically 20%.

A new and improved method in which the second scatterer with the occluding ring assembly is replaced by a "contoured filter," a bimaterial scattering foil, has successfully been developed at the HCL [17] and adapted at LLUMC. The design of the bimaterial filter is illustrated in Figure 1b. A foil made of a high-Z material (e.g., lead), which decreases in thickness from the center towards the outside, scatters more particles from the central ray towards the outside than in the reverse direction, thus flattening the Gaussian distribution produced by the first scatterer. The different energy losses of particles traversing the foil at different distances from the center are compensated for by combining the high-Z and strongly scattering foil with a foil made from a low-Z material (e.g., Lucite) which produces much less scattering. By increasing the thickness of the Lucite from the center towards the outside one can keep the energy loss for all particles constant, independent of the distance to the central ray, while simultaneously achieving the desired scattering properties. The bimaterial scattering system avoids the loss of beam particles, in contrast to an occluding ring assembly, and achieves beam utilization efficiencies approaching 50%. The idea of using two materials with different scattering and energy absorbing properties has also been applied to the modulator wheel [18] as shown in Figure 1a. Beam particles traversing a modulator wheel made from low-Z material are scattered to a varying degree depending on how much material they traverse. By attaching lead foils of appropriate thickness to each step of the modulator wheel the scattering strengths of all wheel segments can be equalized while still providing the needed range modulation. The compensated modulator can then be used as the first scatterer. That way, the range modulator is placed where the beam diameter is smallest and the angular confusion is significantly reduced [5, 9, 18] improving the lateral dose fall-off.

For the modulation of proton beams it has been proposed [19] to use one modulator wheel to provide a range of spread-out Bragg peak widths. The idea is to switch the beam "on" when the steps with the correct thickness are in the beam and to switch the beam "off" at other times. In general, this method does not work for beams of ions heavier than protons which exhibit a tail dose beyond the Bragg peak due to fragments.

A scattering system with a fixed compensated modulator and a bimaterial contoured filter provides dose distributions with the optimal uniformity, in depth and laterally, only for a specific beam energy. The versatility of the system can be greatly improved by installing sets of modulator

wheels and scattering foils such that they can be remotely moved into the beam line. A complete scattering package is under development at the Harvard Cyclotron Laboratory [20]. One of its innovative features is the variable positioning of the contoured filters which are mounted on rails for adjusting the scattering configuration for different beam energies.

Dynamic Beam Spreading Systems

Large treatment fields can also be formed from narrowly focused beams by magnetic deflection. Magnetic beam spreading methods have been investigated and developed for mainly two reasons. First, they offer more flexibility then the passive scattering methods. Different field sizes can be generated and different beam energies can be handled by simply changing the magnet currents. Second, magnetic methods allow to minimize the amount of material in the beam thus avoiding the degradation of the beam quality caused by energy straggling and the generation of unwanted radiation through nuclear reactions. For ion beams the energy straggling due to scattering foils can generally be neglected. The relatively modest amount of material does not significantly change the clinical beam parameters, in particular, the width of the distal fall-off. For proton beams nuclear reactions in the scattering foils lead to a small loss of primary protons and the generation of neutrons. Both effects are usually unimportant. Although in specific situations additional shielding may be required, the neutron contribution from the scattering foils is minor compared with other neutron sources in the treatment room.

For beams of heavier ions the situation is quite different. Here the main problem associated with the use of scattering foils is nuclear fragmentation of the primary beam particles. Due to their lower charge the fragments exhibit a lower specific energy loss than the primary particles which results in a longer range and a dose beyond the Bragg peak, i.e., a degradation of the beam quality. This disadvantage is exacerbated by the fact that beams of heavier ions require more scattering material than proton beams in order to produce the same scattering angle distributions. Various magnetic beam spreading methods and their advantages and disadvantages are discussed below.

Dynamic beam spreading systems use dipole magnets in order to generate large fields by deflecting a narrow pencil beam and distributing the beam particles evenly. The first such system was tried more than 35 years ago [21]. It utilized a pair of dipole magnets with orthogonal magnetic fields. The beam was steered by currents of sawtooth waveform causing it to describe a periodical pattern in a plane orthogonal to the beam axis. Though the principle was successfully demonstrated the system was never used in a clinical program.

Extensively used in the heavy ion clinical trial at the Lawrence Berkeley Laboratory (LBL) was the so-called "wobbler" system [22]. Since beam fragmentation is of great importance for heavy ion beams, the development of magnetic beam spreading systems aimed at enhancing the quality of the radiation field was a major focus of the technical development efforts at LBL. The wobbler, schematically shown in Figure 2, consists of two dipole magnets powered sinusoidally with a 90° phase difference. This results in a circular motion of the beam around the zero-field beam axis. By changing the magnetic field strength in both magnets ring-shaped dose distributions with different radii can be deposited. Their superposition results in a uniform field if the correct amount of dose is delivered in each ring. The wobbler system maximizes the beam utilization efficiency for circular radiation fields for two reasons: first, no beam particles are absorbed or lost besides the ones scattered outside the target area and absorbed in the patient collimator; second, the diameter of the field can easily be adjusted by changing the magnet currents to fit the size of the target volume.

A dynamic beam spreading system like the wobbler is inherently more complex than a passive scattering system. Beam position and intensity have to be carefully monitored and controlled. Small deviations from the concentricity of the rings, i.e., differences of more than 0.5 mm between the positions of the centers, can cause a significant tilt in the dose distribution. For exam-

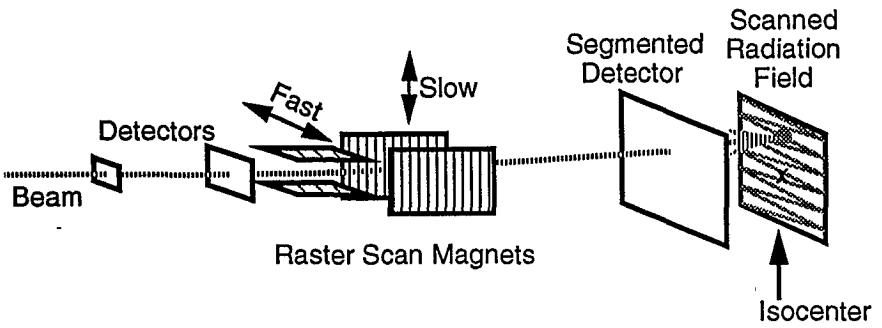

Fig. 3. Scheme of the LBL raster scanning beam delivery system

ple, a shift of 1 mm between the center of the outermost ring and the inner wobbles can lead to a dose difference between the two opposing sides of the radiation field of about 7%, comparable to what is observed for a double scattering system with occluding rings. Similarly, the ions must be uniformly distributed around each ring and the total number of particles in each ring must be within typically ± 2% of the request for satisfying the dose uniformity requirement of ± 2% for the combined field. At the Bevalac synchrotron at LBL this was achieved by running the wobbler at a frequency of 60 Hz and delivering at least several beam spills at each magnet current setting. The beam was clamped off within less than a wobbled beam rotation, when the desired number of ions at that wobbler setting had been delivered.

In order to monitor the actually delivered dose distribution, real time dosimetry devices with a sufficient spatial resolution, for example highly segmented ionization chambers, are needed [23]. Wobbler systems are installed at the Heavy Ion Medical Accelerator (HIMAC) at Chiba, Japan [24].

Many other patterns are also well suited for "painting" uniform dose distributions with a narrow beam. Raster scanning systems have been developed at several institutions [25–27]. The LBL system [9, 28], shown schematically in Figure 3, employed two dipole magnets for deflecting the beam in two orthogonal directions. The magnets were mounted such that they could be rotated up to 90°. However, in the following it is assumed that the beam was scanned horizontally and vertically as indicated in Figure 3. The system was matched to the pulse structure of the Bevalac accelerator, a 1-second spill every 4 seconds. An entire port was scanned in one beam pulse sweeping the field vertically in less than the accelerator spill time. The horizontal scan was performed at a constant scan speed of 2400 cm/s, equivalent to a frequency of 30 Hz for a ± 20 cm field. The resulting scanning pattern produces a uniform dose distribution of better than ± 2.5%, within one complete scan, provided the distance between parallel lines is smaller than the sigma of the Gaussian beam profile. The total number of scans necessary for a treatment depends not only on the maximum available beam current, which determines how much dose can be delivered per scan, but also on how well the beam current and the spill structure can be controlled. It may be necessary to scan the field many times in order to average out dose variations due to fluctuations in the beam current and to deliver the requested total dose within acceptable error margins. The basic field shape of a raster scanning system is a rectangle, the aspect ratio of which can be varied by adjusting the maximum fields in the scanning magnets. This leads, in general, to a better beam utilization efficiency than circular fields. Contrary to double scattering systems or circular wobbler systems, the uniformity of the dose distribution is not affected by small variations in the position of the zero-field central beam axis from one beam pulse to the next during the treatment, since the field is completely painted within every beam pulse.

Three-Dimensional Conformal Dose Delivery

With the beam delivery techniques discussed in the previous sections a high degree of conformation of the high dose region to the target volume is achieved. However, normal tissues upstream of the target volume receive an unnecessary dose when the width of the SOBP is fixed across the field (cf. Fig. 4a). The fixed modulation method causes the spread-out Bragg peak to cover, in general, some volume upstream of the tumor. Techniques for avoiding this are discussed in this section. The potential clinical benefits associated with the improvement in dose localization have been investigated in a number of studies [29–32].

The variable modulation method (Fig. 4b) employs a multileaf collimator whose leaves can be repositioned many times during a treatment. Using a slightly spread Bragg peak the target region is covered in layers, starting from the distal end, by reducing the range of the beam in a stepwise fashion. Each layer is shaped by the multileaf collimator which leads to the trimming of the unwanted radiation. The optimal value of the width of the miniature SOBP, i.e., the thickness of a layer, depends on the desired treatment time, size and shape of the target volume.

The variable Bragg peak modulation as described above works only with proton beams. For heavy ion beams, which suffer from fragmentation and exhibit a tail in the depth-dose distribution beyond the Bragg peak, the tail dose associated with an upstream layer contributes to the dose in the layer behind it producing a nonuniform dose distribution there. However, in this case the desired uniform dose throughout the target volume can be achieved as the sum of nonuniform distributions deposited in each layer. A beam scanning system, which allows varying the dose as a function of position, is needed for delivering such dose distributions (Fig. 5).

Beam scanning techniques are being developed and implemented for treatments with heavier ions as well as for proton therapy because of their unique flexibility and capability in shap-

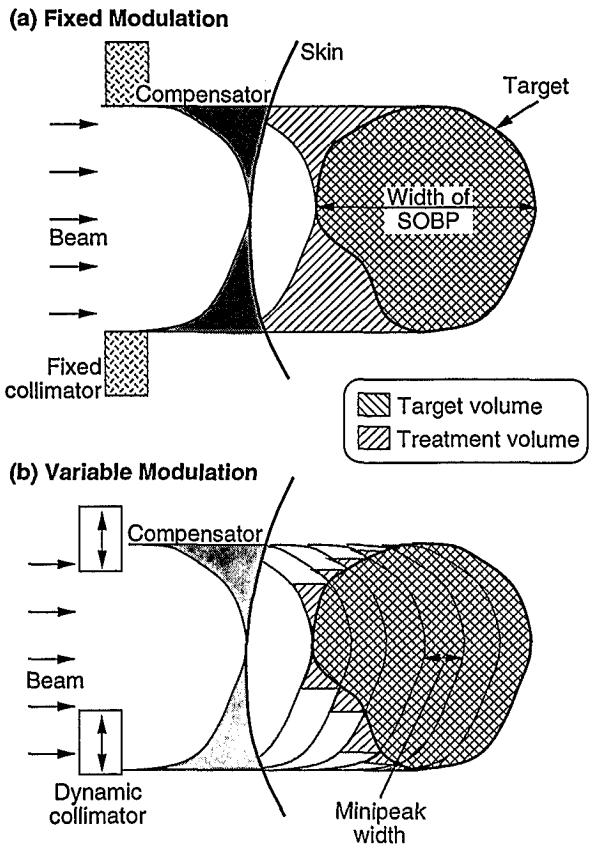

Fig. 4. **a)** Fixed modulation method producing a cylindrical treatment volume which is equal in length to the thickest part of the target volume. **b)** Variable modulation method using a multileaf collimator to trim the treatment volume

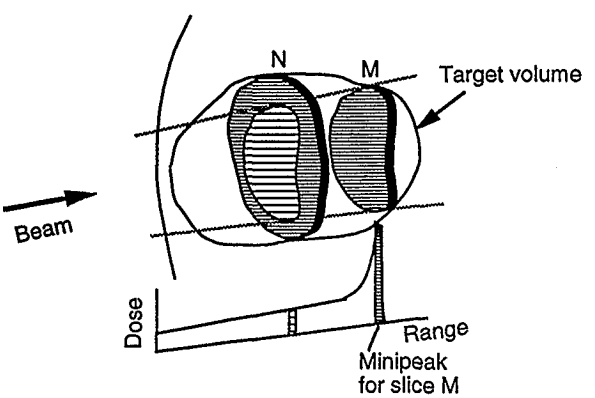

Fig. 5. Schematic view of three-dimensional conformal therapy delivery illustrating different dose regions in a target volume scanned in axially stacked layers

ing three-dimensional dose distributions. The maximum lateral dose gradient which can be achieved depends on the diameter of the beam. Pencil beam scanning offers full electronic control of the dose delivery and eliminates the need for patient collimators and compensating boli.

A beam scanning system which is used for three-dimensional conformal dose delivery must control the dose deposition as a function of beam position much more tightly than a scanning system which is used for simply spreading the beam into a flat distribution The raster scanning system developed at LBL for the heavy ion radiotherapy program [9, 28, 33] achieved the necessary control of the dose deposition by modulating the scanning speed. The depth scan was performed by inserting range shifting material in the beam. The data for controlling the scan speed, which is proportional to the inverse of the dose for a constant beam current, were downloaded for all layers into the memory of the raster scanner interface before the start of the treatment. Also implemented was the capability of modulating the beam extraction from the accelerator, i.e., the beam current. This provided an alternative method of controlling the dose delivery, made it possible not to deposit dose in a particular region, and increased the dynamic range when used in conjunction with the scan speed modulation. A multileaf collimator was added to the LBL system for safety reasons and for providing the option of treating with a relatively wide beam by using the multileaf collimator for defining the lateral radiation field boundaries. Provided that the pencil beam is narrow enough such a device is not needed. In fact, the narrowest lateral fall-offs can be realized with optimized pencil beam scans without a field defining collimator. Although the LBL scanning system in its conformal treatment delivery configuration was tested and dose distributions were measured in phantoms, it was never clinically implemented due to the shutdown of the Bevalac in 1992.

A second major motivation for the development of beam scanning systems is the possibility of realizing a compact isocentric gantry which has a significantly smaller diameter than conventional ones by incorporating the beam scanning into the last section of the gantry optic. This approach has been taken at the PSI in Villigen where the gantry diameter could be reduced to 4 meters compared to the 12 meter diameter of the world's first gantry for proton therapy in Loma Linda (cf. Chapter 23 for details).

PSI's scanning system is operated in the spot scanning (also called voxel scanning) mode. Magnet current, patient positioner, and energy absorber are set for filling a certain voxel before the beam is switched on. When the predetermined number of protons has been delivered, the beam is switched off by energizing a kicker magnet and the beam centroid is moved to the next position or voxel. The fastest scanning direction is the magnetic beam scan, the second fastest the range shifting or depth scan, and the least frequent scan movement is the one of the patient. The voxel scanning method differs from raster scanning in that it is not a continuous scan but the beam is switched off before being moved to the next voxel. Since no radiation is being delivered during the magnet setting time until the new position has been established, voxel scanning may lead to longer treatment times than raster scanning.

At GSI Darmstadt (Germany) a raster scanning system has been developed for a planned clinical program for heavy ion radiotherapy (see also Chapter 36). The goal is to build an active beam delivery system based on magnetic beam scanning and on energy variation by the accelerator for conformal treatments. The target volume is scanned in layers which are stacked in depth. When a layer has been scanned the new beam energy for irradiating the next layer is requested. The lateral scan is performed by two dipole magnets located 12 m upstream of the patient location. Each layer is scanned in a zig-zag fashion (Fig. 3) but the path of the beam is optimized in order to accommodate irregularly shaped areas. Additional scan lines which provide a shortcut to the next regular line along the border of the target area are introduced. The scan is digitally controlled based on 4096 possible beam positions in each dimension and the beam is moved in a series of small discrete steps. The incoming beam is integrated and a signal is generated when a precalculated value corresponding to the desired dose at the current position has been reached. Then the beam is moved at maximum speed to

the next position where it stays until the desired dose has been delivered. The dose delivered during the sweep is counted as deposited at the following voxel. Since the step size is small compared to the beam diameter, the error introduced is negligible. In contrast to the spot or voxel scanning method the beam is not switched off during the move to the new position. It should also be noted that the step size is much smaller than that in spot scanning systems. The validity of the GSI concept has not only been shown in theoretical studies but also confirmed by the delivery and measurements of a variety of test dose distributions [26, 34].

Conclusion

Beam scanning techniques offer not only conformal treatments and a way of constructing compact gantries, but also a natural way of delivering dose distributions which are shaped according to the results of an optimization procedure. It has been shown that the probability for local control can be maximized while not exceeding given complication rates by optimizing the dose distribution based on biological models [1, 35]. As part of the treatment planning process a biological objective function is maximized (or minimized) by adjusting the Bragg peak density. The optimized Bragg peak density can directly be translated into a scanning pattern and dose values for each voxel. It is important to note that, in general, the optimization procedures based on biological models result in non-uniform dose distributions in the tumor volume and variable dose fall-offs in adjacent healthy organs. Such dose distributions are difficult to produce without pencil beam scanning.

On the other hand, pencil beam scanning has a number of disadvantages compared to simpler beam spreading methods. The sequential irradiation of the target volume leads to longer treatment times, the irradiation process must be much more tightly controlled, the dosimetric requirements are much greater since the dose deposition must be measured with sufficient spatial and temporal resolution, patient and organ immobilization are of greater importance [36], and the treatment planning process must include sophisticated optimization procedures if the advantages of pencil beam scanning are to be exploited.

At the present time, passive beam spreading methods still have a lot of usefulness. They provide excellent field uniformity, good beam utilization, and the flexibility to handle different beam energies. For proton beams variable modulation can be achieved in combination with a multileaf collimator. Beam delivery systems with passive beam spreading and field shaping devices are most easily implemented. Dosimetric requirements are much less stringent and treatments can, in principle, be performed without a sophisticated control system.

However, strong arguments can be made that pencil beam scanning will be a preferred beam delivery method in the future. This method has the potential for administering superior treatments based on optimized dose distributions and it will allow proton therapy to stay ahead of the advances being made in conformal photon therapy. New tools needed for optimizing treatments, dose distributions and scanning patterns [37–40] are being developed and will be available in the near future (cf. also Chapter 30). Biological models and mathematical optimization procedures, mainly aimed at three-dimensional conformal photon therapy but also applicable to ion beam therapy, are being studied and fast workstations which are able to perform the extensive calculations are entering the market.

Furthermore, once the technical challenges as presented by the need for the fast and complex control of the beam scan have been mastered, the best treatments can be delivered with the greatest convenience. Optimized scanning patterns, which will automatically be translated into the control parameters for the beam scanning system, will be included in the output of the treatment planning process. The treatments will be electronically controlled freeing the therapists from the cumbersome handling of mechanical devices such as range compensating boli and patient collimators. Instead, they will be able to focus on patient care.

Both, hardware and software developments are necessary in order to realize this vision. Hardware improvements are mainly needed in the areas of fast beam monitoring and dosimetry, and

fast beam current and beam position control. The availability of treatment planning and optimization software and computer codes for translating the treatment plan into instructions for the beam delivery control system will be crucial for making three-dimensional pencil beam scanning a routine method in a clinical setting.

References

1 Källman, P., Lind, B.K., and Brahme, A. An algorithm for maximizing the probability of complication-free tumor control in radiation therapy. Phys. Med. Biol. 37, 871–890, 1992.

2 Slater, J. M., Archambeau, J.O., Miller, D.W., Notarus, M.I., Preston, W., and Slater, J.D. The Proton Treatment Center at Loma Linda University Medical Center: Rationale for and description of its development. Int. J. Rad. Oncol. Biol. Phys. 22, 383–389, 1992.

3 Bragg, W.H. and Kleeman, R. On the ionization curves of radium. Phil. Mag. 8, 726–738, 1904.

4 Lyman, J.T. Computer modeling of heavy charged-particle beams, in Pions and Heavy Ion Radiotherapy: Pre-Clinical and Clinical Studies, Skarsgard, L.D. (ed.) Elsevier, New York, 1983, p. 139.

5 Ludewigt, B.A., Chu, W.T., Phillips, H.M., and Renner, T.R. Accelerated helium-ion beams for radiotherapy and stereotactic radiosurgery. Med. Phys. 18, 36–42, 1991.

6 Wilson, R.R. Radiological use of fast protons. Radiology 47, 487–491 1946.

7 Koehler, A.M., Schneider, R.J., and Sisterson, J.M. Range modulators for protons and heavy ions. Nucl. Instr. Meth. 131, 437–440, 1975.

8 Coutrakon, G., Bauman, M., Lesyna, D., Miller, D., Nusbaum, J., Slater, J., Johanning, J., Miranda, J., DeLuca, P.M., Siebers, Jr., Siebers, J., and Ludewigt, B. A prototype beam delivery system for the proton medical accelerator at Loma Linda. Med. Phys. 18, 1093–1099, 1991.

9 Chu, W.T., Ludewigt, B.A., and Renner, T.R. Instrumentation for treatment of cancer using proton and light-ion beams. Rev. Sci. Instr. 64, 8, 2055–2122, 1993.

10 Larsson, B. Pre-therapeutic physical experiments with high energy protons. Brit. J. Radiol. 34, 143–151, 1961.

11 Blokhin, S.I., Goldin, L.L., Kleinbok, Y.L., Lomanov, M.F., Onosovsky, K.K., Pavlonsky L.M., and Khoroshkov, V.S. Dose field formation on proton beam accelerator ITEP. Med. Radiol. (Moscow) 15, 64–68, 1970.

12 Inada, T., Hayakawa, Y., Maruhash, A., Ohara, K., Kitagawa, T., Akisada, M., Kawachi, K., and Kanai, T. Vertical proton beam irradiation control system for cancer therapy. Jpn. Acta Radiol. 44, 844–853, 1984.

13 Carlsson, J. and Rosander, D. Effects of multiple scattering on proton beams in radiotherapy. Phys. Med. Biol. 18, 633–640, 1973.

14 Koehler, A.M., Schneider, R.J., and Sisterson, J.M. Flattening of proton dose distributions of large-field radiotherapy. Med. Phys. 4, 297–301, 1977.

15 Gottschalk, B. Capabilities of passive beam-spreading techniques, in Proc. Fifth PTCOG Meeting and the International Workshop on Biomedical Accelerators, December 1–2, 1986, Lawrence Berkeley Laboratory, Berkeley, CA, LBL-22962, 1986, pp. 161–168 .

16 Crowe, K., Kanstein, L., Lyman, J.T., and Yeater, F. A. large field medical beam at the 184-inch synchrocyclotron, Lawrence Berkeley Laboratory, LBL-4235, 1975.

17 Gottschalk, B. and Wagner, M.S. Contoured scatterer for proton dose flattening. Harvard Cyclotron Laboratory, A Preliminary Report 3/29/89, 1989.

18 Gottschalk, B., Koehler, A.M., and Wagner, M.S. Upstream scattering modulation in proton therapy beams, in Proc. International Heavy Particle Therapy Workshop, Paul Scherrer Institute, September 18–20, 1989, Blattmann, H. (ed.), Villigen, Switzerland, PSI-Bericht 69, 1989, pp. 19–23.

19 Gottschalk, B., Koehler, A.M., and Wagner, M.S. private communication 1993.

20 Wagner, M.S. Upstream absorber and modulator. Press at the NIRS Int. Sem. on the Applic. of Heavy Ion Accel. to Radiat. Therapy of Cancer, PTcog XXI, Chiba, Japan, Nov. 14–16, 1994.

21 Larsson, B., Leksell, L., Rexed, B., and Sourander, P. Effect of high energy protons on the spinal cord. Acta Radiol. 51, 52–64, 1959.

22 Renner, T.R. and Chu, W.T. Wobbler facility for biomedical experiments. Med. Phys. 14, 825–834, 1987.

23 Renner, T.R., Chu, W.T., Ludewigt, B.A., Nyman, M.A., and Stradtner, R. Multisegmented ionization chamber dosimetry system for light ion beams. Nucl. Instr. Meth. Phys. Res. A281, 640–648, 1989.

24 Kawachi, K., Kanai, T., Endo M., Hirao, Y., and Tsunemoto, H. Radiation oncological facilities of the HIMAC. Jpn. Soc. Ther. Radiol. Oncol. 1, 19–29, 1989.

25 Blattmann, H., Coray, A., Pedroni, E., and E. Greiner, E. Spot scanning for 250 MeV protons. Strahlenther. Onkol. 166, 45–48, 1990.

26 Haberer, T., Becher, W., Schardt, D., and Kraft, G. Magnetic scanning system for heavy ion therapy. Nucl. Instr. Meth. Phys. Res. A330, 296–305, 1993.

27 Kanai, T., Kawachi, K., Kumamoto, Y., Ogawa, H., Yamada, T., Matsuzawa, H., and Inada, T. Spot scanning system for proton radiotherapy. Med. Phys. 7, 365–369, 1980.

28 Renner, T.R., Chu, W., Ludewigt, B., Halliwell, J., Nyman, M., Singh, R.P., Stover, G.D., and Stradtner, R. Preliminary results of a raster scanning beam delivery system, in Proc. IEEE Part. Accel. Conf., Accelerator and Technology, Chicago, March 1989, pp. 672–674.

29 Chen, G.T.Y., Pitluck, S., and Lyman, J.T. Heavy charged-particle treatment planning, in Biological and

Medical Research with Accelerated Heavy Ions at the Bevalac, 1977–1980, Pirruccello, M.C. and Tobias, C.A. (eds.), Lawrence Berkeley Laboratory, LBL-11220, UC-48, 1980, pp. 325–331.

30 Urie, M.M. and Goitein, M. Variable versus fixed modulation of proton beams for treatments in the cranium. Med. Phys. 16, 593–601, 1989.

31 Blattmann, H., Munkel, G., Coray, A., Böhringer, T., Karasawa, K., Magdeburg, W., Nakagawa, K., Pedroni, E., Phillips, M., Scheib, S., and Seelentag, W. Accelerator plan for medical treatment with charged particles at Kyoto University, in Proc. NIRS Int. Workshop on Heavy Charged Particle Therapy and Related Subjects. Itano A. and Kanai, T. (eds.), Chiba, Japan, July 4–5, 1991, pp. 44–51.

32 Castro, J.R., Petti, P.L., Daftari, I.K., Collier, J.M., Renner, T., Ludewigt, B., Chu, W., Pitluck, S., Fleming, T., Alonso, J., and Blakely, E. Clinical gain from improved beam delivery systems. Radiat. Environ. Biophys. 31, 233–240, 1992.

33 Chu, W.T., Ludewigt, B.A., Marks, K.M., Nyman, M.A., Renner, T.R., Singh, R.P., and Stradtner, R. Three-dimensional conformal therapy using light-ion beams, in Proc. NIRS Int. Workshop on Heavy Charged Particle Therapy and Related Subjects, Itano. A. and Kanai, T. (eds.), Chiba, Japan, July 4–5, 1991, pp. 110–123.

34 Haberer, T. Entwicklung eines magnetischen Strahlführungssystems zur tumorkonformen Strahlentherapie mit schweren geladenen Teilchen (Diss.). GSI-94–09, Gesellschaft für Schwerionenforschung, Report June 1994.

35 Brahme, A., Källman, P., and Lind, B.K. Optimization of proton and heavy ion therapy using an adaptive inversion algorithm. Radiother. Oncol. 15, 189–197, 1989.

36 Phillips, M.H., Pedroni, E., Blattmann, H., Boehringer, T., Coray, A., and Scheib, S. Effects of respiratory motion on dose uniformity with a charged particle scanning method. Phys. Med. Biol. 37, 223–234, 1992.

37 Niemierko, A., Urie, M., and Goitein, M. Optimization of 3D-radiation therapy with both physical and biological end points and constraints. Int. J. Rad. Oncol. Biol. Phys. 23, 99–108, 1992.

38 Webb, S. Optimization by simulated annealing of three-dimensional, conformal treatment planning for radiation fields defined by a multileaf collimator: II. Inclusion of two-dimensional modulation of the X-ray intensity. Phys. Med. Biol. 37, 1689–1704, 1992.

39 Jackson, A., Kutcher, G.J., and Yorke, E.D. Probability of radiation-induced complications for normal tissues with parallel architectures subject to non-uniform irradiation. Med. Phys. 20, 613–625, 1993.

40 Holmes, T. and Mackie, T.R. A filtered backprojection dose calculation method for inverse treatment planning. Med. Phys. 21, 303–313, 1994.

25 Radiation Detectors

W. T. CHU

Lawrence Berkeley Laboratory, University of California, CA, Berkeley, USA

Introduction

Ion beam treatments of humans with radiation require accurate, reliable, and safe methods for controlling the ion beams. An accurate delivery of the prescribed dose is essential for achieving the desired cure and preventing an overdose of radiation. In principle, if the beam is properly tuned and the beam delivery is functioning correctly, one absolute or properly-calibrated radiation detector should be sufficient for measuring the delivered dose. In practice, however, depending on the complexity of the beam delivery system, several detectors, with possibly many subdivided detection elements, are needed for achieving the required level of accuracy and safety.

Radiation detectors that are clinically used perform three main functions:

1. real-time measurement of the delivered dose to the patient in order to terminate the irradiation at the prescribed dose,
2. measurement of the spatial distribution of the radiation delivered in order to ensure that the patient prescription is satisfied,
3. measurement of radiation field parameters at selected points along the beam line for controlling the beam delivery system.

The last function is required as ion beams from the accelerator undergo range changes, spatial deflections, and nuclear interactions before reaching the patient.

From a utilitarian point of view, the radiation detectors may be categorized according to their applications, such as detectors for absolute calibration measurements, dose detectors whose signals are proportional to absorbed dose, radiation detectors that can be used to measure dose after being calibrated for a particular type of radiation, and specialized detectors which measure properties of individual particles, e.g., lineal energy transfer (LET) of the projectile particle. Basic dosimetric detectors are usually used in an integrating mode, but their time response must meet the rapidity requirements of termination of the irradiation procedures. Fast detector response is also called for in controlling dynamic beam delivery or measurement of the time structure of extracted beams from an accelerator. In order to measure the dose delivered to the patient precisely, the dose detectors must measure a quantity proportional to the dose imparted to the patient. They must achieve this without significantly perturbing the radiation field, i.e., without degrading the radiation quality. For light ion beams, which contain many particle species with a wide range of LET values due to fragmentation of the projectile particles, the dose detectors must measure the dose independent of the LET distribution in the beam. Large radiation detectors with fine spatial resolution are important for comparing the prescribed and delivered radiation distributions over the entire treatment area. A required dose accuracy for clinical purposes of $\pm 2.5\%$, measured over a large dynamic range of approximately six orders of magnitude, adds to the complexity of monitoring the radiation.

Many of the radiation detectors described in this chapter have been developed for single particle detection in nuclear physics measurements. Several have been used in the dosimetry of con-

ventional radiation (photons and electrons). How these detectors are used in ion beam therapy is the subject of this chapter. The radiation detectors used in ion beam therapy were described in a recent review article [1], therefore, in this chapter new materials are described more extensively while others are briefly discussed for completeness.

Ionization Chambers

At many ion beam therapy facilities, ionization chambers [2] are often used as the primary dose measuring devices because of their accuracy, reliability and ease of operation. When an ion beam traverses an ionization chamber, it produces ionizations in the gas, which are proportional to the energy loss by the beam, which is in turn approximately proportional to the dose absorbed by the detector. This dose can then be related to the absorbed dose in another medium, such as human tissue, by the ratio of the stopping power of the gas to that of the medium. The ionization charge, Q [Coulomb], produced by the beam passing through such a chamber is proportional to the absorbed dose, D [Gy], which is given by the Bragg-Gray equation [3]:

$$Q = D\varrho V/W$$

where ϱ [kg/m^3] is the mass density, V [m^3] the volume, and W [eV] the ionization energy needed to produce an ion pair. Hence, D can be obtained by measuring Q if the value of W is known.

Therefore, the accuracy of the dose measured using ionization chambers is limited by the accuracy of the W-value. The accurate knowledge of W is particularly important if intercomparisons of clinical results from various centers are to be made. Recently, there have been many studies for accurate determination of the W-values [4–7]. Based on the results of these studies, many facilities have agreed to use a W-value of 34.5 ± 0.7 eV [8] for proton beams (cf. also Chapter 26). The W-value varies for different particle types and velocities. This becomes a critical issue when using heavier ion beams because the beams generally contain a mixture of particles (fragments) at various energies produced in the beam modifying devices. For heavier ions the W-value of 33.7 eV is used [9].

Transmission Ionization Chambers

The most common type of ionization chamber used in ion beam therapy is the transmission type. A typical chamber consists of two parallel planes with an electric field applied between them for collection of ionization charges [10]. The effective mass of the chamber per unit area must be reduced so that the chamber has little effect on scattering or fragmenting the beam particles. A typical chamber is schematically depicted in Figure 1, which is composed of the support body, gas windows, signal and high-voltage planes, and the electrical and gas connections. Thin, nonconducting (e.g., Kapton) foils make up beam entrance and exit windows enclosing a gas volume. Additional foils define a pair of parallel planes and create a known ionization volume. One foil is connected to a high voltage source and the other, a collecting foil, is connected to appropriate elec-

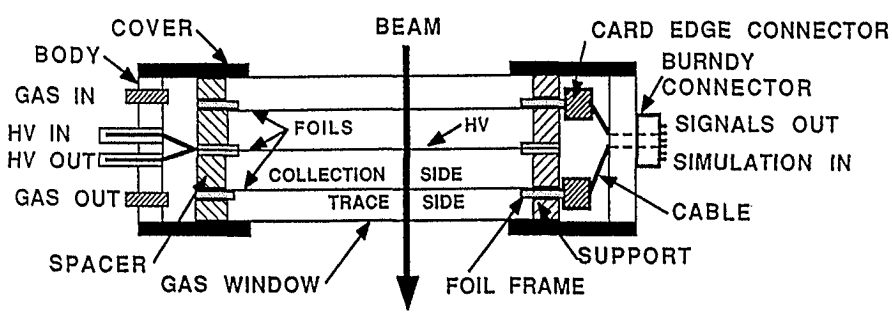

Fig. 1. A cross-section of a typical transmission ionization chamber

tronics for measuring the ionization charge. The properties of the gas used in these chambers determine ionization yield and recombination probability of the charge carriers before their collection.

Gases such as nitrogen, air, tissue-equivalent gas, and argon have been regularly used in ionization chambers. Nitrogen gas or air are most commonly used because their ionization potential, W-value, and stopping power ratio of gas to tissue, (S_m), are better known and their saturation levels are acceptable at beam intensities used for ion beam therapy. Air is also practical because its temperature and pressure variations can be easily measured and corrected for and the humidity of the air has a negligible effect on the detector response. At high beam intensities where saturation effects become important, an inert gas which does not form negative ions, such as Ar or He, can be used. For example, recombination effects for Ne ions would not be expected up to ~200 Gy/s for Ar gas as compared to ~20 Gy/s with air. For higher yields Xe gas can be used with a lower W-value and a higher density. For fast response times He gas has been used because of its higher ion drift velocity.

Thimble Ionization Chambers

As a direct measurement of dose in the patient is not practical, the dosimeters are calibrated against a reference ionization detector, usually a thimble ionization chamber, placed inside a phantom target volume in conditions similar to an actual treatment.

Thimble ionization chambers are spherical or cylindrical chambers made from conductive plastic with a center stem for charge collection. The plastic walls are typically a few mm thick and the sensitive volumes are usually between 0.1 cm^3 and 1.0 cm^3 or greater. Smaller chambers afford better spatial resolution, but are less sensitive. Such detectors serve as practical calibration devices after they are calibrated against a national standard, such as the one at the National Institute of Standards and Technology in the US. These chambers are primarily used with air or a tissue-equivalent gas as the ionization medium.

Segmented Ionization Chambers

When radiation fields are larger than a few centimeters across, it is necessary to pay close attention to the field uniformity. An ionization chamber with segmented collection elements located as close as possible to the patient is best suited in providing the desired on-line information. Segmentation of the collecting planes provides a means of obtaining information on spatial dose distribution. The number of elements can range from several to a few thousand and their geometric arrangement can be tailored to suit the beam spreading system. For example, a collecting element segmented into a set of concentric rings can measure beam profiles with cylindrical symmetry [11].

Other geometric arrangements can be constructed to measure the beam profiles that lack cylindrical symmetries. Examples are the 19 hexagonal elements (5 cm across) arranged in honeycomb fashion (Fig. 2) and the 144-element chamber (a 12×12 array of 2.5 cm $\times$ 2.5 cm areas) both used at LBL [10], and the 400-element chamber (a 20×20 array of 1 cm $\times$ 1 cm areas) at Loma Linda University Medical Center (LLUMC), Loma Linda, California [12]. In these chambers, the signals are extracted through thin traces located on the opposite side of the foil. Holes drilled through the foil, which are then plated through, allow connections between the elements and traces, as schematically shown in Figure 2. This method avoids collection of charge on these traces by placing them away from any electric field.

The 3600-Element Chamber

An ionization chamber with a sensitive area of 30 cm $\times$ 30 cm with 0.5 cm spatial resolution was built at LBL by dividing the collecting plane into a 60×60 array of 5 mm $\times$ 5 mm areas [13]. The detector was specifically designed to minimize its impact on the beam and the space it occupies in the beam line; its physical thickness is 5 cm and the water-equivalent thickness 2 mm. The main difficulty to be overcome was the crowded condition of bringing out signal leads from the 3600 collection areas. This problem was solved by plac-

ing the signal leads in four different planes of laminated material as in the multilayer construction technique developed for printed circuit technology. As a result, the spacings between the leads are made as large as 0.2 mm.

Charge Integrators

Energetic ions traversing an ionization chamber produce a charge output proportional to the deposited dose. Because the clinical beams from an accelerator have temporal structures, measuring the dose means measuring the total charge as an integral of a fluctuating current. The electronics for these devices are generally some form of charge integrator with a response time fast enough for control purposes.

A form of charge integrator that is particularly well suited for ion beam therapy applications is the one which issues a pulse for every fixed increment of input charge (e.g., 10 pC). A standard circuit for this purpose is the charge-balancing current integrator or recycling integrator [14]. When used with digital electronics these circuits measure the dose with the advantages of a large dynamic range, exceptional linearity, and excellent noise immunity.

Typical radiation doses used for ion beam therapy range from approx. 1 mGy to 10 Gy. As an illustration, an ionization chamber using nitrogen gas at atmospheric pressure and room temperature with a 1.0 cm^3 volume exposed to such doses produces between 35 pC to 0.35 μC. Accounting for the variation in volumes that are used in an ionization chamber requires the current integrator to be able to measure as little as 10 pC and as large as 3.5 μC. The rate at which this dose can be delivered can vary from 10^{-3} to 1 Gy/s and even higher instantaneous dose rates. The electronics may saturate at these high dose rates. As saturation leads to an inaccurate dose measurement, some means of detecting a saturation condition must be provided.

Secondary Emission Monitors (SEMs)

A typical SEM consists of a set of parallel foils (e.g., 6 μm thick aluminum foils separated by 3 mm) in a vacuum enclosure. The foils alternate between collection foils and bias foils. The more foils are used, the greater is the signal. The number of secondary electrons produced by traversing ions depends on the energy deposited in the layer, called the escape zone. The work function of the

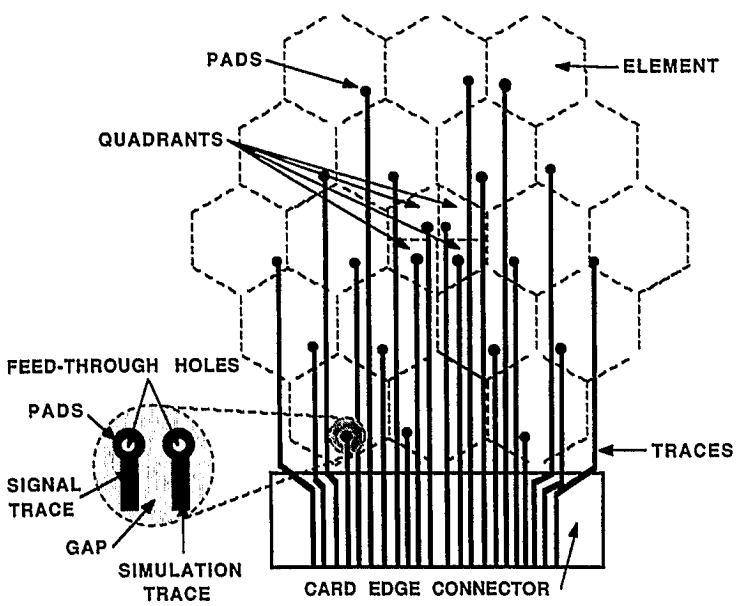

Fig. 2. A schematic drawing of the LBL 19-element segmented ionization chamber. The segmented collection elements are shown in dotted lines and the signal traces in solid lines. The collecting elements and the signal traces are on the opposite sides of the insulating foil. The electric connections are made via holes in the foil which are plated through

material and the condition of the surface determine the thickness of this escape zone. Electron production scales linearly with foil thickness up to the point where electrons do not escape the foil. Good vacuum in the chamber is important for keeping the foil surfaces free of absorbed material which can affect the secondary electron emission. Pressure below 1 mPa reduces the ionization of the residual gas to an acceptable level; however, the better the vacuum the more consistent the performance. A vacuum of 1 μPa is routinely used for the purpose of beam line monitoring. A bias voltage of approximately –50 V is applied to the bias foils to ensure nearly complete collection of the electrons which have energies less than 25 eV.

Dose measuring accuracy of an SEM can be better than 1% and the long-term stability of its output is excellent. A calibration of the SEM can be done against a calibrated ionization chamber or by using the foil activation technique, a calorimeter, or a Faraday cup.

As mentioned above, at high dose rate saturation in ionization chambers can be a major problem in their use as dose-detecting devices. SEMs can serve as alternative detectors to ionization chambers. Saturation in SEMs has not been seen in electron-beam current densities of up to tens of mA/cm^2, making their use ideal in situations where there is a concern about ionization chamber saturation. The SEM outputs are linear until space charge effects become important, which has been estimated to be above 10^9 Gy/s. Another advantage of a SEM detector is its fast response time, which is determined by the travel time of the electrons rather than the slower migration time of ions in an ionization chamber. Responses in the nanosecond time scale are possible. Their major disadvantage is the low yield of secondary electrons per primary particle compared with ionization chambers, that limits their use for low beam particle fluxes.

Wire Chambers

In the simplest form, a wire chamber consists of two planes of evenly spaced parallel wires separated by a given distance, with the intervening volume filled with gas. One wire plane is used as the signal plane, and the other as the high-voltage plane. The high-voltage plane can also be a solid foil conductor instead of a plane of parallel wires. While the common application of wire chambers in particle physics is to detect traversing particles on a particle-by-particle basis, in ion beam therapy applications wire chambers are more often used as integrating devices that integrate spatially along a wire as well as temporarily during an irradiation procedure. Typical clinical ion beam intensities are between 0.1 pA and 0.1 mA.

Wire chambers are typically operated in a proportional mode where a multiplication of the initial ionization occurs, but can be operated in an ionization mode where the gain is unity. In the former mode, multiplication of the initial ionization occurs when the ionized electrons, accelerated by the strong potential gradient around a wire, cause further ionization. The gain is dependent on the type and pressure of the gas, the wire spacing, and the high voltage. By decreasing the wire spacings, increased spatial resolution can be achieved at the price of decreased gain due to the decrease in potential gradient around the wires. Wire spacing as coarse as 6 mm and as fine as 0.2 mm are practical. Gold-coated beryllium/copper wires of 50 μm diameter are often used because of their longevity and mechanical stability in the beam. Common gases used in such devices are air, argon, or gas mixtures such as 10% argon and 90% CO_2. Atmospheric pressure is a convenient gas pressure; however, lower as well as higher pressures have been used. The principles of construction and operation of wire chambers have been discussed widely [15].

Two planes of sense wires placed orthogonally can show the horizontal and vertical projections of the beam profile. The centroid and the width of the beam can be computed in each plane for beam-tuning purposes. Monitoring beam profiles is important for efficiently transporting the ion beams and obtaining the correct dose distributions with the beam delivery system. Typically, a wire chamber is positioned upstream of the beam delivery system and a second wire chamber is located downstream of the delivery system, near the patient. The active area of the second chamber is typically large to accommodate the large radiation fields.

MEDUSA

A multi wire, multiplane wire chamber, called the Medical Dose Uniformity Sampler (MEDUSA), was developed at LBL to reconstruct the two-dimensional dose profile of a beam [16]. It has 16 wire planes, each of which has 64 wires separated by 4 mm. Each plane samples the beam profile projected into the particular wire direction, which is offset by 11.25 degrees (180 degrees divided into 16 equal angles) from adjacent planes. Based on the 16 projected profile data sets, MEDUSA reconstructs the two-dimensional dose profile within a circular area of 256 mm diameter. The reconstruction of the two-dimensional image relies on the 'filtered back projection' algorithm.

Diodes and Diode Arrays

The usefulness of diodes as dose detectors derives from their small size [17]. Measuring dose distributions with fine spatial resolution is difficult with ionization chambers, but simple with diodes which intrinsically have small active areas. As a solid, they absorb a lot more dose in a small volume. Generally speaking, there are two disparate applications of diodes in a typical ion beam therapy facility: Efficient mapping of large dose fields, where the feasibility of a diode array is paramount, and mapping of very small dose fields (e.g., for eye treatments), where ionization chambers may be too large to serve. A calibration of the diode must be done before use since they suffer radiation damage over extended exposure. They are, however, excellent for relative measurements over short time periods. Arrays of diodes have successfully been used for measuring profiles of radiation fields and Bragg ionization curves [18].

Junction diodes, connected to an electrometer which keeps the voltage across the diode nearly equal to zero, exhibit a current (in the 'reverse' direction) nearly proportional to the dose rate over a wide range [19]. There is extensive literature on this subject; however, most of it is about photon and electron beam applications [20]. Nearly any diode will work; power rectifiers, small-signal diodes, microwave diodes, LEDs and photodiodes have all been used. Their advantages are small size, low cost, ruggedness and simplicity of use (no polarizing voltage). Their disadvantages include sensitivity to electrometer voltage burden, decline of output with accumulated dose, and small temperature and dose rate effects.

Commercial diodes for electronics are N-type. P-type diodes built especially for dosimetry are available. They exhibit less radiation damage and smaller dose rate effect [20], but their cost almost rules them out for large arrays.

The associated electrometer is usually an integrator, to measure total charge produced in a monitored exposure. Diodes place a special demand on the electrometer, and their use may be frustrating unless one takes into account that the voltage burden (voltage appearing at the integrator input during normal operation) is critically important. This is not the case with either an ionization chamber or a Faraday cup. This voltage, appearing across the effective resistance of the diode, causes a drift current which will vary with time and temperature unless the electrometer amplifier is carefully chosen. Many popular commercial electrometers are inadequate in this regard but it is not difficult to find an inexpensive operational amplifier (e.g., the Texas Instruments TLC27L2) which is suitable [21]. Unfortunately this leaves the potential user (especially of diode arrays) with an in-house construction project. A 64-channel integrator has been designed, developed and tested at the Harvard Cyclotron Laboratory (HCL), and is available on request.

Otherwise, the use of diode arrays is straightforward. They should feed an array of integrators which is scanned, digitized and read out using some standard scheme, e.g., RS-232 or CAMAC. Each channel should be read out before and after the exposure so that the difference can be taken. Also, in lengthy experiments one should calibrate the diodes before and after the run and keep track of the dose so that final corrections can be made. As the degradation of sensitivity with integrated dose is initially larger, it helps to preirradiate the diodes to approx. 1000 Gy.

The sensitivity range of diodes is significant; e.g., roughly 140 pC/cGy for a 1N4004 (1-A rectifier), 100 pC/cGy for the Hamamatsu S2164 pho-

todiode, 10 pC/cGy for a typical small-signal diode, and 1 pC/cGy for one element of an ELB-1001HDA 10-element LED array useful in mapping very small fields. These numbers will decrease substantially over the useful life of the diode. For comparison, a 0.05 cm^3 thimble ionization chamber registers about 10 pC/cGy.

When mapping large fields of high-energy ions the diode package makes no difference, but for precise work (especially near end-of-range) the photodiode, with its thin and precisely known covering layer, is an elegant package. Of course, photodiodes and LEDs must be carefully light-proofed. Exposed conductors should be covered with coil dope or RTV sealant so that charge is not picked up from ionized air. Depending on the environment, electrostatic shielding (aluminum foil crimped to the shield of the output cable) may be needed. RG-178B/U miniature Teflon insulated cable works well in this and other low signal applications because the cable itself produces little signal when exposed to radiation or when flexed. Avoid connectors, except coaxial types, wherever they might be exposed to radiation.

The use of single diodes for precise dose measurements, though convenient, is somewhat problematic. Koehler [19] reported about 8% more output from a particular diode (long since unavailable) than from a parallel-plate ionization chamber in the Bragg-peak region, when the two were made to agree in the 'entrance' region. If a thimble chamber is used as the reference dosimeter additional geometric effects come into play, and total discrepancies of approx. 15% (diode vs. thimble chamber at the Bragg peak) are found at HCL [22]. At present, there is a wealth of (sometimes contradictory) observations, but very few published. One can only conclude that there is an energy-dependent problem – diodes and ionization chambers, more often than not, exhibit different Bragg curves – that different diodes seem to give different results, as do different ionization chambers, and that the problem may lie with the diodes, the ionization chambers, or both. Energy dependence in proton beam dosimetry at the 5–10% level simply requires further study.

At HCL a dose scanner within a water phantom has been developed. A small water phantom with approximately 15 cm × 15 cm entrance window and 18 cm depth along the proton beam is supported on a three-axis computer-controlled positioning system that can quickly and reproducibly place the tank anywhere in a therapy field. Within the tank, a fourth axis controls the depth of a detector module containing a thimble ionization chamber, an 8 × 6 array of diodes, a 'stair-step' array of diodes for depth detection, and 3 diodes for edge scanning. The system can be manually controlled either locally or remotely, or by a computer command file.

The system takes advantage of the reduced scattering of protons vis-à-vis photons to use a much smaller tank. It is only necessary to ensure that any detector within the tank is surrounded laterally by a radius R of water (or plastic) such that any beam conditions outside of R have an insignificant effect on the dose at the detector. For 160 MeV protons, R = 2 cm is sufficient for most situations but R = 5 cm was chosen for a wide safety margin. The weight of the resulting tank is small enough to move the entire tank and position the detectors laterally after moving from a parking position out of the way of patients undergoing therapy. Deployment of the tank which remains filled with water, aligned with the beam, and connected to the necessary integrators and electrometer can be accomplished in about a minute. Quicker and more detailed scans of patient treatment beams are the result.

The detector module supports the various detectors in a dry environment, surrounded by plastic, within the water tank. An Exradin T1 tissue-equivalent ionization chamber is laterally centered in the module, but with only a small amount of plastic window upstream. The chamber is connected to an electrometer (Keithley 617) about 30 m away, operated in the floating mode. An array of 48 photodiodes (Hamamatsu S2164) in 6 columns of 8 diodes with 10 mm column spacing and 8 mm row spacing are connected to a 64-channel integrator with very low input voltage burden using individual 3 m coaxial cables (RG174). The diode connections to the coaxial cable are concealed in RTV silicon, the entire module is electrically shielded with silver paint, and protected from light by an additional coat of black paint. Edge-mounted diodes are used for

lateral scans of beams with very sharp penumbra. A stairstep of 8 diodes spanning 16 mm in depth in 2 mm steps is used to quickly measure a depth dose in a region of relatively uniform depth.

The Exradin ionization chamber is used for routine beam line checks as well as individual patient therapy beam calibrations. The diodes are used for more detailed scans and for apertures too small to be accurately measured by a larger ionization chamber. The diodes can be recalibrated automatically in 2 minutes by a sequence that measures the dose in the central region of a flat field using the ionization chamber and then serially brings the diodes into the same region in four groups to be calibrated. This procedure is necessitated by the inevitable radiation damage to the diodes, and must be repeated frequently only if large volume scans at high accuracy are required. Figure 3 shows a depth scan using a row of 8 diodes with points taken every 1 mm of depth in the region of the Bragg peak. The alignment of the data points from diode to diode at the distal 50% shows that the variation in depth is about 0.1 mm of water. This regularity, together with accurate lateral diode positioning and ease of calibration, results in large data sets that display continuity over the many diodes involved in the scan.

Other Types of Radiation Detectors

Several types of devices other than ionization chambers, SEMs, wire chambers, and diodes have been successfully used in ion beam therapy applications. Each, as discussed below, has its special application.

Semiconductor Detectors

Aside from the use of diodes, semiconductor detectors are used for many different purposes in ion beam therapy applications.

Semiconductor detectors such as Si surface barrier detectors or thin Ge detectors are excellent for measuring the energy loss of a particle since they have high sensitivity, and their response is independent of the particle type and proportional to the energy deposited. A much smaller amount of energy is required to produce an electron-hole pair compared to ~35 eV needed in a gas ionization chamber to produce an ion pair. However, they do suffer from a pulse height defect associated with large energy depositions leading to recombination of electron-hole pairs. A Ge crystal of sufficient thickness to stop

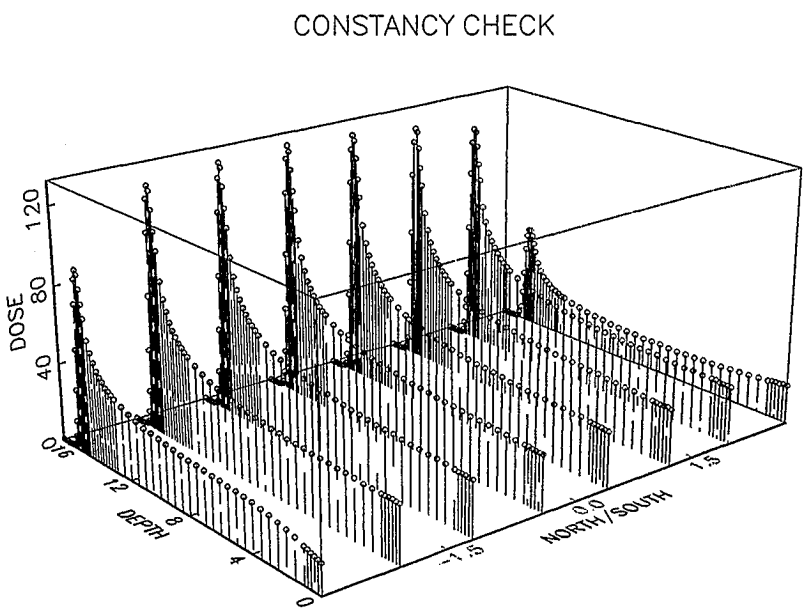

Fig. 3. A depth scan obtained using the HCL diode array. The Bragg curves are taken at every 1 mm (near the peaks) and 2 mm (on the plateaus) interval using a row of eight diodes. Courtesy of M. Wagner, HCL

an incoming particle can serve as a total energy detector. Ge detectors have excellent particle energy resolution, typically dE/E $\approx$ 0.1%, but radiation damage can lead to a degradation in their energy resolution. These detectors are used primarily for single particle detection and are not suitable for measurements at normal clinical beam intensities.

The biological damages due to high-LET radiation cannot completely be described by the dose and average LET. The actual composition of the beam in terms of the particle types and their relative contributions to the biological damages must be determined. A particle detector system known as the BERKLET, has been developed at LBL in order to identify the particle charge, but not mass, along with its residual energy and LET [23]. The system consists of a 300 μm thick Si detector followed by a 5.5 cm thick Ge detector. The two detectors, operated in coincidence, measure the dE/dx and the total energy of the particle, respectively. The total energy that can be measured in the Ge detector corresponds to a particle with an 18.7 cm penetration in water. Another application at LBL of solid-state detectors is the use of position-sensitive Si detectors to measure multiple Coulomb scattering and compare the data against several scattering formulas [24].

Scintillators

In high-energy and nuclear physics experiments, scintillators have been used extensively for single particle detection. In ion beam therapy, they have been used primarily for beam controls because of their fast response times and large dynamic ranges of operation when used in conjunction with phototubes. Large beam currents cause radiation damages to the solid scintillators, which limit their lifetime and affect their response. A Xe gas scintillator has been used to control the beam at Loma Linda [25]. As light production in the scintillator is not simply proportional to the energy loss of the particle due to quenching, their use as a dose detector requires special calibration. Recently, they have been used in conjunction with charge-coupled devices (CCD) to measure the lateral uniformity of a radiation field and to measure the scintillation light as a function of depth for range verification [26].

Calorimeters

The temperature rise of a material from energy deposited in it by an ion beam may be used for absolute dose measurement. Water temperature increases by 2.4×10^{-4} per Gray of deposited dose; but, making an accurate measurement is difficult. Calorimeters are no practical means of measuring dose for on-line clinical dosimetry, but rather serve as calibration standards (see subsequent chapter for details).

Faraday Cups

Faraday cups measure the number of particles by measuring the charges collected on an electrically isolated and evacuated container which stops the beam [27]. When monoenergetic ions impinge upon the Faraday cup, the dose is calculated from the measured number of particles per unit area and the mass stopping power of the particle at the given energy in tissue.

Film

Film is the most economical method for measuring spatial dose distributions with the finest spatial resolution available, yet it is not a rapid instrument. The spatial resolution achievable with film is limited by the resolution of the digitizing procedure, the speed of which is in turn limited by the time required for digitization and data reduction. The darkening of the film, i.e., optical density, after exposure to an ion beam can be used to measure the dose. In retrospective studies at LBL, film is shown to provide better than ±5% absolute dose accuracy if the development conditions are closely controlled; however, few rely on film for clinical dosimetry. The optical density depends more on the particle fluence than the dose deposited. In other words, it depends on the LET of the particles. For this reason, film is primarily a relative dose detector and is used for

measuring lateral dose distributions rather than depth-dose distributions which exhibit pronounced LET dependence.

Thermoluminescent Dosimeters (TLDs)

TLDs are inorganic materials, such as LiF or CaF_2, that do not scintillate promptly, but rather trap electron-hole pairs created from the exposure to ionizing radiation. Upon heating the exposed material, the trapped electrons can escape, leading to light emission which can be detected, and related to the absorbed dose.

Chemical Dosimeters

In chemical dosimetry, radiation dose is determined by measuring the chemical change produced in an irradiated medium. The most well-known chemical dosimeter is the Fricke dosimeter, which determines the dose by measuring the ferric-ion yield from the oxidation of Fe^{2+} to Fe^{3+} by the interaction of the ionization and the ferrous-ion. The measurement of optical density of the irradiated solution at a specific wavelength can be interpreted in terms of the ferric-ion density, which is in turn related to the dose.

One of the recent developments in ion beam dosimetry is the application of alanine compound. Radiation changes the chemical structure of alanine crystals, and the degrees of the chemical changes can be determined by analyzing the Zeeman hyperfine molecular levels through electron spin resonance (ESR). Its advantages are portability, tissue-equivalence, and minimal fading at ambient temperature which provides permanent irradiation record. Its LET dependence and reproducibility are still to be investigated [28].

Nuclear Activation

Foil activation utilizes the ion beam undergoing a nuclear reaction of a known cross-section in a foil of a known thickness. The radioactive yield can then be measured by means of its decay over time, which determines the initial beam intensity, and hence the imparted dose. For example, the reaction

$$^{12}C + p \rightarrow {}^{11}C + p + n$$

has been used to determine absolute fluence and absorbed dose of protons for therapy. This method is used more for verification than on-line analysis.

As a variation of the above method, in vivo dosimetry for assessing the integral dose of an ion beam irradiation has been studied by detecting the decay products of ^{11}C, ^{13}N and ^{15}O from tissue activation [29].

Solid-State Nuclear Track Detectors

The passage of energetic ions through most insulators forms narrow regions of radiation damages, called 'latent tracks'. In crystals, such a track may be detected by viewing with an electron microscope; in polymers by means of special coloring of the track. A more practical method is to use plastic sheets and to etch the latent tracks selectively, which can subsequently be viewed with an optical microscope. Plastics such as CR39 have been extensively used to measure the LET distribution of heavy ion beams [30]. Measurements of an individual track left by traversing or stopping heavy charged particles in plastic detectors render information about their dE/dx, charge and mass number and sometimes velocity. Recently, the use of solid-state nuclear track detectors in nuclear physics has been reviewed [31], and lists of commercial sources of most commonly used material for solid-state nuclear track detectors are found in publications [32].

Concluding Remarks

Many accurate and reliable radiation detectors have been developed and used in ion beam therapy applications. However, important questions that must still be answered remain for complete understanding. For example, the discrepancies in the Bragg curves obtained by different detectors, such as diodes and ionization chambers, should

be explained. Some areas of future developments in radiation detectors are the development of dose detectors which can provide a spatial resolution ($\approx$ 1 mm) sufficient for reconstruction of dose distributions deposited in a patient using pencil-beam scanning, development of two-dimensional amorphous silicon detector arrays, new detectors such as the use of scintillating material or Fricke gels for three-dimensional dose measurements with a high spatial resolution.

Acknowledgments

The author wishes to express his gratitude to Bernard Gottschalk and Miles Wagner of the Harvard Cyclotron Laboratory for providing unpublished materials on diode detectors for inclusion in this article. This work is supported by the Director, Office of Energy Research, Energy Research Laboratory Technology Transfer Program, of the U.S. Department of Energy under Contract No. DE-AC03–76SF00098.

References

1 Chu, W.T., Ludewigt, B.A., and Renner, T.R. Instrumentation for treatment of cancer using proton and light-ion beams. Rev. Sci. Instr. 64, 2055–2122, 1993.
2 Boag, J.W. Ionization chambers, in Radiation Dosimetry, Attix, F.H. and Roesch, W.C. (eds.), Academic Press, New York, 1966, pp. 1–72.
3 Bragg, L. An ionization method for the absolute measurement of gamma-ray energy. Proc. Roy. Soc. Ser. A156, 578, 1936.
4 Thomas, D.J. and Burke, M.W. Value measurements for protons in tissue-equivalent gas and its constituent gases. Phys. Med. Biol. 30, 1201–1213, 1985.
5 Petti, P.L., Verhey, L., and Wilson, R. A measurement of W for 150 MeV protons in nitrogen and argon. Phys. Med. Biol. 31, 1129–1138, 1986.
6 Seuntjens, J. Palmans, H., Verhaegen, F., Denis, J.-M., Vynckier, S., and Thierens, H. Water calorimetry for clinical proton beams, presented at NPL Calorimetry Workshop, Teddington, UK, October 13–15, 1994.
7 Vatnitsky, S.M. and Siebers, J.V. Comparison of water calorimeter with reference ionization chamber dosimetry in high-energy photon and proton beams, presented at NPL Calorimetry Workshop, Teddington, UK, October 13–15, 1994.
8 Verhey, L., private communication, 1995.
9 American Association of Physicists in Medicine, Protocol for Heavy Charged-Particle Beam Dosimetry, A Report of Task Group 20, Radiation Therapy Committee, AAPM Report 16, Am. Inst. Phys., New York, 1986.
10 Renner, T.R., Chu, W.T., Ludewigt, B.A., Nyman, M.A., and Stradtner, R. Multisegmented ionization chamber dosimetry system for light ion beams. Nucl. Instr. Meth. Phys. Res. A281, 640–648, 1989.
11 Lyman, J.T., Howard, J., and Windsor, A.A. Heavy charged-particle beam monitoring with segmented ionization chambers. Med. Phys. 2, 163, 1975.
12 Coutrakon, G., Bauman, M., Lesyna, D., Miller, D., Nusbaum, J., Slater, J., Johanning, J., Miranda, J., DeLuca P.M., Siebers, J., and Ludewigt, B. A prototype beam delivery system for the proton medical accelerator at Loma Linda. Med. Phys. 18, 1093–1099, 1991.
13 Chu, W.T., Ludewigt, B.A., Marks, K.M., Nyman, M.A., Renner, T.R., Singh, R.P., and Stradtner, R. Three-Dimensional conformal therapy using light-ion beams, in Proc. NIRS Int. Workshop on Heavy Charged Particle Therapy and Related Subjects, Itano, A. and Kanai, T. (eds.), Chiba, Japan, July 4–5, 1991, pp. 110–123.
14 Gottschalk, B. Charge-balancing current integrator with large dynamic range. Nucl. Instr. Meth. 207, 417–421, 1983.
15 Sauli, F. Principles of Operation of Multiwire Proportional and Drift Chambers, CERN 77–09, European Organization for Nuclear Research, Geneva, Switzerland, May 3, 1977.
16 Chu, W.T., Alonso, J.R., and Tobias, C.A. Heavy ion beam studies and imaging with a multiplane multiwire proportional chamber. IEEE Trans. Nucl. Sci. NS-28, 2198–2200, 1981.
17 Fowler, J.W. Solid state electrical conductivity dosimeters, in Radiation Dosimetry, Attix, F.H. and Roesch, W.C. (eds.), Academic Press, New York, 1966, pp. 291–324.
18 Gottschalk, B. Calibrating Dosimeter Arrays, HCL Technical Report, Note 6/10/88, Harvard Cyclotron Laboratory, Cambridge, MA, 1988.
19 Koehler, A.M. Dosimetry of proton beams using small diodes. Radiat. Res. Suppl. 7, 53–64, 1967.
20 Rikner, G. and Grusell, E. General specifications for silicon semiconductors for use in radiation dosimetry. Phys. Med. Biol. 32, 1109–1117, 1987.
21 Gottschalk, B. Resetting a current integrator with the supply lines. Nucl. Instr. Meth. A297, 534–535, 1990.
22 Wagner, M.S., private communication, 1994.
23 Llacer, J., Schmidt, J.B., and Tobias, C.A., Characterization of fragmented heavy-ion beams using a three-stage telescope detector: Detector configuration and instrumentation. Med. Phys. 17, 158–162, 1990.
24 Wong, M., Schimmerling, W., Phillips, M.H., Ludewigt, B.A., Landis, D.A., Walton, J.T., and Curtis, S.B. The multiple scattering of very heavy charged particles. Med. Phys. 17, 163–171, 1990.
25 Coutrakon, G., Miller, D., Kross, B.J., Anderson, D.F., DeLuca, P., and Siebers, J. A beam intensity monitor for the Loma Linda cancer therapy proton accelerator. Med. Phys. 18, 817–820, 1991.

26 Coutrakon, G., Miller, D., Wong, J., Gere, L., and Binns, R. Characterization of the Loma Linda proton beam using a plastic scintillator and CCD camera readout. Med. Phys. 17, 543, 1990.
27 Vynckier, S., Meulders, J.-P., Robert, P., and Wambersie, A. The proton therapy program at the cyclotron "Cyclone" of Louvain-la-Neuve (First Dosimetric Results). J. Eur. Radioth. 5, 245–247, 1984.
28 Gall, K. Alanine ESR dosimeters, April 1993, presented at the XVIIIth PTCOG meeting, Nice, France 1993.
29 Graffman, S. and Jung, B. ^{11}C and ^{15}O induced in the mouse by 175 MeV protons. Acta Radiol. Ther. Phys. Biol. 14, 113–126, 1975.
30 Ogura, K., Benton, E.V., Frank, A.L., and Atallah, T.M. Proton response of CR39. Nucl. Tracks Radiat. Meas. 12, 527–530, 1986.
31 Tret'yakova, S.P. Solid-state nuclear track detectors and their use in experimental nuclear physics. Sov. J. Part. Nucl. 23, 156–186, 1992.
32 Durrani, S.A. and Bull, R.K. Solid State Nuclear Track Detection. Principles, Methods, and Applications. Pergamon Press, Oxford, England, 1987.

26 Dosimetry Techniques for Ion Beams

S. VYNCKIER

Université Catholique de Louvain, Cliniques Universitaires St-Luc, Brussels, Belgium

Introduction

Dosimetry of a therapy beam means determination of the absorbed dose at a point of reference and measurement of dose distributions in a tissue-equivalent phantom. The first is essential in order to verify the prescriptions of the protocol whereas the latter is indispensable for planning and quality assurance purposes. The choice of a particular dosimeter will depend on several factors, such as the accuracy and sensitivity desired, and the size of the detector with respect to beam size and gradients involved.

Ion beam dosimetry can be performed using different types of dosimeters including calorimeters, ionization chambers, or Faraday cups [1, 2], see also preceding chapter). National standard dosimetry laboratories will not provide, however, a standard for the dosimetry of ion beams. In order to achieve uniformity on an international level, the use of an ionization chamber, calibrated in terms of air-kerma in a ^{60}Co beam has to be considered.

In conventional photon dosimetry the calorimeter [3, 4] yields the smallest uncertainty in the determination of the absorbed dose, as the measured quantity is the heat equivalent of absorbed energy. Although the use of calorimeters for dosimetry is cumbersome and not suitable for daily practice, research with calorimeters should be encouraged and continued.

Faraday cup measurements are based on the determination of the ion beam fluence. In practice, these Faraday cup measurements are combined with an ionization chamber, exposed to air, in order to calibrate the ionization chamber for later dose determinations in a phantom. This method requires a perfect monoenergetic beam. Moreover, the efficiency of the determination of the fluence will be susceptible to the design of the cup, i.e., wall thickness, quality of the vacuum, guard ring bias voltage, etc. [1, 2, 5].

Practical dosimetry for conventional therapy beams is based on ionization chambers used under well defined conditions. Ionization chambers provide accuracy as well as convenience in use. They can be compared to other dosimetric methods and, if used under these well defined conditions, they will provide uniformity in beam dosimetry, which is one of the main goals of the recommendations.

For ion beam dosimetry, a "Protocol for Heavy Charged Particle Beam Dosimetry" exists which was developed by Task Group 20 of the American Association of Physicists in Medicine (AAPM) [6]. This protocol describes the methods and recommendations for the determination of the absorbed dose in a heavy charged particle beam. With respect to proton beams, a "Code of Practice for Clinical Proton dosimetry" [7, 8] was written by a working group of the European Clinical Heavy Particle Dosimetry (ECHED) association.

The following paragraphs will summerize the basic principles and recommendations for the dose determination in a proton beam, based on the "Code of Practice for Clinical Proton dosimetry" [7, 8]. This code recommends the use of a water calorimeter as reference instrument or, if not available, an ionization chamber, calibrated in terms of air-kerma in a ^{60}Co beam. These principles can also be applied to other heavy charged particle beams. However, so far there is no inter-

national consensus for adopting the values of the basic physical parameters in a charged particle beam. Moreover, the uncertainty on the W-value (i.e., the mean energy to produce an ion pair in the cavity gas) [9] is rather large for ion beams. Some recommendations can be found in the AAPM Report 16 [6]. Therefore, it should be recommended that for ion beams, other than protons, the ionization chamber be calibrated directly with respect to a calorimeter in terms of absorbed dose.

Measurement Conditions for Ionization Chamber Dosimetry in a Proton Beam

At present, there are two major types of clinical applications of proton beams [10–12]: low-energy protons (E_p <90 MeV), for the treatment of ocular melanomas [13, 14] and higher energy protons (E_p > 150 MeV) for the treatment of large and/or deep-seated tumors. For the former kind of treatment, small field sizes (field area 15 cm^2) and high dose rates (dD/dt >10 Gy/min) are applied whereas in the latter, conventional field sizes with conventional dose rates as utilized in photon or electron radiotherapy are employed.

Ionization Chamber Specification

In principle, any type of reliable ionization chamber, as used for photon dosimetry, can be employed. However, most of the medical physicists performing proton dosimetry are using tissue-equivalent (TE) ionization chambers, made of A-150 [1, 7, 8]. Therefore, the formalism developed here is typically for TE ionization chambers. For other types [15, 16], the formalism should be adapted, accordingly.

The choice of the cavity gas in the ionization chamber is strongly dependent on the knowledge of the $(W_{gas})_p$ value for proton beams. Due to its simplicity, preference should be given to air. Recently, Hiraoka et al. [17] measured the $(W_{gas})_p$ ratios in a 70 MeV proton beam for different gases. As a result the $(W_{gas})_p$ for air can be obtained from determinations in another gas, as for instance N_2. All formalism that will follow is only valid for air, used as cavity gas.

Table 1. A_{wall} factors for tissue-equivalent ionization chambers

Ionization Chamber	Chamber Volume (cm^3)	A_{wall}
Exradin T1	0.05	0.992
FW IC18	0.1	0.991
Exradin T2	0.5	0.985
FWT IC 17	1.0	0.983

Proton Energy and Absorbed Dose Specification

For ionization dosimetry in a proton beam, mass stopping power ratios need to be known (see below). However, these ratios vary slowly with energy (Table 2). A clinical proton beam with a spread-out Bragg peak (SOBP) will not be

Table 2. Mass stopping powers for water and air and their ratio. From Ref. 18

Proton energy (MeV)	Mass stopping powers (MeV cm^2 g^{-1})		
	water	air	water/air
10	45.67	40.06	1.1400
20	26.07	22.94	1.1364
30	18.76	16.53	1.1349
40	14.88	13.12	1.1341
50	12.45	10.99	1.1328
60	10.78	9.517	1.1327
70	9.559	8.443	1.1322
80	8.625	7.620	1.1319
90	7.888	6.970	1.1317
100	7.289	6.443	1.1313
125	6.192	5.475	1.1310
150	5.445	4.816	1.1306
175	4.903	4.338	1.1302
200	4.492	3.976	1.1298
225	4.170	3.691	1.1298
250	3.911	3.462	1.1297
275	3.698	3.275	1.1292
300	3.520	3.118	1.1289
350	3.241	2.871	1.1289
400	3.032	2.687	1.1284

monoenergetic and knowledge of the mean energy or the proton energy spectrum at the calibration point is requested. The energy of the proton beam can be specified with its effective energy $(E_p)_{eff}$, if the energy spectrum or the residual range at the point of interest is unknown. The effective energy can be defined as the energy of the monoenergetic protons which have a continuous slowing down approximation (CSDA) range in water equal to the residual range behind the middle of the SOBP. CSDA energy range data for proton beams in different materials are found in the ICRU 49 [18].

The effective energy is only a rough representation of the energy spectrum, but can easily be obtained from dosimetric data. Water is used as material for absorbed dose specification as in the case of photon and electron beams, since the mass stopping power ratios for different tissues relative to water do not deviate to much from unity [19].

Reference Phantom Material and Reference Depth for Measurement

In clinical dosimetry, phantom materials should be closely matched to tissue, i.e., they should have very similar absorption and scattering properties for the radiation beam considered. They are used for two purposes: to simulate the presence of tissue when determining the absorbed dose under reference conditions (reference field size, reference depth, etc.) and secondly, to obtain basic dose distributions, e.g., percent depth doses, off-axis data and isodose contours.

Absorbed dose for proton beams is specified in water and so, by preference, calibration measurements should be performed in water. However, for simplicity, routine output checks can always be performed in an acrylic phantom (PMMA or "solid water") as long as the depth of measurement is scaled to the SOBP in water. This scaling can be obtained from the CSDA ranges in the different materials which can be found in ICRU 49 [18].

The center of the SOBP is a region of dose uniformity. Therefore, calibration should be performed in the middle of the SOBP or – if no SOBP is produced (spot scanning) – in a region of high dose uniformity.

Determination of the Absorbed Proton Dose by a ^{60}Co-calibrated Ionization Chamber

Determination of the absorbed dose using ionization chambers is based on the Bragg-Gray cavity theory [20]

$$D = \frac{Q}{m} \times \frac{W}{e} \times s_{w,g} \qquad (1)$$

where D is the dose to the wall surrounding the cavity, m the mass of the gas in the cavity, W the energy required to form an ion pair in the gas and $s_{w,g}$ the mass stopping power ratio of the wall material, w to the gas, g. The assumptions for the application of the Bragg-Gray relation are standard, i.e., the dimensions of the cavity are small compared to the range of the particles that ionize the gas and the presence of the cavity does not disturb the proton fluence.

Calibration of the Ionization Chamber in a Photon Beam

Calibration of an ionization chamber for proton dosimetry can be performed by exposure to a ^{60}Co-gamma beam in free air (or to an equivalent 2 MV X-ray beam). The calibration must then be obtained by comparison with another ionization chamber calibrated to a reference source of a national standard laboratory. National standard laboratories provide either air-kerma calibration factors, N_K (Gy/reading) or exposure calibration factors, N_x (C/(kg × reading)). The air-kerma calibration factor and the exposure calibration factor are related by:

$$N_K = \frac{N_x(W_{air}/e)_c}{1-g} \qquad (2)$$

where g is the fraction of energy of secondary charged particles that is converted to Bremsstrahlung in air. The index c stands for calibration beam.

By application of the Bragg-Gray cavity theory for an ionization chamber filled with air, the mass

of the gas (m_{air}) in the cavity of the chamber can be obtained from the ^{60}Co-calibration through:

$$m_{air} = \frac{(W_{air}/e)_c \times [(\overline{L}/\varrho)^{A-150}_{air}]_c \, [(\overline{\mu}_{en}/\varrho)^{air}_{A-150}]_c}{N_k \, (1-g) \times A_{wall}} \quad (3)$$

or when using an exposure calibration factor:

$$m_{air} = \frac{[(\overline{L}/\varrho)^{A-150}_{air}]_c \, [(\overline{\mu}_{en}/\varrho)^{air}_{A-150}]_c}{N_x \times A_{wall}} \quad (4)$$

In Equations (3) and (4), A_{wall} is a factor that corrects the chamber response for the absorption and scattering in the chamber wall, its build-up cap and stem during the calibration in air in the ^{60}Co beam, $(W_{air}/e)_c$ is the average energy expense per ion pair formed in dry air by the photon calibration source, $[(\overline{\mu}_{en}/\varrho)^{air}_{A-150}]_c$ is the mean energy absorption coefficient ratio of wall material (A-150) to air for ^{60}Co and $[(\overline{L}/\varrho)^{A-150}_{air}]_c$ is the mean restricted collision mass stopping power ratio of air to wall material for the slowing down spectrum of electrons released by the calibration radiation.

The mass of the gas (m_{air}) can be related to the cavity-gas calibration factor, N_{gas}, known from the American protocol (AAPM, Report 21) for absorbed dose determination from high energy photon and electron beams [16]:

$$N_{gas} = N_{air} = \frac{(W_{air}/e)_c}{m_{air}} \quad (5)$$

or:

$$N_{air} = A_{wall} \times (1-g) \times N_K \times [(\overline{L}/\varrho)^{air}_{A-150}]_c \times [(\overline{\mu}_{en}/\varrho)^{A-150}_{air}]_c \quad (6)$$

Since most national standard laboratories are providing air-kerma calibration factors, it is recommended to use Equations (3) or (4) for the calibration expression.

Ionization Chamber Dosimetry in Proton Beams

Substitution of these calibration factors in the general Bragg-Gray formula, applied during the measurement with this ionization chamber in a phantom, irradiated with the proton beam, will yield (by combination of Equations (1) and (3)) the absorbed dose to the chamber wall (A-150), D_{A-150}:

$$D_{A-150} = M_{corr} \times N_K \times (1-g) \times A_{wall} \times [(\overline{\mu}_{en}/\varrho)^{water}_{air}]_c \times \frac{(W_{air}/e)_p}{(W_{air}/e)_c} \times \frac{[(\overline{S}/\varrho)^{A-150}_{air}]_p}{[(\overline{L}/\varrho)^{A-150}_{air}]_c \times [(\overline{\mu}_{en}/\varrho)^{water}_{A-150}]_c} \quad (7)$$

In this equation $(W_{air}/e)_c$ is the average energy expense per ion pair formed in dry air by the proton source, $[(\overline{S}/\varrho)^{A-150}_{air}]_p$ is the mass stopping power ratio of air to the wall material (A-150) at the proton energy considered and M_{corr} is the chamber reading corrected for ambient conditions such as temperature, pressure, ion collection etc. The absorbed dose to water is then obtained from Equation (7) by multiplication with the mass stopping power ratio of water to A-150:

$$D_{water} = M_{corr} \times N_K \times (1-g) \times A_{wall} \times \frac{(W_{air}/e)_p}{(W_{air}/e)_c} \times \frac{[(\overline{S}/\varrho)^{water}_{air}]_p}{[(\overline{L}/\varrho)^{A-150}_{air}]_c \times [(\overline{\mu}_{en}/\varrho)^{air}_{A-150}]_c} \quad (8)$$

Under these conditions the absorbed dose in a proton beam, measured with an ionization chamber can be written in the following simple formula

$$D_{water} = M_{corr} \times N_K \times C_p \quad (9)$$

with:

$$C_p = A_{wall} \times [(\overline{S}/\varrho)^{water}_{air}]_p \times k \quad (10)$$

In this equation A_{wall} is a chamber-dependent factor, $[(\overline{S}/\varrho)^{water}_{air}]_p$ a proton energy-dependent factor and k a constant whose expression is

$$k = (1-g) \times \frac{(W_{air}/e)_p}{(W_{air}/e)_c} \times \frac{[(\overline{\mu}_{en}/\varrho)^{A-150}_{air}]_c}{[(\overline{L}/\varrho)^{A-150}_{air}]_c} = (1-g) \times \frac{(W_{air}/e)_p}{(W_{air}/e)_c} \times k_m \quad (11)$$

In this Equation k_m is the parameter that corrects for the non-air equivalence of the chamber wall and build-up cap.

If other ionization chambers are used, as recommended in the IAEA Report 277 or AAPM Report 21 [15, 16] with wall and build-up cap constructed from different materials, then the wall correction factor, also known as the k_{att} factor, can be found in the paper from Nath and Schultz [21] or in the existing photon dosimetry protocols.

For these ionization chambers Equations (3) to (12) are not valid and the non-air equivalence of the wall and build-up cap should be corrected by the k_m value

$$k_m = \{ \alpha \times [(\bar{L}/\varrho)^{wall}_{air}]_c \times [(\bar{\mu}_{en}/\varrho)^{air}_{wall}]_c + (1-\alpha) \times [(\bar{L}/\varrho)^{cap}_{air}]_c \times [(\bar{\mu}_{en}/\varrho)^{air}_{cap}]_c \}^{-1} \quad (12)$$

where α is the fraction of ionization due to electrons set in motion in the chamber wall during calibration. Values for these quantities for different ionization chambers can be found in existing photon dosimetry protocols [15, 16].

The values of all physical parameters in order to obtain the absorbed dose and their uncertainties are discussed in the following section. Utilizing the values given there, k is equal to 0.993 for A-150 ionization chambers.

Correction Factors on the Ionization Chamber Reading

In Equation (9) M_{corr} is the corrected reading and is obtained from the true reading, M, by

$$M_{corr} = M \times \prod_i p_i \quad (13)$$

with $\prod_i p_i$ the product of factors in order to correct the electrometer reading to the charge produced in the cavity under standard temperature and pressure conditions. It is defined as

$$\prod_i p_i = p_{T,P} \times p_{hum} \times \frac{(p_{pol})_p}{(p_{pol})_c} \times \frac{(p_{ion})_p}{(p_{ion})_c} \times p_j \quad (14)$$

The indices p and c refer to the proton beam and calibration beam, respectively. The parameters are

- $p_{T,P}$, temperature and pressure correction factor correcting the reading with respect to the reference temperature and pressure. Reference temperature and pressure are generally equal to 20 °C and 101.3 kPa.
- p_{hum}, humidity correction factor. It corrects the chamber reading from ambient air to dry air conditions. A value of 1.0025 [22] which corresponds to 50% humidity can be used. An alternative way is to flush the ionization chamber with dry air.
- $(p_{pol})_{p,c}$, polarity correction factor. It corrects for the change in chamber reading as a result of a change in polarity of the polarizing voltage. For most of the recommended tissue-equivalent ionization chambers this effect is small in the calibration beam as well as in the proton beam.
- $(p_{ion})_{p,c}$, ion recombination correction factor. This factor corrects for any losses in charge due to recombinations. If the calibration beam is ^{60}Co this effect is negligible. For the pulsed radiations the effect can be calculated from Boag's theory [23]. Proton beams are produced by different types of accelerators, including those that have a brief duty cycle. Therefore, the recombination effect $(p_{ion})_p$ should be checked by measuring the saturation curve.
- p_j, product of any other correction factors such as electrometer calibration, leakage currents, cable length etc.

Physical Parameters for Ionization Chamber Dosimetry and Estimation of the Uncertainties

The uncertainty in the measurement of the absorbed dose in proton beams is mainly influenced by the uncertainty on the $(W_{air})_p$ value (Tab. 3). Up to now, some measurements are available for this parameter [9, 17, 24–26]. On the other hand, continuing efforts are being made [27–31] with different types of calorimeters. Comparison of calorimeter dosimetry with ionization dosimetry will yield more information with regard to physical parameters. The parameters that follow are typically for tissue-equivalent ionization chambers made of A-150 and filled

Table 3. Comparison of absorbed dose determinations with ion chambers and calorimeters

Calorimeter material	Proton beam energy (MeV)	D_{ion}/D_{cal}	Center and reference
A-150	51.9	1.015	Orsay – LPRI [28]
A-150	32.6	1.003	Orsay – LPRI [28]
A-150	186	1.024	Orsay – LPRI [28]
water	160	1.01	Boston – MGH [27]
water	180	1.022	Loma Linda [30]
water	47	1.027	Louvain-Ghent [31]

with air, as discussed above. For other ionization chambers the values can be found in photon dosimetry protocols [15, 16].

Physical Factors Used in Calibration

Most of the factors to be used are, at present, recommended uniformly in the different photon dosimetry protocols

- g: the most recent value for the fraction of energy of secondary charged particles, converted to Bremsstrahlung for the calibration beam is 0.003 [32].
- $(W_{air})_c$: the value for the average energy expense per ion pair in dry air for the calibration beam is 33.97 ± 0.06 J/C [33].
- $[(\overline{\mu}_{en}/\varrho)^{A-150}_{air}]_c$: the mean energy absorption coefficients for photon energies near 1 MeV are taken from Hubbell or the ICRU 46 [19, 34]. The ratio of air to A-150 is 1.101.
- $[(\overline{L}/\varrho)^{A-150}_{air}]_c$: the mean restricted collision mass stopping powers are found in the ICRU 46 or for instance the AAPM protocol. The ratio for air to A-150 is 1.145.

Ionization Chamber-Dependent Factors

- A_{wall}: values for the wall correction factor for commercially available tissue-equivalent ionization chambers (A-150 wall + buid-up cap with a total thickness of 0.59 g/cm^2) are taken from Gastorf et al. [35] and shown in Table 1. The uncertainty was estimated by Rogers et al. [36].

Proton Beam-Dependent Factors

- $[(\overline{S}/\varrho)^{water}_{air}]_p$: in the past, stopping powers for protons were taken from tables of Janni [37]. Recently, the ICRU published stopping power values for monoenergetic proton beams for different materials [18]. Mass stopping power ratios must be calculated from these tables. For ionization chamber dosimetry only the mass stopping power ratio air to water has to be known. This ratio varies only slightly with energy. The proton beam energy is specified with its effective energy $(E_p)_{eff}$. Table 2 shows the stopping power values for water and air and their ratio.
- $(W_{air})_p$: the $(W_{air})_p$ value yields the greatest uncertainty and its choice is susceptible to discussion. A value of 34.3 J/C is recommended by the AAPM [1, 6], whereas the ECHED protocol [7, 8] together with the Japanese centers [38] recommends a value of 35.2 J/C, based on ICRU data [9]. Measurements of $(W_{N_2})_p$ were performed recently at Boston [24] and at Louvain [25, 26]. They found values of 36.3 J/C at 150 MeV and 36.84 J/C at 65 MeV, respectively, which is close to the ICRU value for nitrogen of 36.5 J/C. Hiraoka et al. [17] measured relative W-values for air to nitrogen at 70 MeV. Assuming a value of 36.5 J/C for nitrogen (taken from the ICRU) their mesurements confirmed the recommended value of the ICRU of 35.2 J/C. In the absence of further experiments, the value of 35.2 J/C for $(W_{air})_p$ can be used at all energies. At present, water calorimeters results have become available [27, 28, 30, 31]. These measurements indicate (Table 3) a difference of approximately 2% between the ionization chambers (applying a value of 35.2 J/C for $(W_{air})_p$) and the calorimeter. This would mean that in the future a ± 2% lower value for $(W_{air})_p$ might be recommended or a supplementary correction factor of –2% should be

Table 4. Estimation of the uncertainties (1SD) in measurements of absorbed dose for proton beams by an ionization chamber calibrated in air-kerma

Source	Symbol	Relative uncertainty (%)
Electrometer reading	M	0.1
Reading correction factor	$\prod_i p_i$	0.2
Air-kerma calibration factor	N_K	1.0
A_{wall} correlation factor	A_{wall}	0.2
Mass stopping power ratios	$[(\bar{S}/\varrho)^{water}_{air}]_p$	1.2
Average energy required to form an ion pair for protons	$(W_{air}/e)_p$	4.0
Average energy required to form an ion pair for the calibration beam	$(W_{air}/e)_c$	0.2
Ratio of the photon mass absorption coefficients	$[(\bar{\mu}_{en}/\varrho)^{A-150}_{air}]_c$	0.1
Ratio of the mean restricted collision mass stopping powers	$[(\bar{L}/\varrho)^{A-150}_{air}]_c$	0.1
Overall uncertainty on the absorbed dose in water for proton beams	D_{water}	4.3

applied in order to obtain agreement between calovimetry and ionization chamber dosimetry. Final recommendations will be given in an ICRU report on proton dosimetry, which is in preparation [39].

Under these conditions, the overall uncertainty on the absorbed dose in water, utilizing a tissue-equivalent ionization chamber shown in Table 4, is assessed to be equal to 4.3%. The uncertainties which were not discussed here, were taken from the discusions in ICRU 45 [40].

The overall uncertainty for dose determinations in proton beams is larger than for photon or electron beams but comparable to neutron beams [40, 41]. On the other hand, the uncertainty of determining the absorbed dose with a calorimeter is smaller (±2%) [4] and depends on the uncertainty of the assumed heat defect of the calorimeter material (water or A-150 plastic).

For the measurement of the absorbed dose in other heavy charged particle beams, the ionization chamber should be calibrated directly with reference to a calorimeter.

Relative Dosimetry

Acquisitions of absorbed dose distributions are neccesary for two purposes:

- as basic beam parameters for planning purposes (supplementary corrections for the RBE variation as a function of energy will be necessary for ion beams)
- for quality control procedures (beam alignment, symmetry, flatness and beam energy).

The detectors used should, therefore, respond to several criteria:

- the dose distributions should be as in tissue or the neccesary corrections to tissue should be possible
- the detectors should be small with respect to the steep dose gradients of the heavy charged particle beams
- heavy charged particle beams will also show large variations in LET, (even for proton beams, large variations in LET might be expected at the end of their range); therefore, the detectors should not show any LET effect
- they need to have the appropriate dose sensitivity and a linear dose response.

It will not be easy to find a detector responding correctly to these criteria. Several detectors are commonly used in conventional photon or electron beams for relative dosimetry.

Small Ionization Chambers

They have the advantage that the principles explained in the preceding chapters can be applied. They will yield the exact dosimetry result, if the correct factors are applied. If thimble chambers are not small enough with respect to the dose gradients a combination with parallel-plate ionization chambers should be considered. These parallel-plate ionization chambers will have a perfect definition of the measurement point as a function of depth.

Thermoluminescence Dosimeters (TLD)

Several types of thermoluminescence dosimeters are used for dosimetry in conventional radiotherapy; most commonly are LiF:Mg:Ti, CaF_2:Tm and $CaSO_4$ phosphors. All these materials have their own dosimetry characteristics, as far as dose response and sensitivity, tissue-equivalence, or temperature response (glow curve) are concerned. When these phosphors are treated carefully (i.e., standard conditions for annealing, reading, and calibration) a precision of ±3 % can be achieved [42].

For ion beam therapy extra care must be taken as to the LET-dependence of these materials. The average distance between ionizing events along the track can become much less than the distance between the nearest trapping centers. For LiF a strong decrease of dose sensitivity with increasing LET has been observed [43–46] for ion and neutron beams. These phosphors will also show a decreasing supralinearity with increasing LET [47] and an LET-dependent glow curve. For LiF the height of peak no. 6 (≈285 °C) is much more LET-dependent than the other peaks as was observed with protons and other ion beams [48, 49]. An even more pronounced effect has found for CaF_2:Tm phosphors. For these phosphors, an analysis of the ratio of peak 3 (≈150 °C) and 5 (≈240 °C) allows an indication of the beam quality [50, 51].

Photographic Film Emulsion

Films also show a very strong LET-dependence. It is related to the film dose sensitivity and consequently to its grain size [52]. Therefore, it will not be possible to use them for depth-dose determinations. The decrease of the film sensitivity might even be more important than the increase of dose as a function of depth. On the other hand, films still have their usefulness for field mapping. When the beam composition does not change significantly perpendicular to the beam direction, analysis of the optical density of the film yields acceptable results for the determination of the beam profile. In this case, it is possible to exploit fully the advantages of film dosimetry including good spatial resolution and the availability of storable hard copies.

Silicon Diode Detectors

Silicon diode detectors are used in various dosimetric situations: In conventional radiotherapy they serve as in-vivo detectors [53] or as detectors for relative dosimetry [54]. In any case, one can benefit from their excellent spatial resolution and dose sensitivity (cf. preceding chapter for details). For ion beam dosimetry, Si-diodes can be used under the same conditions. However, it is known that they will loose their sensitivity with the accumulation of dose. Rikner [54] has observed a reduction of 30 % in sensitivity after a proton dose of 10 kGy. Care must further be taken because of small differences which have been observed between the Si- and ion chamber response when measuring depth-dose data in proton beams [55, 56]. These differences cannot be explained by variations of the stopping power ratio with energy.

Other Detectors

Other detectors, such as activation detectors, diamond detectors, alanine or radiographic films might be useful for different clinical dosimetry tasks (cf. preceding chapter). Their dosimetry characteristics are, at present, studied [57, 58]. However, not even for proton beams enough data are available at this moment to report on.

References

1 Verhey, L., Koehler, A.M., McDonald, J.C., Goitein, M., Ma, I-C., Schneider, R.J., and Wagner, M. The determination of the absorbed dose in a proton beam for purposes of charged-particle radiation therapy. Radiat. Res. 79, 34–54, 1979.

2 Vynckier, S., Meulders, J.P., Robert, P., and Wambersie, A. The proton therapy program at the cyclotron "Cyclone" of Louvain-la-Neuve (first dosimetric results). J. Eur. Radiother. 5, 245–247, 1984.

3 McDonald, J.C. and Domen, S.R. A-150 plastic radiometric calorimetry for charged particles and other radiation. Nucl. Instr. Meth. Phys. Res. 752, 35–40, 1986.

4 Caumes, J. and Simoen, J.P. A TE-calorimeter as a primary standard for neutron absorbed dose calibrations. J. Eur. Radiother. 5, 235–239, 1984.

5 Kacperek, A. and Bonnet, D.E. Development of a Faraday cup for proton beam dosimetry at the MRC cyclotron unit at Clatterbridge, in Proc. Int. Heavy Particle Therapy Workshop, Blattmann H. (ed.), PSI report 69, 53–56, 1990.

6 AAPM Report 16, Protocol for Heavy Charged-Particle Therapy Beam Dosimetry. A Report of Task Group 20, Am. Inst. Phys., New York, 1986.

7 Vynckier, S., Bonnett, D.E., and Jones, D.T.L. Code of practice for clinical proton dosimetry. Radiother. Oncol. 20, 53–63, 1991.

8 Vynckier, S., Bonnett, D.E., and Jones, D.T.L. Supplement to the code of practice for clinical proton dosimetry. Radiother. Oncol. 32, 174–179, 1994.

9 ICRU Report 31, Average Energy Required to Produce an Ion Pair, Bethesda, Maryland, 1979.

10 Falkmer, F., Fors, B., Larsson, B., Lindell, A., Naeslund, J., and Stenson, S. Pilot study on proton irradiations of human carcinoma. Acta Radiol. 58, 33–51, 1962.

11 Suit, H., Goitein, M., Munzenrider, J., Verhey, L., Blitzer, P., Gragoudas, E., Koehler, A.M., Urie, M., Gentry, R., Shipley W., Urano M., Duttenhaven, J., and Wagner, M. Evaluation of the clinical applicability of proton beams in definitive fractionated radiation therapy. Int. J. Radiat. Oncol. Biol. Phys. 8, 2199–2205, 1982.

12 Graffman, G., Brahme, A., and Larsson, B. Proton radiotherapy with the Uppsala cyclotron. Experience and plans. Strahlentherapie 161, 259–260, 1985.

13 Gragoudas, E.S., Goitein, M., Verhey, L., Munzenrider, J., Suit, H.D., and Koehler, A. Proton beam irradiations: An alternative to enucleation for intraocular melanomas. Ophtalmol. 87, 571–581, 1980.

14 Goitein, M., Gentry, R., and Koehler, A.M. Energy of proton accelerator necessary for proton treatment of the choroidal melanomas. Int. J. Radiat. Oncol. Biol. Phys. 9, 259–260, 1983.

15 IAEA Report 277, Absorbed Dose Determination in Photon and Electron Beams, IAEA Vienna, 1987.

16 AAPM, Task Group 21, A protocol for the determination of the absorbed dose from high-energy photon and electron beams. Med. Phys. 10, 741–771, 1983.

17 Hiraoka, T., Kawashima, K., and Hoshino, K. Determination of differential W-values for proton, deuteron, ^{3}He and ^{60}Co gamma-ray beams in several gases. Phys. Med. Biol. 33, Suppl. 1, 131, 1988.

18 ICRU Report 49, Stopping Powers for Proton and Alfa Particles, Bethesda, Maryland, 1993.

19 ICRU report 46, Photon, electron, proton and neutron interaction data for body tissues, Bethesda, Maryland, 1992.

20 Gray, L.H. Ionization method for absolute measurements of gamma-ray energy. Proc. Royal Soc. (London) A156, 578, 1936.

21 Nath, R. and Schultz, R.J. Calculated response and wall correction factors for ionization chambers exposed to ^{60}Co gamma rays. Med. Phys. 8, 85, 1981.

22 Schultz, R.J., Almond, P.R., Kutcher, G., Loevinger, R., Nath, R., Rogers, D.W.O., Suntharalingam, N., and Wright, K.A. Clarification of the AAPM Task Group 21 protocol. Med. Phys. 13, 755–759, 1986.

23 Boag, J.W. and Currant, J. Current collection and ionic recombination in small cylindrical ionization chambers exposed to pulsed radiation. Br. J. Radiol. 104, 5219–5226, 1980.

24 Petti, P.L., Verhey, L., and Wilson, R. A measurement of w for 150 MeV protons in nitrogen and argon. Phys. Med. Biol. 31, 1129–1138, 1986.

25 Denis, J.M., Slypen, I., Tilquin, I., and Meulders, J.P. Average ionization energy, w, for 65 MeV protons in nitrogen, in Proc. EPAC 90, Nice 1990, pp. 15–16.

26 Denis, J.M., Slypen, I., Tilquin, I., and Meulders, J.P. Mesure de l'énergie moyenne, w, de l'azote par des protons de 65 MeV, Rapport Cyclotron, Louvain-la-Neuve, 57–58, 1990.

27 Schultz, R.J., Verhey, L., Saiful Huq, M., and Venkataramanan, N. Water calorimeter dosimetry for 160 MeV protons. Phys. Med. Biol. 37, 947–953, 1992.

28 Daures, J. Mesures calorimétriques et ionométriques effectuées dans les faisceaux de protonthérapie d'Orsay. Récapitulatif des mesures, personal communications, LPRI/93/114/JJ/JD, 1993.

29 Bridier, A., Delacroix, S., Daures, J., Vynckier, S., Kacperek, A., Mazal, A., Herault, J., Brassard, N., Sabattier, R., and Rosenwald, J.C. Détermination de la dose absorbée dans les faisceaux de particules lourdes chargées, Résumés de la XXXII-ème congrès de la Sociètè Française des Physiciens d'Hôpital.

30 Vatnitski, S.M. and Siebers, J.V. Comparison of water calorimeter with reference ionization chamber dosimetry in high photon and proton beams. Pres. at the NPL Calorimetry Workshop, NPL, Teddington, UK, October 12–14, 1994.

31 Seuntjens, J., Palmans, H., Verhaegen, F., Vynckier, S., Denis, J-M., and Thierens, H. Water calorimeter dosimetry for 90 MeV protons, presented at NPL Calorimetry Workshop, Euromet. Project No. 298, NPL, Teddington, UK, October 13–15, 1994.

32 Boutillon, M. Values of g for Photon Energies. CCEMRI Report (I)/85–18, Offilib, 1985.

33 Boutillon, M. and Perroche-Roux, A. M. Re-evaluation of the W-value for electrons in dry air. Phys. Med. Biol. 32, 213–219, 1987.

34 Hubbell, J.H. Photon mass attenuation and energy absorption coefficients from 1 keV to 20 MeV. Int. J. Radiat. Isot. 33, 1269, 1982.

35 Gastorf, R., Humphries, L., and Rozenfeld, M. Cylindrical chamber dimensions and the corresponding values of A_{wall} and $N_{gas}/(N_X A_{ion})$. Med. Phys. 13, 751–754, 1986.

36 Rogers, D.W.O., Biclajew, A.F., and Nahum, A.E. Ion chamber response and A_{wall} correction factors in a ^{60}Co beam by Monte Carlo simulation. Phys. Med. Biol. 30, 429–443, 1985.

37 Janni, J.F. Proton range-energy tables, 1 keV–10 GeV, part I, Atomic Data and Nuclear Data Tables 27, 147–339, 1982.

38 Hayakawa, Y. and Schechtman, H. Comments on the value of the average energy expended per ion pair formed in air for a proton beam recommended by the AAPM. Med. Phys. 15, 778, 1988.
39 ICRU Report Clinical Proton Dosimetry. Part 1: Beam Production Beam Delivery and Measurement of Absorbed Dose (in preparation).
40 ICRU Report 45 Clinical Neutron Dosimetry, Part I: Absorbed Dose in a Patient Treated by External Beams of Fast Neutrons, Bethesda, Maryland, 1989.
41 Mijnheer, B.J., Battermann, J.J., and Wambersie, A. What degree of accuracy is required and can be achieved in photon and neutron therapy? Radiother. Oncol. 8, 237–252, 1987.
42 McKinlay, A.F. Thermoluminescence dosimetry. Med. Phys. Handbooks 5, Adam Hilger, Bristol 1981.
43 Tochilin, E., Goldstein, N., and Lyman, J.T. The quality and LET dependence of three thermoluminescence dosimeters and their potential use as secondary standards, in Proc. 2nd Int. Conf. of Luminescence Dosimetry, USAEC and ORNL Conf. 680920, 1968, p. 424.
44 Hoffmann, W., Möller, G., Blattmann, H., and Saltzmann, M. Pion dosimetry with thermoluminescence materials. Phys. Med. Biol. 25, 913–921, 1980.
45 Chu, C.L., Hogstrom, K.R., Chen, G.T.Y., and Hilko, R.A. Thermo-luminescence of ^{7}LiF in therapeutic high-linear-energy-transfer charged particle beams. Phys. Med. Biol. 31, 145–160, 1986.
46 Hocini, B., Djeffal, S., Vynckier, S., and Wambersie, A. Response of ^{7}LiF thermoluminescent dosimeters to clinical neutron beams with energies ranging from d(14)+Be to p(65)+Be. Rad. Prot. Dosim. 23, 417–419, 1988.
47 Suntharalingam, N. and Cameron, J.R. Thermoluminescent response of lithium fluoride to radiations with different LET. Phys. Med. Biol. 14, 397–410, 1969.
48 Discroll, C.M. Studies of the effect of LET on the thermoluminescent properties of thin lithium fluoride layers. Phys. Med. Biol. 23, 777–781, 1978.
49 Vynckier, S., Vaerman, C., Delcoigne, B., Denis, J.M., and Wambersie, A. Response of LiF:Mg,Ti (TLD100) dosimeters to clinical proton beams of 85 MeV, in Proc. Int. Heavy Particle Therapy Workshop, Blattmann H. (ed.), PSI-Bericht-111, Switzerland, 26–28 March, 1991, pp. 136–138.
50 Hamal, M., Loncol, Th., de Patoul, N., Denis, J.-M., and Vynckier, S. Caractéristiques dosimétriques des détecteurs thermoluminescents CaF_2:Tm dans des faisceaux de neutrons et protons. Rapport d'activité 1993, Institut de Physique Nucléaire UCL, Louvain-la-Neuve, Belgium 1993, pp. 80–88.
51 Hoffman, W. and Prediger, G. Heavy particle dosimetry with high temperature peaks of CaF_2:Tm and LiF phosphors. Rad. Prot. Dosim. 6, 149–152, 1984.
52 Attix, F.H. Introduction to Radiological Physics and Radiation Dosimetry, J. Wiley & Sons, New York, 1986.
53 Leunens, G., Van Dam, J., Dutreix A., and van der Scheuren, E. Quality assurance in radiotherapy by in-vivo dosimetry 1: Entrance dose measurements, a reliable procedure. Radiother. Oncol. 17, 141–151, 1990.
54 Rikner, G. Silicon diodes as detectors in relative dosimetry of photon, electron and proton radiation fields, Ph.D. Thesis, Uppsala, Sweden, 1983.
55 Raju, M.R. The use of a miniature silicon diode as radiation dosimeter. Phys. Med. Biol. 11, 371, 1966.
56 Koehler, A.M. Dosimetry of proton beams using small silicon diodes. Rad. Res., Suppl. 7, 53,1967.
57 Vatnitski, S.M., Miller, D.W., Siebers, J.V., and Moyers, M.F. Application of solid state detectors for dosimetry of therapeutic protons beams. Med. Phys. 22, 469–473, 1995.
58 Olsen, K.J. and Hansen, J.W. Experimental and calculated effectiveness of a radiographic dye film to stopping 21 MeV ^{7}Li and 64 MeV ^{16}O ions. Nucl. Instr. Meth. B5, 494–504, 1984.

Control Systems for Ion Beam Radiotherapy Facilities

T. RENNER, M. NYMAN, and R. P. SINGH

Lawrence Berkeley Laboratory, Berkeley, CA, USA

Introduction

The advent of hospital-based ion beam radiotherapy facilities has recently focused attention on their requirements [1, 2]. The control system for patient treatments in these facilities is central to the safe and accurate realization of this type of radiotherapy.

A control system for charged particle radiotherapy ensures patient safety, controls the patient treatment, measures compliance of the actual treatment with the prescribed one, and provides feedback to the treatment planning process. In the future, this latter role will expand in several ways. Data obtained through patient dosimetry or other imaging methods will provide information for refining treatment plans. Radioactive beam imaging or PET scanning of isotopes produced within the patient by the particle beam will provide more accurate pictures of the actual treatment volume and its changes during the course of treatment [3, 4]. With the expanding role of 3D-conformal radiotherapy, accurate characterization of the treatment delivery system will be required to calculate treatment plans. These new technologies will require a treatment control system with a solid foundation. A description of such a foundation will be given.

This work is, in large part, an outgrowth of the work of the heavy particle radiotherapy program at the Lawrence Berkeley Laboratory. The history of this system began in 1979, with the development of a system architecture that could be used to treat patients and provide a basis for future development and growth in the technology of beam delivery. The system, which originally ran on a PDP 11–45, eventually ran on five kinds of computers over the last fourteen years, and was robust enough to support several kinds of beam delivery systems. A double scattering system, the wobbler beam delivery system, the first raster scanning beam delivery system and a three-dimensional conformal therapy delivery system have been controlled with it [5, 6]. In addition, the system operated two separate treatment rooms and one biological research facility. It has been used with pulsed beams from a synchrotron and continuous beams from a cyclotron. Our experience with this control system is condensed into a set of functional requirements. No attempt has been made to impose a particular implementation.

Overview of Individual Functions

The functions required for the control of a patient irradiation fall into three categories: a set for beam delivery, a set for beam production, and a set of ancillary functions. They are further subdivided as follows:

- Functions for beam delivery

  Interlocks are conditions which are prerequisites for an irradiation and are expected to be steady state during an irradiation.
  Beam modification is the process of tailoring the radiation field for a particular irradiation.
  Beam measurement dynamically determines radiation field parameters for beam control purposes.

Software beam delivery control comprises the software control algorithms and procedures that determine, set, and control the system parameters for a particular irradiation.
Hardware beam delivery control comprises the hardware control functions necessary for the initiation, termination and control of an irradiation. Often key control functions, such as starting and stopping of the beam, are implemented in both software and hardware for increased safety and reliability.
Monitoring is the verification of critical conditions during an irradiation.

- Beam production functions

  Accelerator and transport control conducts the generation and transport of the beam to a treatment room.
  The *accelerator interface* consists of a switch function for connecting the accelerator and a treatment delivery system, and a communication link between accelerator and treatment delivery systems. It also provides the capability of independent operation of the accelerator and the treatment control systems.
  The *timing* subsystem creates a set of time points which drive the sequence of events for both accelerator control and treatment control.
  Beam abort/halt terminates the delivery of beam into a treatment room.

- Ancillary functions

  The *human interface* provides displays of pertinent information for the medical and operations personnel.
  Simulation mimics measurement information and status to allow testing of the system operation without the use of beam.
  Dispatching is the process of allocating the accelerator to a particular treatment room.
  The *prescription server* serves as the conduit between the treatment planning system and the treatment control system.
  Archiving is the nonvolatile recording of both raw and processed data sufficient to: reconstruct a patient treatment, provide an accumulative history of each patient's treatments and create a data base for accelerator and treatment control system operation. A schematic overview of the treatment control process is shown in Figure 1. The relationship of these functions with one another is shown in Figure 2.

General Discussion of Individual Functions

As seen in Figure 1 the line of information is from the treatment planning system to the treatment control system to the accelerator control system. Rather than following this information flow, the

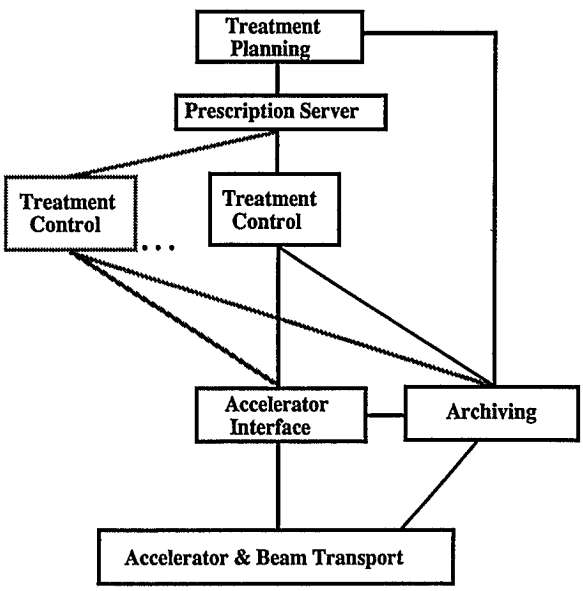

Fig. 1. Overview of the treatment control system. A prescription created by the treatment planning system resides in the prescription server until needed by the treatment control system. The prescription in this context is the information necessary for the delivery system to deliver the dose distribution specified in the treatment plan. A method for communicating with the accelerator and beam transport control system is embodied in the accelerator interface. All relevant data, parameters, tunes, and set points are recorded in archiving. The lighter lines indicate that several independent treatment control systems are possible

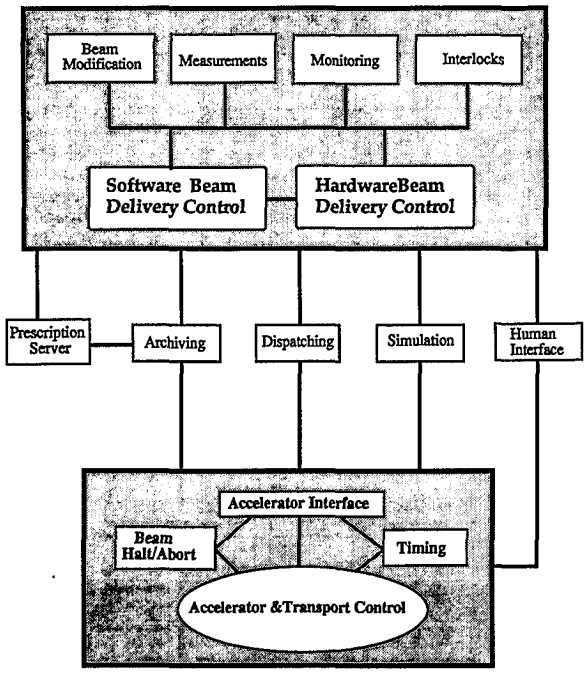

Fig. 2. *Relationship of control system functions.* This schematic diagram shows the relationship between functions found in a treatment control system

discussion will start with the heart of any radiotherapy system, the functions related to beam delivery.

Interlocks

As stated before, the prerequisite, steady state conditions of the treatment system that are not unique to a particular treatment and must be met before an irradiation commences, are interlocks. These interlocks are generally independent of the control of a device and their status is visible to operations and medical personnel. Several examples of such conditions requiring interlocks are:

1. personnel radiation safety circuits that restrict access to radiation areas,
2. the assignment of the accelerator to a particular treatment room,
3. the control system being in a simulation mode,
4. diagnostic X-ray equipment in the beam line, or
5. power supplies whose malfunction can cause harm to a patient and which must be operational before a treatment is allowed to begin.

Beam Modification

Modification of the beam by the control system occurs for each treatment and involves devices such as: collimators, range shifters, lateral spreading devices, range modulators, and a gantry/patient positioner. The fail-safe control and status of these devices are required for patient safety. For example patient-specific collimators need to be identified and their position monitored. For variable collimators, the size and shape has to be controlled to the required resolution within some specified time window. The physical position (location and rotation) of such a collimator is monitored if it is variable.

For changing the beam range, by accelerator energy changes and/or by mechanical degraders, the energy range and step size must be controlled to satisfy the treatment specifications. If compensation of the range is accomplished with a mechanical bolus a means of identifying the patient-specific bolus is important. Large numbers of patients being treated in several treatment rooms mandates a method of verification independent of human verification.

During patient treatments the ion beam is laterally spread out to produce the desired dose distribution. The methods of accomplishing this usually, involve several control parameters. For active systems, these parameters can include: the target shape (e.g., a boundary/shape matrix of the port), a matrix for controlling beam motion and position and possibly a beam current modulation matrix that can be a function of beam position. Double, single, or bi-material scattering systems also require verification of their parameters if they are adjustable on a patient-by-patient basis.

Energy modulation to produce a modulated depth dose distribution, whether achieved electrically or mechanically, and whether discrete or continuously variable, needs to be done on an appropriate time scale by the control system. Monitoring of all relevant parameters necessary

to insure the correct beam energy is critical for a safe treatment. For example, accelerator energy changes require an established set of machine and beam transport parameters for each energy to be used. Consequently, monitoring by the treatment control system of critical accelerator parameters is necessary.

The patient positioner/gantry position is operated with a particular resolution, extent of motion and accuracy of patient positioning. The speed and the extent of movement must be controlled to prevent damage to the device or injury to the patient and only executed with proper human authorization. A manual override of any computer control of such devices is essential, as is monitoring to insure the correct position is maintained at all times during an irradiation.

Beam Measurement

The beam measurement function dynamically determines the radiation field parameters for controlling the treatment and insuring it is delivered correctly. Measurements before the beam undergoes any of the kinds of modification discussed previously, insure the beam characteristics are correct before entering the beam delivery system. After the appropriate modification, an additional measurement as close to the patient as possible, insures the beam modification is correct and more accurately measures what the patient is actually receiving. Such measurements are performed on three time scales as defined below.

A *system unit of time* or clock cycle is the basic unit that allows accurate control of the dose being delivered to the patient. Typically this is in the millisecond or faster time scale. A *dosimetry cycle*, which is on the time-scale of a second, is the set of operations, triggered cyclically by the timing system, and which involve the collection, display and monitoring of data. During this cycle a snap-shot of the system performance allows periodic assessment and archiving of the state of the system. Quantities typically measured on this time scale are: the beam current, the transverse dose profile and centroid before and after beam modification, and the integrated delivered dose at isocenter. The third time-scale is the entire *treatment time* during which the delivered integrated dose at isocenter is measured by at least two independent detectors. Treatment times are on the scale of one to three minutes. During this time a verification of the beam range is also performed.

Software Beam Delivery Control

Software beam delivery control consists of the software procedures and control algorithms which determine and control the parameters for a particular type of irradiation. Figure 3 shows schematically the relationship of the components of this function. Included in this function are several kinds of irradiation procedures which, in general, satisfy the following requirements:

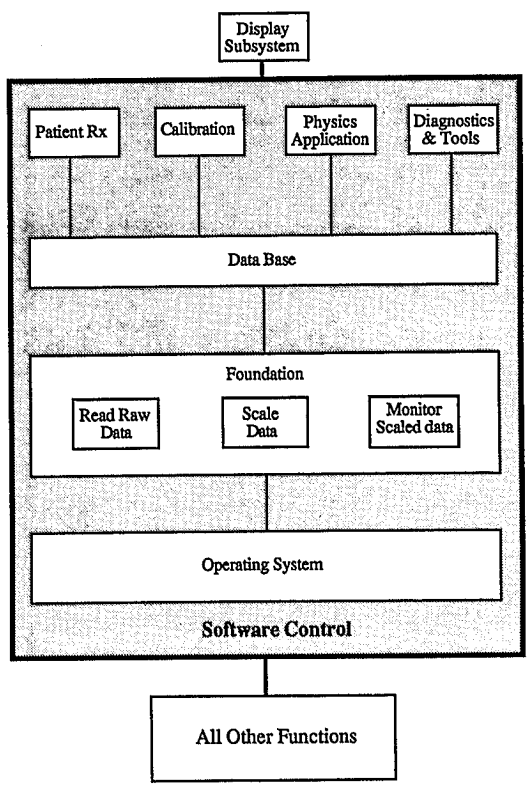

Fig. 3. Software control function scheme. This shows a set of applications which draw on a data base updated by a set of primitive functions which collect, scale, and monitor data in a cyclic fashion. Input from various control system functions are shown, e.g. monitoring, accelerator interface, etc.

1. critical parameters are verified before an irradiation begins,
2. the startup time for a procedure is minimized,
3. the time from initiating an irradiation (turning the beam on) to the actual commencement of the irradiation (beam on target) is minimized,
4. information determined as representative of the state of the treatment is presented to medical and operations personnel every dosimetry cycle.

Three types of irradiation procedures are particularly useful: a treatment procedure for performing a therapeutic irradiation or for exposing diagnostic film for patient alignment purposes, a calibration procedure for determining calibration factors of dosimeters for an irradiation procedure, and physics application procedures for dosimetry measurements.

The treatment procedure involves several tasks. The first task acquires dosimetry calibration information from the calibration procedure described below. Patient set-up parameters are verified against the patient's prescription and hardware parameters set to desired values, e.g., gantry/patient positioner parameters. The state of the interlocks and gantry/patient positioner settings are important to verify before and during the treatment. To recover from an interruption caused by a computer failure, the state of the system is saved on disk every dosimetry cycle. An abort of the irradiation is initiated upon normal completion of an irradiation. This occurs when all the steps of a procedure have been finished, or upon detection of any fault condition. To guard against a software procedure failing without terminating the treatment, an acknowledgment within an appropriate time window of a procedure-specific watchdog occurs every dosimetry cycle. Failure of such acknowledgment leads to an abort of the treatment by the hardware beam delivery control function. Any abort of the treatment (by human intervention, interlock dropout, critical hardware failure, monitoring veto, computer watchdog acknowledgment failure, or a preset scaler trigger) should preserve the state of the system. Support of an immediate resumption or resumption at a later time provides the necessary clinical option of how to proceed with a treatment after an abort. The time to recover from an interruption needs to be prompt and the maximum dose uncertainty after recovery should not exceed the dose delivered in a dosimetry cycle. At the end of a patient treatment, the treatment data is archived and a summary to the appropriate medical personnel is provided.

The calibration procedure establishes the conversion of the raw measured data to delivered dose in several contexts. Two important tasks of this function are calibrating an individual detector against a certified dosimeter and creating a calibration reference for the dosimetry system. On a daily basis the dosimetry system response is then compared against this calibration reference. Most importantly the calibration procedure measures the dosimetry system response relative to a certified dosimeter placed at isocenter within an appropriate phantom target volume. This establishes the calibration for a patient specific radiation treatment setup. Calibration of a patient treatment can also be extrapolated from a measured database provided the dosimetry system behavior and beam characteristics are sufficiently reproducible or can be compensated for. Dose measurements are required to be traceable to a fundamental standard using well-established calibration procedures [7].

Physics application procedures are used to characterize the beam and radiation field properties. Frequently, a measurement over an entire treatment, a part of an entire treatment, a sequence of individual steps of an irradiation or even an unmodified beam irradiation is required. Dose measurements in a water phantom in any of three orthogonal axes is a standard technique supported by these procedures. The ability to terminate the irradiation based on time, monitor units or dose is also advantageous. Both permanent dosimetry detectors and those installed only for a particular experiment, e.g., a diode, calorimeter or scintillator, are often used for beam and radiation field characterizations with these applications. Additional features that are useful are the ability to enable or disable specific beam monitoring, to set beam modification devices, to interrupt a measurement and resume it without loss of data, and to connect additional devices through I/O ports.

Diagnostic tools are also important for troubleshooting and verifying the proper working of the system. These aids are used continuously or upon demand and often concurrently with other procedures. Their access is generally restricted.

Hardware Beam Delivery Control

Hardware beam delivery control comprises the functions necessary for starting, stopping and controlling an irradiation as shown in Figure 4. Since the time frame for controlling the irradiation can be too short for computer control, dedicated hardware is often required or at least advisable for redundancy and reliability. Starting an irradiation requires all interlocks are satisfied, all watchdogs acknowledged, and all monitoring vetoes absent. An irradiation can then be initiated after the proper authorization from a qualified person is given, and the beam abort/halt system is under the control of the treatment control system. Computer-read scalers and preset scalers connected to the beam measurement system track the delivered dose. The beam enable/disable logic based on input from numerous sources initiates an abort of the beam as shown in Figure 4. Device controllers provide computer and manual control of the operation of a device, and status on its operation. Full closed loop control of a device is desirable where feasible and appropriate.

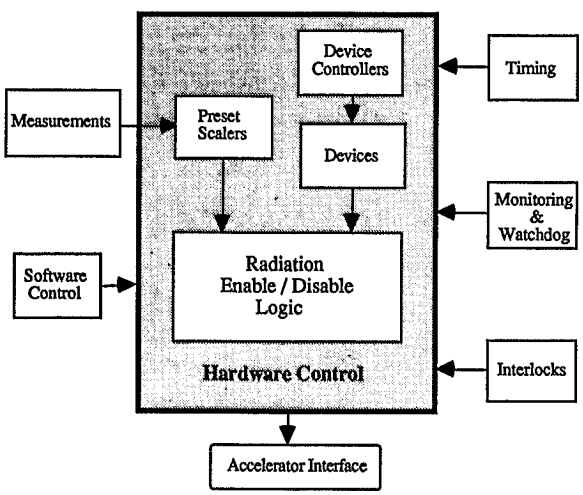

Fig. 4. Hardware control function scheme. Preset scalers, device status, timing faults, monitored parameters, interlock failure, watchdog acknowledgment failure, and software flags are input to the logic which enables and triggers the beam abort/halt system

Stopping an irradiation, as discussed below, involves a halt or an abort action initiated by the hardware beam delivery control. Several conditions can stop an irradiation: an interruption initiated by a qualified person, a preset scaler trigger, a fault signal from a critical device controller, a broken interlock, a failure of a watchdog acknowledgment, or any hardware or software monitoring veto. Continuation of the irradiation after its interruption is synchronized with the dosimetry cycle. The contribution of errors due to the interruption process to any dose error should be clinically acceptable.

Monitoring

Monitoring is an independent function for overseeing critical conditions and parameters during an irradiation. It is not a monolithic system, but rather a function contained within other functions and components of the treatment control system. The conditions and parameters monitored can involve beam modification devices, radiation properties, or accelerator parameters. Monitoring is capable of vetoing an operation and terminating an irradiation, but is not designed for initiating an action or controlling a device. Monitoring also contains the watchdog function which is a hardware-driven periodic check of a software operation. Watchdogs are armed by the system timing signal. The software operation in turn acknowledges the hardware component within a required time or else an abort of the beam is initiated. Upon acknowledgment, a handshake between the two parts is performed and the watchdog rearmed. The computer operation, the treatment procedure, and particular displays are examples of software operations requiring watchdogs.

Monitoring by the treatment control system also involves verification of critical accelerator parameters, separate from any verification performed for accelerator control purposes. Some parameters may require monitoring every acceler-

ator cycle or even continuously. These can include beam time structure, beam energy or rigidity, beam current, beam alignment and profile at the exit of the accelerator.

Critical beam modifying device parameters are also monitored at least every dosimetry cycle as are the radiation properties before and after these devices. The beam range or a quantity from which the range can be inferred, the beam current, the beam alignment (position and angle), and the beam profile are commonly monitored. In addition, after the beam modifying devices, the delivered dose and the radiation field compliance with the prescribed field are monitored. The beam transport system switchyard is also important to monitor, e.g., magnetic fields and magnet currents, as is the part of the beam transport system involved in the abort/halt function.

Accelerator and Beam Transport Control

The generation and travel of the particle beam with the desired characteristics to a treatment room is managed by the accelerator control system. This involves, besides an accelerator, the control of an ion generator, an injection system for initial acceleration and transport of particles to the accelerator, an extraction system for removing the beam from the accelerator, a beam transport system for channeling the particles to the desired treatment room, and a timing reference for process control. The performance of each of these parts is monitored and a watchdog function performed, where necessary, to insure a part is operative. A monitoring system that insures correct and safe operation, and a system for saving and restoring control parameters are also necessary parts. Measurement of beam properties and critical device parameters are also critical to this control function.

Communication links between the various accelerator control parts and their corresponding components employ several types of communication links including:

1. a data line for the exchange of information between subsystems and for stamping data as a certain type (e.g., real beam data, simulated data),
2. a timing line for synchronizing particular operations and procedures and time stamping data for control and archiving purposes,
3. a fast protection line that synchronizes several actions to halt/abort the beam.

Temporarily saving and restoring a partial or complete set of accelerator control parameters (e.g., machine tune) allows efficient switching between treatment rooms. Long term archiving of the accelerator parameters is advantageous for reconstructing the state of the system, creating an operational database for determining new operating conditions and for diagnosing problems.

Simulation in the accelerator system can also be useful for hardware and software testing without actual beam acceleration or magnet operation. Such a system must, of course, be interlocked and simulation status provided to the accelerator control system and the dispatching function. A blatant visual indication of simulation operation is also prudent.

Accelerator Interface

The accelerator interface is a software and hardware switch for connecting the accelerator and a treatment room. The software switch gives exclusive use of the accelerator to a particular treatment room. Similarly a hardware switch allows hardware signals only from the chosen treatment room to go between that treatment room and the accelerator. The extraction status, the abort/halt status, the beam energy, current, position, shape, and the necessary beam transport data (e.g., beam transmission, position, shape) are sent to the treatment control system while parameters, such as the desired energy and intensity, are sent to the accelerator control system via this accelerator interface.

Timing

The timing function drives the cycles of both the accelerator control and treatment control, including the dosimetry cycle, via a dedicated communication line. A loss or variation in this timing function as detected by a watchdog warrants the abort of the beam.

Beam Abort/Halt

The most important function is the beam abort/halt function which stops the delivery of a beam into a treatment room upon human command. Starting of an irradiation is in some sense the undoing of this function whose design must be fail-safe and the status of its state of operation known at all times. Any reasonable design includes redundant methods for stopping the beam (e.g., the beam transport system de-energized for fail-safe reasons, the beam extraction system turned off, a beam stop inserted at the accelerator and treatment room) and a means of easily activating this all critical function. The distinction between an abort and a halt is important and will now be discussed.

With a response time that satisfies clinical dose compliance specifications, a halt turns the beam off when: activated by a qualified person (e.g., by pushing a halt button), undesirable patient motion is detected, or a step in an irradiation procedure is completed. The end of a halt occurs at the removal of a halt request and is synchronized with the dosimetry cycle.

An abort first halts the beam and then inserts a physical beam-stop. Continuing the irradiation is not possible by simple removal of the abort request. An abort is intentionally a more drastic form of treatment interruption, requiring a well-defined set of steps to start the treatment again. An action by a qualified person, completion of an irradiation procedure, loss of any interlock, or the monitoring system's detection of anomalies potentially hazardous to the patient (e.g., unwanted gantry rotation) are situations that should cause an abort.

Special, dedicated hardwired links for aborting the beam are advisable along with buttons at appropriate locations. Reset of the beam abort control circuits should be independently performed by the accelerator and treatment control systems to insure both are ready to proceed.

Human Interface

The human interface connects the control system and the medical or operations personnel via the information displays shown in Table 1. These displays provide the medical and operations personnel with graphics and alphanumeric displays of data, development and diagnostic tools, visual hardware-status displays, error notification, or alarms. Refreshing the displays at least once per dosimetry cycle allows human surveillance of the progress of the treatment. Acknowledgment of a watchdog by critical displays insures the beam

Table 1. Human Interface Displays

Display	Provides	Location			
		Control Console	Setup room	Treatment room	Accelerator Control Room
Pretreatment information	Prescription information	√	√	√	
Irradiation information	Information on a treatment in progress				√
Irradiation summary	Results/summary of a single irradiation	√			
Treatment summary	Summary of treatments for a specified patient	√			
Facility Status and Scheduling	Status of patient treatments and accelerator operations	√	√		√
Beam Delivery	Information on the beam delivery system operation	√			√
Measurement Data	Numerical/ graphical display of data	√			
Alarms and Error Notification	Information of error conditions and alarms	√			

will be aborted if the displays are not updating. Direct visual hardware status, visual and auditory alarms, and a means of archiving errors are needed for debugging and trouble shooting.

Simulation

A means of testing the treatment control system or the accelerator control system without the actual use of beam is an invaluable capability. The simulation function generates measurement and status information that mimics real beam data for this purpose. This function clearly must be fully interlocked at the lowest possible level of its implementation to prevent confusion of real and simulated beam. Before its use, a handshake with the dispatcher verifying the treatment room is "off-line" is prudent, as is an interlock of the beam transport to prevent beam inadvertently entering the room. If a beam stop is used for each treatment room it should be inserted and deactivated.

Simulation also generates beam-modification device control and status information, accelerator parameter values and responses, beam abort/halt control and status information, beam-stop and beam transport status, timing signals and necessary monitoring status of the accelerator systems and treatment control systems. Simulation of the monitoring function may require the capability of suppressing some monitoring function vetoes, but those functions must be enabled when leaving the simulation mode.

Dispatching

For multiple treatment room facilities a method is required for deciding which room will receive beam from the accelerator. This function is called the dispatching function. The dispatching function receives requests from treatment rooms, assesses the availability of accelerator and beam transport systems, and allocates the use of the accelerator to a treatment room. The allocation is based on an algorithm which could be as simple as "first come first serve" or complex following a preset queuing algorithm. After a first mutual check ("handshaking") between the treatment and accelerator control systems this function sets the accelerator interface switches to allow communication between the treatment and accelerator systems. This gives exclusive use of the accelerator to a certain treatment room until released by the treatment control. An abort or halt does not release the use of the accelerator.

The Prescription Server

The prescription server is the link between the treatment planning system and the treatment control system for the exchange of the necessary information such as the beam delivery parameters for a treatment. Because this information is confidential and critical to a patient treatment, it is necessary to prevent unauthorized or inadvertent alteration of treatment parameters. By having the treatment plan reside outside the control system, verification of patient-specific parameters can be done before being transferred and executed by the treatment system. Results of each delivered treatment, which are useful feedback for refining the treatment plan, can be stored on this server. By having such a server the patient prescription information can be used by any treatment room. This allows greater flexibility and improved efficiency in scheduling treatments.

Archiving

A summary of the treatment including the delivered dose and a record of all critical raw and processed data are kept for each dosimetry and accelerator cycle. This process, called archiving, is a nonvolatile method of preserving information. In case of a system crash or treatment interruption, a system recovery or treatment resumption can be performed from this information. Clinical information, such as the patient identification, tumor dose for both an individual treatment and accumulative treatments and the names of personnel involved in the treatment, is archived. Protection of archived information from unauthorized or inadvertent modification is obviously important. Archived data is also needed for the creation and

refinement of the parametrization of control system variables, treatment planning and research analysis.

Conclusion

The safety of a radiation therapy facility is decisively determined by its control system. The general functions are needed in a treatment control system, but the true measure of such a system is in its implementation. To achieve the desired safety, reliability and flexibility, three basic design principles are important: fail-safe design, redundant design and fault-tolerant design. Fail-safe design requires that, at each level of implementation, the most probable failures will result in a safe state. No single hardware or software failure leads to a system failure or a compromise of safety. Redundant design decreases the probability of system failure from a particular failure mode by repeating a design implementation. Fault-tolerant design is achieved by computing or measuring a variable in several ways rather than simply redundantly. This increases the safety of the control system, adds to its monitoring capability and aids in diagnosing problems. It is from the use of these guiding principles that this summation is based on and the success of a control system is accredited.

References

1 Chu, W.T., Staples, J.W., Ludewigt, B.A., Renner, T.R., Singh, R.P., Nyman, M.A., Collier, J.M., Daftari, I.K., Kubo, H., Petti, P.L., Verhey, L.J., Castro, J. R., and Alonso, J.R. Performance Specifications for Proton Medical Facility, Lawrence Berkeley Laboratory Report LBL-33749, March 1993.

2 Gall, K.P., Verhey, L., Alonso, J., Castro, J., Collier, J.M., Chu, W., Daftari, I., Goitein, M., Kubo, H., Ludewigt, B., Munzenrider, J., Petti, P., Renner, T., Rosenthal, S., Smith, A., Staples, J., Suit H., and Thornton, A. State of the art? New proton medical facilities for the Massachusetts General Hospital and the University of California Davis Medical Center. Nucl. Instr. Meth. Phys. Res. B79, 881–884, 1993.

3 Llacer, L., Chatterjee, A., Batho, E.K., and Poskanzer, J.A. IEEE Trans. Nucl. Sci. NS-30, 61–625, 1983.

4 Bennett, G.W., Archambeau, J.O., Archambeau, B.E., Meltzer, J.I., and Wingate, C.L. Visualization and transport of positron emission from proton activation in vivo. Science 200, 1151–1152, 1978.

5 Renner, T.R. and Chu, W.T. Wobbler facility for biomedical experiments. Med. Phys. 14, 825–834, 1987.

6 Chu, W.T., Bercovitz, J.H., Halliwell, J.B., Ludewigt, B.A., Marks, K.M., Nyman, M.A., Renner, T.R., Singh, R.P., Stover, G.D., and Stradtner, R. Three-dimensional conformal therapy using light-ion beams, Digest of the World Congress on Medical Physics and Biomedical Engineering, Kyoto, Japan, July 7–12, 1991. Med. Biol. Eng. Comp. 29, Suppl. Part 2, 776, 1991.

7 AAPM Radiat. Therapy Comm. (Task Group 21), A protocol for the determination of absorbed dose from high energy photon and electron beams. Med. Phys. 10, 741–771, 1983.

VI. Patient Positioning and Treatment Planning

28 Imaging and Tumor Localization

W. SCHLEGEL and J. PROSS*

Deutsches Krebsforschungszentrum (DKFZ), Heidelberg, Germany

Introduction

Computer-assisted radiation treatment planning (RTP), and especially the newly developed three-dimensional treatment planning techniques, provide a tool to find the optimum configuration of radiation beams for the treatment of an individual patient. In clinical practice, RTP has traditionally been based on two-dimensional sectional representations of the treatment of the patient. However, the shape of the tumor and adjacent uninvolved anatomical structures may vary substantially from one section to another. The sectional two-dimensional planning approach may lead to uncertainties in localizing the volume and target volume as well as internal organs, a problem that can still be considered to be one of the most frequent sources of error in the whole radiation treatment procedure.

Today, the situation is gradually changing due to several technical developments, among which the advent of whole-body X-ray computed tomography (CT) and magnetic resonance imaging (MRI) are the most important. With the availability of CT and MRI, the ability to visualize anatomical structures in detail has been tremendously improved.

In order to take full advantage of these new imaging developments within the field of radiation therapy, new tools have to be developed and evaluated that permit easy and precise extraction of the therapy-relevant information from 3D-images, 3D-display of anatomical structures, and computer simulation for accurate placement of radiation beams. This contribution focuses on the application of computers in the step that is currently considered the bottleneck of three-dimensional treatment planning: segmentation of therapy-relevant anatomical structures.

Therapy-Relevant Anatomical Structures

Of all the therapy-relevant structures, two volumes should be defined prior to treatment planning (Fig.1): the *gross tumor volume* (GTV) and the *clinical target volume* (CTV).

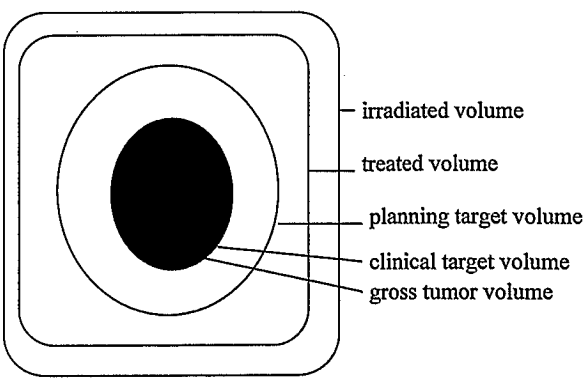

Fig. 1. Schematic illustration of the different volumes in radiotherapy planning: gross tumor volume (GTV) denotes the demonstrated tumor, clinical target volume (CTV) denotes the demonstrated tumor (when present) and also volumes with suspected subclinical tumor, the planning target volume (PTV) consists of the CTV and a margin to account for variations in size, shape and position relative to the treatment beam. The treatment volume receives the tumor dose or the dose considered important for local cure or palliation, and the irradiated volume is the volume which receives a dose considered important for normal tissue tolerance

* present address: Fa. Leibinger GmbH, Freiburg, Germany

During the treatment planning process, further volumes can be described, including the *planning target volume* (PTV) and the *organs at risk* (OARs). The final result of the treatment planning process are the *treated volume* and the *irradiated volume* [1].

The Gross Tumor Volume

The GTV comprises all the tissue that can be recognized and identified as tumor tissue within the tomographic images. The identification of tumor tissue may be based on different criteria, e.g., enhanced or decreased soft tissue contrast in the MR or CT images, with well-defined, blurred or even invisible margins (after subtotal or total tumor resection). Further criteria for the definition of the tumor volume are the displacement of neighboring anatomical structures or the appearance of edematous tissue.

The Clinical Target Volume and the Planning Target Volume

After defining the GTV, the CTV and the PTV have to be defined. The PTV is the volume that has to be completely covered by the therapeutic dose during the irradiation of the patient. It includes the CTV, i.e., the gross tumor volume, plus possible tumor extensions, possible sites of metastasis such as lymphatic regions in the vicinity of the tumor volume, preferred paths of further tumor growth and a so-called "safety margin" around the tumor. This safety region is essential as it takes into account the uncertainties during the irradiation of the patient caused by patient movement and/or inaccurate patient alignment. Tumor and target volume definition remain critical quantities which depend on histological and anatomical classification of tumor and safety margins.

Organs at Risk

The goal of radiotherapy is not only to apply a high radiation dose to the tumor, but also to avoid side effects in the surrounding healthy tissue, especially in those anatomical structures that will not tolerate radiation burdens above certain critical doses.

These non-target tissues or OARs are the third important type of therapy-relevant volume that has to be defined during the treatment planning process. For targets in the skull brain stem, white matter, optic nerve, eyes, or lenses are examples of OARs. There are several good reasons for a complete and accurate segmentation of OARs:

1. The geometrical shape and the location of the three-dimensional surfaces of the OARs can subsequently be used to optimize the position, shapes, and incidence angles of the radiation fields.
2. It is possible to precalculate the dose distribution within the target volumes, and, by adjusting the irradiation technique, minimize the physical dose in the critical areas.
3. With the help of radiobiological models, it is possible to estimate the risk of radiation injury (the treatment-related morbidity probability or TRMP) of critical organs and the probability for tumor control (tumor control probability or TCP).

Optimization of radiation treatment plans on the basis of TCPs and TRMPs seems much more promising than just a geometrical and physical consideration of the treatment planning problem. To make this biological treatment planning a routine tool in the future requires procedures for individual three-dimensional image segmentation for the definition of critical organs or even functional subunits of critical organs in addition to more elaborate and realistic radiobiological models.

Tumor tissue not included in the target volume will – with high probability – be underdosed. Unconsidered OARs, on the other hand, may eventually be overexposed. Errors, inaccuracies, and omissions made during the first step of image segmentation, influence the effectiveness of the treatment plan and the outcome of the whole radiotherapeutic process dramatically. This shows the importance of optimal treatment planning in radiotherapy.

Segmentation of Target Volumes and Organs at Risk

The method currently used in clinical practice for extracting 3D-information from CT and MR images is manual segmentation of the respective data sets. A three-dimensional image may consist of 20 to 60 slices. As many as ten or more structures may need to be outlined on each of these images. This is a major effort, if carried out for every patient. Until now, there have been few automatic tools available in clinical practice to facilitate this process and speed it up. However, some groups are developing fast and user-friendly three-dimensional image segmentation and modeling tools [2–7]. One of these systems will subsequently be described in some detail to characterize the state of the art in manual segmentation.

A Manual Tool for 3D-Segmentation

An interactive workstation program called TOMAS (=tool for manual segmentation) has been developed at the German Cancer Research Center (DKFZ) [4]. It is an example of an advanced program for 3D-segmentation of tumor volumes, target volumes, and organs at risk and is routinely applied in radiation treatment planning.

The program considers the following issues of tomographic image segmentation:

- image presentation
- efficient segmentation tools for drawing on tomographic images
- layout of the user interface
- visualization of the segmentation results

Image Presentation

Figure 2 shows the different sections of tomographic images. Three small windows appear at the top of the display screen. One presents the image data in the original form which is transversal for CT and transversal, sagittal, or frontal (depending on the image acquisition mode) for MRI. The two other small windows display multiplanar reconstructed views of the image data. One of the three views can be selected for presentation in the larger working window (see Fig. 2, bottom).

The spatial position of an actual section is indicated by reference lines in the two other corresponding views. The reference lines can also be used to select an interesting slice simply by moving the line with the computer mouse to the requested position. This method allows the radiotherapist to get an impression of the patient's anatomy in all three dimensions.

The working window is used to outline anatomical structures on the images. For the segmentation of small structures, the images can be enlarged up to a factor of eight of their original size. The area to zoom in upon is selected interactively by moving a rectangle on the image. A presentation with a high zoom factor can be smoothed by low-pass filtering.

The Segmentation Tools

Segmentation of three-dimensional images into tumor volumes, target volumes, and organs at risk is performed in the working window by contouring "regions of interest" in successive transversal, sagittal, or frontal sections with a tomographic image as background. The drawing instrument is the computer mouse. Three different drawing functions are available: free-hand, polygon drawing, and ellipse drawing.

When drawing free-hand, a line on the screen follows the movements of the mouse. Unwanted lines can be deleted at any time. It is often necessary to keep a well-defined safety margin to an anatomical structure, e.g., for the definition of the target volumes. For this purpose, the cursor can be changed into a circle with the center being the active point and the radius corresponding to the desired boundary. Polygons can be drawn by labelling, only the corner points. With the help of a spline interpolation, additional points can be regarded. This way, it is quite easy to create naturally shaped curves that approximate anatomical structures. To segment structures with nearly elliptical shape, e.g., the eyes or the lenses, it is convenient to use the circle and ellipse-drawing functions. This significantly reduces the time needed for outlining these objects.

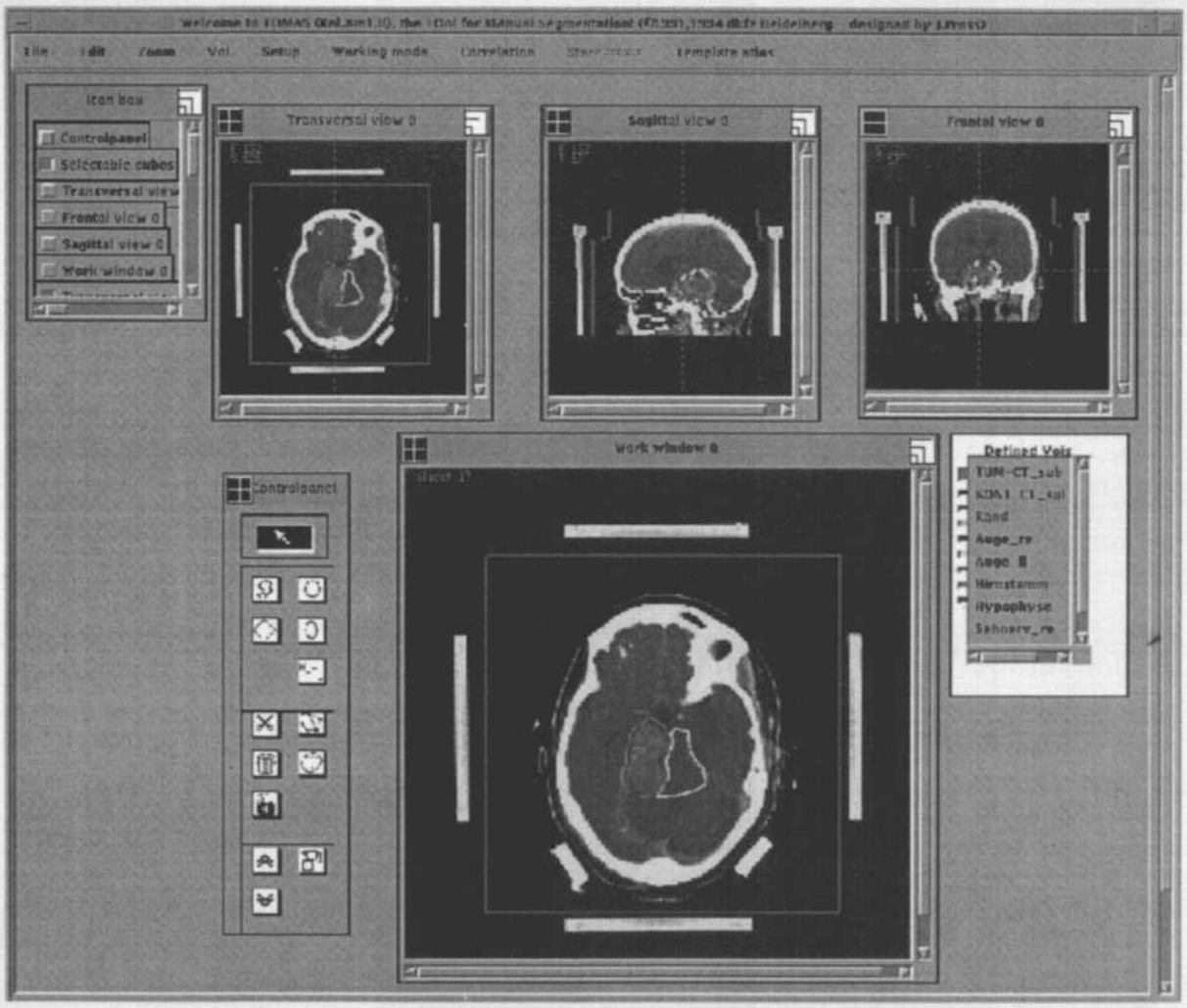

Fig. 2. User interface for manual segmentation of the Program TOMAS [2]

All manually drawn objects are "mouse-sensitive" and can be selected simply by clicking with the left mouse button on an object's outline. Selected objects can be moved, copied, or deleted interactively. It is also possible to scale and edit objects by clicking the mouse button on special control points and to move them to the required position.

As contours of an anatomical structure are often similar for adjacent slices (spacing between slices is usually 2–8 mm) the copy and edit functions are very convenient for three-dimensional segmentation of medical images. After a region has been drawn manually in the first slice to cut the anatomical structure of interest, it is copied to a neighboring slice. Usually, only small parts of the contours need then to be edited or redrawn to match the structure of the object in the new slice.

The interactive delineation of contours is a time-consuming task. A contour interpolation feature is therefore included in the program to calculate the preliminary contour in a slice, if contours in adjacent slices have already been defined. The interpolation algorithm is based on triangulation of the surface defined by two contours. With this feature, volumes of interest are defined as follows:

- the region of interest in the first, central, and last slices of the CT or MRI data set are outlined
- the program interpolates preliminary contours in all intermediate slices
- the contour in an intermediate slice is checked; if the interpolation is unsatisfactory, the contour is edited with the described functions
- the program reinterpolates in all slices where no user-defined contours exist.

Layout of the User Interface

All user interface objects may be manipulated by computer mouse. Functions of the program can be started simply by activating the mouse on icons in a control panel or by selecting entries of pull-down menus. Dialogs with the user are handled by dialog boxes.

A dialog box consists of interactive elements such as text entry fields, radio boxes, list and scale boxes. All program functions are displayed and the user can fully concentrate on working on the screen. This user-friendly interface makes the program easy to use even for inexperienced users.

Visualization

During and at the end of the segmentation procedure, it is important to have the possibility of checking the shape and the consistency of the volume under consideration, preferably in a three-dimensional view. Three visualization aids are currently implemented in the program:

- A contour drawn in the working window is also shown in the corresponding small overview window. The other two overview windows show the intersection of the previous and current contours with the slices perpendicular to the slice in the working window.
- A fifth window may be opened that shows a selection of up to 16 CT or MRI images with the contours of different previously segmented volumes.
- A perspective view of the different contour stacks can be accessed which provides a three-dimensional impression of the segmented volumes.

The Future: Semi-Automatic and Automatic Segmentation Tools

It is obvious that the manual contouring procedure is very time-consuming for the radiotherapist, in particular, when 3D-pictures are to be built-up. More sophisticated computer algorithms are requested to automate this process as far as possible. Only then can more patients benefit from a fully three-dimensional treatment, which is to improve tumor control and reduce side effects.

The remainder of this paper reports on work which has been carried out to achieve this goal.

Image Processing Approaches for Segmentation of Therapy-Relevant Volumes

Besides manual segmentation, objects with sufficient grey-level contrast can be segmented automatically using a threshold-based contouring algorithm. This algorithm, which is commonly used in image segmentation, has been very helpful in defining the outline contour of a patient and in segmenting bony structures or lung tissue in CT images. However, it fails completely for more complex objects with only small grey-level differences to the surrounding tissue.

Image segmentation on the basis of edge definition looks for local discontinuities in the grey-level intensity function of the image [3]. These local discontinuities (i.e., sites of high gradient) characterize abrupt intensity variations which often indicate the presence of an object in the image. Many techniques for edge detection have been developed. Their purpose is to describe an image by a set of points which constitute the boundaries of different objects in the image.

A second type of image segmentation identifies homogeneous regions in the image [7]. The

idea behind this approach is to describe the image by segmenting it into sets of points that possess a certain homogeneity. Different classes of homogeneity have been used to characterize "standard" regions, for example, smooth regions with uniform contrast or only slowly varying intensity or textured regions which can be detected on the basis of their typical structure pattern.

From a theoretical point of view, edge and region detection are complementary, in the sense that knowledge of the edges allows to deduce the regions and vice versa. However, in practice the two methods give rise to different algorithms that produce different results, each having its own peculiarities. The edge detector uses information from a limited number of points with a high image intensity gradient, whereas the region detector exploits information from many more points and can fill gaps left by an edge detector.

Some simple images can be satisfactorily segmented using edges alone, even though gaps may appear where imaging noise disrupts the performance of the edge detector. The boundaries of smooth regions may identify edges untraceable by an edge detector; however, they may be false, and without physical significance.

Rather than using edge and region detectors alone, it should, therefore, be attempted whenever possible, to combine their information in order to produce a more reliable result.

In classical low-level segmentation approaches such as automatic edge detection or region-growing methods, problems occur when the contrast between a structure and its background is low. Unfortunately, OARs and their background yield very often in CT and occasionally in MR images of low contrast. This is usually no problem for the human expert who will contour in such cases on the basis of additional anatomical knowledge.

Most OARs of the head are very similar from patient to patient as far as size and shape are concerned. This well-known fact led to the idea of using anatomical models for different medical applications [8–12]. To support the contouring process of the OARs of the head we have developed methods to fit individual patient data three-dimensionally by a standardized anatomical model.

The Anatomical Model-Based Segmentation Approach

The anatomical template atlas was established based on a high-resolution MR data set of a healthy individual. This data set consists of 128 slices (256×256 pixels) with an isotropic voxel size of approx. 1 mm and shows no significant anatomical deviations (Fig. 3). In this data set an experienced therapist defined the contours of all therapy-relevant OARs manually slice by slice. The next step was a 3D-surface model (Fig. 3) generated by triangulation of the contours of subsequent slices according to the method of Boissonnat [13]. The surface representation is a very compact method of data handling and permits usage of the model in real time. At present, the anatomical template atlas includes the following structures: outlines of the head, brain, cerebellum, eyes, optic nerves, chiasm, brain stem and pituitary gland.

Adapting the template atlas to individual brains is carried out in two steps: the model is first aligned globally to compensate for different positioning of patient and model during image acquisition. In the second step, the anatomical variations in brain size and shape between patient and model are taken into consideration.

A prerequisite for the global alignment of patient and model is to define a common reference coordinate system which allows to quantify the difference in position and orientation between the two. The bicommissural coordinate system according to Talairach and Tournoux [8] is an internationally accepted intracerebral coordinate system (Fig. 4), which serves this purpose. We use it in a variation of Schütz et al. [14].

Talairach et al. came to the conclusion that the anatomical variation between different individual brains is smaller when scaled to their proportional coordinate system. This system consists of 6 cuboids for each hemisphere. The cuboids are defined on the basis of the maximum extension of the brain and two lines (VCA and VCP) through the commissures (CA and CP in Fig. 4) which are perpendicular to the bicommissural plane.

To evaluate the template atlas approach, we integrated a sample implementation of the template atlas into the TOMAS program [15]. The 2D-

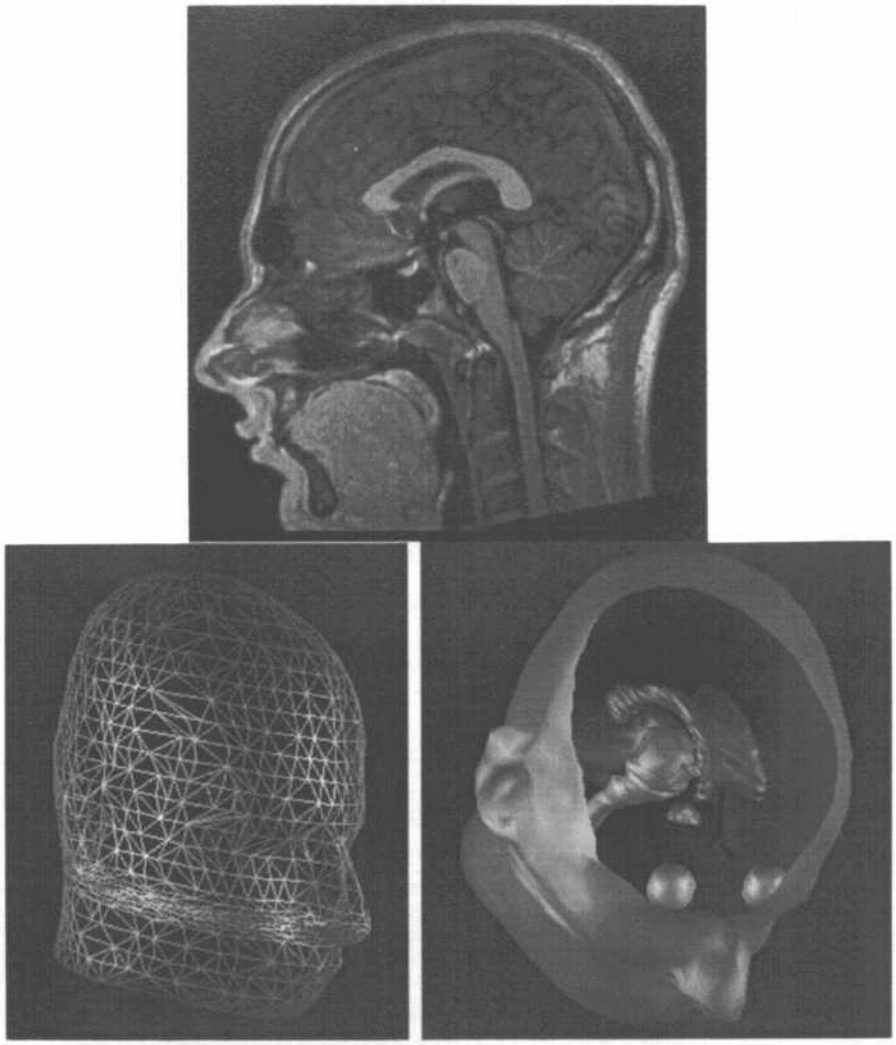

Fig. 3. Top: Sagittal section of the MR data set which serves as basis for the template atlas.
Bottom left: Triangulated network model of the head surface.
Bottom right: Template atlas model shown as shaded surfaces

atlas contours can be interactively moved and rotated in order to align the model to the patient's position and orientation. This way, variations in brain size and shape can be considered. A complete interactive matching procedure is illustrated in Figures 5 through 7. Figure 5 shows the starting position with model and patient more or less randomly oriented to each other. In a first step, the model is aligned to the patient's position in the axial section (Fig. 6, left). Subsequently, the axial rotation (Fig. 6, middle) can be compensated in a sagittal section (Fig.6, right). After this global alignment, position and orientation of model and patient correspond quite well. An interactive proportional scaling is carried out (Fig. 7, left) to compensate anatomical variations. The result is shown in the middle of Figure 7: model and patient match fairly good. A separate translation and rotation of the eyes and the optic nerves improved the result even further to the level illustrated on the right hand side of Figure 7.

In a first evaluation, the model-based segmentation approach was tested with 17 clinical patient data sets selected at random.

The first criterion was the time needed for the model-based approach as compared to the con-

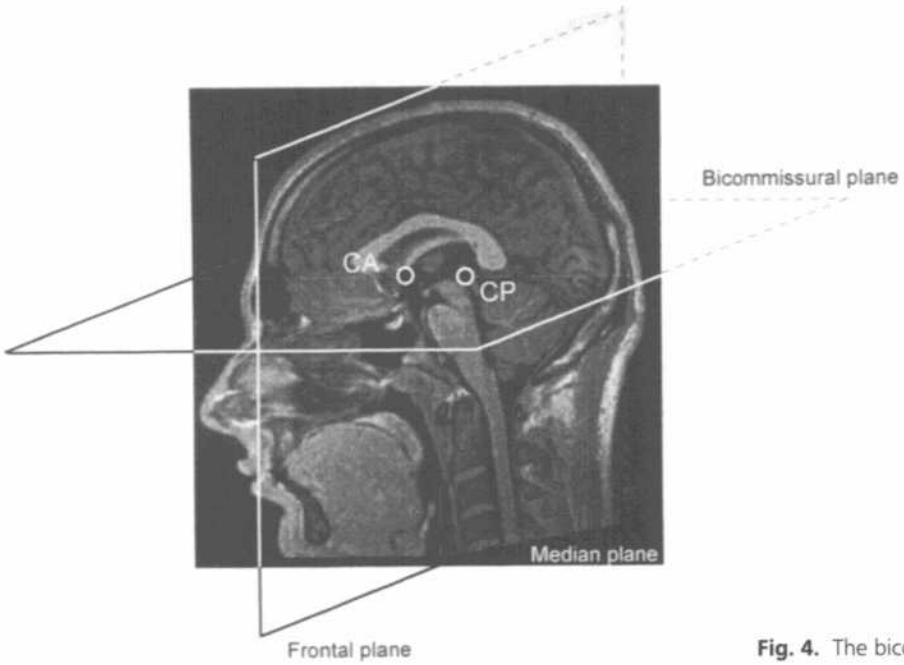

Fig. 4. The bicommissural coordinate system

ventional manual segmentation. The mean segmentation time with the model-based approach ran up to 8 minutes making it 2–3 times faster than the manual method which requires 15 to 30 minutes depending on the number of slices.

Concerning the accuracy, we found only a 10% difference between the model-based approach and the interpersonal variability even though 5 of the 17 test data sets had the brain stem displaced by a tumor. Non-linear deformations like this cannot be modelled with the slice-by-slice linear scaling approach of the proportional scaling method.

The study also showed, that in nearly all cases the contours of the eyes could be used for therapy planning without any modification. In case of the brain stem and the pituitary gland nearly 70% of the contours were suitable without modification and 25% after a simple translation. However,

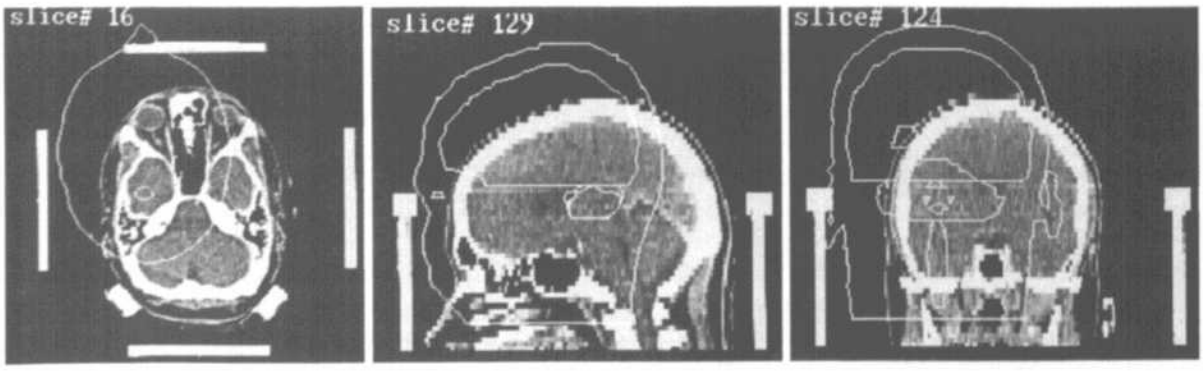

Fig. 5. Starting position of the anatomical model relative to the patient's image data set

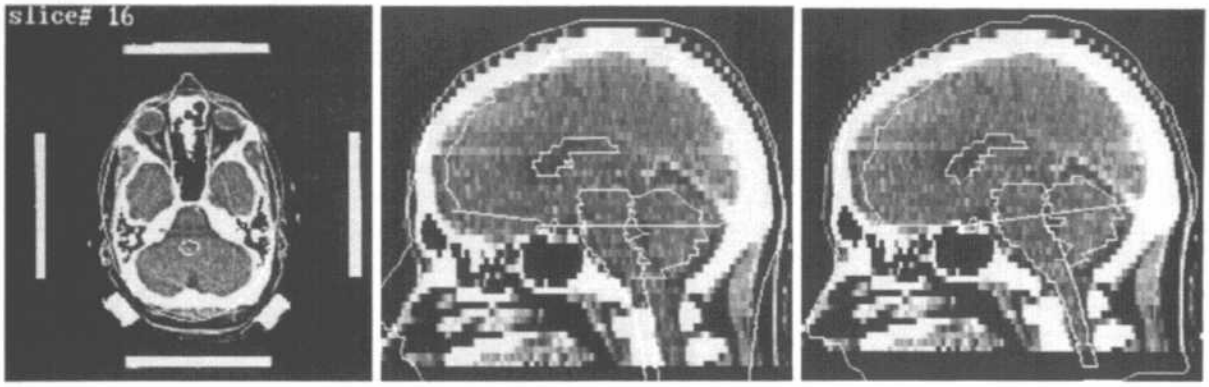

Fig. 6. Different intermediate matching steps for the global alignment

most contours of the optic nerves were inacceptable. The reason for this is the small size of the optic nerves which are poorly visualized in CT images with a 4 mm slice distance (e.g., partial volume effects). Their classification is highly subjective and, therefore, problematic.

Summary

Defining the tumor volume, target volume and organs at risk in CT or MRI data sets is one of the most critical steps in three-dimensional radiotherapy treatment planning. The accuracy with which the volumes can be detected and the required time for the delineation are still far beyond the clinical wishes.

Replacing time-consuming manual image segmentation by computer-assisted interactive image segmentation is a means to facilitate the process. The computer relieves the user of much of the tedious work, and enables the operator to use clinical judgement to achieve the desired result. The approaches described in this chapter are currently subjected to extensive clinical evaluation. First experience shows, that the existing problems can be solved at least for lesions in the head and neck area.

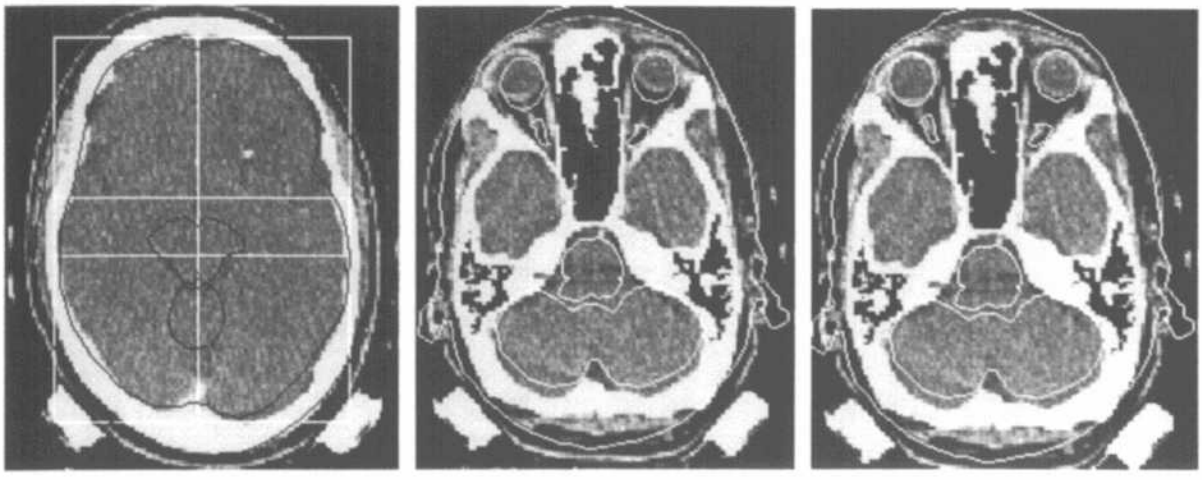

Fig. 7. Different intermediate matching steps to compensate anatomical variations

References

1 Landberg, T. Prescribing, recording and reporting photon beam therapy. Report 50, 1992.

2 Goitein, M. and Abrams, M. Multi-dimensional treatment planning: I. Delineation of Anatomy. Int. J. Radiat. Oncol. Biol. Phys. 9, 777–787, 1983.

3 Elliott, P., Knapman, J.M., and Schlegel, W. Interactive image segmentation for radiation treatment planning. IBM Systems Journal 31, 620–634, 1992.

4 Pross, J. Tool for manual segmentation of volumes in multi-modality 3D imaging, in Three-Dimensional Treatment Planning, Minet, P. (ed.), European Association of Radiology, Liège, 1993. pp. 245–252.

5 Dowsett, R.J., Galvin, M.J., Cheng, E., Smith, R., Epperson, R., Harris, R., Henze, G., Needham, M., Payne, R., Peterson, M.A., Skinner, A.L., and Reynolds, A. Contouring structures for 3-dimensional treatment planning. Int. J. Radiat. Oncol. Biol. Phys. 22, 1083–1088, 1992.

6 Fontana, F., Bonomi, A., and Vernazza, G. Innovative interactive methods for image segmentation, in Proc. of Computer-Assisted Radiology (CAR) 1993, Lembke, H.U., Inamura, K., Jaffe, C.C., and Felix, R. (eds.) Springer Verlag Berlin, 1993, pp. 321–327.

7 Sivewright, G.J., Knapman, J.M., Dickson, W., and Elliott, P.J. Interactive image segmentation applied to CT and MR images, in Proc. of Computer-Assisted Radiology (CAR) 1993, Lembke, H.U., Inamura, K., Jaffe, C.C., and Felix, R. (eds.) Springer Verlag Berlin, 1993, pp. 328–333.

8 Talairach J. and Tournoux P. Co-planar Stereotaxic Atlas of the Human Brain. Thieme, Stuttgart New York, 1988.

9 Greitz, T., Bohm, C., Holte, S., and Eriksson, L. A computerized brain atlas: Construction, anatomical content, and some applications. J. Comput. Assist. Tomogr. 15, 26–38, 1991.

10 Höhne, K.H., Pommert, A., Riemer, M., Schiemann, T., Schubert, R., Tiede, U., and Lierse, W. Framework for the generation of 3D anatomical atlases, in Visualization in Biomedical Computing 1992, Robb, R.A. (ed.), SPIE Proc. Series, Vol. 1808, 1992, pp. 510–519.

11 Kall, B.A., Kelly, P.J., Goerss, S., and Frieder G. Methodology and clinical experience with computed tomography and a computer-resident stereotactic atlas. Neurosurg. 17, 400–407, 1985.

12 Lehmann, E.D., Hawkes, D.J., Hill, D.L.G., Bird, C.F., Robinson, G.P., Colchester, A.C.F., and Maisey M.N. Computer-aided interpretation of SPECT images of the brain using an MRI-derived 3D neuroanatomical atlas. Med. Inform. 16, 151–166, 1991.

13 Boissonnat, J.D. Shape reconstruction from planar cross sections. Computer vision, Graphics, and Image Processing 44, 1–29, 1988.

14 Schütz, T., Vogt, H., Gerke, M., and Kretschmann H.-J. MatchVox-A workstation for computer-assisted neuroimaging, in Proc. of Computer-Assisted Radiology (CAR) 1991, Lembke, H.U., Rhodes, M.L., Jaffe, C.C., and Felix, R. (eds.), Springer-Verlag, Berlin, 1991, pp. 711–715.

15 Pross, J., Bendl, R., and Schlegel, W. TOMAS: A TOol for MAnual Segmentation based on multiple image data sets, in Proc. of the XIth Int. Conf. on the Use of Computers in Radiation Therapy, Hounsell, A.R., Wilkinson, J.M., and Williams, P.C. (eds.), Manchester, 1994, pp. 192–193.

29 Treatment Planning for Proton Beams

M. URIE*

Massachusetts General Hospital, Boston, MA, USA

Introduction

The specific energy deposition characteristics of protons offer the potential of dose distributions which conform more closely to target volumes than can X-rays, but also place higher requirements on the planning of treatments.

These requirements imply the use of reproducible immobilization techniques compatible with the diagnostic imaging modalities and treatment planning imaging studies of fine resolution.

The treatment planning system must be able to handle large volumes of data, perform the necessary calculations, provide the pattern for the required field defining devices and information for a correct positioning of the patient.

Presently, X-ray CT is the only imaging modality available which can provide the data needed to calculate the required range of protons. No MR echo sequence has been developed which can reliably be translated into proton stopping powers, nor are there other 3D-imaging techniques on the horizon which will. Hence treatment planning for proton therapy is based on CT. Exceptions are "shoot-through" techniques in which high energy protons are used and no attempt is made to not treat distal tissues by controlling their range, and secondly a few sites in which the entire pathlength of the protons is through homogeneous tissue of well-known composition and target volumes are regularly shaped.

A brief discussion of treatment planning for eye tumors with non-CT based patient information can be found in Chapter 13. In this chapter the discussion will concentrate on treatment planning based on CT information with the intent to conform the range and modulation of the protons to the target volumes.

Acquisition and Processing of Imaging Data

To treat most target volumes, passage through heterogeneities in the body is required. For proton therapy the position of each heterodense structure and its density must be defined; the range of the protons for any portal must be calculated and then compensated for in order to achieve the desired dose distribution pattern in the individual patient at each treatment session. Presently CT is the only method available to obtain these necessary data.

Converting CT Data into Proton Stopping Powers

CT data are acquired with highly filtered 120–140 kVp X-rays (effective energy of ca. 90 kVp). The mathematically reconstructed Hounsfield units represent the linear attenuation coefficients of these X-rays. These linear attenuation coefficients need to be converted into proton stopping powers in order to calculate the energy or range, required. Most treatment planning systems calculate the areal density by integrating the radiographic pathlength from the effective proton source to the distal target volume, and converting

* present address: University of Massachusetts Medical Center, Worcester, MA, USA

the Hounsfield unit of each encountered voxel into a stopping power using a look-up table.

Historically, the conversion table was empirically established at the Massachusetts General Hospital and Harvard Cyclotron Laboratory using fresh cadaver parts; the accuracy of predicting the protons' range with these data was estimated to be ca. 3.5% (unpublished data). More recent work using proton radiography and an animal's head [1] has examined the accuracy of different conversion tables. For a relatively homogeneous lateral brain irradiation, measurements and calculations based on a tissue substitute conversion table had a rms deviation of 2.5 mm, with a maximum of 11.1 mm. Correcting the table for tissue substitute composition (oxygen/hydrogen content) the rms deviation was reduced to 1.9 mm (maximum 6.0 mm). This is still substantial and most likely due to the effects of atomic composition of the tissues. By adjusting the Hounsfield units for specific organ composition (brain, bone, etc.) and using the tissue substitute corrected for composition conversion table, the rms deviation was reduced to 1.0 mm, with a maximum of 2.3 mm. This approach uses theoretical values of tissue composition. Another suggestion [2] has been to deduce this elemental composition by using dual energy CT scans. This is an accepted technique but as yet not routinely incorporated into planning treatments for proton therapy. Instead, usually a single energy CT scan is acquired and uncertainties in the range compensated for when prescribing the required penetration by adding a few millimeters or approx. 3% of the maximum range to assure target volume coverage.

CT data include the effects of statistical variations. They vary from time to time, with the field of view, and sometimes within the field of view. It is highly recommended that phantom studies be performed regularly to characterize the particular CT scanner being used for treatment planning scans and to include phantom material of well known composition in each patient scan. The treatment planning system should have the tools to scale the conversion table for each individual patient study.

Spatial Resolution

The extent to which inhomogeneities can be compensated for depends on a number of factors, including the scattering characteristics of the protons, the size and density of the inhomogeneities, the amount of physiological and anatomical movements, the stability of the patient, and finally, the ability to reproduce the set-up from CT scan to treatment and from treatment to treatment. In general, it is very difficult to achieve a reproducibility better than 2 mm, 3–5 mm is more common. However, it is better to take into account these variations intentionally with mathematical techniques than to be limited by the spatial resolution of the planning study.

The in-plane spatial resolution of present CT scanners is typically 0.4–1 mm, depending on the field of view. The spatial resolution along the longitudinal body axis is determined by the slice thickness and spacing. The thinner the slices, the greater the spatial resolution but the noisier the data; also there is a greater volume of data to be handled.

Sampling theory predicts better spatial resolution by overlapping the slices, i.e., to acquire 3 mm thick slices at 1.5 mm increments. Studies performed at Massachusetts General Hospital (unpublished data) concluded that the increased resolution was not significant enough clinically for proton therapy to justify the doubling of the data. Hence, unless very specific anatomy or fiducial markers are being localized, contiguous 2 or 3 mm thick slices are judged to be appropriate for treatment planning in the head; 3 or 5 mm is usually adequate for the body.

Treatment planning systems need to calculate the areal density from the effective proton source to the target volume. CT scans must therefore include all materials in the beam path, including any immobilization material which will be there when the patient is treated. Scans are performed with the patient in the immobilization device, in the treatment position, with a large enough field of view to encompass the entire patient circumference and extending far enough superior and inferior of the target volume to allow calculation of range for oblique fields.

Most proton therapy centers have fixed beam lines; the majority are horizontal. To deliver posteriorly and anteriorly oblique fields, patients are treated in seated or standing positions. Studies performed at MGH comparing CT scans taken with the patient supine to the patient seated have shown that intracranial contents shift with respect to the bony landmarks less than 2 mm between the two (unpublished data). However, below the base of skull, not only do the relative positions of the bony structures change but also the soft tissue thickness varies significantly between the two positions, in spite of apparently tightly conforming immobilization devices. These changes can vary significantly and unpredictably from patient to patient, even in the neck. In the thorax, abdomen, and pelvis these changes are much greater; planning studies in these sites must, therefore, be performed in the treatment position and in the immobilization device.

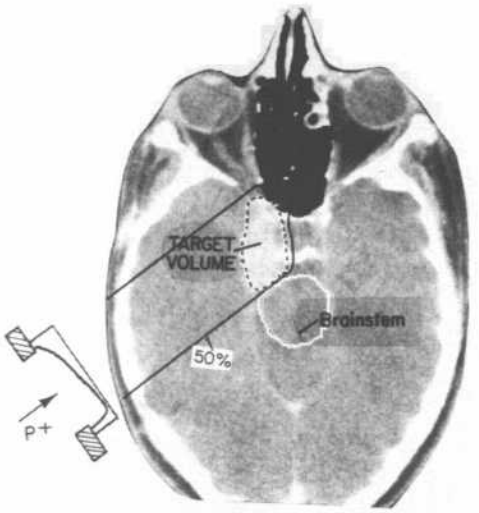

Fig. 1. Axial CT section in the head with the target volume and brain stem delineated. No immobilization material is apparent; the skin would be defined as entrance surface. A posterior oblique portal, shown schematically, would maximize target volume coverage while limiting the brain stem surface to 50% dose. The potential variation in range-modifying bolus thickness is illustrated, as is the potential air gap if the bolus is not contoured to the patient surface

Delineaton and Segmentation of Volumes of Interest

After the CT data are loaded into the treatment planning system, several steps are necessary before designing treatment portals. First, the data for this particular scan need to be scaled for the conversion table to proton stopping powers. Typically the Hounsfield units of the included phantom material (water, bone equivalent, etc.) are sampled and the conversion table uniformly adjusted by giving air, water, and bone values.

Secondly, the surface from which the proton range will be calculated needs to be delineated. Often this is the skin surface, but should include the immobilization material if it will be in place for the treatment. Automatic segmentation techniques may be useful, but their results need to be reviewed carefully and edited if necessary.

Thirdly, target volumes and normal tissues of particular interest need to be delineated (Fig. 1). Computer extraction techniques may be an aid for certain normal tissues, but their results again need to be reviewed carefully (cf. preceding chapter).

It is essential prior to beginning portal selection and design to know the prescribed dose to the target volume(s), the maximum tolerable doses to critical normal tissues, and the partial volume dose constraints to any organ.

Portal Selection

Although much work is underway for computer-assisted and optimized selection of portals, currently this work is done by experienced planners. Taking into consideration the overall aim of the therapy, i.e., to achieve the desired dose to the target and to limit the normal tissue doses, the planner develops on overall strategy. Typically 3 to 4 portals per target are selected from an overall 3D-visualization of the target(s) and its relationship to these normal tissues. Entrance directions are preferentially selected such that they do not overlap, e.g., right lateral, left lateral, posterior, and vertex fields.

The beam's eye view (BEV) display [3] is a valuable tool allowing 3D-visualization of any and all delineated volumes of interest (VOIs). In BEV, the relative geometries of the VOIs are

viewed and the patient's position interactively modified to optimize treatment of the target and sparing of normal tissues. The VOIs may be displayed as linear segments, wire frames, translucent volumes and/or solid structures.

Target volumes often have a geometrical relationship to critical normal tissues which suggest one, or two, optimal beam angles to minimize normal tissue doses. It is usually not desirable to employ only these one or two fields because tissues in the path still receive more dose than is desirable, since entrance doses are >75% in typically modulated beams.

Design of a Single Field

Having selected a portal direction in the BEV, a field-defining aperture may be designed. The geometrical projection of the aperture edge usually corresponds to the 50% dose decrement; margins need to be added around the target to account for the penumbra width from the 50% to the prescribed dose level (typically 90–95%) and to account for set-up uncertainties.

Penumbra width for proton beams varies with the beam line parameters. It increases with increasing scattering material in the beam line and with depth within the patient. Usually, a median depth to the target volume is estimated for a preliminary design of the aperture and the set-up uncertainty for this portal is estimated (typically 3–5 mm). Most planning systems have the ability to outline the projection of the target volume from the BEV and to add a margin around this projection, which can then become the aperture. Most programs also allow viewing the projection of this aperture on the axial CT slices and on sagittal, coronal and oblique planes reconstructed from the axial slices. Viewing this projection allows the planner to make any modifications which were not appreciated in the BEV.

Having defined the field shape perpendicular to the beam with the aperture, the ranges required for the protons throughout the field need to be calculated. Not only is the range to the most distal target from the entrance surface needed, but also the extent in depth of the target in order to know how much the Bragg peak needs to be spread out (modulated). This calculation is performed with the correct perspective from the effective proton source. It is usually done on a regular grid at a spacing commensurate with the spatial resolution of the scan and the scattering characteristics of protons (typically 1 to 2 mm). Since the treatment portal extends outside the target volume – to account for penumbra and set-up margin – an extrapolation scheme (radial is the most common) is required in this region.

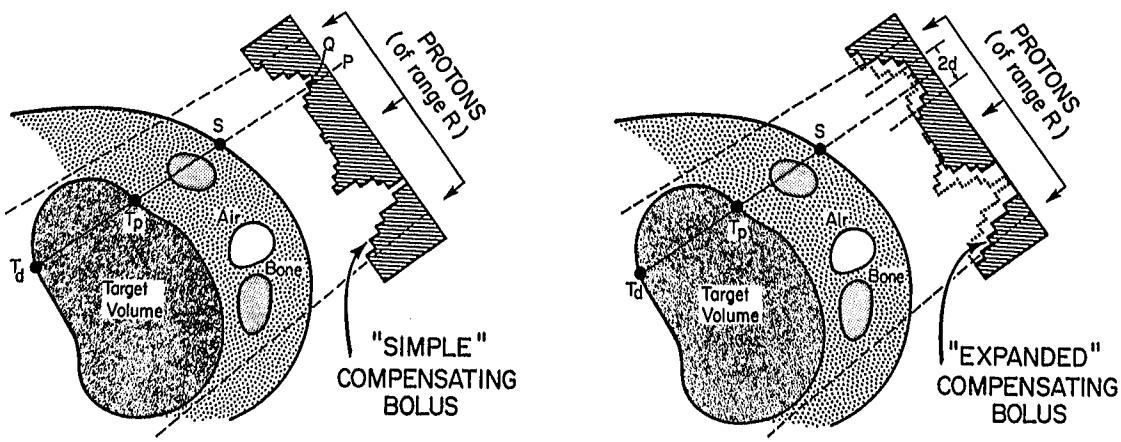

Fig. 2. Design of a bolus for protons of range R to compensate for surface and target irregularities and tissue heterogeneities. Left: Sample line ray along which a line integral is performed to obtain the water-equivalent areal density between the skin (s) and the proximal (T_p) and distal (T_d) target volume surfaces. Right: Expansion of the bolus to ensure target volume treatment within positioning and motion uncertainties of distance d

The result of this calculation is a matrix of required ranges and modulation. In a passively scattered beam, the maximum range throughout the field defines the energy required of the incident beam. The difference of each matrix point from this maximum range defines the thickness of the range-modifying bolus throughout the field (Fig. 2a, left). The thickness is zero at the point of maximum range.

In present planning systems, this calculation is only a radiographic pathlength calculation. There are no estimates of Coulomb scattering of the protons nor of range straggling. It is also a point-by-point calculation, presuming that the beam and beam-modifying devices can be aligned perfectly with the patient as defined at the time of the CT scan. However, there is always some uncertainty in the reproducibility of the patient positioning and in the alignment. To assure target volume treatment or normal tissue sparing, this misalignment needs to be addressed.

One approach has been described by Urie et al. [4] and is illustrated in Figure 2, on the right. Assuming an uncertainty of a given amount, e.g., 3 mm, the range-modifying bolus can be "expanded" to assure target volume coverage. At each point in the raw radiographic pathlength matrix of required range, the neighborhood within a radius of that uncertainty is examined and the range at that point replaced with the greatest range found within the neighborhood. This process is repeated at each point. The resultant matrix of "expanded" range requirements will assure adequate range as long as the patient is aligned within the given uncertainty. Typically, the radius for "expansion" is the same as the margin added to the aperture for set-up uncertainty. The counterside of this approach is that if the patient is "perfectly" aligned, the protons will overpenetrate into normal tissues.

Having "expanded" the range-modifying bolus, the required modulation of the beam needs to be recalculated. In passively scattered beams, the modulation is uniform throughout the field and the maximum required modulation is used. In scanned beams, the "expanded" modulation needs to be incorporated.

Multi-Portal Design

The protons' characteristic of a well-defined range and steep dose fall-off not only spares distal normal tissues but also allows the use of multiple proton portals from different angles to treat a target volume uniformly while delivering essentially no dose to a critical normal tissue it envelops. The basic principle is to treat part of the target volume with one field, using beam edge to stay off the critical structure and another field (or fields) to treat the remainder of the target and have the protons range out in the penumbra of the first field [5].

Figure 3 shows an example for discussion. The target volume abuts and wraps around the brain stem. The first proton portal is a lateral, which treats the target volume anterior of the cord. The range and the range-modifying bolus are calcu-

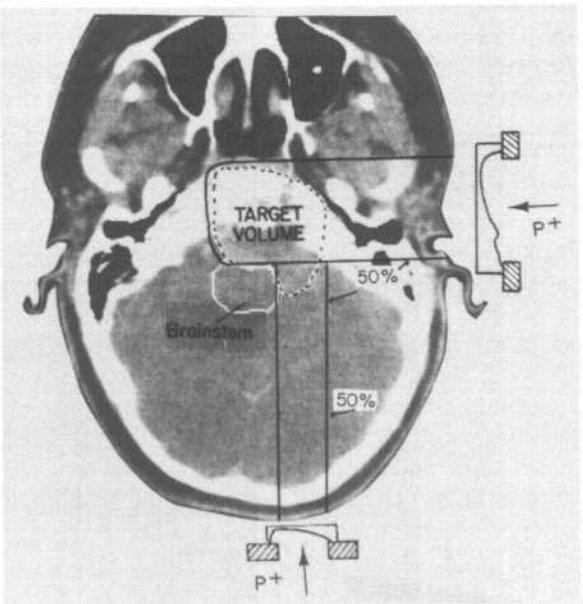

Fig. 3. Axial CT section with a target volume (dotted line) which wraps around and abuts the brain stem (solid white line). Fields are illustrated to treat the target volume uniformly while sparing the brain stem. The lateral field treats the target anterior of the brain stem, placing 50% of the prescribed dose level on the brain stem surface. The posterior field treats the target lateral to the brain stem not included in the lateral field and stops in the penumbra of the lateral field

lated as if it were a standard single field. Set-up and penumbra margin are added in all regions except the brain stem. To treat the target on the lateral side of the brain stem a posterior proton field is designed. Again, the field edge is used to limit the brain stem dose (50% to the surface in this example). To define the range and the range modifying bolus, a new target volume is defined. For this posterior portal, the distal part of the new target volume is the field edge of the lateral field; the proximal portion is the actual target volume lateral of the cord.

Because the distal fall-off and the lateral penumbra are not identical in most proton beam lines, there is no perfect match of the two at the abutment junction. A dose non-uniformity results. How to match them is a clinical judgment; whether to accept a "hot" region of likely overtreatment or to accept a potentially "cool" region near the junction line needs to be decided by the physician. A reasonable and common solution is to match the nominal 50% dose decrement lines, i.e., to prescribe the range of the posterior field to be the raw calculated range to the new target volume minus the 95% to 50% distal fall-off distance (typically 2 mm).

In the planning algorithms which "expand" the raw range-modifying bolus to assure target volume coverage, the effect in these situations can be a significant region of probable overtreatment. At the edges of the fields a significant overshoot may occur if the entrance surface is curved, such as in the neck. This effect can be minimized by defining the new target volume discussed above to extend laterally outside the field. In Figure 3, the target volume is extended laterally to the mid brain stem and medially approx. 1 cm into the petrous ridge. This modified new target volume is solely for calculational purposes to pull the range of the protons back as desired. The "expansion" of the range-modifying bolus may cause likely regions of overtreatment, particularly in regions with significant inhomogeneities. The radius of "expansion" may therefore require reduction for this posterior field but must be consistent with set-up uncertainty.

The overall result of these combinations of fields is a very low dose to the brain stem, a sharp gradient dose to the target volume abutting the brain stem, and a nearly uniform dose to the remainder of the target volume except at the abutment junction. This technique is a particularly powerful tool to treat tumors to higher doses than normal tissues in close proximity can tolerate. Because of inadequacies in present dose calculation algorithms and because of imperfect match of distal fall-off to lateral penumbra, it is recommended that, if significant dose (e.g., >10 Gy) is to be delivered with this type of multiple-field treatment, alternative abutment junctions be used. In Figure 3, for example, the posterior field could treat all the target lateral to the brain stem and the opposite lateral field could be designed to stop in its lateral penumbra. This spreads the regions of potential "hot" and "cold" regions into two junction regions, reducing the absolute dose of potential over- or under-treatment.

Developing the "Best" Plan

Often there are several overall approaches to deliver the dose to the target while maintaining tolerable doses to normal tissues. Which is the "best" remains a clinical decision, though there are attempts to model biological responses, of both tumors and normal tissues, and use these to "optimize" the treatment plan.

Tools to aid in evaluation of a plan and to compare plans are essential. The vast amount of data from 3D-planning systems soon becomes overwhelming without summary and comparison tools. Capabilities of planning systems which have proven particularly useful [5, 6] include

- side-by-side displays (different plans shown on the same slice),
- dose difference displays (dose distributions of two plans subtracted and regions and amounts of difference displayed),
- dose statistics (average dose, maximum dose, minimum dose, etc.),
- dose-volume histograms of volumes of interest,
- predictions of modeling of tumor control probability (TCP) and normal tissue complication probability (NTCP).

Delivering the Planned Treatment

Having developed the desired treatment, several steps are involved in assuring it is delivered as planned. First, the beam modifying devices, aperture and range modifying bolus need to be fabricated and the beam line correctly configured for energy and modulation. Usually, the portal/patient specific devices are milled or poured according to computer files generated in the planning system.

To position the patient correctly for the portal designed from the planning study with the required degree of accuracy (2–3 mm typically) is not a small effort. The technique most widely used is to align the patient to bony landmarks and/or fiducial markers using diagnostic radiographs, and to compare these to radiographs calculated from the CT planning scan. These digitally reconstructed radiographs (DRRs) are calculated with the correct magnification and perspective for each film, and measurements of appropriate landmarks are used to assure the patient is correctly aligned. Often standard orthogonal projections (lateral and anterior-posterior) are used for the initial set-up of the patient and a portal film taken to confirm correct alignment when all rotations have been incorporated.

Several algorithms are available to calculate the required DRRs. Some use interpolation (smoothing) algorithms, or separate "bony" Hounsfield units from "soft tissue" Hounsfield units and allow different relative contrast. Whichever algorithm is employed, the resultant image must be available for high quality output. Radiographic film using either an optical or laser printer output is presently the method of choice to obtain films to compare to the set-up radiographs. Techniques for computer-aided registration are being implemented in some treatment facilities [7]. Using well-defined landmarks and/or fiducial markers identified on orthogonal radiographs, computer programs aid in defining the translations and rotations needed on a day-to-day basis for correct patient alignment. In the near future, digital radiographs should be able to be compared to DRRs electronically and these assessments made without hardcopy.

To be able to display VOIs and points of interest on the DRRs is a useful tool. Fiducial markers and specific bony landmarks should be delineated on the axial slices and displayed on the DRRs. A portal DRR, showing the correct alignment of the anatomy with respect to the central axis and the aperture, is extremely valuable to confirm final positioning correctness prior to treating the patient.

Caveats and Other Considerations

Present planning systems do not have dose calculation algorithms which accurately predict the dose when protons pass through heterogeneous tissues in the actual treatment situation. These inadequacies must be kept in mind when planning the treatment and reviewing the dose display.

The penumbra of a proton field is not uniform with depth in the patient. It broadens predictably as protons pass through homogeneous material. This is accurately modeled by most planning systems. The effects of heterogeneities on the lateral penumbra, however, are not taken into account by present dose algorithms.

Penumbra characteristics are very dependent upon beam line configurations and any material in the beam path. In passively scattered beams with energy variability, the 80%–20% distance may be < 1 mm (at 5 cm depth in water). The energy is often degraded by placing absorbers in the beam line. For example, a cyclotron-generated beam with single output energy of 20 g/cm^2 may need to be degraded to a penetration of 12 g/cm^2 by placing 8 g/cm^2 absorber in the beam path. The absorber introduces angular confusion to the protons and the penumbra is broadened; even when using low-Z materials such as lucite to minimize the scattering angles, the penumbra may be broadened to 4–5 mm (at 5 cm depth in water) with 8–10 cm of in-line absorber [8].

In passively scattered beams, the Bragg peak is modulated in depth to create a region of uniform dose great enough to encompass the target. Different schemes are employed, including modulator wheels and wobblers (cf. Chapter 24), but all introduce additional material into the beam line. Hence, scattering of protons occurs, adversely affecting the lateral penumbra.

To minimize the degradation of the penumbra, energy absorbers and modulation devices are placed as far upstream (away from the patient) as possible. But field-defining apertures and range-modifying boluses should be as close to the patient as possible. An air gap introduces a region in which the effects of angular confusion of the protons are magnified. Ideally, the range-modifying bolus should be shaped to conform to the patient's surface and just touch it; the aperture should be on the surface.

In present delivery systems, the range-modifying bolus often has one flat surface, which is attached to the downstream side of the aperture (Fig. 1). There may be gaps between portions of the bolus and the patient and the aperture may be offset significantly from the patient's surface, depending upon the range-modifying bolus' thickness. The thickness of the bolus and the width of the air gap affect the lateral penumbra [8]. Present planning systems do not have dose calculation algorithms which accurately reflect these factors, though some do approximate corrections to the nominal penumbra. This limitation must be kept in mind when reviewing the dose distributions, particularly if field edges are being used to limit doses to certain critical structures.

The effects of heterogeneities on the range of proton beams have been theoretically and empirically studied but are presently not incorporated into dose calculation algorithms in treatment planning systems. In general, the primary effect of protons passing through heterogeneities is to increase the spread of their effective ranges as they are scattered, resulting in a less steep dose gradient distally.

The effect of a slab of heterogeneity is well understood and modeled. It modifies the penetration of the proton beam. The effect of a heterogeneous edge is dependent upon its density and thickness [9]. In principle, large dose perturbations can develop behind edge discontinuities and such discontinuities can reinforce each other; in practice, the effects of overlying tissue and beam divergence strongly modify the dose perturbations in parallel beams. The effects of thin "slivers" of heterogeneities parallel to the beam may be either under- or over-estimated from radiographic pathlength calculations on CT [10, 11]. As the sliver becomes thinner, the dose distal to the "expected" end of range increases until it is ca. 70% for a 1 mm wide sliver (Fig. 4). Concomitantly, the dose is reduced within the proximal region of the depth dose distribution, due to

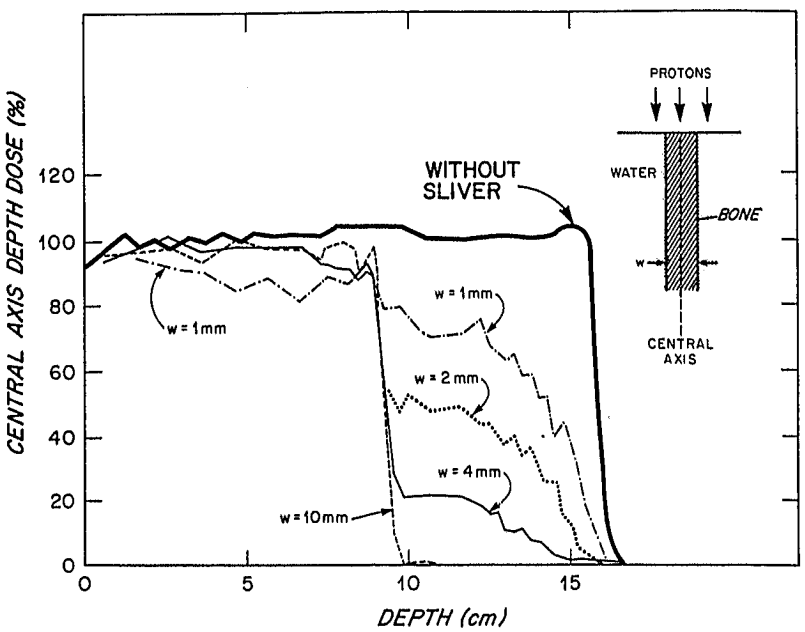

Fig. 4. The effects of a thick inhomogeneity on the distal range of a proton beam. A short (2.5 cm long) sliver at 7.5 cm depth in water causes perturbations in the central axis depth dose; the perturbations for slivers 10, 4, 2, and 1 mm thick are shown

preferential scattering of protons out of the sliver.

Inadequacies of CT to define precisely the fine-anatomical structure, e.g., mastoid air cells, and the limitations of dose algorithms which do not account for Coulomb scattering of protons result in a significant error in the end-of-range dose prediction in some structures. Phantom studies [12] and animal studies [1] have shown that the distance from the distal 80% to 20% may be spread from the water measured 4–5 mm to >20 mm in such cases (Fig. 5). Keeping this in mind when reviewing dose distributions is essential, and it may be advisable to select portal directions which minimize passage through such heterogeneities.

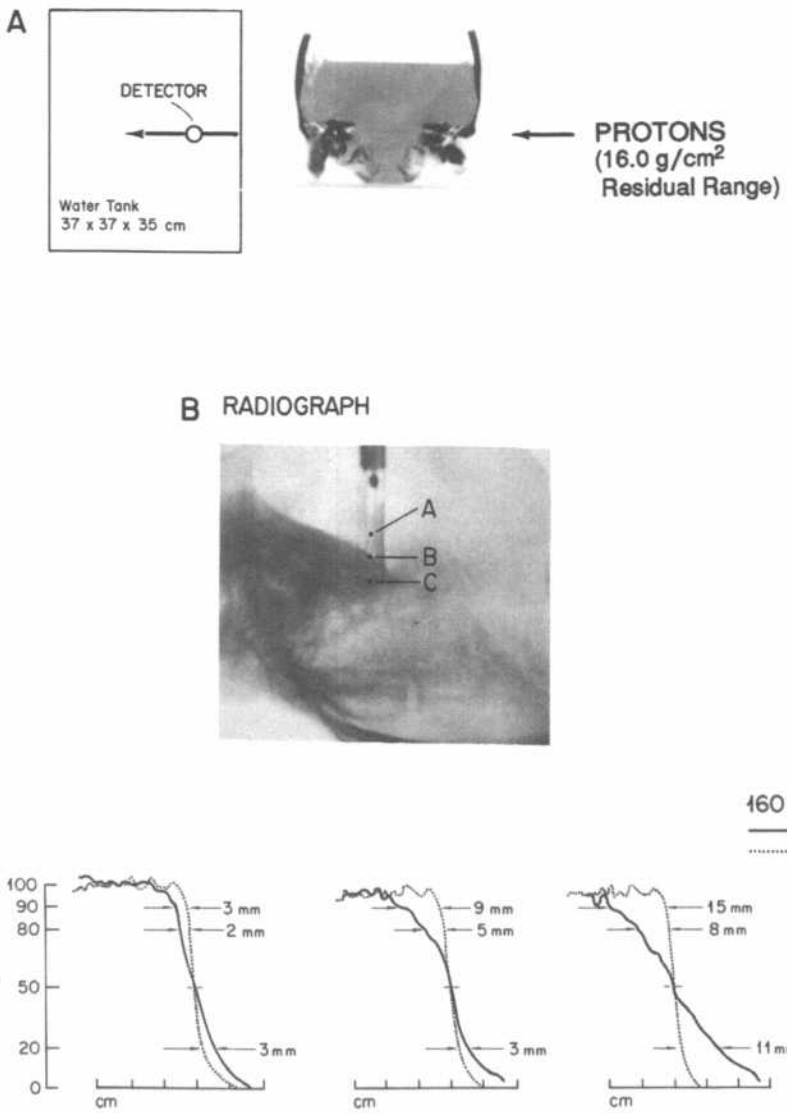

Fig. 5. The effects of multiple fine heterogeneities on the end of range of protons. A) Measurement technique shown schematically in a coronal plane. B) Lateral radiograph indicating the measurement points and the RAS-1 diode in position for depth-dose distribution A. C) Depth-dose distributions at the three points in (B) compared to those measured in water (dotted line). The numbers are the mm distances between the 90%, 80% and 20% dose decrement in the two cases

Besides heterogeneities, air gaps between the range-modifying bolus and the patient will affect the intended stopping pattern of the protons as well. The protons are scattered as they pass through the range-modifying bolus (usually lucite or wax) and an air space acts as a region to magnify the increased angular confusion of the beams. The effect of this scattering is to smooth the desired effects of the compensating bolus [13]. Designing immobilization devices to allow the range-modifying bolus to be very near to the patient and to conform the bolus to the patient contour are important to maximize the distal tailoring of the dose distribution.

No present dose algorithm used for treatment planning adequately models the effects of heterogeneities on the range of protons. In general, broad beam algorithms make only first approximations for these effects on penumbra and ignore end-of-range effects. Pencil beam algorithms do better with the penumbra and make first order approximations to the distal effects. Monte Carlo techniques can account for all of these effects, but presently require too much computing time to be practical for patient planning. In general, dose gradients appear to be sharper and better defined than they really are. This must be kept in mind when reviewing plans and making clinical decisions about treatments.

It is therefore extremely useful for the planning system to be able to estimate and display the likely range of uncertainty in its calculations. The effect of imperfect patient set-up, imperfect conversion from CT data to range of protons, and imperfect dose algorithms are more dramatic for proton therapy than for X-ray therapy. The potential advantage of a well-defined range for a given proton beam also implies a great disadvantage if it is not accurately calculated and controlled, either because the intended target may not be treated at all or distal normal tissues not be spared as intended.

An estimate of the total uncertainty in the dose displayed by the treatment planning system is essential in order for physicians to make clinical judgments. One method to estimate this uncertainty has been implemented at MGH [4, 14]. This method displays the dose as calculated to be the nominal dose; it then estimates, incorporating the set-up uncertainty and the CT conversion uncertainty, the greatest and least likely dose at each point. Although not directly estimating the straggling of protons and the degradation of the sharp fall-off in dose distally when passing through heterogeneities, theoretical [14] and experimental studies [4, 12] have shown that the distal doses in these situations are encompassed

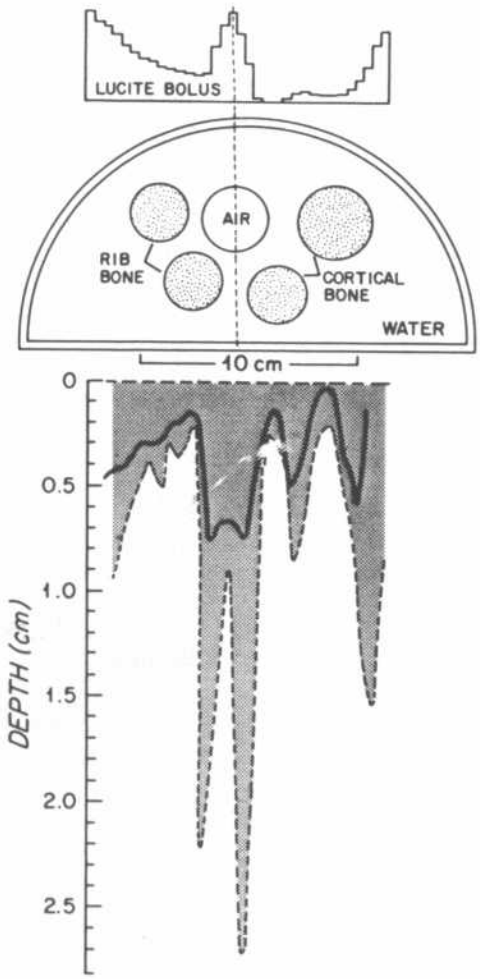

Fig. 6. Contour depths of the distal 50% dose behind a phantom with multiple heterogeneities. The range-modifying bolus was calculated to stop the protons at a uniform depth (zero) and then "expanded" by 3 mm. The ranges of depths in which the 50% contour is predicted to be as long as the range-modifying bolus and "patient" are aligned within 3 mm is indicated by the shaded region. The depths of the 50% contour for the "correctly" aligned situation is shown by the solid line

between the estimated greatest and least likely penetration (Fig. 6).

In Figure 3, for instance, the distal dose gradient (80%–20%) of the lateral field is known to be degraded to approx. 20 mm in the petrous region. The uncertainty calculations would encompass this. The true 80% would be more distal than the "minimum" 80% displayed and the true 20% would be more proximal than the "maximum" 20% displayed.

This method has its drawbacks and is not the only approach. However, it is believed to be extremely important for proton therapy to give the clinicians an estimate of the likely ranges of dose at a particular point.

Conclusions

Proton therapy offers the potential of better conformation of physical dose to target volumes, with a higher probability of tumor control or a decreased probability of treatment related complications. This has been demonstrated for a few sites and is being explored at many others. But to achieve these improvements requires attention to detail and significant efforts at patient positioning, treatment planning, and treatment delivery.

Each patient's treatment must be planned individually, from CT data for nearly all disease sites. An adequate treatment planning system must allow definition of the target volumes and normal tissues of particular interest. It must permit delineation of the field-defining aperture, calculation of the required range, the range-modifying bolus, and the amount of required spread of the Bragg peak throughout each portal, and finally, it needs to provide information for correct patient positioning which has to be assured at each treatment session.

References

1 Schneider, U. and Pedroni, E. Proton radiography as a tool for quality control in proton therapy. Subm. to Med. Phys.

2 Goitein, M. Compensation for inhomogeneities in charged particle radiotherapy using computed tomography. Int. J. Radiat. Oncol. Biol. Phys. 4, 499–508, 1978.

3 Goitein, M., Abrams, M., Rowell, D., Pollari, H., and Wiles, J. Multi-dimensional treatment planning: II. Beam's eye view, back projection and projection through CT sections. Int. J. Radiat. Oncol. Biol. Phys. 9, 789–797, 1983.

4 Urie, M., Goitein, M., and Wagner, M. Compensating for heterogeneities in proton radiation therapy. Phys. Med. Biol. 29, 553–556, 1984.

5 Collaborative Working Group on the Evaluation of Treatment Planning for External Photon Beam Radiotherapy, Report. Int. J. Radiat. Oncol. Biol. Phys. 21, 1991.

6 Goitein, M., Urie, M., Munzenrider, J., Gentry, R., Lyman, J., Chen, G., Castro, J., Maor, M., Stafford, P., Sontag, M., Altschuler, M., Block, P., Chu, J., Richter, M., Smith, A., and Zink, S. Evaluation of treatment planning for particle beam radiotherapy. Final Report of National Cancer Institute contracts NOI-CM27532, IA YOI-CM20110, NOI-CM27531, and NOI-CM27539, 1987.

7 Gall, K., Verhey, L., and Wagner, M. Automating proton therapy patient positioning I. REPOman. Abstracts of PTCOG XVI meeting, Vancouver, BC, Canada, March 30–31, 1992, p. 2.

8 Urie, M.M., Sisterson, J.M., Koehler, A.M., Goitein, M., and Zoesman, J. Proton beam penumbra: effects of separation between patient and beam modifying devices. Med. Phys. 13, 734–741, 1986.

9 Goitein, M. and Sisterson J. The influence of thick inhomogeneities on charged particle beams. Radiat. Res. 74, 217–230, 1978.

10 Goitein, M., Chen, G.T.Y., Ting, J.Y., Schneider, R.J., and Sisterson, J.M. Measurements and calculations of the influence of thin inhomogeneities on charged particle beams. Med. Phys. 5, 265–273, 1978.

11 Goitein, M. A technique for calculating the influence of thin inhomogeneities on charged particle beams. Med. Phys. 5, 258–264, 1978.

12 Urie, M., Goitein, M., Holley, W., and Chen, G. Degradation of the Bragg peak due to inhomogeneities, Phys. Med. Biol. 31, 1–15, 1986.

13 Sisterson, J.M., Urie, M.M., Koehler, A.M., and Goitein, M. Precise shaping of the distal edge of proton beams: the effects of air gaps between compensating bolus and patient. Phys. Med. Biol. 34, 1309–1315, 1989.

14 Goitein, M. Calculation of the uncertainty in the dose delivered during radiation therapy. Med. Phys. 12, 608–612, 1985.

30 Developments in Ion Beam Therapy Planning and Treatment Optimization

A. BRAHME, P. KÄLLMAN, and A. TILIKIDIS

Dept. of Medical Radiation Physics, Karolinska Institute and Stockholm University, Stockholm, Sweden

Introduction

Ion beams pose special problems in treatment planning due to the significant depth variation of the radiobiological and microdosimetric properties of these beams. It is a fairly straightforward problem to develop fixed and standardized range modulation protocols to deliver a uniform biological effect or absorbed dose to extended, essentially rectangular target volumes [1]. A fixed range modulation could be generated using ridge filters, linear, rotary or hydraulic range shifters or by energy modulation of the extracted beam from the accelerator. When using a fixed range modulation, the distal part of the dose distribution could always be conformed to the target volume by advanced bolus techniques. However, to make full use of the radiobiological and physical advantages of ion beams it is advantageous to perform a careful three-dimensional scanning of the beam and predominantly locate Bragg peaks in the target volume as illustrated in Figure 1 [2–5]. This fact becomes increasingly important as the ionization density is increased beyond that of protons. Therefore, accurate radiotherapy optimization is a very complex problem where the special radiobiological and dosimetric properties of the ion beams have to be taken into account to maximize the probability to control the tumor growth without inducing severe damage to healthy normal tissues. In the present chapter the emphasis is therefore on the use of radiobiological optimization methods rather than on, for example, the use of modern three-dimensional diagnostic techniques and advanced bolus design.

From a mathematical point of view, classical radiation therapy planning is basically a forward process that tries to answer the question: How will the absorbed dose and the biological effect in the target volume and surrounding normal tissues be distributed for a given target volume, associated normal patient geometry and suggested configuration of the incident beams? Classical radiation therapy optimization is, therefore, generally a trial and error process, where gradually improved dose plans can be found by trying an increasing number of incident beams in gradually improved configurations [6, 7].

However, in mathematical terminology, radiation therapy optimization is fundamentally an inverse problem. This is so, because what we really want to find, is the optimum combination of incident beams for a given target and normal tissue geometry. More exactly, the planning process should answer the question: which configuration of energy, particle species and shape of the incident beams is best for clinical tumor control with minimal damage to normal tissues? At least under the assumption that the desired dose to the target volume or the geometrical and radiobiological properties of the tumor and normal tissues of the patient are known, it should be possible to find the optimal irradiation technique by inverse therapy planning methods [7–10].

Strictly speaking, there is no such thing as a generally acceptable and truly optimal treatment plan, because there are so many clinical factors that are specific for each patient and for the responsible radiotherapeutic team and all of them have to be taken into account in the optimization. The principal problem is that most of these fac-

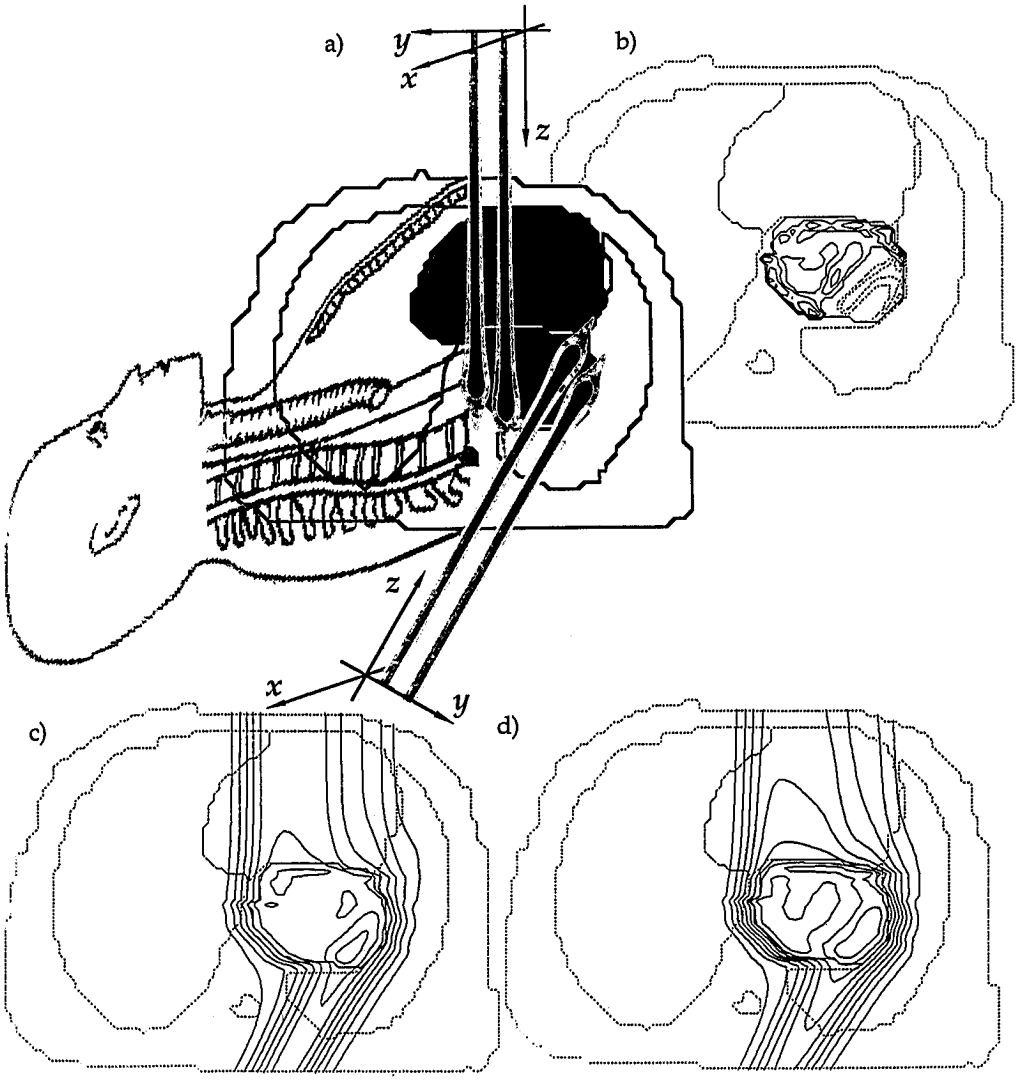

Fig. 1. The irradiation geometry for an optimized two-field neon ion technique applied to an esophagus cancer is shown in (**a**). The optimum Bragg peak density for the two beams are shown in (**b**). The solid curve pertains to the anterior beam and the dotted to the oblique posterior beam. Note that the algorithm produces a high Bragg peak density in the target volume but also that the regions for the two fields are different. The physical dose distribution is shown in (**c**) and the resultant biologically equivalent dose distribution in (**d**). The isodoses are in photon-equivalent Gray from 10 and up in steps of 10

tors concern incompatible entities which cannot be compared on a common scale. In the general case, the number of degrees of freedom in the selection of incident beam directions, beam profiles, particle types and energy modulations is also very large. In clinical practice it is, therefore, difficult to integrate all advantageous and adverse radiation effects on the patient to maximize the clinical outcome, for example, in terms of the quality of life of the patient. In a given clinical setting, such factors as the simplicity of the irradiation technique and the accuracy in dose delivery, often have a strong impact and may sometimes disqualify very complex plans. In general, a strict mathematical optimization is, therefore, not even practical, and several simplifications have to be made.

Due to the considerable variations in radiation quality along the range of the particles (Figs. 2 and 3) the optimal use of heavy ion beams will almost always require complex three-dimensional scanning patterns. The method presented here has the potential to optimally combine a very large number ($\sim 10^6$) of pencil beams of ions of varying energy, ion species and angle of incidence on the tumor such that the probability to eradicate the tumor without causing severe damage to normal tissues is maximized.

Instead of prescribing a certain dose distribution in the target volume, approximately known radiobiological dose response relations for the tumor and the normal tissues can be used to find the optimal dose distribution with regard to complication-free tumor control. For this purpose we have developed a radiobiological model that describes the response of tumors and normal tissues to non-uniform irradiation. The model is based on clinically established dose response data as expressed by the dose causing 50% probability of response, D_{50}, the relative seriality of the tissue, S, and the steepest value of the normalized dose response gradient, γ (cf. Tab. 1). It is important that the model accurately describes the volume dependence of the dose response relation. The new algorithm is able to use known dose response relations to minimize the irradiation of sensitive normal tissues while simultaneously eradicating all tumor cells. With such an algorithm and suitable heavy ion beams, almost any target volume can be clinically controlled by external beam irradiation. Several methods capable of delivering the three-dimensional scanning patterns are available and have been discussed extensively elsewhere [4, 5, 11, 12].

Table 1. The radiobiological parameters in the Neon treatment presented in Figure 1

Organ	D_{50} [Gy]	γ	s
Tumor	55	2.8	–
Lung	24.5	2.1	0.0061
Heart	49.2	3.0	0.2
Spinal cord	60	1.8	1.0
Surrounding normal tissue	80	2.1	1.0

Theory

The RBE for Radiation Fields with Large LET Variations

The relative biological effectiveness may quite accurately be described by an integral over the relative biological effectiveness for each interval

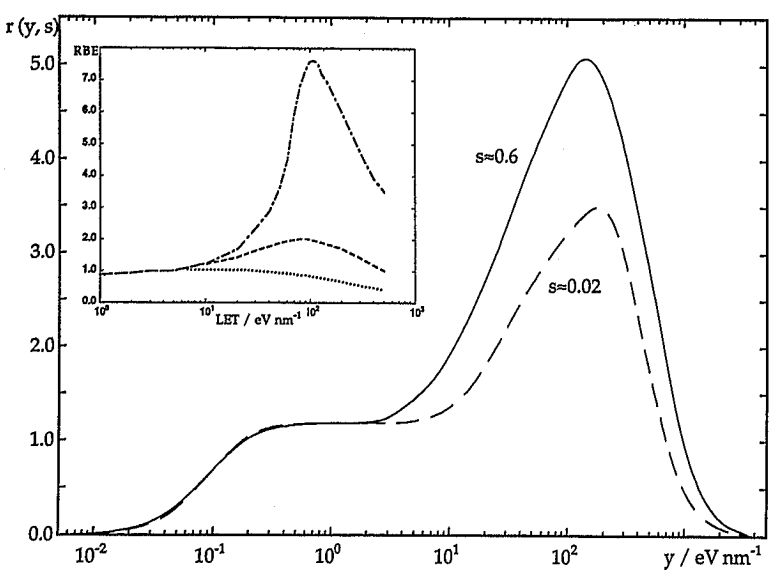

Fig. 2. The biological response functions for high ($s \approx 0.6$) and low ($s \approx 0.02$) survival levels (solid and broken curves, respectively) calculated using microdosimetric single event distributions and experimental RBE values for the radiation qualities taken from [14]. In the insert, RBE values for single track lethal damage (dash dotted curve), DNA double strand breaks (broken curve) and DNA single strand breaks (dotted curve) are shown for comparison (redrawn from [22])

of lineal energy dy of the microdosimetric distribution of energy imparted within each individual biological target for the particular radiation quality. The relative biological effectiveness for energy transfers in the interval y to y+dy will not only depend on the lineal energy y, but also on the actual survival level of interest as illustrated in Figure 2. It should be kept in mind here that the survival at the lineal energy y is based on the assumption that the survival level of interest is reached by dose delivered solely at that lineal energy. This means that the biological effect due to the energy deposited in the interval y to y+dy is independent of the dose delivered at other lineal energy intervals, and that an equivalent dose exisists at y that gives the same survival as the entire microdosimetric spectrum. This is obviously an approximation that we have to make for the calculations to be manageable and to avoid having to calculate the possible complex interactions of high- and low-LET damage. Based on this simplifying assumption the RBE at survival level s may be described by the mathematical formulation:

$$\mathrm{RBE}(s) = \int_0^\infty r(y, s)d(y)dy \qquad (1)$$

where r(y, s) is the relative biological effectiveness at the survival level s at the lineal energy y and d(y) dy is the relative dose contribution in the lineal energy interval dy around y [13, 14]. The relative biological effictiveness r(y, s) as a function of the lineal energy over the range 10^{-2}–10^3 eV/nm have been determined by a deconvolution technique by Tilikidis and Brahme [15]. As seen from Figure 2 the r(y, s) distribution has its maximum in the range 100–200 eV/nm, where the differences between different survival levels also are the largest.

The Integral Equation of Radiation Therapy

The total three-dimensional absorbed dose distribution in the patient from the incident fluence distribution of charged particles may be described by an integral over its constituent pencil beams through the integral relationship:

$$D(r) = \int\int\int\int\int \pi_{\Omega,E}(r,\varrho)\Phi_{ion}(\varrho)d\Omega dE d^2\varrho \qquad (2)$$

where $\Phi_{ion}(p)$ is the incident fluence distribution of the ion beam at points ϱ on the patient surface and π is the pencil beam energy deposition kernels. By combining Equations (1) and (2) with the pencil beams π differential in lineal energy y, the low-LET equivalent dose distribution for the entire lineal energy distribution delivered to the patient may be written as

$$D_{eq}(r) = \int\int\int\int\int\int \frac{\partial \pi_{\Omega,E}(r,\varrho,y)}{\partial y} r(y,s)\Phi_{ion}(\varrho)d\Omega dE dy d^2\varrho \qquad (3)$$

Equation (3) may be used to calculate the equivalent dose distribution and the associated relative biological effect.

The Dose Response Relation for High-LET Beams

The variation in y along the particle tracks will not only modify the macroscopic absorbed dose distribution required to obtain a specific biological effect, but also the local microscopic variance of the spatial dose distribution. On the organ level the dose response may be described by Poisson statistics and quantified by the dose causing 50% probability of a given effect, D_{50}, and the normalized dose response gradient γ [16]:

$$P(D) = 2^{-e^{e\gamma(1-D/D_{50})}} \qquad (4)$$

If the LET is increased beyond the low-LET region, the D_{50} value will decrease due to the increasing RBE. However, the decrease in dose and the increased energy deposition density with LET will also cause an increase in the microscopic variance for a certain radiation effect as illustrated in Figure 3a both for helium and neon ion beams. An increase in the microscopic variances of the beam will leave the D_{50} value largely unchanged but the steepness of the dose response

gradient γ will decrease so that the dose response curve becomes shallower than for example in a low-LET beam as shown in Figure 3b. The γ-value will decrease with increasing macro- and microdosimetric variance as described by [9, 15, 17]:

$$\gamma = \frac{1}{\sqrt{2\pi(\sigma_B^2 + \sigma_D^2 + \sigma_\mu^2)}} \quad (5)$$

where σ_B^2 is the intrinsic variance in biological response, σ_D^2 he variance due to the macroscopic absorbed dose distribution and $\sigma_\mu^2$the mean microdosimetric variance determined by the properties of the particle species. The microscopic variance basically depends both on variations of the mean absorbed dose level and radiation quality changes according to

$$\sigma_\mu^2 = \sigma_{\mu,D}^2 + \sigma_{\mu,Q}^2 \quad (6)$$

as shown in detail for helium and neon ion beams in Figure 3a.

If an organ or a tumor is irradiated with a heterogeneous LET distribution the overall response may be calculated based on the D_{50} and γ-values for each volume element. For a tumor we obtain

$$P_B = \prod_{i=1}^{M} P\,(D_{50,i} \cdot \gamma_i) \quad (7)$$

The probability of normal tissue injury, P_I, can similarly be calculated by considering the relative seriality of the tissue [16]. A suitable objective function for the optimization is the probability of achieving complication-free tumor control, P_+, which for high LET beams may be approximated by [17]:

$$P_+ = P_B(1-P_I) \quad (8)$$

Normally, the tumor is given an absorbed dose above $D_{50,t}$ and the normal tissues a dose below $D_{50,n}$. Consequently, part of the benefit obtained with high LET radiations will be counteracted by their shallower dose response relation and lower γ-value caused by their higher microscopic variance. This is shown in Figure 3b where the decreased tumor control at high doses and the increased risk for severe complications at low doses may reduce the therapeutic window for high-LET beams. Equations (1) through (5) may be used to quantify the complex response of different organs and tumors to the high-LET components of the beam.

The Optimization Procedure

A general optimization procedure for inverse radiation therapy planning has recently been developed [9, 10] by maximization of a biological objective function [9, 16, 18, 19]. The integral in Equation (2) may be rewritten in matrix form so that the three-dimensional dose distribution d is given by:

$$d = \Pi\Phi \quad (9)$$

where Φ is the fluence of the incident pencil beams and Π is the pencil beam energy deposition matrix describing the energy deposition in the patient for each one of the incident pencil beams. Therefore Π represents a mapping from R^2 to R^3, i.e., from the fluence incident on the patient surface to the three-dimensional dose distribution inside the patient. The probability to achieve complication-free tumor control may now be maximized by an efficient steepest descent algorithm which searches for the maximum of P_+ along the direction of the gradient of P_+ with respect to the fluence Φ. This gradient of P_+ is given by:

$$\nabla_\Phi P_+(d) = \frac{\partial(d)}{\partial\Phi}\nabla_d P_+(d) = \Pi^T\nabla_d P_+(d) \quad (10)$$

The iterative scheme for maximization of P_+ now becomes:

$$\Phi^{k+1} = C\,[\Phi^k + A\Pi^T\nabla_d P_+(d^k)] \quad (11)$$

The detailed properties of this algorithm are described by Gustafsson [10, 20].

Results

To illustrate the power of the algorithm in combining high- and low-LET dose contributions in the optimization procedure, it has for simplicity

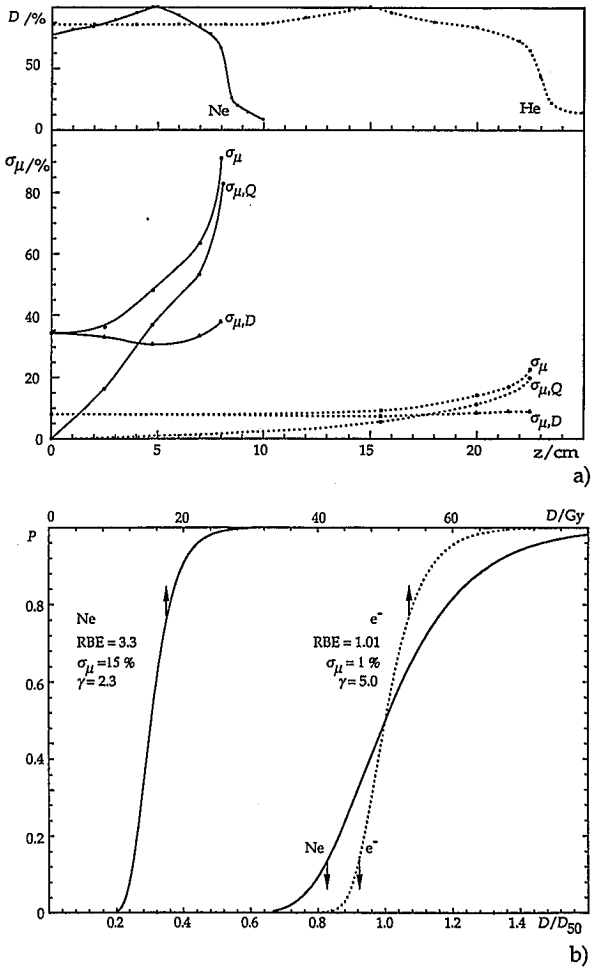

Fig. 3. (**a**) Depth dependence of the relative standard deviation of the microscopic energy deposition and its radiation quality and dose-level dependent components for Ne^{10+} (solid lines) and He^{2+} (dashed lines) beams. For He the variance is just slightly higher than for X-rays [14] whereas the Ne-ions show considerable quality changes with depth. (**b**) The influence of the microdosimetric relative standard deviation on the steepness of the dose response relation is quite high for high-LET beams

been applied to a one-dimensional case with a tumor containing a central 10 % hypoxic cell fraction. The treatment is performed with a mixed beam schedule of neutrons and photons. The result would also approximately pertain to a combination of Ne-ions and proton beams, for example. Radiation response data for the neutrons have been extracted from Guichard et al. [21] and the data for the neutron energy deposition kernel were taken from Moyers [22]. In Figure 4 the resultant dose distributions for the neutron and photon components are shown. It is seen that for a hypoxic tumor the algorithm prefers to use the low OER of the neutrons to eradicate the central hypoxic cells, whereas the photons are applied to the well oxygenated periphery of the tumor volume. This represents an interesting application of a biological objective function, where the radiosensitivity of each subpopulation of cells is considered. Also seen in the figure is that the total absorbed dose in Gray is lower in the central region, reflecting the higher RBE of the neutrons. Finally, the biologically equivalent dose is plotted, and the resultant dose distribution when only photons are used for treatment. With photons alone the hypoxic fraction becomes more difficult to handle. The complication-free control P_+ is about 90 % with the mixed beam and only 65 % with low-LET alone, even if the photon-equivalent dose is much higher than for the mixed schedule.

In order to illustrate some of the problems encountered in scanned particle beam therapy optimization with physical objective functions [4, 7], the use of protons on both a simple and a more complex target volume is shown in Figures 5 and 6, respectively. The build-up properties are illustrated by choosing a simple triangular prism as the first target volume irradiated laterally by a single proton field and trying to get a uniform dose throughout the target. The desired dose distribution in one slice through the target volume is shown in Figure 5b. By using the energy deposition kernel from Figure 5a and the triangular target dose distribution as input into the algorithm (Π and d, respectively), the Bragg peak density (see Eq. 9) in Figure 5c is obtained. Finally, the resultant dose distribution in the target area is illustrated in Figure 5d. An excellent and uniform coverage of the target volume is obtained by this treatment technique. The required range modulation of the proton beam is obtained directly from scanning density in Figure 5c which, in principle, describes the optimal density of Bragg peaks inside the target volume. As the range modulation increases towards the broad part of the triangular target as seen from the direction of the inci-

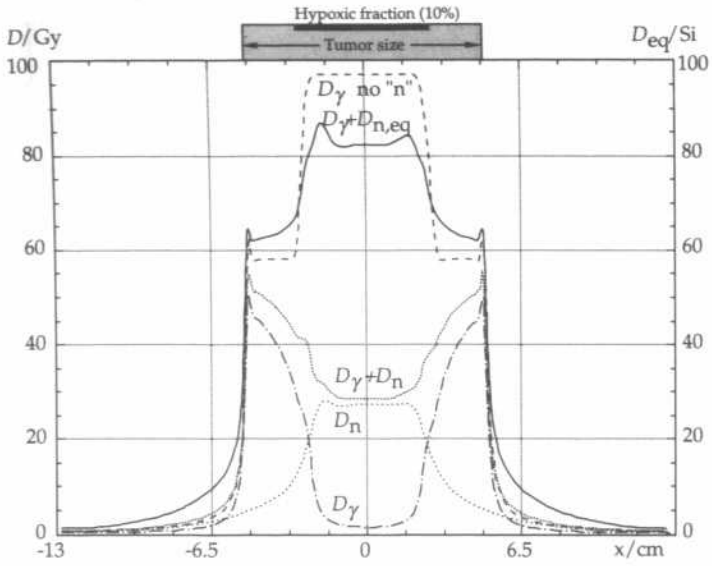

Fig. 4. The optimum dose distributions for a mixed beam treatment technique with neutrons and photons. In the central part of the tumor, there is a 10% fraction of hypoxic cells. The optimum photon dose distribution fraction is dashed dotted and the physical neutron absorbed dose distribution (in Gray), is dotted. The low OER of the neutrons is obviously used to effectively eradicate the hypoxic cells. The total absorbed dose distribution in Gy is the densely dotted curve and the total distribution of the biologically equivalent dose, considering the higher RBE of the neutrons is the solid line. The upper dashed curve is the resultant optimum dose distribution, if only photons are used in the optimization procedure

dent beam, the surface dose in the beam increases rapidly (Fig. 5d). It is clear that the surface dose level is minimized, if the target volume is irradiated from the direction where the depth range covered by the target is minimal.

In the present case it was assumed that all proton beams are incident along the same direction, so no explicit angular dependence is included in Equations (9)–(11). An angular dependence could be introduced here at the cost of considerably increased computation times. However, for proton beam therapy the best directions of incidence are generally quite obvious and an analytical angular optimization is most often not required.

A more complex target volume consisting of an advanced cervix cancer with involved regional lymph nodes is illustrated in Figure 6. The desired absorbed dose distribution in the target volume is shown in Figure 6a. Using a single incident beam on this more complex target results in a rather high entrance dose level as seen in Figures 6b and c. In Figure 6b, an arbitrary direction has been selected, represented here by 150°. Interestingly, the required dose distribution in the target volume is very well reproduced for arbitrary beam entrance angles. The only way to reduce the relative dose in the entrance region, beside choosing the optimum direction of incidence, is to use two or more beam portals. This is illustrated in Figure 6d, where the resultant dose distribution using a three-field treatment technique is shown. The entrance dose level is now below 25% of the target dose. This should be sufficiently low for most organs at risk. It can also be seen that the dose in the bladder and rectum is fairly low with this three-field irradiation technique.

It should be pointed out here that all results are obtained with a simple proton beam model in a single slice through the target volume. In principle, experimental pencil proton beam data should be used in a clinical setting to increase the accuracy. Furthermore, a full three-dimensional optimization is possible in the entire target volume as the algorithm in Equation (11) is, in principle, n-dimensional (for this case n = 3 is sufficient).

In order to illustrate the value of biological objective functions in the algorithm [5, 7], we have applied it to Ne-ion beams in the esophagus configuration of Figure 1. The calculation was performed in a tomographic slice through the thorax region, where both lobes of lung, heart and spinal cord are the principal organs at risk. It is almost impossible to treat the entire target without having to irradiate through at least one of these organs. In our previous study [5] we chose

the spinal cord and the heart as entrance regions, because they have the highest D_{50} values. The resultant dose distribution is shown in Figure 1. The dose response data used in the optimization are given in Table 1. In this case both the anterior and oblique posterior fields were allowed to deliver arbitrary dose distributions. It is interesting that it is biologically advantageous to irradiate different parts of the target from the two directions selected to save the cord [5]. The resultant P_+ is 94% and irradiation of the spinal cord is almost totally avoided by the oblique posterior field.

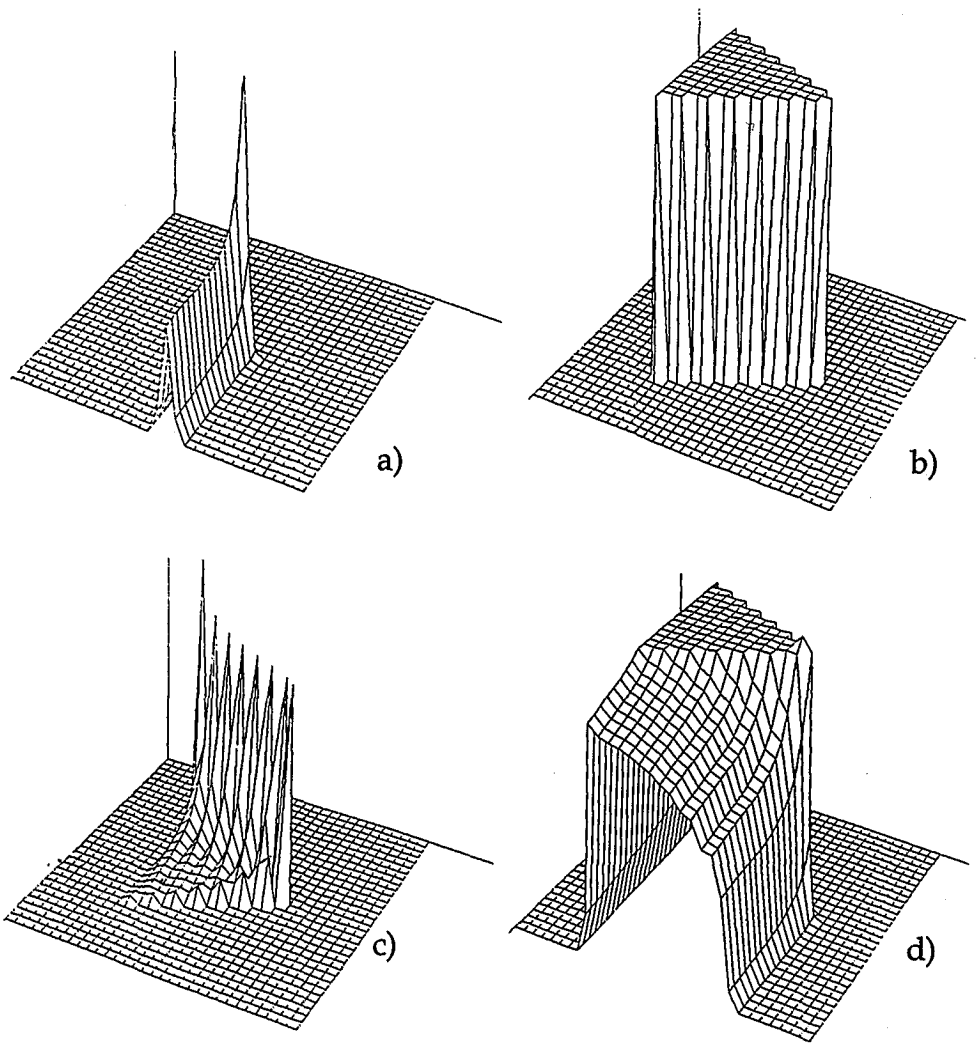

Fig. 5. Isometric plot of the dose distribution (vertical axis) in one slice of a triangular target volume. In (**a**), the elementary proton beam is shown with its Bragg peak at the center of the 32 × 32 pixel slice. The desired dose distribution in the triangular target volume and the required Bragg peak irradiation density is given in (**b**) and (**c**), respectively. The resultant dose distribution in the slice is finally presented in (**d**) with a very good conformation to the desired target dose distribution in (b). The effect of varying depth modulation on the surface dose is particularly striking

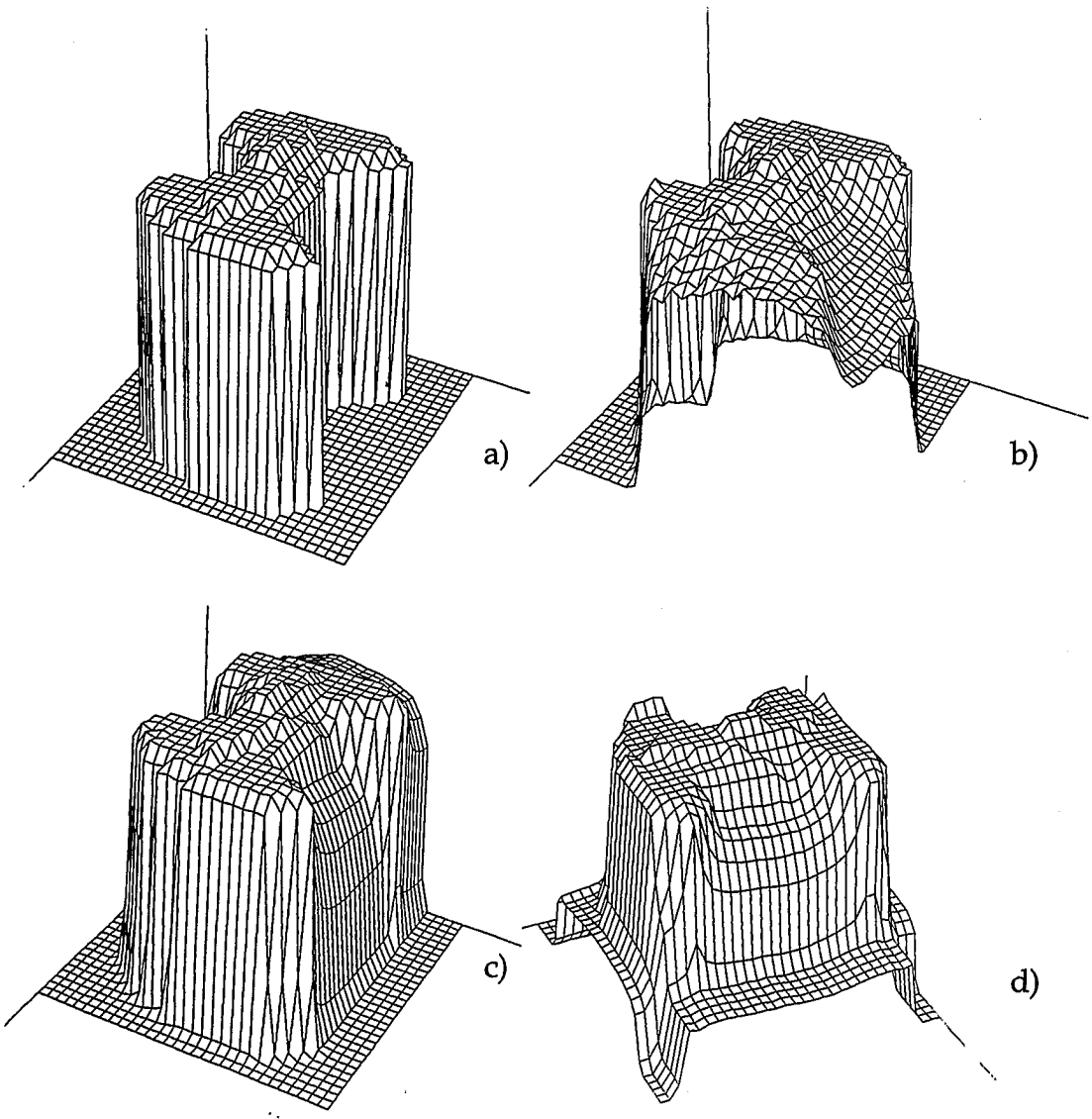

Fig. 6. (**a**) The desired dose distribution in one slice through a complex cervix cancer. In this case the dose to the regional lymph nodes is slightly lower than to the gross target volume. (**b**) The resultant dose distribution from a single proton beam incident at 150°. (**c**) The resultant dose distribution from a single beam at 0°. (**d**) The resultant dose distribution for a three-field technique with beams at 0°, 90°, and 180°

Conclusions

Ion beams provide unique possibilities to treat complex heterogeneous target volumes by external beams. To fully exploit the radiobiological properties of these beams, optimization algorithms with biological objective functions are required. It is also recognized that uncritical use of high-LET beams may lead to increased damage to normal tissues and a decreased therapeutic window as compared with low-LET beams. The optimal combination of low- and high-LET dose delivery is essential to maximize the control probability of hypoxic tumors particularly when sur-

rounded by an infiltratively growing well oxygenated subclinical disease. In general, it is then desirable to eradicate the hypoxic tumor compartment by the high-LET Bragg peak part of light ion beams whereas low-LET beams such as electrons, photons or protons are best suited for the often well oxygenated microscopic spread. With 3D-scanning as beam delivery mode, low-LET proton beams are ideally suited, as they allow an accurate combination with light ion beams exhibiting a high LET. This might be the ideal mixed beam treatment schedule of the future for complex hypoxic tumors with invasive growth.

References

1 Raju, M.R. Heavy particle radiotherapy. Academic Press Inc., New York, 1980.
2 Brahme, A. Physical and biological aspects on the optimum choice of radiation modality. Acta Radiol. Oncol. 21, 469–479, 1982.
3 Goitein, M. and Chen, G.T.Y. Beam scanning for heavy charged particle radiotherapy. Med. Phys. 10, 831–840, 1983.
4 Brahme, A. Källman, P., and Lind, B. Optimization of proton and heavy ion therapy using an adaptive inversion algorithm. Radiother. Oncol. 15, 189–197, 1989.
5 Brahme, A., Källman, P., and Lind, B.K. Optimization of the probability of achieving complication free tumor control using a 3D pencil beam scanning technique for protons and heavy ions. Proc. NIRS Int. Workshop on Heavy Charged Particle Therapy and Related Subjects. Itano, A. Kanai, T. (eds.), Chiba, Japan, 1991, pp. 124–142.
6 Brahme, A., Lind, B.K., and Källman, P. Inverse radiation therapy planning as a tool for 3D dose optimization. Physica Medica, 6, 53–68, 1990.
7 Brahme, A. Treatment optimization using physical and biological objective functions, in Radiation Therapy Physics, Smith, A. (ed.) Berlin, Springer, 1995, pp. 209–246.
8 Brahme, A. and Ågren, A.-K. Optimal dose distribution for eradication of heterogeneous tumors. Acta Oncol. 26, 377–385, 1987.
9 Källman, P., Lind, B.K., and Brahme, A. An algorithm for maximizing the probability of complication-free tumour control in radiation therapy. Phys. Med. Biol. 37, 871–890, 1992.
10 Gustafsson, A., Lind, B.K., and Brahme, A. A generalized pencil beam algorithm for optimization of radiation therapy. Med. Phys. 21, 343–356, 1994.
11 Jongen Y. and Lannoye G. A new concept of isocentric gantry for IBA's cyclotron based proton therapy facility. Proc. of PTCOG XII, Loma Linda, CA, May 7–9, 1990.
12 Montelius, A., Blomquist, E., Naeser, P., Brahme, A., Carlsson, J., Carlsson, A.-C., Graffmann, S., Grussel, E., Hallén, S., Jakobson, P., Jung, B., Larsson, B., Nilsson, B., Rikner, G., Russell, K., and Svensson, R. The narrow proton therapy unit at The Svedberg Laboratory in Uppsala. Acta Oncol. 30, 739–745, 1990.
13 Pihet, P., Menzel, H., Schmidt, R., Beauduin, M., and Wambersie, A. Biological weighting function for RBE specification on neutron therapy beams. Intercomparison of 9 European centres. Rad. Prot. Dosim. 31, 437–442, 1990.
14 Tilikidis, A, Lind, B, Näfstadius, P., and Brahme, A. Microdosimetric investigation on the biological effectiveness of 50 MV scanned bremsstrahlung beams. Int. J. Radiat. Biol., in press, 1995.
15 Tilikidis, A. and Brahme, A. Microdosimetric description of beam quality and biological effectiveness in radiation therapy. Acta Oncol. 33, 457–469 1994.
16 Källman, P., Ågren, A., and Brahme, A. Tumor and normal tissue responses to fractionated non-uniform dose delivery. Int. J. Rad. Biol. 62, 249–262, 1992.
17 Brahme, A. Dosimetric precision requirements in radiation therapy. Acta Radiol. Oncol. 23, 379–391, 1984.
18 Ågren, A., Brahme, A., and Turesson, I. Optimization of uncomplicated control for head and neck tumors. Int. J. Radiat. Oncol. Biol. Phys. 19, 1077–1085, 1990.
19 Ågren, A., Källman, P., and Brahme, A. Determination of the relative seriality of a tissue from its response to non-uniform dose delivery. To be published in Proc. Int. Workshop on Modelling in Clinical Radiobiology, Würzburg, 1995.
20 Gustafsson, A., Svensson, R., Lind, B.K., and Brahme, A. Simultaneous optimization of dynamic multileaf collimation, beam filters and scanning patterns using a generalized pencil beam algorithm. Med. Phys., in press, 1995.
21 Guichard, M., Gueulette, J., Laublin, G., Wambersie, A., and Malaise, E.P. The comparative response of human fibroblasts EMT6 and V79 cells to 50 MeV neutrons. Int. J. Radiat. Oncol. Biol. Phys. 4, 621–627, 1978.
22 Moyers, M.F., Horton, J.L., and Boyer, A.L. A scatter model for fast neutron beams using convolution of diffusion kernels. Rad. Prot. Dosim. 23, 475–478, 1988.
23 Barendsen, G.W. Mechanisms of cell reproductive death and shapes of radiation dose-survival curves of mammalian cells. Int. J. Radiat. Biol. 57, 885–896, 1990.

31 Proton Radiography

U. Schneider*

Paul Scherrer Institut, Villigen, Switzerland

Introduction

The use of protons for radiography was first suggested by Wilson [1] in 1946, but it was not until the 60's that charged particles, as opposed to X-rays, were first used to produce high contrast radiographs. Proton radiography and tomography were virtually abandoned as diagnostic tools due to the success of X-ray computed tomography. Interest in proton radiography is now growing in the light of the increasing success of radiotherapy with protons.

More proton therapy facilities will be available in the future and the use of proton radiography and proton tomography for both diagnostic purposes and for quality control in proton therapy should be therefore investigated from the point of view of the increased availability of proton sources with adequate energy (up to 270 MeV). Proton diagnostic images are characterized by a high density resolution and low dose to the patient. The main disadvantage is the poor spatial resolution as compared to conventional X-ray images. As opposed to photons, proton radiographic images contain additional information on the range of the protons traversing the patient which could be important for therapy and can be used for proton treatment verification.

There are in principle two methods of taking proton radiographies: Nuclear scattering radiography (NSR) and transmission radiography. NSR makes use of the scattering of high energy protons (500–1000 MeV) at the target nuclei. Only one exposure is needed to obtain a three-dimensional reconstruction of the object [2,3]. However, this method can only be used for diagnostic purposes since the images contain no range information. Also, as only scattered protons are detected, unnecessary dose is delivered to the patient. Another disadvantage of this method is the high energy required. This will exclude typical clinical proton accelerators, because such machines will provide only slightly higher energies than are used for proton treatments. For these reasons this article is restricted to proton transmission radiography. With this method, the integrated density along the particle path can be measured, as can local variations of the density, by using the same technique as for X-ray computed tomography.

* Present address: Ludwig-Maximilians-Universität, Munich, Germany

Basic Properties of Proton Radiography

Multiple Coulomb Scattering and Spatial Resolution

The limiting factor affecting position resolution is given by the multiple Coulomb scattering of the protons in the patient. Protons undergo numerous small angle deflections caused by their interaction with the Coulomb fields of the atoms of the traversed material. The cumulative effect of these random deflections can be modelled to a first approximation by a Gaussian angular distribution. This multiple Coulomb scattering determines the spatial resolution of proton radiography and is, therefore, the limiting factor for the

utilization of proton radiography as a diagnostic tool. A detailed discussion of the spatial resolution of proton radiography is given by Mustafa and Jackson [4] and Schneider and Pedroni [5]. They concluded that a spatial resolution of 1 mm can be achieved by measuring the coordinates of the entrance and exit points for each proton. The resultant resolution is poorer than that of X-ray images, but is good enough for quality control purposes in proton therapy. As the underlying physics of proton therapy is essentially the same as for radiography, no improvement in spatial resolution is required.

Energy Loss and Density Resolution

The attenuation of a beam of monochromatic protons passing through homogeneous matter is small until the protons reach the end of their range. The dotted line in Figure 1 shows the flux curve for protons, neglecting nuclear interactions, which demonstrates the steep fall-off that is found in the last portion of the proton range. Thus a small change in the thickness of an absorber will result in a large change in the number of particles which pass through it. The steepness of that slope is given by the range straggling of protons passing through matter and is characterized by the sensitivity of the range measurement.

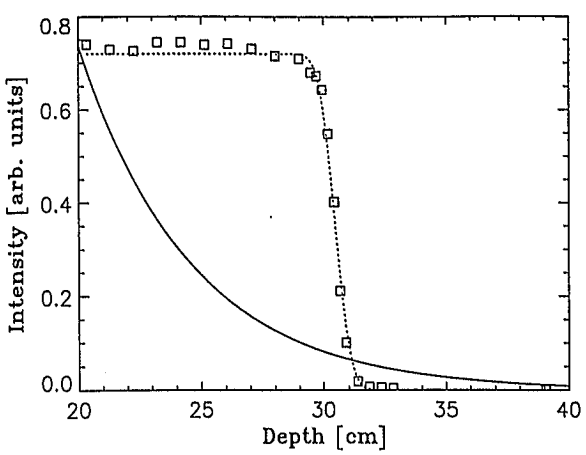

Fig. 1. Flux of 219 MeV protons (dotted line) and 50 keV photons (solid line) passing through water. The symbols represent measurements [18]

The range measurement of each individual proton can either be achieved by measuring directly the range with, for example, a range telescope or by measuring the energy and transforming these into proton ranges. Whether range detection or energy detection is the better choice depends on the sensitivity of the detector. For comparison, Figure 1 shows the transmission of X-rays where the flux is attenuated in a near-exponential fashion with increasing depth in the absorber.

Measurements have been performed where variations in integral density as small as 0.05% could be detected with low dose to the patient [6, 7]. With the same dose applied to the patient, one can detect changes in effective absorber thickness that are considerably smaller than those observable with other radiographic techniques. Such a density resolution is the result of the characteristic loss of energy of protons passing through matter. For protons with energies of the order of 200 MeV, loss of kinetic energy results from ionization of atoms in matter. This energy loss per centimeter, called the stopping power, can be calculated from the well known Bethe-Bloch equation. For protons, it reads

$$\frac{dE}{dx} = Kn_o\frac{1}{\beta^2}\left[\ln\left(\frac{2m_ec^2\beta^2}{(1-\beta^2)I}\right) - \beta^2\right] \qquad (1)$$

where K is a constant, n_o the electron density of the target material, β the velocity of the proton in units of the speed of light ($\beta = v/c$), I the mean ionization energy of the target atoms and m_e the mass of the electron.

The energy loss of protons is thus mainly dependent on the electron density of the traversed matter and on the ionization potential. The value I is approx. $16\ Z^{0.9}$ [eV], Z being the atomic number of the target material. The electron density n_o is a function of the physical density ϱ, the atomic number Z and atomic mass A ($n_o \sim \varrho Z/A$). For most materials in humans, Z/A is relatively constant and the stopping power is proportional to the physical density ϱ, in contrast to the mass absorption coefficient for X-rays, which varies in a complicated manner with Z and A.

It is a further characteristic of protons that they loose kinetic energy in discrete steps by interaction with atomic electrons. As this process

is statistically determined, a monoenergetic beam of protons shows an energy spread after passing through a homogeneous medium. For 215 MeV protons passing through biological material, the standard deviation of this statistical process, expressed as a percentage of the mean range, is approximately 1.1. This factor determines the inherent physical limit for the density resolution of a single detected proton. The density resolution increases with the number of detected protons per pixel according to the usual statistical laws (Fig. 2). The data were produced by taking images from a homogeneous water bath with different proton statistics. The solid line comes from calculation (including the detector energy resolution); the squares represent experimental results.

Energy Deposition and Dose to the Patient

The Bethe-Bloch formula (Eqn. 1) reveals that the stopping power of a proton increases as it slows down. Hence the largest amount of the proton's energy is deposited at the end of its range. Since for proton radiography the proton is stopped in the detection system most of the dose is deposited there and not in the patient. The applied dose for a proton image of 25 x 15 cm^2 size obtained with roughly one million events was calculated to be 0.01 mGy. A X-ray radiograph with both the same spatial and density resolution, would result in a 10 to 20 times higher dose.

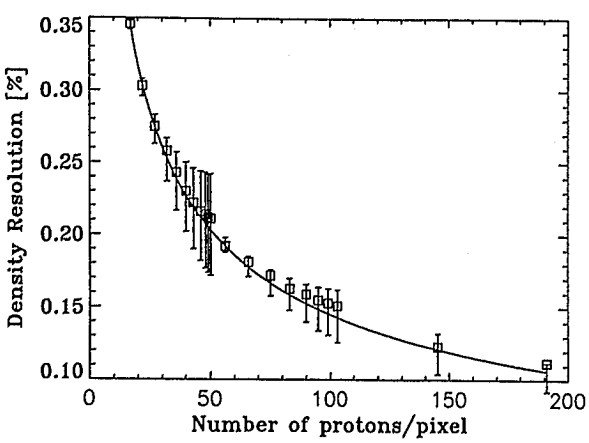

Fig. 2. Plot of the density resolution as a function of the number of detected particles per pixel. The symbols represent measurements in a homogeneous water phantom with different statistics. The solid line is the calculated prediction [18]

Heavy Charged Particle Radiography

Due to their physical properties, heavy charged particles are also interesting for radiography [8, 9]. Since resolution in depth is inversely proportional to the particle mass, it is clear that resolution improves with increasing projectile mass. The same is true for the spatial resolution, which also improves with increasing particle mass.

On the other hand, the dose deposited by heavier ions is higher than for lighter ions, since the energies required for heavy ion beams to penetrate thicknesses of the order of a patient's width are several hundred MeV per nucleon. At these energies, heavy ions undergo nuclear collisions which increase the dose to the patient. In Table 1 the spatial and depth resolutions and dose to the patient are listed for different particles for energies resulting in a total range of 300 mm in water. It can be seen that the improved spatial and density resolution which can be obtained with heavier particles is counteracted by an increased dose to the patient.

Proton Radiography and Tomography for Diagnostic Purposes

Proton radiography and tomography for diagnostic purposes was investigated in the 1970's [6, 7, 10]. The motivation for these studies was to obtain images of low contrast lesions in human

Table 1. Calculated spatial resolution, density resolution and dose to the patient for charged particles with a total range of 300 mm [27]. All results are normalized to unity for protons

Particle	Energy per nucleon MeV/u	Spatial resolution	Density resolution	Average dose to the patient
p	219	1.0	1.0	1.0
^{4}He	219	0.50	0.50	1.01
^{12}C	427	0.28	0.26	1.53
^{16}O	514	0.24	0.22	1.69
^{20}Ne	590	0.21	0.19	1.80

specimens superior to conventional X-ray techniques. In addition, the dose advantage of proton radiography over X-rays encouraged these authors.

Much of the early work was done by Koehler and Steward [6, 7] at the Harvard Cyclotron. They used a scattered 160 MeV proton beam and detected the images by exposing photographic films, located in the steep slope of the proton flux shown in Figure 1. With this apparatus they could visualize and differentiate soft body tissues, including pathological states significantly better than with X-rays. As Figure 3 illustrates, they were able to resolve, e.g., brain tumors and deep-seated grey matter (basal ganglia). Blood clots from stroke patients could also be visualized since blood is significantly more dense than brain tissue. Thus, in the case of the brain, it may be possible to obtain better information on the general nature of a tumor or a stroke. Koehler and Steward also obtained images from fresh human mastectomy specimens and with low doses they could detect changes in tissue density and small satellite tumors. In addition, brain slices containing lesions due to multiple sclerosis were detected as being more transparent to protons than to the surrounding tissue.

The proton radiographic work was afterwards extended using scanning systems and plastic scintillation counters to measure the proton flux [11, 12]. In these reports diagnostically useful proton radiographs of mastectomy and heart specimens were obtained with a low surface dose of only 0.45 mGy. For comparison, a typical dose for X-ray mammography is around 40 mGy.

In the late 1970's and early 1980's systems for obtaining proton CT images were developed [8, 13–16]. These systems have the advantage of using the high density contrast of protons to detect local variations in density as opposed to projected images. Proton CT images may also be used for proton radiotherapy treatment planning since, in contrast to X-ray CTs, they contain direct information on relative proton stopping power, which is used to calculate the range of the treatment beams. The detection equipment for such systems consisted either of multiwire proportional chambers to detect the spatial information and range telescopes for the density information [8, 13, 14] or of collimators plus a magnetic spectrometer [15, 16]. The studies showed that proton tomography yielded results similar to the X-ray CT reconstruction while exposing the sample to a lower radiation.

Proton Radiography for the Verification of Proton Treatments

The more precise a radiation therapy treatment is, the more important is the quality control of patient treatments [17, 18]. A first important task

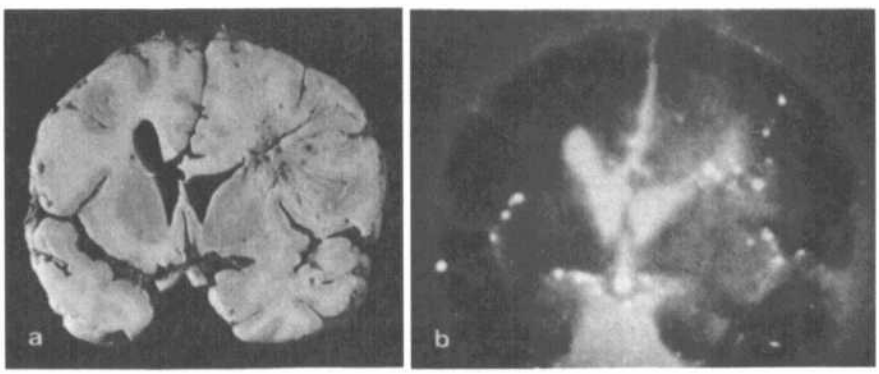

Fig. 3. (**a**) Front view of a coronal slice 1 cm thick of a human brain fixed in formalin. Note the glioblastoma multiforme in the white matter of the hemisphere on the right, with swelling of the hemisphere and distortion of the ventricular system. (**b**) Proton radiograph taken with a Polaroid TLX film. Note the lower density in the tumor area and the visualization of the basal ganglia. The white spots are air bubbles. With kind permission of Andreas M. Koehler [7] and Science

is to check the correct positioning of the patient with respect to the beam. Another requirement is the verification of the range and range variations of the protons, as the calculated proton dose distribution is based on the predicted range of protons in the patient. Proton radiography can fulfil both requirements simultaneously. Proton images produced by range information and range uncertainty information as a function of the proton position can be compared to the predicted results of the treatment planning algorithm.

Sources of range errors include: uncertainties in the computer tomographic data, which are the basis of the treatment planning program, and errors occurring in the treatment planning software [18,19,20]. Range variations due to inhomogeneity interfaces parallel to the beam are also very difficult to predict by the treatment planning software [21]. Such uncertainties in range can result in target misses and overdosage of critical tissue. Proton radiography can help to solve these problems or at least provide a better understanding.

Verification of Patient Positioning

Inaccurate positioning of the patient can result in damage of critical structures or target misses. The usual way of checking the patient positioning before irradiation is to provide X-ray radiographies of the patient in the treatment position and to compare these images with digitally reconstructed radiographs (DRRs) from the CT data used for treatment planning.

Another possibility is to take proton radiographies. The expected advantage is that the images can be taken exactly under the same geometrical conditions as the treatment itself. Hence, the images are true proton-beam's-eye-view projections, as opposed to X-ray images which are conical projections from a given point source. Studies have been made [18] to verify the accuracy of proton radiography in proton therapy. It has been found that, by matching the proton radiographs with images produced from the corresponding CT information, a positioning precision of the order of the voxel size of the image could be obtained. Thus, proton radiography could be a useful tool for verifying the position of the patient in proton therapy.

Detection of Range Uncertainties

Effects due to density inhomogeneities in the traversed material can influence the range of protons. Neglecting them may result in cold spots in the target volume or an unintentional dose to critical structures distal to the target volume.

A proton which passes close to an interface between low and high density tissues can take, due to multiple Coulomb scattering, either the path through the low or through the high density material. In the absence of multiple Coulomb scattering, the inhomogeneities would simply shift the range of protons by a distance equal to the integrated density along the path. However, the effect of multiple Coulomb scattering leads protons which enter and leave the sample through the same entrance and exit points to follow different trajectories and thus to cause range uncertainties. Similar range uncertainties are present also for therapy and can produce significant errors in the dose distribution. Proton radiographs detect the range variations for the whole body and may be used to select the most appropriate direction for an irradiation or to determine the size of the safety margins around the tumor volume.

Urie et al. [21] used heavy ion radiography (carbon and neon) to obtain the shape of the Bragg peak behind the head and the abdomen of a patient. The neon Bragg peak was degraded at the base of the skull from 3 mm to 15 mm and the carbon Bragg peak showed a broadening in regions of the gastrointestinal (GI) tract from 12 mm to 32 mm. Schneider and Pedroni [18] used a 219 MeV proton beam in tissue specimens and an Alderson phantom, respectively. Images of the standard deviation of the proton range spectra in each pixel were taken to study quantitatively the range variations of protons traversing inhomogeneities. Figure 4 shows, as an example for such an image, the DRR of the Alderson phantom head. The colours, which indicate the standard deviation of the range spectra designate the regions with additional straggling caused by inhomogeneities. As can be seen, range uncertainties of over 15 mm occur in regions where the protons passed close to tissue characterized by a strong density gradient orthogonal to the beam. Such critical situations in the Alderson head are listed in Table 2.

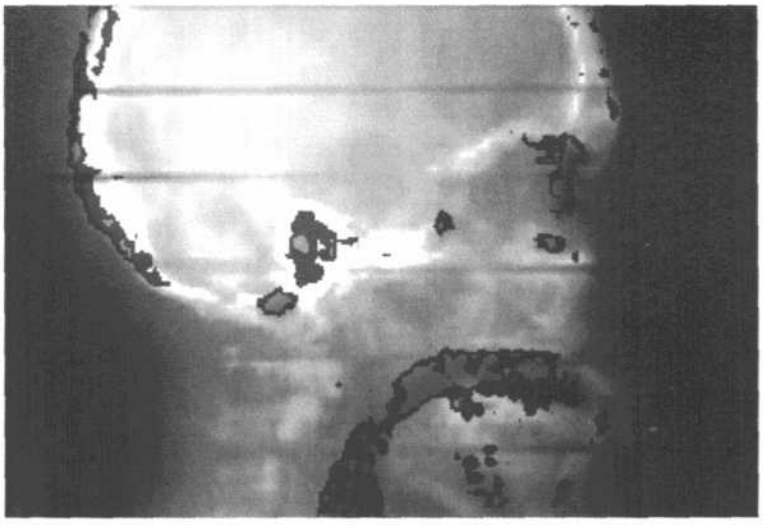

Fig. 4. Digitally reconstructed radiograph (DRR) of the Alderson head. The colours indicate range uncertainties of the protons measured by proton radiography (red: >15 mm, 15 mm > blue > 10 mm, 10 mm > yellow > 5 mm) [18]

Table 2. Range uncertainties measured with proton radiography in the head of the Alderson phantom. Data taken from [18]

Site of passing proton beam	Maximum uncertainty (mm)	Mean uncertainty (mm)
Oral cavity and mandible ramus	25.6	17.4
Mastoid air cells and sigmoid sinus	22.2	16.7
Frontal sinus	22.0	15.7
Tangential to skull	19.0	12.0
Mastoid air cells and bone brain interfaces	18.5	15.3
Sphenoid sinus	18.2	12.5
Maxillary sinus and ethmoid air cells	16.8	13.3

It should be noted that the radiographies in both reports [18, 21] were obtained from charged particles traversing the whole head whereas in a treatment situation, one is interested in the range variation caused by protons stopping in the head. Hence these measurements give an upper limit for the range error which can occur during treatment.

Range variation measurements should be helpful in estimating the necessary safety margins around the target volume, especially, if a tumor is located behind structures which can cause large range variations. Range variations can influence the dose distribution for proton treatments and proton radiography can be used for measuring these uncertainties and may help to find optimal beam directions.

Range Measurement

Computer tomographic images of a patient represent the basic information for the proton therapy treatment planning program. CT data are used to define the position of the target volume and of the critical structures and to quantify the inhomogeneities which are in the path of the proton beam. The CT images are taken with photon beams and are therefore images of photon attenuation data. The proton therapy treatment planning software calculates the dose distribution on the basis of a range calculation for the protons and, therefore, needs data which can be used to describe the interaction of the proton beam with the patient's tissue. The photon attenuation coefficients of the CT data have, therefore, to be converted into a water-equivalent path length, the so-called relative proton stopping power, in order to provide the residual range for the proton beam. This relation between stopping power and Hounsfield values is not unique and it raises the question, how well one can predict ranges using calibrated CT data in practice.

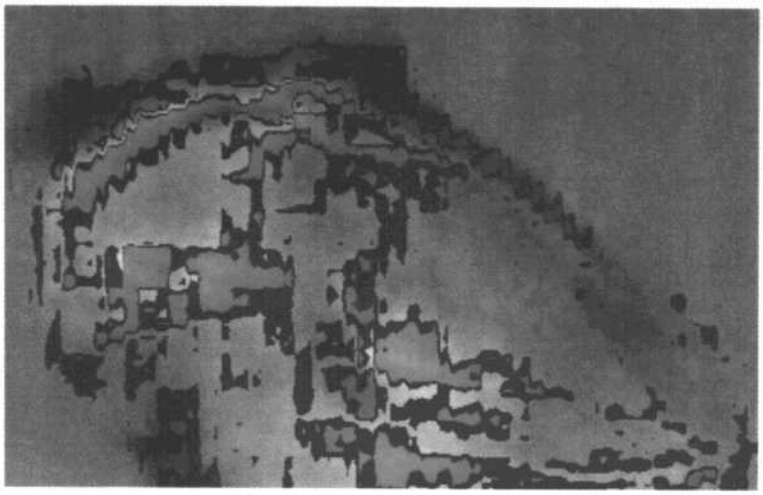

Fig. 5. Proton range image of a sheep's head. The colours indicate range differences between calculated DRR and experimental proton radiography (red: $|r| > 7mm$, blue: $7mm > |r| > 2.5mm$, yellow: $2,5mm > |r| > 0.7mm$) [18]

Experiments concerning the influence of all these errors have been reported. They were either done in vitro with conventional dose measurements [19, 20] or in vivo with proton radiography [18]. Chen et al. [20] measured the Bragg peak shift in an abdomen slice of the Alderson phantom and compared the result with the range calculation based on their CT calibration. They obtained differences between measurements and calculation of about 5% of the traversed matter. Alpen et al. [19] also measured the Bragg peak shift of neon and helium beams in a frozen dog for seven selected target locations. They obtained errors of up to 11% between CT range and measured range. They concluded that large deviations appeared where bone or air filled cavities were in the beam path. Recently, the author [18] has measured range calibrated proton radiographies of a sheep's head (Fig. 5) and compared these to the calculated projections, computed from the calibrated CT data, transverse to the beam. In this study, the proton radiographs were used to improve the range calculation, by a variation of the relation between CT units and relative stopping power [22, 23]. The colours in Figure 5 mark regions of the sheep which correspond to differences between predicted and measured range for a certain CT calibration. Such proton images give both, information about the amplidute of range errors and about its dependence on the penetrated tissue type. The maximum deviation between calculated and predicted range for a typical treatment of a brain tumor could be reduced with the help of such measurements by a factor of 4 and the mean deviation by a factor of 3, respectively.

Thus, a precise check of the calculated range is important for precise proton treatments. Proton radiography can provide better calibrations for CT data and can help to reduce errors in the calculated dose distributions for therapy.

Conclusion

Proton radiography and tomography can be carried out at lower doses for a given density resolution than those occurring in routine X-ray examinations or can produce images with the same dose to the patient but with an improved density resolution. The high density resolution of proton images can be used to detect diagnostically important differences in soft tissues which cannot be seen in conventional X-ray radiographies. The limiting spatial resolution for projected radiographies, due to multiple Coulomb scattering, can be improved if the positional information of the protons is taken in coincidence and the additional spatial knowledge is used to reconstruct the projected images. In addition, significant improvements in the spatial resolution of proton tomographies may be expected by using special algorithms

which include such reconstruction methods, instead of the conventional algorithms used in X-ray tomography. For clinical use of proton radiography, an accelerator with adequate proton energies is required. Such a diagnostic tool could be attached to a therapy machine to prove the accuracy of each individual treatment.

Acknowledgement

I wish to acknowledge the helpful comments and suggestions made by Eros Pedroni, Andy Koehler and Ken Hanson.

References

1 Wilson, R.R. Radiological use of fast protons. Radiology 47, 487–491, 1946.
2 Charpak, G., Majewski, S., Perrin, Y., Saudinos, J., Sauli, F., Townsend, D., and Vinciarelli, J. Further results in nuclear scattering radiography. Phys. Med. Biol. 21, 941–948, 1976.
3 Saudinos, J., Charpak, G., Sauli, F., Townsend, D., and Vinciarelli, J. Nuclear scattering applied to radiography. Phys. Med. Biol. 20, 890–905, 1975.
4 Mustafa, A. and Jackson, D. Small-angle multiple scattering and spatial resolution in charged particle tomography. Phys. Med. Biol. 26, 461–472, 1981.
5 Schneider, U. and Pedroni, E. Multiple Coulomb scattering and spatial resolution in proton radiography. Med. Phys. 21, 1657–1663, 1994.
6 Koehler, A.M. and Steward, V.W. Proton radiographic detection of strokes. Nature 245, 38–40, 1973.
7 Koehler, A.M. and Steward, V.W. Proton beam radiography in tumor detection. Science 179, 913–914, 1973.
8 Crowe, K.M., Budinger, T.F., Cahoon, J.L., Elischer, V.P., Huesman, R.H., and Kanstei, L.H. Axial scanning with 900 MeV alpha particles. IEEE Transactions on Nuclear Science NS-22, 1752–1754, 1975.
9 Tobias, C.A., Benton, E.V., Capp, M.P., Chatterjee, A., Cruty, M.R., and Henke, R.P. Particle radiography and autoactivation. Int. J. Radiat. Oncol. Biol. Phys. 3, 35–44, 1977.
10 Cormack, A.M. and Koehler, A.M. Quantitative proton tomography: Preliminary experiments. Phys. Med. Biol. 21, 560–569, 1976.
11 Kramer, S.L., Moffett, D.R., Martin, R.L., Colton, E.P., and Steward, V.W. Proton radiography. Radiology 135, 483, 1980.
12 Mofett, D.R., Colton, E.P., Concaildi, E.W., Hoffman, E.W., Klem, R.D., Knott, M.J., Kramer, S.L., Martin, R.L., Parker, E.F., Passi, A.R., Schultz, P.F., Stockley, R.L., and Timm, R.E. Initial test of a proton radiographic system. IEEE Transactions on Nuclear Sciences NS-22, 1749–1751, 1975.
13 Hanson, K.M., Bradbury, J. N., Cannon, T.M., Hutson, R.L., Laubacher, D.B., Macek, R.J., Paciotti, M.A., and Taylor, C.A. Computed tomography using proton energy loss. Phys. Med. Biol. 26, 965–983, 1981.
14 Hanson, K.M., Bradbury, J.N., Koeppe, R.A., Macek, R.J., Machen, D.R., Morgado, R., Paciotti, M.A., Sandford, S.A., and Steward, V.W. Proton computed tomography of human specimens. Phys. Med. Biol. 27, 25–36, 1982.
15 Akisada, M., Ohashi, J., Kondo, K., Kurihara, D., Miyashita, S., Tachikawa, A., Takada, Y., and Takikawa, K. Conceptual design of proton computed tomography with magnetic spectrometer. Jap. J. Appl. Phys. 22, 752–758, 1983.
16 Takada, Y. and Abe, I. Multiple pencil beams for proton computed tomography. Nucl. Instr. Meth. Phys. Res. A262, 511–521, 1987.
17 Goitein, M. Calculation of the uncertainty in the dose delivered during radiation therapy. Med. Phys. 12, 608–612, 1985.
18 Schneider, U. and Pedroni, E. Proton radiography as a tool for quality control in proton therapy. Med. Phys. 22, 353–363, 1995.
19 Alpen, E., Saunders, D., Chatterjee, A., Llacer, J., Chen, G., and Scherer, J. A comparison of water-equivalent thickness measurements: CT method vs. heavy ion beam technique. Brit. J. Radiol. 58, 542–548, 1985.
20 Chen, G., Singh, R., Castro, J., Lyman, J., and Quivey, J. Treatment planning for heavy ion radiotherapy. Int. J. Radiat. Biol. Phys. 5, 1809–1819, 1979.
21 Urie, M., Goitein, M., Holley, W., and Chen, G. Degradation of the Bragg peak due to inhomogeneities. Phys. Med. Biol. 31, 1–15, 1986.
22 Moyers, M., Miller, D., Siebers, J., Galindo, R., Sun, S., Sardesai, M., and Chan L. Water equivalence of various materials for 155 to 250 MeV protons, priv. communication, 1993.
23 Mustafa, A. and Jackson, D. The relation between X-ray CT numbers and charged particle stopping powers and its significance for radiotherapy treatment planning. Phys. Med. Biol. 28, 169–176, 1983.
24 Cookson, J.A. Radiography with protons. Naturwissenschaften 61, 184–219, 1979.
25 Curry, J. and Steward, V.W. Establishment of a beam line at the Fermi National Accelerator Laboratory for proton radiography. Med. Phys. 5, 188–195, 1978.
26 Tourovsky, A., Pedroni, E., and Schneider, U. Monte Carlo codes for proton radiography and treatment planning (Status Report). PSI Life Sciences, Annual Report Annex II, 20–22, 1993.
27 Barrett, R.C. and Jackson, D.F. in Nuclear Sizes and Structure, Oxford University Press, 1977, Chapter 8.

32 Compensation of Target Motion

T. Okumura, H. Tsuji, and H. Tsujii

Proton Medical Research Center, University of Tsukuba, Tsukuba-shi, Japan

Introduction

During the last decade developments in diagnostics and treatment planning have been achieved which permit individualized three-dimensional dose delivery. In this context, special attention has been payed to the issue of how close treatment volumes can be approximated and how much dose can be delivered safely to target volumes.

Ion beam therapy is expected to play an important role in such 3D-approaches, since the physical characteristics of ion beams provide an excellent dose distribution [1]. Much work has been contributed to the design of optimal treatment systems for ion beam therapy. This effort resulted, e.g., in a successful local control of uveal melanoma, intracranial and skull-base tumors [2,3]. If we expect to achieve the same results in other tumors, e.g., of the thoraco-abdominal area, however, some problems have to be solved first and compensation of target motion is one of them.

Although CT or MRI imaging techniques allow to optimize treatment plans for conformation therapy, such images are usually static ones. For the treatment of thoraco-abdominal targets, images are obtained from patients interrupting respiration or keeping, occasionally, decubital or prone postures. But, the organs of the thoracoabdominal area show various kinds of motion during the treatment period and motion of the abdominal organs may result in dose uncertainties near the edge of the treatment field. Managing such target fluctuation is the key to success for 3D-treatment of these tumors.

Accurate compensation of target motion will lead to minimization of the treatment volume and dose-limiting organs can be spared from irradiation, avoiding serious treatment morbidities.

It should be emphasized, however, that compensation of target motion does not compensate for inaccurate target localization and lacking reproducibility of daily treatment conditions. The importance of reproducible immobilization of the patients and reliable target localization techniques will be discussed elsewhere in this book. This chapter will concentrate on organ motions during the treatment itself and ways to compensate them.

Types of Organ Motion

Despite the fact that accurate and precise positioning can be achieved with casting and other immobilization techniques, there are several kinds of target motion which are a result of physical or physiological characteristics of the organ. Some of them are static and others change continuously over the treatment time. According to their nature they can be classified into five basic categories:

- gravity or position-related movements
- displacement or deformation by pressure
- gut movements
- respiration-related motions
- vascular pulsation

The first two categories are relatively latent motions whereas the others are continuous or ongoing.

There are only a few published papers describing the issue and there is still insufficient knowledge to make compensated treatment planning of mobile targets a reality. Movement of the eye ball or tongue is very important one to be handled as well, but it is rather a problem of immobilization than compensation.

Gravity or Position-Related Movements

Gravity-related movement is observed in every organ. It is a movement or displacement as a function of the patient position. Once it happens, the three-dimensional relationship between the target and the surrounding organs are maintained until the patient changes his/her position again. For treatment positions other than horizontally supine this might cause problems. When a patient's skull is rotated, e.g., there is a possibility of intracranial motions relative to the skull and the beam line. Movements of intracranial structures of the order of 0.5 to 1.5 mm were detected by Serago and colleagues [4]. Concerning the thoraco-abdominal organs, Tsujii et al. [5] reported that the position of most abdominal organs was displaced caudally in the prone vs. the supine position. The displacement was demonstrated even for pancreatic tumors which are retroperitoneal and more or less adherent to the surrounding structures. These kinds of movements, do not matter too much, as long as the treatment planning is based on CTs obtained in the treatment position.

Displacement or Deformation by Pressure

Displacement or deformation of an organ by pressure is usually observed in organs of the pelvic space. The bladder can change its size and shape considerably, depending on the volume of urine and the pressure from the surrounding gut.

Turner and colleagues [6] investigated the degree of bladder movement during the course of radiotherapy by comparing initial planning CTs with subsequent pelvic CTs performed at weekly intervals during the treatment period. They found that the projected size of the bladder ranged from 16.2 to 80.9 cm^2 and patients with large bladders on the planning CT were more likely to have a change in the bladder size than those with small bladders. A wall displacement of at least 1.5 cm was observed in 60% (18/30) of the cases. There was no chronological pattern of displacement through patients' treatments and all walls were approximately at equal risk of movement. Patients who had posterior margin changes of at least 1.5 cm were also likely to have equally large (>2 cm) rectal diameter changes.

Arimoto and colleagues [7] reported an interesting technique to assume the localization of intrapelvic tumors. They suggested to adjust primarily the daily treatment field settings according to the daily location of the internal target recognizable by metallic fiducials implanted in the tumor site. Then they request the bladder to be emptied and refilled with a defined amount of water to standardize the effective internal body density. With this approach, localized proton boost irradiations could play an important part in the multidisciplinary treatment of locally invasive bladder cancer aiming at the conservation of the bladder [8].

Gut Movement

The alimentary tract – with the exception of the intrathoracic esophagus and lower rectum – is barely a good candidate for conformation therapy by ion beams; not only because its tolerance to radiation is relatively low, but also because it can change its shape and position any moment depending on its contents and peristaltic motion. The gut is also quite mobile, because of its loose fixation to mesenteries. It is, therefore, quite difficult to reproduce the shape and position of the intestinal loops at every treatment session.

These difficulties lead to chronological and geographical inhomogeneities in the region where the ion beams pass through. Urie and co-workers [9] investigated the effects of highly inhomogenous regions, such as the base of skull and abdomen, on the depth-dose characteristics of charged particle beams. They determined the stopping distribution of carbon ions passing through intestinal loops and derived the corresponding Bragg peak distributions. The full width at half maxi-

mum (FWHM) of the Bragg peak (nominally 5.5 mm) was found to be greater than 25 mm at air-soft-tissue interfaces. According to the authors a Bragg peak may not look like a Bragg peak on the distal side of a complex inhomogeneity. Such effects of tissue inhomogeneity along the beam path which may influence the dose distribution need to be further analyzed. This issue is also of relevance in the treatment of pancreas tumors.

Concerning the esophagus, Sugahara and coworkers investigated the displacement of the esophagus in the field-localization process [10]. It is discussed here, even though it might be classified as a position-related rather than an involuntary type of movement.

Measurements of corrected distances on a total of 177 localization attempts disclosed that a correction by >5 mm was necessary in 30.6% and by >10 mm in 10.2% of all localization attempts. Correction of more than 5 mm was required even in 66.7% of 60 localizations in patients older than 80 years. They recommended the use of a real-time verification system for precise and frequent target localization [11], in particular, for patients with high risk factors, i.e. high age, tumor in the lower esophagus or primary lesion T1.

Respiration-Related Motions

Respiratory motion can be considered as the most important motion to be compensated for, because of its repetition and its close relation to the major thoraco-abdominal organs, such as the lung, liver, pancreas and the kidneys.

A major benefit of ion beam therapy is the possibility to minimize the treatment volume. Several studies [12–16] investigating the amplitude of respiration-related organ motion yielded a value of approx. 20 mm in cranio-caudal direction (Tab. 1). It is, therefore, much too big to be ignored, because in ion beam therapy, the safety margins around the tumor volume are usually set to only 5 mm. Without a special technique, a 20 mm longer treatment field in cranio-caudal direction would be necessary in order to deliver the prescribed dose to the target volume. Moerland and colleagues [16] calculated the dose distribution taking the kidney motion into account and they concluded that widening of the penumbra can occur near the edge of the kidney in a situation like this.

Not only the position of the target, but the electron density along the beam path can alter due to respiration movements, although Henkelman and Mah reported that dose variations around the breathing cycle are less than 5% in the case of lung cancer treated with photon therapy [17].

Respiratory motion is a slower phenomenon than vascular pulsation, and more regular than the peristaltic movements of the gut. It is, there-

Table 1. Amplitude of respiration-related organ motion

Investigation	Organ	Method of Measurement	Organ Motion Mean and Range
Weiss (19)	Liver	Scintigraphy	11 mm (8–14)
	Diaphragm	Fluoroscopy	13 mm (8–18)
Nishioka (21)	Diaphragm	Fluoroscopy	12 mm (0–40)
Suramo (20)	Liver	Ultrasound	25 mm (10–40)
	Pancreas		20 mm (10–30)
	L. kidney		19 mm (10–40)
	R. kidney		19 mm (10–40)
Moerland (23)	L. kidney	MRI	2 to 24 mm
	R. kidney		4 to 35 mm
Schwartz (22)	L. kidney	MRI	max: 39 mm
	R. kidney		max: 39 mm

fore, best suited for technical compensation means. Some clinical trials using a compensation technique for respiratory motion in the treatment of liver tumors have recently begun at the University of Tsukuba [18, 19].

Techniques for Compensation of Continuous Organ Motions

There are different methods of beam modulation in ion beam therapy, e.g., scattering and fixed range modulation [20, 21] or several kinds of variable modulation using scanning techniques [22–24]. The method of compensation of continu-

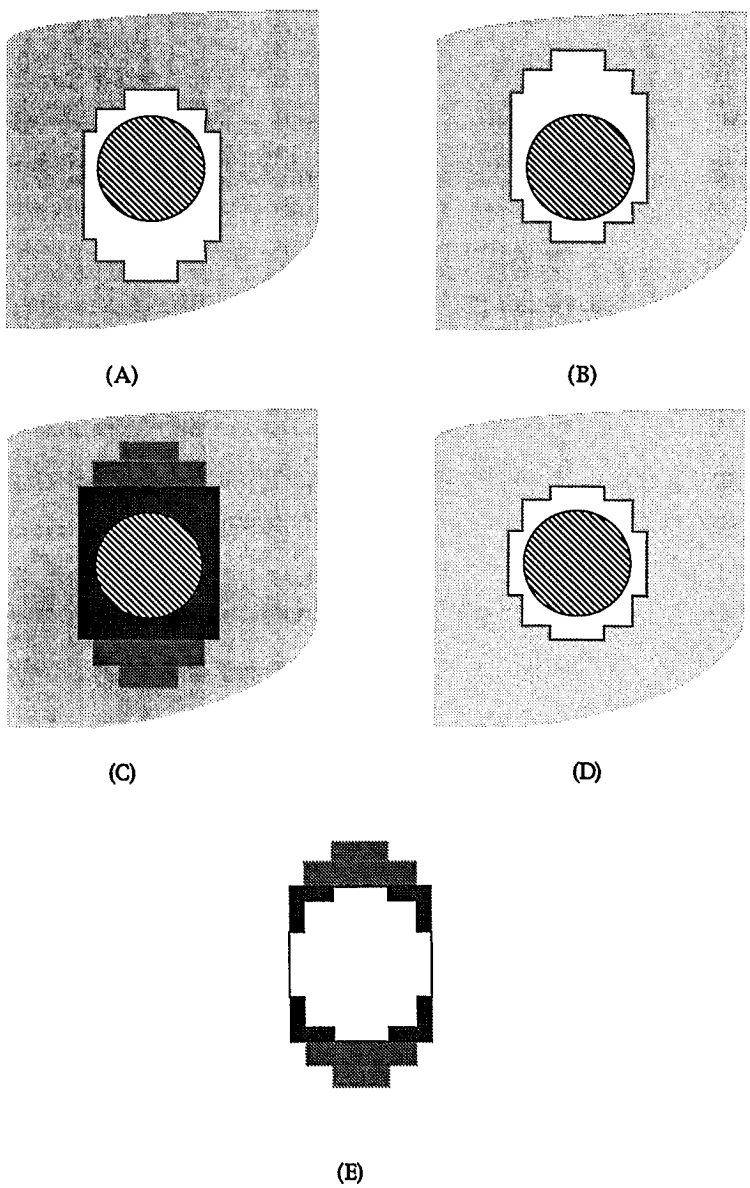

Fig. 1. Schematic representation of the respiration-gated irradiation system ReGIS. An elongated treatment field in craniocaudal dimension (open area with multileaf collimation) covers the target volume (shaded circle) in both, expiration (A) and inhalation (B) phase. Respiratory motion creates dose inhomogeneity in the treatment volume as demonstrated in grayscale (C). Intermittent irradiation with ReGIS allows for minimum treatment field (D). Normal liver tissue surrounding the target volume (shaded area) is effectively spared by means of ReGIS (E)

ous target motions depends on the beam modulation technique applied at a certain facility.

A possible technique of compensation compatible with fixed range modulation is intermittent beam delivery [25], or synchronous movement of the treatment couch with motion of the target. For facilities applying a scanning system, target-oriented variable scanning or some kind of mechanical method to reduce organ motion, such as abdominal fixation [26] would be appropriate.

A Respiration-Gated Irradiation System

Although there are other possible ways to compensate respiratory motion, intermittent irradiation seems to be the simplest and most reliable technique in clinical use (Fig. 1).

Ohara and co-workers developed a respiration-gated irradiation system (ReGIS) for electron linear accelerators [25, 27]. Inada and colleagues adapted the system for proton synchrotron usage [28]. So far, it has been utilized clinically in the treatment of liver tumors [29].

ReGIS is a computer controlled irradiation system triggered by signals that coincide with respiratory motion. The system consists of two components, the monitoring system of the patient's respiration and the triggering system for the proton synchrotron.

Initially, Ohara used an airbag to measure respiratory motion [25], but the big device sometimes overlapped with the treatment field of upper abdominal tumors. A small strain gauge ($4 \times 2\ cm^2$) is available now for monitoring the tension of the abdominal wall which changes parallel with respiration. The strain gauge converts the tension of the abdominal surface into electric signals which, in turn, are amplified and transferred to a signal-control unit. Following the offset and span control, the signals are digitized and transformed into a respiratory curve by a central processing unit (CPU). The operator can set a gate signal at an arbitrary point in the respiration curve displayed on a cathode ray tube (CRT) monitor, and checks, in parallel, the movement of the target fluoroscopically.

The gate signals – one for opening the gate the other for closing it – are usually set to late exhale and early inhalation phase, during which protons are delivered. With this timing, the movement of the diaphragm is minimal and its position is most reproducible as compared to other phases [30].

The signals from ReGIS are sent upstream to the ion source and protons are delivered by a fast-cycling synchrotron which responds to the triggering signal within milliseconds [28]. By using this system the maximum shift of the target can be restricted to 5 mm during the beam delivery period.

A comparative planning was made for a patient with a hepatocellular carcinoma in the right lobe of the liver to estimate the benefit of ReGIS. The maximum diameter of the tumor was 5 cm, and it shifted approx. 2 cm in cephalo-caudal direction. One of the treatment plans was designed to cover the target volume with minimum margins, assuming that successful synchronized irradiation could be performed. The other plan was designed with safety margins which were 2 cm longer at both, cephalic and caudal ends, considering the target's respiration-related fluctuation. The dose-volume curves resulting from the two model calculations are shown in Figure 2. It is obvious that the normal liver tissue surrounding the target is effectively spared by means of ReGIS.

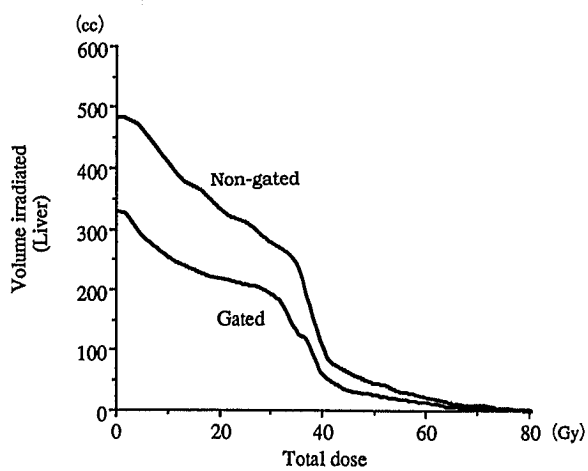

Fig. 2. Comparative dose-volume histograms for normal liver tissue in the treatment of a liver tumor with (gated) and without (non-gated) contribution of a respiration-gated irradiation system. The diameter of the liver tumor, and respiration-related tumor shift were assumed to be 5 cm and 2 cm, respectively

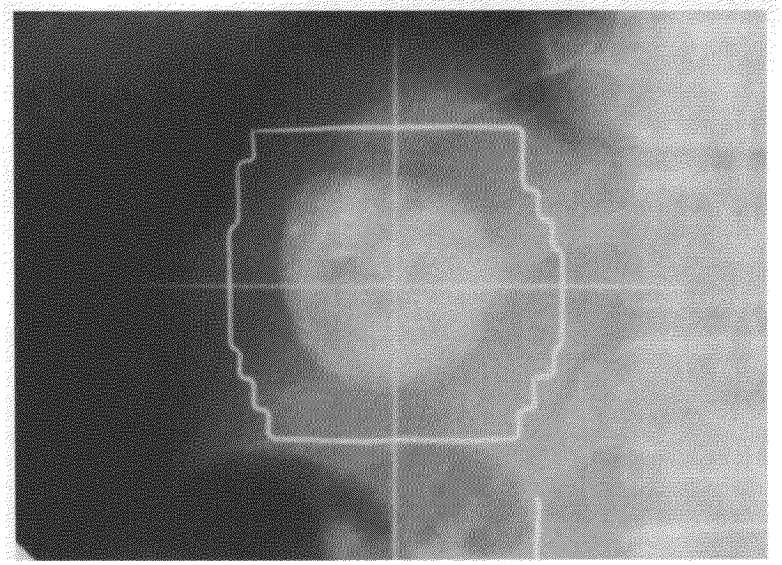

Fig. 3. Example of the treatment portal for a nodular hepatocellular carcinoma with contribution of the respiration-gated irradiation system ReGIS. The nodule was pretreated by transarterial embolotherapy with oily contrast agent

In an actual treatment plan (Fig. 3), the radiation therapists delineate the target volume with 5–10 mm margins on consecutive transaxial CT images of 5 mm thickness. In cephalo-caudal dimension, additional target outlines are prepared for each end, which create the three-dimensional safety margins. For the cephalic end, the same target outline is delineated as for the juxta-caudal scan. For the caudal end, one more imaginary target is prepared, taking into account the respiration-related fluctuation. This way, a 10 mm margin is considered for the caudal end. In case the tumor is located at the caudal surface of the liver facing the small or large intestine, no additional target outline is considered at the caudal end of the treatment volume in order not to induce radiation-related enterocolitis or ulcer.

Vascular Pulsation

In general, peripheral vascular pulsation does not matter, because it is so minute that it does not affect the shape of the target volume. However, pulsation of the heart should not be neglected. The risk of radiation-induced damage to the coronary artery or myocard after mediastinal irradiation (e.g, Hodgkin's disease [31]) has been reported in many articles. Subclinical myocardial damage [32, 33] or luminal narrowing of coronary arteries [34] might have occured, even if a long-term survivor does not show clinical symptoms. It is quite reasonable to apply ion beam therapy to mediastinal treatments, because this way it can be assumed that an irradiation of the heart can be avoided. A person with an invasive thymoma or lung cancer contacting the heart would be a good candidate for ion beam therapy in this respect.

There are not enough data about the amplitude of heart-beat-induced organ movements. An analysis using ultra-fast CT or ECG-gated MRI would be necessary. The pulsation of the heart is among the most difficult movements to compensate for, since it is a very rapid movement and the correlation with breathing and pulsation complicates it even more.

An Integrated System of Patient Immobilization and Motion Control

The theoretical advantage of ion beams over photons, e.g., their improved physical dose distribution [1, 35] and partly higher relative biological effectiveness [36, 37, 38] are quite convincing. Treatment planning supported by modern computer technology can bring out much of their advantage. However, their clinical advantage

cannot be realized without accurate patient positioning, target localization, and compensation of the target motion. Minimizing patient movements is imperative if the prescribed dose is to be delivered with certainty to the intended target volume. This is why patients should be immobilized with various kinds of casts or shells. The next step is to compensate internal target motions as described in this chapter. Finally, it has to be verified if the treatment can be performed as planned. This target localization and field verification process must be rapid, responsive and reliable, since the target motion does not always keep the same pattern. In this respect, internal fiducial and real-time fluoroscopic field verification systems can be helpful [11].

It can be concluded that optimum ion beam therapy cannot go without an integrated treatment system which assures proper patient immobilization, compensation of target motions, and field verification.

References

1 Koehler, A.M. and Preston, W.M. Protons in radiation therapy. Radiology 104, 191–195, 1972.
2 Suit, H. and Urie, M. Proton beams in radiation therapy. JNCI 84, 155–164, 1992.
3 Linstadt, D., Castro, J., Char, D., Decker, M., Ahn, D., Petti, P., Nowakowski, V., Quivey, J., and Phillips T.L Long-term results of helium ion irradiation of uveal melanoma. Int J. Radiat. Oncol. Biol. Phys. 19, 613–618, 1990.
4 Serago, C., Okunieff, P., Gall, K., Fullerton, B., Urie, M., and Rosenthal, S. Measurement of intracranial motions. Presented at XVII. Proton Therapy Cooperative Meeting, Loma Linda, Oct. 26–27, 1992.
5 Tsujii, H., Bagshaw, M.A., Smith, A.R., von Essen, C.F., Mettler, F.A., and Kligerman, M.M. Localization of structures for pion radiotherapy by computerized tomography and orthodiagraphic projection. Int. J. Radiat. Oncol. Biol. Phys. 6, 319–325, 1980.
6 Turner, S.L., Swindell, R., Bowl, N., Read, G., and Cowan, R.A. Bladder movement during radiotherapy for bladder cancer: Clinical implications for computerised treatment planning. Proc. of the XIth Int. Conference on the Use of Computers in Radiation Therapy 1994, Hounsell, A.R., Wilkinson, J.M., and Williams, P.C. (eds.), Manchester, UK, pp. 206–207, 1994.
7 Arimoto,T., Kitagawa,T., Inada,T., Maruhashi,A., Hayakawa,Y., and Sato, M. Some trials in PARMS for the accurate tumor localization and treatment set-ups in fractionated proton therapy. Nippon Acta Radiol. 48, 444–453, 1988.
8 Tsujii, H., Akaza, H., Ohtani M., Tsuji, H., Okumura, T., Ohara, K., and Koiso, K. Preliminary results of bladder-preserving therapy with definitive radiotherapy and intraarterial infusion of chemotherapy. Strahlenther. Onkol. 170, 531–537, 1994.
9 Urie, M., Goitein, M., Holley, W.R., and Chen, G.T.Y. Degradation of the Bragg peak due to inhomogeneities. Phys. Med. Biol. 31, 1–15, 1986.
10 Sugahara, S., Tsujii, H., Tsuji, H., Tatsuzaki, H., Ohara, K., and Itai, Y. The value of frequent positioning of treatment field in radiotherapy of esophageal cancer. Nippon Acta Radiol. 52, 1308–1314, 1992.
11 Tsujii, H., Inada, T., Maruhashi, A., Hayakawa, Y., Tsuji, H., Ohara, K., Akisada, M., and Kitagawa, T. Field localization and verification system for proton beam radiotherapy in deep-seated tumors. Nippon Acta Radiol. 49, 622–629, 1989.
12 Weiss, P.H., Baker, J.M., and Potchen, E.J. Assessment of hepatic respiratory excursion. J. Nucl. Med. 13, 758–759, 1972.
13 Suramo, I., Päivänsalo, M., and Myllylä, V. Craniocaudal movements of the liver, pancreas and kidneys in respiration. Acta Radiol. 25, 129–131, 1984.
14 Nishioka, M., Fujioka, T., Sakurai, M., Nakajima, T., and Onoyama, Y. Movement of the diaphragm during radiation treatment. J. Jpn. Soc. Ther. Radiol. Oncol. 3, 35–39, 1991.
15 Schwartz, L.H., Richaud, J., Buffat, L., and Touboul, E. Kidney mobility during respiration. Presented at XVIII. Proton Therapy Cooperative Meeting, Orsay-Nice, Apr. 16–19, 1993.
16 Moerland, M.A., van den Bergh, A.C.M., Bhagwandien, R., Janssen, W.M., Bakker, C.J.G., Lagendijk, J.J.W., and Battermann, J.J. The influence of respiration-induced motion of the kidneys on the accuracy of radiotherapy treatment planning, a magnetic resonance imaging study. Radiother. Oncol. 30, 150–154, 1994.
17 Henkelman, R.M. and Mah, K. How important is breathing in radiation therapy of the thorax? Int. J. Radiat. Oncol. Biol. Phys. 8, 2005–2010, 1982.
18 Tsujii, H., Tsuji, H., Inada, T., Maruhashi, A., Hayakawa, Y., Takada, Y., Tada, J., Fukumoto, S., Tatsuzaki, H., Ohara, K., and Kitagawa, T. Clinical results of fractionated proton therapy. Int. J. Radiat. Oncol. Biol. Phys. 25, 49–60, 1992.
19 Matsuzaki,Y., Osuga, T., Saito, Y., Chuganji, Y., Tanaka, N., Shoda, J., Tsuji, H., and Tsujii, H. A new, effective, and safe therapeutic option using proton irradiation for hepatocellular carcinoma. Gastroenterology 106, 1032–1041, 1994.
20 Koehler, A.M., Schneider, R.J., and Sisterson, J.M. Range modulators for protons and heavy ions. Nucl. Instr. Meth. 131, 437–440, 1975.
21 Koehler, A.M., Schneider, R.J., and Sisterson, J.M. Flattening of proton dose distributions for large-field radiotherapy. Med. Phys. 4, 297–301, 1977.

22 Goitein, M. and Chen, G.T. Beam scanning for heavy charged particle radiotherapy. Med. Phys. 10,831–840, 1983 .
23 Hiraoka, T., Kawashima, K., Hoshino, K., Kawachi, K., Kanai, T., and Matsuzawa, H. Dose distributions for proton spot scanning beams: Effect by range modulators. Nippon Acta Radiol. 43,1214–1223, 1983.
24 Blattmann, H., Coray, A., Pedroni, E., and Greiner, R. Spot scanning for 250 MeV protons. Strahlenther. Onkol. 166,45–48, 1990.
25 Ohara, K., Okumura, T., Akisada, M., Inada, T., Mori, T., Yokota, H., and Caraguas, M.J.B. Irradiation synchronized with respiration gate. Int. J. Radiat. Oncol. Biol. Phys. 17, 853–857, 1989.
26 Munkel, G., Blattmann, H., Scheib, S., Lomax, A., Pedroni, E., and Ulmer, U. Abdominal fixation – a way to reduce organ motions and to minimize mismatching between target and high dose volume. Presented at XVIII. Proton Therapy Cooperative Meeting, Orsay-Nice, Apr. 16–19, 1993.
27 Ohara, K., Kubota, S., Akisada, M., Inada, T., Kitagawa, T., Okumura, T., and Kure, F. Irradiation synchronized with respiratory cycle. Nippon Acta Radiol. 47, 488–496, 1987.
28 Inada, T., Tsuji, H., Hayakawa, Y., Maruhashi, A., and Tsujii, H. Proton irradiation synchronized with respiratory cycle. Nippon Acta Radiol. 52, 1161–1167, 1992.
29 Okumura, T., Tsuji, H., Hayakawa, Y., Maruhashi, A., Inada, T., and Tsujii, H. Respiration-gated irradiation system for proton radiotherapy. Proc. XIth Int. Conference on the Use of Computers in Radiation Therapy, 1994, Hounsell, A.R., Wilkinson, J. M., and Williams, P.C. (eds.) Manchester, UK 1994, pp. 358–359.
30 Wade, O.L. Movements of the thoracic cage and diaphragm in respiration. J. Physiol. 124, 193–212, 1954.
31 Gustavsson, A., Eskilsson, J., Landberg, T., Svahn Tapper, G., White, T., Wollmer, P., and Akerman, M. Late cardiac effects after mantle radiotherapy in patients with Hodgkin's disease. Ann. Oncol. 1, 355–363, 1990.
32 Stewart, J.R. and Fajardo, L.F. Radiation-induced heart disease: An update. Prog. Cardiovas. Dis. 27, 173–194, 1984.
33 Maunoury, C., Pierga, J.Y., Valette, H., Tchernia, G., Cosset, J.M., and Desgrez, A. Myocardial perfusion damage after mediastinal irradiation of Hodgkin's disease: A thallium-201 single photon emission tomography study. Eur. J. Nucl. Med. 19, 871–873, 1992.
34 Brosius, F.C., Waller, B.F., and Roberts, W.C. Radiation heart disease. Analysis of 16 young (aged 15 to 33 years) necropsy patients who received over 3,500 rads to the heart. Am. J. Med. 70, 519–530, 1981.
35 Suit, H. and Goitein, M. Dose-limiting tissues in relation to types and location of tumours: Implications for efforts to improve radiation dose distributions. Eur. J. Cancer 10, 217–224, 1974.
36 Tenforde, T.S., Tenforde, S.D., Crabtree, K.E., Parks, D.L., Schilling, W.A., Parr, S.S., Flynn, M.J., Howard, J., Lyman, J.T., and Curtis, S.B. RBE values for radiation-induced growth delay in rat rhabdomyosarcoma tumors exposed to plateau and peak carbon, neon and argon ions. Int. J. Radiat. Oncol. Biol. Phys. 7, 217–222, 1981.
37 von Essen, C.F., Blattmann, H., Crawford, J.F,. Fessenden, P., Pedroni, E., Perret, C., Salzmann, M., Shortt, K., and Walder, E. The PIOTRON: Initial performance, preparation and experience with pion therapy. Int. J. Radiat. Oncol. Biol. Phys. 8, 1499–1509, 1982.
38 Urano, M., Verhey, L.J., Goitein, M., Tepper, J.E., Suit, H.D., Mendiondo, O., Gragoudas, E.S., and Koehler, A. Relative biological effectiveness of modulated proton beams in various murine tissues. Int. J. Radiat. Oncol. Biol. Phys. 10, 509–514, 1984.

VII. Individual Facilities

33 Factors Considered in Developing the World's First Hospital-Based Proton Beam Facility

J. M. SLATER, J. O. ARCHAMBEAU, D. W. MILLER, and J. D. SLATER

Loma Linda University Medical Center, Loma Linda, CA, USA

Introduction

Proton beams provide superb control of dose distributions and the opportunity for increasing disease control while decreasing the incidence of normal tissue morbidity. A complete therapy facility, including three isocentric gantries, a horizontal beam line and an eye beam line, now exists at Loma Linda University Medical Center's (LLUMC) Proton Treatment Center. In addition, a research room with three additional beam lines is available, reserving the clinical facilities for their intended purpose. The developmental history of the facility has been presented elsewhere [1, 2]; this chapter attempts to highlight salient aspects of the developmental process and emphasize the important lessons learned, both of which may interest others contemplating development of similar facilities.

Historical Background at LLUMC

LLUMC's interest in proton beam radiation therapy began in the early 1970's with the desire to seek therapeutic dose distributions superior to those obtainable with photon, neutron and electron irradiation. Literature existed which suggested that heavy charged particles provided this potential [3]. In addition, clinical studies of proton and helium ion therapy had suggested the clinical value of particle therapy [4–6]. At that time, however, because patients' anatomy could not be imaged adequately and isodose distributions could not be superimposed precisely on anatomic images, the macrodosimetric advantages proffered by heavy charged particles could not be exploited comprehensively.

Improved imaging modalities began to become available after 1970. Ultrasound imaging appeared first; with its appearance, LLUMC investigators developed a system which used the digitized information as a basis for superimposing anatomic and dose-distribution data. When CT scans became available, the ultrasound-based treatment planning system was modified to employ CT digital information [7, 8].

As the 1970's progressed into the 1980's, computer-assisted therapy planning became more precise and widely used [9, 10]. Large-field proton and helium ion therapy developed at Harvard Cyclotron Laboratory (HCL) and Lawrence Berkeley Laboratory (LBL) [11, 12]. These advances were considered by investigators at LLUMC. By early 1984, based on the need to improve results obtainable with conventional radiation and the protons' potential to improve those results, a decision was made to develop a hospital-based, therapy-dedicated proton beam facility. In subsequent months, discussions were held among faculty, administrators and trustees of LLUMC and Loma Linda University (LLU) concerning the cost of constructing a facility, potential benefits, and future needs. In late 1984 the decision was made to proceed to the planning phase. Accordingly, LLUMC approached investigators at Argonne National Laboratory and other institutions, with inquiries about building such a facility; these inquiries led to plans to convene a meeting at Fermilab in January 1985. At that time, ideas were exchanged about accelerators,

facilities and clinical trials. This meeting was the nucleus of the Proton Therapy Co-operative Group (PTCOG), which formed less than a year later. PTCOG is an international, informal, unfinanced consulting and user group of engineers, physicists, biologists, and physicians, all sharing a common interest in proton radiotherapy.

PTCOG developed the design requirements for an accelerator, beam transport system and treatment room delivery system suitable for a hospital-based facility. By 1987, meeting these requirements seemed doable. LLU and LLUMC authorized a conceptual design study, which was completed by Fermilab and LLU/LLUMC staff in 1987. Subsequently LLUMC contracted with Fermilab for an engineering design of the accelerator and transport system; LLUMC, working with other laboratories and industry, developed the engineering design of the delivery system and facility.

Overall Design Considerations in Planning the Facility

From the outset, it was clear that the entire project: building, accelerator, delivery systems and patient care areas, needed to be designed as an integrated whole. A structure was required which would both house the treatment delivery systems and efficiently manage patient flow. Close collaboration between the architectural and equipment design teams was imperative, because the shielding concrete and steel walls could not be adjusted, being once in place, nor could there be any significant changes in equipment design to accommodate building errors. Accordingly, the various engineering design teams accomplished their tasks in a collegial manner; regular intercommunication among teams and team members was maintained. Eight teams were formed, each having tasks relevant to the overall engineering design; LLUMC, LLU, Fermilab and NBBJ, the architectural firm, provided staff for each team. Weekly meetings were supplemented by monthly meetings with hospital and university administrators, and periodic meetings were held with outside reviewers; these meetings helped to keep the teams communicating and aware of progress and problems. Timely development was emphasized; timing in planning, fabrication and installation was as important to the project's success as the successful operation of its component parts, because of the high monthly construction costs. Pre-building arrangements with the LLUMC purchasing department, suppliers, labor unions, and all primary and secondary contractors avoided costly delays and disputes and resulted in the ability to take early partial occupancy for installation of certain heavy subsystems.

The building was designed to treat patients safely and efficiently. It was also designed to: be erected within its budget; provide facilities for patient, practitioner and scientist, for education and research; and be modifiable, to accept new technology. Design requirements stemmed from clinical treatment, research and educational needs, plus marketing and financial projections. These resulted in a facility with five therapy beam lines in four rooms, as well as a separate research room containing three beam lines. Clinics, treatment rooms, patient preparation areas, waiting rooms, animal research facilities and offices were sited to promote optimal efficiency.

Accelerator and Beam Control Considerations

The heart of the LLUMC therapy system is the synchrotron. Fermilab and Department of Energy administrative and engineering staff played essential roles in transforming the accelerator from a laboratory instrument to a treatment tool. Traditional synchrotron performance and reliability had to be retained while reducing size. Commercial and industrial support facilitated the transfer and integrated the synchrotron with the beam transport and delivery systems.

Proton accelerators suitable for physics research usually are large and expensive to operate and maintain. A hospital-based proton accelerator must be compact, reliable, require little maintenance, and operate at low cost. The flux intensity must be sufficient to keep each patient's treatment time short. Beam energy must be rap-

idly variable to permit total flexibility in beam delivery. At LLUMC, these requirements suggested a synchrotron rather than a linear accelerator or cyclotron.

The LLUMC machine satisfies minimum space requirements. Its dipole magnets bend the protons in their correct orbit and provide horizontal and vertical focusing, thus conserving space by eliminating additional focusing quadrupole magnets. A compact radiofrequency quadrupole (RFQ) injector accelerates a low-energy (35 keV) proton beam to 2 MeV in a 1.6 meter distance, simultaneously focusing and accelerating the beam. The synchrotron provides a pulsed, 300-msec beam to the designated treatment room every 2.2 sec. In the ring, the protons gain energy with each turn until they reach a maximum energy of 70–250 MeV; at that point, the magnetic dipole field and RF frequency are held constant until the protons are extracted and transported to the treatment rooms. After extraction, the magnetic dipole fields return to injection level for the next batch of 2 MeV protons.

The beam is under computer control from its origin in the synchrotron until delivery to the patient, save for independent safety interlocks. All control processors are synchronized within microseconds by global timing signals propagated from one clock. The accelerator's control system can be divided conceptually into a low-level analogue RF system and a high-level digital system. The former, a closed-loop system, keeps the beam centered in the ring during the acceleration cycle. The latter controls beam energy and extraction, and directs the beam to delivery systems in the treatment and calibration rooms. The system contains multi-segmented, retractable ion chambers, placed along the beam line, to monitor beam centering and cross-sectional shape. Beam loss monitors within the beam transport area emit an audible alarm and stop the beam when an unsafe condition is detected.

Users configure the system by selecting a beam line, beam energy, and gantry angle; in doing so, they retrieve required magnet settings from the system database. The control system accepts beam parameters from several subsystems, such as treatment rooms, and responds to commands in real time. The lowest level of interface displays the settings and status of every device in the beam transport system and permits the user to reset or switch any device on or off, enabling engineers at remote locations to diagnose and repair problems. Every device has built-in self-test functions for early detection of malfunctions.

Treatment Planning and Delivery Considerations

Since a proton beam's main advantage derives from its ability to shape the dose distribution conform to the target, each patient's treatment plan must describe a set of optimum treatment portals and beam-modifying devices. These optima are achieved by studying three-dimensional computer simulations of patient treatment using different beam configurations and modifiers; the set of beams selected provides the best potential for tumor control with minimal damage to surrounding normal tissues. Three-dimensional planning requires a set of CT images to define the location and shape of target volumes and radiation-sensitive normal tissues, as well as a three-dimensional matrix of effective tissue densities for proton beam absorption. Other data, particularly magnetic resonance images, help determine the condition of normal structures and the extent of disease. Using this information, each treatment beam is designed to penetrate the body to a specified margin beyond the target volume or to irradiate a specified portion of a target volume. A tissue compensator and rotating range-modulator wheel are employed to shape the range distribution within each field.

Treatment planning is performed with three-dimensional planning software acquired from HCL [9, 10] and modified by LLU engineers. A dedicated CT scanner supplies the planning images. Shapes of treatment portal apertures and tissue compensators are generated by the planning system. Apertures are made from cerrobend alloy in Styrofoam molds made with a computer-controlled cutter. Tissue compensators are fabricated on a numerically controlled milling machine. The treatment planning system overlays isodose distributions on CT images and produces dose-

volume histograms in preparation for routine stereotactic fractionated treatments.

The LLUMC facility uses rotating gantries, which allow one to select beam entry angles without changing the patient's position. A cork-screw beam optics system, suggested by HCL investigators [13], minimizes the axial dimension of the rotating structure. Beam range is controlled by energy and range-shift selection. Lateral spreading of the beam is accomplished by dual scattering foils. A scanned beam system, to yield large conformal treatment fields with no scatterer range loss, is planned.

The beam delivery system monitors the dose delivered to the patient and terminates irradiation within approximately 2% of the desired dose. In addition to the primary dose-monitoring function, backup systems monitor dose delivered, the shape of the beam profile, and overall field uniformity. If any preset tolerance is exceeded during treatment, the control system terminates patient exposure.

The beam delivery system also protects the patient from human, hardware and software errors. A database contains the identification codes of modulator wheels, range-shifting blocks, tissue compensators and apertures for all treatment portals, for every patient. Bar codes attached to these devices must be scanned and must agree with the database before treatment can begin. Similarly, other patient setup parameters, including gantry angle and aperture position, must agree with database values. Measurements obtained from magnetic field probes located in the dipole bending magnets are compared with the database to assure that the correct beam energy is supplied. The control system monitors the location of all movable devices in the beam delivery system, checks for software and electronic error conditions, and monitors total treatment time. One independent dose monitor is set by the operator prior to each treatment.

Research Considerations

Proton beam therapy follows the continuum of improved dose delivery that has historically been observed from low-voltage radiation therapy through supervoltage equipment [14]. It can be used whenever conventional external beam radiation therapy is appropriate, either alone or in multimodality regimes. It was developed to exploit in the clinic the advantageous proton beam dose distribution and to improve the therapeutic ratio. Such exploitation requires clinical studies to document results. To develop optimal proton therapy techniques, multi-institutional cooperative studies are essential. Towards this end, the Proton Radiation Oncology Group (PROG) was organized by LLUMC, HCL and LBL. PROG currently conducts cooperative trials in CNS and in head and neck tumors. Initial treatment site studies, using conventional time-dose fractionation schedules, were primarily concerned with treatment of patients with chondrosarcomas and chordomas of the base of the skull and the cervical spine and showed improved control rates. A PROG multi-institutional study is thus underway, randomizing the dose for patients having those tumors and skull base and cervical spine meningiomas. Proton boost doses are also being used to treat paraspinal tumors, including chondrosarcomas and thoracic and abdominopelvic soft tissue sarcomas.

Protons are being used to decrease the dose to surrounding normal brain in children and adults. Studies are being conducted to evaluate potential neuroendocrine, ophthalmic and neuropsychiatric late effects.

Accelerated fractionation schedules are being studied in selected head and neck tumors, using photons and protons. Initially, a concomitant boost technique is being used to evaluate locally advanced tumors of the oropharynx and paranasal sinuses. These PROG multi-institutional phase I/II studies use significantly higher doses, delivered in a shorter period of time, than has been done with photons; proton boosts limit the extent of normal tissue treated.

Hypofractionated treatment plans are used to treat choroidal melanomas. Proton treatment in this anatomic site presently delivers doses in the range of 70 CGE (cobalt-gray equivalent) in five fractions over 7 or 8 days. The control rate has exceeded 95% [15]. A randomized PROG study is in progress, comparing 70 Gy in five fractions to 50 Gy in five fractions for selected patients to

determine whether the dose reduction reduces visual loss.

Proton radiosurgery is being performed in conjunction with the neurosurgery and neuroradiology departments at Stanford University Medical Center and LBL's Department of Life Sciences, to treat patients with arteriovenous malformations (AVMs). Compared to radiosurgery performed on a linear accelerator or gamma knife, charged particles can localize the dose while treating larger fields, without the need for overlapping isocenters or a large dose gradient in the target volume. Protons are being evaluated for large AVMs that have been unsuccessfully treated with other forms of radiosurgery. Other radiosurgical approaches are being evaluated, including proton beams for isolated brain metastases and to boost the dose for high-grade gliomas.

The potential of protons is being evaluated in other sites, including early-stage, non-small-cell, medically inoperable lung cancer, isolated paraaortic lymph nodes, and other pediatric tumors including retinoblastoma and selected rhabdomyosarcomas. Encouraging preliminary results from other proton institutions, wherein patients with isolated liver metastases and unresectable hepatocellular carcinomas have been treated, have led to the development of LLUMC protocols for these clinical entities.

The LLUMC research program also includes basic radiobiological and physics investigations aimed at identifying areas for clinical study, and exploring the micro- and macrodosimetric characteristics of proton beams for the purpose of employing the beam optimally. Recent studies on the LLU beam suggest that previously unrealized microdosimetric benefits may be possible [16].

Conclusion

The LLUMC experience evolved from pioneering work done at other institutions and broke new ground in: the development and use of a synchrotron designed specifically for a hospital; isocentric gantries to deliver the beam; patient immobilization systems for routine stereotactic therapy; and a computer-driven scheduling and charting system. Some aspects of the experience might be relevant to those contemplating future patient-dedicated facilities.

The LLUMC facility was conceived as a place where the capabilities of proton beams could be exploited optimally for patient treatment. The planning process was conducted with that objective in mind and conceptual designs were flexible, to encourage ideas that would meet the facility's fundamental goal. The three gantries reflect that flexibility. It was recognized that a gantry would contribute to precise delivery because multiple portals could be more easily achieved without moving the patient. A flexible design approach allowed for consideration of more than one gantry.

Along with underlying flexibility in the conceptual design stage, a team approach was essential. The role of LLUMC's consultants, particularly within PTCOG, was very important. They added experience and expertise, and provided a collegial atmosphere in which ideas could be discussed. The team concept was essential in the active development stage, as well. Once decisions were made concerning hardware, software and construction, the challenge became one of realizing the conceptual designs. Several teams were formed, each with responsibility for some aspect of the overall project, yet each charged also with keeping the larger goal in focus. Clear and constant communication among team members and among teams was maintained in order to maintain that focus; this "task force" approach was maintained throughout the development of the facility, and continues today.

Since optimal exploitation of protons for treatment was the underlying goal, a prime tenet of facility design was to optimize patient flow while conducting the basic and clinical research required to characterize protons' behavior in tissue and identify potential applications beyond those for which protons were already used. A separate research facility, with its own beams, grew from this intent. Research was regarded as essential, since proton beam therapy, while no longer in its infancy, could be said to be in its adolescence. It has the potential to be used for localized solid tumors in almost any anatomic site, but basic and clinical research are required to determine specific applications.

References

1 Slater, J.M., Miller, D.W., and Archambeau, J.O. Development of a hospital-based proton beam treatment center. Int. J. Radiat. Oncol. Biol. Phys. 14, 761–775, 1988.

2 Slater, J.M., Archambeau, J.O., Miller, D.W., Notarus, M., Preston, W., and Slater, J.D. The proton treatment center at Loma Linda University Medical Center: Rationale for and description of its development. Int. J. Radiat. Oncol. Biol. Phys. 22, 383–389, 1991.

3 Wilson, R.R. Radiological use of fast protons. Radiology 47, 487–491, 1946.

4 Kjellberg, R.N., Shintani, A., Frantz, A.G., and Kliman, B. Proton beam therapy in acromegaly. New Eng. J. Med. 309, 689–695, 1968.

5 Kliman, B., Kjellberg, R.N., Swisher, B., and Butler, W. Proton beam therapy of acromegaly: A 20-year experience. Prog. Endocr. Res. Ther. 1, 191–211, 1984.

6 Tobias, C.A., Roberts, J.E., Lawrence, J.H., Low-Beer, B.V.A., Anger, H.O., Born, J.L., McCombs, R., and Huggins, C. Irradiation hypophysectomy and related studies using 340 MeV protons and 190 MeV deuterons. Peaceful Uses of Atomic Energy 10, 95–96, 1956.

7 Slater, J.M., Neilsen, I.R., Chu, W.T., Carlsen, E.N., and Chrispens, J.E. Radiotherapy planning using ultrasound/sonic graph pen/computer system. Cancer 34, 96–99, 1974.

8 Neilsen, I.R., Slater, J.M., and Chu, W.T. An interactive system for radiation treatment planning utilizing computed tomography data as input to the planning process. Medinfo 80: Proc. Second World Conference on Medical Informatics. North-Holland, Amsterdam, 1980; p. 1072 (abstract).

9 Goitein, M. and Abrams, M. Multi-dimensional treatment planning: I. Delineation of anatomy. Int. J. Radiat. Oncol. Biol. Phys. 9, 777–787, 1983.

10 Goitein, M., Abrams, M., Rowell, D., Pollari, H., and Wiles, J. Multi-dimensional treatment planning: II. Beam's-eye view, back projection, and projection through CT scans. Int. J. Radiat. Oncol. Biol. Phys. 9, 789–797, 1983.

11 Suit, H.D., Goitein, M., Munzenrider, J.E., Verhey, L., Gragoudas, E., Koehler, A.M., Urano, M., Shipley, W.U., Linggood, R.M., Friedberg, C., and Wagner, M. Clinical experience with proton beam radiation therapy. J. Canad. Assoc. Radiol. 31, 35–39, 1980.

12 Saunders, W.M., Chen, G.T.Y., Austin-Seymour, M., Castro, J.R., Collier, M., Gauger, G., Gutin, P., Phillips, T.L., Pitluck, S., Walton, R.E., and Zink, S.R. Precision, high-dose radiotherapy: II. Helium ion treatment of tumors adjacent to critical central nervous system structures. Int. J. Radiat. Oncol. Biol. Phys. 11, 1339–1347, 1985.

13 Koehler, A.M. Preliminary design study for a corkscrew gantry. Proc. 5th PTCOG Meeting: International Workshop on Biomedical Accelerators. Lawrence Berkeley Laboratory, Dec 1–2, 1986, LBL-Report 22962, Lawrence Berkeley Laboratory, 1987, pp. 147–158.

14 Berry, R.J. Therapeutic uses of X-rays. Int. J. Radiat. Biol. 51, 873–895, 1987.

15 Gragoudas, E.S., Seddon, J.M., Egan, K., Munzenrider, J., Austin-Seymour, M., Goitein, M., Verhey, L., and Koehler, A. Long-term results of proton beam irradiated uveal melanomas. Ophthal. 94, 349–353, 1987.

16 Robertson, J.B., Glisson, W.C., Archambeau, J.O., Miller, D.W., Moyers, M.F., Siebers, J.F., Slater, J.M., and Dicello, J.F. The relative biological effectiveness of attenuated protons, in Biologic Effects and Physics of Solar and Galactic Cosmic Radiation, Part B. Swenberg, C.E., Hornack, G., and Stassinopoulos, E.G. (eds.) Plenum Press, New York, 1993, pp. 853–858.

34 HIMAC – A New Start for Heavy Ions

K. KAWACHI

National Institute of Radiological Sciences (NIRS), Chiba-shi, Japan

Introduction

The Heavy Ion Medical Accelerator in Chiba (HIMAC) was completed in 1993, and since June 1994 heavy ion therapy has made a new start at this facility after the close-down of the BEVALAC accelerator at the Lawrence Berkeley Laboratory (LBL) in Berkeley, California in 1992. The HIMAC is the first heavy ion accelerator in the world dedicated exclusively to medicine, and its design parameters are based on the radiation oncological requirements summarized in Table 1.

Based on results of radiological studies and clinical trials at the LBL, the ion species for the HIMAC were chosen in the atomic number range of 2 (helium) to 18 (argon). From clinical experience in conventional radiation therapy at the NIRS a maximum range of 30 cm in soft tissue appeared sufficient for any type of deep-seated tumor and a dose rate of 5 Gy/min should permit completion of typical treatment fractions within one minute. The maximum field size of the beam – 22 cm in diameter – was also selected based on clinical experience at the NIRS. The usage of both, vertical and horizontal beams is considered as another essential aspect of the facility which assures a highly controlled dose distribution with heavy ions.

Table 1. Medical requirements for HIMAC

Particle species	He to Ar
Penetrating range	30 cm in tissue
Dose rate	5 Gy/min
Max.field size	22 cm Ø
Beam direction	vertical & horizontal

The accelerator specifications are derived from the above mentioned radiation oncological requirements (see Tab. 2). The maximum accelerating energy was determined from the range-energy relationship for silicon which is one of the heaviest ions considered for treatment of deep-seated, radioresistant tumors. For ions lighter than silicon the chosen 800 MeV/u provide a considerable greater range in tissue than the required 30 cm. To satisfy this requirement, a synchrotron was chosen as main accelerator. The beam intensities for the various ion species to be extracted from the synchrotron ring were estimated from the expected dose rate. But since the pulse rate of most synchrotrons is of the order of one pulse per couple of seconds, it was necessary to design the time structure of the beam with a long flat-top intensity during the pulses in order to achieve precise dose control.

The most suitable accelerator complex for the HIMAC facility was determined by taking into account the most reliable accelerator technology existing in those days and not the least cost performance. The total layout of the HIMAC facility (Fig. 1) consists of two types of ion sources, an RFQ and an Alvarez linac, two synchrotron rings, high energy beam transport lines, and irradiation sites for treatment and experimental work.

Table 2. Accelerator specification

Ion species	He to Ar
Maximum energy	800 MeV/u (for $\varepsilon = 0.5$)
Minimum energy	100 MeV/u (for $\varepsilon = 0.5$)
Beam intensity	2.0×10^9 pps/ring (for C)
Duty factor	20 %/ring
Repetition rate	0.5 Hz/ring

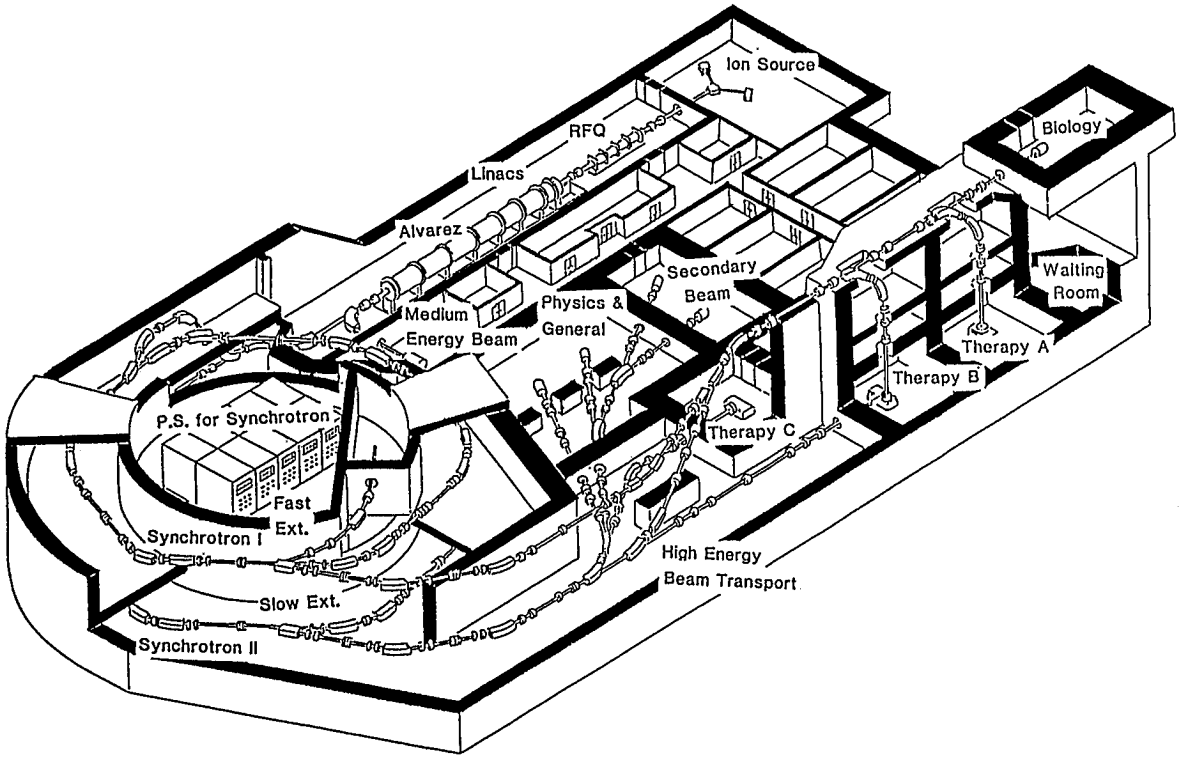

Fig. 1. A general view of the HIMAC facility

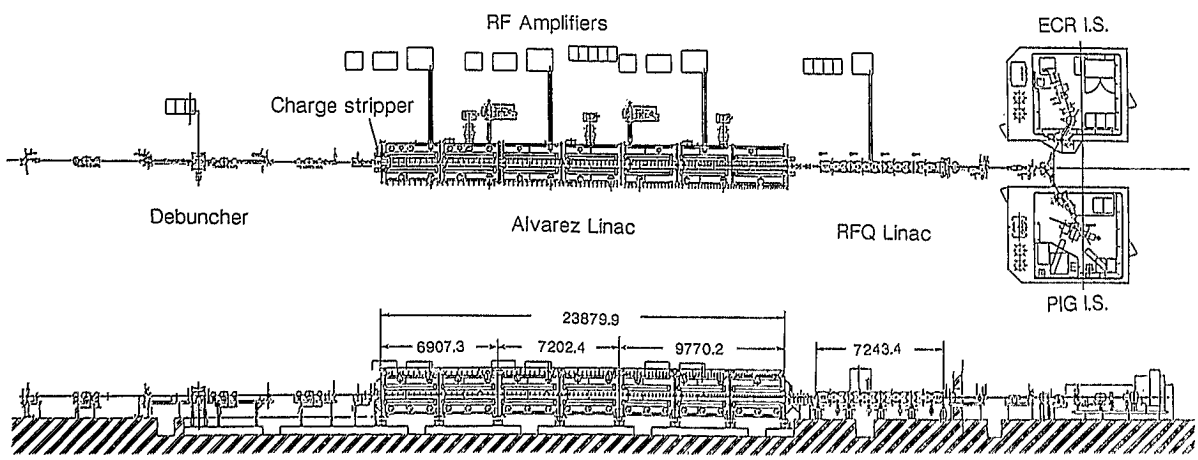

Fig. 2. Layout of the injector system

The Injector System

The injector system comprises two types of ion sources, an RFQ linac, and Alvarez linac and a debuncher cavity which is installed in a medium energy beam transport line (Fig. 2).

The two ion sources. which are a PIG (Penning ion gauge) ion source and an ECR (electron cyclotron resonance) ion source are both available in order to keep operation for the medical facility reliable and stable. Initially, the ECR source which is basically maintenance-free was proposed for heavier ions, such as neon, silicon or argon, whereas the PIG source was proposed for the lighter ions, including helium, carbon or neon. However, it has been found that both ion sources are able to produce enough intensity of all the ions, so that each ion source can serve as back-up for the other.

The extracted beam contains only ions (selected by an analyzing magnet) with a charge-to-mass ratio of 1/7 to 1/2. These ions are further accelerated at DC acceleration gaps and focused by solenoid and electrostatic quadrupole lenses.

Coming from the ion source, the heavy ions are injected with 8 keV/u into a pre-injector radio-frequency quadrupole (RFQ) (total length: 7.3 m, cavity diameter: 0.6 m). The output energy of the RFQ linac is 800 keV/u. Other parameters are summerized in Table 3.

The ions accelerated by the RFQ linac are fed into an Alvarez linac which is the most suitable injector system for the low duty-factor synchrotron. The Alvarez linac is separated into three cavities with a diameter of about 2.2 m and a total length of about 24 m. It has 106 drift tubes in the cavities: each tube is supported by horizontal and vertical stems, and equipped with a quadrupole magnet for beam focusing. Its operating frequency is 100 MHz, the same as that of the RFQ linac. Ions are accelerated to 6 MeV/u by the Alvarez linac and passed through a carbon foil to obtain fully-stripped ions of the accelerator. Fully stripped ions from the Alvarez linac can also be fed into a medium-energy beam irradiation room for low-energy heavy ion experiments. Table 4 lists the major parameters of the Alvarez linac.

Table 3. Summary of RFQ linac parameters

Input energy	8 keV/u
Output energy	800 keV/u
Charge-to-mass ratio	1/7–1/2
Operating frequency	100 MHz
Vane length	725 cm
Cavity diameter	58.8 cm
Maximum field	205 kV/cm
Peak RF power	260 kW (70 % Q)

Table 4. Summary of Alvarez linac parameters

Input energy	0.8 MeV/u
Output energy	6.0 MeV/u
Charge-to-mass ratio	1/7–1/2
Operating frequency	100 MHz
Structure	3 independent RF cavities
Focusing sequence	FODO
Cavity length	9.77/7.20/6.91 m
Cavity diameter	2.20/2.18/2.16 m
Number of drift tubes	56/28/22
Peak RF power	840/830/770 kW (75 % Q)

The Main Accelerator

The main accelerator comprises a pair of separated-function type synchrotron rings (Fig. 3). The two stacked rings consist of identical components and are separated by a shielding floor. The average diameter of the rings is about 41 m, and the circumference about 130 m. Both rings have identical lattice structure, a multi-turn injection channel and a slow extraction channel. In addition, the lower ring will have a second injection system for high energies and fast extracted ions, and the upper ring a fast extraction system. Both rings and the junction beam line have a flexible design to accommodate possible future extensions.

The injection energy into the synchrotron rings is 6 MeV/u. The output energy is continuously variable from 100 to 800 MeV/u for ions with a charge-to-mass ratio of 1/2 (cf. Tab. 5). The variable energy is a very important feature for patient treatment because it reduces the amount of low-LET secondary particles (produced by fragmentation) and will be able to provide the best dose distribution to a target using the most appropriate heavy ions. Both synchrotron rings operate with a

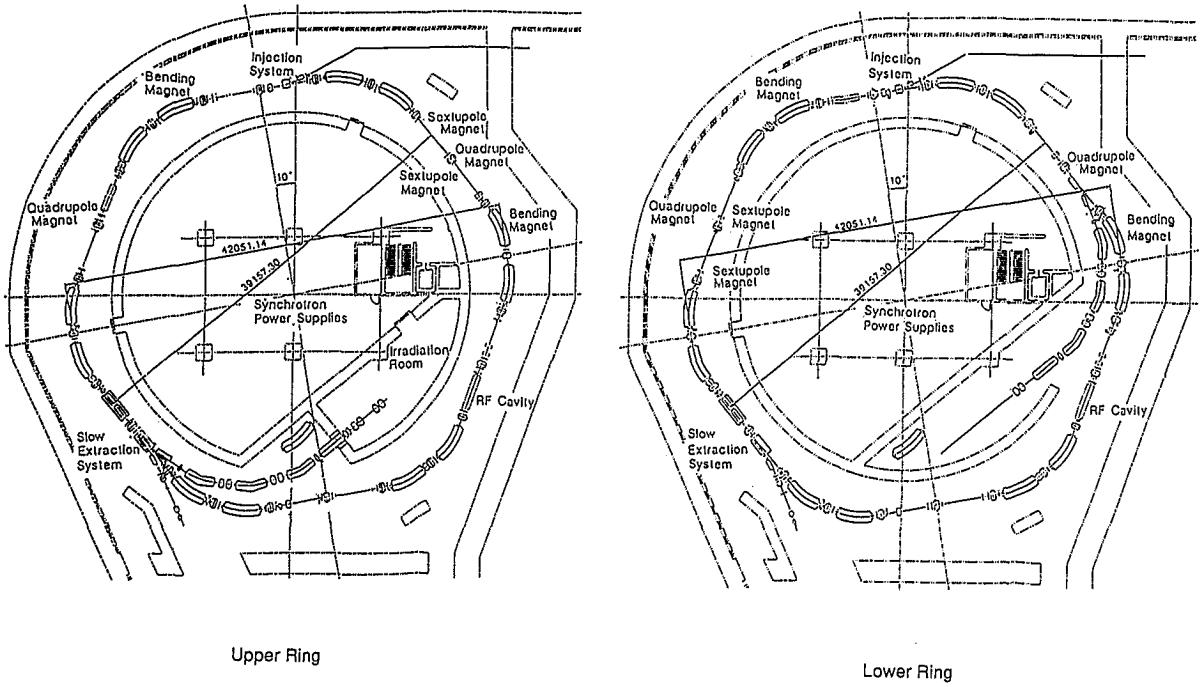

Fig. 3. A plan view of the synchrotron rings

repetition frequency of 0.3 to 1.5 Hz, but with a phase difference of one half period; this feature will greatly contribute to reducing the reactive power fluctuation.

Table 5. Summary of synchrotron parameters

Injection energy	6 MeV/u
Maximum energy	800 MeV/u (for q/A=1/2)
Lattice structure	FODO
Maximum rigidity	9.73 Tm
Periodicity	6
Cells per period	2
Circumference	129.6 m
Number of dipole magnets	12 (3.4 m each)
Dipole field (min/max)	0.11/1.5 T
Number of quadrupole magnets	24 (0.4 m each)
Quadrupole gradient (min/max)	0.4/7.4 T/m
Repetition rate	0.3–1.5 Hz
Revolution frequency	0.262–1.948 MHz
Rise/flat-top time	0.7/0.4 s (at 0.5 Hz, 600 MeV/u)

The High-Energy Beam Transport System

The accelerator system and all irradiation ports are connected by a high-energy beam transport system. Layouts of the high-energy beam transport lines are shown in Figure 4. Each beam extracted from the upper or lower ring will be dedicated to a vertical or horizontal beam line. The horizontal lines provide beams to two treatment rooms (B and C), to a physical or general irradiation area, and a secondary beam room; however, on special occasions, the main horizontal beam line can be joined to the vertical line. The vertical lines provide vertical beams to two treatment rooms (A and B) and horizontal beams to a biological irradiation area. The huge vertical beam lines represent one of the most desired radiation therapy features of the whole system.

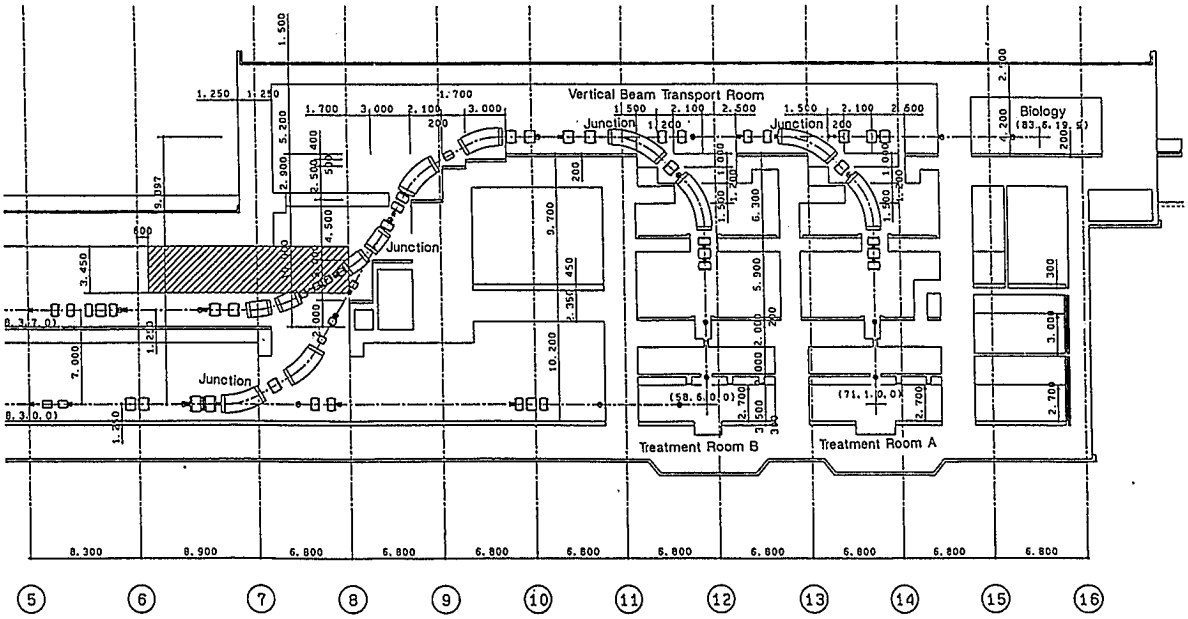

Fig. 4 a. A cross sectional view of the vertical beam lines

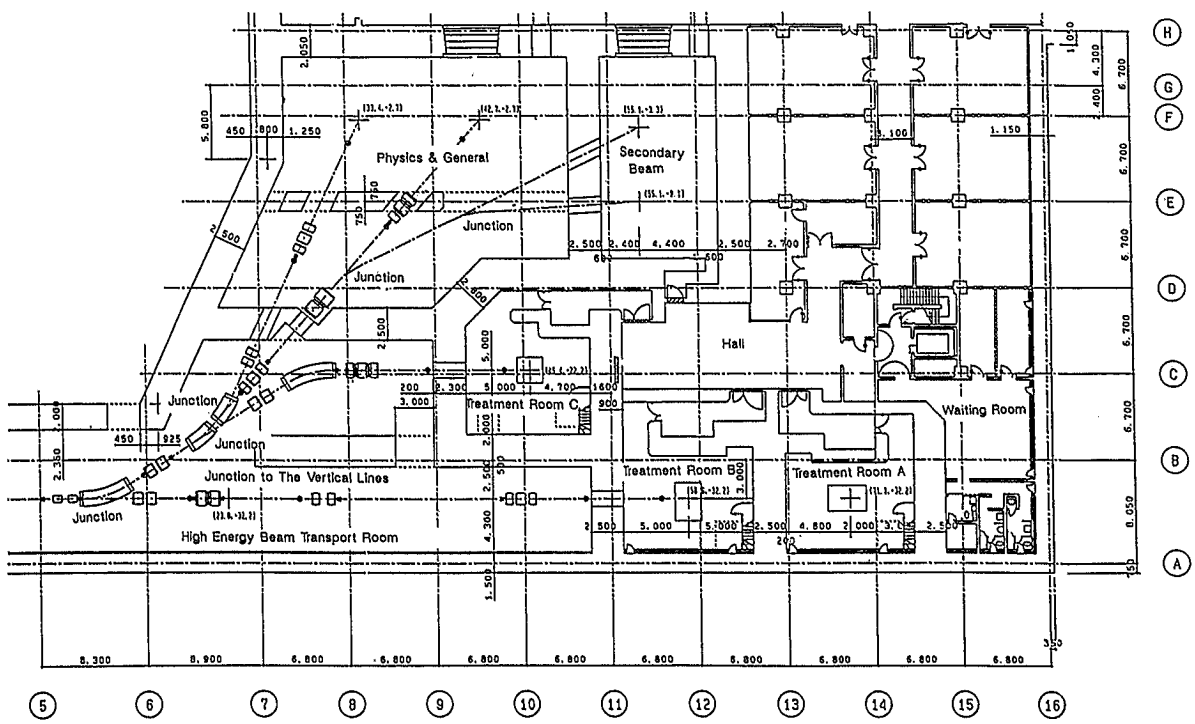

Fig. 4 b. Arrangement plan of the horizontal beam lines

The Beam Delivery System

Several devices including a pair of scanning magnets, a scatterer changer, a neutron shutter, a range shifter, a ridge filter, a block collimator, a multi-leaf collimator and several beam monitoring devices make up the beam delivery system. Figure 5 shows the typical beam line arrangement of treatment room B.

The scanning magnets and thin scatterers generate large uniform irradiation fields. The scanning magnets are orthogonal bending magnets which can support wobbler as well as raster or spot scanning, according to the use of suitable power supplies. In the beginning, our uniform fields will be generated by a combination of beam wobbling and scattering which is relatively fast, yields uniform fields and less nuclear fragments than scattering alone.

The electrical power supplies for the scanning magnets feed the sinusoidal current with a frequency of 62.8 Hz, which is selected to avoid nonuniformity due to pickup of noise synchronized with the line frequency. With the 90-degree phase difference between the two magnets, the wobbler magnets give rise to the circular rotation of the beam spot at the isocenter.

The ridge filter spreads out the narrow Bragg peak up to the size of the tumor. Individual filters can be selected from the ridge filter changer, a large circular rotational frame for up to seven different aluminum or copper filters.

The range shifter uses absorbers to fine-tune the ion range to conform with the depth of the tumor. They are nothing but energy degraders of different thicknesses. Nine lucite absorbers, 0.5 to 128 mm thick, are combined to the desired thickness by computer control.

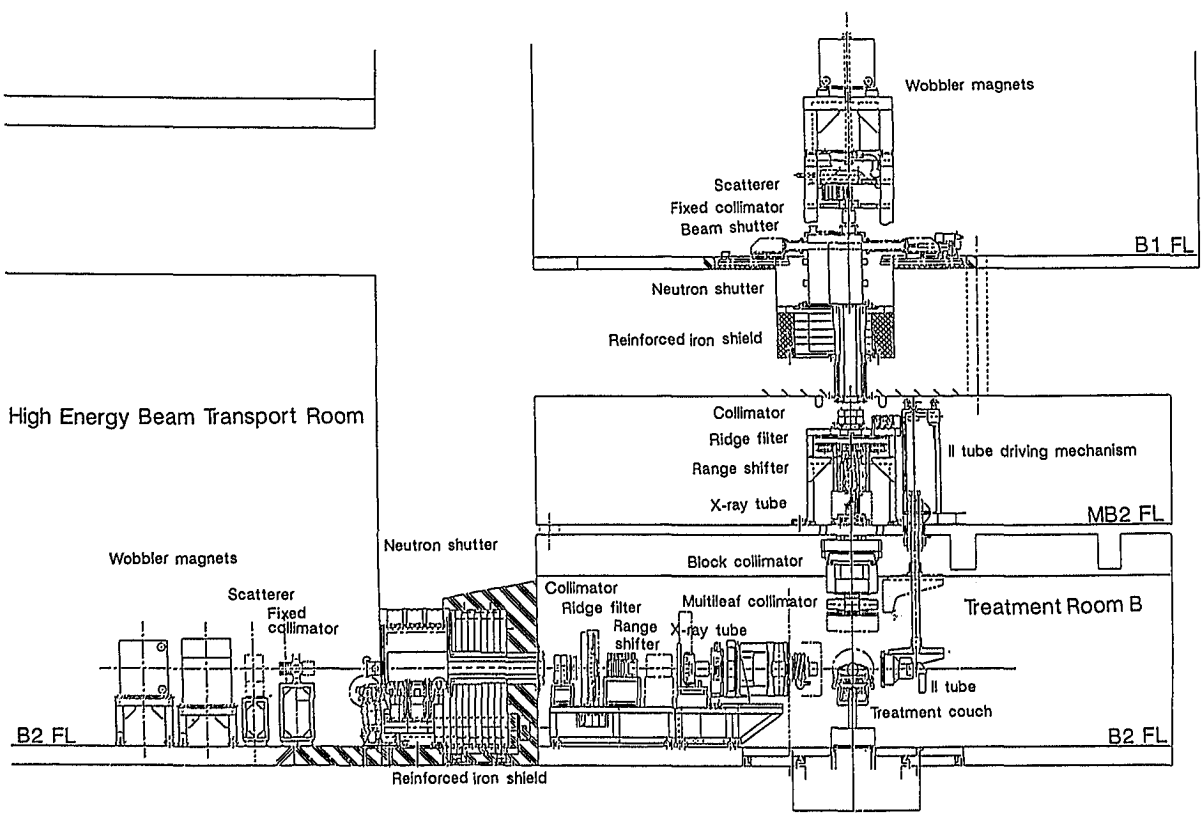

Fig. 5. Arrangement plan of the irradiation devices for treatment room B

The Al block collimator is composed of 4 slit-leaves (20 cm thick) which roughly cut off most of the irrelevant portion of the spread-out beam. It reduces the production of neutrons and induced activities as compared to the steel leaves of the multileaf collimator. The multileaf collimator is a field-shaping device which tailors the beam according to the perpendicular cross-section of the tumor. The maximum opening between two opposite leaves is 22 cm. Each leaf has a 16 cm stroke. The irradiation field size is 15×22 cm^2 at maximum. There are 23 leaves at each side of the aperture. The height of each leaf is 6.25 mm, the thickness along the beam direction 14 cm. The clearance between neighboring leaves is within 0.20 mm. Each leaf has two step stairs along the beam path to block the beam passing straight through the gap between neighboring leaves.

In order to measure and record the irradiation dose, the principal and substitutional ionization chambers are placed separately as dose monitors. The flatness monitor comprises 25 segmented sensitive parts in an ionization chamber. These are continuously monitored to keep the beam intensity distribution uniform in the irradiated area. All these devices are operated under computer control and the signals are monitored and displayed on a graphic panel on a pulse-to-pulse basis.

The Patient Positioning System

Patient positioning devices for accurate patient set-up have been installed in each treatment room. There are laser pointers, a light localizer, X-ray tubes, image intensifier tubes, a treatment couch, patient immobilization aids and an X-ray CT. The laser pointer is an indicator of the beam center for heavy ion treatment. The light localizer is the projector of the parallel light and placed into the beam line alternatively with the X-ray-tube. It is used to check the setting of the multileaf collimator by projecting the shape on the patient. X-ray tubes and image intensifier tubes are set perpendicularly to each other, one of them being the beam's eye view. They are used to verify the beam direction and the target volume position using certain reference numbers of anatomical landmarks. By comparing the positions of the landmarks on the X-ray image taken at the time of patient positioning on the couch and those on the reference image from the digitally reconstructed radiographs which were generated at the time of treatment planning the displacement of the patient's couch can be determined. The couch can automatically be adjusted by the patient positioning computer which is linked to the image verification device. The X-ray CT is used for a final verification of the density and the range of the ions in the patient body immediately before the treatment.

Future Developments at the HIMAC

The heavy ion research project does not only include clinical trials of heavy ion therapy, but focuses as well on basic research in medical physics, radiation biology, and radiation chemistry. Therefore, it is very important that the HIMAC facility is flexible enough to allow for different eventualities in future extensions.

One idea is to produce radioactive beams for treatment as well as diagnosis. They could be produced just before the junction of the horizontal and vertical beam lines. In this case, the junction line would be used for analyzing the section of secondary beams, and the selected radioactive beam could be used as vertical treatment beam. This feature seems very important for radiation therapy, since it permits precise verification of an irradiated volume with the treatment beam.

An effective and sophisticated parallel use of the two synchrotron rings requires some technological improvements which could provide the following:

- simultaneous irradiation with a horizontal and a vertical beam in treatment room B
- two beams used simultaneously in different treatment rooms or experimental irradiation areas
- joining the upper and the lower beam lines to reduce beam failure probability to some degree.

If the junction beam line between the two rings (a fast extracted beam from the upper ring injected into the lower one) is completed, the following feature could be expected:

- two-stage cascade acceleration for ions heavier than argon by adding a stripper foil to the extended junction beam line.

It might also be possible to use the lower ring as a storage ring for the upper synchrotron. This could be interesting for the following plans:

- to accumulate radioactive beams in the lower ring for treatment and verification with the same beam
- to treat patients for a very short time with a single shot of an accumulated stable heavy ion.

Sophisticated 3D-irradiation with the spot scanning method will also be pursued. It requests, however, a range shifter unit and upgraded power supplies for the scanning magnets. The procedure has been verified with proton beams from the NIRS medical cyclotron. Three-dimensional irradiation treatment does not only require a special beam delivery system, but also a very advanced 3D-treatment planning program which takes physical dose distribution and biological effects into account. Although the 3D- treatment planning program is under development, its final completion will take some time until the necessary experimental data have been compiled at the HIMAC.

Conclusions

The construction of the accelerator facilities and the HIMAC building started in 1988. The entire facility was completed in 1993 and in June of 1994 the first patient was treated. For the time being, HIMAC will be the only medically dedicated heavy ion accelerator in the world. NIRS is indebted to many colleagues from abroad who contributed important developments to the facility. HIMAC will continue to be open for domestic and international research collaborations, and appreciates joined clinical trials.

35

New Developments at PSI

H. BLATTMANN

Paul Scherrer Institute, Division of Radiation Medicine, Villigen, Switzerland

Introduction

Heavy charged particles have been recognized several decades ago to have favorable characteristics for radiation therapy [1, 2] and more than 15 000 patients have been treated in the meantime at various facilities with ions and pions. When the 590 MeV proton accelerator at Villigen was planned in the sixties, pions were regarded as probably the most promising particles for radiation therapy with a superior physical dose distribution and an increased biological effectiveness.

Already the first layout of the experimental hall of the PSI (then SIN) included a biomedical treatment site [3]. A vertical beam line was in operation only half a year after the first beam of 590 MeV had been extracted from the accelerator at the end of 1974. After a period of physical and biological measurements, it was realized that the dose rate was low and that it was unlikely to increase in a reasonable time. It was, therefore, decided to build a dedicated beam line of higher dose rate for medical applications. Dosimetric measurements, including determination of energy spectra of secondary particles, emitted after capture of negative pions in biologically relevant nuclei, and microdosimetric studies in the beam were continued. Radiobiological experiments, primarily on sensitive systems like eggs of Drosophila, Vicia faba bean roots, and mammalian cell cultures were performed.

In 1975, after a study of various options for a new medical beam line with increased dose rate, a solution was chosen which was based on the Stanford Medical Pion Generator (SMPG) [4], and was given the name Piotron [5]. The geometrical properties of this device, i.e., 60 beams in a vertical plane focused onto the axis of the Piotron, and the fact that the 60 superconducting coils were connected in series, resulting in an equal range for each beam, limited the choice of treatment techniques to dynamic scanning of the target volume by ring or spot scan.

Experience from the Pion Project

In the pion project of PSI, a spot scanning technique was developed, and the first patients were treated in early 1981. The dose rate achievable in the Piotron was approx. 0.2 Gy/l/min, if all 60 beams were used. With this application technique it was not only possible to get a homogeneous physical dose distribution throughout the target volume, but also a fairly homogeneous biologically effective dose. RBE corrections were considered to be unnecessary for 60 beam irradiations.

Treatment planning was based on CT scans taken in steps of 5 to 10 mm accross the entire target volume [6]. To guarantee the same geometry for treatment planning and irradiation, the patient was scanned in the same couch as was used for treatment. In each of the CT-slices the contour of the target volume was entered. The desired dose distribution consisted then of a homogeneous dose inside this target volume and a rapid fall-off outside. The dose distribution was optimized using a χ^2-algorithm. The individual treatment plans were verified by dose measurements in selected points of phantoms. In addition, whenever possible, in-vivo dosimeters were

placed in the target volume during treatment. Biological experiments performed in different geometries [7], intercomparisons with other centers [8], and clinical experience were used to decide on the treatment dose.

Pions were expected to yield substantially better results than photons due to their radiobiological advantages, especially for tumors with fractions of anoxic cells. The fractionation scheme selected had to be close to a known fractionation scheme for conventional photon radiation with a low number of fractions for logistics reasons. 20 fractions in 5 weeks were compared with results from the Manchester technique using 20 fractions in 4 weeks. In a dose escalation program the optimal total dose was determined as 33 Gy, which was used for most treatments throughout the entire program [9, 10]. As many of the initial patients had bladder tumors, it was possible to verify the dose in the target volume with in vivo dosimetry, an important aspect for a new technique with individually shaped target volumes.

The treatment with pions was assumed to protect normal tissues adjacent to the target volume better than conventional radiation, due to the favorable physical dose distribution and a drop in biological efficiency outside the high dose volume. With increasing experience it became obvious, that the radiation quality to the normal tissue inside and to some extent outside the target volume was the same as for the tumor cells.

In contrast to TRIUMF, PSI never intended to perform any randomized trials in the pion project. They seemed out of scope because of the limited number of treatments feasible at our physics facility, not attached to a large hospital.

As treatments at a research institute are substantially more expensive than conventional radiotherapy, it was the aim to treat primarily indications which could not be treated satisfactorily with conventional means. Very encouraging results were found especially for large, mostly irregularly shaped tumors, which could not be treated with curative doses of other radiations. For specific groups, e.g., large retroperitoneal soft tissue and bone sarcoma, conformation radiotherapy with pions could be regarded as the treatment of choice [9]. Even though these rare indications would not justify a clinical pion therapy facility, the necessary effort was in good relation to the result. It is yet not possible to decide conclusively if the results are a consequence of the increased RBE of pions, the dose conformation treatment, or a combination of both. For soft tissue sarcoma, a comparison with results from the literature suggests a combined effect. While a conversion factor of two from a 20-fraction pion treatment to a 35-fraction photon treatment could explain normal tissue reaction as well as tumor reaction for many of the treated tumors, the converted dose of 66 Gy for large sarcomas of two liter volume was still far below the 80 Gy, needed in photon therapy [11].

An important experience gained in the pion therapy project was to recognize the significance of conformation treatment which permitted higher doses in the target volume and the flexibility to distribute the dose outside the target volume according to the different sensitivities of the adjacent normal structures. The spherical spot in the Piotron, with its moderate fall-off, made it, however, often impossible to yield enough sparing of a specific neighbouring tissue.

Treatment of Ocular Melanoma with 72 MeV Protons

In parallel to the pion project, a proton therapy project for ocular melanoma was established in 1984. It has since been running successfully [12]. The injector cyclotron of PSI is particularly well suited for this therapy as the range of the protons (3 cm) is sufficient and the distal fall-off excellent. Proton therapy of ocular melanoma is an exceptionally favorable situation for proton radiotherapy as the target volume is small and well delineated, close to the surface and generally inoperable. Close to the target volume, there are critical structures which can be spared best with protons. The small target volume can be treated in a few fractions to a tumoricidal dose, resulting in a local control of the order of 95% or more without jeopardizing normal tissue tolerance. The short overall treatment time of only one week makes it easy for a research facility to accomo-

date regular treatment periods into the schedule of a multiuser accelerator, and it is also of advantage for the patients, who often come from far.

With only one week beam time per month, approximately two hundred patients per year are treated in the OPTIS program at PSI; so far, more than 1600 patients from many different countries in Europe have been treated. Due to the low frequency of ocular melanoma, a dedicated accelerator in a hospital could economically only be justified if other indications would be treated. The research activities of the OPTIS group focus, therefore, on evaluating new indications for this irradiation technique. In addition to the treatment of ocular melanoma, the beam line also serves for detector tests for the high-energy proton therapy project, and since 1993 it has also been used for radiotherapy of selected tumors in a veterinary radiooncology program (cf. Chapter 10).

High-Energy Proton Therapy Project

As a result of the experience with pion therapy and proton therapy of ocular melanoma, a proton therapy delivery system was planned to provide the same flexibility concerning dose application as modern clinical installations.

The application technique developed at the PSI is based on a discrete pencil beam scanning on three orthogonal axes [13–15]. The first and fastest movement is performed by magnetic scanning with a sweeper magnet, the second movement is done by a mechanical range shifter in steps of 5 mm in tissue and the slowest movement translates the patient in the direction perpendicular to the protons' path. Each of the approx. 10 000 spots per liter is deposited statically in an average time of 12 msec to a precision of one percent (Fig. 1). The dose fall-off for a single port, laterally and distally is of the order of 10 mm (90–10 %).

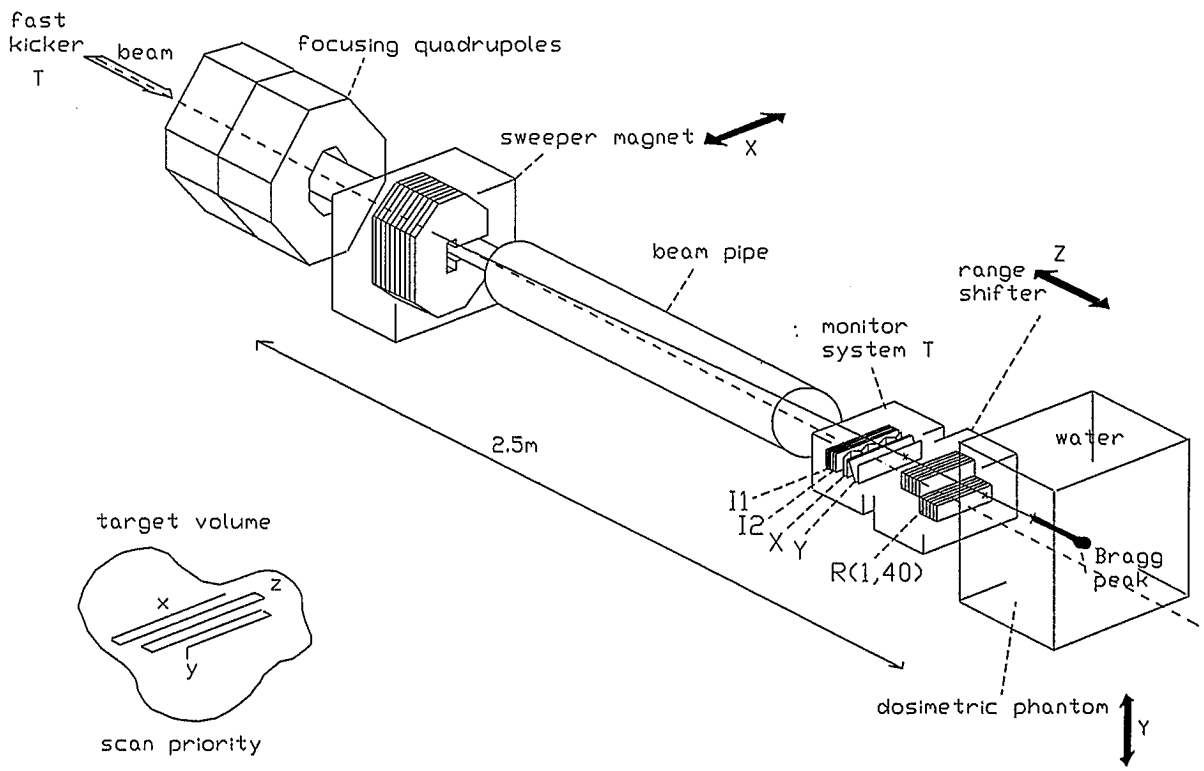

Fig. 1. Principle of the discrete voxel scanning for protons at PSI. Description in the text

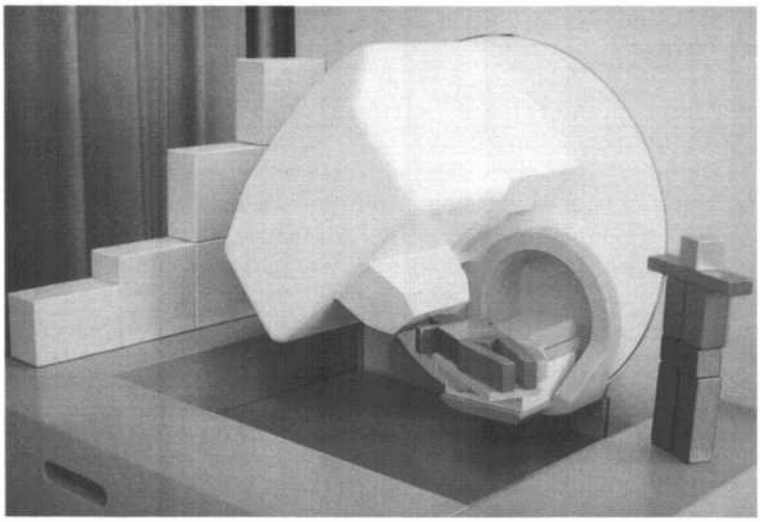

Fig. 2. View of the gantry (wooden model)

A customized treatment planning program has been developed for the special characteristics of the scanning technique. The first version of this program is running and has been tested on geometrical target volumes in the beam period 1992 [16]. The dose is optimized by computer control; in a water phantom, a homogeneity of close to 1% in the target volume has been achieved.

The monitoring and dosimetry system, too, had to be adapted to the scanning application technique with a fast response time to control each spot to the design goal of 1% homogeneity. For absolute dosimetry, a Faraday cup and a water calorimeter will be used in parallel to calibrated ionization chambers.

An isocentric gantry with a diameter of only 4 m has been installed and has undergone testing with beam since spring 1994. The gantry is equally versatile in selecting treatment ports as a modern clinical linear accelerator.

Isocentric Beam Delivery for Deep-Seated Tumors

The target volume conform treatment technique tested in the horizontal beam line can now be performed on an isocentric gantry (Fig. 2). In general, multiport irradiations will be performed. In the present version of the treatment planning software each port is optimized individually. The treatment time per port will not be longer than for conventional linac therapy.

The design and realization of the gantry was a challenging project, well suited for a medical physics group at a research institute. The problems had to be solved in close contact to medical application not generally possible in an industrial environment. PSI with its expertise in physics, engineering, radiobiology and radiooncology, and with a proton beam of the appropriate energy has been a very valuable frame for such an endeavor.

The small size of the gantry is a result of the limited space available for the project in the experimental hall. But the solution found, may be particularly well suited for hospitals, where space is often very limited, too. Apart from the 590 MeV accelerator, the facility can be considered a prototype for a hospital-based installation. Experience can be gained using the novel application technique, treatment planning, but also the patient preparation technique, which is optimized for an efficient use of the limited beam time. We expect to prove that voxel scanning is a very efficient technique for conformation therapy in terms of staff requirements and material costs. Individual collimators and compensators, necessary for irradiation with scattered proton beams, are needed only in special cases. Treatment by several ports per patient can be done without

time-consuming realignments, which would be necessary for photon treatment or for scattered proton beam treatment with beam modification hardware.

Special requirements arise from the high demands on a precision treatment with a dynamic application technique. Patient or organ movement have been identified to be of special relevance in the treatment with the voxel scanning technique [17]. Fixation techniques and position verification systems are, therefore, evaluated and under development especially for deep-seated tumors in the abdomen. One of the techniques is proton radiography. It can serve as means to check energy loss calculations in the treatment planning program as well as position verification method under treatment conditions (cf. Chapter 31). As it needs a higher proton energy than the therapeutic beam to traverse the patient completely, it is of interest to investigate if this tool would be worthwhile in a clinical facility and justify higher costs for the accelerator.

Even though it is usually not the primary goal of a medical program at a research facility to accumulate large patient numbers, it is possible to determine the effort per patient and extrapolate it to a clinical environment.

The radiotherapy project at PSI is only marginally hampered by the fact that the irradiations are performed at a physics institute with only limited medical infrastructure. The anticipated indications can, in general, be performed on an outpatient basis. A regional hospital is available for those needing hospitalization.

Status of the Experimental Radiotherapy Program

Beam optics measurements of the gantry beam line and measurements in a water phantom have been performed to check the beam characteristics and provide input for the treatment planning program. Measurements in phantoms with density inhomogeneities will follow for single beams and entire treatment plans.

As part of an extended experimental program on the treatment of spontaneous tumors in dogs, a first animal was treated in fall 1994 (Fig. 3) to study the entire chain of individual steps from diagnostics with individual moulage and computer tomography to treatment planning, dose verification, fractionated treatment, and follow-up. A relatively simple geometry was selected.

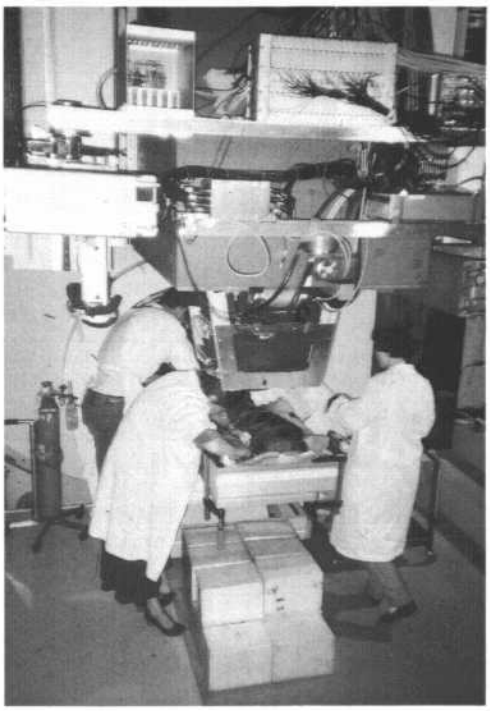

Fig. 3. Treatment of the first dog patient on the gantry. The beam is coming from above, visible is the 90° bending magnet and the nozzle. The anaesthetized dog is positioned in the mould, TLDs and ionization chambers are mounted to check the skin dose

In a ten-fraction treatment an infiltrative lipoma of approx. one liter in the hind leg of a dog of 33 kg was treated with a dose of 36 CGE (Cobalt-Gray equivalent), assuming a RBE of 1.1 for protons. Even though the target volume was almost the entire leg, the target dose was defined three-dimensionally on a series of CT slices to spare a small amount of skin cranially. One single port with a vertical beam was used. The dose distribution calculated for this treatment was verified by measurements with ionization chambers in a solid plexiglass block and by exposing X-ray films at various depths in a plexiglass stack perpendicular to the incoming protons. For each fraction, verification films were taken proximally and distally to the leg.

The main goal of this first treatment was to verify that nothing unexpected happened – neither in terms of early reactions nor in late reactions – before a larger number of animals will be treated starting early 1995.

Protons are considered a low-LET (linear energy transfer) radiation with a similar RBE (relative biological effectiveness) as photons used in conventional radiotherapy (cf. Chapter 3). For the dynamic application technique developed at PSI, some uncertainty arises from the high dose rate (10^4 Gy/min) in the pencil beam. Although it is not expected that this yields RBE values significantly different from proton therapy experience at other centers, biological experiments are planned by the Institute for Medical Radiobiology of the University of Zurich. Mammalian cells will be exposed to various doses under typical radiotherapy conditions. These experiments will be supplemented by fractionated whole-body irradiation of mice for the intestinal crypt cell assay. Both types of experiments can be considered biological dosimetry.

The Clinical Program

The aim of the clinical program is to find indications for which the dose distribution of proton conformation therapy is significantly better than for any other treatment modality. The basis of comparison might be elaborate photon therapy techniques with multiport, irregularly shaped fields with or without boost treatment, photon conformation therapy with multileaf collimators, or external beam therapy combined with brachytherapy.

Intercomparisons of treatment plans for proton and photon radiotherapy have been started already, using the Voxel Plan treatment planning software from the German Cancer Research Center (DKFZ), Heidelberg [18]. Preference will be given to cases where the difference in dose distribution seems large enough to expect improved therapy results with a moderate number of patients treated.

It is generally agreed upon that proton beams, due to their excellent distal dose fall-off, are of special value when a radiation-sensitive normal structure is located directly adjacent to the target volume. This is of special importance, if, e.g., a port has to be chosen, which points directly towards the normal structure.

Another goal of the clinical program is to find indications which are significantly better treated with conformation proton therapy than with scattered proton beam therapy using fixed range modulation.

Large, deep-seated, irregularly shaped target volumes have high priority for three-dimensional scanning, as for this category the impact of dose shaping is most pronounced with a substantially lower integral dose than conformation photon therapy can yield. For small volumes, even if the shape is irregular, the advantage might be limited as only modest amounts of normal tissues would be included in the high-dose volume. Large numbers of patients would be needed to document the modest improvement expected in this case.

Special attention has also to be paid to the frequency of the indications selected, as one of the goals is to demonstrate that the small gantry and the dynamic beam application are interesting solutions for routine use in a hospital with a wide spectrum of indications, and that the technique serves a real need in radiation therapy. Finally, it is our attempt to prove that the technique is feasible, practical and can be performed with a modest effort in manpower per patient.

The clinical program is being designed by a "Proton Therapy Users Group", formed several years ago. Most of the radiooncology departments of Switzerland are collaborating in this group [19]. They will provide the patient base for the project and decide on the protocols for the treatment of the various indications.

Proton Radiosurgery

PSI plans to set up a beam line for cross-fire irradiations of small volumes for functional surgery in a similar way as was done in Uppsala in the late 50's.

Radiosurgery is performed in single fractions (cf. Chapter 16). This is one reason, why the program is ideally suited for external users, e.g., neurosurgical groups. It is also expected that the

program opens new areas of research to the PET program at PSI, specializing in brain research.

The 590 MeV protons of the ring cyclotron of PSI are perfectly appropriate for cross-firing technique [20]. In the area of the former pion therapy project a beam of up to 20 μA is available, suitable for functional radiosurgery in the brain. By degrading or scattering, the intensity would be reduced to the desired dose rate. A horizontal, collimated beam would be available using a stereotactic frame and a precise chair with five degrees of freedom. Beam diameters of approx. 1 to 20 mm would be feasible. The dedicated beam line for proton radiosurgery would be an ideal supplement for the proton gantry. The time-consuming positioning for the radiosurgery sessions would also occur in a separate area, increasing the efficiency and availability of the gantry beam line.

Conclusion

A radiotherapy project at a research accelerator facility is strongly influenced by the operation conditions of the accelerator, and the competition with other user groups for beam time or specific beam requirements. Unstable beam is frequently the result of tuning for higher beam currents. Limited availability of the beam is often the consequence of shut-down periods, scheduled to improve the performance of the accelerator for the basic research users. Compromises made in the design of beam lines, may lead, for example, to reduced flexibility in selection of treatment angles. But only if the same flexibility as for modern hospital equipment is available, the test conditions for a new radiation source are really sound.

Tighter dose distributions feasible with proton conformation therapy will in many cases enable higher doses per fraction reducing the overall time of the treatment and hence the costs. The favorable dose distributions should yield better clinical results and hence justify higher facility costs.

Conformation therapy by voxel scanning is characterized by minimal individual patient hardware, which saves time and costs. This is of special relevance for future routine operation in a hospital environment. The design of a very compact gantry may be particularly well suited for hospital facilities.

A medical project at a research facility should concentrate on developing new techniques rather than accumulating large numbers of patients. Randomized trials which often require hundreds of patients for each treatment arm – especially if only modest changes in cure rates are expected – are, therefore, generally out of scope [21]. Instead, the focus should be on demonstrating the potential of proton therapy for indications which cannot be treated satisfactorily by existing radiation types. Treatments which promise improvements and for which it would be unethical to perform a randomized trial would be ideal candidates.

Establishing the proton therapy sites at PSI has been an interdisciplinary task involving not only many different groups inside the institute but also many links to other University institutes as the Institute for Biomedical Techniques at the ETH and University of Zurich, the Institute of Medical Radiobiology, and the Veterinary School of the University of Zurich. Many contributions from University groups from Switzerland and other countries are appreciated.

References

1 Fowler, P.H. and Perkins, D.H. The possibility of therapeutic applications of beams of negative pi-mesons. Nature 189, 524–528, 1961.
2 Wilson, R.R. Radiological use of fast protons. Radiology 47, 487–491, 1946.
3 Horst, W. and Conrad, B. Radiotherapie des Krebses mit negativen Pi-Mesonen. Fortschritte auf dem Gebiete der Röntgenstrahlen 105, 299–321, 1966.
4 Boyd, D., Schwettman, H.A., and Simpson, J. A large acceptance pion channel for cancer therapy. Nucl. Instr. Meth. 11, 315–331, 1973.
5 Von Essen, C.F., Blattmann, H., Crawford, J.F., Fessenden, P., Pedroni, E., Perret, C., Salzmann, M., and Walder, E. The Piotron: Initial performance, preparation and experience with pion therapy. Int. J. Radiat. Oncol. Biol. Phys. 8, 1499–1509, 1982.
6 Pedroni, E., Blattmann, H., Salzmann, M., Walder, E., Crawford, J.F., Dietlicher, R., Cordt, I., Schäppi, K., von Essen, C.F., and Perret, C. Treatment planning and dosimetry for the pi-meson therapy facility at SIN, in Proc. Int. Conf. on the Application of Physics to Medicine and Biology. Alberi, G, Bajzer, Z., and Baxa, P. (eds.), World Scientific, Singapore, 1983, pp. 1–25.

7 Jüling-Pohlit, L., Blattmann, H., Pedroni, E., and Pohlit, W. The RBE of negative pions in the treatment of tumors with different volumes. Strahlenther. Onkol. 169, 394–404, 1993.
8 Raju, M.R. Heavy Particle Radiotherapy, Academic Press, New York, 1980.
9 Greiner, R.H., Blattmann, H.J., Thum, P., Coray, A., Crawford, J.F., Kann, R.H., Munkel, G., Pedroni, E., von Essen, C.F., and Zimmermann, A. Dynamic pion irradiation of unresectable soft tissue sarcomas. Int. J. Radiat. Oncol. Biol. Phys. 17, 1077–1083, 1989.
10 Greiner, R., Blattmann, H., Thum, P., Bösiger, P., Coray, A., Kann, R., Lahtinen, T., Reinhardt, H., von Essen, C.F., and Zimmermann, A. Anaplastic astrocytoma and glioblastoma: Pion irradiation with the dynamic conformation technique at the Swiss Institute for Nuclear Research (SIN). Radiother. Oncol. 17, 37–46, 1990.
11 Perez, C.A. and Brady, L.W., Overview, in Principles and Practice of Radiation Oncology, 2nd Ed., Perez, C.A. and Brady, L.W. (eds.) 1992, pp.1–63.
12 Egger, E., Zografos, L., Perret, C., and Gailloud, C. Proton beam irradiation of choroidal melanomas at PSI: Technique and results, in Medical Radiology – Diagnostic Imaging and Radiation Oncology, Radiotherapy of Intraocular and Orbital Tumors, Alberti, W. E. and Sagerman, R. H. (eds.) Springer Verlag, 1993, 57–72.
13 Blattmann, H., Coray, A., Pedroni, E., and Greiner, R. Spot scanning for 250 MeV protons. Strahlenther. Onkol. 166, 45–48, 1990.
14 Blattmann, H. Beam delivery systems for charged particles. Radiat. Envir. Biophys. 31, 219–231, 1992.
15 Pedroni, E., Bacher, R., Blattmann, H., Böhringer, T., Coray, A., Lomax, A., Lin, S., Munkel, G., Scheib, S., Schneider, U., and Tourovsky, A. The 200 MeV Proton therapy project at PSI: Conceptual design and practical realization. Subm. to Med. Phys. 22, 37–53, 1995.
16 Scheib, S. and Pedroni, E. Dose calculation and optimization for 3D conformal voxel scanning. Radiat. Envir. Biophys. 31, 251–256, 1992.
17 Phillips, M.H., Pedroni, E., Blattmann, H., Böhringer, T., Coray, A., and Scheib, S. Effects of respiratory motion on dose uniformity with a charged particle scanning method. Phys. Med. Biol. 37, 223–234, 1992.
18 Schlegel, W., Pastyr, O., Bortfeld, T., Becker, G., Schad, L., Gademann, G., and Lorenz, W.J. Computer systems and mechanical tools for stereotactically guided conformation therapy with linear accelerators. Int. J. Radiat. Oncol. Biol. Phys. 24, 781–787, 1992.
19 Greiner, R., Blattmann, H., Häfliger, J.-M., Lütolf, U.M., and Mirimanoff, R.O. Strahlentherapie mit hochenergetischen Protonen. Schweiz. Krebsbulletin 9, 8–11, 1989.
20 Larsson, B., Leksell, L., and Rexed, B. The use of high energy protons for cerebral surgery in man. Acta Chir. Scand. 125, 1–7, 1963.
21 Bentzen, S.M. Radiobiological considerations in the design of clinical trials. Radiother. Oncol. 32, 1–11, 1994.

36 Heavy Ion Therapy at GSI

G. KRAFT

Gesellschaft für Schwerionenforschung (GSI), Darmstadt, and University of Kassel, Kassel, Germany

Introduction

Plans to include heavy ion therapy to the scientific program of GSI date back to the first proposal for a heavy ion synchrotron (Schwer-Ionen-Synchrotron, SIS) submitted to the German Ministry of Research and Technology in July 1979 [1]. In this paper the two main advantages of heavy charged particles were emphasized: their superior depth-dose distribution and the high biological efficiency at the end of the particle range. At the second GSI Workshop on Heavy Charged Particles in Biology and Medicine 1981, a group formed to promote the idea of heavy ion radiotherapy. It consisted mostly of German physicians from Heidelberg, Hamburg, Gießen and Frankfurt, but with connections to LBL Berkeley, USA, the Radiotherapy Department of the Catholic University of Louvain-la-Neuve, Belgium and the SIN (now PSI), Villigen, Switzerland. In 1981, the original SIS-proposal was upgraded to 10 GeV/u mainly for physical reasons. However, it failed and the medical meetings were discontinued after a change in the GSI directorship. A new SIS-proposal was submitted in March 1984, comprising a storage ring that allowed many novel experiments in atomic and nuclear physics [2]. It was accepted mainly because of the new physical concept, but the final layout of the facility included an experimental area for biophysical experiments, as well.

In 1989, during the constuction period of the SIS, a proposal for the medical use of the heavy ion beams was jointly prepared by the Heidelberg Radiological Clinic, the German Cancer Research Center (DKFZ) and GSI. But at that time the German govern ment preferred a European solution and did not fund the proposal. With support from the EULIMA project, preparatory work was started. But it was not sufficient to build a therapy unit.

The first radiobiology experiments with relativistic heavy ions were performed in 1991 mostly in time-sharing mode with other physics experiments. The "peaceful coexistence" of physics and radiobiology experiments promoted the idea – after another change in the GSI directorship – to use the ion beams of SIS not only for pretherapeutic work, but to install a unit for Heavy Ion Therapy at GSI (HITAG) for the treatment of 70 to 100 patients per year. This new proposal, jointly prepared with the University Clinic and the German Cancer Research Center, both at Heidelberg, was submitted to the German Ministry of Research and Technology in May 1993 [3]. It stressed the new techniques for tumor conform treatment which the GSI had developed in the meantime, and the new insights into radiobiology which the biophysics experiments at SIS and other accelerators had prompted.
The experience of LBL with heavy ions has indicated superior treatment results for certain tumors as compared to conventional therapy, but a comparable outcome to proton therapy as performed at Harvard, for example [4]. As protons are assumed not to have an elevated biological effictiveness in contrast to the heavier ions, identical clinical results at Berkeley and Harvard would suggest that the potential of heavy ions cannot be exploited clinically in an adequate way.

One reason for this result could be that LBL's irradiation technique permitted an essential part of the high-LET dose to be spread outside the

tumor volume limiting the tolerance level, another that the high-LET component of the heavier particles observed in vitro has been overestimated. Therefore, in the HITAG project most effort has been put on developing a strictly tumor conform dose delivery system and an advanced understanding of the radiobiological effects that are relevant for the increased biological efficiency of the particles.

In the following sections the novel approach to tumor conform treatment using intensity-controlled raster scanning, its limitations and consequences for the treatment planning and the safety system are given. In addition, requirements concerning the physical and biological characterization of the particle beams are summarized. Finally, a technical description of the layout and the future perspective of the heavy ion therapy at GSI is given.

Tumor Conform Treatment and the Problems of Beam Delivery

An extensive compilation of the various methods of beam shaping for therapy has been published by Blattmann [5]. They can be categorized into the following two groups:

- beam spreading techniques which affect the lateral and longitudinal direction simultaneously. This is mostly done by passive beam-forming elements like scattering systems, range modulators, etc.
- active beam spreading methods using fast magnetic scanning combined with an adequate energy variation for a tumor conform treatment.

The major advantage of a passive system is that the beam quality delivered to the patient is largely independent of the beam quality delivered from the accelerator to the spreading system: intensity and emittance fluctuations do not influence the scattering process and the spread-out beam in the target volume does not have inhomogeneities caused by these fluctuations. Secondly, the radiation field in the target area has a cylindrical symmetry which allows to measure the relative biological effectiveness (RBE) for the various penetration depths and to assign RBE values depending only on the penetration depth but independent of the lateral extension of the target volume.

A major disadvantage of the passive methods, however, is the cylindrical shape of the radiation field which encloses the tumor in a very crude way, affecting a large fraction of healthy tissue by the biologically highly efficient stopping ions when irradiating irregularly shaped tumors, for example. Consequently, the tolerance of this healthy tissue determines the maximum tumor dose and possibly the success of the treatment. Finally, passive beam spreading is also costly because it requires individually tailored beam shaping moduls for every patient.

Strict tumor conform treatment is very easy to understand in its conception (Fig. 1): the treatment volume is dissected into slices of equal thickness and each slice is treated separately by moving the beam over the cross sectional area. After having treated the most distal slice, the energy is reduced and the preceding slice is treated in the same way. The outline of consecutive slices can be different, so that tumors of arbitrary shapes can be treated in this manner following exactly their outer contours.

Simple as it sounds, this method of tumor conform treatment raises many problems concerning the delivery control and distribution of a pencil beam. Applying the desired physical dose pattern and even more difficult, assigning the proper RBE value to each point of the target volume are the critical issues.

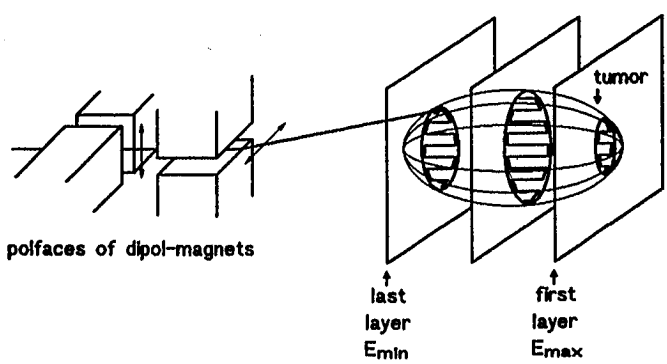

Fig. 1. Schematic view of the magnetic scanning system. The tumor volume is dissected into layers of equal thickness and each layer is treated separately by "painting" the necessary dose with a pencil beam

Intensity-Controlled Raster Scanning

For target conform dose delivery, a prototype of a magnetic scanning system for lateral beam deflection has been used in the biology cave of SIS in combination with the active energy variation by the accelerator for range variation.

In various experiments, it has been shown that an energy variation from pulse to pulse (≈ 2 s) is possible. This includes tuning the beamline to the experimental cave [6]. Figure 2 shows a scanning pattern taken with four different energies delivered within a time sequence of three seconds between the individual steps. However, a major problem of a pure active energy variation mode is the small width of the Bragg peak that would require more than 200 energies to cover a range between 2 and 30 cm. For such a close spacing between the different layers the particle covering of each layer is small and difficult to measure in the position sensitive ionization chamber. Therefore, additional systems for widening the Bragg peak to approximately 3 mm FWHM have to be considered. This will reduce the number of different energies and in consequence the machine settings to a more reasonable number, and the beam intensity produces more reasonable currents in the transmission detectors.

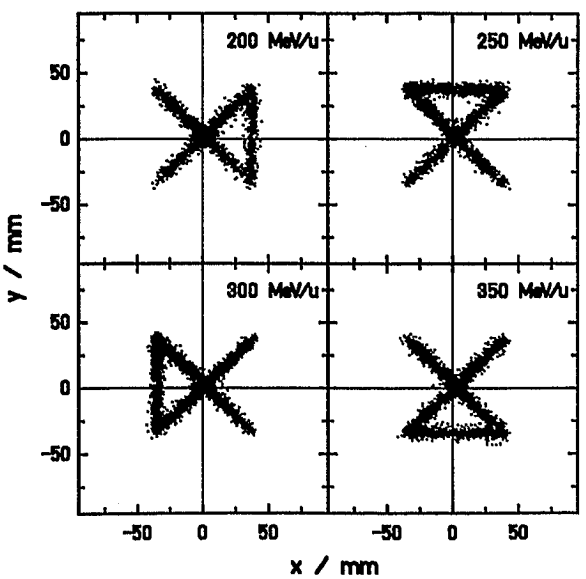

Fig. 2. By combining beam scanning and energy variation, simple figures were produced to test the performance of the scanning system and the quality of the beam. The energy was changed in the accelerator from pulse to pulse within 3 seconds and the beam line was tuned in the same rhythm

The lateral beam deflection is a more difficult issue for tumor conform treatment. As the treatment of the more distal layers preirradiates the proximal ones, at least partially, the latter have to be treated inhomogeneously in order to achieve a homogeneous dose or inactivation effect in the total volume. In addition, beam fluctuations from the accelerator have to be compensated for in order to achieve the desired particle number in each spot. Two different strategies, raster and voxel (or spot) scanning, have been proposed to cope with these problems [6].

For voxel scanning each slice of the target volume is dissected into discrete volume elements (voxels) for which the necessary number of particles is delivered separately by turning off the intensity when the beam is moved from one voxel to another. In the raster scan mode, the beam is moved continuously without turning it on and off. The deposited dose is adjusted by changing the "writing velocity" according to the beam intensity and particle covering.

Extensive calculations have shown [6] that with both approaches, raster or voxel scanning, the same quality of particle covering of any irregular shaped cross sectional area can be obtained. Moreover, in the practical realization both methods become very similar. For voxel scanning an optimal pathway from spot to spot has to be given. This is obviously the connection between neighboring spots, i.e., a more or less continuous pathway. For raster scanning the given pathway has to be digitized into coordinate elements that can be stored in a computer. The only difference between the two solutions is, therefore, whether the beam has or has not to be turned off while moving from spot to spot.

If the distance beween consecutive voxels is much smaller than the diameter of the beam, the dose delivered during moving from one voxel to the next is small and interrupting the beam is not necessary. Slight over- or underexposures of a voxel can be compensated when exposing the next.

A digitized version of an intensity-controlled raster scan, i.e., a hybrid system of raster and voxel scanning has been realized at the biophysics cave at GSI (details are given in [6]). In this set-up, the beam is guided by two magnets in x- and y-direction and the beam intensity is measured by a transmission counter.

The beam path in a single slice is dissected into up to 16000 elements and the writing velocity (maximum 1 cm/msec) of the beam is controlled by an ionization chamber as transmission counter. It has been demonstrated that the use of a transmission counter to control the writing velocity is also a very elegant and efficient method to cope with the intensity fluctuations of the extracted beam from the accelerator. First experiments showed that particle coverings with a homogeneity of 5% or better can be produced, even if the incoming beam has large intensity fluctuations (Fig. 3). But in the same way and with the same accuracy any desired inhomogeneous distribution can be produced as well. This is necessary, e.g., when a three-dimensional volume has to be exposed to a certain isodose or biological isoeffect with low intensities in the midsection and higher intensities at the borderline.

Inhomogeneous radiation exposures have been used to produce three-dimensional, spherical volumes. In a water tank (as tissue equivalent) a spherical volume of 6 cm in diameter, was exposed to an isodose of carbon ions [7]. CR 39 nuclear track detectors immersed in the water were used to record the dose. 30 particle energies were necessary to produce the variation in depth and for each particle range up to several hundred spots were irradiated. The particle covering in the equatorial plane and a photograph of the total exposed volume are shown in Figures 4a and b, respectively. The result of this experiment fully confirms the expectation that tumor conform treatment can be performed by an intensity-controlled raster scanning system. In the near future, this technique will be refined to treat any arbitrary shaped volume.

On-line Control of the Beam by Positron Emission Tomography

Precise beam delivery needs precise control. Heavy ions can be monitored using the production of radioactive isotopes that decay by positron emission. The β^+-annihilation can be localized by measuring the two coincident 511 keV gamma-quanta in two adjacent gamma-cameras. As the positrons are mainly emitted isotropically with respect to the beam direction, the center of the observed distribution of positron emission corresponds to the stopping point of the radioactive isotope.

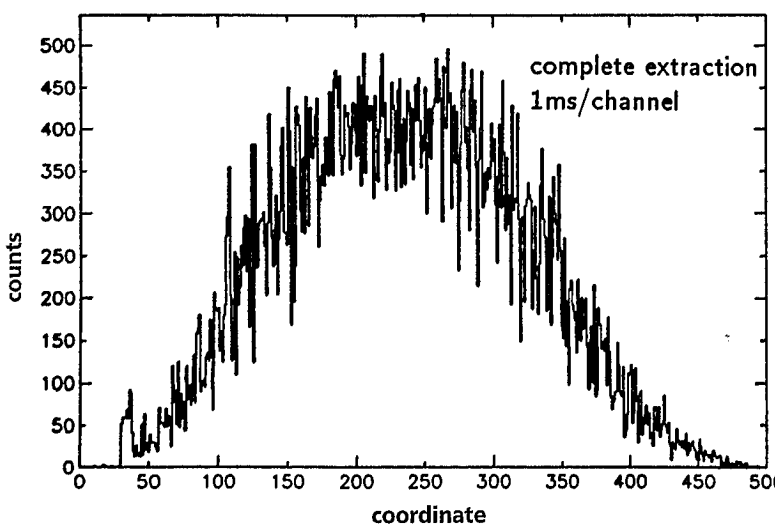

Fig. 3. Time profile of the extracted beam of SIS. The beam intensity is given as a function of the extraction time. The feed back system of the raster scan is able to adjust the "writing velocity" to these functions

Originally, a beam of radioactive β^+-emitting ions was used to verify the treatment plan prior to therapy [8]. At Lawrence Berkeley Laboratory, this approach was successfully applied in cases, where the treatment volume was close to a critical organ such as the spinal cord.

Meanwhile, is has been demonstrated in phantom measurements that β^+-radioactivity produced by a stable beam is sufficient to monitor the stopping points of the projectile ions [9]. Beams of stable ions undergo nuclear reactions, including projectile and target fragmentation. Most likely are stripping reactions which lead to lighter ions, a fraction of which are β^+-isotopes. In the case of target fragmentation, these β^+-emitters are smeared out over the particle path. For the projectile fragmentation the β^+-isotopes have nearly the same range due to their similar mass-to-charge ratio and the strongly forward-peaked reaction kinematics. In Figure 5 the induced β^+-activity of a Ne-beam implanted into a plastic block is compared with the calculated range distribution and with the range of the primary Ne-beam. From the β^+-distribution the range of the stable Ne-ions can be calculated with high accuracy and compared to the treatment plan. The PET technique to verify the treatment plan can also be used for other light ions, includ-

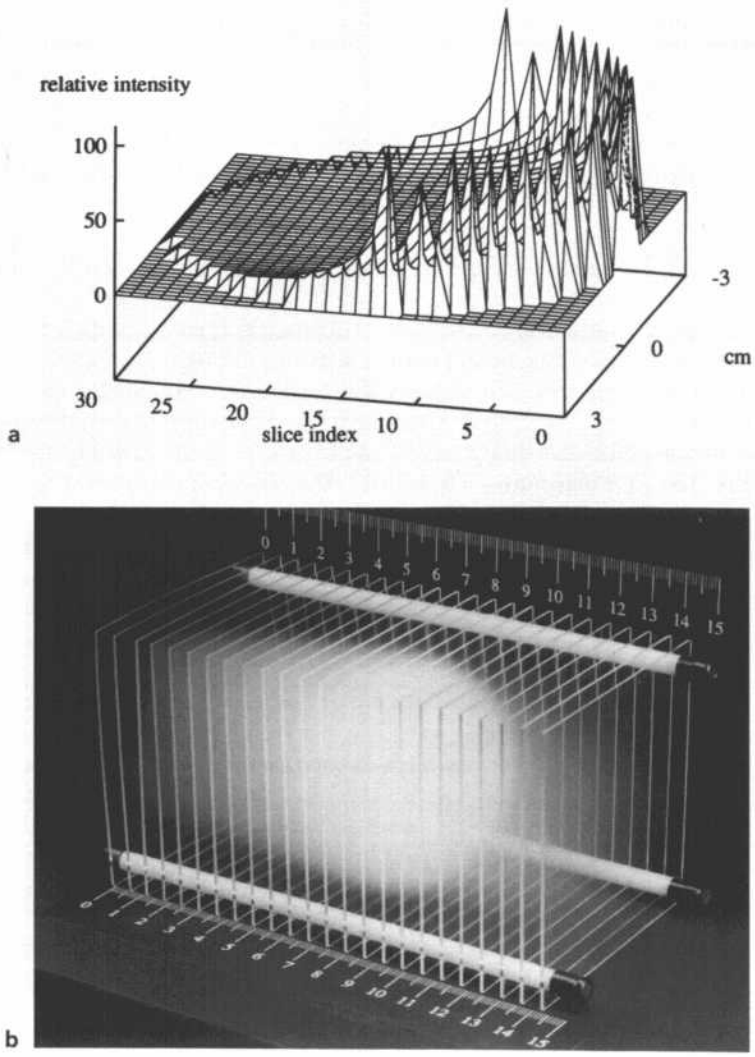

Fig. 4. A sphere of 6 cm in diameter was located in a water phantom (depth 9–15 cm) and exposed to a carbon beam [7]. **a**) Particle covering in the equatorial plane of the volume, **b**) photograph of a recording of the dose by nuclear track detectors. A small dose is visible in the entrance channel on the left

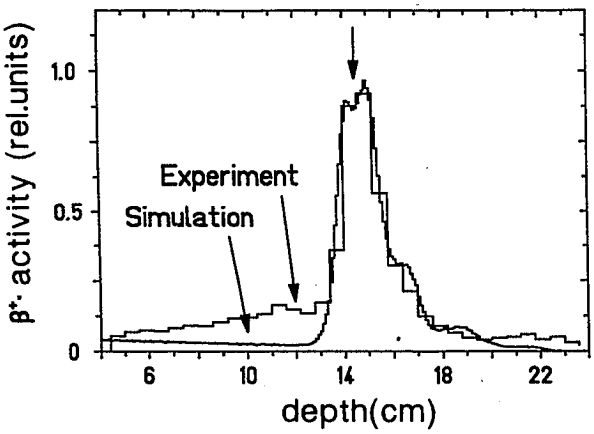

Fig. 5. Measured and calculated profiles of β^+-emitting isotopes are compared with the range of the primary stable ^{20}Ne beam as indicated by the short arrow [9]

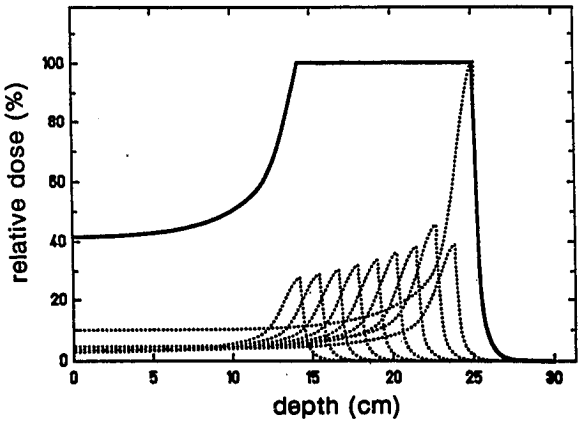

Fig. 6. Schematic representation of a homogeneous dose distribution over an extended target volume produced by superposition of individual Bragg peaks

ing oxygen, nitrogen or carbon ions, but not for helium ions or protons. It should be mentioned that measuring the β^+-activity during the beam spill is not possible, due to a high background activity. However, the off-spill time intervals are sufficient for PET analysis.

Figure 5 illustrates another problem of dose localization for the heavier ions: with increasing atomic number more and more lighter fragments are produced. They have a longer range than the primary beam causing a long tail of dose behind the Bragg maximum. Therefore, the excellent dose distribution of the heavy charged particles deteriorates for ions heavier than neon.

Physical and Biological Beam Characterization

Detailed knowledge of the physical and biological interactions of the beam with the target material is extremely important when using beam scanning methods to achieve a tumor conform target volume.

In an arbitrarily shaped target volume the composition of the particle field differs from point to point. This is due, first of all, to the fact that beams of different energies have to be superimposed to achieve the desired depth distribution (Fig. 6). Therefore, particles of different energies contribute to the biological effect in each point. Secondly, the composition in atomic number of the primary beam is changed to a large extent by nuclear fragmentation. For a carbon beam with penetration depth of 15 cm in tissue, e.g., approximately 50% of the primary carbon ions undergo nuclear reactions which yield lighter fragments down to protons [10]. Therefore, in each target point the particle field consists of various contributions of particles having atomic numbers from the primary ions down to protons and a complex energy distribution.

Extended measurements of beam fragmentation in thick water targets have been performed at the fragment separator (FRS) at GSI. Because of the double separation mode of the FRS, it was possible in a first target to produce all isotopes of medical interest simultaneously and then to follow their fragmentation in tissue-equivalent targets using a complex analysis system for energy and atomic number [10]. These measurements showed that fragmentation in the second and third generation, i.e., the fragmentation of reaction products contributes significantly to the total amount of reaction products (Fig. 7).

Based on a proper parametrization of the beam fragmentation and taking into account the energy loss and straggling of the ions, the composition of the particle field can be described by a

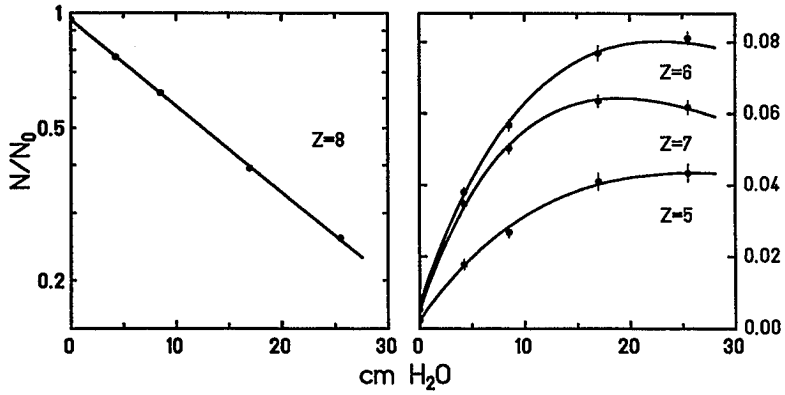

Fig. 7. Nuclear fragmentation of heavy ions. Left: Decrease of the primary ions by nuclear reactions as function of the penetration depth. Right: Build-up of the heavier reaction products with increasing penetration depth in water [10]

distribution function f(Z, E, x, y, z) of the atomic number Z, the energy E, and the position coordinates x, y and z. The dose D(x, y, z) deposited by such a particle distribution in a small subvolume centered around x, y, z is then given by

$$D(x, y, z) = \iint f(Z, E, x, y, z) \times LET(Z, E)\, dE\, dZ$$

This dose distribution for the individual elements of the target volume can be measured using a position-sensitive counter as control of the desired particle covering in each point of the target volume and to verify the distribution function f(Z, E, x, y, z). But the dose distribution D(x, y, z) cannot be used to calculate directly the biological effect, because the relative biological effetiveness RBE(x, y, z) is also a strong function of the atomic number and energy of the particles. [11]. The proper RBE in each target point requires, therefore, knowledge of the composition of the given dose in atomic number and energy. In reality, the situation is even more complex because the RBE further depends on biological parameters like dose level and dose fractionation scheme, and most important, on the tissue type. A solution of this problem is only possible using an elaborate theoretical approach [12] as described in detail in Chapter 6.

Technical Realization of the HITAG Project

The heavy ion sychrotron SIS can accelerate all ions from helium to uranium to energies between 80 MeV/u and more than 1 GeV/u. For the medically relevant lighter ions, such as carbon or oxygen, intensities of some 10^9 particles per spill are available. This particle flux is sufficient to produce a dose of a few Gray per liter in five to ten spills or within 10 to 20 seconds.

In each spill only a few tenths of a second are needed for acceleration while the beam can be extracted by resonance extraction – stochastic would be better – over a few seconds. The energy from SIS can be changed from pulse to pulse. Because of the high flexibility of the synchrotron, it is planned to treat the patients in time-sharing with the physics experiments in four two-week periods per year and to operate the SIS with two different ion sources, one with carbon for patient treatment, the other with the ions for the physical experiments. With the raster scan method, one fraction should be administered within less than five minutes, whereas patient positioning might take much longer (20–40 minutes). Therefore, the dead-time for the physics experiments will not exceed 10 minutes per hour.

In order to minimize possible conflict between the physical experiments and medical treatments, a dedicated medical cave has been constructed and will be connected to an annex housing a control room for the beam delivery to the medical

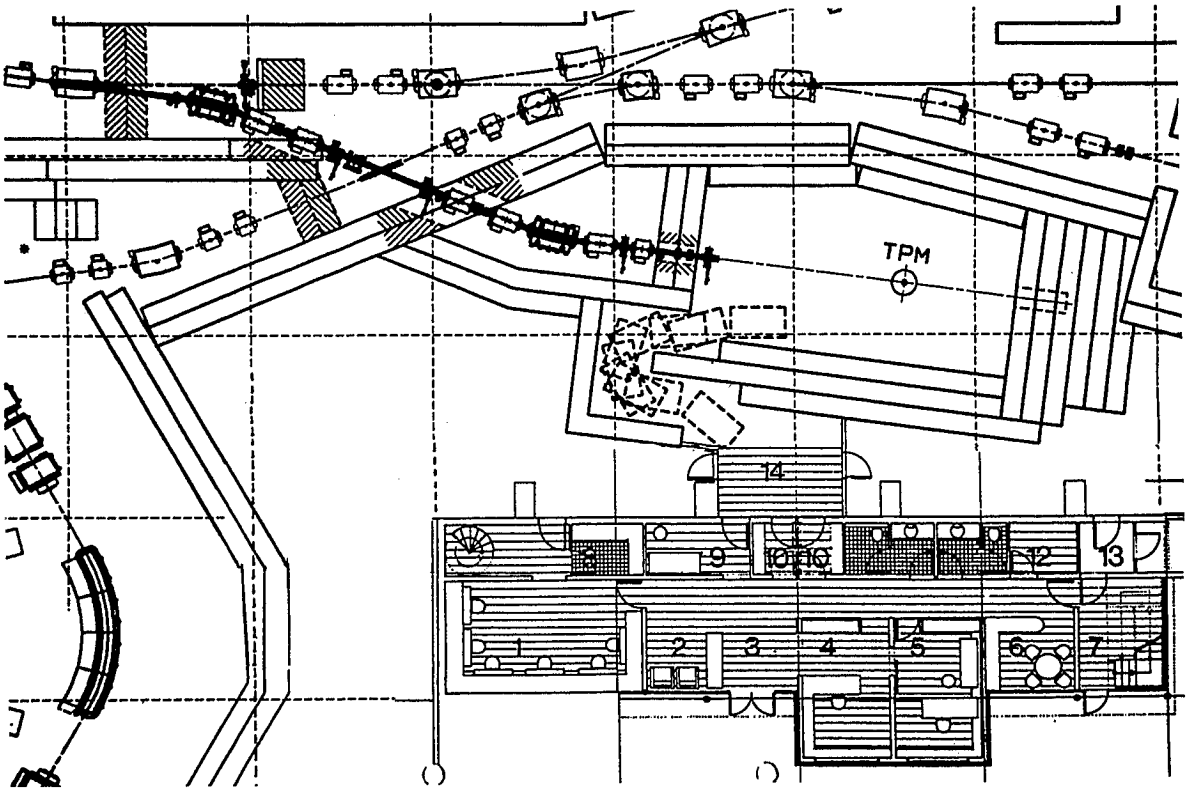

Fig. 8. Medical cave at the SIS with beam line to the treatment room (TPM) and an annex for the control room and medical rooms

room and other rooms necessary for physicians and patients including waiting rooms, examination rooms and offices (Fig 8). However, the main examinations and diagnosis of the patients will be performed at the Radiological Clinic Heidelberg which will also decide on the clinical preferences and the patient selection.

Safety System

The use of a pencil beam with high local efficiency for tumor killing requires special precautions to guarantee that the beam meets the desired specifications and is always located at the correct position in the target volume. To achieve this, a complete set of detectors and controls will be installed to trace the beam. In order to avoid uncontrolled movements of the beam during the resonant extraction, the beam line between accelerator and scanning magnets is set to non-dispersive (achromatic) beam transport. This is especially necessary for the last part of the transport system where the beam is bent from the main beam line into the medical cave by two symmetric dipol magnets and pairs of quadrupols symmetric to the dipols. However, an intermediate energy dispersive focus is produced between the dipols which represents an image of the final focus in the patient. Location and diameter of the beam can be monitored in a non-destructive way using scintillator paddels as beam scratchers at the intermediate focus. In addition, a set of two independent, position-sensitive counters just in front of the patient monitor the beam on-line during exposure. One of these detectors, a multi-wire chamber driven in ionization mode measures the localization of the center of the beam and its diameter within 100 μs. These data are compared with the precalculated irradiation pattern within

less than half a millisecond and if differences are observed, the beam can be stopped within another half a millisecond. During the abortion time less than 1 mGy is deposited assuming a dose rate of 2 Gy per 10 seconds. This represents an infinitesimally small dose when compared to the total dose. A sensitive ionization chamber is dedicated for clinical dosimetry, measuring the absolute dose in each position of the patient entrance. The data of these transmission detectors together with the previously reported PET system guarantee a precise control of the deposited dose.

Another important safety feature is the asymmetric layout of the raster scan system. When the magnets of the scan system are not powered, the beam will pass by the patient and be stopped in a beam dump. Only if the scan magnets are powered correctly, the beam is directed to the patient. In case of an unexpected failure of the scan system, the beam will automatically move away from the patient. In addition to these special safety elements for the scanned pencil beam, the usual precautions for radiation safety will be followed.

Time Frame of HITAG

According to the 1993 [3] proposal, the first patient treatment is foreseen for 1996. In summer of 1994, the concrete shielding of the medical cave was completed and the beam line components were assembled in winter 1994/95. First tests are scheduled for summer 1995. The PET system has undergone testing at the FZR Dresden and the components for treatment planning, i.e., the physical and biological beam characterization are to be put together at GSI to be included into an existing planning program ("Voxelplan") of the German Cancer Research Center. Experiments in which the in vitro results are to be transferred to various tissue types are under way. From mid 1995 the interplay of all components and the treatment program are to be tested in sham treatments of an anthropomorphic phantom and in a few animal experiments. Considering the progress, it should be possible to begin with patient treatments as scheduled in 1996.

References

1 SIS eine Beschleunigeranlage für relativistische schwere Ionen, Darmstadt, GSI, July 1979.
2 Die Ausbaupläne der GSI, Darmstadt, GSI, March 1984.
3 Kraft, G. und Gademann, G. Einrichtung einer experimentellen Strahlentherapie bei der GSI Darmstadt, GSI Report 93–23, 1993.
4 Wambersie, A. The future of high-LET radiation in cancer therapy, in Proc. of the EULIMA Workshop on the Potential Value of Light Ion Beam Therapy, Chauvel, P. and Wambersie, A. (eds.), EUR 12165 EN Brussels, 1989, pp. XIX–LV.
5 Blattmann, H. Beam delivery systems for charged particles. Radiat. Environ. Biophys. 31, 219–231, 1992.
6 Haberer, Th., Becher, W., Schardt, D., and Kraft, G. Magnetic scanning system for heavy ion therapy. Nucl. Instr. Meth. Phys. Res. A330, 296–305, 1993.
7 Weber, U. GSI Nachrichten 11, 6, 1993.
8 Llacer, J., Schmidt, J.B., and Tobias, C.A. Characterization of fragmented heavy-ion beams using a three-stage telescope detector: measurements of 670 MeV/amu Ne-beams. Med. Phys. 17, 151–167, 1990.
9 Enghardt, W., Fromm, W.D., Geissel, H., Keller, H., Kraft, G., Magel, A., Manfraß, P., Münzenberg, G., Nickel, F., Pawelke, F., Schardt, D., Scheidenberger, C., and Sobiella, M. The spatial distribution of positron-emitting nuclei generated by relativistic light ions. Phys. Med. Biol. 37, 2127–2131, 1992.
10 Schall, I., Schardt, D., Kraft, D., Magel, A., Mohar, M.F., Münzenberg, G., Nickel, F., Scheidenberger, C., Schwab, W., Kankeleit, E., and Fukumura, A. Nuclear fragmentaion of light ion beams in water. GSI, 93–1, 337, 1993.
11 Kraft, G. The radiobiological and physical basis for radiotherapy with protons and heavier ions, Strahlenther. Onkol. 166, 10–13, 1990.
12 Scholz M. and Kraft, G. A parameter-free track-structure model for heavy action cross sections, in Biophysical Modelling of Radiation Effects, Chadwick, K.H., Moschini, G., and Varma, M.N. (eds.), Adam Hilger, Bristol, 1992, pp. 185–192.

37

NAC – The Only Proton Therapy Facility in the Southern Hemisphere

D. T. L. JONES

National Accelerator Centre, Faure, South Africa

Introduction

The only heavy particle therapy facility in the Southern Hemisphere is at the South African National Accelerator Centre (NAC) at Faure, about 35 km from downtown Cape Town [1–4]. Although patients were first treated on September 6, 1988 on the p(66)/Be neutron therapy unit [5, 6], routine treatment only began in 1989, while proton therapy was first undertaken in the NAC's 200 MeV horizontal beam on September 10, 1993 [7]. It is possibly the only facility in the world where both high-energy neutrons and high-energy protons have been used for patient treatment. The NAC facilities were planned specifically to provide research opportunities in natural sciences for users from all over the country and other parts of the world, to supply high-energy nuclear particles for radiation therapy and to produce radioisotopes, primarily for medical applications.

Following a detailed study of the feasibility of a centralized accelerator facility for South Africa, the NAC was officially established on April 1, 1977. It took another 10 years for the local team to complete the design and construction of the new accelerators and other facilities, before routine operation could commence. Approximately 18 months later, neutron therapy (which for historical reasons had priority as far as radiation therapy was concerned) commenced, following extensive dosimetric and radiobiological measurements [8–10]. Once neutron therapy was established as a routine procedure [4, 11], attention was given to the development of the proton therapy facilities. Today NAC's facilities are utilized by more than 200 medical specialists and scientists from many disciplines and institutes in South Africa and abroad. Included in this number are more than 50 post-graduate students.

The NAC is probably unique in the sense that it was designed from the outset as a multidisciplinary facility to meet the often conflicting requirements (in terms of beam quality) for nuclear physics experiments and proton therapy on the one hand, and isotope production and neutron therapy on the other hand. Although many dedicated accelerator facilities for medical applications have been constructed, medical facilities at nuclear physics installations have previously been added on as an afterthought and have often been inadequate, inefficient or inconvenient as clinical centers.

Operation of the Facilities

The layout of the radiation areas is shown in Figure 1. All the major facilities, with the exception of the neutron therapy unit (Elven Precision Ltd., Crawley, U.K.), were designed locally. They include a solid-pole light-ion injector cyclotron (SPC1) and a variable-energy separated-sector cyclotron (SSC), capable of accelerating protons to a maximum energy of 200 MeV, while a heavy- and polarized-ion injector cyclotron (SPC2) is nearing completion and should be fully operational by August 1994.

A 6 MV CN Van de Graaff accelerator (located in a separate building), which has been in use for more than 30 years, is utilized mainly for applied research. The medical complex includes three

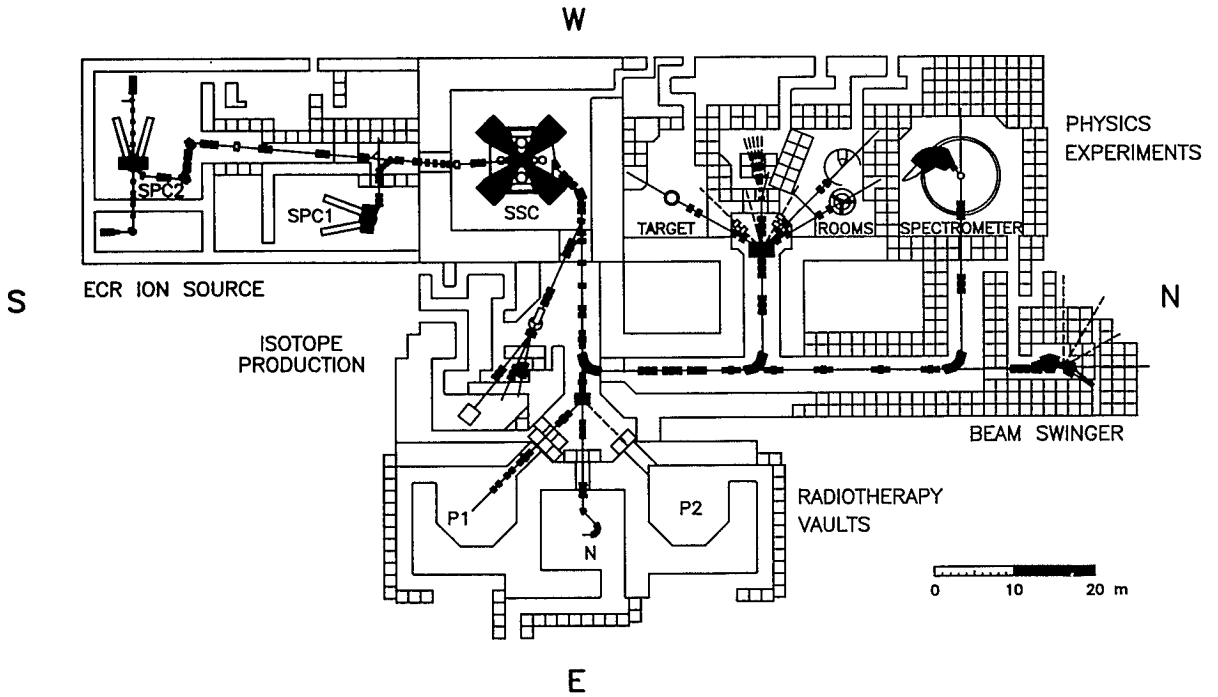

Fig. 1. Layout of the NAC radiation areas. The isocentric neutron therapy unit is located in vault N, while the horizontal proton therapy facility is located in vault P1. Vault P2 is empty at present. SSC: separated-sector cyclotron, SPC1: solid-pole cyclotron #1, SPC2: solid-pole cyclotron #2

radiotherapy treatment vaults, laboratories, offices, patient service areas, full medical physics and radiobiology facilities (including provision for experimental animals) as well as a 30-bed on-site hospital. One of the treatment vaults (N) contains the p(66)/Be isocentric neutron therapy unit on which more than 600 patients have been treated, while the 200 MeV horizontal beam proton therapy facility occupies a second vault (P1). A second proton therapy beam line (possibly isocentric) is foreseen for the third vault (P2). Operating theaters are located close to this vault for use in possible future intraoperative proton therapy procedures.

At present proton therapy takes place only on one day of the week while research, development and quality control procedures on the proton therapy facility are undertaken the previous night after the energy has been changed from 66 MeV to 200 MeV. The rest of the available beam time is taken up by radioisotope production with 66 MeV proton beams (two nights), neutron therapy (3 days), and physics research (weekends).

All patients, including those from other parts of the country and from neighboring territories, are referred to the NAC through either Groote Schuur Hospital (University of Cape Town) or Tygerberg Hospital (University of Stellenbosch). Both teaching hospitals are about 25 min by road from the NAC. They treat more than 5 000 new radiotherapy patients annually. At present all patient assessment and treatment planning is undertaken at the hospitals. Although most patients are housed in the on-site hospital for the duration of their treatments, others attend as out-patients.

The Proton Therapy Unit

The proton therapy facility can at present only be used for the treatment of head and neck lesions. It consists essentially of a beam delivery system, a treatment chair linked to an automatic positioning system and various field verification devices.

A schematic layout of the existing beam delivery system, which was originally developed (in conjunction with the NAC's Accelerator Group) for crossfire plateau irradiations, is shown in Figure 2. The beam line is 1.25 m above floor level. Most of the components are mounted on bearings on a precision optical bench and their positions can easily be changed. Furthermore, they can be retracted from and inserted into the beam by remotely-controlled pneumatic pistons. The total distance between the vacuum window and the isocenter is 7 m.

The proton beam exits the vacuum through a 0.025 mm thick Havar window. A double scatterer plus occluding ring system [12] is used to flatten the proton beam. The beam delivery system is designed for a maximum field diameter of 10 cm. The first scatterer (#1) is located immediately downstream of the vacuum window and is a 1 mm thick lead plate. The occluding rings (50 mm thick brass) are mounted on the second scatterer (#2) which is a 1 mm thick brass plate. This assembly is located 2.9 m downstream of the first scatterer. The central stopper has a radius of 1.34 cm, while the inner and outer radii of the concentric ring are 2.42 and 3.61 cm, respectively. This beam spreading system is currently used for all field sizes.

The double scattering system being used is extremely sensitive to beam positioning and it was found essential to install an automated control system. The beam is controlled by two computerized feedback systems acting on two sets (#1 and #2) of xy steering magnets. The first feedback system uses a multiwire ionization chamber (MWIC #1) with 2 mm resolution which monitors the beam position in the x and y directions perpendicular to the beam axis. The steering magnets (set #1) for this system are located 2.8 m upstream of MWIC #1. The second feedback system uses the signals from a quadrisegmented transmission ionization chamber which monitors the beam symmetry and is located close to the patient. This second feedback system operates on the downstream steering magnets (set #2). The first feedback system uses information from the MWIC (#1) located between these two latter steering magnets and ensures that the beam is aligned with the beam axis at this point. This dual feedback system ensures a very stable and symmetrical beam. A second MWIC (#2) with 3 mm resolution is installed in front of the occluding rings and is only used to display the beam profile at this point. The segmented ionization chamber system (Lawrence Berkeley Laboratory, California) also includes an electrode made up of 12 concentric rings which provides information on the beam profile assuming azimuthal symmetry.

There are 3 antiscatter collimators (#1, #2, #3) in the beam as shown in Figure 2. The front face of the final (patient) collimator (#4) is located 27.5 cm upstream of the isocenter. Fixed inserts, which can either be custom-made or of a standard shape, fit into the final collimator

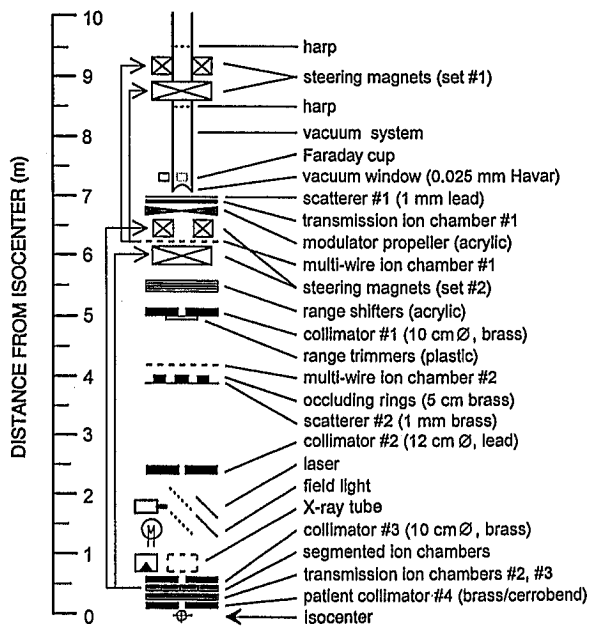

Fig. 2. Layout of the 200 MeV horizontal proton therapy beam modification system. The drawing is not to scale, but all the beam line components are shown in their approximate positions

assembly which can rotate around the beam axis in order to align non-circular collimators with the planned treatment field. This assembly cannot be moved closer to the isocenter, as it will get in the way of the cameras of the patient positioning system (see below). The collimator inserts are made of brass (5 cm thick) or low-melting-point alloy (6 cm thick). Front- and back-pointer lasers and a field-defining light are used to indicate the beam axis and to project the shape of the final collimator onto the patient, respectively. Lateral lasers are also provided. There are mounting posts at various positions along the beam axis for locating a theodolite, which is used for precise alignment of the beamline components and for accurately checking the patient position if required. A coaxial X-ray tube can be mounted close to the patient collimator and is used for verification of the treatment fields.

A dual transmission ionization chamber system (#2) (5 μm thick aluminized mylar foils, 5 mm separation) located immediately upstream of the patient collimator is used to monitor the dose delivered. Redundant dose information can also be obtained from the segmented ionization chambers. A single transmission ionization chamber (#1) (5 μm thick aluminized mylar foils, 1 mm separation) located immediately downstream of scatterer #1 is used for experimental purposes and to provide the reference signal for dose distribution measurements. All these monitors are filled with ambient air.

The transmission ionization chambers used for dose monitoring are calibrated against air-filled A-150 tissue-equivalent ionization chambers according to the Supplement of the "Code of Practice for Clinical Proton Dosimetry" ([13, 14], see also Chapter 26). Dose rates which are used clinically are about 3 Gy/min. To achieve this dose rate in the plateau region of an unmodulated beam (dose measured at a depth of 5 cm in water) a beam current of about 15 nA is required. The total mass in the path of the beam between the vacuum system and the isocenter is about 2.0 g/cm^2 corresponding to an energy loss of about 9 MeV for a beam with a nominal incident energy of 200 MeV. Since the beam energy cannot be reproduced exactly week by week, plastic range-trimmer plates, 0.6 mg/cm^2 thick, are placed on collimator #1 in order to routinely produce a residual range of 24 cm in water (distal 50% level) for patient treatment. For spread-out Bragg peak (SOBP) therapy, additional acrylic range-shifter plates are manually inserted just upstream of collimator #1 to achieve the required range. Wax compensators, to correct for oblique incidence in SOBP treatments, are sometimes used. They are mounted on the downstream face of the patient collimator. With existing hospital planning systems only rudimentary heterogeneity corrections can be made, so distal edge compensation has not yet been implemented. Microswitches sense whether the movable beam line components are in their correct positions and this information is interlocked with the safety system. A bar code system to identify and verify treatment field specific components such as collimator, propeller (see below), range shifters etc. is under development.

Figure 3 shows a typical isodose curve for an unmodulated 10 cm diameter beam with a resid-

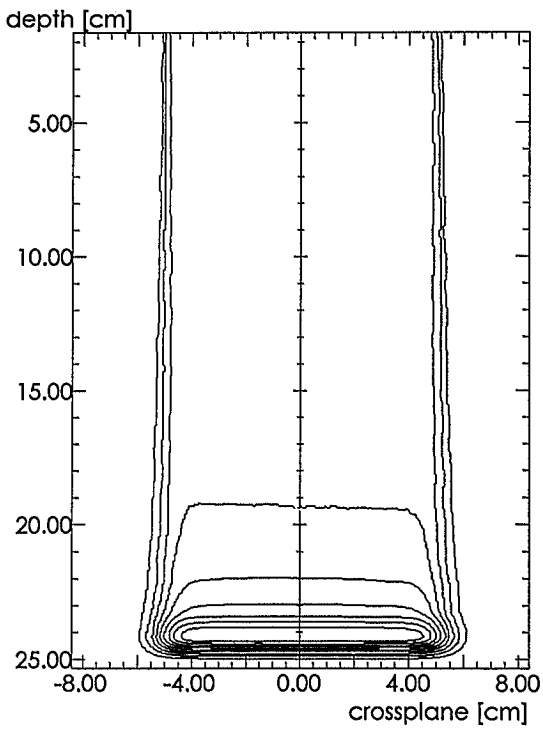

Fig. 3. Isodose distribution measured in water with a 0.01 cm^3 tissue-equivalent ionization chamber in an unmodulated proton beam with a 10 cm diameter collimator. The 10% to 90% isodoses in 10% steps are shown

Table 1. Beam data for an unmodulated proton beam with a 10 cm diameter collimator

Depth in water (cm)	Flatness[a] (%)	Integral symmetry[b]	Penumbra (cm)		Beam widths (cm)	
			90%/10%	80%/20%	50%	90%
2.2	1.0	0.6	0.36	0.22	10.23	9.84
7.4	0.7	0.4	0.54	0.33	10.31	9.75
12.6	0.5	0.3	0.76	0.47	10.38	9.63
17.8	1.4	0.6	1.09	0.69	10.43	9.41
24.2 (peak)	3.0	0.3	1.57	1.02	10.48	8.85

[a] Over 80% of field size [b] Between 50% dose levels

ual range of 24.5 cm. The full width at half-maximum (FWHM) of the Bragg peak is 2.4 cm, while the 90–10% and 80–20% distal fall-offs are 0.60 and 0.40 cm, respectively. The entrance to peak ratio is 0.28. Information about the flatness, symmetry and penumbrae for this beam is given in Table 1.

For SOBP therapy the Bragg peak is spread out longitudinally by using a "propeller" made up of different thicknesses of acrylic and which is rotated in the proton beam [15]. The propellers are designed on the basis of measurements of the attenuation of a monoenergetic beam in different thicknesses of acrylic placed at the position of the propeller. Figure 4 shows measured 4.5 and 11 cm SOBPs (90% dose level) together with the calculated contributions from the individual monoenergetic range-shifted curves. The dose uniformity over the flat regions is ± 1.0%.

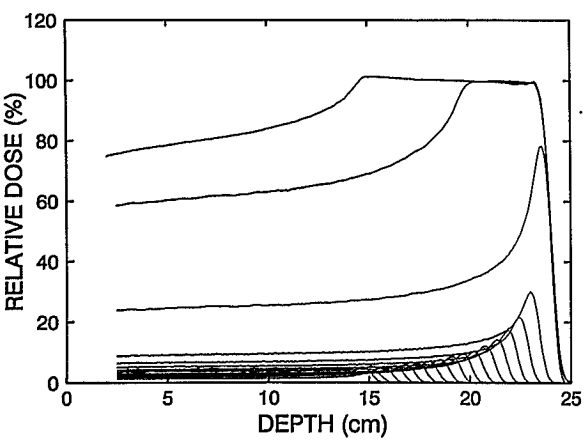

Fig. 4. Proton depth-dose curves measured in water with a 0.01 cm^3 tissue-equivalent ionization chamber in range-modulated proton beams with 10 cm diameter collimators. The calculated contributions of the individual range-shifted monoenergetic curves which are used to design the modulator propellers are also shown. The Bragg peaks are spread out over 4.5 cm and 11 cm (90% dose level), respectively

Several radiobiological [16, 17] and microdosimetric [18, 19] measurements have been made in both monoenergetic and modulated 200 MeV proton beams. Proton dosimetry intercomparisons have been undertaken at various overseas centers [20, 21]. The results obtained by the different participants with tissue-equivalent ionization chambers agree very well. Dosimetry and biological intercomparisons have recently been undertaken at NAC with groups from Louvain-la-Neuve, Belgium and Tsukuba, Japan [22, 23]. These latter data are still being evaluated, but early indications are that the results obtained are excellent. For example the RBEs, based on the mouse jejunal crypt cell assay, were found to vary from 1.11 in the plateau region to 1.23 at the distal edge of the SOBP [23], consistent with earlier measurements in other proton therapy beams [24].

The patient support and positioning system [25, 26] used at the NAC was jointly designed by the Departments of Mechanical Engineering and Surveying and Geodetic Engineering of the University of Cape Town. A special feature of the treatment "chair" (in which the patient can assume any position from sitting upright to lying down) is that it can retract completely beneath the floor. A trolley which runs on a set of rails can quickly and accurately be positioned over the

chair. There is also a set of rails on the trolley itself which enables dosimetry equipment (e.g., water phantom) to be accurately located on the trolley. There are several "parking bays" in the treatment room for storing the dosimetry equipment when not in use and from which the equipment can be wheeled directly onto the trolley.

The patient positioning system makes use of real-time stereophotogrammetric (SPG) techniques and is linked to the patient support system (chair) which is a computerized adjustable system with 5 degrees of freedom (3 translations, vertical rotation, backrest rotation). When a patient undergoes a CT scan to locate the treatment volume, small radiopaque reference targets (1 mm diameter ball bearings) are affixed to a custom-made plastic mask which fits the patient's head precisely. From the scan three-dimensional co-ordinates for all the targets are determined relative to a reference point in the treatment volume. This reference point is normally taken as the treatment isocenter. Retroreflective markers 8 mm in diameter are then fixed accurately on the mask exactly over the radiopaque markers. A close-fitting back section is made for each patient's mask and fixed to the fully adjustable chair headrest. In order to compensate for the chair's lack of a roll motion, the patient's head often has to be tilted slightly from the vertical to allow positioning to be accomplished.

During the patient positioning stage, a set of three charge-coupled device (CCD) TV cameras capture video images through a frame grabber of the retroreflective markers on the patient mask. These images are then analyzed by a personal computer using SPG techniques. Since the positions of the video cameras and the direction of the proton beam are accurately known in space, it is possible to calculate the position of the reference point in the treatment volume, relative to the beam axis. The effects of camera distortions, aspect ratio and perspective are taken into account in the calculations. The co-ordinates of the beam entry point are also required and are obtained from the treatment planning program. Spatial corrections to align the vector between the beam entry point and the reference point (isocenter), with the beam axis are then sent from the SPG computer to a second personal computer which controls the chair. Computer-controlled stepper motors move the chair by the required amounts (x, y and z translation accuracy is within 0.1 mm; vertical and backrest rotation accuracy is within 0.1°) to bring the treatment vector directly into the proton beam. Additional information regarding the rotation angle of the final patient collimator is also calculated by the first (SPG) computer. The collimator angle is at present manually set. It takes typically 2–3 iterations from an arbitrary location to align the patient in the required position.

Once the patient is properly positioned, according to preset tolerances of the beam entry point, tumor and reference targets (normally 0.5 mm) the position is checked by means of the front- and back-pointer lasers or with theodolites. This can be verified, and the collimator rotation angle checked, by means of a double-exposure coaxial portal X-radiograph; one exposure is taken with the collimator out of the beam to show the anatomy while for the second exposure the collimator is in position to show its outline and orientation. For this second exposure the X-ray tube is moved upstream so that, if required, the magnification can be matched to that of the anatomical exposure. A typical such radiograph is shown in Figure 5. If everything is correct, the system is set to monitor the positions of all the reflective targets and hence the position of the reference point in the treatment volume as well as the beam entry point. The beam can then be switched on and will be switched off automatically if any of these points moves by more than a preset amount (normally 1 mm).

A total of eight CCD video cameras are positioned approx. 2.5 m from the isocenter at different angles symmetrically around the beam line. Only three cameras can be used at a time and they must find at least three reflective targets, common to at least two cameras. A calibration frame with retroreflective targets of which the three-dimensional co-ordinates have been accurately surveyed relative to the beam axis is placed over the isocenter and is used to fix the positions of the eight cameras in space. The calibration frame can be placed accurately and reproducibly in its surveyed position to facilitate the camera calibration procedure. A second accurately

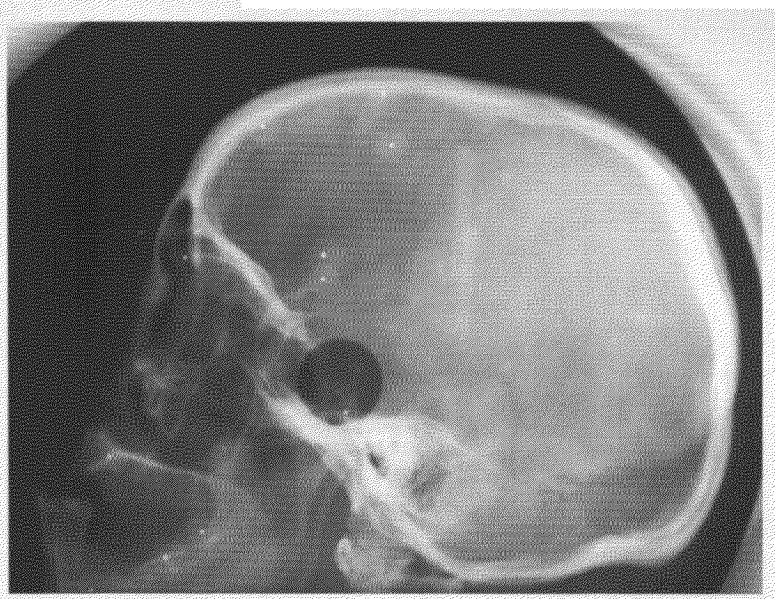

Fig. 5. Typical verification double-exposure X-radiograph with the collimator outline superimposed on the anatomical image. In this case the collimator magnification factor was 2.2. The 1 mm diameter ball-bearings imbedded in the patient's mask are clearly visible

surveyed small frame is placed on the chair backrest and is used to check the operation of the system. Both these latter procedures are done daily to ensure accurate patient positioning. A treatment field can typically be set up in less than 10 minutes. A complete treatment simulation for each patient is done on the day preceding treatment to ensure that no problems occur during treatment. The analysis of the portal radiographs taken for the limited number of patients treated so far indicates that the registration between the reference points on the masks and the anatomical landmarks varies by less than 1 mm during the course of the treatment.

The Clinical Proton Program

As noted above proton therapy was initiated on September 10, 1993. The clinical program for the treatment of small intracranial lesions and of tumors of the base of the skull commenced with the plateau crossfire technique so as to enable staff to familiarize themselves with the SPG positioning system and with the associated complex treatment planning and patient set-up procedures. The first SOBP treatment was performed on February 18, 1994. Treatments are at present given on Fridays only. The number of fields per treatment ranges from 1 to 5 and the total treatment time from 20 minutes to 2 hours depending on the complexity of the set-up, number of verification films and patient movement during treatment. The procedures for preparing the patient for treatment are labour-intensive and time-consuming and account for the relatively small number of patients treated to date. Up to June 30, 1994, 26 patients (65 fractions, 229 fields) had been treated, of which 10 underwent SOBP treatments. Information concerning the lesions treated until then, is given in Table 2. They include 10 metastatic brain tumors, 4 meningiomas, 5 arteriovenous malformations, 1 acoustic neuroma, 2 skull base tumors, 3 gliomas and 1 pituitary adenoma. Lesion volumes range from 0.6 to 43 mm^3 and the total doses from 12 Gy to 60 Gy given in 1 to 4 weekly fractions. To reduce normal tissue morbidity in large volumes or pre-irradiated lesions, fractionated doses have been given according to the scheme proposed by Brenner et al. [27].

Consideration is at present being given to increasing the beam time available for proton therapy. A fractionation schedule which includes 3 fractions per week of both protons and neutrons can be accomodated without seriously compro-

Table 2. Proton treatment details (30 June 1994)

Pathology	Number of patients	Volume of lesion (cm^3)	Total dose/ fractions	Number of fields
Brain metastasis	10	0.6–10.6	18 Gy/1–25 Gy/2	1–4
Meningioma	4	8.0–36.0	12 Gy/2–34 Gy/3	2–4
Arteriovenous malformation	5	3.8–43.0	14 Gy/3–34 Gy/2	3–5
Acoustic neuroma	1	13.6	24 Gy/3	4
Skull base tumor	2	9.2–25.0	21 Gy/3	4–5
Glioma	3	6.6–33.0	15 Gy/3–24 Gy/4	1–5
Pituitary adenoma	1	1.1	60 Gy/3	4

mising the other main NAC activities. Another constraint is the time taken to change beam energy (which is approx. 2.5 hours on average at present).

As soon as more beam time can be made available for proton irradiation, more sophisticated fractionated treatments are foreseen. These will include larger tumors of the brain and base of skull, e.g., craniopharyngiomas and chordomas, as well as boosts to head and neck tumors like the tonsil, antrum, orbit and thyroid. In addition, modification of the patient support and beam delivery systems will enable boost doses to be given to pelvic tumors like the prostate, rectum, cervix and anus. Furthermore, because of the unparalled facilities available at the NAC, proton boosts of neutron treatments are possible and such treatments, possibly for the first time in the world, will commence shortly. Since it is a very rare disease in South Africa it is not a viable proposition to develop a dedicated beamline for the treatment of ocular melanomas.

Summary

The neutron therapy clinical program continues to accrue 120 –130 patients annually and provides a significant proportion of the current world-wide neutron therapy patient load. With its constant patient accrual and reliable operation the NAC's neutron therapy unit is an extremely viable facility and will doubtlessly provide significant input into defining the role of this modality.

The unique stereophotogrammetric patient positioning system ensures precise, reproducible and quick patient set-up for proton therapy of intracranial and head and neck lesions. Furthermore, since it is a non-invasive procedure, fractionated treatments can be routinely given. Preparations for patient treatment are, however, time-consuming and efforts will be made to streamline this. Possible improvements which will be investigated include the manufacture of a multileaf collimator system and the use of bite-blocks carrying a standard co-ordinated frame for patient fixation and positioning.

Because of the small, but significant increase in RBE with depth along the spread-out Bragg peak, it may be necessary to optimize the therapeutic advantage of the beam by designing the modulation propellers to give a uniform biological dose across the SOBP as is done with heavier ions. The nearly DC nature of the cyclotron beam makes the implementation of beam scanning much less demanding than with slowly-pulsed synchrotron beams and investigation of such a beam-spreading system is warranted.

Within a few years it is hoped to install another proton beam delivery system in the third treatment vault. This could be isocentrically mounted and would permit intraoperative therapy as operating theaters have been built in close proximity. It is interesting to note that with some very minor alterations both the Loma Linda University Medical Center's cork-screw gantry and the Paul Scherrer Institute's compact gantry (for details cf. previous chapters) can be accomodated in this vault.

Because of its unique position as the only particle therapy facility in Africa and in the Southern Hemisphere, its superb facilities and on-site tech-

nological and scientific expertise, the excellent medical services available at the local referring hospitals, and the wide spectrum of clinical material available in the region, there is no doubt that the NAC is destined to play a major role in determining the future role of both high-energy neutrons and protons in radiation treatment.

References

1 Jones, D.T.L. Proposed medical applications of the NAC facilities. S. Afr. J. Sci. 78, 149–153, 1982.

2 Jones, D.T.L. Progress with the 200 MeV cyclotron facility at the National Accelerator Centre, in Proc. 5th Symp. Neutron Dosimetry, Neuherberg, Munich, EUR 9762 EN, Vol. II, Commission of the European Communities, Luxembourg, 1984, pp. 989–998.

3 Jones, D.T.L. and Yudelev, M. Particle therapy at the National Accelerator Centre: Progress and Plans, in Proc. Int. Heavy Particle Therapy Workshop, PSI, Villigen, Switzerland, 1989. Blattmann, H. (ed.); PSI Bericht Nr. 69, 1990, pp. 77–80.

4 Schmitt, G., Levin, V., Mills, E.E.D., and Jones, D.T.L. The neutron and proton therapy project at Faure, RSA, in Proc. Proton Radiotherapy Workshop, PSI, Villigen, Switzerland, 1991. Blattmann, H. (ed.); PSI Bericht Nr. 111, 1991, pp. 61–62.

5 Jones, D.T.L. Particles for patients. Nuclear Active 40, 30–36, 1989.

6 Scharf, W.H. Biomedical Particle Accelerators. AIP Press, New York, 1994, pp. 462–469.

7 Vernimmen, F., Wilson, J., and Schmitt, G. The proton therapy clinical programme. NAC Annual Report, NAC/AR/94–01, National Accelerator Centre, Faure, South Africa, 1994, § 9.4.

8 Jones, D.T.L., Yudelev, M., and Hendrikse, W.L.J. Physical characteristics of the South African high energy neutron therapy facility. Radiat. Prot. Dosim. 23, 365–368, 1988.

9 Jones, D.T.L. and Yudelev, M. Neutron dosimetry measurements in a p(66)/Be(40) clinical beam, in Proc. Int. Heavy Particle Therapy Workshop, PSI, Villigen, Switzerland, 1989. Blattmann, H. (ed.), PSI Bericht Nr. 69, 1990, pp. 149–151.

10 Böhm, L., Blekkenhorst, G., Slabbert, J.P., Verheye, F., Jones, D.T.L., and Yudelev, M. RBE and OER - measurements on the p(66)+Be neutron beam at Faure, South Africa, Strahlenther. Onkol. 168, 42–47, 1992.

11 Stannard, C., Vernimmen, F., van Wijk, L., Brennan, S., and Alberts, A. The neutron therapy clinical programme. NAC Annual Report, NAC/AR/94–01, National Accelerator Centre, Faure, South Africa, 1994, § 9.2.

12 Koehler, A.M., Schneider, R.J., and Sisterson J.M. Flattening of proton dose distributions for large-field radiotherapy. Med. Phys. 4, 297–301, 1977.

13 Vynckier, S., Bonnett, D.E., and Jones, D.T.L. Supplement to the code of practice for clinical proton dosimetry. Radioth. Oncol. 32, 174–179, 1994.

14 Vynckier, S., Bonnett, D.E., and Jones, D.T.L. Code of practice for clinical proton dosimetry. Radiother. Oncol. 20, 53–63, 1991.

15 Koehler, A.M., Schneider, R.J., and Sisterson, J.M. Range modulators for protons and heavy ions. Nucl. Instr. Meth. 131, 437–440, 1975.

16 Slabbert, J.P., Jones, D.T.L., Vernimmen, F., Schreuder, A.N., Jones, H.L., and Renan, M. Preliminary radiobiological measurements in 66 and 200 MeV proton beams. NAC Annual Report, NAC/AR/93–01, National Accelerator Centre, Faure, South Africa, 1993, § 10.3.5.

17 Slabbert, J.P., Jones, D.T.L., Schreuder, N., Jones, H.L., Symons, J., and Hough, J.H. Variations in biological effectiveness with depth in a 200 MeV proton beam. NAC Annual Report, NAC/AR/94–01, National Accelerator Centre, Faure, South Africa, 1994, § 10.3.1.

18 Binns, P.J., Hough, J.H., Jones, D.T.L., and Schreuder, A.N. Microdose spectra for protons of different LET. NAC Annual Report, NAC/AR/93–01, National Accelerator Centre, Faure, South Africa, 1993, § 10.2.5.

19 Hough, J.H. and Binns, P.J. Quality variations in a modulated proton beam. NAC Annual Report, NAC/AR/94–01, National Accelerator Centre, Faure, South Africa, 1994, § 10.2.1.

20 Jones, D.T.L., Kacperek, A., Vynckier, S., Mazal A., Delacroix, S., and Nauraye, C. A European proton dosimetry intercomparison. NAC Annual Report, NAC/AR/92–01, National Accelerator Centre, Faure, South Africa, 1992, § 10.1.2.

21 Schreuder, A.N., Mazal, A., Nauraye, C., Delacroix, S., Bridier, A., Gall, K., Wagner, M., and Beatty, J. Dosimetry intercomparisons at CPO, France and HCL, U.S.A. NAC Annual Report, NAC/AR/94–01, National Accelerator Centre, Faure, South Africa, 1994, § 10.1.2.

22 Jones, D.T.L., Schreuder, A.N., Symons, J.E., Vynckier, S., Hayakawa, Y., and Maruhashi, A. Proton dosimetry intercomparison at NAC. NAC Annual Report, NAC/AR/94–01, National Accelerator Centre, Faure, South Africa, 1994, § 10.1.1.

23 Böhm, L., Gueulette, J., De Coster, B.M., Serafin, A. Verheye, F., Vynckier, S., Wambersie, A., Slabbert, J.P., Symons, J.E., Schreuder, A.N., and Jones, D.T.L. Biological effectiveness of 200 MeV protons at various depths using irradiation of mouse jejunal crypt cells: An international intercomparison. NAC Annual Report, NAC/AR/94–01, National Accelerator Centre, Faure, South Africa, 1994, § 10.3.9.

24 Tepper, J., Verhey, L., Goitein, M., and Suit, H.D., In vivo determinations of RBE in a high energy modulated proton beam using normal tissue reactions and fractionated dose schedules. Int. J. Radiat. Oncol. Biol. Phys. 2, 1117–1122, 1977.

25 van der Vlugt, G. and Rüther, H. A real-time photogrammetric system for patient positioning in proton therapy. Int. Arch. Photogram. Remote Sensing 28, 880–885, 1992.
26 Levin, C.V., Hough, J., Adams, L.P., Boonzaier, D., Rüther, H., and Wynchank, S. Determining locations of intracerebral lesions for proton therapy. Phys. Med. Biol. 38, 1393–1401, 1993.
27 Brenner, D.J., Martel, M.K., and Hall, E.J. Fractionated regimens for stereotactic radiotherapy of recurrent tumors of the brain. Int. J. Radiat. Oncol. Biol. Phys. 21, 819–824, 1991.

38 Ophthalmological Proton Facilities

A. KACPEREK

Douglas Cyclotron Unit, Clatterbridge Centre for Oncology (CCO), Wirral, United Kingdom

Introduction

At the time of writing, over 5000 patients have been treated with protons for ocular lesions. Centers which are active in this work within the western hemisphere are shown in Table 1. Most of these treatments have concerned uveal melanoma which is a relatively rare condition but still represents a significant workload for the small number of proton therapy centers. Other ocular and extraocular conditions including choroidal haemangiomas or retinal blastomas are also being treated at some of the centers.

The efficacy of proton treatment may be gauged from the number of new centers and those at the planning stage. Most proton therapy facilities are located in nuclear research centers, but Clatterbridge (CCO) and Loma Linda (LLUMC) are hospital-based facilities.

Much of the pioneering development work has been carried out in the USA [1, 2] at Harvard (HCL) and Berkeley (LBL) and in Switzerland at the Paul Scherrer Institute (PSI) [3]. Their designs have influenced treatment beam line development in most centers. Some design differences have evolved, mainly in response to local factors, influencing beam production techniques and resulting in variations in the physical parameters. Hence, no two facilities are identical.

The following sections will illustrate the common features of treatment centers as well as the differences in construction, beam flattening, range modifying devices and patient position recording. Much of the physical data, where kindly made available, are obtained by local measurement techniques. Therefore, a direct comparison is not appropriate, although these data can be considered a basis for informed discussion.

Table 1. Active proton eye therapy centers excluding Russia, up to September 1994

Center	Location	Country	Patient numbers*	Year of 1st treatment	Other treatments
HCL	Cambridge	USA	2061	1975	deep-seated tumors
NIRS	**Chiba	Japan	40	1979	neutron therapy
PSI	Villigen	Switzerland	1700	1984	deep-seated tumors
TSL	Uppsala	Sweden	20	1989	deep-seated tumors
CCO	Clatterbridge	UK	550	1989	neutron therapy
LLUMC	Loma Linda	USA	32	1990	deep-seated tumors
CAL	Nice	France	410	1990	neutron therapy
CPO	Orsay	France	450	1990	deep-seated tumors
LLN	Louvain***	Belgium	8	1991	neutron therapy
UCD	Davis	USA	4	1994	none

* June 1994 ** facility has vertical beam line *** Intraocular treatments

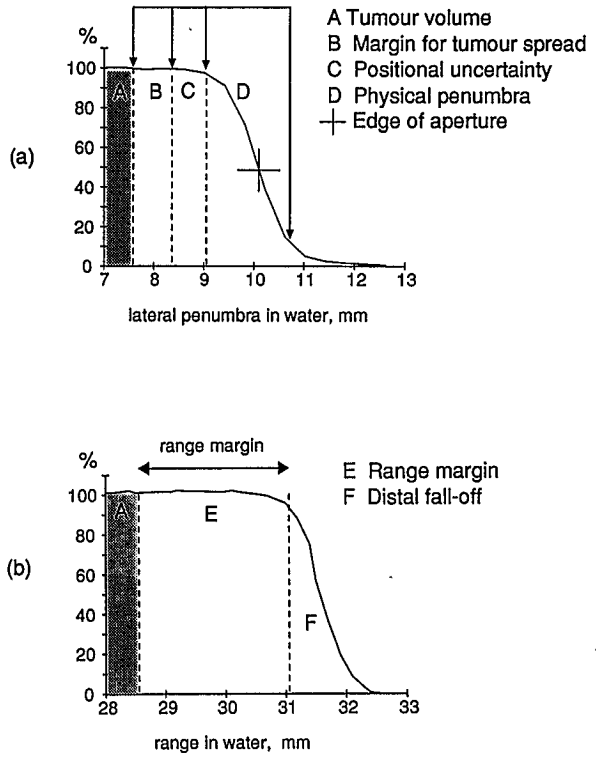

Fig. 1. Sketches showing the components of **a)** lateral and **b)** range margins

Proton eye therapy permits the use of a single port treatment to irradiate a defined target volume whilst sparing sensitive eye structures and skin surface. The precise conformation of the high dose region to the target volume, which may be of several cubic centimeters, necessitates accurate localization of the tumor and reproducible patient positioning for each treatment fraction.

The target volume consists of a defined tumor volume and a margin. The size and composition of this margin has been discussed by Goitein and Miller [4] and is illustrated in Figure 1. It consists principally of:

1. lateral penumbra and distal fall-off
2. microscopic tumor spread
3. estimated positioning precision and movement during treatment

The first factor is dependent on the beam characteristics specific to each facility. Tumor spread is thought to be about 1 mm beyond the edge of the tumor volume, although anecdotal evidence suggests that this spread may be greater for larger tumors. The third factor depends on the patient stillness, the stability of the chair construction and the immobilization device.

This is a simple description and it may not appropriate to adopt concepts and terminology used in mainstream radiotherapy [5]. For example, some ophthalmological centers define only visible tumor whilst others include cellular spread. Therefore, each treatment facility must be aware of the biological and physical factors affecting the volume to be treated and select appropriate margins.

Beam Characteristics

Five centers participated in a comparison of measured beam characteristics. Measurements were made at the therapy position of a patient eye, using local scanners and measurement devices as shown in Tables 2 and 3.

Table 2. Penumbra measurements using a 20 mm collimator. The modulated beam was of approx. 30 mm range and 18 mm modulation

Center	Full energy beam		Modulated beam		Diode type
	90%–10%	80%–20%	90%–10%	80%–20%	
HCL	1.40	0.80	1.60	1.10	MC459
PSI	0.90	0.60	1.60	1.10	1N4007
CCO	1.05	0.65	1.75	1.10	BPW34
CAL	1.60	1.00	2.40	1.50	BPW34
CPO	1.15	0.70	1.90	1.25	1N4006

Table 3. Distal fall-off measurements for pure Bragg peak and modulated depth-doses

Center	Pure Bragg peak		Modulated beam		Measurement device
	90%–10%	80%–20%	90%–10%	80%–20%	
HCL	3.40	2.45	4.40	2.90	diode RET2
PSI	1.10	0.75	1.20	0.90	diode; 1N4007
CCO	0.90	0.50	0.90	0.75	diode; BPW34
LLUMC	1.60	1.20	1.70	1.66	PP (home)
CAL	0.80	0.75	1.28	0.90	diode; BPW34
CPO	2.30	1.55	2.80	1.80	IC, 0.14 cm^3, (Wellhofer)
	2.00	1.40	2.30	1.50	IC, PPC (NACP)

IC = ionization chamber PPC = parallel plate chamber

Lateral penumbra and distal fall-off characteristics were measured for the case of an unmodulated full energy beam and a spread-out Bragg peak (SOBP) beam which would be used for eye therapy. The measurements were performed with a 20 mm diameter final collimator in water or by using plastic absorbers. In the latter case, results were corrected to water depth using simple density correction.

Profiles

The transverse beam measurements of the full energy and modulated proton beams were performed in the horizontal direction only. For clarity, the scans are shown separately for each facility in Figure 2. The lateral profiles of the SOBP were obtained by scanning across the middle of the constant dose region, which corresponds to a range of approximately 21 mm. The air gap was the same in both measurements.

Clearly, the penumbra estimations are influenced by the choice of the normalization point. No definition of appropriate beam flatness is proposed but it is remarked that the data in Figure 2 show a deviation of better than ± 3% over 80% of the central incident field. The slight depressions in the CCO and PSI profiles may be due to attenuation by axial cross-wires. The beam line parameters which affect the beam penumbra are shown in Tables 4 and 5. The use of X-ray verification film may provide a relatively simple means of comparing profiles of full-energy, unmodulated beams, which is of limited value. Ionization density effects would preclude the accurate use of film for profiles in modulated beams.

Table 4. Beam line characteristics of eye therapy centers

Center	Machine energy MeV	Energy in treatment room MeV	Type of passive scattering	Distance scatter-exit* mm	Distance modulator-exit mm	Distance of beam in air mm
HCL	160	69	single, Lexan**	1100	1260	1685
PSI	72	61	single, Pb	1435	1445	1600
CCO	62.5	62.5	double, W	1450	1250	1410
TSL	200	72	double, brass	1765	470	2350
LLUMC	250	100	single, Pb	1120	1294	1669
CAL	65	65	single, Ta	8000	1930	2040
CPO	200	76.1	single, Pb	1480	2060	2410

* distance between the beam flattening foil(s) and the patient collimator; for double-foil systems measurement is from the second scatter foil

** 11.6 cm used to reduce initial beam energy

Table 5. Modulator characteristics of centers

Center	Modulator type	Construction material	Step size, mm	Range-shifter material	Range-shifter step size, mm	Maximum field size, mm
HCL	propeller	Lucite	6–9	Lucite	continuous	38
PSI	propeller*	Al**	continuous	Al	continuous	34
CCO	propeller	Perspex	0.84	Perspex***	0.20	34
TSL	propeller	polystyrene	1.25	polystrene	continuous***	50
LLUMC	propeller	polycarbonate	1.8–2.0	Lucite	continuous	30
CAL	propeller	Perspex	0.84	Perspex	0.20	34
CPO	propeller	Lucite	1.00	Lucite	0.10	40

* 18-segment adjustable propeller; range shifter and modulator combined
** includes Cu-inserts for anterior sparing
*** range shifters < 1mm are of Al foil
**** system of sliding wedges

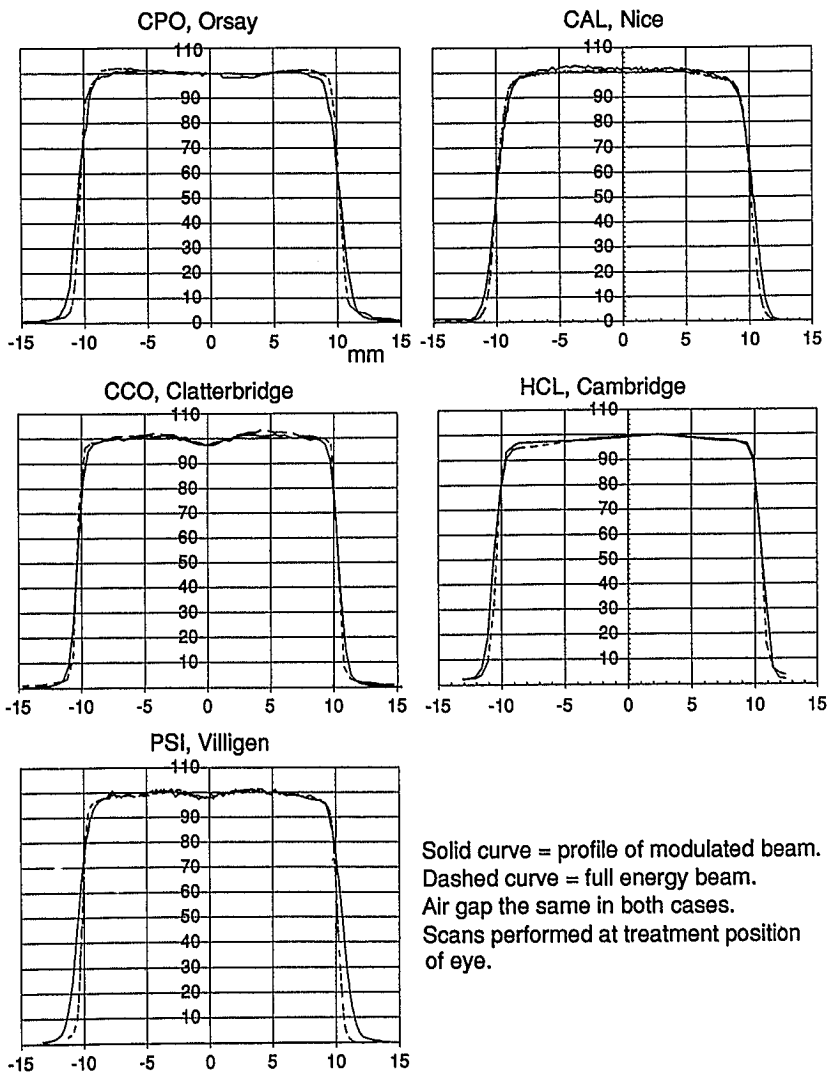

Fig. 2. Lateral scans of modulated (solid line) and unmodulated (dashed line) therapy beams

Depth-Doses

Figure 3 shows the SOBPs measured from five centers. The distal fall-off measurements and devices used are presented in Table 3. All measurements were carried out with plastic absorbers and corrected to water-equivalent depth. The entrance doses varied between 62 and 75%. The fall-offs are greater in the case of SOBPs than for the pure Bragg peak depth-doses since there is a contribution to the primary, least absorbed peak, from the second Bragg peak. For 80% of the constant dose region, the deviation is less than ± 2%.

It must be emphasized that these data are preliminary and drawing significant conclusions is not appropriate. Their quality depends on the measurement devices, some of which are indicated in the tables. However, the data constitute a first step in defining beam qualities between proton therapy centers.

Designs of Beam Lines

The effect of the positioning of beam modifying devices has been studied [6–8] and reviewed by Gottschalk [9]. Various parameters affect the final beam quality including:

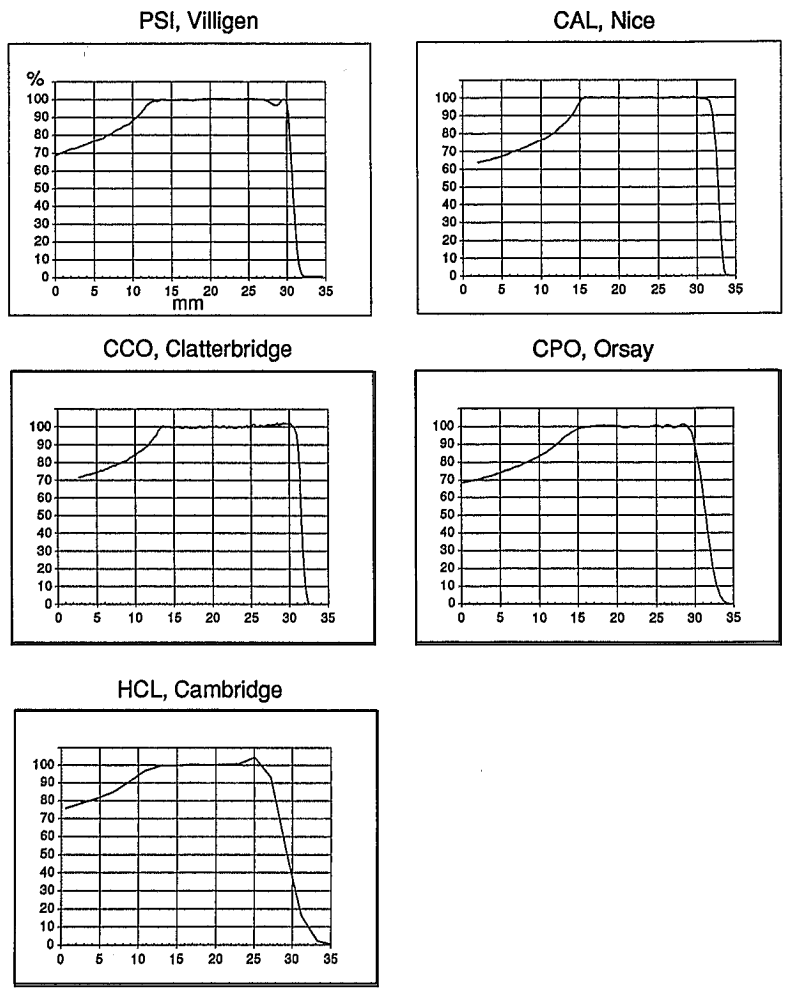

Fig. 3. Modulated proton depth-doses for eye therapy. Normalized to mm in water

1. distance from scattering (homogenizing) foils to exit,
2. distance from range modifying devices to exit,
3. amount of gross energy degradation,
4. distance traveled in air of proton beam,
5. in-beam devices (e.g., parallel-plate chambers, cross-wires, vacuum windows).

Factors 1 and 2 affect the beam divergence. In 3, gross range absorbers, which reduce high energy beams to approximately 70 MeV, can be shown to affect the range straggling, hence the width of the Bragg peak. Factor 4 causes energy loss of approximately 1 MeV/m in air at 65 MeV, which is an important consideration for centers limited in maximum beam energy.

Scattering Foils and Beam Flattening

The use of thin foils of high atomic number to produce beam flattening by scattering is common as shown in Table 4. Multiple Coulomb scattering of protons is approximately proportional to the square root of the atomic number, the thickness of the material and the reciprocal of the incident proton energy. The resultant, approximately Gaussian, lateral proton distribution is trimmed by the primary collimators, leaving a small central portion sufficiently uniform for therapy use. A longer effective source distance would improve flattening at the expense of beam intensity. Beam defocusing, prior to the scattering foil, has been used additionally to improve uniformity. It is widely recognized that the single foil technique is relatively insensitive to beam steering drift but at the cost of some beam range loss and intensity-to-dose efficiency.

For centers limited in maximum energy or beam intensity, a double scattering foil technique was discussed [9, 10]. This technique uses two very thin foils with an occluding stopper on the second foil, however, the resultant beam uniformity is more susceptible to beam steering drift. The Svedberg Laboratory (TSL) at Uppsala has adopted a non-uniform second scattering foil for their eye therapy beam line [11, 12].

Checking and Safety Procedures

Apart from dosimetry checks, each center has also different checks and priorities. The following items are common in many centers:

- modulator speed detector and range shifter check,
- detection of film holder or other equipment temporarily in beam,
- collimator check,
- treatment emergency stop button.

A bar code system based on checking that the correct patient mask, collimator and modulator/range shifter combination is used at the Loma Linda University Medical Center (LLUMC). Unenclosed beam lines may require measures to ensure no occlusion of the beam. At some centers, the accelerator is used to provide proton beams at high beam currents for other purposes, e.g., neutron therapy or radioisotope production. Different methods have been adopted to avoid high proton dose rates, e.g., the CCO has a power-limited ion source supply, PSI has an additional upstream scattering foil which reduces the beam current by 90% [3].

Patient Positioning and Observation During Treatment

A close-circuit television camera (CCTV) with close-up lens is used at an angle to the beam axis to observe the eye during treatment. To improve image contrast and minimize patient distraction, some centers use infrared lighting conditions (cf. Table 6). The most effective camera position to detect eye movement is along the eye gaze axis at a similar position to the LED fixation light. This is employed at facilities having long nozzles or extended collimator tubes, e.g., HCL and TSL. Alternatively, viewing via a mirror down the beam line is used but requires the collimator to be sufficiently large to observe the eye features [3].

Perforated thermosetting mask material (e.g., Aquaplast or Orfit) is used by most centers to immobilize the patient head. It has the advantage of rapidity and is reusable [13]. The bite-block

Table 6. Various parameters related to patient treatment

Center	Isocenter mm	Height above floor mm	Image recording method	Monitoring during treatment	Head restraint	Dental bite block
HCL	70	1335	Polaroid with video	infrared light, CCTV	mask with back	yes
NIRS	50	vertical beam	X-ray film	CCTV	mask only	no
PSI	70	1550	Polaroid	infrared light, CCTV	mask with back	yes
TSL	70	1500	Polaroid	normal light, CCTV	head strap	yes
CCO	70	1520	Polaroid	normal light, CCTV	mask with back	yes
LLUMC	70	1500	Polaroid	infrared light, CCTV	mask with back	yes
CAL	70	1455	Polaroid	normal and infrared light, CCTV	mask with back	yes
CPO	70	1400	X-ray film	infrared light, CCTV	mask	yes

consists of common dental compound mounted on an aluminum plate, which is attached onto the mask holder which in turn is attached either onto the patient chair or the therapy beam line. The TSL at Uppsala uses an adjustable U-shape restraint with an adjustable forehead strap [11].

The standard treatment chair moves in three orthogonal directions; some chairs have a further independent adjustment for patient height where the mask holder is attached to the chair. The chairs also have rotation around the vertical axis and an angular adjustment to the mask holder. Several facilities have extra degrees of freedom such as chair tilt (at CPO and TSL), which are used for eye and other treatment modalities.

Polaroid, and in some cases image intensifiers, provide images of the radio-opaque tumor and beam cross-wires. The amount of position correction is decided by comparing images with an overlay generated by the EYEPLAN program as shown in Figure 4. If the treatment is interrupted further position films are taken. The final hard-copy is used for patient documentation. Non-clip treatments use field light positioning or laser lights with prescribed landmarks. Verhey et al. [13] have measured a mean eye movement during treatment of 0.5 mm ± 0.3 mm. At the CCO the uncertainty of the positioning check is estimated subjectively at 0.25 mm, mainly due to film and overlay resolution. Similar estimates have been made at the CPO [14]. The degree of patient movement encountered at each facility is a combination of factors which include the immobilization devices, the chair rigidity, patient condition and efficacy of the eye-monitoring device.

A LED (light-emitting diode) mounted on an azimuthal stalk provides the direction of patient gaze which has been determined from the planning program. For patients with poor vision in both eyes some centers use personalized contact lenses acting as eye suction devices to control the gaze direction. If healthy eye fixation is used, non-parallel vision may cause an apparent shift in gaze angle. This is usually observed at simulation and corrected for at the therapy planning stage.

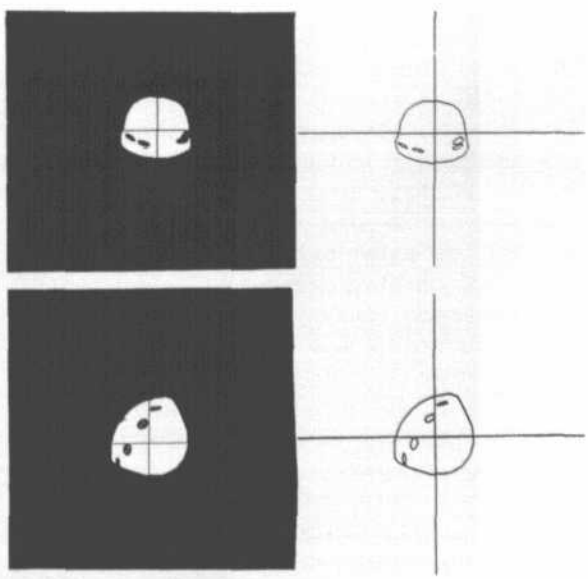

Fig. 4. Axial views of patient clips, collimators, cross-wires and tantalum clips. On the right are the EYEPLAN generated overlays used for positional checks

Planning Program

EYEPLAN is an interactive, three-dimensional therapy planning program which was developed at the Massachusetts General Hospital for eye tumor therapy using either proton beams [4] or radioactive plaques. Subsequently, improvements were made at PSI [15]. Further development, particularly in ease of use and the modelling of eyelids has been made at Clatterbridge [16].

The EYEPLAN program serves to create a model of the patient eye and of the size and location of the tumor. Following simulation, the program allows the planner to determine the limits of eye fixation angle and finally to optimize the treatment plan for an individual patient. The computer eye model is constructed from physical measurements of the eye such as the eye-axis length, limbus and lens diameter. The position of tantalum (Ta) scleral clips geographically locates the tumor on the choroidal surface using measurements obtained at time of surgery. Their number can vary from three to five depending on tumor size. The clip positions on the patient simulation photographs are entered into the EYEPLAN program either manually or, much more conveniently, by using a high resolution digitizer pad (accuracy < 0.1mm).

The tumor base dimensions and shape are deduced from clinical fundus photographs, clinical drawings and ultrasonography. Whilst this may not affect directly tumor treatment, an incorrect model will cause unwitting irradiation of healthy eye tissue. Ultrasound, CT and MR imaging are used to provide patient eye and tumor information. Patient MR eye scans with Ta clips are performed at the CCO when clinical data are inconsistent. The program can incorporate different densities for the components of the eye although this option has not been implemented by any center. At present, single whole eye densities of either 1.00 or 1.05 are assumed, based on the densities of individual eye components including the lesion [17].

Wedges, made of aluminum or plastic, are used by many centers, mainly to reduce the irradiated volume within the eye and, less frequently, to minimize dose to sensitive eye structures. Up to two wedges can be incorporated into a patient plan (Fig. 5). In situations where eyelids cannot satisfactorily be retracted, one or both eyelids can be modelled with a variety of geometrical shapes. The range and modulation is recalculated for every adjustment of wedge and eyelid shape. Some measurements of the effect of wedges have been performed at PSI [3] and Clatterbridge [18].

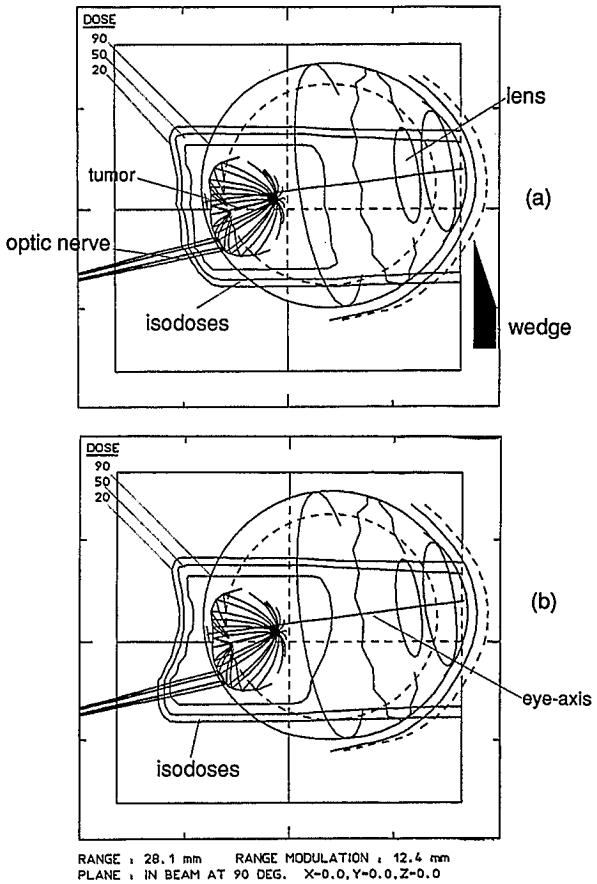

Fig. 5. EYEPLAN horizontal views of isocontours with (**a**) and without (**b**) wedge.

Boluses, of toughened dental wax, are sometimes used to provide a flat surface in regions of irregular geometry, e.g., at the inner canthus.

At present, many centers employ Digital VAX computers with a VMS operating system. Color graphics terminals such as the Tektronix 4105A, to visualize both images and text, are used or are emulated for instance, on a M4400 (Microcolour Graphics) terminal. At Clatterbridge, a DEC

Alpha (Model 2000/300) workstation has been installed for eye planning, giving a five-fold speed increase over the previous Micro VAX II. PSI uses a VAX 4000/60 for planning with an X-windows environment.

Treatment of Superficial Eye Lesions

Several treatments involving superficial regions in the eye have been performed which do not use radio-opaque markers. Presently, they include iris melanomas and tumors of the conjunctiva.

These treatments are given by means of field light or laser light localization. For iris melanomas care is taken to minimize irradiation of the ciliary body; this can be done by reducing the proton range to a depth of a few millimeters. Proton treatments of the conjunctiva have been given as a boost to electron therapy. At Centre Antoine Lacassagne (CAL) at Nice, a novel, hemispherical compensator has been proposed for the conjunctival treatments, which permits superficial irradiation of the uvea behind eyelids [19]. PSI uses simple boluses to protect the lens. The very short ranges and sharp fall-offs obtained using deuterons (requiring little in-beam absorbers, hence sharper fall-off) of 37 MeV have been discussed by PSI [20].

Radiation Doses

Fractionation regimes vary from 4 fractions (fx) in 4 days to 5 fx in 7 to 8 days, and were determined originally by beam time availability especially if a center had other treatments or beam time users as in nuclear research facilities. Table 7 shows the prescribed doses at each center which vary from 70 CGE (Cobalt-Gray equivalent) to 53.8 Gy.

Proton dose calibrations are performed either directly by a standards laboratory or with a local secondary standard which can be traced to a national standards laboratory. The frequency of such calibrations varies from 6 to 12 months. Methods such as calorimetry and Faraday cup dosimetry are the subject of a separate chapter of this book (Chapter 26). Intercenter dosimetry comparisons provide a check of dosimetry techniques used at each center. Usually, groups of ionization chambers are irradiated in the beam of the host center under identical conditions. In addition, ^{60}Co irradiations may be performed to obtain local air-kerma values and to check for any chamber performance changes due to transport. In the future, other ways of intercomparing beam dose and quality may include alanine dosimetry and film exposures, although these methods are subject to non-linearity due to ionization density effects.

Table 8 shows the checks practised prior to patient treatment at the various facilities. The checks reflect the machine characteristics at each facility, e.g., lack of proton energy or of beam steering stability. Table 8 shows as well the in-beam dose monitors which are calibrated for each patient treatment. At least two devices are used at each center. The choice of monitor is guided by local criteria such as thin-walled ionization chambers for low proton energy loss or SEMs to minimize problems associated with pulsed beams.

Table 7. Treatment details of eye facilities

Center	Prescribed dose, Gy	Number of fractions	Period of treatment	Margins aperture, mm	range, mm	Wedges, boluses
HCL	50 or 70*	5	7–8 days	3.0	2.5–3.0	none
NIRS	70*	5	5 weeks	3.0	3.0	none
PSI	54.5	4	4 days	2.0	2.5	aluminum, no
TSL	54.6	4	4 days	3.0	2.5–3.0	plastic, no
CCO	53.1	4	4 days	2.5	2.5 (2.0)	aluminum, no
LLUMC	70*	5	7 days	3.0	3.0	none
CAL	53.1	4	4 days	2.5	0–2.5	Lucite, wax
CPO	54.5	4	4 days	2.5	2.5	Lucite, plastic

* indicates Cobalt-Gray equivalent

Table 8. Treatment beam checks

Center	Beam flatness	Range and modulator checks	Dosimetry checks	Dose rate Gy/min	Duration sec	In-beam dose monitors
HCL	rarely	each treatment	each treatment	10–24	30–90	2 PPC, unsealed
PSI	daily	each treatment	each treatment	20–60	10–30	2 PPC, unsealed
CCO	each treatment	weekly	each treatment	12–35	15–40	2 PPC, unsealed
TSL	each treatment	each treatment	each treatment	32–41	20–25	4 diodes
LLUMC	rarely	weekly	daily	5–8	120–180	SEM/PPC
CAL	daily	weekly	daily	approx. 40	20	2 PPC, unsealed
CPO	daily	daily	daily	13–42	20–64	2 PPC, unsealed

PPC = parallel plate chambers
SEM = secondary emission chamber

Most centers have used copper or brass collimators for low induced radioactivity and ease of machining considerations. Several centers use graphite primary collimators as the carbon causes minimal proton scattering and the induced ^{11}C activity has a short half-life. Neutron shielding consisting of iron or paraffin wax is used particularly near beam scattering foils and primary collimators.

Measurements of patients at the CCO have shown no neutron doses above 0.2 mSv and no detectable photon doses using film badge dosimeters placed on the abdomen of the patients during treatment, although an earlier beam line configuration showed slightly higher doses [18]. PSI has examined stray neutron doses in the proximity of the patient head using superheated drop detectors and have indicated doses of 1 mSv behind the head and up to 16 mSv on the temple during a full treatment course [21]. Patients completing treatment had induced dose rates of less than 1 μSv/h.

Discussion

It is clear that interest in treating eye malignancies with proton beams is growing rapidly. The pioneering centers such as Harvard and PSI have been a source of invaluable help to newer proton treatment facilities. However, much valuable information and experience from all facilities remains unpublished.

The advantageous conformal characteristics of proton radiation require a precise knowledge of the localization and shape of the tumor volume and the dimensions of the treatment eye, all of which is incorporated into the eye treatment plan. The irradiation of healthy eye tissue is minimized, where possible, by optimization of the patient gaze angle, but is also dependent on selected treatment margins of which the lateral penumbra and distal fall-off of the beam are important components.

There is a variation in the prescribed dose and fractionation regime between the various centers which may mean that the best dose and fractionation pattern is not yet determined. Also, this makes precise comparison of patient outcomes between facilities difficult to interpret.

This work provides a preliminary overview of some physical parameters in the construction of proton eye beam lines and their effect on the therapeutic beam. Other factors affecting the precision of the treatments may differ at each center. Most centers are subject to different local constraints such as operational space, access to beam time, beam energy and stability. Therefore, there is a different optimum design solution as each facility responds to these local conditions.

Acknowledgements

I thank the following for discussions and for measurement data: E. Egger, Paul Scherrer Institute, Villigen, N. Brassart, Centre Antoine Lacassagne, Nice, A. Mazal, Centre de Protonthérapie d'Orsay, Orsay and J. Burns, Harvard Cyclotron Laboratory, Cambridge. I appreciated the generous assistance of J. Sisterson, A. Montelius, D. Miller, P. Chauvel, A. Wambersie, T. Nakano, M. Sheen, and J. Shaw.

References

1 Sisterson, J.M. and Johnson, K.N. As we approach 3000: Proton radiation therapy at the Harvard Cyclotron Laboratory. Am. Assoc. Med. Dosim. XI, 21–30, 1986.
2 Gragoudas, E.S., Goitein, M., Koehler, A.M., Verhey, L.J., Tepper, J., Suit, H.D., Brockhurst, R., and Constable, J.J. Proton irradiation of small choroidal malignant melanomas. Am. J. Ophthalmol. 83, 665–673, 1977.
3 Egger, E., Zografos, L., Perret, C., and Gailloud, C., Proton beam irradiation of choroidal melanomas at the PSI: Technique and results, in Medical Radiology: Radiotherapy of Intraocular and Orbital Tumors. Alberti, W. E. and Sagerman, R. H. (eds.), Springer-Verlag, Berlin, Heidelberg, 1993, pp. 57–72.
4 Goitein, M. and Miller, T. Planning proton therapy of the eye. Med. Phys. 10, 275–283, 1983.
5 ICRU Report 50. Prescribing, Recording and Reporting Beam Therapy. International Commission on Radiation Units and Measurements, Maryland, Bethesda, USA, 1993
6 Urie, M.M., Sisterson, J.M., Koehler, A.M., Goitein, M., and Zoeman, J. Proton beam penumbra: Effects of separation between patient and beam modifying devices. Med. Phys. 13, 734–741, 1986.
7 Bonnett, D.E., Kacperek, A., and Sheen, M.A. Characteristics of a 62 MeV proton therapy beam, in Proc. 2nd European Particle Accelerator Conference, Nice, France, 1990, pp. S12–S14.
8 Nauraye, C., Mazal, A., Delacroix, S., Bridier, A., Chavaudra, J., and Rosenwald, J.C. An experimental approach to the design of a scattering system for a proton therapy beam line dedicated to ophthalmological applications. Accept. for publ. in Int. J. Radiat. Oncol. Biol. Phys. 1995.
9 Gottschalk, B. Double Scattering with Optimum Dose Uniformity in Proton Radiotherapy. Harvard Cyclotron Technical Note PTA 8/1/86, Harvard Cyclotron Laboratory, Cambridge, USA, 1986. Also in Abstracts of PTCOG XX meeting, Chester, May 16–18, 1994, Particle Newsletter 14, July 1994.
10 Koehler, A.M., Schneider, R.J., and Sisterson, J.M. Flattening of proton dose distributions for large-field radiotherapy. Med. Phys. 4, 297–301, 1977.
11 Montelius, A., Blomqvist, E., Naeser, P., Brahme, A., Carlsson, J., Carlsson, A-C., Graffman, S., Grusell, E., Hallen, S., Jakobsson, P., Jung, B., Larsson, B., Nilsson, B., Rikner, G., Russell, K., and Svensson, R. The narrow proton beam therapy unit at the Svedberg Laboratory in Uppsala, Acta Oncol. 30, 730–745, 1991.
12 Grusell, E., Montelius, A., Brahme, A., Rikner, G., and Russell, K. A general solution to charged particle beam flattening using an optimized dual-scattering-foil technique, with application to proton therapy beams. Phys. Med. Biol. 39, 2201–2216, 1994.
13 Verhey, L., Goitein, M., McNulty, P., Munzenrider, J.E., and Suit, H.D. Precise positioning of patients for radiotherapy. Int. J. Radiat. Oncol. Biol. Phys. 8, 289–294, 1982.
14 Delacroix, S., Mazal, A., Brassart, N., Ozeer, R., Nauraye, C., Lacroix, F., Biensan, S., Schlienger, P., and Chauvel, P. Controle du positionnement des patients lors du traitement du mélanome de la choroïde par un faisceau de protons de 73 MeV. XXXIIeme Congrès de la Société Française des Physiciens d'Hôpital, 3–5 juin 1993. Bull. Cancer/Radiothérapie 80, pp. 267–282.
15 Perret, C., Greiner, R., Zografos, L., and Gailloud, C. Die Behandlung intraokularer Melanome mit Protonen am Paul Scherrer Institut (PSI). Juli 1988. ID PSI/2000.
16 Sheen, M.A. Review of EYEPLAN at Clatterbridge. Abstracts of XX PTCOG meeting at Chester, UK, May 16–18, 1994. Also earlier work presented at XVIII PTCOG meeting at Nice, France, April 19, 1993.
17 ICRP Report of the Task Group on Reference Man. Publication 23, Pergamon, Oxford, UK 1975.
18 Bonnett, D.E., Kacperek, A., Sheen, M.A., Goodall, R., and Saxton, T.E. The 62 MeV proton beam for the treatment of ocular melanoma at Clatterbridge. Br. J. Radiol. 66, 907–914, 1993.
19 Chauvel, P., Caujolle, J.P., Sauerwein, W., Friedrichs, W., Brassart, N., and Herault, J. Protontherapy as a possible salvage treatment for conjunctival melanomas, in Proc. Int. Symp. on Intraocular and Epibulbar Tumors, Firenze, March, 3–5, 1994, Frezzotti, R., Balestrazzi, E., Falco, L., and Esente, S., (eds.), Moduzzi Editore, 1994, pp. 171–181.
20 Egger, E. Development of a Light Ion Beam for the Treatment of Superficial Malignant Lesions of the Eye. Internal Report. TM-21–92–01. Paul Scherrer Institute, Villigen, Switzerland, Sept.1992.
21 d'Errico, F. and Egger, E. Superheated drop (bubble) detector tests with proton therapy beams, in Particles Newsletter 14, Abstracts of PTCOG XX, Chester, May 16–18, 1994, pp. 12–13.

39 Facilities Under Construction, Planned and Proposed

J. M. SISTERSON

Harvard Cyclotron Laboratory, Harvard University, Cambridge, MA, USA

Introduction

World-wide, there were 15 operating proton therapy facilities and one pion beam facility at the end of 1993 [1]. Only one facility is located in a hospital setting with an accelerator designed and built for proton radiation therapy. There is great interest world-wide in building dedicated proton and ion beam therapy facilities in a hospital setting, or in adapting accelerators at existing research facilities to provide therapy beam lines.

Four new projects are expected to come on line in 1994. Two of these projects – at the Paul Scherrer Institute in Villigen, Switzerland and the HIMAC facility at Chiba, Japan – have been discussed in detail in preceding chapters.

Brief descriptions are given in this chapter of eleven facilities that are

1) completed and started operation in 1994,
2) under construction and expect to treat the first patient in 1994 or 1995,
3) fully funded, but have not yet started construction,
4) proceeding with testing concepts and building equipment while additional funding is sought,
5) at the stage of actively seeking funding as the feasibility and design studies are complete. All these facilities hope to begin operations by the year 2000, if funding is obtained.

One project is already operating at the UC Davis Eye Facility, University of California, Davis California, USA, where the first patient was treated in May 1994. Projects nearing completion are at the TRIUMF Eye Facility, TRIUMF, University of British Columbia, Vancouver, Canada, where it is hoped to treat the first patient by the end of 1994 and The Berlin Eye Treatment Facility, Berlin, Germany where the first patient treatment is expected in 1995.

The Northeast Proton Therapy Center (NPTC), Massachusetts General Hospital in Boston, Massachusetts, USA will begin construction in 1995, and the first patient treatment is expected to be in 1998. At the Ion Beam Therapy Project at COSY-Jülich, Jülich, Germany, the experimental program is in progress. At the Moscow Proton Therapy Facility, Moscow, Russia, components are being built and the Eye Treatment Facility at Munich, Germany, has recently installed their post-accelerator.

There are several proposed facilities that have completed the planning and feasibility study stage and now (August 1994) funds are being sought to build all or part of the facilities. These include the Centre for Oncological Hadrontherapy, Italy, the Proton Therapy Facility in Groningen, Netherlands, the Regional Proton Therapy Facility for the North Carolina State University (NCSU) Centennial Campus, North Carolina, USA and the proton therapy centers of Proton Development N.A., Inc., Illinois, USA.

The UC Davis Eye Facility, USA

A proton eye treatment facility has recently been completed at the 76-inch cyclotron at the Crocker Nuclear Laboratory on the campus of the University of California, Davis. This cyclotron, originally built by E.O. Lawrence in 1937 was used by

Dr. Stone for the early neutron radiotherapy trials at Lawrence Berkeley Laboratory. It was also used to produce some of the heavy, short lived nuclei, like Seaborgium, which was recently named. The cyclotron was moved to Davis in the early 70's and converted into an isochronous cyclotron, with a maximum energy of 68.5 MeV protons. It also is being used for heavy ion physics research. The eye treatment facility at Davis was built by personnel from the Lawrence Berkeley Laboratory. Most of the beam line elements were from the Helium ion beam line at the Bevalac. The facility is being operated by the Department of Radiation Oncology at the University of California.

With the variable water absorber in place, the maximum penetration of the proton beam is 30 mm. The field is flat to within ± 3% over 3 cm and ± 5% over 5 cm diameter. Modulator wheels have been constructed from plastic using diode depth-dose scans as the source of calculation data. The treatment dose rate has been set to be 6 Gy/min, using less than 1% of the maximum beam intensity of the cyclotron.

As of June 30, 1994, 4 patients have been treated. The treatment protocol calls for 48 Gy in 4 fractions given over 4 days. Approximately 15 treatment weeks will be used during the first year of operation, treating a total of approximately 40–50 patients.

The TRIUMF Eye Facility, Canada

The development of the proton facility for the treatment of ocular tumors at TRIUMF in collaboration with the British Columbia Cancer Agency and the University of British Columbia Department of Ophthalmology approaches its final stage. Recently, the installation of beam delivery and monitoring devices at the proton channel (2C) was completed and the first patient treatment is anticipated by the end of 1994.

The layout of the beam line follows closely the standard set-ups of existing facilities. The beam of 70 MeV protons, with an extracted current of 1–5 nA in order to achieve the required dose rate of 15–30 Gy/min, is monitored by a system of standard devices, consisting of 1) a secondary emission monitor (SEM) watching for beam bursts, 2) a profile wire chamber for first beam alignment and 3) a multipurpose ionization chamber complex with an independent transmission foil as a backup and a quadrant foil for the detection of lateral beam displacements. The delivery of the clinically required dose profiles is achieved by a conventional system of a single scattering foil 1/32 inch of Pb), various collimators and the standard range shifter and range modulator devices. The various components were successfully tested in March 1994. The installation of the two crucial remaining hardware components, the control console and the treatment chair, as well as the final testing of the control software was expected to be completed in early July 94.

The acquisition of dosimetry data as required for treatment planning with the code EYEPLAN was almost completed by mid 1994. Relative proton dosimetry data were obtained by using diode detectors in a water phantom. For a stable cyclotron tune dose calibrations and dose profiles were observed to be reproducible within 1% and 2–3%, respectively. A dose uniformity of ± 2% was achieved for spread-out Bragg peaks (SOBP) of plateau widths ranging from 5–20 mm. Furthermore, first RBE measurements were recently completed and analyzed, indicating an average RBE of 1.2 ± 0.1 for a SOBP of 20 mm.

Further ongoing developments in treatment planning and dosimetry at TRIUMF are related to the eye facility as well as to the proposed treatment site for larger fields. For the eye project, various options to improve the standard treatment planning procedure are investigated, e.g., computer automated search for eye fixation angles or the benefits of a treatment with two different ports. For larger fields, the feasibility of quantitative in vivo proton dosimetry with PET techniques is under study. Furthermore, a collaboration with the German Cancer Research Center (DKFZ) in Heidelberg was started to develop a three-dimensional dose algorithm for proton therapy of larger fields. The long term aim of this work is to create a unified 3D-treatment planning system for photon and proton therapy by integrating the developed proton dose algorithms into the three-dimensional photon treatment planning system VOXELPLAN of the DKFZ.

The Berlin Eye Treatment Facility, Germany

A collaboration between the Eye Clinic of the Klinikum Steglitz (Free University Berlin), the Radiotherapy Department of the Charité (Humboldt University) and the Hahn-Meitner-Institut (HMI) has recently been initiated to establish a facility for the treatment of ocular melanoma with proton beams at the Ion Beam Laboratory of the HMI. Funding of this facility will be provided by the Klinikum Steglitz.

The accelerator of the Ion Beam Laboratory of the HMI consists of a 6 MV single-ended Van de Graaff injector coupled to a four-sector isochronous cyclotron. The machine has been in operation since 1978 for nuclear and solid state physics. Positive ions from hydrogen to xenon can be produced in the ECR source of the Van de Graaff injector. Heavy ions can be accelerated to energies of $30 \times A$ (MeV), A being the ion's mass. Due to improvements of the HF-system of the cyclotron in 1988–89, protons can be accelerated up to a maximum energy of 72 MeV which is suitable for the treatment of ocular melanomas. Measurements using a beam of 72 MeV protons and tests of the beam delivery reliability have been carried out since summer 1993.

An existing beam line was modified for experiments with only the 72 MeV proton beam. A 50 mm tantalum foil mounted 18 m upstream of the planned treatment place is used for spreading the beam laterally. Depth-dose curves of a collimated beam in water show Bragg peak-to-entrance dose ratios of 5:1. The measured relative dose fluctuations across the lateral beam profiles in water are smaller than 5%. Measured energy spectra of the proton beam show the full energy peak at 72 MeV and a continuous background with approx. 5% of the total intensity.

A therapy control room and a patient waiting room with a separate entrance to the treatment area are planned and have to be added to the cyclotron building. The first treatments are planned for late 1995. The cyclotron will then be used one week per month for proton therapy of ocular melanoma which should give a treatment capacity of approximately 150 patients/year.

The Northeast Proton Therapy Center (NPTC), USA

The Northeast Proton Therapy Center (NPTC) will be built on the Massachusetts General Hospital (MGH) campus. The current schedule calls for the commissioning of the proton therapy equipment to be completed on July 1, 1998, and for patient treatments to begin immediately thereafter. Funds for the NPTC, which are being shared between MGH and the National Cancer Institute, have been secured and the major contracts have been signed.

Bechtel Corporation will be the design/building contractor. Bechtel, providing total project management services and construction management, is teamed with Tsoi/Kobus & Associates, Architect; McNamara/Salvia, Inc., Structural Engineer; McPhail Associates, Geotechnical Engineer; and John Moriarty & Associates, Construction Contractor. Bechtel will build a two-level facility, one underground, having three treatment rooms, at least one and probably two with gantries and the other(s) being equipped with fixed beams and capable of gantry installation. The layout for the treatment level is shown in Figure 1.

IBA, Belgium – teamed with General Atomics and the University of Louvain – was selected as the equipment vendor. IBA will deliver a high-field, room temperature cyclotron which will produce 235 MeV protons with a continuous beam intensity of up to 300 nA (see Chapter 22). The maximum energy corresponds to a depth range of about 34 g/cm^2 in the absence of absorbing or lateral beam spreading elements in the beam line. If passive scattering methodology is used to achieve a 25 cm $\times$ 25 cm field size, the depth of penetration would be about 28 g/cm^2. In addition to a passive beam spreading system, IBA will build a beam wobbling system to achieve large treatment fields. Using the wobbler, a penetration of 32 g/cm^2 can be achieved for a field size of 25 cm $\times$ 25 cm. A variable energy degrader will be integrated with the cyclotron which will allow energy changes from 235 MeV down to 70 MeV in a few seconds.

General Atomics will construct the beam lines, gantries and patient positioners. The gantries will

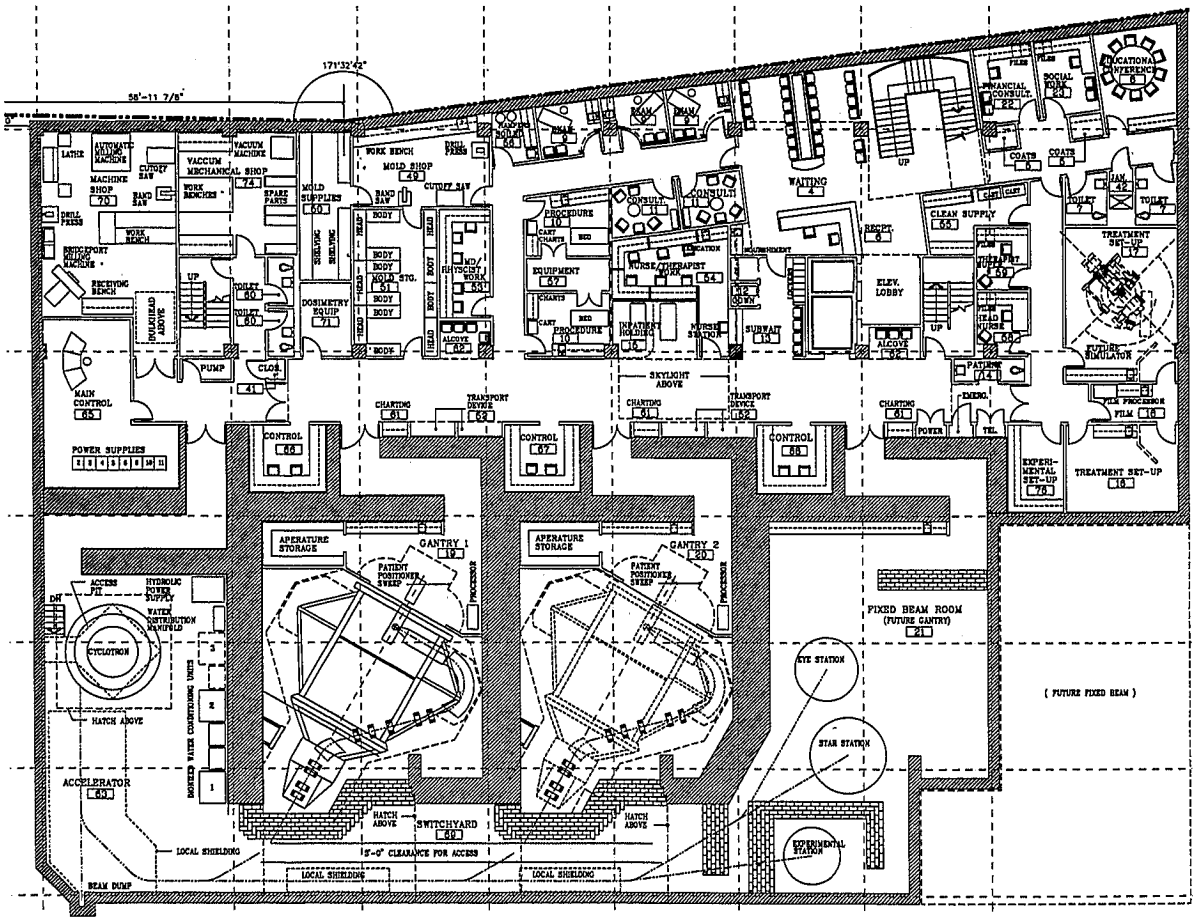

Fig. 1. Layout of the treatment level of the Northeast Proton Therapy Center

be conventional in design. The patient positioners will be designed to meet the particular needs and precision requirements of proton therapy. The isocentric gantries will have a 360-degree rotational capability with beam delivery elements designed to bend the proton beam achromatically while allowing for different focusing conditions. The flexibility in focusing conditions will accommodate both passive beam spreading and pencil beam scanning. The beam lines and gantries will accommodate rapid energy changes and switching among treatment rooms.

The beam delivery nozzles will be designed by the Cyclotron Research Center of the University of Louvain in collaboration with their proton therapy group and members of the Harvard Cyclotron Laboratory and will be manufactured by IBA. The design will be based on the beam spreading technology developed by Gottschalk et al. at the Harvard Cyclotron Laboratory [2]. The nozzle will contain an XY sweeping magnet, appropriate for beam wobbling. The transition to raster scanning will be straightforward.

The NPTC is expected to treat 400 patients during the first year. This patient load is planned to increase to 750 by the fifth year and 1000 by the tenth year of operation. New clinical research protocols for the NPTC are being written and a transition plan for moving the clinical operations from the Harvard Cyclotron Laboratory to the NPTC is being formulated.

The Ion Beam Therapy Project at COSY-Jülich, Germany

On April 1, 1993 the cooler synchrotron and storage ring COSY-Jülich was officially inaugurated. COSY has been built primarily for medium energy physics but its characteristics are well suited for radiation therapy.

Protons injected into COSY at an energy of 40 MeV can be accelerated up to 2.5 GeV. Heavier ions such as carbon, oxygen and neon can be accelerated in the medically necessary intensity and energy range ($\approx 10^8$ particles/s and E = 400–500 MeV/u), but this option will not be used during the first few years.

At present, COSY can store approx. 2×10^{10} protons and accelerates them up to 1.4 GeV/c or ca. 750 MeV kinetic energy. Except for the stochastic cooling expected in spring 1995, COSY should be fully developed by summer 1994 and can store up to 2×10^{11} protons. The expected beam intensity is 5×10^9 protons/s at maximum energy and 2×10^{10} at 200 MeV, respectively.

Other features that make COSY particularly suited for therapeutic application are an ultraslow extraction mode (spill times up to 1000 s), a low beam emittance (2.5 π mm mrad vert. and horiz.) and a high momentum stability during beam pulses and from pulse to pulse ($\Delta p/p = 10^{-3}$). Intensity fluctuations of less than 10% during a pulse and a reproducibility of approx. 1% is expected. The duty cycle should typically be 50% for a repetition rate of 0.5 Hz.

The medical program at COSY (COSY-med) comprises four main topics:

1) the technical physics program responsible for design and development of the beam delivery and scanning system, the patient positioning, control and safety systems,
2) the radiation physics program for beam characterization, (in vivo) dosimetry and irradiation planning,
3) the technical infrastructure program for the integration of the therapy site into the COSY building, the design and construction of the necessary annex,

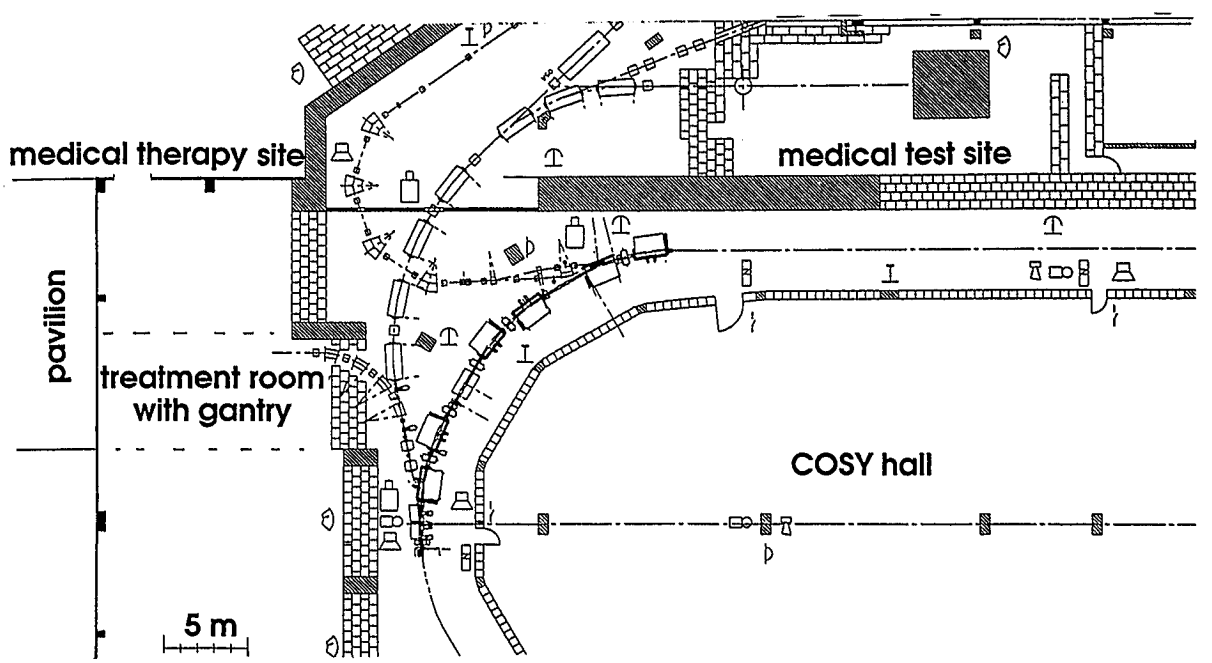

Fig. 2. Layout of the medical area within the COSY facility

4) the biomedical program to characterize the COSY beam biologically, develop clinically relevant assays and optimize tumor imaging.

The projected investment costs for the therapy project are approximately $9 million which will have to come mostly from additional funding on top of the present KFA budget.

Two areas of the COSY facility are reserved for the medical program as shown in Figure 2. Site I is going to be used as experimental area for the pretherapeutic physical and biological program. Site II will be the actual therapy area with patient preparation and treatment room.

The test site I will be equipped with a horizontal beam line providing the same beam quality as at the therapy site. Preparations for the first experiments for beam characterization are under way. A water and a double wedge solid phantom are ready for use with various detector systems. A microstrip and a Si-ring detector, fibre hodoscopes and a 1/2 inch tissue-equivalent proportional counter have already been tested in ion beams. Number of particles, beam profile, energy distribution, absolute dose, dose profile in air and tissue-equivalent phantoms are the parameters to be measured with proton beams between 50 and 250 MeV. Good spatial resolution and detailed information about the contributions of the individual primary and secondary beam components are the priority in this study. In addition, a comparison of cooled and uncooled beams is planned.

The wide range of energies provided by COSY and the ability to change the energy actively from pulse to pulse in small steps without using beam degrading absorber materials has guided the design of the therapy site. A rotating gantry will allow the same flexibility in choosing the treatment angle(s) as in conventional irradiation and a 3D-scanning system is foreseen for tumor conform treatment. Design and cost comparisons for the beam delivery system have now started. The projected therapy site is spacious but a compact beam line system will be designed as model for possible use in a hospital environment.

COSY is a research accelerator mainly used by nuclear physicists, so only a limited number of patients can be treated. The goal will be to treat about 100 well selected cases per year, concentrating on a few indications and to choose tumors with well diagnosable borders close to critical structures (e.g., irregularly shaped head and neck tumors, pediatric tumors). The advantageous dose distribution and steep dose gradient of the ion beam would be most beneficial for the treatment of larger, deep-seated tumors for which treatment modalities need to be developed. Collaborations to define these clinical studies are planned with several nearby University Hospitals.

The Moscow Proton Therapy Facility, Russia

In Russia, the Institute of Theoretical and Experimental Physics (ITEP) in collaboration with other scientific and clinical centers, has been designing and manufacturing equipment for the

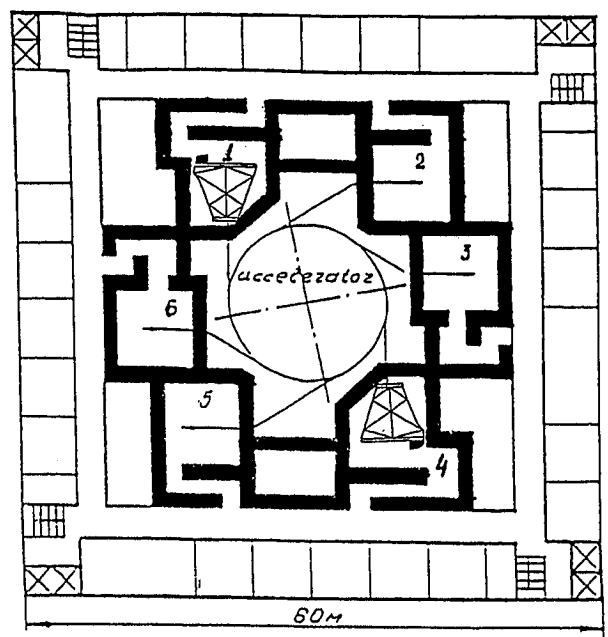

Fig. 3. Top view of a version of the Moscow Proton Therapy Facility (PTF) with two gantries. The treatment rooms are as follows: fully rotational gantries in rooms 1 and 4; intracranial irradiation in room 2; eye treatments in room 5; gynecological treatments in room 6; research and development in room 3. The beams in rooms 2, 3, 5 and 6, are fixed horizontal ones. The total area for the accelerator, beam channels and treatment rooms, is 1300 m^2

Moscow Proton Therapy Facility (PTF). The PTF project has two distinctive features. A synchrotron accelerating H^--ions as the medical accelerator has been chosen [3–5], and a circular arrangement for the treatment rooms around the accelerator selected, as shown in Figure 3.

These choices were made for the following reasons: The most modern methods of conformal dose delivery, have been based on the use of three-dimensional scanning systems receiving a narrow pencil beam at their entrance. The recharge system of beam ejection from the H^--synchrotron presupposes the production of such a narrow beam with extremely small (10^{-7} m rad) phase volume, immediately behind the ejection system. Thus, the H^--synchrotron makes it possible to get the required beam easily, without additional collimation, particle loss, or increase of radiation level. Moreover, the delivery of a beam with small cross section and divergence to the treatment rooms can be made using cheap, light and small-aperture proton channels, lenses and magnets. This is particularly important for the design of the gantry. The weight ratio of the Moscow project gantry and the gantry in Loma Linda, is better than 1:10 (7 tons vs. 90 tons).

The circular structure of the PTF allows the treatment rooms to be very close to the accelerator which makes the proton channels very short. Therefore, the PTF footprint and the number of lenses and magnets are minimized. Thus the areas occupied by the accelerator, beam channels and six treatment rooms in the Moscow project, have the ratio of 1:1.5 to those occupied by the Loma Linda facility with its five treatment rooms. In addition, each proton channel (starting from the beam ejection system) and each treatment room, works independently, but they can operate in parallel. The energy and intensity of the beam in each pulse sent successively to the treatment rooms, are also chosen individually. The basic parameters are given in Table 1.

Any combination is possible for the number of treatment rooms with horizontal fixed beams and with gantry systems.

Table 1. Basic Parameters of the Moscow PTF.

Energy of external proton beams	variable, up to 250 MeV
Number of particles per pulse	up to 3×10^{10}
Repetition rate	3 Hz
Ejection time	200 ms
Dose field dimensions provided by the gantry	up to 30×30 cm^2
Number of treatment rooms	6

The Eye Treatment Facility at Munich, Germany

The two Munich Universities, Ludwig-Maximilians-Universität and Technische-Universität München, operate a 14 MV tandem Van de Graaff accelerator for nuclear physics research. Recently, a post-accelerator, TRITRON, has been installed to extend the nuclear physics program. TRITRON is an ambitious new accelerator type using superconducting bending magnets and superconducting acceleration cavities operating at $T \leq 4.5$ K (liquid helium). Protons have the longest range of particles accelerated by TRITRON and the maximum energy should reach 70 MeV. It is planned to install an eye-treatment facility and to perform selected dosimetry studies in collaboration with the radiotherapy group of the University of Regensburg.

The Centre for Oncological Hadrontherapy, Italy

A feasibility study has just been completed [6] for a hospital-based hadrontherapy facility to be built in Italy. A request for financing is now being submitted to the authorities. The facility hopes to treat 1000 patients/year in 5 treatment rooms served by a H^-/light ion synchrotron. The facility will have:

1) two rooms equipped with isocentric gantries capable of transporting protons up to 250 MeV,

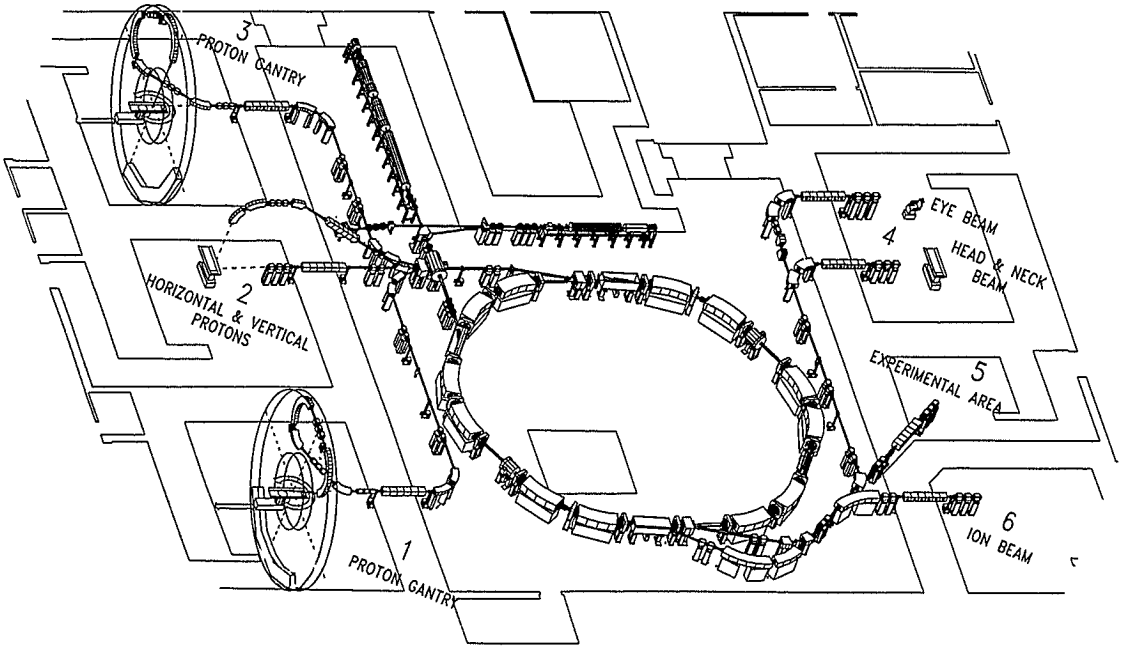

Fig. 4. Layout of the Centre for Oncological Hadrontherapy

2) one room with two 250 MeV proton beams, one horizontal and one vertical pointing down,
3) one room with two horizontal beam lines, one for irradiations of eye tumors and one mainly devoted to head and neck treatments,
4) one room with a horizontal beam for experiments using both protons and light ions (dosimetry, radiobiology, calibrations, etc.),
5) one room devoted to future light ion treatments,
6) two smaller rooms served by the 11 MeV proton beam from the injector, one for the production of positron emitting radionuclides for PET uses, the other for thermal neutron production for boron neutron capture therapy (BNCT). The layout of the facility is shown in Figure 4.

The complex will have two buildings: one above ground with conventional facilities and office space, and a heavily shielded area underground (the "bunker") housing the accelerator and the treatment rooms which will have a surface area of about 3500 m^2 and a maximum height of about 15 m to accommodate the gantry rooms. The rooms for BNCT and for radionuclide production will be on the lowest floor.

The accelerator is a H^--synchrotron (which will also accelerate protons) capable of providing 60–250 MeV proton beams with an average intensity of about 10 nA. Injection in the synchrotron is at 11 MeV from a linac (RFQ + DTL). The design includes the possibility to upgrade the machine in order to accelerate fully stripped light ions up to $^{16}0$ to a final energy in the range of 120–400 MeV/u with minor interventions on the ring and the addition of a second ion source and injector.

The main advantages of accelerating H^- are:

1) the simplicity of the ejection system based on a thin target (stripping foil),
2) the very small transverse emittances (of the order of 0.1 π mm mrad) of the extracted beams which can be obtained with a small stripping target. This allows the weight of the gantry magnets to be reduced, due to their smaller required aperture,
3) the possibility of controlling the extracted beam intensity by a feedback from a monitor

in the beam line to the dipoles driving the beam to the stripping foil. The allowed time constant for such direct feedback is fundamentally much shorter than for resonant extraction.

The synchrotron is provided with multiple extraction: two charge-exchange extraction systems for H^-, one resonant extraction for protons and one fast extraction port to be used as beam abort. The extraction of H^--ions is achieved by smoothly driving the circulating beam against a small beryllium or carbon foil, by a local orbit bump. A short bending magnet placed just after the stripping foil separates the protons from the circulating H^--ions.

Two treatment rooms will be equipped with an isocentric gantry of the "cork-screw" type, similar to that installed at the Loma Linda University Medical Center in California, but of reduced weight. The outer diameter of the proposed gantry is about 11 m with a distance between the exit of the last dipole and the isocenter of 3.4 m. The gantry optics are achromatic and designed to fully exploit the small beam size. The estimated vertical aperture of the dipole magnets is 2 cm. The weight of the magnets is estimated to be about 6 t and the overall weight of the gantry is expected not to exceed 25 t.

The Proton Therapy Facility in the Netherlands

In 1995 the new AGOR cyclotron will be commissioned at the nuclear physics laboratory "Kernfysisch Versneller Instituut" (KVI) in Groningen, the Netherlands. The cyclotron was built in Orsay, France, jointly by the French and Dutch science agencies (AGOR: Accelerator Groningen Orsay). In April 1994 the machine produced its first beam and it has passed the acceptance tests successfully. During 1994, the cyclotron was disassembled and transported to Groningen where it is expected to be ready for the first experiments in the summer of 1995.

The cyclotron is equipped with superconducting coils, which makes the machine relatively compact. Various heavy ions can be accelerated to kinetic energies of 600 q^2/A (MeV) with q and A being the charge and mass of the ion. Protons can be produced with a maximum energy of 200 MeV. The availability of 200 MeV protons provides a unique opportunity to introduce proton therapy in the Netherlands and to contribute to the international need for proton therapy facilities.

A collaboration between the Radiotherapy Departments of the University Hospitals in Groningen and Utrecht, the Daniel den Hoed Kliniek in Rotterdam, the Radiobiology group of the University of Groningen and KVI has been initiated to plan a research facility for radiotherapy with proton beams at the KVI. The facility should serve as a pilot project for a possible clinical use of protons in radiotherapy. The planned facility consists of a dedicated beam line and a "beam swinger" gantry in the KVI building.

The various users of the cyclotron have agreed upon a beam-time sharing schedule with 24 weeks of beam time for proton therapy. The facility should be able to treat about 250 patients per year.

Since high quality proton therapy touches the limits of present (medical) technology, a multidisciplinary research program will be initiated. A program for the development of special instrumentation has been started in collaboration with clinical physicists from the participating hospitals.

During the operational phase, medical research, consisting of several clinical studies, and radiobiological research will be performed in an international collaboration. It is estimated that in the Netherlands about 1000 patients per year have indications for proton therapy.

Presently, a detailed inventory is being made of the different projects, both in the medical field (e.g., patient selection, dose distributions) and in (clinical) physics (e.g., design of the gantry, dosimetry, treatment planning). Proposals for the proton therapy project and the associated research programs have been submitted to various Dutch funding agencies. It is anticipated that, after funding has been achieved, it will take another three years to set up the facility.

A Regional Proton Therapy Facility for the North Carolina State University Centennial Campus, USA

NC STAR is a proposed project to be built on the new "Centennial Campus" of North Carolina State University (NCSU) in Raleigh. The major components are two synchrotron rings. One ring, the booster, has a dual mission. It must boost (accelerate) electrons to full energy (2.5 GeV) for injection into the second (storage) ring. The electron storage ring is an intense light source which will support various research and applied programs utilizing powerful synchrotron radiation in the X-ray, ultraviolet and far infrared regions involving collaboration between universities, state and federal agencies, and advanced technology industries. The acceleration and injection of electrons will require only a small percentage of the time available on the booster ring. Most of the operating time would therefore be available for a second purpose, such as to accelerate protons and deliver them to an on-site, dedicated cancer treatment clinic. The clinic will be operated by the Radiation Oncology Department of the UNC School of Medicine.

At NC STAR, protons would be produced in a duoplasmatron ion source, preaccelerated to 15 MeV in two linac stages, injected into the booster synchrotron, accelerated to the desired energy (70 MeV to 250 MeV, nominally), extracted, and transported to the patient treatment area. The booster synchrotron can generate protons of over 1700 MeV, but shielding costs will limit the energy to a much lower value. The present booster design will accommodate H^--ions which have certain advantages over protons with regard to the properties of the extracted beam. However, it is not thought that the associated cost savings would compensate for the more stringent (i.e., expensive) vacuum requirements of H^--ion beams compared to the base vacuum needed for electron acceleration. The relatively high rigidity (8.3 Tm) of the booster makes it suitable as a heavy ion accelerator, e.g., for carbon ion therapy, which might be an option in the future.

Protons will be delivered to patients in treatment rooms in a clinical setting where they will be attended by a professional staff as in a hospital-based oncology department. The facility will feature two beam delivery systems: 1) a fixed beam to treat patients with tumors in the head and neck areas; a special chair with multiple adjustments will be used for patient positioning; and 2) a gantry system to treat patients with deep body tumors.

The Centennial Campus site in Raleigh is approximately 30 minutes on interstate highway from the UNC School of Medicine in Chapel Hill. The remote facility will be supported by a full staff of physicians and attendants, and it will house essential ancillary equipment such as computers for retrieving patient records and treatment plans. Thus, the NC STAR-based facility will be a well-designed remote site with a number of highly favorable local factors that favor this particular project, including significant cost savings.

Proton Development N.A., Inc., USA

Proton Development N.A., Inc. is in the process of arranging financing for the purpose of establishing the first of nineteen Medical Proton Therapy Facilities in the Chicago area and the remaining eighteen throughout the United States. Each facility will be on the campus of a major teaching medical complex and will have four treatment rooms, three gantries and one head, neck and eye horizontal beam room.

The facilities will be run as commercial enterprises. Each will have two CT units, an MRI unit, a business office, examination rooms and offices for medical educational centers. Each medical school will have an office in the building so that they can treat their own patients. At the first facility, for example, there will be seven offices, since there are seven medical schools in Chicago.

A business plan has been completed which includes an economic feasibility study in real dollars. Operating costs have been projected between $4.9 million to $14 million per year depending on the hours of operation. The projected budget for the first facility is $106 million, significantly larger than what has been quoted by not-for-profit/government and church supported

institutions. These projections include treating over 2000 patients per year with a staff of 150 personnel to cover approximately 92 hours of operation per week.

Acknowledgements

The author wishes to thank the following colleagues for their reports which contain most recent, partly unpublished data on the various facilities: J. de Boer, Ludwig-Maximilians-Universität; S. Carb, Proton Development N.A., Inc.; J. Heese, Hahn-Meitner-Institut, Berlin; U. Linz, Forschungszentrum Jülich; R. Mowat, North Carolina State University; V. S. Khoroshkov and K. K. Onosovsky, ITEP, Moscow; U. Oelfke, TRIUMF, University of British Columbia; J.M. Schippers, KVI, and B.G. Szabó, University Hospital, Groningen; M. Silari, CNR, Milan, Italy; A. Smith, Northeast Proton Therapy Center, Boston; and L. Verhey, University of California, San Francisco.

References

1 Sisterson J.M. (ed.) Particles 14; July 1994, p.10.
2 Gottschalk, B. Capabilities of passive beam-spreading techniques, in Proc. of the 5th PTCOG Meeting and the Int. Workshop on Biomedical Accelerators, Dec. 1–2, 1986, LBL-Report-22962, pp. 161–168.
3 Khoroshkov, V.S., Onosovsky, K.K., Breev, V.M., Goldin, L.L., Kleinbock, Y.L., Lomanov, M.F., Lyulevitch, V.I., Vorontsov, I.A., Klenov, G.I., Rybalko, V.S., and Ivanov, Yu.S. Soviet Project of PTF. Proc. of the NIRS Int. Workshop on Heavy Charged Particle Therapy and Related Subjects. Chiba, Japan, July 4–5, 1991, pp. 204–212.
4 Khoroshkov, V.S. and Onosovsky, K.K. H^--Synchrotron for Proton Therapy Facility, in Proc. of the NIRS Int. Workshop on Heavy Charged Particle Therapy and Related Subjects, Chiba, Japan, July 4–5, 1991, pp. 213–220.
5 Khoroshkov, V.S., Goldin, L.L., Onosovsky, K.K., and Klenov, G.I. The USSR Project of a Proton Therapy Facility. Digest of the World Congress on Medical Physics and Biomedical Engineering, XVI Int. Conf. on Medical and Biological Engineering, and IX Int. Conf. on Medical Physics. Kyoto, Japan, July 7–12, 1991, p.50.
6 Amaldi, U. and Silari, M. (eds.), The TERA Project and the Centre for Oncological Hadrontherapy, INFN-LNF-SIS Ufficio Publicazioni, Frascati, Italy, 1994.

Subject Index